

Dissertation zur Erlangung des Doktorgrades der Fakultät für Chemie und Pharmazie
der Ludwig-Maximilians-Universität München

**Structural Analyses of Antibiotic Resistance Mechanisms by
Cryo Electron Microscopy**



Stefan Arenz
aus
Tettnang, Deutschland

2015

Erklärung

Diese Dissertation wurde im Sinne von § 7 der Promotionsordnung vom 28. November 2011 von Herrn Prof. Dr. Roland Beckmann betreut.

Eidesstattliche Versicherung

Diese Dissertation wurde eigenständig und ohne unerlaubte Hilfe erarbeitet.

München,

Stefan Arenz

Dissertation eingereicht am 21.05.2015

1. Gutachter: Herr Prof. Dr. Roland Beckmann
2. Gutachter: Herr Dr. Daniel N. Wilson

Mündliche Prüfung am 15.07.2015

Table of Contents

ACKNOWLEDGEMENTS	1
LIST OF ORIGINAL PUBLICATIONS	2
CONTRIBUTIONS REPORT.....	3
ABBREVIATIONS.....	5
SUMMARY	7
1 INTRODUCTION	8
1.1 <i>The Bacterial Ribosome.....</i>	8
1.2 <i>The Translation Cycle.....</i>	10
1.2.1 Initiation.....	11
1.2.2 Elongation.....	14
1.2.3 Termination.....	23
1.2.4 Recycling.....	27
1.3 <i>Antibiotics.....</i>	28
1.3.1 Proline-rich Antimicrobial Peptides	31
1.3.2 Tetracyclines	32
1.3.3 Macrolides	35
2 OBJECTIVES OF THESE STUDIES.....	50
3 CUMULATIVE THESIS: SUMMARY OF PUBLICATIONS	52
3.1 <i>Publication 1 Structural Basis for the Interaction of Protein S1 with the Escherichia coli Ribosome</i>	52
3.2 <i>Publication 2 The Proline-rich Antimicrobial Peptide Onc112 Inhibits Translation by Blocking and Destabilizing the Post-initiation Complex</i>	53
3.3 <i>Publication 3 Tetracycline Antibiotics and Resistance Mechanisms.....</i>	54
3.4 <i>Publication 4 Cryo-EM Structure of the Tetracycline Resistance Protein TetM in Complex with a Translating Ribosome at 3.9 Å Resolution.....</i>	55
3.5 <i>Publication 5 Molecular Basis for Erythromycin-dependent Ribosome Stalling During Translation of the ErmBL Leader Peptide.....</i>	56
3.6 <i>Publication 6 Drug Sensing by the Ribosome Induces Translational Arrest via Active Site Perturbation</i>	58
3.7 <i>Publication 7 Alternate Conformation of a Nascent Chain in the Ribosomal Tunnel Induces P-tRNA Perturbation and Inhibition of Peptide Bond Formation</i>	59
4 DISCUSSION	61
4.1 <i>Interaction of Protein S1 with the Escherichia coli Ribosome</i>	61
4.2 <i>Proline-rich antimicrobial peptides.....</i>	63
4.3 <i>TetM-mediated Tetracycline Resistance.....</i>	64
4.4 <i>Macrolide-dependent Ribosome Stalling</i>	66
5 REFERENCES	74
6 PUBLICATIONS	103

Acknowledgements

First of all, I want to thank Dr. Daniel N. Wilson for accepting me as a PhD student in his lab. I am deeply grateful for your continuous, excellent and strong support during my PhD, for many inspiring scientific discussions, for your constant advice, for giving me the opportunity to accept challenges like conference talks, for so many valuable experiences and of course for the great times during trips, including the best reuben pastrami sandwich on earth! Thank you for being such a great scientific and personal mentor, I honestly enjoy working in your lab.

I want to thank Prof. Roland Beckmann for all the expertise, valuable advice and support and for providing such an excellent scientific environment, which makes research possible! I further want to thank Dr. Otto Berninghausen, Charlotte Ungewickell and Susanne Rieder for great cryo-EM image data sets and their support with everything concerning EM. Special thanks go to all our collaborators, especially to Dr. Nora Vazquez-Laslop and to Prof. Alexander Mankin for numerous discussions and ideas regarding all Erm-projects.

Further I want to thank: Daniel Sohmen, for supervising me during my practical and during my master thesis, for many discussions, for a lot of help with so many things and for always answering all my questions; Dr. Agata Starosta for a lot of help with biochemical experiments, for many excellent ideas and permanent advice; Dr. Julian Deeng and Dr. Sibylle Franckenberg for introducing me into image processing; Dr. Bertrand Beckert for tremendous help with certain Perl scripts; Dr. Lukas Bischoff and Dr. Stephan Wickles for many fruitful discussions and help with image processing; Andre Heuer for organizing numerous events; Dr. Birgitta Beatrix, for helping me taking care for the centrifuges; Ingegerd Walz for organizing everything outside the lab; Heidemarie Sieber for permanent help with orders; Thanks to all people I forgot to mention for forgiving me. Generally, I want to thank all present and past members of the Wilson and the Beckmann group, for parties, fun and the extraordinary nice and supportive atmosphere!

My biggest thanks go to Susi, for her love and for her everlasting support, and to my family, especially to my parents who made everything possible!

List of Original Publications

Publication 1

Konstantin Byrgazov, Irina Grishkovskaya, **Stefan Arenz**, Nicolas Coudevylle, Hannes Temmel, Daniel N. Wilson, Kristina Djinovic-Carugo and Isabella Moll (2014). Structural basis for the interaction of protein S1 with the *Escherichia coli* ribosome. *Nucleic Acids Research*. 43, 661-673.

Publication 2

Carolin A. Seefeldt*, Fabian Nguyen*, Stéphanie Antunes*, Natacha Pérébasquine, Michael Graf, **Stefan Arenz**, Kishore K. Inampudi, Céline Douat, Gilles Guichard, Daniel N. Wilson and Axel C. Innis (2015). The proline-rich antimicrobial peptide Onc112 inhibits translation by blocking and destabilizing the post-initiation complex. *Nature Structural & Molecular Biology*. 10.1038/nsmb.3034.

Publication 3

Fabian Nguyen, Agata L. Starosta, **Stefan Arenz**, Daniel Sohmen, Alexandra Dönhöfer and Daniel N. Wilson (2014). Tetracycline antibiotics and resistance mechanisms. *Biological Chemistry*. 395, 559-575.

Publication 4

Stefan Arenz, Fabian Nguyen, Roland Beckmann and Daniel N. Wilson (2014). Cryo-EM structure of the tetracycline resistance protein TetM in complex with a translating ribosome at 3.9 Å resolution. *Proceedings of the National Academy of Sciences*. 112, 5401-5406.

Publication 5

Stefan Arenz, Haripriya Ramu, Pulkit Gupta, Otto Berninghausen, Roland Beckmann, Nora Vázquez-Laslop, Alexander S. Mankin and Daniel N. Wilson (2014). Molecular basis for erythromycin-dependent ribosome stalling during translation of the ErmBL leader peptide. *Nature Communications*. 5: 3501.

Publication 6

Stefan Arenz, Sezen Meydan, Agata L. Starosta, Otto Berninghausen, Roland Beckmann, Nora Vázquez-Laslop and Daniel N. Wilson (2014). Drug Sensing by the Ribosome Induces Translational Arrest via Active Site Perturbation. *Molecular Cell*. 56, 446-452.

Publication 7

Stefan Arenz, C. Axel Innis, Roland Beckmann and Daniel N. Wilson (2015). Alternate conformation of a nascent chain in the ribosomal tunnel induces P-tRNA perturbation and inhibition of peptide bond formation. *Unpublished manuscript*.

*These authors contributed equally to this work.

Contributions Report

This dissertation comprises work, which was conducted during my PhD research from March 2012 to June 2015 in the lab of Dr. Daniel N. Wilson at the Gene Center of the Ludwig-Maximilians University Munich. Some projects were done in collaboration with scientists from the labs of Prof. Roland Beckmann (Munich, Germany), Prof. Isabella Moll (Vienna, Austria), Prof. Kristina Djinovic-Carugo (Vienna, Austria), Prof. Gilles Guichard (Bordeaux, France), Prof. C. Axel Innis (Bordeaux, France) and Prof. Alexander S. Mankin (Chicago, USA).

Publication 1 (Byrgazov et al., 2014)

This publication reports the structural basis for the interaction of ribosomal protein S1 with the *E. coli* ribosome. I prepared the ErmCL-stalled ribosome complex, performed the cryo-EM analysis and visualized domains D1 and D2 of S1 on the ribosome. I docked the crystal structures into the density and contributed to interpretation of the map. I prepared figures 3, 6, S3, S4 and contributed to writing this manuscript.

Publication 2 (Seefeldt, Nguyen, Antunes et al., 2015)

This publication comprises the first structure of the proline-rich antimicrobial peptide Onc112 bound to the *Thermus thermophilus* ribosome as well as biochemical analyses, unraveling the mode of Onc112-mediated translation inhibition. I performed the disome assays showing that Onc112 destabilizes the 70S post-initiation complex and prepared figures 4b-e of the manuscript.

Publication 3 (Nguyen et al., 2014)

This publication reviews the development of first-, second- and third-generation tetracyclines, their mode of ribosome binding, their mechanism of action as well as diverse tetracycline resistance mechanisms, such as drug efflux, drug modification, target mutation and ribosome protection. I prepared figure 6 and contributed to writing this manuscript.

Publication 4 (Arenz et al., 2015)

This publication reports a cryo-EM structure of TetM in complex with a translating ribosome at 3.9 Å resolution. I prepared the TetM•RNC complex, performed the cryo-EM analysis, reconstructed and refined the complex and built the model for the TetM-bound ribosome. I contributed to data interpretation and the design of *in vitro* translation experiments. I prepared all figures and helped writing this manuscript.

Publication 5 (Arenz et al., 2014)

This publication reports the molecular basis for erythromycin-dependent ribosome stalling during translation of the ErmBL leader peptide. I used the disome system to purify ErmBL-SRCs and performed the cryo-EM analysis to reconstruct the ErmBL-SRC. Beside my contribution to interpret the map and biochemical data, I built the molecular model for ErmBL-SRC. I prepared all figures and helped writing this manuscript.

Publication 6 (Arenz et al., 2014)

This publication provides the first near-atomic resolution structure of a drug-stalled ribosome and unravels how drug sensing by the ribosome induces translational arrest during translation of the ErmCL leader peptide via active site perturbation. I used the previously established disome system to purify ErmCL-SRCs and performed the cryo-EM analysis to reconstruct the ErmCL-SRC. I performed the model building for ErmCL-SRC and contributed to interpretation of structural and biochemical data, prepared all figures and assisted in writing this manuscript.

Publication 7 (Arenz et al., unpublished manuscript)

This publication, reporting a 3.1-3.6 Å reconstruction of the ErmBL-SRC, provides structural insight into the complex interplay between the ErmBL nascent polypeptide, the ribosome and the tunnel-bound drug at a yet unachieved level of detail, allowing our previously proposed model for ErmBL-mediated translation arrest to be revised. I used the previously established disome system to purify ErmBL-SRCs and performed the cryo-EM analysis to reconstruct the ErmBL-SRC. After refinement of the map, I generated and refined a molecular model for the complete ErmBL-SRC. I contributed to interpretation of the data, prepared all figures and helped writing this manuscript.

Abbreviations

2D	two-dimensional
A	adenine
AAP	arginine attenuator peptide
aa-tRNA	aminoacyl-tRNA
A-site	acceptor site
ASL	anticodon stem loop
C	cytosine
CMV	cytomegalovirus
DC	decoding center
Cs	spherical aberration
CTH	C-terminal helix
DNA	deoxyribonucleic acid
EF	elongation factor
EM	electron microscopy
Erm	erythromycin methyltransferase
E-site	exit site
FRET	fluorescence resonance energy transfer
G	guanine
GAC	GTPase-associated center
GDP	guanosin-5'-diphosphate
GTP	guanosin-5'-triphosphate
h#	helix # of small ribosomal subunit
H#	helix# of large ribosomal subunit
IC	initiation complex
IF	initiation factor
kDa	kilodalton
LSU	large subunit
MDa	megadalton
MIC	minimal inhibition concentration

MRSA	methicillin resistant <i>Staphylococcus aureus</i>
NMR	nuclear magnetic resonance
OB	oligosaccharide/oligonucleotide-binding
ORF	open reading frame
Pi	inorganic phosphate
PrAMP	proline-rich antimicrobial peptide
P-site	peptidyl site
PTC	peptidyl transferase center
POST	post-translocation
PRE	pre-translocation
RF	release factor
RNA	ribonucleic acid
mRNA	messenger RNA
rRNA	ribosomal RNA
tRNA	transfer RNA
lmRNA	leaderless messenger RNA
RNC	ribosome nascent chain complex
RPP	ribosome protection protein
rProtein	ribosomal protein
RRF	ribosome recycling factor
SD	Shine-Dalgarno
SRC	stalled ribosome complex
SRL	sarcin-ricin loop
SSU	small subunit
T	thymine
U	uracil
UTR	untranslated region

Summary

The ribosome translates the genetic code stored in the codon sequence of the mRNA into proteins, which represents a central step in all living organisms. Using cryo electron microscopy (cryo-EM) this work sheds light on several aspects of translation. We provide the first structural basis for the interaction of ribosomal protein S1 with the ribosome, extending our insight into how S1 enables translation initiation on highly structured mRNAs. Since the ribosome is the major target for antibiotics within bacterial cells, we unraveled how the proline-rich antimicrobial peptide Onc112, representing a potentially new class of clinically used antibiotics, binds to the ribosome and inhibits translation. Bacterial resistance to all classes of clinically used antibiotics is quickly spreading and represents a major threat to public health. We gained profound insight into the molecular mechanism of the widespread ribosome protection protein (RPP) TetM-mediated tetracycline resistance, by obtaining a high-resolution cryo-EM reconstruction of TetM bound to a translating ribosome. Another mechanism by which bacteria become resistant is based on the principle of target modification. For example, specialized Erm-type methyltransferases methylate the macrolide binding site within the ribosome exit tunnel and thus confer macrolide resistance. Expression of these resistance enzymes is strictly regulated by drug-dependent translation attenuation on short upstream open reading frames encoding leader peptides. Thereby, the amino acid sequence of the nascent peptide, together with the presence of macrolides, is a crucial determinant necessary for stalling to occur. By using cryo-EM on stalled ribosome complexes (SRCs), we unraveled for the first time how the nascent leader peptide intimately interacts with the ribosome and the tunnel-bound macrolide to generate a stalling signal, which is then communicated to the peptidyl transferase center (PTC) to arrest translation of the leader peptide, thus leading to induction of expression of the resistance enzyme. Moreover, we revealed that depending on the amino acid sequence of the nascent peptide, the mechanisms by which the ribosomal PTC gets inactivated is completely distinct.

1 Introduction

Almost 50 years ago, Francis Crick published the hypothesis of the central dogma of molecular biology (Crick, 1970). The central dogma describes that sequential genetic information stored in DNA is transferred from DNA polymers to RNA polymers to amino acid polymers, so called proteins. During transcription, genetic information stored as DNA sequence is transcribed into the corresponding RNA sequence by specialized DNA-dependent RNA polymerases. RNA molecules play numerous roles in the cell. They can act as regulators of gene expression, serve as structural scaffolds or function as enzymes. The destination of most of the cellular RNA molecules is to carry the genetic code to build a specific protein. Such RNA molecules are called messenger RNAs (mRNAs). In the process of translation, macromolecular machines read the genetic code stored in nucleotide triplets (codons) (Crick et al., 1961) of the mRNA sequence and translate this information into an amino acid sequence of a protein. The macromolecular machines responsible for translation were discovered in 1955 by George Palade on electron microscopy images of acinar cells of rat pancreas (Palade, 1955) and were initially named Palade particles. Later, these particles were renamed to “Ribosomes” (McQuillen et al., 1959). The function of ribosomes is conserved in all three domains of life, however species-specific differences in their molecular architecture exist. These differences are exploited for example by various antibiotics that exclusively bind and inhibit prokaryotic ribosomes.

1.1 The Bacterial Ribosome

In all three kingdoms of life, the ribosome is responsible for the biosynthesis of polypeptides by translation of mRNA sequences. The bacterial ribosome consists of the 30S subunit (small subunit, SSU) and the 50S subunit (large subunit, LSU) that reversibly join together to form the 70S ribosome with a total molecular mass of approximately 2.5 megadalton (MDa). In bacteria, such as *Escherichia coli*, the 30S ribosomal subunit is composed of the 16S ribosomal RNA (rRNA) and 21 ribosomal proteins (rProteins), whereas the 50S ribosomal subunit is formed by 23S rRNA, 5S rRNA and 33 rProteins (**Fig. 1**). The two subunits have different roles during

translation. The SSU harbors the decoding center (DC), which is responsible for decoding the genetic information stored in the codon sequence of mRNA, whereas the LSU of the ribosome harbors the peptidyl transferase center (PTC), which is the active site of the ribosome for linking amino acids together to form the polypeptide chain (**Fig. 1**). Similar to the decoding center, the PTC is composed predominantly of rRNA, leading to the suggestion that the ribosome is a ribozyme (Ban et al., 2000; Cech, 2000; Hansen et al., 2002c; Harms et al., 2001; Nissen et al., 2000; Noller, 2012; Schlünzen et al., 2001). The N-terminus of the closest ribosomal protein L27 comes within 8-10 angstroms (Å) of the PTC (Voorhees et al., 2009) and is not essential for catalysis, since cells expressing N-terminal truncation mutants of L27 are still viable, although their growth rate is severely affected (Maguire et al., 2005). Therefore L27 certainly contributes to proper PTC function, which is underlined by the recent suggestion that the N-terminus L27 not only is involved in proper tRNA positioning (Voorhees et al., 2009), but is also directly involved in a proton wire mechanism enabling peptide bond formation (Polikanov et al., 2014b).

Amino acids are delivered to the ribosome bound to adaptor molecules called transfer-RNA molecules (tRNAs). The tRNAs contain anticodons, which recognize specifically the codons on the mRNA that encode the amino acids linked to the tRNAs. The correctness of the interaction between the anticodon of the tRNA and the codon of the mRNA is monitored by the DC of the small subunit. The ribosome possesses three binding sites for tRNAs at the subunit interface, namely the acceptor site (A-site), the peptidyl site (P-site) and the exit site (E-site) (**Fig. 1**). During translation, the tRNAs sequentially move from the A-site to the P-site to the E-site before they dissociate from the ribosome. The growing polypeptide is attached to the P-site tRNA (peptidyl-tRNA) and passes through the 100 Å long and 15-30 Å wide exit tunnel located in the 50S subunit. Hydrolysis detaches the newly synthesized polypeptide from the P-site tRNA allowing its dissociation from the ribosome (Schmeing and Ramakrishnan, 2009).

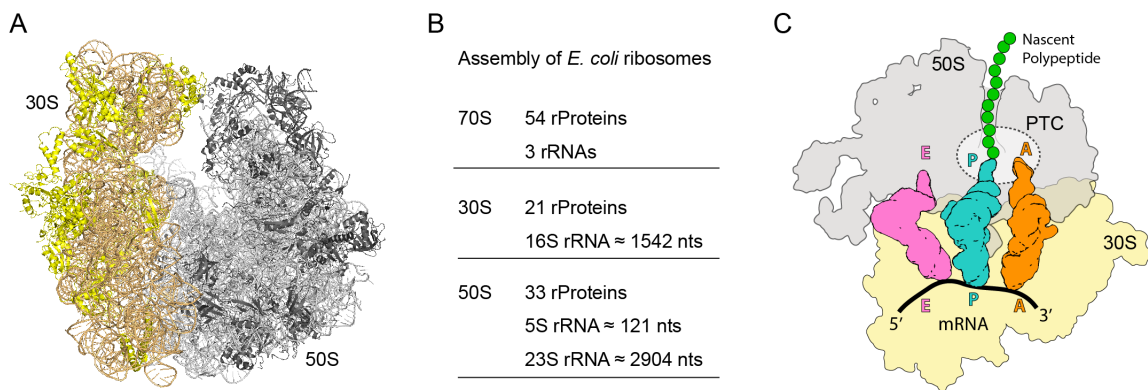


Figure 1 | The prokaryotic ribosome. (A) Overview of the *Escherichia coli* 70S ribosome (Dunkle et al., 2011) with 30S subunit colored in yellow and 50S subunit in grey. (B) Table of assembly components of the 70S ribosome as well as the 30S and 50S subunits. (C) Schematic representation of the prokaryotic ribosome bound with three tRNAs showing the 30S subunit (yellow), 50S subunit (grey), A-site tRNA (orange), P-site tRNA (cyan), E-site tRNA (pink) and mRNA (black). The PTC on the 50S subunit is depicted as dashed-lined sphere.

1.2 The Translation Cycle

Translation is a cyclic reaction that can be divided into four steps: Initiation, Elongation, Termination and Recycling (**Fig. 2**). Initiation of translation involves 30S-mediated start site recognition on the mRNA and subsequent joining of the 50S subunit to form the 70S complex. During elongation, aminoacyl-tRNAs (aa-tRNAs) are delivered to the A-site of the ribosome and bring along the next amino acid for incorporation into the nascent polypeptide chain. The PTC thereby catalyzes the formation of a new peptide bond between the A-site amino acid and the C-terminus of the nascent polypeptide, which is elongated by one amino acid. After peptide bond formation, the tRNAs are translocated from the A- to the P-site and from the P- to the E-site, respectively. Thereby the mRNA advances by three nucleotides, which places the next codon in the A-site and thus allows for the next cycle of translation elongation. The elongation cycle continues until a stop codon, rather than a sense codon, enters the A-site. Stop codon-mediated hydrolysis of the peptidyl-tRNA leads to termination of translation and subsequent ribosome recycling. Recycling includes splitting of the 70S complex into the SSU and the LSU to allow re-initiation on the next mRNA molecule. In the following sections 1.2.1-1.2.4 the four steps of the translation cycle will be described in detail.

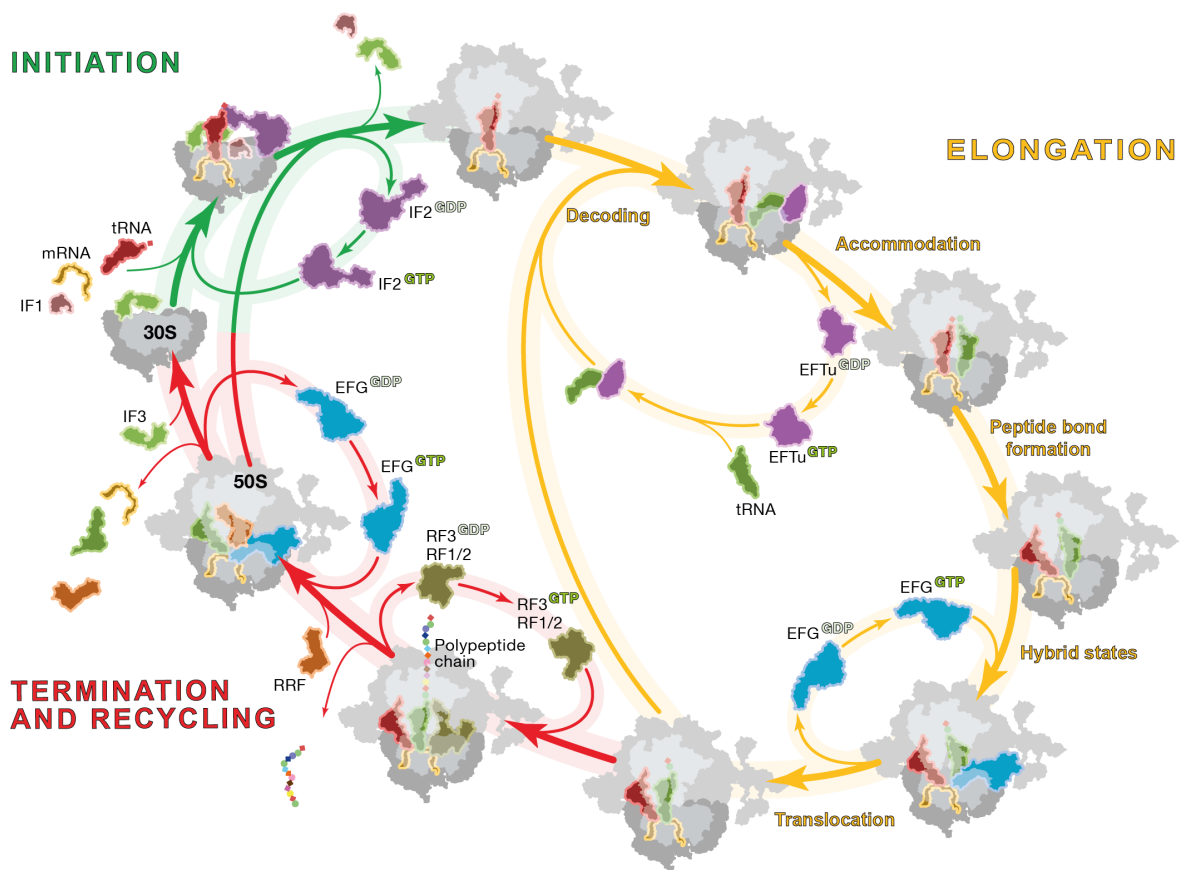


Figure 2 | Overview of the prokaryotic translation cycle. During Initiation (green), the 70S-IC is formed, involving IF1, IF2, IF3, mRNA, initiator tRNA and both 30S and 50S ribosomal subunits. In the Elongation phase, incoming tRNAs are delivered by EF-Tu to the A-site of the ribosome. After accommodation of the A-site tRNA, the ribosome catalyzes peptide bond formation and transfers the peptide attached to the P-site tRNA onto the A-site tRNA, thereby elongating the nascent peptide by one amino acid. The ribosome adopts the ratcheted state with tRNAs in hybrid states. EF-G mediates translocation of the mRNA by one codon and translocation of the tRNAs from the A- to the P and from the P- to the E-site. If a sense codon is displayed in the empty A-site, a new round of the elongation cycle occurs. As soon as a stop codon emerges in the A-site, translation Termination is mediated by the action of RF1, RF2 and RF3. During ribosome Recycling, RRF and EF-G cooperate to split the ribosome for translation initiation on the next mRNA. Figure modified from (Sohmen et al., 2009).

1.2.1 Initiation

Initiation of translation is the rate-limiting step during translation of mRNA molecules into proteins (Laursen et al., 2005). Prokaryotic translation initiation requires formation of the 30S initiation complex (30S-IC), which involves the three initiation factors IF1, IF2 and IF3, as well as mRNA and the formylated initiator fMet-tRNA_{fMet} (**Fig. 3**). The methionyl-tRNA transformylase-mediated formylation of the initiator tRNA distinguishes initiator fMet-tRNA_{fMet} from elongation Met-tRNA^{Met}

(Guillon et al., 1992; Lee et al., 1991; Seong and RajBhandary, 1987). The main goal of 30S-IC formation is to position the initiator fMet-tRNA^{fMet} in a P/I state (peptidyl/initiation state) binding the start codon of the mRNA in the P-site of the SSU (Allen et al., 2005; Antoun et al., 2006; Julian et al., 2011). Subsequently, the LSU joins to form the 70S initiation complex (70S-IC) (**Fig. 3**). 70S-IC formation is accompanied by the dissociation of initiation factors IF1-3 from the ribosome, leaving the fMet-tRNA^{fMet} positioned in the P/P state and thereby priming the ribosome for initiation of translation elongation (Marshall et al., 2009).

During initiation, IF1 and IF3 ensure fidelity of the process, whereas IF2 recruits fMet-tRNA^{fMet}. IF3 binds to the E-site of the 30S subunit (**Fig. 3**) to form the IF3-30S complex and thereby prevents premature 50S subunit joining before association with IF1, IF2, mRNA and initiator tRNA (Dallas and Noller, 2001; Grunberg-Manago et al., 1975; Karimi et al., 1999; Subramanian and Davis, 1970). The interaction of the Shine-Dalgarno (SD) sequence (Shine and Dalgarno, 1974) of canonical mRNAs with the 3' end of the 16S rRNA (anti-SD) places the start codon in the P-site and allows for subsequent association of fMet-tRNA^{fMet}, IF1 and IF2 (Demeshkina et al., 2010; Jenner et al., 2010b; Kaminishi et al., 2007). Discrimination of the initiator tRNA is performed by IF3 through monitoring of three unique G:C base pairs in fMet-tRNA^{fMet} (Hartz et al., 1990; Hartz et al., 1989; O'Connor et al., 2001; Risuleo et al., 1976; Sussman et al., 1996). Furthermore, the presence of IF3 is required to ensure the fidelity of the codon-anticodon interaction in the P-site of the SSU (Milon et al., 2008). IF1 binds at the A-site of the SSU (Carter et al., 2001; Julian et al., 2011; Simonetti et al., 2008) where it stabilizes IF2 binding (Moreno et al., 1999) and accelerates IF2 dependent fMet-tRNA^{fMet} recruitment (Gualerzi and Pon, 1990; Laursen et al., 2005; Zucker and Hershey, 1986). The GTPase IF2 binds to the acceptor stem and to the fMet moiety of the initiator fMet-tRNA^{fMet} (Guenneugues et al., 2000), as well as to IF1 and ribosomal protein S12 (Julian et al., 2011). Notably, the interaction between IF1 and IF2 is not conserved (Kapralou et al., 2008). Binding of initiation factors to the SSU stabilizes a swiveled conformation of the head with respect to the body (Julian et al., 2011). The LSU joins the 30S-IC in ratcheted conformation to form the 70S-IC (Allen et al., 2005). Formation of the 70S-IC activates GTP hydrolysis by IF2, which leads to unratcheting of the ribosome allowing the conformational transition of the

fMet-tRNA_f^{Met} from the P/I state to the accommodated P/P-state. At the same time, the IF's dissociate from the complex thus turning the ribosome into its translation elongation competent conformation (Marshall et al., 2009).

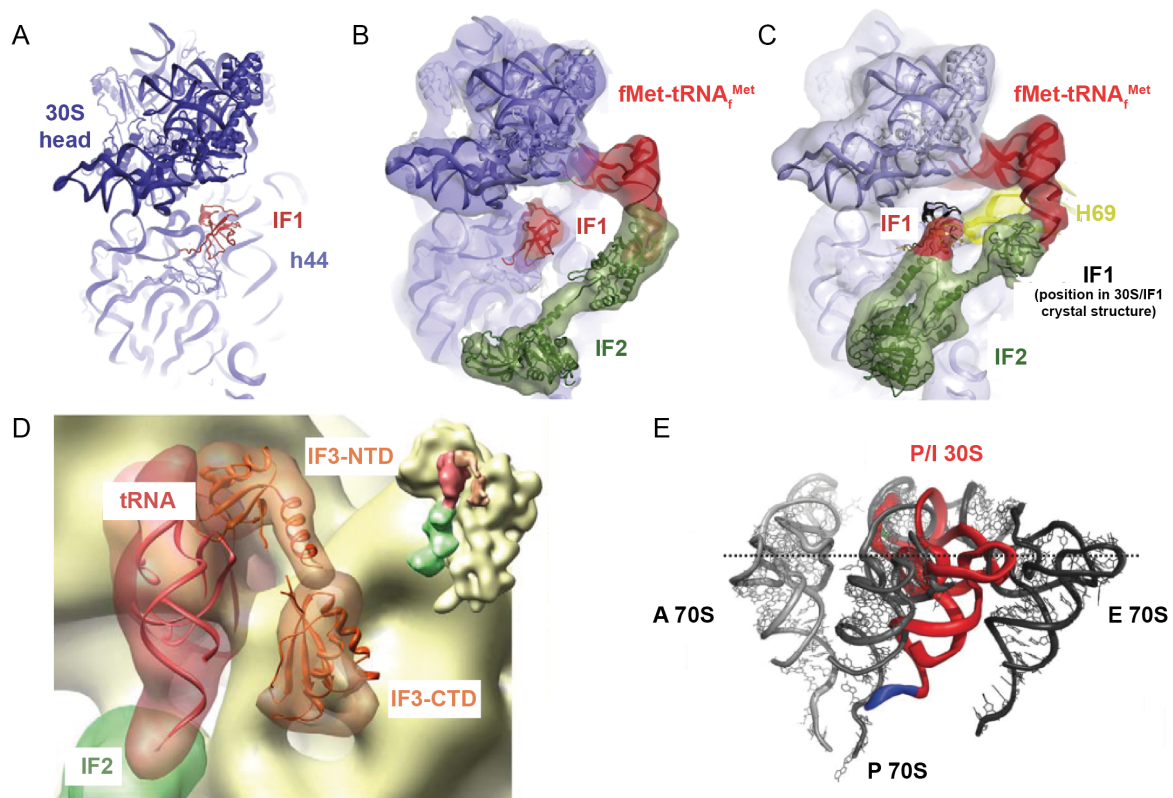


Figure 3 | Localization of IF1, IF2 and IF3 in prokaryotic 30S- and 70S-initiation complexes. (A) Crystal structure of IF1 (red) bound to the 30S subunit (blue) (Carter et al., 2001). (B) Cryo-EM structure of 30S-IC with IF1 (red), fMet-tRNA_f^{Met} (red) and IF2 (green) (Simonetti et al., 2008). (C) Cryo-EM structure of the 70S-IC (Allen et al., 2005) with IF1 (red), fMet-tRNA_f^{Met} (red), IF2 (green), H69 (yellow, occupies the density annotated as IF3 in (Allen et al., 2005)) and overlay of shifted IF1 position (black) in (A). (D) Cryo-EM structure of the 30S-IC showing density for IF3 (orange) (Julian et al., 2011). (E) Comparison of tRNA position in the 30S-IC (30S•mRNA•fMet-tRNA_f^{Met}•IF1•IF2•GTP) (Simonetti et al., 2008) with those observed in 70S post-initiation complex (Yusupova et al., 2006). Figure modified from (Julian et al., 2011; Myasnikov et al., 2009; Simonetti et al., 2008).

During canonical initiation, initial mRNA recognition and unfolding of structured mRNAs is a crucial step preceding 30S-IC formation. Interestingly, the ribosomal protein S1 plays a major role in these early steps of translation. Ribosomal protein S1 is the largest ribosomal protein with a mass of 61.1 kDa and is essential for translation initiation in Gram-negative bacteria (Sorensen et al., 1998). S1 contributes to an initial positioning of the mRNA at the ribosome by interaction with their A/U

rich 5' untranslated region (UTR) (Boni et al., 1991). Furthermore S1 was shown to have an implication in unfolding secondary structures of certain mRNAs and thus enables 30S-IC formation on highly structured mRNAs (Duval et al., 2013; Qu et al., 2012). However, translation initiation on leaderless mRNAs (lmRNAs) lacking the 5' UTR does not depend on S1 (Moll et al., 2002; Tedin et al., 1997). Due to the intrinsic flexibility of the six-domain protein, complete structural information regarding its binding mode to the ribosome has remained elusive. Publication 1 of this cumulative thesis provides the first insight into the structural basis for the interaction of protein S1 with the *Escherichia coli* ribosome (Byrgazov et al., 2015).

1.2.2 Elongation

Unlike initiation, termination and recycling, the translation elongation cycle is conserved in all three kingdoms of life. After initiation, the ribosomal P-site is occupied by the initiator fMet-tRNA^{Met} whereas the A-site remains empty. The next aa-tRNA is delivered to the empty A-site as a ternary complex together with GTPase elongation factor Tu (EF-Tu) and its cofactor guanosin-5'-triphosphate (GTP) (Fischer et al., 2015; Schmeing et al., 2009; Schuette et al., 2009; Voorhees and Ramakrishnan, 2013). Initial binding of the ternary complex is mediated by interaction of EF-Tu with ribosomal protein L7/L12 and notably is mRNA independent (Diaconu et al., 2005; Rodnina et al., 1996). The ternary complex binds in a conformation that allows the anticodon stem loop (ASL) of the tRNA to bind into the decoding center on the SSU whereas the aminoacylated 3'-acceptor stem is still bound to EF-Tu. In this state, the tRNA is bound in the A/T state and adopts a bent conformation (Blanchard et al., 2004a; Fischer et al., 2015; Schmeing et al., 2009; Schuette et al., 2009; Stark et al., 1997; Valle et al., 2002).

Decoding of mRNA codons by complementary anticodons of cognate tRNAs links the genetic code directly to the amino acid sequence of encoded proteins. To ensure translational fidelity, the ribosome discriminates between cognate and non-cognate tRNA binding by monitoring the interaction between the A-site codon of the mRNA and the anticodon of the tRNA (still bound to EF-Tu) within the decoding center (Ogle and Ramakrishnan, 2005). Binding of a cognate tRNA leads to complementary Watson-Crick base-pair codon-anticodon interactions. Following

codon recognition, nucleotides A1492 and A1493 (*E. coli* numbering is used throughout this thesis) adopt a conformation flipped-out of helix 44 (h44) of the 16S rRNA and together with G530 monitor the correct Watson-Crick geometry of the first two base-pairs of the codon-anticodon interaction in the form of A-minor motifs (Nissen et al., 2001; Ogle et al., 2001). At the third nucleotide position of the codon a wobble pair (e.g. G•U) is tolerated. This allows a single tRNA to decode multiple codons that only differ in the third anticodon position, thus providing an explanation for the degeneracy of the genetic code (Crick, 1966). Recognition of a correct codon-anticodon interaction triggers large-scale conformational changes in the ribosome that induce a domain closure of the 30S involving movement of the shoulder towards EF-Tu. These structural rearrangements are propagated to EF-Tu, which ultimately leads to stimulation of GTP hydrolysis (Ogle et al., 2002; Schmeing et al., 2011; Schuette et al., 2009; Voorhees et al., 2010). GTPase activity is controlled by positioning the catalytic histidine 84 (H84) of EF-Tu in proximity to the phosphate of A2662 of the sarcin-ricin loop (SRL) in H95 of the 23S rRNA. This enables H84 to coordinate a water molecule for nucleophilic attack on the γ -phosphate of GTP, which is then hydrolyzed (Voorhees et al., 2010). GTP hydrolysis and inorganic phosphate (P_i) release cause structural rearrangements in EF-Tu leading to dissociation of EF-Tu from the ribosome and thus allowing the tRNA to transition from the A/T-state into the A/A-state. During accommodation, the acceptor stem of the tRNA moves into the A-site of the PTC in the large ribosomal subunit (Blanchard et al., 2004c; Douthwaite et al., 1983; Sanbonmatsu et al., 2005; Schmeing et al., 2009; Voorhees et al., 2010). This process is accelerated by supporting conformational rearrangements in the LSU that establish guiding interactions with the anticodon stem loop and the elbow region of the tRNA (Jenner et al., 2010a).

For a long time the hypothesis was widely accepted that exclusively the binding of cognate tRNAs induce the domain closure on the SSU, leading to higher rates of GTP hydrolysis for cognate compared with near-cognate or non-cognate tRNA binding (Gromadski and Rodnina, 2004; Ogle et al., 2001; Ogle et al., 2002; Pape et al., 1999). However, the initial structural studies were based on crystal structures of 30S subunits in complex with incomplete U₆ hexanucleotide mRNA molecules and ASL mimicking tRNAs (Ogle et al., 2001; Ogle et al., 2002). Notably, the P-site codon

was mimicked by the 3' end of the 16S rRNA, which forced the U₆ mRNA to exclusively bind to the A-site and downstream, creating an artificial conformation where the mRNA was not covalently linked between the A-site and the P-site codons. Moreover, clear density for the near-cognate ASL and codon could only be observed in the presence of paromomycin (Ogle et al., 2002), which might effect the mismatch conformation on the 30S. Recent crystal structures of complete cognate or near-cognate tRNAs bound to the full 70S ribosome, both of which induced the closed conformation of the SSU, are challenging the hypothesis of how the ribosome distinguishes cognate tRNAs from near-cognate or non-cognate tRNAs (Demeshkina et al., 2012). The authors suggest that despite extensive contacts with the A-minor groove of the codon-anticodon helix, nucleotides A1492, A1493 and G530 do not discriminate cognate and near-cognate tRNAs, since they appear not to directly monitor the correct Watson-Crick geometry (Demeshkina et al., 2012), as suggested previously (Ogle et al., 2001; Ogle et al., 2002). Interestingly these structures show that the ribosome forces a G•U wobble pair at the first or second codon position to adopt Watson-Crick base pair geometry (**Fig. 4**). To achieve Watson-Crick geometry, the ribosome stabilizes an energetically unfavorable tautomer of the nucleotide. The authors suggested that this energetic penalty is then used by the ribosome to discriminate cognate from near-cognate tRNAs (Demeshkina et al., 2012).

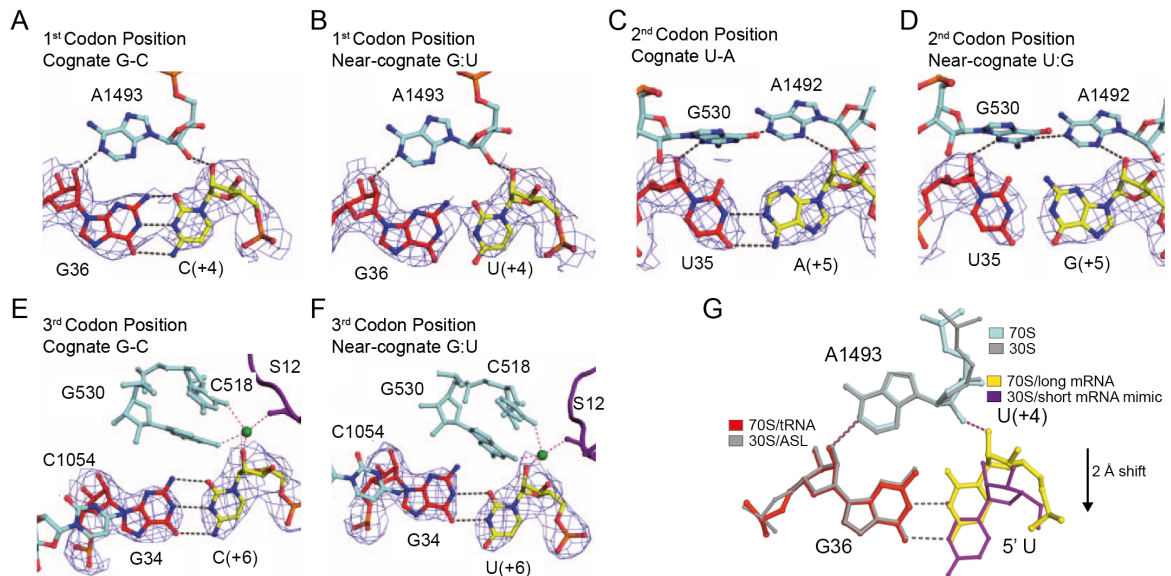


Figure 4 | Codon-anticodon interactions in the decoding center of the 70S ribosome. (A-F) Codon-anticodon interactions at the (A,B) first, (C,D) second and (E,F) third codon position of (A,C,E) cognate and (B,D,F) near-cognate tRNAs. **(G)** Superposition of near-cognate codon-anticodon interactions from the 70S structure (Demeshkina et al., 2012) with a 30 nucleotide-long mRNA and from the 30S structure (Ogle et al., 2001) with a short mRNA fragment, showing the shift of the first nucleotide of the A-site codon and the static nature of A1493. Figure modified from (Demeshkina et al., 2012).

Peptide bond formation between the incoming amino acid attached to the A-site tRNA and the nascent polypeptide attached to the P-site tRNA represents the main function of the ribosome. Upon accommodation of the A-site tRNA, the PTC located in domain V of the 23S rRNA catalyzes the peptidyl transfer reaction rapidly, with a rate that is approximately 2×10^7 -fold increased compared with the rate of spontaneous peptide bond formation in solution (Sievers et al., 2004). The ribosome is supposed to act as an entropy trap by precisely positioning the aminoacylated tRNA CCA-end substrates for trans-esterification and formation of a new peptide bond (Sievers et al., 2004). In line with this hypothesis, the 50S subunit alone retains the ability to catalyze peptide bond formation even in the absence of elongation factors (Monro, 1967; Schmeing et al., 2002; Traut and Monro, 1964; Wohlgemuth et al., 2006). Positioning of the tRNAs is facilitated by stabilizing interactions between 23S rRNA nucleotides and the tRNA CCA-ends. The P-site CCA end is stabilized by Watson-Crick base pairs of nucleotides C74 and C75 with P-loop nucleotides G2251 and G2252, respectively, whereas A76 stacks onto the ribose of A2451 and hydrogen bonds with A2450. The A-site C74 and C75 interact with A-loop nucleotides, whereby

C74 stacks upon U2555 and C75 forms a Watson-Crick base pair with G2553. A76 interacts with G2583 in form of a class I A-minor motif (Hansen et al., 2002c; Kim and Green, 1999; Nissen et al., 2000; Polikanov et al., 2014b; Voorhees et al., 2009).

Proper tRNA accommodation into the A-site leads to conformational changes within the PTC, as revealed by crystal structures of *Haloarcula marismortui* 50S subunits bound with minimal CCA analogs (Schmeing et al., 2005a; Schmeing et al., 2005d). Namely, 23S rRNA nucleotides G2583, U2584, U2585 undergo a shift of 1-2 Å, while U2506 rotates by 90° to provide space for A-tRNA accommodation into the PTC (Schmeing et al., 2005a; Schmeing et al., 2005d). These conformational changes convert the PTC into its induced state by exposing the peptidyl-tRNA ester for peptide bond formation, which occurs through nucleophilic attack of the α -amino group of the A-tRNA onto the carbonyl-carbon of the aminoacyl ester of the peptidyl-tRNA in the P-site (Polikanov et al., 2014b). Recent crystal structures of *Thermus thermophilus* 70S ribosomes in the pre- and post-catalysis state revealed that the PTC adopts the same conformation when complete tRNA substrates are bound (Polikanov et al., 2014b; Voorhees et al., 2009).

The nature of the chemical mechanism of peptide bond formation has been under debate for many years. Three different catalytic mechanisms have been proposed, ranging from acid-base catalysis (Muth et al., 2000; Nissen et al., 2000) over substrate-assisted catalysis (Dorner et al., 2003; Weinger et al., 2004) to the now generally accepted hypothesis that the ribosome acts as an entropic trap to facilitate the reaction (Sievers et al., 2004). Despite initial suggestions, biochemical evidence showed that the N6 atom of 23S rRNA nucleotide A2451 located in hydrogen-bonding distance to the α -amino group is not essential for peptide bond formation (Muth et al., 2000; Nissen et al., 2000; Polacek et al., 2001; Youngman et al., 2004). These findings strongly argue against a possible acid-base catalysis reaction for peptide bond formation (Bieling et al., 2006).

The rate-limiting step during catalysis is the formation of a transition state following nucleophilic attack of the α -amino group onto the carbonyl-carbon of the peptidyl-tRNA (Hiller et al., 2011; Kuhlenkoetter et al., 2011). Rapid break-down of the transition state transfers the peptide from the P-site tRNA onto the amino acid attached to the A-site tRNA, leaving a peptidyl-tRNA in the A-site and a deacylated

tRNA in the P-site. However, the precise contributions of residues within the PTC during peptide bond formation still remain unclear, as does the structural nature of the intermediate state (Hiller et al., 2011; Kingery et al., 2008; Kuhlenkoetter et al., 2011; Schmeing et al., 2005a).

Recent advances in understanding the molecular mechanism of peptide bond formation are based on high-resolution crystal structures of a *Thermus thermophilus* 70S ribosome in both pre-attack and post-catalysis states (Polikanov et al., 2014b). Three water molecules trapped in the PTC before catalysis allowed the authors to suggest a proton wire mechanism that couples aa-tRNA accommodation and peptide bond formation (**Fig. 5**). Both tRNAs, 23S rRNA nucleotides A2451, U2584, C2063 and A2602 as well as the N-terminus of ribosomal protein L27 contribute to the coordination of the water molecules. L27 and N6 of A2602 activate a water molecule (W1) to initiate the proton wire via the 2' OH of A2451 to the 2' OH of the P-site A76, which deprotonates the α -amino group for concerted nucleophilic attack onto the ester carbonyl carbon (**Fig. 5**). The tetrahedral intermediate state is stabilized by a second water molecule (W2), which donates a proton to the negatively charged ester carbonyl carbon. Breakdown of the intermediate state occurs via protonation of the 3' ester oxygen of the leaving group via a third water (W3) and a partially reversed proton wire via the 2'OH of P-site A76, the 2'OH of A2451 back to W1 (Polikanov et al., 2014b) (**Fig. 5**). The concerted action of de-protonation of the α -amino group and the nucleophilic attack is in agreement with previous reports (Kingery et al., 2008), as well as the tetrahedral structure of the intermediate state (Hiller et al., 2011). The central role of the 2'OH of the P-site A76 during peptide bond formation is in agreement with structural (Hansen et al., 2001) and biochemical evidence showing that substitution of this hydroxyl-group by fluorine or hydrogen leads to a 10^2 - 10^6 -fold reduction of the catalysis rate (Dorner et al., 2003; Weinger et al., 2004; Zaher et al., 2011). However, translation experiments performed in the presence of desoxy-A76 tRNA^{Ser} showed that production of full peptides was still possible, but notably at lower rates (Koch et al., 2008). L27 is the nearest ribosomal protein to the PTC and is supposed to contribute to catalysis by stabilizing the 23S rRNA as well as both tRNAs (Voorhees et al., 2009) and by coordination and activation of W1 (Polikanov et al.,

2014b). Consistently, deletion or N-terminal truncation of L27 by three amino acids decreases the rate of translation (Maguire et al., 2005).

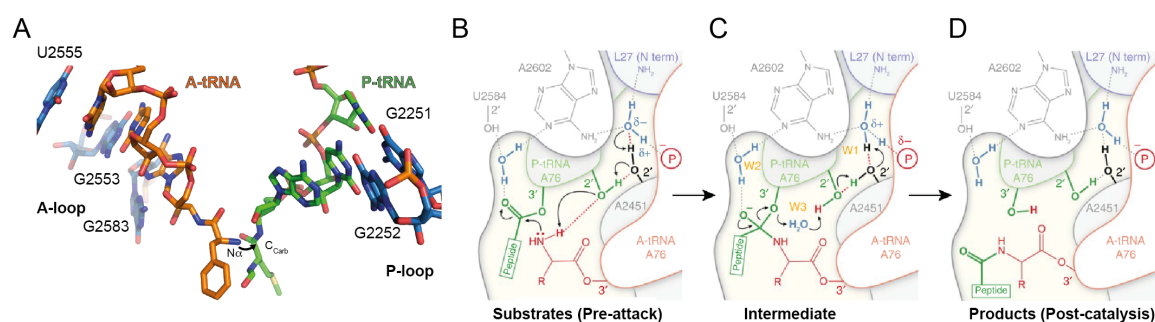


Figure 5 | Possible pathway for peptide bond formation. (A) Overview of CCA-ends of A-site tRNA (orange) and P-site tRNA (green) in the pre-peptide bond formation state (Polikanov et al., 2014b). (B) Simultaneous deprotonation of the A-site tRNA α -amine and nucleophilic attack onto the P-site tRNA carbonyl carbon. (C) Formation of a tetrahedral intermediate state with water molecules (yellow) involved in proton transfer along a proton wire. (D) Breakdown of the intermediate state via partial reversal of the proton transfer results in peptidyl-tRNA in the A-site and deacylated tRNA in the P-site. Figure modified from (Polikanov et al., 2014b).

Translocation. After peptide bond formation, the A-site is bound by the peptidyl-tRNA lengthened by one amino acid and the P-site is bound by deacylated tRNA. In order to allow the next round of elongation, the tRNAs together with the mRNA have to move with respect to the ribosome, namely to shift the peptidyl-tRNA from the A-site to the P-site and the deacylated tRNA from the P-site to the E-site. The mRNA shifts precisely by one codon, placing the next codon in the A-site. Translocation is catalyzed by the GTPase elongation factor G (EF-G) and provides an empty A-site, which in turn allows binding and accommodation of the next cognate aa-tRNA and thus the elongation cycle to proceed. However, the ribosome has an intrinsic capability to translocate tRNAs both forward and backward (Gavrilova et al., 1976; Konevega et al., 2007; Shoji et al., 2006). The function of EF-G is to accelerate and direct the process in forward direction (Frank and Gonzalez, 2010; Rodnina et al., 1997).

In the pre-translocation (PRE) state the 3'-ends of A- and P-site tRNA spontaneously move back and forth between the P- and E-sites on the LSU, respectively, while their ASLs remain anchored within the A- and P-sites on the SSU. This tRNA movement with respect to the LSU but not with respect to the SSU creates A/P and P/E hybrid tRNA binding states (Moazed and Noller, 1989; Munro et al., 2007; Semenov et al.,

1992; Sharma et al., 2004). The spontaneous formation of tRNA hybrid states is driven by decreased affinity for peptidyl-tRNA in the A-site and deacylated tRNA in the P-site by approximately 1000-fold (Semenkov et al., 2000; Sharma et al., 2004). Two independent tRNA hybrid states were identified using single-molecule fluorescence resonance energy transfer (FRET) measurements (Munro et al., 2007). In hybrid state 1 (H1) both tRNAs adopt hybrid states (A/P and P/E), whereas in hybrid state 2, only the P-site tRNA is shifted to the P/E hybrid state while the A-site tRNA adopts the classical A/A conformation (Munro et al., 2007). On the time scale, formation of the A/P hybrid state occurs after the movement of the deacylated tRNA from the P- to the E-site (Pan et al., 2007; Walker et al., 2008). The E-site on the 50S subunit sterically occludes binding of peptidyl-tRNA and thus ensures that translocation occurs only after completed peptide bond formation (Rheinberger and Nierhaus, 1983; Schmeing et al., 2003).

Formation of tRNA hybrid states is coupled to a large-scale conformational rotation (ratcheting) of the SSU $\sim 3\text{-}10^\circ$ counterclockwise relative to the LSU (Agirrezabala et al., 2008; Frank and Agrawal, 2000; Julian et al., 2008; Valle et al., 2003). During the next step of translocation, the mRNA and the ASLs move by one codon with respect to the SSU. This process is catalyzed by the GTPase EF-G, which binds together with GTP and stabilizes the ratcheted state of the ribosome (Blanchard et al., 2004c; Dorner et al., 2006; Munro et al., 2010; Spiegel et al., 2007). It has been shown that EF-G binds to both the ratcheted and non-ratcheted states of the ribosome, but translocation occurs via hybrid state formation for both scenarios (Chen et al., 2011a; Pulk and Cate, 2013).

Rotation around two hinges (Mohan et al., 2014) of the SSU head relative to the body (head swiveling) opens a constriction which allows the passage of the mRNA and ASLs through the SSU (Ratje et al., 2010; Savelsbergh et al., 2000; Yamamoto et al., 2014; Zhang et al., 2009). Domain IV of EF-G, overlapping the A-site on the SSU, is crucial to facilitate GTP-dependent translocation by disrupting interactions of the codon-anticodon duplex with the DC (Liu et al., 2014). Translocation of tRNAs through the ribosome proceeds via a series of intermediate states including intra-subunit hybrid states on the SSU, where the mRNA and ASLs simultaneously bind to the A- and P-site (ap/P) and to the P- and the E-site (pe/E) (Ramrath et al., 2013;

Ratje et al., 2010). Following GTP hydrolysis and P_i release, the 30S head swivel and the ratcheting is reversed, EF-G dissociates and leaves the ribosome in the post-translocation (POST) state with tRNAs bound in the classical P/P and E/E sites (Ermolenko and Noller, 2011; Ratje et al., 2010). The tRNA in the E-site then dissociates spontaneously from the ribosome (Chen et al., 2011b; Semenov et al., 1996; Uemura et al., 2010; Wettstein and Noll, 1965). Yet, dissociation appears to depend on the buffer conditions *in vitro* and hasn't been addressed *in vivo*.

Recently, a plethora of high-resolution crystal structures or cryo electron microscopy reconstructions of EF-G bound to the ribosome in the PRE state (Brilot et al., 2013; Chen et al., 2013; Lin et al., 2015; Pulk and Cate, 2013; Tourigny et al., 2013), in intermediate states (Zhou et al., 2013, 2014) of translocation and in the POST state (Lin et al., 2015) have advanced the current understanding of the precise structural rearrangements during EF-G-catalyzed translocation (**Fig. 6**). The structures of EF-G bound ribosome in the PRE state verified the previous suggestion that the mechanism of GTPase activation is very similar for EF-Tu and EF-G. Interaction with the SRL (H95) opens the hydrophobic gate in the G-domain of EF-G and places the catalytic histidine into the active site, where it initiates hydrolysis of the γ -phosphate from GTP. However, the chemical nature of the hydrolysis reaction is controversially discussed (Chen et al., 2013; Liljas et al., 2011; Tourigny et al., 2013). The latest crystal structures of dityromycin-captured EF-G bound in the PRE and POST states revealed an entirely new conformation of EF-G in the PRE state. Surprisingly, EF-G is bound to the ribosome in a compacted state, where domain IV is buried within EF-G, being far away from the A-site on the SSU (Lin et al., 2015) (**Fig. 6**). This structure could provide novel insight into possible structural transitions of EF-G that might occur during GTPase-dependent translocation. Notably, in this study an EF-G-L9 fusion protein was co-crystallized together with ribosomes. Although the authors claim that the chimeric fusion protein does not interfere with the conformation of EF-G bound in the POST state, it cannot be excluded that the observed PRE state represents a non-physiological state of EF-G bound to the ribosome. Interestingly, recent FRET experiments showed that EF-G adopts predominantly a compact conformation in solution and infrequently transitions to an elongated conformation (Salsi et al., 2015). In contrast, EF-G binding to either pre-translocation or post-

translocation ribosomes stabilizes the elongated form of EF-G, however the data demonstrated that two compacted conformations of EF-G on the ribosome could transiently occur. The authors suggested that EF-G might initially sample the ribosome in a compacted state and transition to the elongated conformation prior to GTP hydrolysis and translocation (Salsi et al., 2015), which supports the structure of the compacted EF-G bound to the PRE state ribosome (Lin et al., 2015).

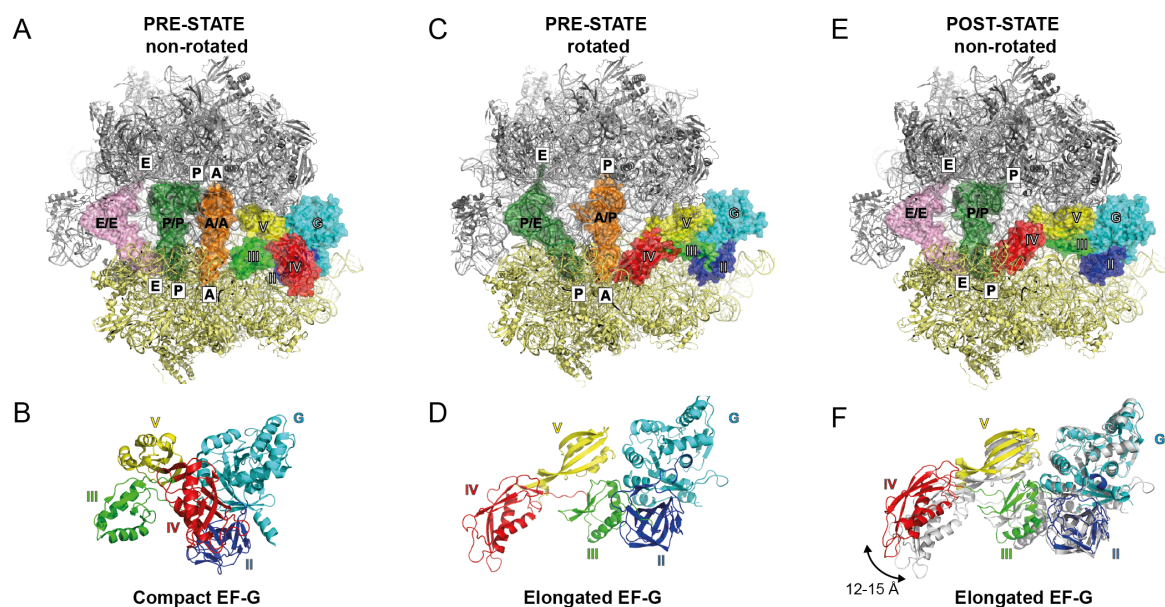


Figure 6 | Conformational rearrangements of EF-G during translocation. (A-F) Overviews and isolated views of EF-G bound in the (A,B) PRE-state to non-rotated ribosomes with EF-G in compact conformation and tRNAs in the A-site (orange), P-site (green) and E-site (pink) (Lin et al., 2015), and (C,D) in the PRE-state to rotated ribosomes bearing a peptidyl-tRNA in the A/T hybrid state (orange) and a deacylated tRNA (pink) in the P/E hybrid state (Brilot et al., 2013), as well as (E,F) in the non-rotated POST state with translocated tRNAs in the P-site (green) and E-site (pink) (Lin et al., 2015). (F) Interdomain rearrangements of EF-G during translocation. Superposition of the PRE-state (grey) and the POST-state conformation of EF-G (color-coded) by alignment of domains I and II of EF-G (Lin et al., 2015).

1.2.3 Termination

Class I termination release factors 1 (RF1) or 2 (RF2) recognize mRNA stop codons in the A-site of the SSU and trigger translation termination by mediating hydrolysis of the P-site peptidyl-tRNA and subsequent peptide release (Caskey et al., 1968; Jin et al., 2010). In a following step, the class I release factors are removed from the ribosome with the help of the GTPase class II release factor RF3 in a GTPase-dependent manner (Freistroffer et al., 1997; Zavialov et al., 2001).

Early mutagenesis studies showed that class I release factors contain two distinct regions responsible for stop codon recognition and peptidyl-tRNA hydrolysis. The conserved GGQ motif was shown to be important for hydrolysis (Frolova et al., 1999; Mora et al., 2003; Seit Nebi et al., 2000; Shaw and Green, 2007), whereas the tripeptide motifs PxT (PAV or PVT) in RF1 and SPF in RF2 appear to be important for stop codon recognition (Ito et al., 2000; Scarlett et al., 2003). RF1 and RF2 differ with respect to stop codon recognition (RF1 recognizes UAG/UAA; RF2 recognizes UGA/UAA) (Scolnick et al., 1968), but both mediate peptidyl-tRNA hydrolysis by placing their universally conserved GGQ-motif into the PTC where it positions and activates a water molecule for nucleophilic attack onto the peptidyl-ester carbonyl carbon (Klaholz, 2011; Petry et al., 2008). Structures of RF1 (Laurberg et al., 2008; Petry et al., 2005) (**Fig. 7**), RF2 (Jin et al., 2010; Klaholz et al., 2003; Korostelev et al., 2008; Petry et al., 2005; Rawat et al., 2003; Weixlbaumer et al., 2008) and RF3 (Gao et al., 2007; Jin et al., 2011; Zhou et al., 2012b) bound to the ribosome have revealed profound insight into the structural determinants of stop codon recognition and translation termination. Selective discrimination of the second codon position A2 (UAG/UAA) by RF1 is mediated hydrogen bonding interactions between P184 and T186 (PxT motif) with the first two stop codon bases (Laurberg et al., 2008) (**Fig. 7**). RF2 monitors the second codon position G2 via interactions between G2 and S193 of the SPF motif, and specifically via interaction of the 2-amino group of G2 (absent in adenines) with residues T203 and S204. The capability of RF2 to recognize both adenine (A2) and a guanine (G2) in the second codon position is based on the flexible character of the serine side chain (SPF motif) that is able to interact either with A2 or G2 (Korostelev et al., 2008; Korostelev et al., 2010; Weixlbaumer et al., 2008). In contrast, specific discrimination of the first codon position U1 (uridine in all three stop codons) is mediated by a common GxxE motif in helix 5 of the release factors. The nucleotide in the third codon position is rotated and stacks on G530 upon RF1/RF2 binding, due to insertion of a conserved histidine (H193 in RF1, H215 in RF2) between codon positions 2 and 3 (**Fig. 7**). RF1 interacts with A3 or G3 by interactions involving T194 and Q181, while RF2 uses the hydroxyl group of T194 to monitor A3 (Korostelev et al., 2008; Korostelev et al., 2010; Laurberg et al., 2008; Weixlbaumer et al., 2008). Binding of release factors induce conformational changes

in the DC (G530, A1492 and A1493) that are distinct compared to those during decoding of sense codons by tRNAs (Ogle et al., 2001; Youngman et al., 2007). For example, stacking interactions between 16S rRNA nucleotide A1493 and 23S rRNA nucleotide A1913 as well as between 16S rRNA nucleotide G530 and the third stop codon base are observed (Korostelev et al., 2008; Laurberg et al., 2008; Weixlbaumer et al., 2008).

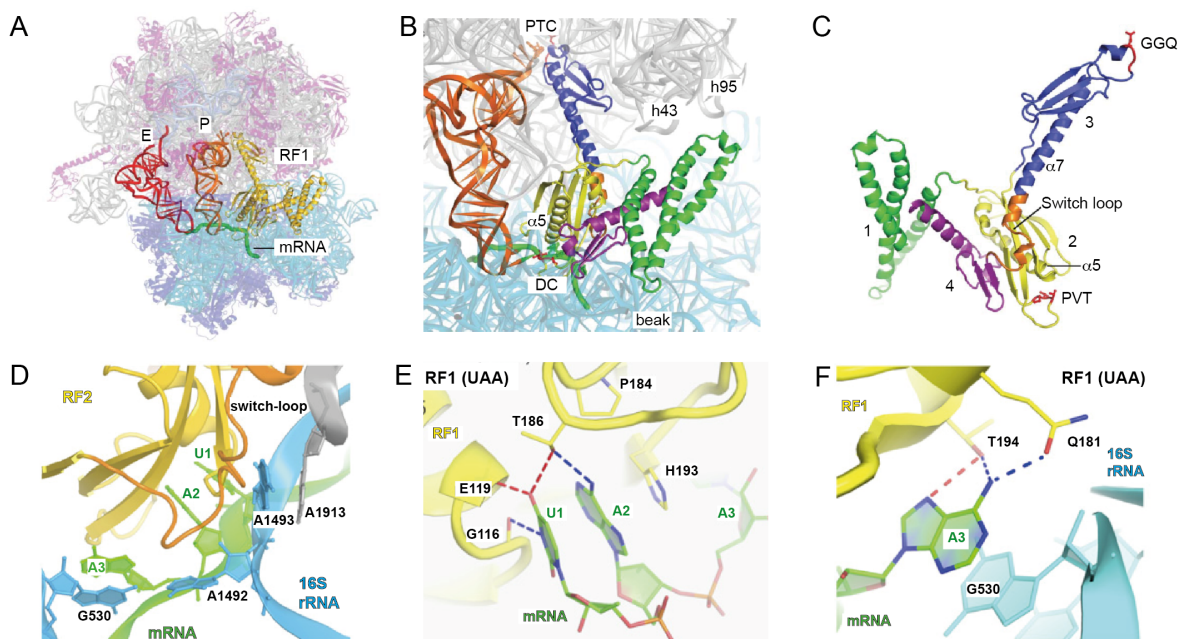


Figure 7 | Decoding of UAA stop codon by release factor 1. (A-B) Overview of RF1 bound to the ribosome with P-site tRNA (orange), E-site tRNA (red) and mRNA (green) (Laurberg et al., 2008). (C) Domain architecture of RF1 with GGQ motif and PVT motif highlighted in red. (D) Conformation of the DC upon RF2 (yellow) binding showing mRNA (green), 16S rRNA nucleotides G530, A1492 and A1493 (blue) and 23S rRNA nucleotide A1913 (grey) (Korostelev et al., 2008). (E) Interaction of RF1 (yellow) with the first two stop codon nucleotides (green) (Laurberg et al., 2008). (F) Interaction of RF1 (yellow) with the third stop codon nucleotide (green) (Laurberg et al., 2008). Figure modified from (Korostelev, 2011; Laurberg et al., 2008).

The conformation of class I release factors in solution was shown to be in an equilibrium between a closed and an open form (Vestergaard et al., 2001; Zoldak et al., 2007). In the closed conformation, the GGQ motif and the PxT/SPF motif are only 23 Å apart from each other. Due to the small distance, simultaneous interaction of the PxT/SPF motif with the stop codon and the GGQ motif with the PTC is not possible (Vestergaard et al., 2001; Zoldak et al., 2007). Ribosome binding induces conformational changes in RF1 and RF2 that stabilize the open conformation, which

allows the concurrent insertion of the GGQ motif into the PTC upon stop codon recognition (Klaholz, 2011). Proper placement of the GGQ motif within the PTC is crucial for hydrolysis of the peptidyl-tRNA and thus release of the newly synthesized peptide (Frolova et al., 1999; Shaw and Green, 2007). The two glycine residues thereby sterically allow the GGQ motif to slip into the PTC, adjacent to the P-site A76 (Shaw and Green, 2007). It has been shown that it is not the amino acid side chain of Q230 of the GGQ motif that is responsible to mediate hydrolysis (Seit-Nebi et al., 2001; Shaw and Green, 2007), but rather the backbone nitrogen of Q230 that accounts for the catalytic activity of RF1 and RF2 by interacting with the 3'OH of A76 (Laurberg et al., 2008). However, loss of the posttranslational N5-methylation of Q230 reduces the efficiency of peptide-release (Dincbas-Renqvist et al., 2000) and therefore favors a model where the glutamine side chain, together with the backbone amine, the 2'OH of A76 and A2451 directly coordinate a water molecule for nucleophilic attack (Jin et al., 2010; Klaholz, 2011; Weixlbaumer et al., 2008).

After hydrolysis of the nascent chain, the class II release factor RF3 binds to the ribosome and promotes dissociation of RF1 and RF2 from the ribosome in a GTP-dependent manner (Freistroffer et al., 1997; Grentzmann et al., 1998). RF3•GTP binding to RF1/RF2•ribosome complexes stabilizes the ratcheted state of the ribosome with tRNAs in hybrid states (Ermolenko et al., 2007; Gao et al., 2007; Jin et al., 2011; Klaholz et al., 2004; Zhou et al., 2012b). The ratcheted conformation of the ribosome creates a series of steric clashes between RF domains I and IV with the L11 stalk and the 30S head, respectively, which are supposed to contribute to the destabilization of the RFs (Gao et al., 2007). However, RF3•GTP binding to POST state ribosomes would result in the same clashes. Together with the architectural similarity between RF3•GDP and EF-TU•GTP, it has been argued that RF3 might bind to the ribosome in its GDP bound conformation (Gao et al., 2007; Zavialov et al., 2001). However, stable binding of RF3•GDP to ribosomes is not observed (Jin et al., 2011; Pel et al., 1998). Possibly, the post-termination ribosome spontaneously adopts the ratcheted state, which is subsequently sampled and stabilized by RF3•GTP, leading to dissociation of RF1 and RF2 (Zhou et al., 2012a). A recent study showed that GTP hydrolysis by RF3 is independent of the functional state of the ribosome and that RF3•GTP binds and hydrolyzes GTP on both pre- and post-termination

complexes. However, peptide release stabilizes RF3•GTP binding to the ribosome due to formation of the ratcheted state of the ribosome (Peske et al., 2014). Interestingly, the binding position of the G domain of RF3 to the SRL (H95) differs from the positions observed for EF-Tu and EF-G (Gao et al., 2009; Schmeing et al., 2009; Voorhees et al., 2010), which suggests more than one common mechanism leading to GTPase activation on translational GTPases exists (Zhou et al., 2012b).

1.2.4 Recycling

After RF3-mediated dissociation of class I release factors, the ribosome is still bound to mRNA and deacylated tRNA in the P-site. Recycling of the mRNA•tRNA•70S complex is necessary to allow a new round of peptide synthesis. During recycling, the ribosome is split into subunits by the combined action of ribosome recycling factor (RRF) and EF-G in a GTP-dependent manner (Agrawal et al., 2004; Hirashima and Kaji, 1973; Karimi et al., 1999; Lancaster et al., 2002; Peske et al., 2005). The first detailed structural insight into RRF binding to ribosomes was based on a crystal structure of domain I of *Escherichia coli* RRF bound to *Deinococcus radiodurans* 50S subunit and allowed a mechanistic description of RRF-induced conformational rearrangements in H69 of intersubunit bridge B2a (Wilson et al., 2005b). A recent crystal structure of RRF bound to a complete ribosome showed that RRF was bound to the ribosomal P-site, stabilizing the ratcheted conformation of the ribosome with deacylated tRNA in the P/E hybrid state (Dunkle et al., 2011; Weixlbaumer et al., 2007). Binding of EF-G to the RRF•mRNA•tRNA•70S complex subsequently splits the ribosome into subunits upon GTP hydrolysis (Barat et al., 2007; Ito et al., 2002; Pai et al., 2008; Peske et al., 2005; Zavialov et al., 2005). Binding of IF3 to the 30S subunit leads to dissociation of mRNA and deacylated tRNA and simultaneously prevents re-association with the 50S subunit (Dallas and Noller, 2001; Grunberg-Manago et al., 1975; Karimi et al., 1999; Singh et al., 2005; Subramanian and Davis, 1970). Thereby, IF3 directly links the last steps in translation termination to the first steps of translation initiation.

1.3 Antibiotics

Antibiotics are small compounds that inhibit bacteria by inducing either cell death (bactericidal antibiotics) or inhibition of growth (bacteriostatic antibiotics). More than 85 years ago, Sir Alexander Fleming discovered the first antibiotic penicillin (Fleming, 1929) in *Penicillium* fungi species, for which he received the Nobel Prize in 1945. Since their discovery, antibiotics revolutionized the field of medicine by using them as potent agents against a huge variety of infectious diseases. However upon exposure, antibiotic resistance among bacteria spreads extraordinary fast, making antibiotics powerless against these pathogens (Hede, 2014). In order to provide an update on the latest in the evolution of antimicrobial resistance and healthcare-associated infection, the Center for Disease Prevention and Control (ECDC) annually publishes an epidemiological report. It is alarming that the percentages of organisms exhibiting antimicrobial resistance to multiple antibiotics continuously increase. For example, the percentile occurrence of methicillin-resistant *Staphylococcus aureus* (MRSA) among *Staphylococcus aureus* isolates is determined to be around 25% in many European countries. Moreover, Gram-negative pathogens like *Escherichia coli* and *Klebsiella pneumoniae*, the major causative organisms of urinary and respiratory tract infection, significantly follow the trend in acquiring multi-drug resistance. Frighteningly, only a few last-line antibiotics, such as carbapenems are available to treat patients infected with multi-drug resistant bacteria. However, also carbapenem-resistant bacteria are already spreading due to frequent carbapenem usage when other antibiotics are non-effective. The fast progression of antibiotic resistance among bacteria greatly emphasizes the importance of discovery and development of new potent antimicrobial agents. Despite the discovery of many classes of antibiotics in the decades after their discovery, only a few antibiotics like lipopeptides and oxazolidinones (Linezolid) (Fischbach and Walsh, 2009) were introduced into medical usage in the past 40 years. In contrast, resistance to all known classes of antibiotics has emerged within only a few years after their introduction into clinical usage (Clatworthy et al., 2007). The huge discrepancy between the development of resistances and the development of new potent antimicrobial agents is a serious threat for public health. It is therefore crucial to study and to understand the molecular mechanisms causing antibiotic resistance. Especially a structural view on

antibiotic target sites paves the way for the development of new antimicrobial agents that overcome bacterial resistance by either synthesis of novel compounds or by chemical modification of known and naturally occurring antibiotics (Kohanski et al., 2010).

The antimicrobial activity of antibiotics is based on their ability to disruptively interfere with a variety of fundamental biochemical processes within the bacterial cell. Cell wall synthesis (β -lactams, glycopeptides, lipopeptides), DNA replication (fluoroquinolones), DNA transcription into RNA (rifamycins) and protein synthesis (aminoglycosides, tetracyclines, macrolides, streptogramins, phenicols) are the major targets for the different classes of antibiotics (Kohanski et al., 2010). The bacterial ribosome is an important target for many classes of antibiotics that inhibit peptide synthesis (Wilson, 2004; Wilson, 2009, 2014). The main antibiotic binding sites within the ribosome are localized to the DC, the PTC, the GTPase-associated center (GAC) and to the peptide exit tunnel. Hence, all four major functions of the ribosome, namely decoding, peptide bond formation, GTPase activation and progression of the nascent chain are subject to antibiotic-mediated inhibition (Wilson, 2009) (**Fig. 8**). Antibiotics binding near the DC on the SSU mainly inhibit translation by interfering with tRNA delivery to the A-site (tetracyclines, streptomycins) or by disturbing EF-G-dependent mRNA and tRNA translocation (aminoglycosides, neomycin, pactamycin, spectinomycin, ampicoumycin A, negamycin, dityromycin, hygromycin B, viomycin, capreomycin), or by blocking initiator tRNA binding to the P-site (edeine, kasugamycin). PTC targeting antibiotics prevent peptide bond formation by overlapping the A-site (chloramphenicol, lincosamides, oxazolidinones, puromycin, sparsomycin), P-site (blasticidin S, bactobolin A) or both A- and P-site (pleuromutilins, streptogramin A). Antibiotics binding to the GAC on the LSU inhibit translation by interfering with binding of the translational GTPases EF-Tu, EF-G and IF2 (thiopeptides). Ribosome exit tunnel-targeting antimicrobial compounds (macrolides, streptogramin B) impair progression of the nascent polypeptide through the LSU, which leads to translation inhibition by peptidyl-tRNA drop-off (Amunts et al., 2015; Bulkley et al., 2014; Polikanov et al., 2014a; Polikanov et al., 2014l; Wilson, 2014).

During my research, I mainly focused on three classes of antibiotics including tetracycline, the founding member of the tetracycline class of antibiotics, erythromycin, the founding member of the macrolide class of antibiotics, and Onc112, a ribosome-targeting proline-rich antimicrobial peptide (PrAMP). Sections 1.3.1-1.3.3 provide a more detailed introduction into these antimicrobial agents.

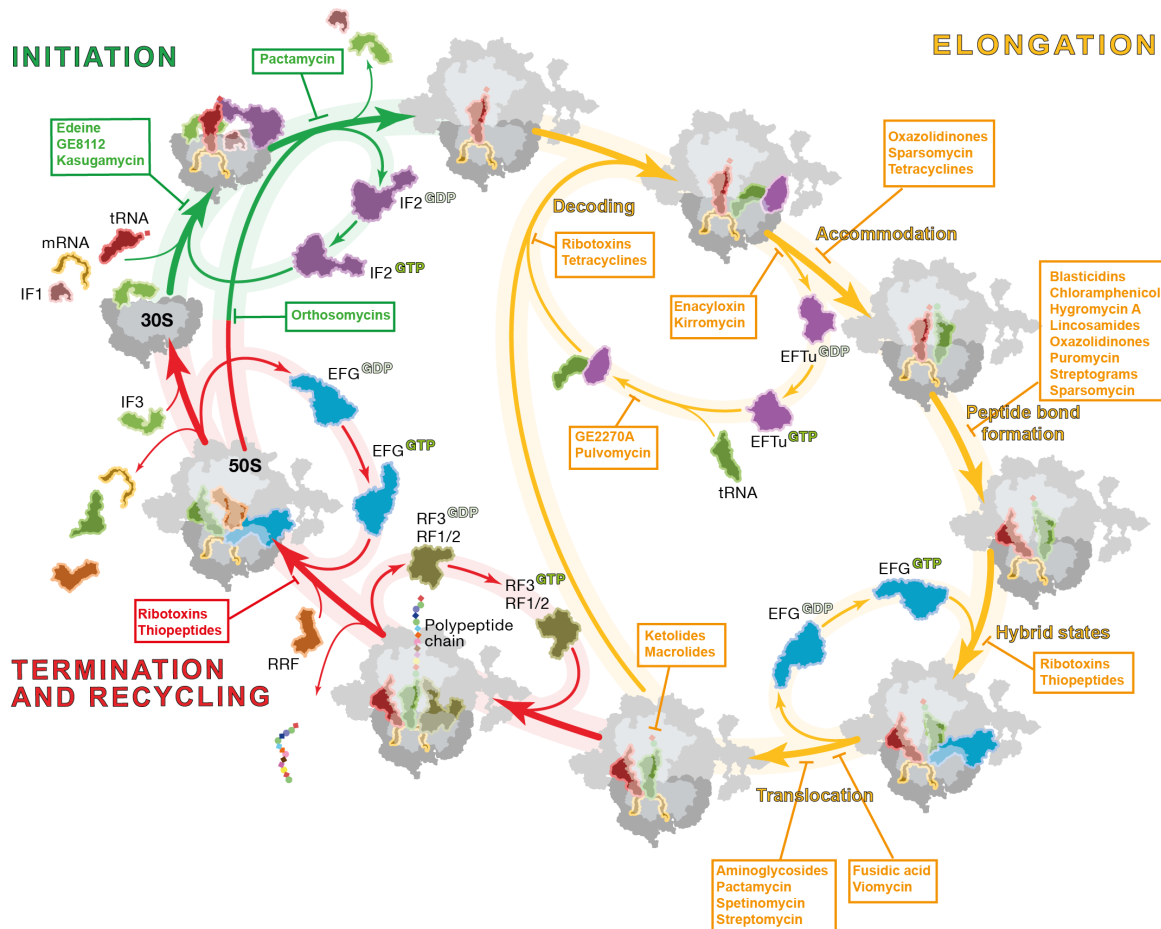


Figure 8 | Overview of antibiotics inhibiting the prokaryotic translation cycle. Overview of antibiotics, inhibiting translation initiation (green), translation elongation (yellow) and translation termination/recycling (red) of the prokaryotic translation cycle. Figure modified from (Sohmen et al., 2009).

1.3.1 Proline-rich Antimicrobial Peptides

Antimicrobial peptides are part of the innate immune response of all multicellular organisms (Andreu and Rivas, 1998; Casteels et al., 1989; Li et al., 2014; Zasloff, 2002). The huge variety of small antimicrobial peptides among the plethora of multicellular organisms can be grouped based on chemical-structural criteria of the peptides (Boman, 1995). In general, antimicrobial peptides fall into two major classes (i) linear peptides and (ii) cyclic peptides. Members of linear peptides can adopt (iii) α -helical or (iv) linear structures due to high content of specific amino acids like proline (Pro), arginine (Arg) or tryptophan (Trp) (Boman, 1995). Among the diversity of peptides with antimicrobial activity, the subclass of proline-rich antimicrobial peptides (PrAMPs) stands out as a potential new weapon to treat bacterial strains that acquired resistances to conventional antibiotics used in clinical practice (Li et al., 2014). Remarkably, PrAMPs specifically inhibit intracellular targets, in contrast to other antimicrobial peptides, which kill pathogens by lysing their cell membrane (Scocchi et al., 2011). Specific inhibition of bacterial growth while leaving eukaryotic cells unaffected is the main basic property characterizing a potent antibiotic. PrAMPs achieve this species specificity and therefore exhibit low toxicity (Hansen et al., 2012), for example, by selective import into bacterial cells through specialized transporters, such as SbmA located in the inner membrane of Gram-negative bacteria, which are absent in mammalian cells (Mattiuzzo et al., 2007; Runti et al., 2013).

Inside the cell, PrAMPs were shown to target the 70 kDa heat shock protein DnaK, leading to protein misfolding (Otvos, 2005). Accordingly, PrAMPs can even inactivate bacterial peptide toxins by inhibiting their proper folding (Otvos et al., 2014). Crystal structures of PrAMPs bound to *Escherichia coli* DnaK provide structural insight into their mode of interaction (Zahn et al., 2013; Zahn et al., 2014). Recently, a new intracellular target for PrAMPs was identified (Krizsan et al., 2014). Due to the low affinity of PrAMPs to the chaperone DnaK and based on the observation, that mutant cells, lacking DnaK, are equally or slightly more susceptible to apidaecins and oncocins, the authors suggested that DnaK is most likely not the biologically relevant target for PrAMPs. Instead, the authors biochemically showed that insect-derived PrAMPs like apidaecins and oncocins bind with nanomolar dissociation constants to the 70S ribosome leading to inhibition of protein synthesis (Krizsan et al., 2014).

Publication 2 of this cumulative thesis reports the first crystal structure of the proline-rich antimicrobial peptide Onc112 bound to *Thermus thermophilus* 70S ribosomes at 3.1 Å resolution. The structure reveals that Onc112 binds within the ribosome exit tunnel and extends towards the PTC, overlapping the A-site and thereby prevents translation by inhibiting A-site tRNA accommodation. Onc112 allows translation initiation, but destabilizes the 70S initiation complex, presumably by mediating fMet-tRNA_f^{Met} dissociation (Seefeldt et al., 2015).

1.3.2 Tetracyclines

In the 1950-1960's, tetracycline antibiotics were introduced into clinical practice as the first class of broad-spectrum antibiotics showing effectivity against both Gram-positive and Gram-negative bacteria. The first members of this class of antibiotics, chlortetracycline (Duggar, 1948), oxytetracycline (Finlay et al., 1950) and tetracycline (Backus et al., 1954; Conover et al., 1953; Perlman et al., 1960) are naturally produced by *Streptomyces* species (the largest genus of actinobacteria) and are therefore called first-generation tetracyclines. All members of this class of antibiotics share a common structural core, consisting of four aromatic rings (naphthacene core) (Stephens et al., 1952). Superior pharmacokinetic properties, water-solubility and oral availability caused tetracyclines to be preferentially used in clinical practice and agriculture to treat bacterial infections. However, due to the extensive use of tetracyclines, bacteria quickly became resistant. To improve pharmacokinetic and antimicrobial activity of tetracyclines, second-generation tetracyclines, such as doxycycline (Stephens et al., 1963) and minocycline (Martell and Boothe, 1967) as well as the third-generation tetracyclines tigecycline (Petersen et al., 1999), omadacycline (Draper et al., 2013) and eravacycline (Grossman et al., 2012), were semi-synthetically produced by chemical modification of their respective parent compounds. Strikingly, third-generation tetracyclines like tigecycline exhibit an increased binding affinity to the ribosome (up to 100-fold) compared to tetracycline (Grossman et al., 2012; Jenner et al., 2013; Olson et al., 2006) and inhibit growth of both susceptible and resistant bacterial strain at similar minimal inhibitory concentrations (Barden et al., 1994; Sum et al., 1994; Testa et al., 1993).

Tetracyclines bind to multiple sites on the ribosome (Anokhina et al., 2004; Brodersen et al., 2000; Pioletti et al., 2001), however the primary binding site (Tet1) is localized to the A-site of the small subunit overlapping the DC (Connell et al., 2002; Jenner et al., 2013). Binding to Tet1 involves multiple hydrogen bonds to the backbone of h34 and h31 of the 16S rRNA, the coordination of two magnesium (Mg^{2+}) ions as well as a stacking interaction of ring D with C1054 (Brodersen et al., 2000; Jenner et al., 2013; Pioletti et al., 2001). These interactions are nucleotide sequence-unspecific and therefore explain the broad-spectrum activity of this class of antibiotics. Tetracyclines inhibit translation by interfering with EF-Tu-mediated tRNA delivery to the ribosome by sterically occluding A-site ASL binding to the DC (Blanchard et al., 2004a; Jenner et al., 2013; Suarez, 1965).

Bacterial resistance to tetracyclines is mainly conferred by four different mechanisms. The most common strategy used by Gram-negative and Gram-positive bacteria is tetracycline efflux i.e. actively pumping the drug out of the cell. Tetracycline efflux pumps (e.g. TetA) act as proton/tetracycline antiporters by exchanging a proton (H^+) for a tetracycline molecule against a concentration gradient (Guillaume et al., 2004; Piddock, 2006). Another strategy conferring tetracycline resistance is the expression of monooxygenase enzymes (e.g. TetX) that inactivate tetracycline by hydroxylation (Speer et al., 1991; Yang et al., 2004). Furthermore, mutations in the 16S ribosomal RNA confer tetracycline resistance. For example the single mutation G1058C in h34 (Ross et al., 1998) as well as the triple mutation A965U/G966U/A967U in h31 (Dailidienė et al., 2002; Trieber and Taylor, 2002) were identified in *Propionibacterium acnes* and *Helicobacter pylori*, respectively. In both cases, tetracycline resistance is mediated by perturbation of the drug binding site causing a significantly decreased affinity of tetracycline to the ribosome (Nonaka et al., 2005). Another class of widespread tetracycline resistance genes encodes so-called ribosome protection proteins (RPPs) that confer resistance by directly dislodging tetracycline from its binding site. The best-studied members of RPPs, *Enterococcus faecalis* TetM and *Campylobacter jejuni* TetO share more than 75% sequence identity. RPPs display homology to the GTPase EF-G (~25% identity and ~35% similarity) and similarly bind to the ribosome in a GTP-dependent manner (Burdett, 1991; Connell et al., 2003a; Dantley et al., 1998; Taylor et al., 1995; Trieber

et al., 1998). Subsequent GTP hydrolysis leads to factor dissociation from the ribosome but is not strictly required for tetracycline release (Burdett, 1991; Connell et al., 2003a; Trieber et al., 1998). Structural information on the binding mode and the molecular mechanism of tetracycline release is based on cryo-EM reconstructions of TetO or TetM bound to empty or non-translating ribosomes at resolutions ranging from 7.2–16 Å (Dönhöfer et al., 2012; Li et al., 2013; Spahn et al., 2001) (**Fig. 9**).

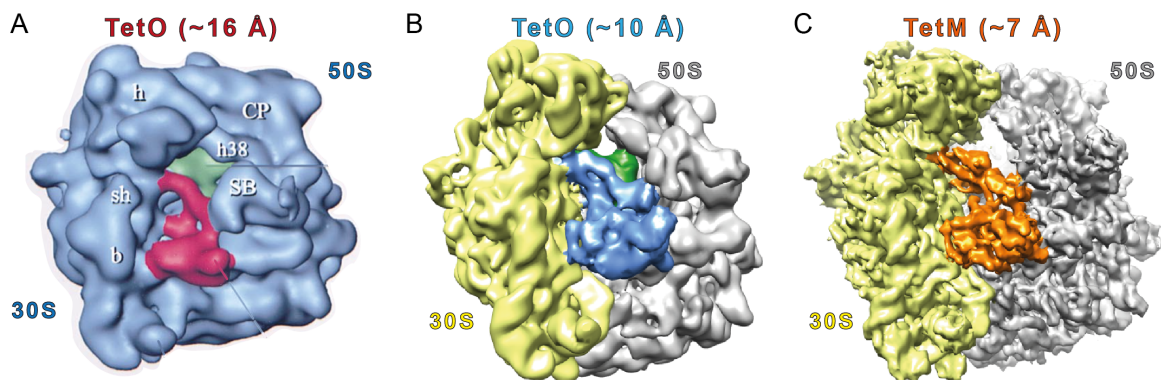


Figure 9 | Overview of available cryo-EM structures of RPP-bound ribosomes. (A) First cryo-EM structure of TetO (red) bound to *E. coli* 70S ribosome (blue) containing P-site tRNA (green) at ~16 Å resolution (Spahn et al., 2001). (B) Cryo-EM structure of TetO (blue) bound to *E. coli* 70S ribosome (30S, yellow; 50S grey, P-site tRNA, green) at ~10 Å resolution (Li et al., 2013). (C) Cryo-EM structure of TetM (orange) bound to vacant *E. coli* 70S ribosome (30S, yellow; 50S grey) at ~7 Å resolution (Dönhöfer et al., 2012).

The initial structure showed TetO bound to the POST state ribosome occupying a similar binding site as EF-G (Spahn et al., 2001). Due to the absence of density near the tetracycline binding site, the mechanism of drug-release was proposed to be indirect (Spahn et al., 2001). The later structures at higher resolution however showed electron density within the A-site on the SSU overlapping the tetracycline binding site and therefore contradicted the previously proposed mechanism and suggested that RPPs directly dislodge tetracycline from its binding site (Dönhöfer et al., 2012; Li et al., 2013). The 7.2 Å resolution structure of TetM bound ribosomes allowed a homology model based on EF-G to be built and docked into the cryo-EM density. The reconstruction revealed that the C-terminal extension in TetM, which is absent in EF-G, adopts a helical structure and binds to the ribosome near the DC (Dönhöfer et al., 2012). The docked homology model further suggested that residues in loop III of TetM domain IV overlap the tetracycline binding site. Mutagenesis

studies identified two tyrosine residues (Y506 and Y507) in loop III of domain IV that are critical for *in vivo* TetM activity, when both are mutated to alanine (Dönhöfer et al., 2012). Similar studies using TetO reported that even the single mutant Y507A abolishes TetO activity, which indicated possible differences between TetM and TetO (Li et al., 2013). Recently, a revision of the TetO Y507A mutation demonstrated only a reduction of the minimal inhibition concentration (MIC) like reported previously for TetM, and only the Y506A/Y507A double mutation abolished TetO activity completely (Nguyen et al., 2014). Due to the high sequence conservation of RPPs in this region, it seems likely that both TetM and TetO retain reduced activity with single mutants of Y507 and that mutation of both Y506 and Y507 is required to abolish activity of RPPs. However, the precise molecular mechanism by which RPPs dislodge tetracycline from the ribosome and in particular the implication of Y506 and Y507 in this process remained unclear due to the limited resolution (Dönhöfer et al., 2012; Li et al., 2013). Publication 4 of this cumulative thesis reports a high-resolution (3.9 Å) cryo-EM reconstruction of TetM bound to translating ribosomes, which provides a much more detailed insight into the interaction of TetM with the *Escherichia coli* ribosome. For example, the structure revealed that a proline residue (P509) located at the tip of loop III is directly involved in tetracycline release and that the two tyrosine residues are instead important for stabilizing the conformation of loop III (Arenz et al., 2015).

1.3.3 Macrolides

Overview. The clinically important class of macrolide antibiotics consists of a number of polyketide compounds, which specifically inhibit many Gram-positive and Gram-negative bacterial pathogens (Gaynor and Mankin, 2003; Kannan and Mankin, 2012; Katz and Ashley, 2005; Mankin, 2008; Poehlsgaard and Douthwaite, 2003; Takashima, 2003; Wilson, 2009, 2014). The first generation macrolide erythromycin A is naturally produced by *Saccharopolyspora erythraea* and represents the first member of macrolides introduced into clinical practice in the 1950's (McGuire et al., 1952). Second-generation macrolides like clarithromycin, roxithromycin and azithromycin are produced semi-synthetically by chemical modification of the parent compounds and show improved pharmacokinetic and antimicrobial properties. The

increasing spread of macrolide resistance has led to the development of third generation macrolides, namely the ketolides (e.g. telithromycin), which are more effective against susceptible as well as some resistant bacterial strains. The chemical structure of macrolides comprises a common 12-16-member macrolactone ring to which different amino sugars are attached to various positions. For example erythromycin consists of the 14-member macrolactone ring with C3'-cladinose and C5'-desosamine sugar modifications. In comparison, the macrolactone ring of the ketolide telithromycin lacks the C3'-cladinose sugar and instead carries a C3'-keto group and a 11,12 cyclic carbamate with an extended alkyl-aryl arm.

Target binding site. Macrolides bind to empty or initiating ribosomes (Contreras and Vazquez, 1977; Pestka, 1974; Tai et al., 1974) at the entrance of the exit tunnel as was suggested via chemical foot-printing showing protection of 23S rRNA nucleotide A2058 and A2059 (Moazed and Noller, 1987; Poulsen et al., 2000; Rodriguez-Fonseca et al., 1995) (**Fig. 10**). Crystal structures of macrolide-bound ribosomes confirmed that the C5'-sugar moiety interacts with nucleotides A2058 and A2059, which places the macrolides near the tunnel entrance in proximity to the tunnel constriction formed by ribosomal proteins L4 and L22, with the macrolactone ring lying flat against the tunnel wall (Bulkley et al., 2010; Dunkle et al., 2010; Hansen et al., 2002a; Tu et al., 2005). This contrasts with an early structure of erythromycin bound to *Deinococcus radiodurans* 50S, which showed a different conformation of the lactone ring, pointing into the tunnel lumen (Schlünzen et al., 2001). Surprisingly, later structures of 14-membered macrolides bound to the *Deinococcus radiodurans* 50S showed the lactone ring lying flat against the tunnel wall (Belousoff et al., 2011; Pyetan et al., 2007). Importantly, species-specific differences in the binding mode of macrolides exist (Wilson, 2011). For example, different binding positions of the alkyl-aryl arm of the ketolide telithromycin were observed in crystal structures of telithromycin bound to *Haloarcula marismortui* and *Deinococcus radiodurans* 50S subunits (Wilson et al., 2005a) and *Escherichia coli* 70S ribosomes (Dunkle et al., 2010). The different binding location of the alkyl-aryl arm can be explained by species-specific differences of the rRNA nucleotides interacting with this moiety (Wilson, 2011).

Mode of action. In general, macrolides inhibit protein synthesis by interfering with the progression of the nascent chain through the ribosome exit tunnel (Tenson et al., 2003). After synthesis of small oligopeptides consisting of 6-8 amino acids, oligopeptidyl-tRNAs drop off of the ribosome (Menninger and Otto, 1982; Otaka and Kaji, 1975; Tenson et al., 2003). Thereby, the length of the oligopeptide chain before induction of drop-off strongly depends on the nature of the macrolide bound within the exit tunnel. For example telithromycin, lacking the C3'-cladinose provides more space for the nascent chain and therefore allows synthesis of longer (9-10 amino acids) oligopeptides before peptidyl-tRNA drop-off (Tenson et al., 2003). However, the general principle that macrolides simply plug the ribosome exit tunnel and prevent total peptide synthesis has been challenged recently by the observation that some peptides were able to bypass the drug in the tunnel and become fully synthesized (Kannan et al., 2012). Interestingly, comparative analyses of cellular protein contents after exposure with either erythromycin or telithromycin showed that telithromycin allowed synthesis of quantitatively more peptides compared to erythromycin (Kannan et al., 2012). This finding makes sense, since the macrolides do not sterically occupy the full diameter of the ribosomal tunnel but instead leave space for the peptide to pass by. Since the ketolide telithromycin does not contain the bulky C3'-cladinose sugar, it seems logical to assume that telithromycin provides more space to the nascent chain to pass by the drug compared to erythromycin and therefore allows synthesis of more proteins. To enable a protein to pass by the macrolide, its N-terminal amino acid residues seem to be important. For example swapping the N-terminal 12 amino acids between the macrolide-insensitive HNS protein and the sensitive OsmC protein rendered OsmC highly resistant to macrolide-induced translation inhibition (Kannan et al., 2012). Due to the absence of sequence homology between the N-termini of macrolide-resistant proteins, it seem likely that the N-termini of macrolide resistant peptides adopt a defined conformation within the exit tunnel that allows their N-termini to thread through the small pore in a drug-obstructed tunnel. Collectively, these findings suggest a far more complex interplay between the amino acid sequence of the nascent chain, the ribosomal tunnel and the macrolide in order to determine the fate of a translating ribosome.

Resistance. Resistance to macrolides can be conferred by a number of different mechanisms (Wilson, 2014). Translation of the originally identified 34 nucleotides long 23S rRNA fragment E-RNA34 (harbors pentapeptide mini-gene coding for the so-called E-peptide) as well as translation of random mini-gene library-derived specific pentapeptides causes low-level macrolide resistance (Tenson and Mankin, 2001; Tenson et al., 1997). However, neither overexpression of the E-peptide nor *in vitro* addition of synthetic E-peptides (Tenson et al., 1996) confers erythromycin resistance, ruling out the possibility that pentapeptides act by directly sequestering the drug. According to the current model, during their own synthesis, the nascent pentapeptides dislodge the drug from its binding site via direct interaction and, following their release, sweep it along to remove it from the ribosome in a “bottle brush” model of action (Lovmar et al., 2006; Tenson and Mankin, 2001; Tenson et al., 1997; Tripathi et al., 1998). This mechanism would provide time for the ribosome to translate cellular mRNAs into polypeptides, which occupy the ribosomal tunnel and thus prevent rebinding of the drug (Andersson and Kurland, 1987). A later study demonstrated that class I release factor-dependent translation termination of the pentapeptide is crucial for erythromycin dissociation from the ribosome (Lovmar et al., 2006). However, the originally identified pentapeptide is encoded within segments of the 23S rRNA that is not normally translated. The association of the rRNA with rProteins as well as extensive secondary structures within the 23S rRNA prevent translation of the 23S rRNA-encoded pentapeptide (Tenson and Mankin, 2001), which raises the question whether erythromycin-resistance proteins represent a biologically relevant resistance mechanism. Spontaneous deletions of specific nucleotides of the 23S rRNA were shown to cause erythromycin resistance (Dam et al., 1996; Douthwaite et al., 1989; Douthwaite et al., 1985), presumably by altering the secondary structure of pentapeptide-containing rRNA regions, which possibly enables pentapeptide expression.

The most frequent resistance mutation A2058G in the 23S rRNA causes high-level resistance to most macrolides, including ketolides (Vester and Douthwaite, 2001), and explains the natural macrolide resistance of eukaryotic ribosomes carrying a guanine nucleotide in this position. However, mutation of A2058 to G does not confer

resistance to yeast ribosomes and thus suggests that more factors are involved in mediating macrolide resistance to eukaryotic ribosomes (Bommakanti et al., 2008). Moreover, A2058G mutation does not confer resistance to ketolides in *Streptococcus pneumoniae* (Canu et al., 2002; Farrell et al., 2003). In *Pneumococcus* species, the resistance mutation A2059G is found more frequently compared to the A2058G mutation (Franceschi et al., 2004; Vester and Douthwaite, 2001). Furthermore, mutations in rProteins L4 and L22 confer macrolide resistance presumably by perturbation of the 23S rRNA conformation comprising the drug-binding site (Chittum and Champney, 1994; Gregory and Dahlberg, 1999; Wittmann et al., 1973). Macrolide efflux mediated by MefA and MsrA macrolide efflux pumps (Roberts et al., 1999; Ross et al., 1990) as well as macrolide modification for example by macrolide phosphorylases of the Mph family are further sources of high-level resistance (Roberts et al., 1999). Modification of 23S rRNA nucleotides by methyltransferases for example is another common strategy conferring macrolide resistance. Methylation of G748 by RlmA (II) methyltransferase renders the producing organism resistant to tylosin (in combination with monomethylated A2058) (Douthwaite et al., 2004). Erythromycin resistance methyltransferases (Erms) methylate or dimethylate the macrolide binding nucleotide A2058 at the N6 position, which would lead to steric clashes with the C5'-monosaccharide and therefore reduces the affinity of macrolides to the ribosome and confers resistance (Hansen et al., 2002a) (**Fig. 10**).

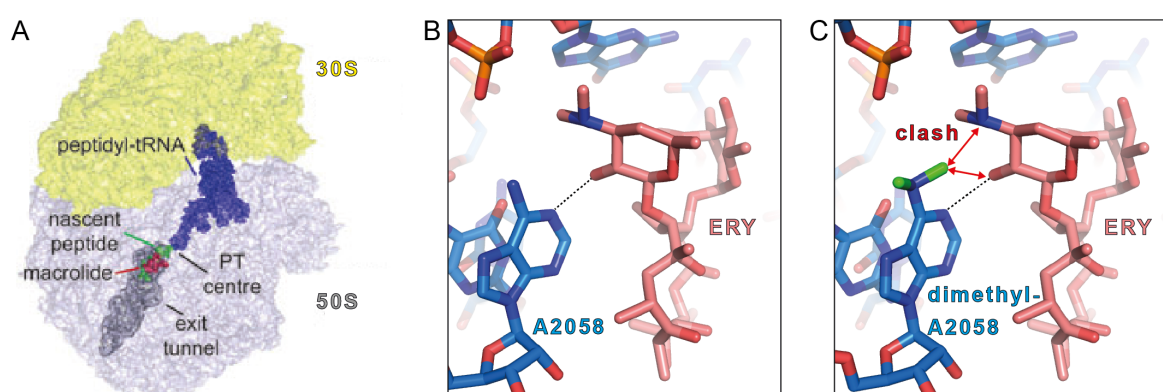


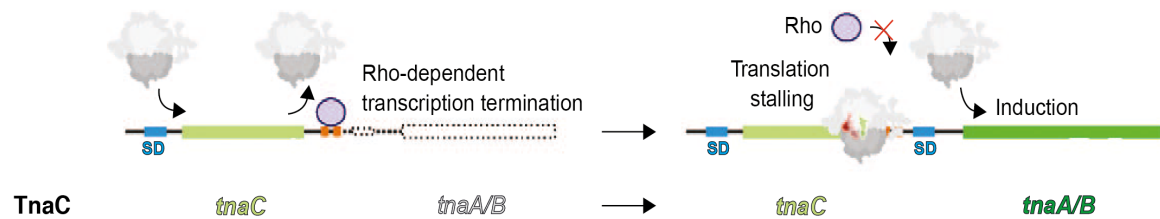
Figure 10 | Overview of the macrolide binding site within the ribosome exit tunnel. (A) Figure modified from (Ramu et al., 2009) showing macrolide (red) within the ribosome exit tunnel (grey) near the PTC (PT center). The nascent peptide is shown in green, the P-site peptidyl-tRNA in blue and the macrolide in red. (B) Erythromycin (red) hydrogen bonds with nucleotide A2058 of the 23S rRNA (Dunkle et al., 2010). (C) Methylation or dimethylation (green) of A2058 by Erm-type methyltransferases interferes with drug binding.

Expression of genes coding for Erms are inducible via macrolide-dependent translation attenuation on upstream open reading frames (Horinouchi and Weisblum, 1980; Iordanescu, 1976; Shivakumar et al., 1980; Weisblum, 1995). This mechanism ensures that expression of the resistance gene is only induced in the presence of the drug. Interestingly, ketolide-mediated induction of ErmC does not use ribosome stalling on ErmCL, but rather ribosome frameshifting at the upstream ORF to induce expression of ErmC (Gupta et al., 2013a). The tight regulation of Erm expression could be explained by the recent finding that permanent methylation of A2058 is associated with a huge fitness cost for the bacterial cell (Gupta et al., 2013b), probably due to de-regulation of translation.

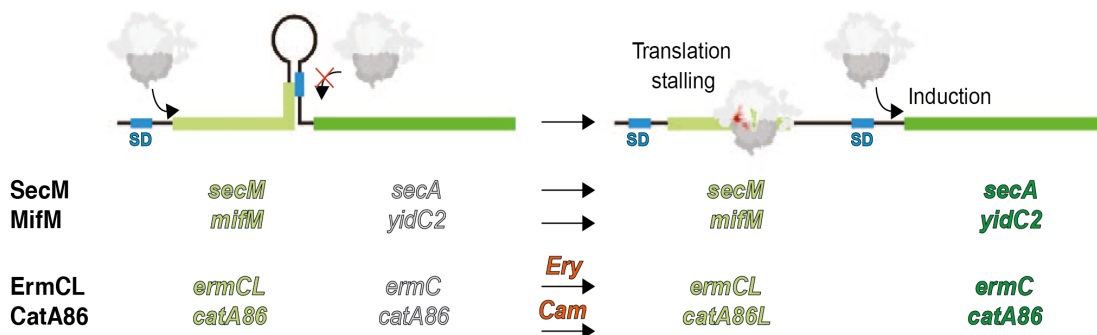
Stalling. In addition to the abilities of macrolides to induce peptidyl-tRNA drop-off or allow synthesis of specific peptides, macrolides can also induce ribosome stalling during translation of specific peptide sequences. The principle of nascent polypeptide-mediated translation attenuation occurs in many organisms to regulate expression of certain genes (Wilson and Beckmann, 2011). Nascent polypeptide-mediated translation regulation can be an intrinsic property of the nascent chain, such that the amino acid sequence of the nascent chain, for example polyproline sequences (Doerfel et al., 2013; Peil et al., 2013; Starosta et al., 2014; Tanner et al., 2009; Ude et al., 2013; Woolstenhulme et al., 2013), is sufficient to slow down the rates of translation and in some cases even induce translation arrest (Ito and Chiba, 2013). Therefore, the ribosome exit tunnel seems not to be just a passive conduit through which nascent polypeptides pass during synthesis, but rather closely monitors and interacts with the amino acid residues of the nascent chain in order to communicate with the PTC to modulate the rate of translation (Wilson and Beckmann, 2011). Nucleotide residues of the 23S rRNA comprising the wall of the ribosomal tunnel could potentially be involved in sensing nascent polypeptides. For example mutation of nucleotides U1782, U2609, A2503, U2586 or A2062 does not influence peptide synthesis, but severely affect the ribosomes ability to halt translation in response to specific nascent polypeptides (Vázquez-Laslop et al., 2011). Ribosome stalling often occurs during translation of small upstream open reading frames (ORFs) to regulate expression of downstream genes in the operon, which are transcriptionally or translationally repressed (**Fig. 11**). Well-studied examples are

the MifM (Chiba et al., 2009; Sohmen et al., 2015) and SecM (Bhushan et al., 2011; Goldman et al., 2015; Gumbart et al., 2012; Nakatogawa and Ito, 2002; Tsai et al., 2014; Wilson and Beckmann, 2011) leader peptides.

A Transcription antitermination via translation termination stalling



B Translation induction via translation elongation stalling



C Translation repression via translation termination stalling

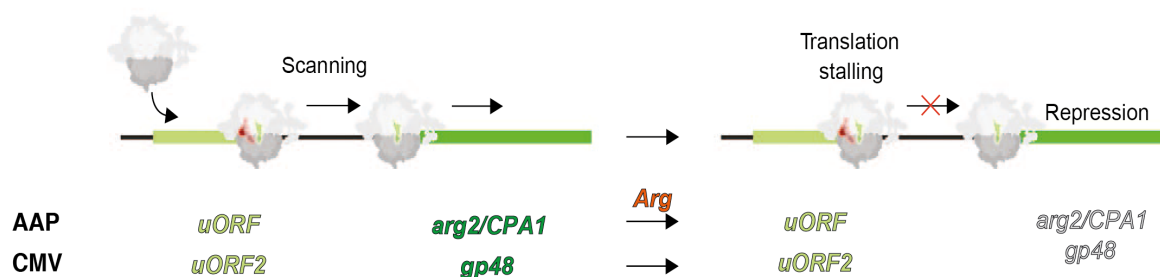


Figure 11 | Regulation of gene expression by ribosome stalling. (A) Ribosome stalling during translation termination on the TnaC leader peptide prevents rho-dependent transcription termination and allows transcription and expression of the downstream *tnaA/B* genes. (B) Ribosome elongation stalling during translation of SecM, MifM, ErmCL and Cat86 leader peptides leads to structural rearrangements of the respective mRNAs, which consequently expose the previously inaccessible Shine-Dalgarno (SD) sequences of the downstream genes allowing their expression. (C) Ribosome stalling during translation termination on upstream open reading frames (uORFs) of cytomegalovirus (CMV) and arginine attenuator peptide (AAP) prevents scanning and thus expression of their respective downstream genes. Figure modified from (Wilson and Beckmann, 2011).

MifM-stalling. The MifM leader peptide consists of 95 amino acids, whereas the C-terminal residues 69-89 were shown to be critical for stalling (Chiba et al., 2009). Interestingly, translation stalls at four specific sites in the MifM leader peptide and biochemical experiments revealed that residues R69, I70, W73, I74, M80, N81, as well as the C-terminal DEED (86-89) motif are important for translation arrest (Chiba and Ito, 2012; Chiba et al., 2009). Surprisingly it was shown, that translation of MifM leads to ribosome stalling in a species-specific manner, as MifM induces stalling on *Bacillus subtilis*, but not on *E. coli* ribosomes (Chiba et al., 2011). Notably, nucleotides comprising the ribosomal tunnel are highly conserved between *B. subtilis* and *E. coli*, which raises the question of how the species-specificity of MifM is achieved. A recent publication reported a high-resolution structure of a MifM-stalled ribosome (**Fig. 12**) with D89 in the P-site, which biochemically identified a single *B. subtilis*-specific residue Met90 of L22 being responsible to modulate the species specificity of MifM (Sohmen et al., 2015). Indirect contact of MifM with L22 Met90 together with further interactions between critical residues of MifM and nucleotides in the ribosomal tunnel possibly stabilize the MifM nascent chain in a special conformation, placing the side chain of Glu87 of MifM in a position, which prevents A-site tRNA accommodation to the PTC and therefore peptide bond formation leading to translation arrest (Sohmen et al., 2015). In the natural context, the ribosome manages to incorporate the next amino acid, although at lower rates (Chiba and Ito, 2012; Chiba et al., 2009), which leads to the assumption that Glu87 is not solely responsible for translation arrest, especially, since single mutation of Glu87 does not prevent stalling to occur (Chiba and Ito, 2012). The observed SD-anti-SD helix in MifM-stalled ribosome complex (SRC) might contribute to the stalling event (Sohmen et al., 2015), similar to induction of ribosome pausing mediated by internal SD-like sequences in bacteria (Li et al., 2012). Notably, MifM-stalled ribosomes are unreactive to release factors (Chiba and Ito, 2012; Chiba et al., 2009), probably due to the steric overlap of A2602 in MifM-SRC with the GGQ motif of RF2, which is proposed to prevent RF2 accommodation into the PTC.

SecM-stalling. The SecM leader peptide sequence is 170 codons long and precedes the downstream gene *secA*. The ribosome stalls during translation of SecM at the 165th codon position with a glycine codon in the P-site and a proline codon in the A-site (Muto et al., 2006; Woolhead et al., 2006). Specific residues within the C-terminal amino acid sequence F₁₅₀XXXXWIXXXXGIRAG₁₆₅ together with the spacing in between them are known to be critical for stalling (Nakatogawa and Ito, 2001, 2002). In detail, cysteine-mutagenesis studies showed that only R163 is indispensable for stalling, whereas the flanking residues play a secondary role, presumably to position R163 into a specific location inside the tunnel (Yap and Bernstein, 2009). It has been shown that the proline-tRNA^{Pro} in the A-site is required for efficient stalling (Muto et al., 2006; Nakatogawa and Ito, 2002), however peptide bond formation between the peptidyl-tRNA and the proline-tRNA^{Pro} in the A-site still occurs slowly (Muto et al., 2006). Biochemical evidence shows that mutation of tunnel components A2058G, A2062U, A2503G (Lawrence et al., 2008; Nakatogawa and Ito, 2002; Vazquez-Laslop et al., 2010) as well as insertion of single adenine residues between A749-A753 and furthermore insertions, deletions or mutations in L22 and L4 (Lawrence et al., 2008; Nakatogawa and Ito, 2002) alleviates ribosome stalling on SecM. Cryo-EM reconstructions of SecM-stalled ribosomes at ~11 Å (Mitra et al., 2005) and ~6 Å resolution (Bhushan et al., 2011) are available (**Fig. 12**). The former structure suggested that the SecM nascent chain induces larger scale conformational changes in the 23S rRNA by interaction with A2058 and A749-A753 (Mitra et al., 2006), which alter the correct geometry in the PTC required for peptide bond formation. The better resolved structure however did not support this cascade of rRNA conformational changes but instead visualized direct interaction between critical residues of SecM with nucleotides of the ribosomal tunnel as well as a shift of 2 Å in the peptidyl-tRNA ester linkage, which moves the peptidyl-ester further away from the A-site tRNA and thereby alters the geometry within the PTC leading to inhibition of peptide bond formation (Bhushan et al., 2011). Within the limitations of a ~6 Å map, SecM appears to interact with nucleotides U2609, U2585 and A2062 comprising the ribosome exit tunnel. A2062 is a highly flexible nucleotide (Fulle and Gohlke, 2009) and is stabilized in a conformation with the base lying flat against the tunnel wall probably via the key interaction with the critical SecM residue Arg163 (Bhushan et al., 2011). By being

stabilized in this defined conformation, A2062 potentially communicates to the PTC via A2503 to inhibit peptide bond formation (Vazquez-Laslop et al., 2010), eventually by shifting the peptidyl-tRNA ester. Supporting the hypothesis, mutation of either A2062 (Vazquez-Laslop et al., 2010) or Arg163 (Nakatogawa and Ito, 2002; Yap and Bernstein, 2009) abolishes SecM-dependent ribosome stalling. Ribosomal stalling could be additionally influenced by the identity of the tRNA in the A-site, since proline naturally shows slower rates of peptide bond formation compared to other amino acids (Pavlov et al., 2009). In contrast to MifM, SecM might therefore affect the P-site rather than the A-site illustrating that nascent peptide-mediated ribosome stalling might be inducible via different mechanisms culminating in inhibition of the PTC.

Further underlining the complex and impressive ability of the ribosome to monitor the amino acid sequence and structure of growing polypeptides, nascent polypeptide-mediated translation regulation can also depend on the presence of a small ligand or cofactor bound in the ribosome exit tunnel (Ramu et al., 2009; Vazquez-Laslop et al., 2011; Vazquez-Laslop et al., 2008). Well-characterized examples are the free L-tryptophan-dependent ribosome stalling during translation of TnaC and the macrolide-dependent ribosome stalling during translation of Erm-type leader peptides.

TnaC-stalling. One of the best-studied examples is the 24 amino acid-long leader peptide TnaC, which requires the presence of free L-tryptophan (L-Trp) for stalling to occur (Bischoff et al., 2014; Gong and Yanofsky, 2002; Seidelt et al., 2009). Unlike for stalling on *Erm* leader peptides, ribosome stalling during translation of TnaC in the presence of free L-Trp does not induce mRNA rearrangements, but rather leads to transcription anti-termination and therefore expression of downstream genes (Gong and Yanofsky, 2002). Ribosomes translating the TnaC leader peptide stall with the last sense codon of TnaC (P24) in the P-site and the UGA stop codon in the A-site. Therefore, unlike MifM of SecM, TnaC induces stalling during translation termination by preventing RF2-mediated peptide release (Gong and Yanofsky, 2002). Numerous biochemical experiments determined residues P24, D16 and W12 of TnaC, as well as their relative spacing, to be critical for the ribosome to respond to free L-Trp by inactivation of the PTC (Cruz-Vera et al., 2005; Cruz-Vera and Yanofsky, 2008; Gong

and Yanofsky, 2002). The first structural insight into TnaC-stalled ribosomes was provided by a cryo-EM reconstruction at 5.8 Å (Seidelt et al., 2009). The structure highlighted that TnaC adopts a defined conformation within the exit tunnel, which stabilizes U2585 and A2602 in defined positions that would sterically prevent accommodation of release factors into the PTC and thereby translation termination (Seidelt et al., 2009). However, despite the identification of critical interactions between TnaC and the ribosomes, the resolution was not sufficient to localize the L-tryptophan cofactor and therefore a detailed explanation of L-Trp-induced ribosome stalling during translation of TnaC remained elusive. Recently, a high-resolution cryo-EM reconstruction of the TnaC-SRC at 3.8 Å (**Fig. 12**) revealed the binding sites of two tryptophan molecules bound within the ribosomal tunnel and provided detailed insight into the interactions between TnaC and components of the ribosomal exit tunnel (Bischoff et al., 2014). Interestingly, the two L-Trp molecules are bound ~15-20 Å distant from the PTC, which contrasts initial suggestions that the tryptophan binding site is located directly within the A-site of the PTC, overlapping the sparsomycin binding site (Cruz-Vera et al., 2006; Cruz-Vera et al., 2007; Cruz-Vera and Yanofsky, 2008). The observed binding site for the L-Trp molecules in proximity to A2058 of the 23S rRNA and I19 of TnaC (Bischoff et al., 2014) nicely agrees with more recent studies suggesting that these two residues play an important role for L-Trp binding and subsequent inhibition of the PTC (Martinez et al., 2014). In detail, the TnaC nascent polypeptide creates two hydrophobic pockets within the exit tunnel to accommodate the two L-Trp molecules W1 and W2. W1 is sandwiched between D21, V20 and I19 of TnaC on the one side, and U2586 on the tunnel side, whereas W2 is bound in a pocket formed by TnaC residues V20 and I15 and by A2058/A2059 of the 23S rRNA. Interestingly, W2 binding to TnaC structurally mimics the ribosome-bound ketolide telithromycin in this region (Dunkle et al., 2010), which induces translational arrest during translation of certain leader peptides (Vázquez-Laslop et al., 2011), suggesting a more general role of A2058/A2059 and U2609/A752 in nascent chain-dependent translation regulation. Accordingly, mutagenesis of U2609, A752 and A2058 severely affects stalling efficiency during translation of TnaC (Cruz-Vera et al., 2005; Cruz-Vera and Yanofsky, 2008; Gong and Yanofsky, 2002). Nucleotides U2585 and A2602 within the PTC adopt positions that would sterically clash with the GGQ

motif of RF2 and thereby interfere with RF2-mediated peptidyl-hydrolysis of the TnaC nascent chain (Bischoff et al., 2014). Collectively, critical amino acid residues in TnaC appear to establish defined interactions with the ribosomal tunnel, thereby forming two binding sites for L-Trp molecules, binding of which is then allosterically communicated to the PTC to stabilize U2585 and A2602 in conformations incompatible with RF2-mediated translation termination. The example of TnaC-stalling clearly illustrates the complexity of the communication between nascent chain, ribosomal tunnel and small molecule co-factors to allosterically inactivate the PTC.

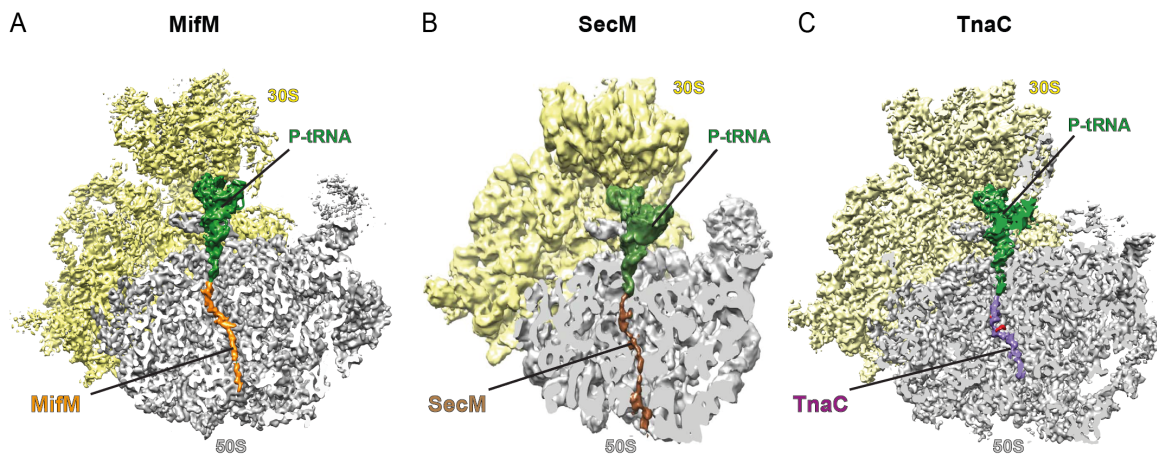


Figure 12 | Overview of cryo-EM structures of MifM-, SecM-, and TnaC-stalled ribosomes. (A-C) Comparison of cryo-EM structures of (A) MifM-SRC (Sohmen et al., 2015), (B) SecM-SRC (Bhushan et al., 2011) and (C) TnaC-SRC (Bischoff et al., 2014), with 50S subunits (grey) cut in order to display the path of the respective nascent polypeptide chains passing through the ribosomal tunnel.

Erm-type-stalling. Macrolide-dependent ribosome stalling during translation of Erm-type leader peptides was initially discovered to regulate expression of the inducible downstream macrolide resistance methyltransferase ErmC (Horinouchi and Weisblum, 1980; Iordanescu, 1976; Shivakumar et al., 1980; Weisblum, 1995). In general, in the absence of erythromycin, ErmC expression is inhibited since the SD sequence and start codon of ErmC are sequestered in a stem loop structure of the mRNA, which prevents translation initiation. At sub-inhibitory concentrations of erythromycin, ribosomes translating the ErmCL leader peptide become stalled, which causes a change in the mRNA secondary structure so that the SD sequence and the start codon of the *ermC* gene become exposed, allowing ribosome binding and

induction of ErmC expression. To date, numerous Erm-type leader sequences regulating downstream resistance genes have been identified in multiple organisms (Ramu et al., 2009; Vázquez-Laslop et al., 2011). Notably, the amino acid sequence of the different leader peptides is very diverse and can be grouped into several classes, depending on a common C-terminal amino acid sequence motif critical for stalling (Ramu et al., 2009; Vázquez-Laslop et al., 2011). Despite the common mechanism used by all Erm-type leader peptides to stall translation in order to induce expression of downstream resistance genes, they vary significantly in terms of biochemical properties, like drug-specificity, A-site tRNA specificity and dependency on certain nucleotides of the ribosomal tunnel (Vázquez-Laslop et al., 2011). How the macrolide-bound ribosome senses the presence of specific structures and amino acid sequences of different nascent polypeptides within the exit tunnel and how these signals are communicated to the PTC to stall translation are hot topics in the field. In general, Erm-type leader peptides are rather short, with stalling sites between codon positions 6-16 (Ramu et al., 2009). For simplicity reasons, the following section focuses on main differences/similarities between ErmAL1 (MCTSI**IAVV**^P-**E**^A; IAVV peptides), ErmBL (MLVFQMR**NVD**^P-**K**^A; miscellaneous peptides), ErmCL (MGIFS**IFVI**^P-**S**^A; IFVI peptides) and ErmDL (M**THSMRL**^P-**R**^A; RLR peptides), representing members of the four main stalling motif classes of Erm-type leader peptides (**stalling motif** = critical residues) (Vázquez-Laslop et al., 2011).

Studies on the ErmDL leader peptide, which belongs to the RLR-class of stalling peptides, revealed that unlike for ErmCL (Vázquez-Laslop et al., 2008), N-terminal truncation of the leader peptide to yield the minimal tripeptide stalling-motif MRL^P-R^A, retains its ability to respond to the presence of both erythromycin and telithromycin (Sothiselvam et al., 2014). The authors claimed that the MRL tripeptide is too short to directly contact the tunnel-bound drug and further could not identify critical residues comprising the tunnel wall. Consequently, the macrolide was suggested to allosterically induce conformations within the PTC, which allow the ribosome to respond to RLR stalling sequences (Sothiselvam et al., 2014). In fact, chemical probing analyses as well as molecular dynamics simulations demonstrated that solely the binding of a macrolide to the ribosome, in the absence of nascent polypeptide, changes the chemical protection pattern and the computed

conformational freedom of nucleotides U2585 and A2602, which play critical roles during peptide bond formation (Schmeing et al., 2005d; Voorhees et al., 2009). Therefore, the authors concluded that drug binding allosterically predisposes the ribosome to respond to specific amino acid sequences of the nascent chain (Sothiselvam et al., 2014). To address the mechanism of macrolide action on a genome-wide level, recent ribosome profiling experiments performed with azithromycin (Davis et al., 2014), erythromycin or telithromycin-treated (Kannan et al., 2014) cells were performed. The profiling data revealed that in the presence of the drug, translation of most genes proceeds past the 5'-codons and is arrested during translation of specific amino acid sequence motifs located more distal in the open reading frames, suggesting that macrolides inhibit protein synthesis in a sequence-specific manner (Davis et al., 2014; Kannan et al., 2014). Interestingly, the profiling experiments identified, amongst others, the stalling motif R/K x R/K, which nicely corresponds to the stalling motif present in RLR-class leader peptides (e.g. ErmDL). However, not every R/K x R/K motif encountered by a drug-bound ribosome induces translation arrest, which suggests that the variable N-terminal context of the R/K x R/K motif is critical to turn the motif into a stalling-motif (Kannan et al., 2014). Moreover, erythromycin (Kannan et al., 2014) or azithromycin-treated (Davis et al., 2014) cells display a broader variety of arrest motifs compared with telithromycin-treated cells (Kannan et al., 2014).

Despite all Erm-type leader peptides requiring the presence of a macrolide bound within the exit tunnel to induce translation arrest, the chemical nature of the macrolide, especially the presence of the C3'-cladinose sugar, plays a role during induction of stalling. For example the C3'-cladinose sugar is crucial to induce stalling during translation of ErmAL1 and ErmCL, whereas in contrast, stalling on ErmBL and ErmDL leader peptides is also inducible by the ketolide telithromycin, which lacks the C3'-cladinose sugar (Sothiselvam et al., 2014; Vazquez-Laslop et al., 2011; Vázquez-Laslop et al., 2011; Vazquez-Laslop et al., 2008). These results suggest that ErmAL1/ErmCL and ErmBL/ErmDL nascent chains might follow different paths within the drug-obstructed ribosome exit tunnel, which might be directed by the presence or absence of the C3'-cladinose sugar of erythromycin. Differences in the path of the nascent chain might lead to different key interactions between the nascent

polypeptides and nucleotides comprising the tunnel wall. For example, mutagenesis of A2062 and A2503 abolishes stalling during translation of ErmAL1 and ErmCL, but has no effect on ErmBL and ErmDL-mediated translation arrest (Vázquez-Laslop et al., 2011; Vazquez-Laslop et al., 2008). Furthermore, differences in the degree of PTC inactivation exist. For example, drug-dependent stalling on ErmAL1 can be alleviated by mutation of the A-site codon to A, F, M or C (Ramu et al., 2011), thus making the A-site selective for accommodation of only certain aa-tRNAs that would lead to peptide bond formation. In contrast, drug-dependent stalling on ErmCL inhibits peptide bond formation irrespective of the identity of the A-site amino acid and therefore induces a restrictive A-site (Ramu et al., 2011). Interestingly, the amino acid in the -2 position (A in ErmAL1; F in ErmCL) plays a critical role in determining the fate of the A-site, since swapping this residue between ErmAL1 and ErmCL turns the A-site selective for ErmCL_F7A (Ramu et al., 2011). However, the structural changes within the PTC leading to this change in A-site specificity remain unclear. Publications 5 (Arenz et al., 2014b), 6 (Arenz et al., 2014a) and 7 (Arenz, 2015) of this cumulative thesis report the first high-resolution cryo-EM structures of drug-stalled ribosomes during translation of ErmBL (Arenz et al., 2014b; Arenz, 2015) and ErmCL (Arenz et al., 2014a) leader peptides, providing the first structural insight into the complex interplay between nascent peptide, the tunnel-bound macrolide and components of the exit tunnel to inactivate the PTC. The structures essentially show that ErmBL and ErmCL nascent chains follow different paths through the ribosome. The ErmCL nascent chain directly senses the presence of erythromycin (Arenz et al., 2014a), whereas the ErmBL nascent peptide adopts a different conformation within the exit tunnel following a path far away from erythromycin. (Arenz et al., 2014b; Arenz, 2015). Moreover, the structures show differences in the conformation of A2062 (Arenz et al., 2014a; Arenz et al., 2014b; Arenz, 2015), which agrees well with biochemical evidence demonstrating the differential importance of this nucleotide for stalling (Vázquez-Laslop et al., 2011; Vazquez-Laslop et al., 2008). Most interestingly, the structures of ErmBL and ErmCL-stalled ribosomes reveal dramatic differences in the conformation of the inactivated PTC, thereby highlighting that ErmBL and ErmCL nascent chains inactivate the PTC via two distinct mechanisms (Arenz et al., 2014a; Arenz et al., 2014b; Arenz, 2015).

2 Objectives of These Studies

Ribosomal protein S1 (Publication 1)

S1 is known to be intrinsically very flexible (Chu and Cantor, 1979; Moore and Laughrea, 1979), explaining the absence of structural data of the full-length protein bound to the ribosome. Previous biochemical experiments suggested that the N-terminal region of S1 (residues 1-106; S1₁₀₆) mediates S1 binding to the ribosome (Byrgazov et al., 2012; Lauber et al., 2012) via interaction with ribosomal protein S2 (Boni et al., 1982; Moll et al., 2002). The aim of this work was to provide a structural basis of the interaction between S1 and S2, which anchors S1 on the ribosome, and to extend our insight into how S1 enables translation initiation of highly structured mRNAs.

Proline-rich antimicrobial peptides (Publication 2)

Proline-rich antimicrobial peptides (PrAMPs) are produced by the innate immune response and exhibit activity against various Gram-negative pathogens. Due to their low toxicity, PrAMPs represent a potent new class of antibiotics. Recently biochemical experiments demonstrated that Onc112, a 19-residue member of the oncocin family of PrAMPs targets the 70S ribosome and inhibits translation (Krizsan et al., 2014). The aim of this project was to obtain a high-resolution structure of an Onc112-bound ribosome to determine the PrAMP binding site on the ribosome and, together with biochemical experiments, to unravel the mode of action by which PrAMPs inhibit translation.

Tetracycline resistance (Publication 3 and 4)

Tetracycline resistance can be mediated by specialized proteins like TetM, which confer resistance by dislodging the clinically important tetracycline from its binding site on the SSU of the ribosome. However, due to the low resolution of previous cryo-EM reconstructions of TetM-bound ribosomes, detailed insight into TetM-mediated

tetracycline resistance remained elusive. By using translating instead of vacant ribosomes as substrates for TetM binding, we aimed to improve complex homogeneity for state-of-the-art cryo-EM analysis. The goal was to obtain a sufficiently high-resolved reconstruction of TetM-bound ribosomes to unravel, together with complementing biochemical experiments, the molecular mechanism by which TetM dislodges tetracycline from its binding site and thus confers resistance.

Macrolide-dependent ribosome stalling (Publications 5, 6 and 7)

The presence of subinhibitory concentrations of clinically important macrolide antibiotics induces ribosome stalling during translation of Erm-type leader peptides, resulting in induction of expression of downstream macrolide resistance genes. Despite a lot of biochemical information on drug-dependent ribosome stalling being available, structural insight into the complex interplay between nascent polypeptide, the ribosomal exit tunnel and the tunnel-bound macrolide was lacking. Here we aimed to rectify this situation by determination of high-resolution cryo-EM structures of drug-stalled ribosomes, providing insight into the molecular mechanism by which translation of Erm-type leader peptides is arrested in the presence of macrolides antibiotics. Moreover, we aimed to address interesting differences among different drug-stalled ribosomes, like drug-specificity and A-site specificity, which strongly depend on the amino acid sequence of the peptide being translated.

3 Cumulative Thesis: Summary of Publications

3.1 Publication 1 | Structural Basis for the Interaction of Protein S1 with the *Escherichia coli* Ribosome

Konstantin Byrgazov, Irina Grishkovskaya, Stefan Arenz, Nicolas Coudevylle, Hannes Temmel, Daniel N. Wilson, Kristina Djinovic-Carugo and Isabella Moll.

Nucleic Acids Research. 43, 661-673 (2014).

The six-domain ribosomal protein S1 is essential for translation initiation in Gram-negative bacteria (Sorensen et al., 1998). Previous experiments suggested that the N-terminal region of S1 (residues 1-106; S1₁₀₆) is necessary and sufficient (Byrgazov et al., 2012; Lauber et al., 2012) for interaction with ribosomal protein S2 (Boni et al., 1982; Moll et al., 2002). However, high-resolution structural information on the binding mode of S1 to the ribosome is unavailable, due to the intrinsic flexibility of the protein. By using a combination of NMR, X-ray crystallography, cryo-EM and biochemical studies, we gained profound insight in the structure and molecular interactions of the N-terminal domain S1 when bound to the ribosome. Multidimensional heteronuclear NMR studies on S1₁₀₆, S1₈₆ and S1₁₉₋₈₆ revealed that the N-terminal (1-18; S1_{NTS}) and C-terminal (87-106) linkers of D1 (19-86) are disordered in solution. *In vivo* binding assays demonstrated that the flexible S1_{NTS} is the crucial element of S1 required for ribosome binding. To unravel the molecular interaction pattern of S1_{NTD (1-86)} to S2, a chimeric fusion protein S2-S1_{NTD} was crystallized. Interestingly, the resulting 2-3 Å structure showed that the S1_{NTS} folds upon binding to S2 and adopts a α -helical structure, which is connected to the four β -stranded globular domain D1 of S1 (S1_{D1}) via a flexible seven amino acid linker. Notably, the fold of S1_{D1} resembles a truncated oligosaccharide/oligonucleotide-binding (OB) fold and is therefore different compared to the OB-fold of D3-D6 of S1. Interaction between S1_{NTD} and S2 is established via both π -stacking interactions involving phenylalanine residues of S1_{NTH} as well as via two salt bridges involving Asp39 and Lys43 of S1_{D1}. Thereby, direct interaction with S1_{D1} stabilizes residues Asp188 and Asp205 of the S2 zinc (Zn²⁺) binding pocket in their Zn²⁺ coordinating

conformation. Pull-down experiments using either tagged ribosomes or tagged S1_{NTD} variants revealed that the S1_{NTD}-D2 interaction is primarily based on π -stacking interactions between S1_{NTH} and S2. *In vitro* competition assays between S1_{NTH} and full length S1 suggested that S1_{NTH} competes with full length S1 for the same binding site. Accordingly, by competing with native S1, addition of 10-to 50-fold molar excess of S1_{NTS} over ribosomes inhibited *in vitro* translation of *ompA* mRNA, which was shown to be strictly dependent on the presence of S1 (Tedin et al., 1997). Furthermore, we determined a cryo-EM structure of a programmed *E. coli* ribosome at 8 Å resolution. Additional density adjacent to S2 was attributed to parts of S1, since S2-based alignment of the S2-S1_{NTD} crystal structure perfectly placed S1_{D1} into one of the additional densities. The cryo-EM structure reveals contact sites between S1_{NTD} and S2 in the same regions as expected from S2-S1_{NTD} crystal structure, as well as additional contacts of S1_{NTD} with the mRNA and the 3'-end of the 16S rRNA. Thereby, the cryo-EM structure suggests that the chimeric S2-S1_{NTD} fusion complex is physiologically relevant.

3.2 Publication 2 | The Proline-rich Antimicrobial Peptide Onc112 Inhibits Translation by Blocking and Destabilizing the Post-initiation Complex

A. Carolin Seefeldt*, Fabian Nguyen*, Stéphanie Antunes*, Natacha Pérébasquine, Michael Graf, Stefan Arenz, Kishore K. Inampudi, Céline Douat, Gilles Guichard, Daniel N. Wilson and C. Axel Innis.

Nature Structural & Molecular Biology. 10.1038/nsmb.3034 (2015).

Innate immune response-derived proline-rich antimicrobial peptides are active against various pathogens and due to their low toxicity represent a potent new class of antibiotics. Onc112, a 19-residue member of the oncocin family of proline-rich antimicrobial peptides, targets the 70S ribosome and inhibits translation (Krizsan et al., 2014). This publication reports a 3.1 Å crystal structure of Onc112 bound to *Thermus thermophilus* 70S ribosomes in complex with deacylated tRNA_f^{Met} in the P-site, providing the first structural insight into the mechanism of Onc112-mediated translation inhibition. We identified Onc112 binding within the upper region of the ribosome exit tunnel in a reverse orientation, such that the N-terminal residues

overlap the binding site for the CCA-end of the A-site tRNA, interfering with A-site tRNA binding and resulting in translation inhibition. Onc112 binding to the ribosome resembles an induced fit, involving stabilization of defined conformations of normally flexible nucleotides U2506, U2585 and A2062. An extensive, stabilizing network of hydrogen bonds between the N-terminal 10 residues and components of the 23S rRNA is observed, whereas the C-terminal residues appear to be flexible. We demonstrated that C-terminally truncated versions of Onc112 retain reduced activity to inhibit *in vitro* translation reactions, but lose their antimicrobial activity *in vivo*. To unravel the mode of Onc112 action, we employed ribosome toe-printing experiments to demonstrate that Onc112 inhibits translation after 70S initiation complex formation. Onc112 further destabilizes the 70S initiation complex, as observed by monitoring disome formation upon translation of a dicistronic mRNA *in vitro* in the presence of Onc112, presumably because Onc112 sterically clashes with fMet-tRNA^{Met} causing it to dissociate from the ribosome. Finally, *in vivo* growth inhibition experiments confirmed that SbmA is indeed the inner membrane transporter necessary for Onc112 uptake into Gram-negative bacteria.

3.3 Publication 3 | Tetracycline Antibiotics and Resistance Mechanisms

Fabian Nguyen, Agata L. Starosta, Stefan Arenz, Daniel Sohmen, Alexandra Dönhöfer and Daniel N. Wilson.

Biological Chemistry. 395, 559-575 (2014).

The ribosome is one of the main targets for antibiotics within a bacterial cell. The large family of tetracycline antibiotics represents one of the most frequently applied class in clinical practice to treat a variety of bacterial infectious diseases. Our publication reviews the development of first-, second- and third-generation members of tetracyclines and describes their mode of ribosome binding and their mechanism of action. Additionally, we review diverse mechanisms that give rise to bacterial resistance to tetracyclines, such as drug efflux, drug modification, target mutation and ribosome protection proteins.

3.4 Publication 4 | Cryo-EM Structure of the Tetracycline Resistance Protein TetM in Complex with a Translating Ribosome at 3.9 Å Resolution

Stefan Arenz, Fabian Nguyen, Roland Beckmann and Daniel N. Wilson.

Proceedings of the National Academy of Sciences. 112, 5401-5406 (2014).

The tetracycline resistance protein TetM belongs to the family of ribosome protection proteins (RPPs) that confer resistance by dislodging the clinically important tetracycline from its binding site on the SSU of the ribosome. Current knowledge about RPP action is based on 7.2-16 Å resolution cryo-EM reconstructions of RPP-bound vacant or non-translating ribosomes. However, due to lack of resolution, detailed insight into RPP-mediated tetracycline resistance remained elusive. By using state-of-the-art cryo-EM and multi-particle reconstruction of ribosome nascent chain complexes (RNCs) bound with TetM, we obtained a 3.9 Å reconstruction of TetM•RNC. The structure allowed TetM contacts with the ribosome to be revealed, a backbone model for TetM bound to an *E. coli* ribosome to be built and the previous model of TetM action to be revised. We overcame previous complex heterogeneity problems (Dönhöfer et al., 2012) by using defined substrate ribosomes (stalled during translation of ErmCL, trapped in non-rotated state, bearing a peptidyl-tRNA in the P-site and an empty A-site) for *Enterococcus faecalis* TetM binding in the presence of the non-hydrolysable GTP analog GDPCP. The structure reveals interaction of the conserved and functionally critical C-terminal helix (CTH) of TetM with A1913 of H69 in the decoding center, which adopts a defined position similar to that observed when A-site tRNA is bound to ribosome. Moreover, decoding center nucleotides A1492 and A1493 appear to flip out of h44 of the 16S rRNA, which confirms the previous suggestion based on the 7.2 Å TetM•70S structure (Dönhöfer et al., 2012), however the splayed conformation of A1492 and A1493 is distinct from all previously observed conformations. Unlike in previous reconstructions of TetM/TetO•70S complexes, the density for loop III of domain IV of TetM was unambiguous and resolved to 3.5 Å resolution, allowing the register and orientation of bulky side chains to be accurately determined. The fully conserved proline residue 509 located at the tip of loop III stacks upon C1054 of h34 comprising the tetracycline binding site

(Brodersen et al., 2000; Jenner et al., 2013; Pioletti et al., 2001) and would sterically clash with ribosome-bound tetracycline. In contrast to previous suggestions that Y506 and Y507 are directly involved in dislodging the drug from the ribosome, analysis of the structure combined with *in vivo* growth inhibition assays of selected TetM loop III mutants provided evidence that Y506 and Y507 are involved in intra-domain interactions that appear to stabilize the functional conformation of loop III. Collectively, we suggest that RPPs use P509 at the tip of loop III instead of Y506/Y507 to interact with the tetracycline binding site nucleotide C1054 and thus to directly dislodge tetracycline from the ribosome.

3.5 Publication 5 | Molecular Basis for Erythromycin-dependent Ribosome Stalling During Translation of the ErmBL Leader Peptide

Stefan Arenz, Haripriya Ramu, Pulkit Gupta, Otto Berninghausen, Roland Beckmann, Nora Vázquez-Laslop, Alexander S. Mankin and Daniel N. Wilson.

Nature Communications. 5: 3501 (2014).

The presence of subinhibitory concentrations of the clinically important macrolide erythromycin induces ribosome stalling during translation of the ErmBL leader peptide, resulting in induction of expression of the downstream macrolide resistance methyltransferase ErmB. We show by northern blotting that the ribosome is unable to catalyze peptide bond formation between the P-site peptidyl-tRNA^{Asp} and the incoming A-site Lys-tRNA^{Lys}, which causes the ribosome to stall during elongation with codon 10 (D10) in the P-site and K11 in the A-site. As a major achievement, our publication provides the first structural insight into drug-dependent stalled ribosome complexes (SRCs) and expands profoundly the mechanistic understanding of the complex interplay between nascent polypeptide, the tunnel-bound drug and nucleotides comprising the tunnel wall to generate a stalling signal, which is then communicated to the PTC to arrest translation. We developed an *in vitro* disome system, which allows highly specific purification of drug-dependent SRCs that cannot be purified using N-terminal affinity tagging due to the short (10 amino acids) nascent peptide residing inside the tunnel. Multiparticle cryo-EM allowed us to obtain a reconstruction of the ErmBL-SRC at 4.5 Å resolution in the ribosomal core, which

meant that our structure was one of best-resolved cryo-EM structures reported at the time, since revolutionizing improvements in the field of cryo-EM like application of direct electron detectors and Cs-correctors were not available to us at that stage. The structure reveals a unique path of the nascent ErmBL peptide, which bypasses the tunnel-bound drug. In perfect agreement with the absence of direct contact between ErmBL and erythromycin, toe-printing experiments confirmed that azalides and even ketolides lacking the C3'-cladinose sugar induce ribosome stalling during translation of ErmBL. Alanine scanning mutagenesis biochemically identified the C-terminal residues R7, V9 and D10 of ErmBL being critical for stalling. Strikingly, based on the structure, these residues appear to interact with nucleotides U2586 (R7) and U2585 (V9, D10) comprising the tunnel wall. Further toe-printing studies confirmed the functional interaction between R7 and U2586, since nucleotide alterations of U2586 restored stalling during translation of the ErmBL R7A mutant. This key interaction between nascent chain and ribosome seems to be communicated to the PTC, where V9 and D10 of ErmBL appear to interact with U2585, thereby stabilizing the uninduced state of the PTC. We proposed that the uninduced conformation of the PTC corrupts accommodation of the A-site bound Lys-tRNA^{Lys} into the PTC resulting in inhibition of peptide bond formation.

3.6 Publication 6 | Drug Sensing by the Ribosome Induces Translational Arrest via Active Site Perturbation

Stefan Arenz, Sezen Meydan, Agata L. Starosta, Otto Berninghausen, Roland Beckmann, Nora Vázquez-Laslop and Daniel N. Wilson.

Molecular Cell. 56, 446-452 (2014).

Ribosome stalling during translation of the *Staphylococcus aureus* ErmCL leader peptide is induced by the clinically important erythromycin and leads to expression of the downstream macrolide resistance methyltransferase ErmC. We modified the previously established *in vitro* disome system to prepare a homogeneous population of ErmCL-SRCs for subsequent analysis by cryo-EM. Using high-quality Cs-corrected cryo-EM images of the ErmCL-SRC derived from a direct electron detector, multiparticle reconstruction yielded a 3.9 Å resolution map of ErmCL-SRC. The high resolution (3.5 Å in the ribosomal core) enabled a detailed view on the conformation of the PTC and the mechanistic interplay between ErmCL, erythromycin and nucleotides of the tunnel wall. Unlike ErmBL, the ErmCL nascent chain appears to directly sense the presence of erythromycin via interaction between the backbones of invariant I6/F7 in ErmCL and the critical C3'-cladinose sugar of erythromycin. Overall, four major sites of interaction between ErmCL and the ribosome are observed, such as critical residues V8/F7 interacting with U2506, invariant I6 interacting with U2586 and presumably I3 interacting with the critical A2062, which is stabilized in a different conformation compared with the ErmBL-SRC. We showed by toe-printing that mutagenesis of U2586 partially rescued the stalling-deficiency of the ErmCL I6A mutant, which suggests a functional interplay between I6 and U2586. The interactions with U2586, U2506, A2062 and the C3'-cladinose sugar of erythromycin stabilize the nascent chain in a conformation, which precludes U2585 to adopt its canonical position and promotes U2585 to flip into a novel, previously unseen conformation. The flipped position of U2585 together with shifted P-site tRNA A76 and shifted nucleotide A2602 perturbs the conformation of the PTC, reducing its ability to stably bind and accommodate A-site tRNA, which culminates in translation arrest.

3.7 Publication 7 | Alternate Conformation of a Nascent Chain in the Ribosomal Tunnel Induces P-tRNA Perturbation and Inhibition of Peptide Bond Formation

Stefan Arenz, C. Axel Innis, Roland Beckmann and Daniel N. Wilson.

Unpublished manuscript (2015).

The previous cryo-EM reconstruction of the ErmBL-SRC (section 3.4) was resolved to 4.5-6.6 Å. At this resolution, neither density for amino acid side chains, nor separation of density for individual rRNA nucleotides can be observed, which profoundly restricts a detailed mechanistic understanding of molecular interactions between amino acid side chains of the nascent ErmBL peptide with individual nucleotides of the tunnel wall and the tunnel-bound macrolide. Based on this relatively low-resolution structure, we suggested that ErmBL stabilizes the PTC in an uninduced conformation, which prevents A-site tRNA accommodation and therefore peptide bond formation. In order to deepen our insight into the mechanism of ErmBL-stalling, we subjected the ErmBL-SRC to state-of-the-art cryo-EM and received high quality, Cs-corrected images acquired by a direct electron detection camera. Two maps of the ErmBL-SRC, in presence and absence of A-site tRNA, were reconstructed and resolved to 3.1-3.6 Å. At this resolution, most amino acid side chains are resolved, density for bases of rRNA is separated, and even the lysine amino acid attached to the A-site tRNA is visible. The drastically improved resolution of the ErmBL-SRC maps allowed us to build a molecular model for ErmBL-SRC and to provide detailed insight into the complex interplay between nascent chain, drug and the ribosome to inactivate the PTC. According to our previous observation, the path of ErmBL adopts the same unique conformation within the tunnel, which allows the nascent chain to bypass erythromycin without contacting it. The high resolution of the map enabled us to identify in total nine hydrogen bonds between the C-terminal residues R7, N8 and D10 of ErmBL with the ribosome exit tunnel, while the N-terminal three residues of ErmBL are flexible and disordered. Notably, the positively charged side chain of the critical ErmBL residue R7 is well resolved and is stabilized within a negatively charged rRNA pocket formed by 23S rRNA nucleotides A2063, A2441, A2439 and U2586. Strikingly, we observed that the side chain of D10, which is esterified to the P-

site tRNA, is rotated by 180 degrees compared with the corresponding side chain positions in all available crystal- and cryo-EM structures with aminoacylated P-site tRNAs, adopting an unexpected, novel and previously unseen conformation. We suggest that the rotation around the very C-terminal residue is a consequence of its context within the ErmBL nascent peptide and that it dictates the path ErmBL follows. Unlike what we proposed in our previous model, the A-site tRNA appears to be fully or near-fully accommodated. Instead, we observed that A76 of the P-site tRNA is shifted by 1-2 Å, which was also noticed at lower resolution. Remarkably, A2602 and the N-terminus of L27 are disordered in the ErmBL-SRC, which contrasts with the observations that both become ordered within a fully functional PTC ready to form a peptide bond. Therefore we propose that in the presence of erythromycin, ErmBL adopts an unusual, rotated conformation, which is stabilized by R7 interactions with the tunnel, to follow an alternate path through the tunnel, bypassing the drug. Contradicting our previous model, ErmBL does not perturb the A-site, but rather the P-site of the PTC (presumably by rotation of the C-terminal D10), which leads to an unfavorable conformation of the PTC being unable to catalyze peptide bond formation.

4 Discussion

4.1 Interaction of Protein S1 with the Escherichia coli Ribosome

The six-domain ribosomal protein S1 is able to unwind model RNA duplexes and secondary structures in the absence of ribosomes (Bear et al., 1976; Kolb et al., 1977; Qu et al., 2012; Rajkowitsch and Schroeder, 2007; Studer and Joseph, 2006; Thomas et al., 1978), as well as to unfold mRNA secondary structures on the ribosome (Duval et al., 2013). S1 is known to be intrinsically very flexible (Chu and Cantor, 1979; Moore and Laughrea, 1979), which made structural analysis of the full-length protein bound to the ribosome impossible. We provide evidence that the N-terminal segment of S1 folds partially into a α -helix upon binding to S2, which is crucial to anchor S1 on the ribosome. In contradiction to previous studies suggesting that D1 and D2 of S1 have no RNA-binding ability (Subramanian, 1983), we observe interaction of D1 with the 3'-end of ribosomal 16S rRNA and mRNA, possibly contributing to the stabilization of S1 on the ribosome. However, due to the low resolution of the cryo-EM map, a detailed account for the residues involved in these interactions remains elusive. Furthermore, we observe additional electron density extending from S1_{D1}, which would fit in dimension to the size of the second domain D2 of S1. Interestingly, this density is directly placed at the entrance of the mRNA channel and the fusion of density strongly suggests interactions between S1_{D2} with both 16S rRNA and the 5'-end of mRNA. The strong interactions between S1_{D1} and S1_{D2} with the ribosome confirm previous studies showing that D1 and D2 of S1 provide the boundary to the ribosome (Subramanian, 1983). Confirming our placement of D1 and D2, a recently published cryo-EM structure of a SecM-stalled ribosome showed density attributable to S1_{D1} and S1_{D2} in the same position compared to our structure (Park et al., 2013). However, a third density similar in size and shape connected to density for S1_{D2} is visible and might represent S1_{D3}, indicating that S1_{D3} could be more stabilized compared to D4-D6 of S1, which agrees with a more recent study showing that D1-D3 of S1 are needed to retain full 30S binding activity of S1 (Duval et al., 2013). The flexibility of D3-D6 of S1 (Boni et al., 1991; Subramanian, 1983) might allow S1 to recruit specific mRNAs to the ribosome at the initiation step. Beside the possibility

that S1 interacts with mRNAs on the ribosome, it was also shown that in some situations S1 interacts with mRNAs in the absence of ribosomes (Qu et al., 2012) and facilitates mRNA delivery to the ribosome (Duval et al., 2013).

According to our crystal structure, residue K43 of S1 interacts directly with D188 of S2, which contributes to the coordination of the Zn^{2+} ion residing in the Zn^{2+} binding pocket of S2. It is tempting to speculate that the S1-S2 interaction can be regulated by the presence or absence of Zn^{2+} . In this regard, the intracellular Zn^{2+} concentration might modulate ribosome specificity to translate leaderless mRNAs (lmRNAs) and thus change the entire translome. It seems likely that depending on the intracellular Zn^{2+} concentration, S1 containing and S1-deficient ribosomes are simultaneously present in the cell. This would contribute to ribosome heterogeneity, which may be important for bacteria to quickly and efficiently adapt to changing environmental conditions. For example during stress conditions in *E. coli*, the toxin MazF is activated and cleaves specific mRNAs at their 5'-end to generate lmRNAs (Vesper et al., 2011). Therefore it seems logical that bacteria down-regulate the association of S1 to the ribosome at increasing concentrations of lmRNAs to ensure their predominant translation. In fact, free S1 accumulates during stationary growth phase (Ramagopal, 1976). It seems likely that S1 binding to the ribosome can be regulated by posttranslational modifications. Accordingly, the acetylation pattern of some ribosomal proteins including S1 and S2 changes in stationary growth phase (Yu et al., 2008). Furthermore it was shown, that residues T2 and S44 of S1 are phosphorylated during growth in minimal medium in the late stationary phase (Soares et al., 2013), which potentially interferes with S1 binding to S2. Detailed biochemical analysis is required to elucidate whether modifications of the N-terminal segment of S1 indeed generates ribosome heterogeneity for fine-tuning protein synthesis. Generation of a high-resolution structure of the first domains of S1 bound to the ribosome, for example, by using direct electron detector-derived high-quality cryo-EM images, would certainly expand out current understanding of the molecular interactions of S1 with the 16S rRNA, mRNA as well as other ribosomal proteins besides S2. However, due to the flexibility of S1, higher resolution might be limited to D1 and possibly D2.

4.2 Proline-rich antimicrobial peptides

Our studies show that the proline-rich antimicrobial peptide Onc112 binds within the ribosome exit tunnel and sterically prevents accommodation of tRNAs into the A-site of the PTC and thereby inhibit translation. Additionally, we provide biochemical evidence that Onc112 inhibits translation at the step after 70S initiation complex formation. Toe-printing assays were used to monitor the position of the ribosome on the mRNA and showed that all ribosomes are positioned with the AUG start codon in the P-site, indicative for initiating ribosome unable to enter the elongation phase. We suggest that Onc112 binding to the ribosome destabilizes the 70S initiation complex by interfering with fMet-tRNA_f^{Met} binding to the ribosomal P-site, which might lead to P-site tRNA destabilization and subsequent dissociation from the ribosome. However, due to the high pH required for crystallization of ribosomes, the initiator tRNA gets hydrolyzed during crystallization, which prevents structural analysis of the interfering interplay between the formyl-methionine residue and Onc112. It seems possible that the binding position of Onc112 to ribosomes containing fMet-tRNA_f^{Met} in the P-site deviates from the binding position observed in our structure bearing deacylated tRNA_f^{Met} in the P-site. However, due to the instability of the complex, simultaneous presence of fMet-tRNA_f^{Met} and Onc112 appears rather unlikely, which makes structural analysis of the complex by other techniques, such as cryo-EM, challenging. We further suggest that positively charged residues within the full-length Onc112, particularly the C-terminus, are necessary for SbmA-mediated import across the inner membrane of Gram-negative pathogens. However it remains unclear by which mechanism Onc112 gets imported into the periplasmic space. Since diffusion of the polar Onc112 through the lipid-bilayer of the outer membrane should be impossible, certain outer membrane pores could facilitate Onc112 import, yet, genomic screens for resistance mutations exclusively identified SbmA as being critical for PrAMP import (Mattiuzzo et al., 2007). Crystal structures of other PrAMPs like drosocin, pyrrocoricin and apidaecin bound to the ribosome are necessary to investigate whether all ribosome-targeting PrAMPs share the same binding site within the ribosome exit tunnel, which seems likely due to their high sequence similarity. The 23S rRNA nucleotides comprising the PrAMP binding site are highly conserved, suggesting that eukaryotic ribosomes might be a target for Onc112

binding, as well. Yet, Onc112 exhibits a low toxicity to eukaryotic cells, possibly due to the absence of the transporter SbmA, responsible for uptake in bacteria. The binding site for Onc112 overlaps with the binding site for other 50S-targeting antibiotics, like chloramphenicol, pleuromutilins, lincosamides and macrolides, therefore resistance mutations for antibiotics like chloramphenicol or erythromycin could confer cross-resistance to PrAMPs. But due to the extended binding interface between Onc112 and several nucleotides of the 23S rRNA, it seems rather unlikely that single rRNA mutations could confer resistance to Onc112. Structural and biochemical analysis of critical residues in these PrAMPs would expand our understanding about the molecular mechanism of ribosome binding and cellular import, which might enable the development of second-generation PrAMPs, which could overcome cross-resistances and exhibit improved pharmacokinetic properties as well as reduced toxicity for application in clinical practice.

4.3 TetM-mediated Tetracycline Resistance

Our structure of TetM-bound RNCs revealed that P509 located at the tip of loop III in domain IV overlaps in position with ring D of tetracycline and thereby dislodges tetracycline from the ribosome to confer resistance. It would be interesting to supplement the complex with tetracycline in order to structurally investigate whether TetM and tetracycline can be bound simultaneously to the ribosome. However, biochemical evidence suggests that TetM removes tetracycline upon binding to the ribosome, since GTP-hydrolysis is not strictly required for drug-release (Burdett, 1996; Trieber et al., 1998). Due to the inability of TetM to confer resistance to third-generation tetracyclines like tigecycline (Bergeron et al., 1996; Chopra, 2002; Grossman et al., 2012; Jenner et al., 2013), the use of tigecycline seems much more likely to capture a state where TetM and the drug are simultaneously bound on the ribosome. Importantly, biochemical evidence that TetM fails to dislodge tigecycline from the ribosome is still lacking. Notably, in the previous reconstruction of the TetM•70S complex, the binding reaction was performed in the additional presence of tigecycline. Despite the low resolution of the map, it could be concluded that presence of TetM and tigecycline are mutually exclusive (Dönhöfer et al., 2012), possibly due to the ability of TetM to remove tigecycline from the ribosome. Since it is proposed that

TetM prevents rebinding of tetracycline by inducing conformational changes of nucleotides comprising the drug binding site (such as C1054) that persist after TetM dissociation (Connell et al., 2003a; Connell et al., 2003d; Connell et al., 2002; Dönhöfer et al., 2012), it might be also possible that these conformational changes selectively prevent rebinding of tetracycline. Tigecycline rebinding may however still be possible due to its higher affinity compared to tetracycline. Within the limits of the resolution of our map, TetM does not appear to induce conformational changes in C1054, but it is possible that such conformational rearrangements occur after GTP hydrolysis and upon TetM dissociation from the ribosome. It is also possible that by stabilizing A1492 and A1493 of the decoding center in the flipped-out conformation, TetM action promotes ternary complex binding similar to the action of the antibiotic paromomycin, before tetracycline rebinding occurs. Collectively, it remains unclear whether tigecycline overcomes TetM action by persisting on the ribosome, or by selectively rebinding to a deformed binding site. Mutagenesis studies of TetM might identify a mutant TetM, which also confers resistance to third-generation tetracyclines, such as tigecycline. At a resolution between 3.5-4.5 Å, many side chains of TetM residues are not visible, which only allowed us to build a backbone model for TetM. One open question that remains addresses the conformational state of the GTPase center of TetM. It seems highly likely that the conformation is very similar to EF-Tu and EF-G, however while TetM displays higher sequence similarity to EF-G, the conformational state on the ribosome resembles closer EF-Tu since ET-Fu also binds a non-ratcheted ribosome. Therefore, differences regarding the position of the catalytic histidine and its interaction with the GTP binding pocket might exist. Despite the observation that our structure exhibits density for the nucleotide GTP, the precise interactions within its binding site remain elusive due to the limiting resolution of the map.

4.4 Macrolide-dependent Ribosome Stalling

Our publications demonstrate that the amino acid sequence of a nascent peptide directly determines its conformation and the path it follows through the erythromycin-bound ribosome exit tunnel. Following a defined path is favored by intimate interactions between the nascent chain and either components of the exit tunnel or erythromycin or both. The placement of the nascent chain within the tunnel, together with its specific interactions generates a stalling signal, which is communicated to PTC to arrest translation by inhibition of peptide bond formation. Interestingly, our studies show that the stalling signal can be diverse and strongly depends on the amino acid sequence of the nascent chain. Remarkably, translation of both ErmBL and ErmCL leads to inhibition of peptide bond formation at the stall-site, but the mechanism of PTC inactivation differs fundamentally. While the ErmBL nascent chain generates a stalling signal that leads to perturbation of the P-site by shifting the A76 ribose of the P-site tRNA, the stalling signal generated by ErmCL is communicated to the A-site, where U2585 rotates by 180° and A2602 together with the P-site tRNA shifts in position, thereby globally deforming the A-site to prevent A-site tRNA accommodation and thereby peptide bond formation. Within the following sections, individual features of drug-stalled ribosomes, like the (i) path of the nascent chain, (ii) contacts within the ribosomal tunnel, (iii) drug-specificity, (iv) conformation of the PTC and (v) A-site specificity, are comparatively discussed.

Paths of nascent chains. The initial map of the ErmBL-SRC was resolved to 4.5 Å in the ribosomal core. At this resolution, the cryo-EM density of the ErmBL nascent polypeptide was fragmented and appears as a thin tube, without hints for the positions of amino acid side chains. Therefore, interactions could only be interpreted based on fusion of density indicating proximity between regions within the nascent chain and regions within the ribosomal tunnel. The absence of fusion of density between ErmBL and the C3'-cladinose sugar of erythromycin suggested that ErmBL does not contact the drug, however, it could not be excluded that a side chain of ErmBL is involved in interacting with erythromycin. In contrast, the recent high-resolution reconstruction of the ErmBL-SRC at 3.1 Å in the ribosomal core allowed a precise atomic model for ErmBL including side chains to be built. Remarkably, the

overall path based on the low-resolution map is nearly identical to the path at higher resolution, indicating that the rough placement of the ErmBL nascent chain in the low-resolution map was valid and reliable. According to the initial reconstruction, the high-resolution map does not indicate direct contact between ErmBL and erythromycin, but it should be noted, that the side chain for residue N8 is not visible in the recent structure. Most favored rotamers of N8 would sterically clash with the desosamine sugar of erythromycin possibly forcing N8 to adopt multiple other less defined states, explaining the absence of density. Most importantly, N8 does not play an important role in stalling since it can be mutated to A without affecting the stalling efficiency (Arenz et al., 2014b), thus making the absence of density for the side chain negligible. The high-resolution structure unambiguously shows that the side chain of D10 is rotated by 180° when compared with the side chain positions observed in all other available structures of ribosomes bearing an acylated P-site tRNA. It seems possible that the rotation around D10 directs the path of ErmBL away from the drug, but it is entirely unclear what causes the rotation and when it occurs during translation. The observation that the C-terminal Asp amino acid in the MifM-SRC adopts the canonical position (Sohmen et al., 2015) suggests that the rotation of D10 in ErmBL is initiated by the presence of erythromycin, which forces ErmBL into a specific conformation, culminating in the rotation of D10. If the rotation is caused by the interplay between drug and peptide, the question remains whether D10 is the first amino acid to rotate, or whether the preceding amino acids V9, N8, R7 were rotated, too? To speculatively answer this question, it seems more likely that D10 is the first amino acid to rotate and that this rotation directly leads to perturbation of the P-site A76 ribose and therefore to inactivation of the PTC. To address this question experimentally, translation of ErmBL could be artificially stopped at various steps preceding the stall-site and each complex could be subjected to cryo-EM to obtain a pseudo time-resolved structural view on translation of the ErmBL leader peptide.

Compared to ErmBL, the ErmCL nascent peptide was resolved to 3.5 Å and follows a fundamentally different path through the ribosomal exit tunnel, directly contacting the C3'-cladinose of erythromycin and overlapping with the canonical position of U2585. At this resolution, bulky side chains can be seen, for example, the

position of the critical F7 is unambiguous. In contrast, side chains of the critical surrounding hydrophobic amino acids I9, V8 and I6 are barely visible. Due to the lack of resolution, atomic details on the interaction between the ErmCL backbone and the C3'-cladinose of erythromycin remain elusive. It should be noted that the N-terminal 1-3 amino acids of both ErmBL and ErmCL appear to be disordered, however, biochemical evidence suggests that they play an important role in stalling, possibly a steric role, since N-terminal truncation mutants fail to induce stalling (Vazquez-Laslop et al., 2008). It remains unclear, how erythromycin contributes to the path of the nascent peptides, but presumably by narrowing down the diameter of the tunnel, the conformational space for the nascent chain to adopt a defined conformation is limited and thereby the nascent chain is forced into its specific intra-tunnel location. It would be interesting to visualize the conformation of the nascent chains in the absence of erythromycin, for example, by stalling the ribosome artificially at the same position during translation of the leader peptide. Artificial stalling could be achieved via different approaches: The mRNA could be truncated after the stall-site, but due to recycling mechanisms in lysate-based *in vitro* translation systems, this approach is limited to the use in the expensive PURE system. Furthermore, truncation of the mRNA would exclude the presence of A-site tRNA, which could contribute to the conformation adopted by the PTC. The more reasonable way to artificially stall ribosomes at a defined site is based on the lack of charged tRNAs decoding the A-site codon, either by deprivation of the A-site encoded amino acid from the system and/or by application of aminoacyl-tRNA synthetase inhibitors, which specifically prevent the A-site tRNA from being charged with the amino acid.

Contacts of the nascent chain. Contacts between the nascent chain and the ribosome and/or the macrolide stabilize the conformation and the path of nascent polypeptides within the ribosome exit tunnel. Based on the low-resolution reconstruction of the ErmBL-SRC, a number of contacts between ErmBL and the ribosome could be identified, at least within the limits of the resolution. Although the identity of the interacting residues remained ambiguous, we proposed interactions between D10/V9 of ErmBL with U2585, R7 with U2586 and an interaction between F4 and U2609. Strikingly, we confirmed these interactions in the high-resolution

reconstruction and were further able to more precisely map the atomic regions involved in these interactions. Based on our initial publication showing a functional interaction between U2586 and R7, we assumed that the side chain of R7 might interact directly with the base of U2586, probably via stacking interaction. In contrast, we observe that the positively charged side chain of R7 appears to interact with the sequence-independent ribose 2'-OH of U2586, which contributes to a negatively charged pocket stabilizing the side chain of R7. Yet, the backbone of R7 potentially hydrogen bonds with the nucleobase of U2586, which might be disrupted by conformational changes upon mutation of R7 to alanine. Therefore we assume that secondary mutations of U2586, which rescue the stalling deficiency of the ErmBL R7A mutant, establish new interactions with the ErmBL backbone and thus stabilize the nascent chain in a conformation that enables the stalling signal to be communicated to the PTC to arrest translation. A major difference between ErmBL and ErmCL is their dependency on the 23S rRNA nucleotides A2062 and A2503. While, ErmCL stalling is strongly reduced in presence of A2062U or A2503G mutations, stalling during translation of ErmBL remains unaffected (Ramu et al., 2009). Accordingly, our structures show that A2062 adopts a very different orientation in ErmCL-SRC compared to ErmBL-SRC, while the position of A2503 is unchanged in both structures. Direct interaction between ErmCL and A2062 is observed, while ErmBL does not interact with A2062, explaining why stalling on ErmBL is not affected by mutation of A2062. ErmCL stabilizes A2062 in a conformation enabling N7 of A2062 to interact with the exocyclic amino group A2503, suggesting that the N-terminus of ErmCL may play a steric role to induce the previously noted interaction between A2062 and A2503 (Vazquez-Laslop et al., 2010). However, within the limits of the resolution, we do not see conformational changes defining previously proposed relays from A2062/A2503 back up to the PTC (Vazquez-Laslop et al., 2010). Thereby, we suggest that A2062/A2503 affect the conformational state of the PTC via the ErmCL nascent chain.

Drug-specificity. Toe-printing experiments show that the C3'-cladinose sugar of erythromycin is crucial to arrest translation on ErmCL since the absence or even small alterations of the cladinose sugar, abolish stalling (Vazquez-Laslop et al., 2011).

In contrast, we show that ribosome stalling during translation of ErmBL is also inducible by ketolides like telithromycin, which lack the C3'-cladinose moiety. The differential drug-specificity of the two peptides is probably due to their differential behavior in sensing the tunnel-bound drug. While ErmCL directly interacts with the cladinose, ErmBL follows a path distant from the cladinose preventing direct interaction.

It would be interesting to investigate whether mutations introduced in the leader peptides are able to modulate their drug-specificity. It is tempting to speculate that mutagenesis of D10 in ErmBL to a bulky amino acid like tyrosine would prevent its unusual rotation due to steric hindrance of the bulky side chain with the ribosomal tunnel. Thereby, the path of the ErmBL nascent chain would be changed and directed closer to the cladinose, which might become crucial for stalling to occur. Furthermore, a structure of ErmBL-SRC in the presence of telithromycin instead of erythromycin would address questions whether ErmBL follows the same path through a ketolide-bound exit tunnel and whether the interaction pattern with the ribosome, or even the mechanism leading to translation arrest, is changed.

Conformation of the PTC. According to our initial model based on the low-resolution map of ErmBL-SRC, the nascent chain stabilizes the uninduced conformation of the PTC, which is incompatible with tRNA accommodation at the A-site. However, the improved resolution of the complex allowed us to more precisely assess the conformational state of the PTC and to revise our model for ErmBL-mediated translation arrest. Despite the high resolution, we cannot unambiguously state that the PTC adopts a fully induced conformation, however the positioning of the α -amino group of the aa-tRNA in the A-site seems to be sufficiently accommodated for nucleophilic attack onto the carbonyl carbon of the P-site ester. According to the recent crystal structure of the ribosome captured in the pre-peptide bond formation state, proton transfer from the attacking nucleophile to water molecule W1 (coordinated by A2602 and L27) via a proton wire formed by the 2'-OH of the P-site A76 ribose and the 2'-OH of A2451 is necessary for peptide bond formation to occur (Polikanov et al., 2014b). In the ErmBL-SRC we observe that the A76 ribose of the P-site tRNA is shifted away from the A-site, possibly breaking the

necessary proton wire network leading to inhibition of peptide bond formation. Since at the given resolution water molecules and protons are not visualized, interpretations regarding an interrupted proton wire remain speculative. However, A2602 and the N-terminus of L27 that coordinate W1 are delocalized in the ErmBL-SRC structure and therefore W1 cannot be coordinated, preventing initial deprotonation of the attacking nucleophile necessary for the catalysis of peptide bond formation. Furthermore, the presence of the aminoacylated tRNA in the A-site and a peptidyl-tRNA in the P-site is alone sufficient to indicate that peptide bond formation has not occurred. X-ray crystallographic structures of the ErmBL-SRC for example might provide resolution sufficient to visualize single water molecules, however due to the basic pH necessary to crystallize ribosomes, it was so far impossible to obtain X-ray structures of RNCs.

Contrasting the mechanism of drug-dependent stalling during translation of ErmBL, the cryo-EM structure of ErmCL-SRC reveals that drug-dependent ErmCL-SRC employ a completely unrelated mechanism of PTC silencing, namely via perturbation of the PTC active site. Thereby, the ErmCL nascent peptide overlaps in position with canonical positions of U2585, promoting an alternative, flipped conformation of U2585 which leads to the loss of a potentially A-site tRNA-stabilizing hydrogen bond between the C4 oxygen of U2585 and the 2'-OH of the A-site A76 ribose. Together with shifts of A2602 and the P-site A76, ErmCL remodels the PTC making it unfavorable for tRNAs to fully accommodate at the A-site of the PTC. The reduced ability of ErmCL-SRC to accommodate tRNAs at the A-site agrees well with the absence of density for A-site tRNA in the cryo-EM map as well as with single-molecule FRET studies showing that ErmCL-SRC less stably binds A-site tRNA (Johansson et al., 2014). This is in contrast to our ErmBL-SRC reconstructions, where stable binding of A-site tRNA was observed. Interestingly, the overall conformational state of the PTC observed in MifM-, TnaC-, ErmBL- and ErmCL-SRC is different for all four structures. The only similarity between ErmCL, TnaC and MifM is the position of A2602, which appears to narrow down the entry cleft for A-site tRNAs, and even prevents accommodation of release factors for MifM and TnaC. Notably, the flipped conformation of U2585 in ErmCL-SRC is not observed in any other ribosome structure solved to date. Therefore it seems likely that different stalling peptides

induce unrelated conformational changes within the PTC, all of which culminate in PTC inactivation.

A-site specificity. We show that mutation of the lysine codon in the A-site of ErmBL to alanine alleviates translation arrest, indicating that ErmBL-mediated ribosome stalling strongly depends on the nature of the amino acid attached to the A-site tRNA. In sharp contrast, the ErmCL-SRC exhibits a restrictive A-site, namely that irrespective of the amino acid attached to the A-site tRNA, the ribosome stalls during translation of ErmCL in the presence of erythromycin. Current knowledge about A-site specificity is based on studies on the ErmAL1 leader peptide (Ramu et al., 2011). Despite the similar hydrophobic C-terminal amino acid sequence of ErmAL1 (IAVV) compared to ErmCL (IFVI), ribosome stalling during translation of ErmAL1, unlike for ErmCL, strongly depends on the nature of the A-site-tRNA. Except for proline, which is known to be a poor peptide acceptor due to its imino-group (Pavlov et al., 2009), a rationale as to how the ribosome distinguishes amino acids to either stall or continue translation of Erm-leader peptides in presence of macrolides is currently unknown. It has been reported that the identity of the amino acid influences aminoacyl-tRNA binding to the ribosome (Fahlman and Uhlenbeck, 2004), however a structural basis about the specific placement of different amino acids in the A-site remains elusive. Remarkably toe-printing experiments using ErmAL1 (selective A-site), ErmCL (restrictive A-site) as well as chimeras of both demonstrated that swapping the amino acid in the -2 position between ErmAL1 (A) and ErmCL (F) renders the A-site of the ErmCL_F7A-SRC selective. This indicates that the -2 position in the nascent chain relative to its C-terminus represents a key element in modulating the A-site specificity. In this regard it is noteworthy to mention that the -2 position in the SecM leader peptide is also crucial for stalling (Yap and Bernstein, 2009), suggesting that drug-dependent ribosome stalling on ErmAL1/ErmCL might share similarities to drug-independent ribosome stalling during translation of SecM (Vazquez-Laslop et al., 2010). Yet, it is unknown, how the identity of a specific amino acid in the -2 position is communicated to the PTC. One explanation addressing this open question derives from our ErmCL-SRC reconstruction. The phenylalanine residue F7 in the -2 position of ErmCL is engaged in a strong stacking interaction with U2506 of the 23S

rRNA. This interaction might stabilize the ErmCL nascent chain in a position overlapping with canonical positions of U2585 and thereby trigger the perturbation of the active site. It is tempting to speculate that mutagenesis of F7 to alanine disrupts this interaction, and thereby presumably influences the path of ErmCL and therefore the extent of PTC perturbation, which possibly renders the A-site selective. Another option is that mutagenesis of F7 to alanine alters the conformation of ErmCL to such an extent, that it allows U2585 to adopt its usual conformation and thereby an entirely different stalling signal is generated and communicated to the PTC, resulting in a selective property of the A-site. Another idea as to how the amino acid in the -2 position affects the A-site specificity is related to the conformational state of U2506. U2506 appears to adopt a defined state upon A-site tRNA accommodation (Schmeing et al., 2005d), which is stabilized by stacking interaction with F7 in ErmCL. It seems possible that the absence of this interaction by the F7A mutation allows flexibility of U2506, which could sterically interfere with the amino acid attached to the A-site tRNA during accommodation and thus arrest translation in an amino acid specific manner. To structurally assess this issue, an ErmCL_F7A-SRC could be generated and analyzed by cryo-EM. It would be interesting to see whether the overall conformation of the nascent chain and/or U2506 is affected by the mutation.

In conclusion, we have demonstrated that ErmBL and ErmCL use two completely different mechanisms by which the ribosomal PTC gets inactivated. A lot more structures of other drug-stalled ribosomes, for example ErmDL- or ErmAL1-SRCs are necessary to understand whether similarities regarding the stalling signal exist, or whether every individual peptide in the tunnel interacts with the drug in an individual way to generate a defined and individual peptide-specific stalling signal that inactivates the PTC via many different ways. Overall, our studies demonstrate that the interplay between nascent polypeptide, the macrolide and nucleotides of the ribosomal tunnel, to generate a stalling signal, which is communicated to the PTC to inhibit peptide bond formation, is extremely complex and highly specific.

5 References

- Agirrezabala, X., Lei, J., Brunelle, J.L., Ortiz-Meoz, R.F., Green, R., and Frank, J. (2008). Visualization of the hybrid state of tRNA binding promoted by spontaneous ratcheting of the ribosome. *Mol Cell* 32, 190-197.
- Agrawal, R., Sharma, M., Kiel, M., Hirokawa, G., Booth, T., Spahn, C., Grassucci, R., Kaji, A., and Frank, J. (2004). Visualization of ribosome-recycling factor on the *Escherichia coli* 70S ribosome: Functional implications. *Proc. Natl Acad. Sci. USA* 101, 8900–8905.
- Allen, G., Zavialov, A., Gursky, R., Ehrenberg, M., and Frank, J. (2005). The cryo-EM structure of a translation initiation complex from *Escherichia coli*. *Cell* 121, 703-712.
- Amunts, A., Fiedorczuk, K., Truong, T.T., Chandler, J., Peter Greenberg, E., and Ramakrishnan, V. (2015). Bactobolin A binds to a site on the 70S ribosome distinct from previously seen antibiotics. *Journal of molecular biology* 427, 753-755.
- Andersson, S., and Kurland, C.G. (1987). Elongating ribosomes in vivo are refractory to erythromycin. *Biochimie* 69, 901-904.
- Andreu, D., and Rivas, L. (1998). Animal antimicrobial peptides: an overview. *Biopolymers* 47, 415-433.
- Anokhina, M.M., Barta, A., Nierhaus, K.H., Spiridonova, V.A., and Kopylov, A.M. (2004). Mapping of the second tetracycline binding site on the ribosomal small subunit of *E.coli*. *Nucleic Acids Res.* 32, 2594-2597.
- Antoun, A., Pavlov, M.Y., Lovmar, M., and Ehrenberg, M. (2006). How initiation factors tune the rate of initiation of protein synthesis in bacteria. *EMBO J.* 25, 2539-2550.
- Arenz, S., Meydan, S., Starosta, A.L., Berninghausen, O., Beckmann, R., Vazquez-Laslop, N., and Wilson, D.N. (2014a). Drug sensing by the ribosome induces translational arrest via active site perturbation. *Mol Cell* 56, 446-452.
- Arenz, S., Nguyen, F., Beckmann, R., and Wilson, D.N. (2015). Cryo-EM structure of the tetracycline resistance protein TetM in complex with a translating ribosome at 3.9-Å resolution. *Proceedings of the National Academy of Sciences of the United States of America* 112, 5401-5406.
- Arenz, S., Ramu, H., Gupta, P., Berninghausen, O., Beckmann, R., Vazquez-Laslop, N., Mankin, A.S., and Wilson, D.N. (2014b). Molecular basis for erythromycin-dependent ribosome stalling during translation of the ErmBL leader peptide. *Nat Commun* 5, 3501.
- Arenz, S., Innis, C. A., Beckmann, R., and Wilson, D. N. (2015). Aternate conformation of a nascent chain in the ribosomal tunnel induces P-tRNA perturbation and inhibition of peptide bond formation. Unpublished manuscript.

- Backus, E.J., Duggar, B.M., and Campbell, T.H. (1954). Variation in *Streptomyces aureofaciens*. *Annals of the New York Academy of Sciences* *60*, 86-101.
- Ban, N., Nissen, P., Hansen, J., Moore, P.B., and Steitz, T.A. (2000). The complete atomic structure of the large ribosomal subunit at 2.4 Å resolution. *Science* *289*, 905-920.
- Barat, C., Datta, P.P., Raj, V.S., Sharma, M.R., Kaji, H., Kaji, A., and Agrawal, R.K. (2007). Progression of the ribosome recycling factor through the ribosome dissociates the two ribosomal subunits. *Mol Cell* *27*, 250-261.
- Barden, T.C., Buckwalter, B.L., Testa, R.T., Petersen, P.J., and Lee, V.J. (1994). "Glycylcyclines". 3. 9-Aminodoxycyclinecarboxamides. *J Med Chem* *37*, 3205-3211.
- Bear, D.G., Ng, R., Van Derveer, D., Johnson, N.P., Thomas, G., Schleich, T., and Noller, H.F. (1976). Alteration of polynucleotide secondary structure by ribosomal protein S1. *Proceedings of the National Academy of Sciences of the United States of America* *73*, 1824-1828.
- Belousoff, M.J., Shapira, T., Bashan, A., Zimmerman, E., Rozenberg, H., Arakawa, K., Kinashi, H., and Yonath, A. (2011). Crystal structure of the synergistic antibiotic pair, lankamycin and lankacidin, in complex with the large ribosomal subunit. *Proceedings of the National Academy of Sciences of the United States of America* *108*, 2177-2182.
- Bergeron, J., Ammirati, M., Danley, D., James, L., Norcia, M., Retsema, J., Strick, C.A., Su, W.G., Sutcliffe, J., and Wondrack, L. (1996). Glycylcyclines bind to the high-affinity tetracycline ribosomal binding site and evade Tet(M)- and Tet(O)-mediated ribosomal protection. *Antimicrob Agents Chemother* *40*, 2226-2228.
- Bhushan, S., Hoffmann, T., Seidelt, B., Frauenfeld, J., Mielke, T., Berninghausen, O., Wilson, D.N., and Beckmann, R. (2011). SecM-stalled ribosomes adopt an altered geometry at the peptidyltransferase center. *PLoS Biol.* *19*, e1000581.
- Bieling, P., Beringer, M., Adio, S., and Rodnina, M.V. (2006). Peptide bond formation does not involve acid-base catalysis by ribosomal residues. *Nat Struct Mol Biol* *13*, 423-428.
- Bischoff, L., Berninghausen, O., and Beckmann, R. (2014). Molecular basis for the ribosome functioning as an L-tryptophan sensor. *Cell Rep* *9*, 469-475.
- Blanchard, S.C., Gonzalez, R.L., Kim, H.D., Chu, S., and Puglisi, J.D. (2004a). tRNA selection and kinetic proofreading in translation. *Nat. Struct. Mol. Biol.* *11*, 1008-1014.
- Blanchard, S.C., Kim, H.D., Gonzalez, R.L., Jr., Puglisi, J.D., and Chu, S. (2004c). tRNA dynamics on the ribosome during translation. *Proc. Natl. Acad. Sci. USA* *101*, 12893-12898.
- Boman, H.G. (1995). Peptide antibiotics and their role in innate immunity. *Annu Rev Immunol* *13*, 61-92.

- Bommakanti, A.S., Lindahl, L., and Zengel, J.M. (2008). Mutation from guanine to adenine in 25S rRNA at the position equivalent to *E. coli* A2058 does not confer erythromycin sensitivity in *Saccharomyces cerevisiae*. *RNA* *14*, 460-464.
- Boni, I.V., Isaeva, D.M., Musychenko, M.L., and Tzareva, N.V. (1991). Ribosome messenger recognition: mRNA target sites for ribosomal protein S1. *Nucleic acids research* *19*, 155-162.
- Boni, I.V., Zlatkin, I.V., and Budowsky, E.I. (1982). Ribosomal protein S1 associates with *Escherichia coli* ribosomal 30-S subunit by means of protein-protein interactions. *Eur J Biochem* *121*, 371-376.
- Brilot, A.F., Korostelev, A.A., Ermolenko, D.N., and Grigorieff, N. (2013). Structure of the ribosome with elongation factor G trapped in the pretranslocation state. *Proceedings of the National Academy of Sciences of the United States of America* *110*, 20994-20999.
- Brodersen, D.E., Clemons, W.M., Carter, A.P., Morgan-Warren, R.J., Wimberly, B.T., and Ramakrishnan, V. (2000). The structural basis for the action of the antibiotics tetracycline, pactamycin, and hygromycin B on the 30S ribosomal subunit. *Cell* *103*, 1143-1154.
- Bulkley, D., Brandi, L., Polikanov, Y.S., Fabbretti, A., O'Connor, M., Gualerzi, C.O., and Steitz, T.A. (2014). The antibiotics dityromycin and GE82832 bind protein S12 and block EF-G-catalyzed translocation. *Cell Rep* *6*, 357-365.
- Bulkley, D., Innis, C.A., Blaha, G., and Steitz, T.A. (2010). Revisiting the structures of several antibiotics bound to the bacterial ribosome. *Proceedings of the National Academy of Sciences of the United States of America* *107*, 17158-17163.
- Burdett, V. (1991). Purification and Characterization of Tet(M), a Protein That Renders Ribosomes Resistant to Tetracycline. *The Journal of biological chemistry* *266*, 2872-2877.
- Burdett, V. (1996). Tet(M)-promoted release of tetracycline from ribosomes is GTP dependent. *Journal of bacteriology* *178*, 3246-3251.
- Byrgazov, K., Grishkovskaya, I., Arenz, S., Coudeville, N., Temmel, H., Wilson, D.N., Djinic-Carugo, K., and Moll, I. (2015). Structural basis for the interaction of protein S1 with the *Escherichia coli* ribosome. *Nucleic acids research* *43*, 661-673.
- Byrgazov, K., Manoharadas, S., Kaberdina, A.C., Vesper, O., and Moll, I. (2012). Direct interaction of the N-terminal domain of ribosomal protein S1 with protein S2 in *Escherichia coli*. *PLoS one* *7*, e32702.
- Canu, A., Malbruny, B., Coquemont, M., Davies, T.A., Appelbaum, P.C., and Leclercq, R. (2002). Diversity of ribosomal mutations conferring resistance to macrolides, clindamycin, streptogramin, and telithromycin in *Streptococcus pneumoniae*. *Antimicrob. Agents Chemother.* *46*, 125-131.

- Carter, A.P., Clemons, W.M., Jr., Brodersen, D.E., Morgan-Warren, R.J., Hartsch, T., Wimberly, B.T., and Ramakrishnan, V. (2001). Crystal structure of an initiation factor bound to the 30S ribosomal subunit. *Science* 291, 498-501.
- Caskey, C.T., Tompkins, R., Scolnick, E., Caryk, T., and Nirenberg, M. (1968). Sequential translation of trinucleotide codons for the initiation and termination of protein synthesis. *Science* 162, 135-138.
- Casteels, P., Ampe, C., Jacobs, F., Vaeck, M., and Tempst, P. (1989). Apidaecins: antibacterial peptides from honeybees. *EMBO J* 8, 2387-2391.
- Cech, T. (2000). Structural biology. The ribosome is a ribozyme. *Science* 289, 878-879.
- Chen, C., Stevens, B., Kaur, J., Cabral, D., Liu, H., Wang, Y., Zhang, H., Rosenblum, G., Smilansky, Z., Goldman, Y.E., *et al.* (2011a). Single-molecule fluorescence measurements of ribosomal translocation dynamics. *Mol Cell* 42, 367-377.
- Chen, C., Stevens, B., Kaur, J., Smilansky, Z., Cooperman, B.S., and Goldman, Y.E. (2011b). Allosteric vs. spontaneous exit-site (E-site) tRNA dissociation early in protein synthesis. *Proceedings of the National Academy of Sciences of the United States of America* 108, 16980-16985.
- Chen, Y., Feng, S., Kumar, V., Ero, R., and Gao, Y.G. (2013). Structure of EF-G-ribosome complex in a pretranslocation state. *Nat Struct Mol Biol* 20, 1077-1084.
- Chiba, S., and Ito, K. (2012). Multisite Ribosomal Stalling: A Unique Mode of Regulatory Nascent Chain Action Revealed for MifM. *Mol. Cell*.
- Chiba, S., Kanamori, T., Ueda, T., Akiyama, Y., Pogliano, K., and Ito, K. (2011). Recruitment of a species-specific translational arrest module to monitor different cellular processes. *Proc. Natl Acad. Sci. USA* 108, 6073-6078.
- Chiba, S., Lamsa, A., and Pogliano, K. (2009). A ribosome-nascent chain sensor of membrane protein biogenesis in *Bacillus subtilis*. *EMBO J.* 28, 3461-3475.
- Chittum, H.S., and Champney, W.S. (1994). Ribosomal protein gene sequence changes in erythromycin-resistant mutants of *Escherichia coli*. *J. Bacteriol.* 176, 6192-6198.
- Chopra, I. (2002). New developments in tetracycline antibiotics: glycylicyclines and tetracycline efflux pump inhibitors. *Drug. Resist. Updates* 5, 119-125.
- Chu, Y.G., and Cantor, C.R. (1979). Segmental flexibility in *Escherichia coli* ribosomal protein S1 as studied by fluorescence polarization. *Nucleic acids research* 6, 2363-2379.
- Clatworthy, A.E., Pierson, E., and Hung, D.T. (2007). Targeting virulence: a new paradigm for antimicrobial therapy. *Nat Chem Biol* 3, 541-548.

- Connell, S.R., Tracz, D.M., Nierhaus, K.H., and Taylor, D.E. (2003a). Ribosomal protection proteins and their mechanism of tetracycline resistance. *Antimicrob. Agents Chemother.* *47*, 3675-3681.
- Connell, S.R., Trieber, C.A., Dinos, G.P., Einfeldt, E., Taylor, D.E., and Nierhaus, K.H. (2003d). Mechanism of Tet(O)-mediated tetracycline resistance. *EMBO J.* *22*, 945-953.
- Connell, S.R., Trieber, C.A., Stelzl, U., Einfeldt, E., Taylor, D.E., and Nierhaus, K.H. (2002). The tetracycline resistance protein Tet(O) perturbs the conformation of the ribosomal decoding centre. *Mol. Microbiol.* *45*, 1463-1472.
- Conover, L.H., Moreland, W.T., English, A.R., Stephens, C.R., and Pilgrim, F.J. (1953). Terramycin. Xi. Tetracycline. *Journal of the American Chemical Society* *75*, 4622-4623.
- Contreras, A., and Vazquez, D. (1977). Cooperative and antagonistic interactions of peptidyl-tRNA and antibiotics with bacterial ribosomes. *Eur. J. Biochem.* *74*, 539-547.
- Crick, F. (1970). Central dogma of molecular biology. *Nature* *227*, 561-563.
- Crick, F.H., Barnett, L., Brenner, S., and Watts-Tobin, R.J. (1961). General nature of the genetic code for proteins. *Nature* *192*, 1227-1232.
- Crick, F.H.C. (1966). Codon-anticodon pairing: The wobble hypothesis. *J. Mol. Biol.* *19*, 548-555.
- Cruz-Vera, L., Rajagopal, S., Squires, C., and Yanofsky, C. (2005). Features of ribosome-peptidyl-tRNA interactions essential for tryptophan induction of tna operon expression. *Mol. Cell* *19*, 333-343.
- Cruz-Vera, L.R., Gong, M., and Yanofsky, C. (2006). Changes produced by bound tryptophan in the ribosome peptidyl transferase center in response to TnaC, a nascent leader peptide. *Proceedings of the National Academy of Sciences of the United States of America* *103*, 3598-3603.
- Cruz-Vera, L.R., New, A., Squires, C., and Yanofsky, C. (2007). Ribosomal features essential for tna operon induction: tryptophan binding at the peptidyl transferase center. *J. Bacteriol.* *189*, 3140-3146.
- Cruz-Vera, L.R., and Yanofsky, C. (2008). Conserved residues Asp16 and Pro24 of TnaC-tRNA^{Pro} participate in tryptophan induction of Tna operon expression. *J. Bacteriol.* *190*, 4791-4797.
- Dailidienė, D., Bertoli, M.T., Miciuleviciene, J., Mukhopadhyay, A.K., Dailidė, G., Pascasio, M.A., Kupcinskis, L., and Berg, D.E. (2002). Emergence of tetracycline resistance in *Helicobacter pylori*: multiple mutational changes in 16S ribosomal DNA and other genetic loci. *Antimicrob Agents Chemother* *46*, 3940-3946.
- Dallas, A., and Noller, H.F. (2001). Interaction of translation initiation factor 3 with the 30S ribosomal subunit. *Mol. Cell* *8*, 855-864.

- Dam, M., Douthwaite, S., Tenson, T., and Mankin, A.S. (1996). Mutations in domain II of 23 S rRNA facilitate translation of a 23 S rRNA-encoded pentapeptide conferring erythromycin resistance. *Journal of molecular biology* *259*, 1-6.
- Dantley, K., Dannelly, H., and Burdett, V. (1998). Binding interaction between Tet(M) and the ribosome: Requirements for binding. *J. Bacteriol.* *180*, 4089-4092.
- Davis, A.R., Gohara, D.W., and Yap, M.N. (2014). Sequence selectivity of macrolide-induced translational attenuation. *Proceedings of the National Academy of Sciences of the United States of America* *111*, 15379-15384.
- Demeshkina, N., Jenner, L., Westhof, E., Yusupov, M., and Yusupova, G. (2012). A new understanding of the decoding principle on the ribosome. *Nature* *484*, 256-259.
- Demeshkina, N., Jenner, L., Yusupova, G., and Yusupov, M. (2010). Interactions of the ribosome with mRNA and tRNA. *Curr Opin Struct Biol.*
- Diaconu, M., Kothe, U., Schlunzen, F., Fischer, N., Harms, J.M., Tonevitsky, A.G., Stark, H., Rodnina, M.V., and Wahl, M.C. (2005). Structural basis for the function of the ribosomal L7/12 stalk in factor binding and GTPase activation. *Cell* *121*, 991-1004.
- Dincbas-Renqvist, V., Engstrom, A., Mora, L., Heurgue-Hamard, V., Buckingham, R., and Ehrenberg, M. (2000). A post-translational modification in the GGQ motif of RF2 from *Escherichia coli* stimulates termination of translation. *EMBO J.* *19*, 6900-6907.
- Doerfel, L.K., Wohlgemuth, I., Kothe, C., Peske, F., Urlaub, H., and Rodnina, M.V. (2013). EF-P is essential for rapid synthesis of proteins containing consecutive proline residues. *Science* *339*, 85-88.
- Dönhöfer, A., Franckenberg, S., Wickles, S., Berninghausen, O., Beckmann, R., and Wilson, D.N. (2012). Structural basis for TetM-mediated tetracycline resistance. *Proc. Natl. Acad. Sci. USA* *109*, 16900-16905.
- Dorner, S., Brunelle, J.L., Sharma, D., and Green, R. (2006). The hybrid state of tRNA binding is an authentic translation elongation intermediate. *Nat Struct Mol Biol* *13*, 234-241.
- Dorner, S., Panuschka, C., Schmid, W., and Barta, A. (2003). Mononucleotide derivatives as ribosomal P-site substrates reveal an important contribution of the 2'-OH to activity. *Nucleic acids research* *31*, 6536-6542.
- Douthwaite, S., Crain, P., Liu, M., and Poehlsgaard, J. (2004). The tylosin-resistance methyltransferase RlmA(II) (TlrB) modifies the N-1 position of 23S rRNA nucleotide G748. *J. Mol. Biol.* *337*, 1073-1077.
- Douthwaite, S., Garrett, R.A., and Wagner, R. (1983). Comparison of E coli tRNA^{Phe} in the free state, in the ternary complex and in the ribosomal A and P sites by chemical probing. *Eur. J. Biochem.* *131*, 261-269.

- Douthwaite, S., Powers, T., Lee, J.Y., and Noller, H.F. (1989). Defining the structural requirements for a helix in 23S ribosomal RNA that confers erythromycin resistance. *J. Mol. Biol.* *209*, 655-665.
- Douthwaite, S., Prince, J.B., and Noller, H.F. (1985). Evidence for functional interaction between domains II and V of 23 S ribosomal RNA from an erythromycin-resistant mutant. *Proc. Natl. Acad. Sci. U. S. A.* *82*, 8330-8334.
- Draper, M.P., Weir, S., Macone, A., Donatelli, J., Trieber, C.A., Tanaka, S.K., and Levy, S.B. (2013). The Mechanism of Action of the Novel Aminomethylcycline Antibiotic Omadacycline. *Antimicrob Agents Chemother.*
- Duggar, B.M. (1948). Aureomycin; a product of the continuing search for new antibiotics. *Annals of the New York Academy of Sciences* *51*, 177-181.
- Dunkle, J.A., Wang, L., Feldman, M.B., Pulk, A., Chen, V.B., Kapral, G.J., Noeske, J., Richardson, J.S., Blanchard, S.C., and Cate, J.H. (2011). Structures of the bacterial ribosome in classical and hybrid states of tRNA binding. *Science* *332*, 981-984.
- Dunkle, J.A., Xiong, L., Mankin, A.S., and Cate, J.H. (2010). Structures of the *Escherichia coli* ribosome with antibiotics bound near the peptidyl transferase center explain spectra of drug action. *Proceedings of the National Academy of Sciences of the United States of America* *107*, 17152-17157.
- Duval, M., Korepanov, A., Fuchsbaue, O., Fechter, P., Haller, A., Fabbretti, A., Choulier, L., Micura, R., Klaholz, B.P., Romby, P., *et al.* (2013). *Escherichia coli* ribosomal protein S1 unfolds structured mRNAs onto the ribosome for active translation initiation. *PLoS biology* *11*, e1001731.
- Ermolenko, D.N., Majumdar, Z.K., Hickerson, R.P., Spiegel, P.C., Clegg, R.M., and Noller, H.F. (2007). Observation of intersubunit movement of the ribosome in solution using FRET. *Journal of molecular biology* *370*, 530-540.
- Ermolenko, D.N., and Noller, H.F. (2011). mRNA translocation occurs during the second step of ribosomal intersubunit rotation. *Nat Struct Mol Biol* *18*, 457-462.
- Fahlman, R.P., and Uhlenbeck, O.C. (2004). Contribution of the esterified amino acid to the binding of aminoacylated tRNAs to the ribosomal P- and A-sites. *Biochemistry* *43*, 7575-7583.
- Farrell, D.J., Douthwaite, S., Morrissey, I., Bakker, S., Poehlsgaard, J., Jakobsen, L., and Felmingham, D. (2003). Macrolide resistance by ribosomal mutation in clinical isolates of *Streptococcus pneumoniae* from the PROTEKT 1999-2000 study. *Antimicrob Agents Chemother* *47*, 1777-1783.
- Finlay, A.C., Hobby, G.L., and *et al.* (1950). Terramycin, a new antibiotic. *Science* *111*, 85.
- Fischbach, M.A., and Walsh, C.T. (2009). Antibiotics for emerging pathogens. *Science* *325*, 1089-1093.

- Fischer, N., Neumann, P., Konevega, A.L., Bock, L.V., Ficner, R., Rodnina, M.V., and Stark, H. (2015). Structure of the *E. coli* ribosome-EF-Tu complex at <3 Å resolution by C-corrected cryo-EM. *Nature*.
- Fleming, A. (1929). On the antibacterial action of cultures of a penicillium, with special reference to their use in the isolation of *B. influenzae*. 1929. *Bulletin of the World Health Organization* 79, 780-790.
- Franceschi, F., Kanyo, Z., Sherer, E., and Sutcliffe, J. (2004). Macrolide resistance from the ribosome perspective. *Curr. Drug Targets Infect. Disord.* 4, 177-191.
- Frank, J., and Agrawal, R.K. (2000). A ratchet-like inter-subunit reorganization of the ribosome during translocation. *Nature* 406, 318-322.
- Frank, J., Jr., and Gonzalez, R.L. (2010). Structure and dynamics of a processive Brownian motor: the translating ribosome. *Annu Rev Biochem* 79, 381-412.
- Freistroffer, D.V., Pavlov, M.Y., MacDougall, J., Buckingham, R.H., and Ehrenberg, M. (1997). Release factor RF3 in *E. coli* accelerates the dissociation of release factors RF1 and RF2 from the ribosome in a GTP-dependent manner. *EMBO J.* 16, 4126-4133.
- Frolova, L., Tsivkovskii, R., Sivolobova, G., Oparina, N., Serpinski, O., Blinov, V., Tatkov, S., and Kisselev, L. (1999). Mutations in the highly conserved GGQ motif of class 1 polypeptide release factors abolish the ability of human eRF1 to trigger peptidyl-tRNA hydrolysis. *RNA* 5, 1014-1020.
- Fulle, S., and Gohlke, H. (2009). Statics of the ribosomal exit tunnel: implications for cotranslational peptide folding, elongation regulation, and antibiotics binding. *Journal of molecular biology* 387, 502-517.
- Gao, H., Zhou, Z., Rawat, U., Huang, C., Bouakaz, L., Wang, C., Cheng, Z., Liu, Y., Zavialov, A., Gursky, R., *et al.* (2007). RF3 induces ribosomal conformational changes responsible for dissociation of class I release factors. *Cell* 129, 929-941.
- Gao, Y.G., Selmer, M., Dunham, C.M., Weixlbaumer, A., Kelley, A.C., and Ramakrishnan, V. (2009). The structure of the ribosome with elongation factor G trapped in the posttranslocational state. *Science* 326, 694-699.
- Gavrilova, L.P., Kostiashekina, O.E., Koteliansky, V.E., Rutkevitch, N.M., and Spirin, A.S. (1976). Factor-free(non-enzymic and factor-dependent systems of translation of polyU by *E coli* ribosomes. *J. Mol. Biol.* 101, 537-552.
- Gaynor, M., and Mankin, A. (2003). Macrolide antibiotics: binding site, mechanism of action, resistance. *Curr. Top. Med.Chem.* 3, 949-961.
- Goldman, D.H., Kaiser, C.M., Milin, A., Righini, M., Tinoco, I., Jr., and Bustamante, C. (2015). Ribosome. Mechanical force releases nascent chain-mediated ribosome arrest in vitro and in vivo. *Science* 348, 457-460.

- Gong, F., and Yanofsky, C. (2002). Instruction of translating ribosome by nascent peptide. *Science* 297, 1864-1867.
- Gregory, S.T., and Dahlberg, A.E. (1999). Erythromycin resistance mutations in ribosomal proteins L22 und L4 perturb the higher order structure of 23S ribosomal RNA. *J. Mol. Biol.* 289, 827-834.
- Grentzmann, G., Kelly, P.J., Laalami, S., Shuda, M., Firpo, M.A., Cenatiempo, Y., and Kaji, A. (1998). Release factor RF-3 GTPase activity acts in disassembly of the ribosome termination complex. *RNA* 4, 973-983.
- Gromadski, K.B., and Rodnina, M.V. (2004). Kinetic determinants of high-fidelity tRNA discrimination on the ribosome. *Mol Cell* 13, 191-200.
- Grossman, T.H., Starosta, A.L., Fyfe, C., O'Brien, W., Rothstein, D.M., Mikolajka, A., Wilson, D.N., and Sutcliffe, J.A. (2012). Target- and resistance-based mechanistic studies with TP-434, a novel fluorocycline antibiotic. *Antimicrob Agents Chemother* 56, 2559-2564.
- Grunberg-Manago, M., Dessen, P., Pantaloni, D., Godefroy-Colburn, T., Wolfe, A.D., and Dondon, J. (1975). Light-scattering studies showing the effect of initiation factors on the reversible dissociation of *Escherichia coli* ribosomes. *J. Mol. Biol.* 94, 461-478.
- Gualerzi, C.O., and Pon, C.L. (1990). Initiation of messenger-RNA translation in prokaryotes. *Biochemistry* 29, 5881-5889.
- Guenneugues, M., Caserta, E., Brandi, L., Spurio, R., Meunier, S., Pon, C.L., Boelens, R., and Gualerzi, C.O. (2000). Mapping the fMet-tRNA^{fMet} binding site of initiation factor IF2. *EMBO J* 19, 5233-5240.
- Guillaume, G., Ledent, V., Moens, W., and Collard, J.M. (2004). Phylogeny of efflux-mediated tetracycline resistance genes and related proteins revisited. *Microb Drug Resist* 10, 11-26.
- Guillon, J.M., Meinnel, T., Mechulam, Y., Lazennec, C., Blanquet, S., and Fayat, G. (1992). Nucleotides of transfer RNA Governing the Specificity of Escherichia-Coli Methionyl-transfer RNA(Met)f Formyltransferase. *Journal of molecular biology* 224, 359-367.
- Gumbart, J., Schreiner, E., Wilson, D.N., Beckmann, R., and Schulten, K. (2012). Mechanisms of SecM-mediated stalling in the ribosome. *Biophysical journal* 103, 331-341.
- Gupta, P., Kannan, K., Mankin, A.S., and Vazquez-Laslop, N. (2013a). Regulation of gene expression by macrolide-induced ribosomal frameshifting. *Mol Cell* 52, 629-642.
- Gupta, P., Sothiselvam, S., Vazquez-Laslop, N., and Mankin, A.S. (2013b). Deregulation of translation due to post-transcriptional modification of rRNA explains why erm genes are inducible. *Nat. Commun.* 4, 1984.

- Hansen, A., Schafer, I., Knappe, D., Seibel, P., and Hoffmann, R. (2012). Intracellular toxicity of proline-rich antimicrobial peptides shuttled into mammalian cells by the cell-penetrating peptide penetratin. *Antimicrob Agents Chemother* 56, 5194-5201.
- Hansen, J.L., Ippolito, J.A., Ban, N., Nissen, P., Moore, P.B., and Steitz, T.A. (2002a). The structures of four macrolide antibiotics bound to the large ribosomal subunit. *Mol. Cell* 10, 117-128.
- Hansen, J.L., Schmeing, T.M., Klein, D.J., Ippolito, J.A., Ban, N., Nissen, P., Freeborn, B., Moore, P.B., and Steitz, T.A. (2001). Progress toward an understanding of the structure and enzymatic mechanism of the large ribosomal subunit. *Cold Spring Harb Symp Quant Biol* 66, 33-42.
- Hansen, J.L., Schmeing, T.M., Moore, P.B., and Steitz, T.A. (2002c). Structural insights into peptide bond formation. *Proc. Natl. Acad. Sci. USA* 99, 11670-11675.
- Harms, J., Schlutzen, F., Zarivach, R., Bashan, A., Gat, S., Agmon, I., Bartels, H., Franceschi, F., and Yonath, A. (2001). High resolution structure of the large ribosomal subunit from a mesophilic eubacterium. *Cell* 107, 679-688.
- Hartz, D., Binkley, J., Hollingsworth, T., and Gold, L. (1990). Domains of initiator transfer RNA and initiation codon crucial for initiator transfer RNA selection by *Escherichia coli* IF3. *Gene Dev.* 4, 1790-1800.
- Hartz, D., McPheeters, D.S., and Gold, L. (1989). Selection of the initiator tRNA by *Escherichia coli* initiation factors. *Genes Dev.* 3, 1899-1912.
- Hede, K. (2014). Antibiotic resistance: An infectious arms race. *Nature* 509, S2-3.
- Hiller, D.A., Singh, V., Zhong, M., and Strobel, S.A. (2011). A two-step chemical mechanism for ribosome-catalysed peptide bond formation. *Nature* 476, 236-239.
- Hirashima, A., and Kaji, A. (1973). Role of elongation factor G and a protein factor on the release of ribosomes from messenger ribonucleic acid. *J. Biol. Chem.* 248, 7580-7587.
- Horinouchi, S., and Weisblum, B. (1980). Posttranscriptional modification of mRNA conformation: mechanism that regulates erythromycin-induced resistance. *Proceedings of the National Academy of Sciences of the United States of America* 77, 7079-7083.
- Iordanescu, S. (1976). Three distinct plasmids originating in the same *Staphylococcus aureus* strain. *Arch Roum Pathol Exp Microbiol* 35, 111-118.
- Ito, K., and Chiba, S. (2013). Arrest peptides: cis-acting modulators of translation. *Annu. Rev. Biochem.* 82, 171-202.
- Ito, K., Fujiwara, T., Toyoda, T., and Nakamura, Y. (2002). Elongation factor G participates in ribosome disassembly by interacting with ribosome recycling factor at their tRNA-mimicry domains. *Mol. Cell* 9, 1263-1272.

- Ito, K., Uno, M., and Nakamura, Y. (2000). A tripeptide 'anticodon' deciphers stop codons in messenger RNA. *Nature* *403*, 680-684.
- Jenner, L., Demeshkina, N., Yusupova, G., and Yusupov, M. (2010a). Structural rearrangements of the ribosome at the tRNA proofreading step. *Nat Struct Mol Biol* *17*, 1072-1078.
- Jenner, L., Starosta, A.L., Terry, D.S., Mikolajka, A., Filonava, L., Yusupov, M., Blanchard, S.C., Wilson, D.N., and Yusupova, G. (2013). Structural basis for potent inhibitory activity of the antibiotic tigecycline during protein synthesis. *Proceedings of the National Academy of Sciences of the United States of America* *110*, 3812-3816.
- Jenner, L.B., Demeshkina, N., Yusupova, G., and Yusupov, M. (2010b). Structural aspects of messenger RNA reading frame maintenance by the ribosome. *Nat Struct Mol Biol* *17*, 555-560.
- Jin, H., Kelley, A.C., Loakes, D., and Ramakrishnan, V. (2010). Structure of the 70S ribosome bound to release factor 2 and a substrate analog provides insights into catalysis of peptide release. *Proceedings of the National Academy of Sciences of the United States of America* *107*, 8593-8598.
- Jin, H., Kelley, A.C., and Ramakrishnan, V. (2011). Crystal structure of the hybrid state of ribosome in complex with the guanosine triphosphatase release factor 3. *Proceedings of the National Academy of Sciences of the United States of America* *108*, 15798-15803.
- Johansson, M., Chen, J., Tsai, A., Kornberg, G., and Puglisi, J.D. (2014). Sequence-Dependent Elongation Dynamics on Macrolide-Bound Ribosomes. *Cell Rep*.
- Julian, P., Konevega, A.L., Scheres, S.H., Lazaro, M., Gil, D., Wintermeyer, W., Rodnina, M.V., and Valle, M. (2008). Structure of ratcheted ribosomes with tRNAs in hybrid states. *Proceedings of the National Academy of Sciences of the United States of America* *105*, 16924-16927.
- Julian, P., Milon, P., Agirrezabala, X., Lasso, G., Gil, D., Rodnina, M.V., and Valle, M. (2011). The Cryo-EM structure of a complete 30S translation initiation complex from *Escherichia coli*. *PLoS biology* *9*, e1001095.
- Kaminishi, T., Wilson, D.N., Takemoto, C., Harms, J.M., Kawazoe, M., Schluenzen, F., Hanawa-Suetsugu, K., Shirouzu, M., Fucini, P., and Yokoyama, S. (2007). A snapshot of the 30S ribosomal subunit capturing mRNA via the Shine-Dalgarno interaction. *Structure* *15*, 289-297.
- Kannan, K., Kanabar, P., Schryer, D., Florin, T., Oh, E., Bahroos, N., Tenson, T., Weissman, J.S., and Mankin, A.S. (2014). The general mode of translation inhibition by macrolide antibiotics. *Proceedings of the National Academy of Sciences of the United States of America* *111*, 15958-15963.

- Kannan, K., and Mankin, A.S. (2012). Macrolide antibiotics in the ribosome exit tunnel: species-specific binding and action. *Annals of the New York Academy of Sciences* 1241, 33-47.
- Kannan, K., Vazquez-Laslop, N., and Mankin, A.S. (2012). Selective protein synthesis by ribosomes with a drug-obstructed exit tunnel. *Cell* 151, 508-520.
- Kapralou, S., Fabbretti, A., Garulli, C., Spurio, R., Gualerzi, C.O., Dahlberg, A.E., and Pon, C.L. (2008). Translation initiation factor IF1 of *Bacillus stearothermophilus* and *Thermus thermophilus* substitute for *Escherichia coli* IF1 in vivo and in vitro without a direct IF1-IF2 interaction. *Molecular microbiology* 70, 1368-1377.
- Karimi, R., Pavlov, M., Buckingham, R., and Ehrenberg, M. (1999). Novel roles for classical factors at the interface between translation termination and initiation. *Mol. Cell* 3, 601-609.
- Katz, L., and Ashley, G.W. (2005). Translation and protein synthesis: macrolides. *Chem Rev* 105, 499-528.
- Kim, D., and Green, R. (1999). Base-pairing between 23S rRNA and tRNA in the ribosomal A site. *Mol Cell* 4, 859-864.
- Kingery, D.A., Pfund, E., Voorhees, R.M., Okuda, K., Wohlgemuth, I., Kitchen, D.E., Rodnina, M.V., and Strobel, S.A. (2008). An uncharged amine in the transition state of the ribosomal peptidyl transfer reaction. *Chemistry & biology* 15, 493-500.
- Klaholz, B., Myasnikov, A., and Van Heel, M. (2004). Visualization of release factor 3 on the ribosome during termination of protein synthesis. *Nature* 427, 862-865.
- Klaholz, B.P. (2011). Molecular recognition and catalysis in translation termination complexes. *Trends Biochem Sci* 36, 282-292.
- Klaholz, B.P., Pape, T., Zavialov, A.V., Myasnikov, A.G., Orlova, E.V., Vestergaard, B., Ehrenberg, M., and Van Heel, M. (2003). Structure of the *Escherichia coli* ribosomal termination complex with release factor 2. *Nature* 421, 90-94.
- Koch, M., Huang, Y., and Sprinzl, M. (2008). Peptide-bond synthesis on the ribosome: no free vicinal hydroxy group required on the terminal ribose residue of peptidyl-tRNA. *Angew Chem Int Ed Engl* 47, 7242-7245.
- Kohanski, M.A., Dwyer, D.J., and Collins, J.J. (2010). How antibiotics kill bacteria: from targets to networks. *Nat Rev Microbiol* 8, 423-435.
- Kolb, A., Hermoso, J.M., Thomas, J.O., and Szer, W. (1977). Nucleic acid helix-unwinding properties of ribosomal protein S1 and the role of S1 in mRNA binding to ribosomes. *Proc. Natl. Acad. Sci. USA* 74, 2379-2383.
- Konevega, A.L., Fischer, N., Semenov, Y.P., Stark, H., Wintermeyer, W., and Rodnina, M.V. (2007). Spontaneous reverse movement of mRNA-bound tRNA through the ribosome. *Nat Struct Mol Biol* 14, 318-324.

- Korostelev, A., Asahara, H., Lancaster, L., Laurberg, M., Hirschi, A., Zhu, J., Trakhanov, S., Scott, W.G., and Noller, H.F. (2008). Crystal structure of a translation termination complex formed with release factor RF2. *Proceedings of the National Academy of Sciences of the United States of America* *105*, 19684-19689.
- Korostelev, A., Zhu, J., Asahara, H., and Noller, H.F. (2010). Recognition of the amber UAG stop codon by release factor RF1. *EMBO J* *29*, 2577-2585.
- Korostelev, A.A. (2011). Structural aspects of translation termination on the ribosome. *RNA* *17*, 1409-1421.
- Krizsan, A., Volke, D., Weinert, S., Strater, N., Knappe, D., and Hoffmann, R. (2014). Insect-derived proline-rich antimicrobial peptides kill bacteria by inhibiting bacterial protein translation at the 70S ribosome. *Angew Chem Int Ed Engl* *53*, 12236-12239.
- Kuhlenkoetter, S., Wintermeyer, W., and Rodnina, M.V. (2011). Different substrate-dependent transition states in the active site of the ribosome. *Nature* *476*, 351-354.
- Lancaster, L., Kiel, M.C., Kaji, A., and Noller, H.F. (2002). Orientation of ribosome recycling factor from directed hydroxyl radical probing. *Cell* *111*, 129-140.
- Lauber, M.A., Rappsilber, J., and Reilly, J.P. (2012). Dynamics of ribosomal protein S1 on a bacterial ribosome with cross-linking and mass spectrometry. *Mol Cell Proteomics* *11*, 1965-1976.
- Laurberg, M., Asahara, H., Korostelev, A., Zhu, J., Trakhanov, S., and Noller, H.F. (2008). Structural basis for translation termination on the 70S ribosome. *Nature* *454*, 852-857.
- Laursen, B.S., Sorensen, H.P., Mortensen, K.K., and Sperling-Petersen, H.U. (2005). Initiation of protein synthesis in bacteria. *Microbiol. Mol. Biol. Rev.* *69*, 101-123.
- Lawrence, M.G., Lindahl, L., and Zengel, J.M. (2008). Effects on translation pausing of alterations in protein and RNA components of the ribosome exit tunnel. *J. Bacteriol.* *190*, 5862-5869.
- Lee, C.P., Seong, B.L., and Rajbhandary, U.L. (1991). Structural and Sequence Elements Important for Recognition of Escherichia-Coli Formylmethionine Transfer RNA by Methionyl-Transfer RNA Transformylase Are Clustered in the Acceptor Stem. *The Journal of biological chemistry* *266*, 18012-18017.
- Li, G.W., Oh, E., and Weissman, J.S. (2012). The anti-Shine-Dalgarno sequence drives translational pausing and codon choice in bacteria. *Nature* *484*, 538-541.
- Li, W., Atkinson, G.C., Thakor, N.S., Allas, U., Lu, C.C., Chan, K.Y., Tenson, T., Schulten, K., Wilson, K.S., Haurlyuk, V., *et al.* (2013). Mechanism of tetracycline resistance by ribosomal protection protein Tet(O). *Nat. Commun.* *4*, 1477.

- Li, W., Tailhades, J., O'Brien-Simpson, N.M., Separovic, F., Otvos, L., Jr., Hossain, M.A., and Wade, J.D. (2014). Proline-rich antimicrobial peptides: potential therapeutics against antibiotic-resistant bacteria. *Amino Acids* *46*, 2287-2294.
- Liljas, A., Ehrenberg, M., and Aqvist, J. (2011). Comment on "The mechanism for activation of GTP hydrolysis on the ribosome". *Science* *333*, 37; author reply 37.
- Lin, J., Gagnon, M.G., Bulkley, D., and Steitz, T.A. (2015). Conformational changes of elongation factor G on the ribosome during tRNA translocation. *Cell* *160*, 219-227.
- Liu, G., Song, G., Zhang, D., Zhang, D., Li, Z., Lyu, Z., Dong, J., Achenbach, J., Gong, W., Zhao, X.S., *et al.* (2014). EF-G catalyzes tRNA translocation by disrupting interactions between decoding center and codon-anticodon duplex. *Nat Struct Mol Biol* *21*, 817-824.
- Lovmar, M., Nilsson, K., Vimberg, V., Tenson, T., Nervall, M., and Ehrenberg, M. (2006). The molecular mechanism of peptide-mediated erythromycin resistance. *J. Biol. Chem.* *281*, 6742-6750.
- Maguire, B.A., Beniaminov, A.D., Ramu, H., Mankin, A.S., and Zimmermann, R.A. (2005). A protein component at the heart of an RNA machine: the importance of protein l27 for the function of the bacterial ribosome. *Mol. Cell* *20*, 427-435.
- Mankin, A.S. (2008). Macrolide myths. *Curr. Opin. Microbiol.* *11*, 414-421.
- Marshall, R.A., Aitken, C.E., and Puglisi, J.D. (2009). GTP hydrolysis by IF2 guides progression of the ribosome into elongation. *Mol Cell* *35*, 37-47.
- Martell, M.J., Jr., and Boothe, J.H. (1967). The 6-deoxytetracyclines. VII. Alkylated aminotetracyclines possessing unique antibacterial activity. *J Med Chem* *10*, 44-46.
- Martinez, A.K., Gordon, E., Sengupta, A., Shirole, N., Klepacki, D., Martinez-Garriga, B., Brown, L.M., Benedik, M.J., Yanofsky, C., Mankin, A.S., *et al.* (2014). Interactions of the TnaC nascent peptide with rRNA in the exit tunnel enable the ribosome to respond to free tryptophan. *Nucleic acids research* *42*, 1245-1256.
- Mattiuzzo, M., Bandiera, A., Gennaro, R., Benincasa, M., Pacor, S., Antcheva, N., and Scocchi, M. (2007). Role of the *Escherichia coli* SbmA in the antimicrobial activity of proline-rich peptides. *Molecular microbiology* *66*, 151-163.
- McGuire, J.M., Bunch, R.L., Anderson, R.C., Boaz, H.E., Flynn, E.H., Powell, H.M., and Smith, J.W. (1952). [Ilotycin, a new antibiotic]. *Schweiz Med Wochenschr* *82*, 1064-1065.
- McQuillen, K., Roberts, R.B., and Britten, R.J. (1959). Synthesis of Nascent Protein by Ribosomes in *Escherichia Coli*. *Proceedings of the National Academy of Sciences of the United States of America* *45*, 1437-1447.

- Menninger, J., and Otto, D. (1982). Erythromycin, carbomycin and spiramycin inhibit protein synthesis by stimulating the dissociation of peptidyl-tRNA from ribosomes. *Antimicrob. Agents Chemother.* *21*, 811-818. .
- Milon, P., Konevega, A.L., Gualerzi, C.O., and Rodnina, M.V. (2008). Kinetic checkpoint at a late step in translation initiation. *Mol. Cell* *30*, 712-720.
- Mitra, K., Schaffitzel, C., Fabiola, F., Chapman, M.S., Ban, N., and Frank, J. (2006). Elongation arrest by SecM via a cascade of ribosomal RNA rearrangements. *Mol Cell* *22*, 533-543.
- Mitra, K., Schaffitzel, C., Shaikh, T., Tama, F., Jenni, S., Brooks, C.L., 3rd, Ban, N., and Frank, J. (2005). Structure of the *E. coli* protein-conducting channel bound to a translating ribosome. *Nature* *438*, 318-324.
- Moazed, D., and Noller, H.F. (1987). Chloramphenicol, erythromycin, carbomycin and vernamycin B protect overlapping sites in the peptidyl transferase region of 23S ribosomal RNA. *Biochimie* *69*, 879-884.
- Moazed, D., and Noller, H.F. (1989). Intermediate states in the movement of transfer RNA in the ribosome. *Nature* *342*, 142-148.
- Mohan, S., Donohue, J.P., and Noller, H.F. (2014). Molecular mechanics of 30S subunit head rotation. *Proceedings of the National Academy of Sciences of the United States of America* *111*, 13325-13330.
- Moll, I., Grill, S., Grundling, A., and Blasi, U. (2002). Effects of ribosomal proteins S1, S2 and the DeaD/CsdA DEAD-box helicase on translation of leaderless and canonical mRNAs in *Escherichia coli*. *Molecular microbiology* *44*, 1387-1396.
- Monro, R.E. (1967). Catalysis of peptide bond formation by 50 S ribosomal subunits from *Escherichia coli*. *Journal of molecular biology* *26*, 147-151.
- Moore, P.B., and Laughrea, M. (1979). The conformational properties of ribosomal protein S1. *Nucleic acids research* *6*, 2355-2361.
- Mora, L., Heurgue-Hamard, V., Champ, S., Ehrenberg, M., Kisselev, L.L., and Buckingham, R.H. (2003). The essential role of the invariant GGQ motif in the function and stability in vivo of bacterial release factors RF1 and RF2. *Mol. Microbiol.* *47*, 267-275.
- Moreno, J.M., Drskjotersen, L., Kristensen, J.E., Mortensen, K.K., and Sperling-Petersen, H.U. (1999). Characterization of the domains of *E. coli* initiation factor IF2 responsible for recognition of the ribosome. *FEBS Lett.* *455*, 130-134.
- Munro, J.B., Altman, R.B., O'Connor, N., and Blanchard, S.C. (2007). Identification of two distinct hybrid state intermediates on the ribosome. *Mol. Cell* *25*, 505-517.
- Munro, J.B., Altman, R.B., Tung, C.S., Sanbonmatsu, K.Y., and Blanchard, S.C. (2010). A fast dynamic mode of the EF-G-bound ribosome. *EMBO J.* *29*, 770-781.

- Muth, G.W., Ortoleva-Donnelly, L., and Strobel, S.A. (2000). A single adenosine with a neutral pKa in the ribosomal peptidyl transferase center. *Science* *289*, 947-950.
- Muto, H., Nakatogawa, H., and Ito, K. (2006). Genetically encoded but nonpolypeptide prolyl-tRNA functions in the A site for SecM-mediated ribosomal stall. *Mol Cell* *22*, 545-552.
- Myasnikov, A.G., Simonetti, A., Marzi, S., and Klaholz, B.P. (2009). Structure-function insights into prokaryotic and eukaryotic translation initiation. *Curr Opin Struct Biol* *19*, 300-309.
- Nakatogawa, H., and Ito, K. (2001). Secretion monitor, SecM, undergoes self-translation arrest in the cytosol. *Mol. Cell* *7*, 185-192.
- Nakatogawa, H., and Ito, K. (2002). The ribosomal exit tunnel functions as a discriminating gate. *Cell* *108*, 629-636.
- Nguyen, F., Starosta, A.L., Arenz, S., Sohmen, D., Donhofer, A., and Wilson, D.N. (2014). Tetracycline antibiotics and resistance mechanisms. *Biol Chem* *395*, 559-575.
- Nissen, P., Hansen, J., Ban, N., Moore, P.B., and Steitz, T.A. (2000). The structural basis of ribosome activity in peptide bond synthesis. *Science* *289*, 920-930.
- Nissen, P., Ippolito, J.A., Ban, N., Moore, P.B., and Steitz, T.A. (2001). RNA tertiary interactions in the large ribosomal subunit: the A-minor motif. *Proc. Natl. Acad. Sci. USA* *98*, 4899-4903.
- Noller, H.F. (2012). Evolution of protein synthesis from an RNA world. *Cold Spring Harb Perspect Biol* *4*, a003681.
- Nonaka, L., Connell, S.R., and Taylor, D.E. (2005). 16S rRNA mutations that confer tetracycline resistance in *Helicobacter pylori* decrease drug binding in *Escherichia coli* ribosomes. *Journal of bacteriology* *187*, 3708-3712.
- O'Connor, M., Gregory, S.T., Rajbhandary, U.L., and Dahlberg, A.E. (2001). Altered discrimination of start codons and initiator tRNAs by mutant initiation factor 3. *Rna A Publication of the Rna Society* *7*, 969-978.
- Ogle, J.M., Brodersen, D.E., Clemons Jr, W.M., Tarry, M.J., Carter, A.P., and Ramakrishnan, V. (2001). Recognition of cognate transfer RNA by the 30S ribosomal subunit. *Science* *292*, 897-902.
- Ogle, J.M., Murphy, F.V., Tarry, M.J., and Ramakrishnan, V. (2002). Selection of tRNA by the ribosome requires a transition from an open to a closed form. *Cell* *111*, 721-732.
- Ogle, J.M., and Ramakrishnan, V. (2005). Structural insights into translational fidelity. *Annu. Rev. Biochem.* *74*, 129-177.

- Olson, M.W., Ruzin, A., Feyfant, E., Rush, T.S., 3rd, O'Connell, J., and Bradford, P.A. (2006). Functional, biophysical, and structural bases for antibacterial activity of tigecycline. *Antimicrob Agents Chemother* *50*, 2156-2166.
- Otaka, T., and Kaji, A. (1975). Release of (oligo)peptidyl-tRNA from ribosomes by erythromycin A. *Proc. Natl. Acad. Sci. USA* *72*, 2649-2652.
- Otvos, L., Jr. (2005). Antibacterial peptides and proteins with multiple cellular targets. *J Pept Sci* *11*, 697-706.
- Otvos, L., Jr., Flick-Smith, H., Fox, M., Ostorhazi, E., Dawson, R.M., and Wade, J.D. (2014). The designer proline-rich antibacterial peptide A3-APO prevents *Bacillus anthracis* mortality by deactivating bacterial toxins. *Protein Pept Lett* *21*, 374-381.
- Pai, R.D., Zhang, W., Schuwirth, B.S., Hirokawa, G., Kaji, H., Kaji, A., and Cate, J.H. (2008). Structural Insights into ribosome recycling factor interactions with the 70S ribosome. *Journal of molecular biology* *376*, 1334-1347.
- Palade, G.E. (1955). A small particulate component of the cytoplasm. *J. Biophys. Biochem. Cytol.* *1*, 59-68.
- Pan, D., Kirillov, S.V., and Cooperman, B.S. (2007). Kinetically competent intermediates in the translocation step of protein synthesis. *Mol Cell* *25*, 519-529.
- Pape, T., Wintermeyer, W., and Rodnina, M. (1999). Induced fit in initial selection and proofreading of aminoacyl-tRNA on the ribosome. *EMBO J* *18*, 3800-3807.
- Park, E., Menetret, J.F., Gumbart, J.C., Ludtke, S.J., Li, W., Whynot, A., Rapoport, T.A., and Akey, C.W. (2013). Structure of the SecY channel during initiation of protein translocation. *Nature*.
- Pavlov, M.Y., Watts, R.E., Tan, Z., Cornish, V.W., Ehrenberg, M., and Forster, A.C. (2009). Slow peptide bond formation by proline and other N-alkylamino acids in translation. *Proceedings of the National Academy of Sciences of the United States of America* *106*, 50-54.
- Peil, L., Starosta, A.L., Lassak, J., Atkinson, G.C., Virumae, K., Spitzer, M., Tenson, T., Jung, K., Remme, J., and Wilson, D.N. (2013). Distinct XPPX sequence motifs induce ribosome stalling, which is rescued by the translation elongation factor EF-P. *Proceedings of the National Academy of Sciences of the United States of America* *110*, 15265-15270.
- Pel, H., Moffat, J., Ito, K., Nakamura, Y., and Tate, W. (1998). *Escherichia coli* release factor 3: Resolving the paradox of a typical G protein structure and atypical function with guanine nucleotides. *RNA* *4*, 47-54.
- Perlman, D., Heuser, L.J., Dutcher, J.D., Barrett, J.M., and Boska, J.A. (1960). Biosynthesis of tetracycline by 5-hydroxy-tetracycline-producing cultures of *Streptomyces rimosus*. *Journal of bacteriology* *80*, 419-420.

- Peske, F., Kuhlenkoetter, S., Rodnina, M.V., and Wintermeyer, W. (2014). Timing of GTP binding and hydrolysis by translation termination factor RF3. *Nucleic acids research* *42*, 1812-1820.
- Peske, F., Rodnina, M., and Wintermeyer, W. (2005). Sequence of steps in ribosome recycling as defined by kinetic analysis. *Mol. Cell* *18*, 403-412.
- Pestka, S. (1974). Binding of [¹⁴C]erythromycin to *Escherichia coli* ribosomes. *Antimicrob Agents Chemother* *6*, 474-478.
- Petersen, P.J., Jacobus, N.V., Weiss, W.J., Sum, P.E., and Testa, R.T. (1999). In vitro and in vivo antibacterial activities of a novel glycylicycline, the 9-t-butylglycylamido derivative of minocycline (GAR-936). *Antimicrob Agents Chemother* *43*, 738-744.
- Petry, S., Brodersen, D., Murphy, F.t., Dunham, C., Selmer, M., Tarry, M., Kelley, A., and Ramakrishnan, V. (2005). Crystal structures of the ribosome in complex with release factors RF1 and RF2 bound to a cognate stop codon. *Cell* *123*, 1255-1266.
- Petry, S., Weixlbaumer, A., and Ramakrishnan, V. (2008). The termination of translation. *Curr Opin Struct Biol* *18*, 70-77.
- Piddock, L.J. (2006). Multidrug-resistance efflux pumps - not just for resistance. *Nat Rev Microbiol* *4*, 629-636.
- Pioletti, M., Schlunzen, F., Harms, J., Zarivach, R., Gluhmann, M., Avila, H., Bashan, A., Bartels, H., Auerbach, T., Jacobi, C., *et al.* (2001). Crystal structures of complexes of the small ribosomal subunit with tetracycline, edeine and IF3. *EMBO J.* *20*, 1829-1839.
- Poehlsgaard, J., and Douthwaite, S. (2003). Macrolide antibiotic interaction and resistance on the bacterial ribosome. *Curr. Opin. Investig. Drugs* *4*, 140-148.
- Polacek, N., Gaynor, M., Yassin, A., and Mankin, A.S. (2001). Ribosomal peptidyl transferase can withstand mutations at the putative catalytic nucleotide. *Nature* *411*, 498-501.
- Polikanov, Y.S., Osterman, I.A., Szal, T., Tashlitsky, V.N., Serebryakova, M.V., Kusocek, P., Bulkley, D., Malanicheva, I.A., Efimenko, T.A., Efremenkova, O.V., *et al.* (2014a). Amicoumacin a inhibits translation by stabilizing mRNA interaction with the ribosome. *Mol Cell* *56*, 531-540.
- Polikanov, Y.S., Steitz, T.A., and Innis, C.A. (2014b). A proton wire to couple aminoacyl-tRNA accommodation and peptide-bond formation on the ribosome. *Nat Struct Mol Biol* *21*, 787-793.
- Polikanov, Y.S., Szal, T., Jiang, F., Gupta, P., Matsuda, R., Shiozuka, M., Steitz, T.A., Vazquez-Laslop, N., and Mankin, A.S. (2014l). Negamycin interferes with decoding and translocation by simultaneous interaction with rRNA and tRNA. *Mol Cell* *56*, 541-550.

- Poulsen, S.M., Kofoed, C., and Vester, B. (2000). Inhibition of the ribosomal peptidyl transferase reaction by the mycarose moiety of the antibiotics carbomycin, spiramycin and tylosin. *J. Mol. Biol.* *304*, 471-481.
- Pulk, A., and Cate, J.H. (2013). Control of ribosomal subunit rotation by elongation factor G. *Science* *340*, 1235970.
- Pyetan, E., Baram, D., Auerbach-Nevo, T., and Yonath, A. (2007). Chemical parameters influencing fine-tuning in the binding of macrolide antibiotics to the ribosomal tunnel. *Pure Appl. Chem.* *79*, 955-968.
- Qu, X., Lancaster, L., Noller, H.F., Bustamante, C., and Tinoco, I., Jr. (2012). Ribosomal protein S1 unwinds double-stranded RNA in multiple steps. *Proceedings of the National Academy of Sciences of the United States of America* *109*, 14458-14463.
- Rajkowitsch, L., and Schroeder, R. (2007). Dissecting RNA chaperone activity. *RNA* *13*, 2053-2060.
- Ramagopal, S. (1976). Accumulation of free ribosomal proteins S1, L7, and L12 in *Escherichia coli*. *Eur J Biochem* *69*, 289-297.
- Ramrath, D.J., Lancaster, L., Sprink, T., Mielke, T., Loerke, J., Noller, H.F., and Spahn, C.M. (2013). Visualization of two transfer RNAs trapped in transit during elongation factor G-mediated translocation. *Proceedings of the National Academy of Sciences of the United States of America* *110*, 20964-20969.
- Ramu, H., Mankin, A., and Vazquez-Laslop, N. (2009). Programmed drug-dependent ribosome stalling. *Molecular microbiology* *71*, 811-824.
- Ramu, H., Vazquez-Laslop, N., Klepacki, D., Dai, Q., Piccirilli, J., Micura, R., and Mankin, A.S. (2011). Nascent peptide in the ribosome exit tunnel affects functional properties of the A-site of the peptidyl transferase center. *Mol Cell* *41*, 321-330.
- Ratje, A.H., Loerke, J., Mikolajka, A., Brunner, M., Hildebrand, P.W., Starosta, A.L., Donhofer, A., Connell, S.R., Fucini, P., Mielke, T., *et al.* (2010). Head swivel on the ribosome facilitates translocation by means of intra-subunit tRNA hybrid sites. *Nature* *468*, 713-716.
- Rawat, U.B., Zavialov, A.V., Sengupta, J., Valle, M., Grassucci, R.A., Linde, J., Vestergaard, B., Ehrenberg, M., and Frank, J. (2003). A cryo-electron microscopic study of ribosome-bound termination factor RF2. *Nature* *421*, 87-90.
- Rheinberger, H.-J., and Nierhaus, K.H. (1983). Testing an alternative model for the ribosomal peptide elongation cycle. *Proc. Natl. Acad. Sci. USA* *80*, 4213-4217.
- Risuleo, G., Gualerzi, C., and Pon, C. (1976). Specificity and properties of the destabilization, induced by initiation factor IF-3, of ternary complexes of the 30S ribosomal subunit. *Eur. J. Biochem.* *67*, 603-613.

- Roberts, M.C., Sutcliffe, J., Courvalin, P., Jensen, L.B., Rood, J., and Seppala, H. (1999). Nomenclature for macrolide and macrolide-lincosamide-streptogramin B resistance determinants. *Antimicrob Agents Chemother* *43*, 2823-2830.
- Rodnina, M.V., Pape, T., Fricke, R., Kuhn, L., and Wintermeyer, W. (1996). Initial binding of the elongation factor Tu center dot GTP center dot aminoacyl-tRNA complex preceding codon recognition on the ribosome. *The Journal of biological chemistry* *271*, 646-652.
- Rodnina, M.V., Savelsbergh, A., Katunin, V.I., and Wintermeyer, W. (1997). Hydrolysis of GTP by elongation factor G drives tRNA movement on the ribosome. *Nature* *385*, 37-41.
- Rodriguez-Fonseca, C., Amils, R., and Garrett, R.A. (1995). Fine structure of the peptidyl transferase centre on 23 S-like rRNAs deduced from chemical probing of antibiotic-ribosome complexes. *J. Mol. Biol.* *247*, 224-235.
- Ross, J.I., Eady, E.A., Cove, J.H., and Cunliffe, W.J. (1998). 16S rRNA mutation associated with tetracycline resistance in a gram- positive bacterium. *Antimicrob Agents Chemother* *42*, 1702-1705.
- Ross, J.I., Eady, E.A., Cove, J.H., Cunliffe, W.J., Baumberg, S., and Wootton, J.C. (1990). Inducible erythromycin resistance in staphylococci is encoded by a member of the ATP-binding transport super-gene family. *Molecular microbiology* *4*, 1207-1214.
- Runti, G., Lopez Ruiz Mdel, C., Stoilova, T., Hussain, R., Jennions, M., Choudhury, H.G., Benincasa, M., Gennaro, R., Beis, K., and Scocchi, M. (2013). Functional characterization of SbmA, a bacterial inner membrane transporter required for importing the antimicrobial peptide Bac7(1-35). *Journal of bacteriology* *195*, 5343-5351.
- Salsi, E., Farah, E., Netter, Z., Dann, J., and Ermolenko, D.N. (2015). Movement of elongation factor G between compact and extended conformations. *Journal of molecular biology* *427*, 454-467.
- Sanbonmatsu, K.Y., Joseph, S., and Tung, C.S. (2005). Simulating movement of tRNA into the ribosome during decoding. *Proceedings of the National Academy of Sciences of the United States of America* *102*, 15854-15859.
- Savelsbergh, A., Matassova, N.B., Rodnina, M.V., and Wintermeyer, W. (2000). Role of domains 4 and 5 in elongation factor G functions on the ribosome. *J. Mol. Biol.* *300*, 951-961.
- Scarlett, D.J., McCaughan, K.K., Wilson, D.N., and Tate, W.P. (2003). Mapping functionally important motifs SPF and GGQ of the decoding release factor RF2 to the *Escherichia coli* ribosome by hydroxyl radical footprinting. Implications for macromolecular mimicry and structural changes in RF2. *J. Biol. Chem.* *278*, 15095-15104.

- Schlünzen, F., Zarivach, R., Harms, J., Bashan, A., Tocilj, A., Albrecht, R., Yonath, A., and Franceschi, F. (2001). Structural basis for the interaction of antibiotics with the peptidyl transferase centre in eubacteria. *Nature* *413*, 814-821.
- Schmeing, T.M., Huang, K.S., Kitchen, D.E., Strobel, S.A., and Steitz, T.A. (2005a). Structural insights into the roles of water and the 2' hydroxyl of the P site tRNA in the peptidyl transferase reaction. *Mol. Cell* *20*, 437-448.
- Schmeing, T.M., Huang, K.S., Strobel, S.A., and Steitz, T.A. (2005d). An induced-fit mechanism to promote peptide bond formation and exclude hydrolysis of peptidyl-tRNA. *Nature* *438*, 520-524.
- Schmeing, T.M., Moore, P.B., and Steitz, T.A. (2003). Structures of deacylated tRNA mimics bound to the E site of the large ribosomal subunit. *RNA* *9*, 1345-1352.
- Schmeing, T.M., and Ramakrishnan, V. (2009). What recent ribosome structures have revealed about the mechanism of translation. *Nature* *461*, 1234-1242.
- Schmeing, T.M., Seila, A.C., Hansen, J.L., Freeborn, B., Soukup, J.K., Scaringe, S.A., Strobel, S.A., Moore, P.B., and Steitz, T.A. (2002). A pre-translocational intermediate in protein synthesis observed in crystals of enzymatically active 50S subunits. *Nat. Struct. Biol.* *9*, 225-230.
- Schmeing, T.M., Voorhees, R.M., Kelley, A.C., Gao, Y.G., Murphy, F.V.t., Weir, J.R., and Ramakrishnan, V. (2009). The crystal structure of the ribosome bound to EF-Tu and aminoacyl-tRNA. *Science* *326*, 688-694.
- Schmeing, T.M., Voorhees, R.M., Kelley, A.C., and Ramakrishnan, V. (2011). How mutations in tRNA distant from the anticodon affect the fidelity of decoding. *Nat. Struct. Mol. Biol.* *18*, 432-436.
- Schuetz, J.C., Murphy, F.V.t., Kelley, A.C., Weir, J.R., Giesebrecht, J., Connell, S.R., Loeke, J., Mielke, T., Zhang, W., Penczek, P.A., *et al.* (2009). GTPase activation of elongation factor EF-Tu by the ribosome during decoding. *Embo J* *28*, 755-765.
- Scocchi, M., Tossi, A., and Gennaro, R. (2011). Proline-rich antimicrobial peptides: converging to a non-lytic mechanism of action. *Cell Mol Life Sci* *68*, 2317-2330.
- Scolnick, E., Tompkins, R., Caskey, T., and Nirenberg, M. (1968). Release factors differing in specificity for terminator codons. *Proc. Natl Acad. Sci. USA* *61*, 768-774.
- Seefeldt, C., Nguyen, F., Antunes, S., Pérébasquine, N., Graf, M., Arenz, S., Inampudi, K., Douat, C., Guichard, G., Wilson, D.N., *et al.* (2015). The Proline-rich Antimicrobial Peptide Onc112 Inhibits Translation by Blocking and Destabilizing the Post-initiation Complex. *Nat Struct Mol Biol.*
- Seidelt, B., Innis, C.A., Wilson, D.N., Gartmann, M., Armache, J.P., Villa, E., Trabuco, L.G., Becker, T., Mielke, T., Schulten, K., *et al.* (2009). Structural insight into nascent polypeptide chain-mediated translational stalling. *Science* *326*, 1412-1415.

- Seit Nebi, A., Frolova, L., Ivanova, N., Poltarau, A., and Kiselev, L. (2000). Mutation of a glutamine residue in the universal tripeptide GGQ in human eRF1 termination factor does not cause complete loss of its activity. *Mol. Biol. (Moscow)* 34, 899-900.
- Seit-Nebi, A., Frolova, L., Justesen, J., and Kisselev, L. (2001). Class-1 translation termination factors: invariant GGQ minidomain is essential for release activity and ribosome binding but not for stop codon recognition. *Nucleic Acids Res.* 29, 3982-3987.
- Semenkov, Y., Shapkina, T., Makhno, V., and Kirillov, S. (1992). Puromycin Reaction for the A-Site-Bound Peptidyl-Transfer RNA. *FEBS Lett* 296, 207-210.
- Semenkov, Y.P., Rodnina, M.V., and Wintermeyer, W. (1996). The "allosteric three-site model" of elongation cannot be confirmed in a well-defined ribosome system from *Escherichia coli*. *Proceedings of the National Academy of Sciences of the United States of America* 93, 12183-12188.
- Semenkov, Y.P., Rodnina, M.V., and Wintermeyer, W. (2000). Energetic contribution of tRNA hybrid state formation to translocation catalysis on the ribosome. *Nat. Struct. Biol.* 7, 1027-1031.
- Seong, B., and RajBhandary, U.L. (1987). *Escherichia coli* formylmethionine tRNA: mutations of GGG:CCC sequence conserved in anticodon stem of initiator tRNAs affect initiation of protein synthesis and conformation of anticodon loop. *Proc. Natl. Acad. Sci. U.S.A.* 84(2), 334-338.
- Sharma, D., Southworth, D.R., and Green, R. (2004). EF-G-independent reactivity of a pre-translocation-state ribosome complex with the aminoacyl tRNA substrate puromycin supports an intermediate (hybrid) state of tRNA binding. *RNA* 10, 102-113.
- Shaw, J.J., and Green, R. (2007). Two distinct components of release factor function uncovered by nucleophile partitioning analysis. *Mol Cell* 28, 458-467.
- Shine, J., and Dalgarno, L. (1974). The 3'-terminal sequence of *E. coli* 16S rRNA: Complementarity to nonsense triplets and ribosome binding sites. *Proc. Natl. Acad. Sci. USA* 71, 1342-1346.
- Shivakumar, A.G., Hahn, J., Grandi, G., Kozlov, Y., and Dubnau, D. (1980). Posttranscriptional regulation of an erythromycin resistance protein specified by plasmic pE194. *Proceedings of the National Academy of Sciences of the United States of America* 77, 3903-3907.
- Shoji, S., Walker, S.E., and Fredrick, K. (2006). Reverse translocation of tRNA in the ribosome. *Mol Cell* 24, 931-942.
- Sievers, A., Beringer, M., Rodnina, M.V., and Wolfenden, R. (2004). The ribosome as an entropy trap. *Proc. Natl. Acad. Sci. U S A* 101, 7897-7901.

- Simonetti, A., Marzi, S., Myasnikov, A.G., Fabbretti, A., Yusupov, M., Gualerzi, C.O., and Klaholz, B.P. (2008). Structure of the 30S translation initiation complex. *Nature* *455*, 416-420.
- Singh, N., Das, G., Seshadri, A., Sangeetha, R., and Varshney, U. (2005). Evidence for a role of initiation factor 3 in recycling of ribosomal complexes stalled on mRNAs in *Escherichia coli*. *Nucleic Acids Res.* *33*, 5591-5601.
- Soares, N.C., Spat, P., Krug, K., and Macek, B. (2013). Global dynamics of the *Escherichia coli* proteome and phosphoproteome during growth in minimal medium. *J Proteome Res* *12*, 2611-2621.
- Sohmen, D., Chiba, S., Shimokawa-Chiba, N., Innis, C.A., Berninghausen, O., Beckmann, R., Ito, K., and Wilson, D.N. (2015). Structure of the *Bacillus subtilis* 70S ribosome reveals the basis for species-specific stalling. *Nat Commun* *6*, 6941.
- Sohmen, D., Harms, J.M., Schlunzen, F., and Wilson, D.N. (2009). Enhanced SnapShot: Antibiotic inhibition of protein synthesis II. *Cell* *139*, 212-212 e211.
- Sorensen, M.A., Fricke, J., and Pedersen, S. (1998). Ribosomal protein S1 is required for translation of most, if not all, natural mRNAs in *Escherichia coli* in vivo. *J. Mol. Biol.* *280*, 561-569.
- Sothiselvam, S., Liu, B., Han, W., Ramu, H., Klepacki, D., Atkinson, G.C., Brauer, A., Remm, M., Tenson, T., Schulten, K., *et al.* (2014). Macrolide antibiotics allosterically predispose the ribosome for translation arrest. *Proceedings of the National Academy of Sciences of the United States of America* *111*, 9804-9809.
- Spahn, C.M., Blaha, G., Agrawal, R.K., Penczek, P., Grassucci, R.A., Trieber, C.A., Connell, S.R., Taylor, D.E., Nierhaus, K.H., and Frank, J. (2001). Localization of the ribosomal protection protein Tet(O) on the ribosome and the mechanism of tetracycline resistance. *Mol. Cell* *7*, 1037-1045.
- Speer, B.S., Bedzyk, L., and Salyers, A.A. (1991). Evidence that a novel tetracycline resistance gene found on two *Bacteroides* transposons encodes an NADP-requiring oxidoreductase. *Journal of bacteriology* *173*, 176-183.
- Spiegel, P.C., Ermolenko, D.N., and Noller, H.F. (2007). Elongation factor G stabilizes the hybrid-state conformation of the 70S ribosome. *RNA* *13*, 1473-1482.
- Stark, H., Rodnina, M.V., Rinkeappell, J., Brimacombe, R., Wintermeyer, W., and Vanheul, M. (1997). Visualization of Elongation Factor Tu On the *Escherichia Coli* Ribosome. *Nature*. *389*, 403-406.
- Starosta, A.L., Lassak, J., Peil, L., Atkinson, G.C., Virumae, K., Tenson, T., Remme, J., Jung, K., and Wilson, D.N. (2014). Translational stalling at polyproline stretches is modulated by the sequence context upstream of the stall site. *Nucleic acids research* *42*, 10711-10719.

- Stephens, C.R., Beereboom, J.J., Rennhard, H.H., Gordon, P.N., Murai, K., Blackwood, R.K., and von Wittenau, M.S. (1963). 6-Deoxytetracyclines. IV.1,2 Preparation, C-6 Stereochemistry, and Reactions. *Journal of the American Chemical Society* *85*, 2643-2652.
- Stephens, C.R., Conover, L.H., Hochstein, F.A., Regna, P.P., Pilgrim, F.J., Brunings, K.J., and Woodward, R.B. (1952). Terramycin. VIII. Structure of aureomycin and terramycin. *J. Am. Chem. Soc.* *74*, 4976-4977.
- Studer, S., and Joseph, S. (2006). Unfolding of mRNA secondary structure by the bacterial translation initiation complex. *Mol. Cell* *22*, 105-115.
- Suarez, G., Nathans D. (1965). Inhibition of aminoacyl-sRNA binding to ribosomes by tetracycline. *Biochemical and biophysical research communications* *18*, 743-750.
- Subramanian, A.-R. (1983). Structure and Functions of Ribosomal Protein S1. *Prog. Nucleic Acid Res. Mol. Biol.* *28*, 101-142.
- Subramanian, A.R., and Davis, B.D. (1970). Activity of initiation factor F3 in dissociating *Escherichia coli* ribosomes. *Nature* *228*, 1273-1275.
- Sum, P.E., Lee, V.J., Testa, R.T., Hlavka, J.J., Ellestad, G.A., Bloom, J.D., Gluzman, Y., and Tally, F.P. (1994). Glycylcyclines. 1. A new generation of potent antibacterial agents through modification of 9-aminotetracyclines. *J Med Chem* *37*, 184-188.
- Sussman, J.K., Simons, E.L., and Simons, R.W. (1996). *Escherichia coli* translation initiation factor 3 discriminates the initiation codon *in vivo*. *Mol. Microbiol.* *21*, 347-360.
- Tai, P.-C., Wallace, B.J., and Davis, B.D. (1974). Selective action of erythromycin on initiating ribosomes. *Biochemistry* *13*, 4653-4659.
- Takashima, H. (2003). Structural consideration of macrolide antibiotics in relation to the ribosomal interaction and drug design. *Curr. Top. Med. Chem.* *3*, 991-999.
- Tanner, D.R., Cariello, D.A., Woolstenhulme, C.J., Broadbent, M.A., and Buskirk, A.R. (2009). Genetic identification of nascent peptides that induce ribosome stalling. *J. Biol. Chem.* *284*, 34809-43818.
- Taylor, D.E., Jerome, L.J., Grewal, J., and Chang, N. (1995). Tet(O), a protein that mediates ribosomal protection to tetracycline, binds, and hydrolyses GTP. *Can J Microbiol* *41*, 965-970.
- Tedin, K., Resch, A., and Blasi, U. (1997). Requirements for ribosomal protein S1 for translation initiation of mRNAs with and without a 5' leader sequence. *Mol. Microbiol.* *25*, 189-199.
- Tenson, T., Deblasio, A., and Mankin, A. (1996). A functional peptide encoded in the *Escherichia coli* 23S rRNA. *Proc Natl Acad Sci USA* *93*, 8796.

- Tenson, T., Lovmar, M., and Ehrenberg, M. (2003). The mechanism of action of macrolides, lincosamides and streptogramin B reveals the nascent peptide exit path in the ribosome. *J. Mol. Biol.* *330*, 1005-1014.
- Tenson, T., and Mankin, A. (2001). Short peptides conferring resistance to macrolide antibiotics. *Peptides* *22*, 1661-1668.
- Tenson, T., Xiong, L.Q., Kloss, P., and Mankin, A.S. (1997). Erythromycin resistance peptides selected from random peptide libraries. *The Journal of biological chemistry* *272*, 17425-17430.
- Testa, R.T., Petersen, P.J., Jacobus, N.V., Sum, P.E., Lee, V.J., and Tally, F.P. (1993). In vitro and In vivo Antibacterial Activities of the Glycylcyclines, a New Class of Semisynthetic Tetracyclines. *Antimicrob Agents Chemother* *37*, 2270-2277.
- Thomas, J.O., Kolb, A., and Szer, W. (1978). Structure of single-stranded nucleic acids in the presence of ribosomal protein S1. *Journal of molecular biology* *123*, 163-176.
- Tourigny, D.S., Fernandez, I.S., Kelley, A.C., and Ramakrishnan, V. (2013). Elongation factor G bound to the ribosome in an intermediate state of translocation. *Science* *340*, 1235490.
- Traut, R.R., and Monro, R.E. (1964). The puromycin reaction and its relation to protein synthesis. *J. Mol. Biol.* *10*, 63-72.
- Trieber, C.A., Burkhardt, N., Nierhaus, K.H., and Taylor, D.E. (1998). Ribosomal Protection from Tetracycline Mediated by Tet(O) Interaction with Ribosomes Is GTP-Dependent. *Biol. Chem.* *379*, 847-855.
- Trieber, C.A., and Taylor, D.E. (2002). Mutations in the 16S rRNA genes of *Helicobacter pylori* mediate resistance to tetracycline. *Journal of bacteriology* *184*, 2131-2140.
- Tripathi, S., Kloss, P.S., and Mankin, A.S. (1998). Ketolide resistance conferred by short peptides. *The Journal of biological chemistry* *273*, 20073-20077.
- Tsai, A., Kornberg, G., Johansson, M., Chen, J., and Puglisi, J.D. (2014). The Dynamics of SecM-Induced Translational Stalling. *Cell Rep.*
- Tu, D., Blaha, G., Moore, P., and Steitz, T. (2005). Structures of MLSBK antibiotics bound to mutated large ribosomal subunits provide a structural explanation for resistance. *Cell* *121*, 257-270.
- Ude, S., Lassak, J., Starosta, A.L., Kraxenberger, T., Wilson, D.N., and Jung, K. (2013). Translation elongation factor EF-P alleviates ribosome stalling at polyproline stretches. *Science* *339*, 82-85.
- Uemura, S., Aitken, C.E., Korlach, J., Flusberg, B.A., Turner, S.W., and Puglisi, J.D. (2010). Real-time tRNA transit on single translating ribosomes at codon resolution. *Nature* *464*, 1012-1017.

- Valle, M., Sengupta, J., Swami, N.K., Grassucci, R.A., Burkhardt, N., Nierhaus, K.H., Agrawal, R.K., and Frank, J. (2002). Cryo-EM reveals an active role for aminoacyl-tRNA in the accommodation process. *EMBO J.* *21*, 3557-3567.
- Valle, M., Zavialov, A., Sengupta, J., Rawat, U., Ehrenberg, M., and Frank, J. (2003). Locking and unlocking of ribosomal motions. *Cell* *114*, 123-134.
- Vazquez-Laslop, N., Klepacki, D., Mulhearn, D.C., Ramu, H., Krasnykh, O., Franzblau, S., and Mankin, A.S. (2011). Role of antibiotic ligand in nascent peptide-dependent ribosome stalling. *Proceedings of the National Academy of Sciences of the United States of America* *108*, 10496-10501.
- Vazquez-Laslop, N., Ramu, H., Klepacki, D., Kannan, K., and Mankin, A.S. (2010). The key function of a conserved and modified rRNA residue in the ribosomal response to the nascent peptide. *EMBO J.* *29*, 3108-3117.
- Vázquez-Laslop, N., Ramu, H., and Mankin, A.S. (2011). Nascent peptide-mediated ribosome stalling promoted by antibiotics. In *Ribosomes. Structure, function, evolution*, M.V. Rodnina, W. Wintermeyer, and R. Green, eds. (Wien, New York: Springer-Verlag), pp. 377-392.
- Vazquez-Laslop, N., Thum, C., and Mankin, A.S. (2008). Molecular mechanism of drug-dependent ribosome stalling. *Mol Cell* *30*, 190-202.
- Vesper, O., Amitai, S., Belitsky, M., Byrgazov, K., Kaberdina, A.C., Engelberg-Kulka, H., and Moll, I. (2011). Selective translation of leaderless mRNAs by specialized ribosomes generated by MazF in *Escherichia coli*. *Cell* *147*, 147-157.
- Vester, B., and Douthwaite, S. (2001). Macrolide resistance conferred by base substitutions in 23S rRNA. *Antimicrob. Agents Chemother.* *45*, 1-12.
- Vestergaard, B., Van, L., Andersen, G., Nyborg, J., Buckingham, R., and Kjeldgaard, M. (2001). Bacterial polypeptide release factor RF2 is structurally distinct from eukaryotic eRF1. *Mol. Cell* *8*, 1375-1382.
- Voorhees, R.M., and Ramakrishnan, V. (2013). Structural basis of the translational elongation cycle. *Annu. Rev. Biochem.* *82*, 203-236.
- Voorhees, R.M., Schmeing, T.M., Kelley, A.C., and Ramakrishnan, V. (2010). The mechanism for activation of GTP hydrolysis on the ribosome. *Science* *330*, 835-838.
- Voorhees, R.M., Weixlbaumer, A., Loakes, D., Kelley, A.C., and Ramakrishnan, V. (2009). Insights into substrate stabilization from snapshots of the peptidyl transferase center of the intact 70S ribosome. *Nat Struct Mol Biol* *16*, 528-533.
- Walker, S.E., Shoji, S., Pan, D., Cooperman, B.S., and Fredrick, K. (2008). Role of hybrid tRNA-binding states in ribosomal translocation. *Proceedings of the National Academy of Sciences of the United States of America* *105*, 9192-9197.

- Weinger, J.S., Parnell, K.M., Dorner, S., Green, R., and Strobel, S.A. (2004). Substrate-assisted catalysis of peptide bond formation by the ribosome. *Nat. Struct. Mol. Biol.* *11*, 1101-1106.
- Weisblum, B. (1995). Insights into erythromycin action from studies of its activity as inducer of resistance. *Antimicrob Agents Chemother* *39*, 797-805.
- Weixlbaumer, A., Jin, H., Neubauer, C., Voorhees, R.M., Petry, S., Kelley, A.C., and Ramakrishnan, V. (2008). Insights into translational termination from the structure of RF2 bound to the ribosome. *Science* *322*, 953-956.
- Weixlbaumer, A., Petry, S., Dunham, C.M., Selmer, M., Kelley, A.C., and Ramakrishnan, V. (2007). Crystal structure of the ribosome recycling factor bound to the ribosome. *Nat. Struct. Mol. Biol.* *14*, 733-737.
- Wettstein, F.O., and Noll, H. (1965). Binding of transfer ribonucleic acid to ribosomes engaged in protein synthesis: Number and properties of ribosomal binding sites. *J. Mol. Biol.* *11*, 35-53.
- Wilson, D.N. (2004). Antibiotics and the inhibition of ribosome function. In *Protein Synthesis and Ribosome Structure*, K. Nierhaus, and D. Wilson, eds. (Weinheim: Wiley-VCH), pp. 449-527.
- Wilson, D.N. (2009). The A-Z of bacterial translation inhibitors. *Crit Rev Biochem Mol Biol* *44*, 393-433.
- Wilson, D.N. (2011). On the specificity of antibiotics targeting the large ribosomal subunit. *Ann. N. Y. Acad. Sci.* *1241*, 1-16.
- Wilson, D.N. (2014). Ribosome-targeting antibiotics and bacterial resistance mechanisms. *Nat. Rev. Microbiol.* *12*, 35-48.
- Wilson, D.N., and Beckmann, R. (2011). The ribosomal tunnel as a functional environment for nascent polypeptide folding and translational stalling. *Curr. Opin. Struct. Biol.* *21*, 1-10.
- Wilson, D.N., Harms, J.M., Nierhaus, K.H., Schlünzen, F., and Fucini, P. (2005a). Species-specific antibiotic-ribosome interactions: Implications for drug development. *Biol. Chem.* *386*, 1239-1252.
- Wilson, D.N., Schlunzen, F., Harms, J.M., Yoshida, T., Ohkubo, T., Albrecht, R., Buerger, J., Kobayashi, Y., and Fucini, P. (2005b). X-ray crystallography study on ribosome recycling: the mechanism of binding and action of RRF on the 50S ribosomal subunit. *EMBO J.* *24*, 251-260.
- Wittmann, H.G., Stoffler, G., Apirion, D., Rosen, L., Tanaka, K., Tamaki, M., Takata, R., Dekio, S., and Otaka, E. (1973). Biochemical and genetic studies on two different types of erythromycin resistant mutants of *Escherichia coli* with altered ribosomal proteins. *Mol. Gen. Genet.* *127*, 175-189.

- Wohlgemuth, I., Beringer, M., and Rodnina, M.V. (2006). Rapid peptide bond formation on isolated 50S ribosomal subunits. *EMBO Rep* 7, 699-703.
- Woolhead, C.A., Johnson, A.E., and Bernstein, H.D. (2006). Translation arrest requires two-way communication between a nascent polypeptide and the ribosome. *Mol Cell* 22, 587-598.
- Woolstenhulme, C.J., Parajuli, S., Healey, D.W., Valverde, D.P., Petersen, E.N., Starosta, A.L., Guydosh, N.R., Johnson, W.E., Wilson, D.N., and Buskirk, A.R. (2013). Nascent peptides that block protein synthesis in bacteria. *Proceedings of the National Academy of Sciences of the United States of America* 110, E878-887.
- Yamamoto, H., Qin, Y., Achenbach, J., Li, C., Kijek, J., Spahn, C.M., and Nierhaus, K.H. (2014). EF-G and EF4: translocation and back-translocation on the bacterial ribosome. *Nat Rev Microbiol* 12, 89-100.
- Yang, W., Moore, I.F., Koteva, K.P., Bareich, D.C., Hughes, D.W., and Wright, G.D. (2004). TetX is a flavin-dependent monooxygenase conferring resistance to tetracycline antibiotics. *The Journal of biological chemistry* 279, 52346-52352.
- Yap, M.N., and Bernstein, H.D. (2009). The plasticity of a translation arrest motif yields insights into nascent polypeptide recognition inside the ribosome tunnel. *Mol Cell* 34, 201-211.
- Youngman, E.M., Brunelle, J.L., Kochaniak, A.B., and Green, R. (2004). The active site of the ribosome is composed of two layers of conserved nucleotides with distinct roles in peptide bond formation and peptide release. *Cell* 117, 589-599.
- Youngman, E.M., He, S.L., Nikstad, L.J., and Green, R. (2007). Stop codon recognition by release factors induces structural rearrangement of the ribosomal decoding center that is productive for peptide release. *Mol Cell* 28, 533-543.
- Yu, B.J., Kim, J.A., Moon, J.H., Ryu, S.E., and Pan, J.G. (2008). The diversity of lysine-acetylated proteins in *Escherichia coli*. *J Microbiol Biotechnol* 18, 1529-1536.
- Yusupova, G., Jenner, L., Rees, B., Moras, D., and Yusupov, M. (2006). Structural basis for messenger RNA movement on the ribosome. *Nature* 444, 391-394.
- Zaher, H.S., Shaw, J.J., Strobel, S.A., and Green, R. (2011). The 2'-OH group of the peptidyl-tRNA stabilizes an active conformation of the ribosomal PTC. *EMBO J* 30, 2445-2453.
- Zahn, M., Berthold, N., Kieslich, B., Knappe, D., Hoffmann, R., and Strater, N. (2013). Structural studies on the forward and reverse binding modes of peptides to the chaperone DnaK. *Journal of molecular biology* 425, 2463-2479.
- Zahn, M., Kieslich, B., Berthold, N., Knappe, D., Hoffmann, R., and Strater, N. (2014). Structural identification of DnaK binding sites within bovine and sheep bactenecin Bac7. *Protein Pept Lett* 21, 407-412.

- Zasloff, M. (2002). Antimicrobial peptides in health and disease. *N Engl J Med* 347, 1199-1200.
- Zavialov, A.V., Buckingham, R.H., and Ehrenberg, M. (2001). A posttermination ribosomal complex is the guanine nucleotide exchange factor for peptide release factor RF3. *Cell* 107, 115-124.
- Zavialov, A.V., Hauryliuk, V.V., and Ehrenberg, M. (2005). Splitting of the posttermination ribosome into subunits by the concerted action of RRF and EF-G. *Mol. Cell* 18, 675-686.
- Zhang, W., Dunkle, J.A., and Cate, J.H. (2009). Structures of the ribosome in intermediate states of ratcheting. *Science* 325, 1014-1017.
- Zhou, J., Korostelev, A., Lancaster, L., and Noller, H.F. (2012a). Crystal structures of 70S ribosomes bound to release factors RF1, RF2 and RF3. *Curr Opin Struct Biol* 22, 733-742.
- Zhou, J., Lancaster, L., Donohue, J.P., and Noller, H.F. (2013). Crystal structures of EF-G-ribosome complexes trapped in intermediate states of translocation. *Science* 340, 1236086.
- Zhou, J., Lancaster, L., Donohue, J.P., and Noller, H.F. (2014). How the ribosome hands the A-site tRNA to the P site during EF-G-catalyzed translocation. *Science* 345, 1188-1191.
- Zhou, J., Lancaster, L., Trakhanov, S., and Noller, H.F. (2012b). Crystal structure of release factor RF3 trapped in the GTP state on a rotated conformation of the ribosome. *RNA* 18, 230-240.
- Zoldak, G., Redecke, L., Svergun, D.I., Konarev, P.V., Voertler, C.S., Dobbek, H., Sedlak, E., and Sprinzl, M. (2007). Release Factors 2 from *Escherichia coli* and *Thermus thermophilus*: structural, spectroscopic and microcalorimetric studies. *Nucleic acids research*.
- Zucker, F.H., and Hershey, J.W.B. (1986). Binding of *Escherichia coli* protein synthesis initiation factor IF1 to 30S ribosomal subunits measured by fluorescence polarization. *Biochemistry* 25, 3682-3690.

6 Publications

2015

1. **Stefan Arenz**, C. Axel Innis, Roland Beckmann and Daniel N. Wilson (2015). Alternate conformation of a nascent chain in the ribosomal tunnel induces P-tRNA perturbation and inhibition of peptide bond formation.
Unpublished manuscript.
2. A. Carolin Seefeldt*, Fabian Nguyen*, Stéphanie Antunes*, Natacha Pérébasquine, Michael Graf, **Stefan Arenz**, Kishore K. Inampudi, Céline Douat, Gilles Guichard, Daniel N. Wilson and C. Axel Innis (2015). The proline-rich antimicrobial peptide Onc112 inhibits translation by blocking and destabilizing the post-initiation complex.
Nature Structural & Molecular Biology. 10.1038/nsmb.3034.

*These authors contributed equally to this work.

2014

3. **Stefan Arenz**, Sezen Meydan, Agata L. Starosta, Otto Berninghausen, Roland Beckmann, Nora Vázquez-Laslop and Daniel N. Wilson (2014). Drug Sensing by the Ribosome Induces Translational Arrest via Active Site Perturbation.
Molecular Cell. 56, 446-452.
4. **Stefan Arenz**, Fabian Nguyen, Roland Beckmann and Daniel N. Wilson (2014). Cryo-EM structure of the tetracycline resistance protein TetM in complex with a translating ribosome at 3.9 Å resolution.
Proceedings of the National Academy of Sciences. 112, 5401-5406.
5. **Stefan Arenz**, Haripriya Ramu, Pulkit Gupta, Otto Berninghausen, Roland Beckmann, Nora Vázquez-Laslop, Alexander S. Mankin and Daniel N. Wilson (2014). Molecular basis for erythromycin-dependent ribosome stalling during translation of the ErmBL leader peptide.
Nature Communications. 5: 3501.
6. Fabian Nguyen, Agata L. Starosta, **Stefan Arenz**, Daniel Sohmen, Alexandra Dönhöfer and Daniel N. Wilson (2014). Tetracycline antibiotics and resistance mechanisms.
Biological Chemistry. 395, 559-575.
7. Konstantin Byrgazov, Irina Grishkovskaya, **Stefan Arenz**, Nicolas Coudevylle, Hannes Temmel, Daniel N. Wilson, Kristina Djinovic-Carugo and Isabella Moll (2014). Structural basis for the interaction of protein S1 with the *Escherichia coli* ribosome.
Nucleic Acids Research. 43, 661-673.

Structural basis for the interaction of protein S1 with the *Escherichia coli* ribosome

Konstantin Byrgazov¹, Irina Grishkovskaya², Stefan Arenz³, Nicolas Coudeville², Hannes Temmel¹, Daniel N. Wilson³, Kristina Djinovic-Carugo^{2,4} and Isabella Moll^{1,*}

¹Department of Microbiology, Immunobiology and Genetics, Max F. Perutz Laboratories, Centre for Molecular Biology, University of Vienna, Dr. Bohrgasse 9/4, 1030 Vienna, Austria, ²Department of Structural and Computational Biology, Max F. Perutz Laboratories, Centre for Molecular Biology, University of Vienna, Campus Vienna Biocenter 5, A-1030 Vienna, Austria, ³Gene Center, Department of Biochemistry and Center for Integrated Protein Science Munich (CiPSM), Ludwig-Maximilians-Universität München, Feodor-Lynen-Strasse 25, 81377 Munich, Germany and ⁴Department of Biochemistry, Faculty of Chemistry and Chemical Technology, University of Ljubljana, Aškerčeva 5, 1000 Ljubljana, Slovenia

Received September 08, 2014; Revised November 21, 2014; Accepted December 04, 2014

ABSTRACT

In Gram-negative bacteria, the multi-domain protein S1 is essential for translation initiation, as it recruits the mRNA and facilitates its localization in the decoding centre. In sharp contrast to its functional importance, S1 is still lacking from the high-resolution structures available for *Escherichia coli* and *Thermus thermophilus* ribosomes and thus the molecular mechanism governing the S1–ribosome interaction has still remained elusive. Here, we present the structure of the N-terminal S1 domain D1 when bound to the ribosome at atomic resolution by using a combination of NMR, X-ray crystallography and cryo-electron microscopy. Together with biochemical assays, the structure reveals that S1 is anchored to the ribosome primarily via a stabilizing π -stacking interaction within the short but conserved N-terminal segment that is flexibly connected to domain D1. This interaction is further stabilized by salt bridges involving the zinc binding pocket of protein S2. Overall, this work provides one hitherto enigmatic piece in the ‘ribosome puzzle’, namely the detailed molecular insight into the topology of the S1–ribosome interface. Moreover, our data suggest novel mechanisms that have the potential to modulate protein synthesis in response to environmental cues by changing the affinity of S1 for the ribosome.

INTRODUCTION

During the last decades the bacterial ribosome was at the centre of numerous research efforts that made great strides

in elucidating the structure of the translational machinery and the process of protein synthesis at the molecular level. In sharp contrast, protein S1, which is essential for translation initiation in Gram-negative bacteria (1), is still lacking from the high-resolution structures available for *Escherichia coli* and *Thermus thermophilus* ribosomes (2). The protein associates late during assembly of the 30S ribosomal subunit (3) and interacts with a pyrimidine-rich region in the 5′ untranslated region (5′UTR) of mRNAs (4). Here, S1 unwinds RNA structures by binding to single-stranded RNA during thermal breathing (5). Thus, the protein shows RNA chaperone activity (6) and is essential for the binding and the accommodation of structured mRNAs into the decoding channel (7). Notably, S1 is dispensable for translation of leaderless mRNAs (lmRNAs) that lack a 5′UTR and hence harbour a 5′-terminal AUG start codon (8,9).

Structurally, S1 is composed of six contiguous domains (D1–D6; Figure 1A), which are connected via linkers providing the flexibility that is likely to play a role in recruitment of mRNA transcripts to the ribosome (10). The structural organization of the single C-terminal domains (D3–D6; Figure 1A), which interact with ssRNA (4,11), was modelled for D3, D4 and D5 (12) and, later on, solved at atomic resolution for D4 and D6 (13). Each of these domains displays an oligosaccharide–oligonucleotide binding (OB)-fold, consisting of two three-stranded antiparallel β -sheets, where strand 1 is shared by both sheets, with an α -helix that packs against the bottom of the barrel, typically oriented lengthwise along the long axis of the β -barrel (14). Immune-electron microscopic studies revealed that domains D3–D6 extend from the platform side of the 30S subunit where the 5′-end of the mRNA would be located (15). In contrast, the two N-terminal domains (D1, D2; Figure 1A) have no detectable RNA-binding activity but rather provide the boundary to the ribosome (11,16). In contrast

*To whom correspondence should be addressed. Tel: +43 1 4277 54606; Fax: +43 1 4277 9546; Email: Isabella.Moll@univie.ac.at

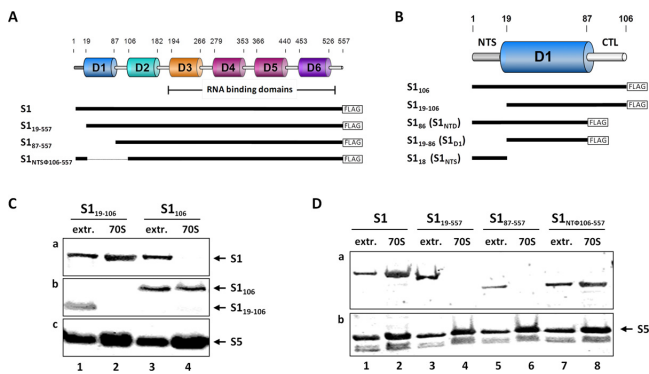


Figure 1. The N-terminal segment is essential for protein S1 to interact with the ribosome *in vivo*. (A) Schematic of the domain organization of protein S1 and the C-terminally FLAG-tagged S1 variants used in the study. (B) The N-terminal domain D1 of protein S1 including the flexible N-terminal segment (NTS) and the C-terminal linker (CTL) is enlarged, and its variants used in the study are depicted below. (C) Equimolar amounts of S30 extracts (lanes 1 and 3) and 70S ribosomes (lanes 2 and 4) purified from *E. coli* strain JE28 synthesizing protein S1_{19–106} (lanes 1 and 2) or protein S1₁₀₆ (lanes 3 and 4) were analysed for the presence of native S1 (panel a) and proteins S1₁₀₆ and S1_{19–106} (panel b) by western blotting using antibodies directed against S1₁₀₆ (18). Western blotting of protein S5 served as loading control (panel c). (D) Equal amounts of S30 extracts (extr.; lanes 1, 3, 5 and 7) and ribosomes (70S; lanes 2, 4, 6 and 8) purified from *E. coli* strain JE28 upon synthesis of FLAG-tagged proteins S1 (lanes 1 and 2), S1_{19–557} (lanes 3 and 4), S1_{87–557} (lanes 5 and 6) or S1_{NTD106–557} (lanes 7 and 8) were analysed for the presence of the respective proteins by western blotting employing anti-FLAG antibodies (panel a). Protein S5 served as loading control (panel b).

to studies that suggest a potential interaction of S1 with the 16S rRNA ((17) and references therein), several lines of evidence indicate that the N-terminal region of S1 comprising 106 amino acids (S1₁₀₆) is sufficient to ensure its assembly to the 30S ribosomal subunit (10,18) by means of protein–protein interactions *via* protein S2 (9,19).

Besides its pivotal role in protein synthesis, S1 acts as a host factor component of the replicase holoenzyme of the bacteriophage Q β (20). Interestingly, this function can be performed by the N-terminal part of the protein comprising domains D1 and D2 (21). During the preparation of this manuscript the structure of the Q β replicase comprising the β -subunit, EF-Tu, EF-Ts and the N-terminal half of S1 was published revealing that domains D1 and D2 function to anchor S1 on the β -subunit (22). However, the structure of S1 when assembled to the ribosome is unknown. Due to the intrinsic flexibility of the protein, ribosomes were intentionally depleted for S1 to facilitate the crystallization process for structural analyses (2). Thus, the molecular mechanism governing the S1-ribosome interaction has still remained elusive. Nevertheless, the *E. coli* S1 protein was tentatively localized on the ribosome based on difference electron density maps between a cryo-electron microscopy (EM) structure of the *E. coli* 70S ribosome containing S1 and a map based on the crystal structure of the *T. thermophilus* 30S that lacked S1 (23). The results suggested that S1 binds within the cleft at the base of the small subunit head and platform; however, the limited resolution prevented any molecular interpretation.

Here, we present the first crystal structure of the N-terminal domain of protein S1 (comprising 86 amino acid residues; hereafter referred to as S1_{NTD}; Figure 1B) in complex with protein S2 at 2.4–3 Å resolution, showing detailed insights into the molecular basis of the S1–ribosome interaction. In addition, we have visualized S1 bound to the ribosome using cryo-EM underpinning the S1–S2 interaction observed in the crystal structure. Together with functional analyses, we demonstrate that a short, but highly conserved, N-terminal segment is the primary ribosome anchoring point for S1. This interaction is further stabilized by salt bridges between the globular fold of S1_{NTD} and S2. Notably, the structure shows that the anchoring helix is connected by a flexible hinge region with domain D1, which mechanistically supports the dynamic movement of S1 when bound to the 30S subunit. Moreover, our functional studies suggest potential mechanisms, which might fine tune the affinity of S1 for the ribosome in response to environmental cues.

MATERIALS AND METHODS

Bacterial strains and plasmids

Escherichia coli strains, plasmids and oligonucleotides used in this study are listed in the Supplementary Tables S1 and S2. Unless otherwise indicated, bacterial cultures were grown in Luria–Bertani (LB) medium supplemented with ampicillin (100 μ g/ml). When appropriate, kanamycin (20 μ g/ml) was added. Growth was monitored by measuring the optical density at 600 nm (OD₆₀₀).

Construction of plasmids

The sequence encoding the HA-tagged version of protein S2 was amplified by polymerase chain reaction (PCR) using primers P1 and P2 employing genomic DNA of *E. coli* strain MG1655 as a template. The respective products were cleaved with NarI and XhoI and cloned under control of the Trc promoter in the corresponding sites of plasmid pProEX–Htb (Life Technologies) resulting in plasmid pProEX–S2–HA. To generate plasmid pProEX–S2–S1_{NTD} for expression of the chimeric protein S2–S1_{NTD}, the sequence encoding protein S1₈₆ was amplified with primers P3 and P4. The PCR product was cleaved with HindIII and ligated between the two HindIII-sites of the plasmid pProEX–S2–HA. Plasmid pPro-S1F (18) was used as a template to construct plasmid pPro-S1_{NTS106–557}F. The coding sequence for the S1 domain D1 was removed employing the Phusion site-directed mutagenesis kit (NEB) using 5'-monophosphorylated primers P5 and P6. Plasmids pPro-S1F and pPro-S1₁₀₆F (18) were used as templates to construct plasmids pPro-S1_{19–557}F and pPro-S1_{19–106}F. The coding sequence for the N-terminal 18 amino acids was removed employing the Phusion site-directed mutagenesis kit (NEB) using 5'-monophosphorylated primers P7 and P8. Plasmids pPro-S1₁₀₆F and pPro-S1_{19–106}F were used as templates to construct plasmids pPro-S1₈₆F and pPro-S1_{19–86}F. The coding sequence for the C-terminal 18 amino acids was removed employing the Phusion site-directed mutagenesis kit (NEB) using 5'-monophosphorylated primers P9 and P10. The plasmid pPro-S1₈₆F was used as a template to

construct plasmids pPro-S1₈₆F encoding variants of S1_{NTD} harbouring the F5A, F9A, D39K and K43E mutations. The respective mutations were introduced employing the Phusion site-directed mutagenesis kit (NEB) using the 5'-monophosphorylated primers P15/P17, P16/P17, P18/P20 and P19/P20, respectively. The sequences encoding proteins S1₁₀₆, S1₈₆ and S1₁₉₋₈₆ were amplified by PCR employing pairs of primers P11/P13, P11/P14 and P12/P14 respectively. The respective products were cleaved with NdeI and XhoI and cloned under control of the T7 promoter in the corresponding sites of plasmid pET22b (Novagen) yielding plasmids pET-S1₁₀₆, pET-S1₈₆ and pET-S1₁₉₋₈₆. All constructs were verified by sequencing (Microsynth).

Overexpression and purification of the chimeric protein S2-S1_{NTD}

Escherichia coli strain Tuner harbouring plasmid pProEX-S2-S1_{NTD} was grown in LB medium at 37°C. Expression of the *rpsB-rpsA_{NTD}* fusion gene was induced by addition of 1 mM Isopropyl-D-thiogalactopyranoside (IPTG). The HIS-tagged chimeric protein S2-S1_{NTD} was purified with the TALON cobalt resin (Clontech) and subsequently treated with AcTEV-protease (Life Technologies) and purified via a HiLoad 26/60 Superdex 200 column (GE Healthcare) to remove the His-tag using a buffer containing 100 mM HEPES (2-[4-(2-hydroxyethyl)piperazin-1-yl]ethanesulfonic acid)-KOH, (Potassium hydroxide) pH 7.4, 6 mM MgCl₂ and 200 mM KCl. The fractions containing the chimeric protein were concentrated with an Amicon ultra centrifugal filter unit (MWCO of 30 kDa; Millipore).

Crystallization, data collection, structure determination and refinement

Crystals of the S2-S1_{NTD} chimeric construct were initially obtained in the crystallization screen JBScreen 7 (Jena Bioscience), using the sitting-drop vapor diffusion technique and a nanodrop-dispensing robot (Phoenix RE; Rigaku Europe, Kent, United Kingdom). Crystallization conditions were optimized to 0.1 M HEPES-KOH, pH 7.4, 3 mM MgCl₂, 7.5% (w/v) PEG 6000, 3% (w/v) 2-methylpentanediol-2,4, 100 mM KCl using the hanging drop vapor diffusion technique at 22°C. The crystals were flash cooled in liquid nitrogen prior to data collection. The data set has been collected at the beamline I04 of the Diamond Light Source at 100 K using a wavelength of 0.98 Å. The data frames were processed using the XDS package (24), and converted to the mtz format with the program AIMLESS (25). In assessing the data quality and establishing the resolution cutoff we relied on criteria based on the correlation coefficient CC1/2 (26). The structure was solved by using the molecular replacement pipeline program BALBES (27), the log file indicated that atomic coordinates of S2 from 30S subunit of *E. coli* (pdb accession code: 2qbf, chain B) and the fragment of hypothetical protein PA5201 from *P. aeruginosa* (pdb accession code: 2oce) were yielded in solution. About 90% of the model was placed using the program AUTOBUILD from Phenix software package (28). The structure was then refined with the REFMAC (29) and Phenix Refine (28) and finally, the rebuilding of structure was done

Table 1. Data collection and refinement statistics

Data collection	
Source	I04, Diamond
Wavelength (Å)	0.98
Resolution (Å)	37.79–2.30 (2.38–2.30) ^a
Space group	P3 ₁ 21
Unit cell (Å, °)	a = b = 87.28 c = 94.36; α = γ = 90; β = 120
Molecules (a.u.)	1
Unique reflections	18 726 (1670)
Completeness (%)	99.0 (91.3)
R _{merge} ^b	0.175 (1.106)
R _{meas} ^c	0.186 (1.238)
R _{pim} ^d	0.063 (0.543)
Multiplicity	8.1 (4.5)
I/sig(I)	7.4 (1.5)
CC (1/2)	0.993 (0.548)
B _{Wilson} (Å ²)	22.1
Refinement	
R _{cryst} ^e /R _{free} ^f (%)	16.3/22.8
rmsd bonds (Å)	0.008
rmsd angles (°)	1.09

^aValues in parentheses are for the highest resolution shell.

$${}^b R_{\text{merge}} = \frac{\sum_{hkl} \sum_{i=1}^N |I_{i(hkl)} - \bar{I}_{(hkl)}|}{\sum_{hkl} \sum_{i=1}^N I_{i(hkl)}}$$

$${}^c R_{\text{meas}} = \frac{\sum_{hkl} \sqrt{N/(N-1)} \sum_{i=1}^N |I_{i(hkl)} - \bar{I}_{(hkl)}|}{\sum_{hkl} \sum_{i=1}^N I_{i(hkl)}}$$

$${}^d R_{\text{pim}} = \frac{\sum_{hkl} \sqrt{1/(N-1)} \sum_{i=1}^N |I_{i(hkl)} - \bar{I}_{(hkl)}|}{\sum_{hkl} \sum_{i=1}^N I_{i(hkl)}}$$

Where $\bar{I}_{(hkl)}$ is the mean intensity of multiple $I_{i(hkl)}$ observations of the symmetry-related reflections, N is the redundancy.

$${}^e R_{\text{cryst}} = \frac{\sum |F_{\text{obs}} - |F_{\text{calc}}||}{\sum |F_{\text{obs}}|}$$

^fR_{free} is the cross-validation R_{factor} computed for the test set of reflections (5%) which are omitted in the refinement process.

using the program Coot (30). Stereochemistry and structure quality were also checked using the program MolProbity (31). The figures were produced using the Pymol software (32). Coordinates have been deposited in the protein data bank (pdb accession code: 4toi). Data collection and refinement statistics are reported in Table 1.

Purification of ribosomal subunits

Ribosomal subunits were purified based on the His-tagged proteins L7/L12 employing Ni-NTA-agarose (33). Briefly, *E. coli* strain JE28 was grown in LB medium supplemented with kanamycin (20 µg/ml). At OD₆₀₀ 0.7–0.9 the culture was harvested by centrifugation at 5000g for 20 min at 4°C. The cell pellet was resuspended in lysis buffer (20 mM Tris-HCl, pH 7.4, 10 mM MgCl₂, 30 mM NH₄Cl, 100 mM KCl, 10 mM Imidazole, 1 unit/ml RNase-free DNase I (Roche), 0.1 mM PMSF (phenylmethanesulfonyl fluoride)). The cells were disrupted by three freeze and thaw cycles and the lysate was cleared by centrifugation at 15 000g for

20 min at 4°C. The extracts were applied to 10 ml of Ni-NTA-agarose (QIAGEN) pre-equilibrated in lysis buffer, and washed by 10 column volumes of washing buffer (20 mM Tris·HCl, pH 7.4, 10 mM MgCl₂, 30 mM NH₄Cl, 150 mM KCl, 20 mM Imidazole). Thereafter, the Ni-NTA-agarose was resuspended in 10 column volumes of dissociation buffer (20 mM Tris·HCl, pH 7.4, 1 mM MgCl₂, 30 mM NH₄Cl, 150 mM KCl, 20 mM Imidazole) and incubated for 8 h at 4°C. The flow-through fractions that contain the 30S ribosomal subunits were collected and the Mg²⁺ concentration was adjusted to 10 mM. The tetra-His-tagged 50S subunits were eluted by 10 column volumes of elution buffer (20 mM Tris·HCl, pH 7.4, 10 mM MgCl₂, 30 mM NH₄Cl, 150 mM KCl, 150 mM Imidazole). The fractions containing ribosomal subunits were dialysed against tight-couple (TICO) buffer (20 mM HEPES–HCl pH 7.6, 6 mM MgCl₂, 30 mM NH₄Cl and 4 mM β-mercaptoethanol) and concentrated using Amicon filter devices (MWCO of 100 kDa; Millipore). Protein S1-depleted 30S ribosomes were prepared by affinity chromatography using poly(U)-Sepharose 4B (Pharmacia) (34).

Co-purification of tetra-His-tagged ribosomes with FLAG-tagged protein S1 variants

Escherichia coli strain JE28 cells harbouring plasmids pProEX-HTb, pPro-S1₈₆F, pPro-S1₁₀₆F, pPro-S1_{19–86}F, pPro-S1_{19–106}F, pPro-S1F, pPro-S1_{19–557}F, pPro-S1_{87–557}F, pPro-S1_{NTSΦ106–557}F, pPro-S1₈₆F_{F5A}, pPro-S1₈₆F_{F9A}, pPro-S1₈₆F_{D39K} and pPro-S1₈₆F_{K43E} were grown in LB broth supplemented with 100 μg/ml ampicillin, 20 μg/ml kanamycin and 0.5% (w/v) glucose. The synthesis of FLAG-tagged protein S1 variants was induced by addition of 0.1 mM IPTG at OD₆₀₀ of 0.30–0.35. One hour thereafter the cells were harvested by centrifugation and lysed by three freeze and thaw cycles in lysis buffer containing 20 mM Tris·HCl, pH 7.4, 10 mM MgCl₂, 30 mM NH₄Cl, 100 mM KCl, 10 mM Imidazole, 0.1 mM PMSF, 1 unit/ml RNase-free DNase I (Roche). After centrifugation at 30 000g for 30 min at 4°C, the extracts were applied to the Ni-NTA agarose (QIAGEN), washed by 10 column volumes of washing buffer (20 mM Tris·HCl, pH 7.4, 10 mM MgCl₂, 30 mM NH₄Cl, 150 mM KCl, 20 mM Imidazole) followed by elution with a buffer containing 20 mM Tris·HCl, pH 7.4, 10 mM MgCl₂, 30 mM NH₄Cl, 150 mM KCl, 150 mM Imidazole. The protein composition of the ribosomes was determined by western blot analysis using anti-FLAG (Abcam), anti-S1₁₀₆ and anti-S5 antibodies.

Purification of ¹⁵N-labelled proteins S1₁₀₆, S1₈₆ and S1_{19–86}

Escherichia coli strain Tuner (DE3) harbouring plasmids pET-S1₁₀₆, pET-S1₈₆ and pET-S1_{19–86} were grown in M9 minimal medium supplemented with ¹⁵NH₄Cl (Sigma, 1 g/l) and 100 μg/ml ampicillin. The synthesis of the respective proteins was induced by addition of 1 mM IPTG at OD₆₀₀ of 0.8–0.9. Two hours thereafter the cells were harvested by centrifugation and lysed by three freeze and thaw cycles in lysis buffer containing 50 mM Na₂HPO₄, pH 8.0, 300 mM NaCl, 10 mM Imidazole, 0.1% Tween-20, 0.5 mg/ml DNase I (Roche), 20 μg/ml RNase A. After centrifugation at 4°C, 30.000g for 30 min, the S30 extracts were

applied to a Ni-NTA agarose, washed by 10 column volumes of washing buffer (50 mM Na₂HPO₄, pH 8.0, 500 mM NaCl, 20 mM Imidazole) followed by elution with elution buffer (50 mM Na₂HPO₄, pH 8.0, 300 mM NaCl, 250 mM imidazole). The eluted fractions were dialysed against phosphate buffered saline (PBS) buffer and a size exclusion fast protein liquid chromatography (FPLC) was performed on a HiLoad Sephadex 75 16/60 column (GE Healthcare). The purified proteins were concentrated using Amicon filter devices (MWCO of 3 kDa; Millipore).

Purification of protein S2-HA

Escherichia coli strain Tuner harbouring plasmid pProEX-S2-HA was grown in M9 minimal medium supplemented with 100 μg/ml ampicillin. The synthesis of protein S2-HA was induced by addition of 0.1 mM IPTG at OD₆₀₀ of 0.5–0.6. Four hours later, the cells were harvested and lysed by three freeze and thaw cycles in lysis buffer containing 50 mM HEPES–KOH, pH 7.4, 3 mM MgCl₂, 200 mM KCl, 10 mM imidazole, 0.1% Tween-20, 0.5 mg/ml DNase I (Roche), 20 μg/ml RNase A. After centrifugation at 100 000g for 30 min at 4°C, the supernatant was applied to Ni-NTA agarose, washed by 10 column volumes of washing buffer (50 mM HEPES–KOH, pH 7.4, 3 mM MgCl₂, 250 mM KCl, 10% (w/v) glycerol, 20 mM imidazole) followed by elution with elution buffer (50 mM HEPES–KOH, pH 7.4, 3 mM MgCl₂, 200 mM KCl, 200 mM imidazole). The eluted proteins were dialysed against 50 mM HEPES–KOH, pH 7.4, 3 mM MgCl₂, 150 mM KCl.

Co-purification analysis

Purified protein S2–HA was incubated with S100 extracts prepared from the *E. coli* strain Tuner over-expressing the different *rpsA* genes as follows. *Escherichia coli* cells carrying the plasmids pProEX-HTb, pPro-S1_{19–86}F or plasmids pPro-S1₈₆F containing the different point mutations (WT, F5A, F9A, D39K or K43E) were grown in LB-Amp (100 μg/ml). 30 min after addition of 0.1 mM IPTG at OD₆₀₀ of 0.4–0.5 the cells were harvested and lysed by three freeze and thaw cycles in lysis buffer (50 mM HEPES–KOH, pH 7.4, 3 mM MgCl₂, 200 mM KCl, 0.1% Tween-20, 0.5 mg/ml DNase I (Roche)). After centrifugation at 100 000g for 60 min at 4°C, the amount of S1 protein variants was determined by quantitative western blotting. The extracts were combined with equimolar amounts of protein S2–HA and incubated at 37°C for 30 min. Co-immunoprecipitation was performed employing anti-ECS antibodies (Bethyl) covalently linked to protein A magnetic beads (Life Technologies). After three washing cycles (50 mM HEPES–KOH, pH 7.4, 3 mM MgCl₂, 100 mM KCl) the proteins were eluted from the beads by boiling in Laemmli buffer, separated on sodium dodecyl sulphate-polyacrylamide gel electrophoresis (SDS-PAGE) and analysed by western blotting employing anti-FLAG (Abcam), anti-HA (Sigma) and anti-S1₁₀₆ antibodies.

Generation and purification of ErmCL-SRC

The 2*XermCL* construct was synthesized (Eurofins, Martinsried, Germany) such that it contained a T7 promoter

followed by a strong ribosome binding site (RBS) spaced by seven nucleotides (nts) to the ATG start codon of the first *ermCL* cistron. A linker of 22 nts separated the stop codon of the first *ermCL* cistron and the start codon of the second *ermCL* cistron. The linker also comprised the strong RBS 7 nts upstream of the ATG start codon of the second *ermCL* cistron, enabling initiation of translation independent from the first *ermCL* cistron. Each *ermCL* cistron encoded amino acids 1–19 corresponding to ErmCL leader peptide (GenBank accession number: V01278) present on macrolide resistance plasmid pE194 (35). The complete sequence of 2*XermCL* construct is:

5'-TAATACGACTCACTATAGGGAGTTTTATAAG
GAGGAAAAAATatgggcatttttagtattttgtaatcagcacagtta
ttataaccaacaaaaataaAGTTTTATAAGGAGGAAAA
AATatgggcatttttagtattttgtaatcagcacagttcattatcaacaaa
caaaaaataa-3' (T7 promoter, italics; RBS, bold; ErmCL
ORF, small letters with GTA codon in P-site of stalled
ribosome shown in bold; Annealing site for complementary
DNA oligonucleotide, underlined). *In vitro* translation of
the 2*xermCL* construct was performed using the Rapid
Translation System RTS 100 *E. coli* HY Kit (Roche; Cat.
no. 3246817). Translations were carried-out in the presence
of 10 μ M erythromycin (ERY) for 1 h at 30°C. Control
reactions were performed in the absence of erythromycin
as well as using a monocistronic *ermCL* construct. Transla-
tion reactions were analysed on sucrose density gradients
(10–55% sucrose in a buffer A, containing 50 mM HEPES-
KOH, pH 7.4, 100 mM KOAc, 25 mM Mg(OAc)₂, 6 mM
 β -mercaptoethanol, 10 μ M erythromycin and 1 \times Com-
plete EDTA-free Protease Inhibitor cocktail (Roche)) by
centrifugation at 154 693g (SW-40 Ti, Beckman Coulter)
for 2.5 h at 4°C. For ErmCL–SRC purification, disome
fractions were collected using a Gradient Station (Bio-
comp) with an Econo UV Monitor (Biorad) and a FC203B
Fraction Collector (Gilson). Purified ErmCL–SRC disomes
were concentrated by centrifugation through Amicon
Ultra-0.5 ml Centrifugal Filters (Millipore) according
to the manufacturer's protocol. To obtain monosomes
of the ErmCL–SRC, a short DNA oligonucleotide (5'-
ttcctcctataaaact-3', Metabion) was annealed to the linker
between the *ermCL* cistrons of the disomes, generating
a DNA–RNA hybrid that could be cleaved by RNase H
(NEB) treatment at 25°C for 1 h.

Negative-stain electron microscopy

Ribosomal particles were diluted in buffer A to a final concentration of 0.5 A₂₆₀/ml. One drop of each sample was deposited on a carbon-coated grid. After 30 s, grids were washed with distilled water and then stained with three drops of 2% aqueous uranyl acetate for 15 s. The remaining liquid was removed by touching the grid with filter paper. Micrographs were taken using a Morgagni transmission electron microscope (FEI), 80 kV, wide angle 1 K CCD at direct magnifications of 72 K. The negative stain electron microscopy was used to prescreen the samples and ensure that the concentration was accurate to obtain an optimal density and distribution of ribosomal particles for the cryo-grids.

Cryo-electron microscopy and single particle reconstruction

Monosomes of the ErmCL–SRC were applied to 2 nm pre-coated Quantifoil R3/3 holey carbon supported grids and vitrified using a Vitrobot Mark IV (FEI Company). Data collection was performed on a Titan Krios transmission electron microscope (TEM) (FEI, Netherlands) under low-dose conditions (~ 20 e⁻/Å²) at a nominal magnification of 75 000 \times with a nominal defocus between -1 and -3.5 μ m. Images were collected at 200 keV at a magnification of 148 721 \times at the plane of CCD using a TemCam-F416 CMOS camera (TVIPS GmbH, 4096 \times 4096 pixel, 15.6 μ m pixel, 1 s/full frame), resulting in an image pixel size of 1.0489 Å (object scale). Data collection was facilitated by the semi-automated software EM-TOOLS (TVIPS GmbH) as described (36). Contrast-transfer functions were determined using the SPIDER TF ED command and recorded images were manually inspected for good areas and power-spectra quality. Data were processed further using the SPIDER software package (37), in combination with an automated workflow as described previously (36). After initial, automated particle selection based on the program SIGNATURE (38) initial alignment was performed with 624 304 particles, using *E. coli* 70S ribosome as a reference structure (39). After removal of noisy particles (76 346 particles; 12%) and non-aligning particles (271 873 particles; 44%), the dataset could be sorted into two main subpopulations: The first subpopulation (153 240 particles; 25%) was defined by the presence of non-stoichiometric densities for tRNAs in the A-, and P-sites. The second, homogeneous subpopulation was defined by the absence of density for the A-tRNA and the presence of stoichiometric density for the P-tRNA (128 846 particles; 21%). This major subpopulation could be refined to an average resolution of 7.9 Å according to the Fourier Shell Correlation (FSC at a cut-off value of 0.5).

Molecular modeling and map-docking procedures

The crystal structure of the 30S subunit (pdb accession code: 3ofo) of the *E. coli* 70S ribosome (40) was fitted as a rigid body into the cryo-EM density map of the ErmCL–SRC using UCSF Chimera (41) (fit in map function). The molecular model for S1_{D1} was based on the crystal structure of the S2–S1_{NTD} complex (Figure 2) and the C-terminus of S1 was extended (amino acids V68–A105) based on a homology model generated by HHPred (42) using the crystal structure of eIF2 α as a template (pdb accession code: 1kl9 (43)). Upon alignment of S2 of the S2–S1_{NTD} complex to S2 of *E. coli* 30S subunit (pdb accession code: 3ofo (40)), S1_{D1} fitted nicely into additional density on the ErmCL–ribosome complex (Figure 3C). The final model was adjusted manually using Coot (30) to fit the density of the ErmCL–ribosome map. Crystal structures of 30S subunits from *T. thermophilus* (pdb accession code: 1j5e (44)) and *E. coli* (pdb accession code: 3ofo (40)) were filtered to comparable resolutions using the Molmap function in Chimera. Difference electron density maps were then calculated in SPIDER (37) by subtracting the filtered map for *T. thermophilus* 30S subunit (pdb accession code: 1j5e (44)) or *E. coli* 30S subunit (pdb accession code: 3ofo (40)) from either EMD-1003 (45) or the ErmCL–SRC map (Supplementary Figure S4A–D).

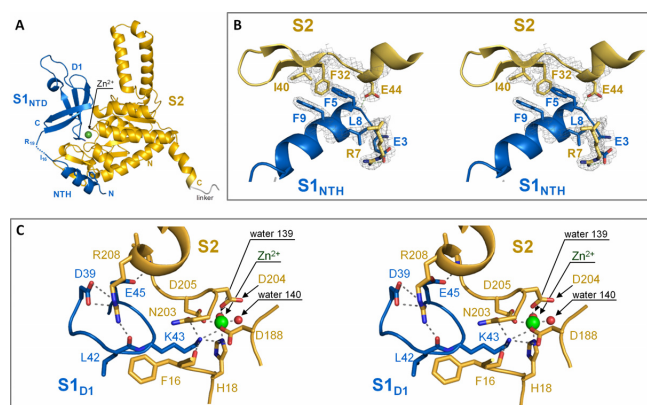


Figure 2. Interaction between S1_NTD and protein S2. (A) Overview showing the S2–S1_NTD complex structure assembled from two protomers, with S1_NTD in blue, S2 in yellow. Zn²⁺ is depicted as a green sphere. This colour code is used throughout the figures. (B) Stereo view showing the close up of the π -stacking interaction with the aromatic ring of Phe32 of protein S2 with Phe5 and Phe9 of S1_NTD. (C) Stereo view showing the salt bridge interactions between the core domain S1_{D1} and the globular domain of S2 involving the Zn²⁺ binding pocket. The water molecules involved in the coordination of the Zn²⁺ ion are shown as red spheres.

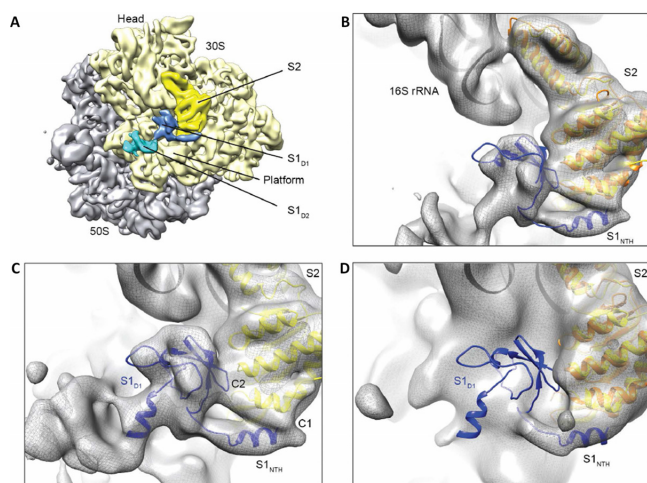


Figure 3. Binding position of S1 on the *E. coli* 70S ribosome. (A) Cryo-EM structure of a translating *E. coli* 70S ribosome containing additional density for domain 1 (S1_{D1}, blue) and domain 2 (S1_{D2}, cyan) of ribosomal protein S1. Density for the large (grey) and small (pale yellow) ribosomal subunit, together with ribosomal protein S2 (bright yellow) is indicated. (B) Initial model for the position of S1_NTD obtained by aligning S2 (yellow) of the chimeric S2–S1_NTD with S2 (orange) from an *E. coli* 30S subunit (pdb accession code: 3of0 (40)) fitted to the cryo-EM map (grey mesh) as a rigid body. (C) Refined model for the complete S1_NTD based on homology with eIF2 α (pdb accession code: 1kl9 (43)) and fitted so as to maintain interactions between S1 and S2 as observed in the chimeric crystal structure, but also constrained by the electron density of the cryo-EM map (grey mesh). (D) The position of S1_NTD (blue) relative to the *E. coli* 70S ribosome at 11 Å (EMD-1003 (45)) based on aligning S2 (yellow) of the chimeric S2–S1_NTD with S2 (orange) from an *E. coli* 30S subunit (pdb accession code: 3of0 (40)) fitted to the cryo-EM map (grey mesh) as a rigid body.

Figure preparation

Figures showing electron densities and atomic models were generated using UCSF Chimera (41) or Pymol (<http://www.pymol.org/>) (32).

In vitro binding of FITC-labelled peptide S1₁₈ to the 30S(-S1) subunit

The FITC–S1₁₈ peptide (FITC–MTESFAQLFEEESLKEIE–COOH) was synthesized by Fmoc *N*-(9-fluorenyl)-methoxycarbonyl solid-phase peptide synthesis and N-terminally labelled with fluorescein isothiocyanate (FITC). The average molecular mass of the peptide was determined to be 2254 Da with an Applied Biosystems Voyager System 1105 mass spectrometer. 40 pmol of 30S(-S1) subunits were incubated either with 80 pmol of native S1 or with 400 pmol of FITC–S1₁₈ in 50 μ l TICO buffer at 37°C for 30 min. After addition of 50 μ l TICO buffer the samples were applied to 100 kDa MWCO Amicon concentrators (Millipore), washed and concentrated to 50 μ l by centrifugation at 10 000g. The retained fractions were subjected to SDS-PAGE analysis. After staining with SYPRO Ruby (Invitrogen) the gels were scanned employing a Typhoon using a 488 nm laser and the filters of 520 nm to detect FITC and 610 nm to detect SYPRO Ruby stained proteins, respectively.

In vitro translation

The *ompA* mRNA was prepared *in vitro* as described (9). The *in vitro* translation was performed using the *E. coli* S30 Extract System for Linear Templates (Promega). The reactions containing 1 μ Ci/ml of [³⁵S]-methionine, 0.2 μ M of *ompA* mRNA and 0.3 μ M of ribosomes were incubated for 60 min at 37°C in the absence or presence of 3 or 30 μ M of purified proteins S1₁₀₆, S1_{87–194} or peptide FITC–S1₁₈, respectively. The reactions were stopped by addition of SDS-protein sample buffer and separated on SDS-PAGE. The dried gels were exposed to a Typhoon Molecular Dynamics PhosphoImager (GE Healthcare) for visualization and quantification.

RESULTS

The N-terminal S1 domain is not a bona fide S1 domain

We first analysed the N-terminal region of S1 (S1₁₀₆), which is pivotal for the interaction with S2 (18), by multidimensional heteronuclear NMR. Of the 96 resonances visible on the ¹H–¹⁵N HSQC spectrum (out of the 104 expected resonances) 59 could be assigned to residues Gly21 to Gly79. The remaining 37 peaks corresponding to residues Met1 to Pro20 and Phe80 to Glu106 (Figure 1B), exhibit the broadness and poor signal-to-noise ratio indicative for structural disorder in solution, which is in agreement with the results of a recent NMR study on the first domain of S1 (46). In addition, the comparison of the ¹H–¹⁵N spectrum of S1₁₀₆ with the spectra of the S1₈₆ (lacking the C-terminal linker, CTL) and S1_{19–86} (lacking both, the CTL and the N-terminal segment, NTS; Figure 1B; Supplementary Figure S1A) revealed that both terminal regions are not part

of the core domain, since the resonances corresponding to residues Gly21 to Gly79 remain unchanged within the three spectra (Supplementary Figure S1A). Finally, using ^1H , ^{15}N and ^{13}C secondary chemical shifts we could determine that the folded core of S1₁₀₆ comprises only four β -strands (Supplementary Figure S1B). In addition, our data show that the N- and C-terminal regions are structurally disordered when S1 is in *apo* form, i.e. when not bound to the ribosome.

The flexible S1_{NTS} is required for ribosome binding

To dissect the role of the flexible S1_{NTS} (residues Met1 to Thr18) and the core domain of S1₁₀₆, we analysed *in vivo* the ribosome binding capacity of the truncated protein variant (S1_{19–106}; Figure 1B). Upon ectopic expression of the *rpsA*₁₀₆ or *rpsA*_{19–106} genes in *E. coli* strain JE28, 70S ribosomes were affinity-purified as described in ‘Materials and Methods’ section. Subsequent western blot analysis revealed that in contrast to S1₁₀₆, which completely abolishes assembly of native S1 by blocking its binding site (Figure 1C, panel a, lane 4), S1_{19–106} neither interacts with the 70S ribosome (Figure 1C, panel b, lane 2), nor interferes with binding of the native protein S1 (Figure 1C, panel a, lane 2). To further verify that the NTS is likewise vital for ribosome binding of full-length protein S1, we repeated the co-purification studies employing a full-length protein S1 lacking the NTS (S1_{19–557}; Figure 1A). Here, the ectopically expressed S1 variants were detected *via* their C-terminal FLAG-tag and therefore distinguishable from the native S1. As expected, and in contrast to full length S1 (Figure 1D, panel a, lane 2), S1_{19–557} does not associate with the ribosome *in vivo* (Figure 1D, panel a, lane 4).

To further assess the role of the NTS for ribosome binding, the NTS was fused to D2–D6 of S1 (S1_{NTS Φ 106–557}; Figure 1A). Consistently, the presence of the NTS enabled ribosome binding of protein S1_{NTS Φ 106–557} lacking domain D1 (Figure 1D, panel a, lane 8), whereas the flexible linker region located between domains D1 and D2 (residues 87–106) did not allow ribosome binding (Figure 1D, panel a, lane 6). Taken together, these results corroborate our assumption that the flexible NTS is the crucial element tethering S1 to the ribosome, whereas the core structure of domain D1 *per se* does not promote binding of S1 to the ribosome.

Crystal structure of the S2–S1_{NTD} complex

Since S1 binds to the ribosome by means of protein-protein interaction *via* protein S2 (9,19), we aimed to crystallize S1_{NTD} in complex with S2. After numerous attempts, we were successful in crystallization of a chimeric protein consisting of protein S2 connected to S1_{NTD} (residues 1 to 86) *via* a five-amino acid long linker (S2–S1_{NTD}; Supplementary Figure S2A). The S2–S1_{NTD} structure was solved and refined to 2–3 Å resolution ($R_{\text{work}}/R_{\text{free}}$ 18.6%/24.8%) with one molecule of S2–S1_{NTD} in the asymmetric unit. Data collection and final refinement statistics are reported in Table 1. The crystal packing analysis showed that the interaction between S2 and S1_{NTD} is formed inter-molecularly between two symmetry related molecules. The molecules are related by a crystallographic 2-fold axis, where S2 interacts with S1_{NTD} of the symmetry mate (Supplementary Figure

S2B). In all subsequent structural analyses and discussions, we will refer to the S2–S1_{NTD} structure of the complex assembled from the two protomers (Figure 2A).

The S2 component retains the two domain organization consisting of a coiled-coil and an α/β globular part (Figure 2A). This structure can be superimposed with the structure of S2 in the context of the *E. coli* 30S subunit (pdb accession code: 2qbf, chain B) with a *root-mean-square deviation (rmsd)* of 1.4 Å over 212 superimposed C α atoms. In agreement with the previous knowledge that S2 is a Zn²⁺ binding protein (47), we also identified the Zn²⁺ binding pocket within the globular domain of S2 (Figure 2A and C). The Zn²⁺ binding site in S2 is partially occupied, Zn²⁺ being octahedrally coordinated by the side-chains of residues Asp188, Asp204, Asp205 and His18 as well as two water molecules. The identity of the metal was confirmed by the presence of a characteristic peak in the anomalous difference Fourier map calculated using the data collected at wavelength 1.28 Å, corresponding to the Zn²⁺ K-edge (Supplementary Figure S2C and D).

The structure of the S1_{NTD} comprises two spatially separated structural motifs (Figure 2A): the 11 N-terminal residues of S1_{NTD} form an α -helix (from here on referred to as S1_{NTH}) that is connected to the four β -stranded globular moiety (from here on referred to as S1_{DI}) *via* a seven amino acid residues flexible linker. Notably, the S1_{NTH} is structurally disordered in the free form (Supplementary Figure S1) and adopts an α -helical conformation upon binding to S2 (Figure 2A and B) through a ‘folding upon binding’ mechanism (48).

Interestingly, a DALI search identified the S1 domain of the RNA binding protein Tex from *Pseudomonas aeruginosa* (49) as the closest structural neighbour of S1_{NTD} (Z-score 5.1, rmsd of 4.9 Å over 56 equivalent C α atoms). The S1 domain of Tex adopts the classical OB fold, and structural comparison shows that the S1_{NTD} displays a truncated OB fold missing the β -strand 5 and the N-terminal part of β -strand 1, which is in the OB fold part of both β -sheets (Supplementary Figure S2G). Further, the α -helix between β -strands 3 and 4 at the bottom of the OB fold barrel is replaced by an 11 amino acid loop. Thus, S1_{DI} is structurally distinct from other S1 domains as exemplified by the comparison with domains D4 (Supplementary Figure S2E) and D6 (Supplementary Figure S2F) of protein S1.

Surprisingly, both the S1_{NTH} and the S1_{DI} contact the globular domain of S2. The aromatic rings of two phenylalanine residues, Phe5 and Phe9 located in the S1_{NTH}, form a stabilizing π -stacking interaction (50) with the aromatic ring of Phe32 located on β -strand 2 of the globular domain of S2 (Figure 2B). In addition, the core domain S1_{DI} interacts with S2 *via* two salt bridges: the side chain of Asp39 of S1_{DI} interacts with Arg208 of S2 (Figure 2C), whereas the side chain of Lys43 of S1_{DI} protrudes towards the Zn²⁺ binding pocket in protein S2 and interacts *via* polar bonds with the side chains of Asp188 and Asp205 thereby stabilizing their Zn²⁺ coordinating position (Figure 2C). Additionally, Lys43 interacts with Asn203 and the C-atom of Phe16, which is involved an aromatic stacking interaction with His15, which is in turn packing with Phe9 in S1_{NTH}. To validate the likelihood of whether these interfaces mediate the interaction in solution, we performed a bioinformatics anal-

ysis with PISA (Protein Surfaces, Interfaces and Assemblies (51)). Probability measures $P_{\Delta G,IF}$ of specific interfaces were derived from the gain in solvation energy upon complex formation, with $P_{\Delta G,IF} > 0.5$ indicating hydrophilic/unspecific and $P_{\Delta G,IF} < 0.5$ to hydrophobic/specific interfaces (Supplementary Table S3). Analysis of the interface between S2 and S1_{NTH} shows that the $P_{\Delta G,IF}$ values (0.176, 0.311) are in the range of probabilities derived from typical protein interfaces (0.1–0.4). In the case of S2 and S1_{NTD} however, the $P_{\Delta G,IF}$ values > 0.7 indicate a less specific interaction with a smaller interface area (Supplementary Table S3), suggesting that the dominant and specific stabilizing interaction in the complex is between S2 and S1_{NTH}. Surprisingly, all protein S2 residues that are involved in interaction with S1_{NTD} are highly conserved within γ -Proteobacteria and Firmicutes (Supplementary Figure S6), despite the lack of a ribosome-bound homolog of S1 in the phylum of Firmicutes. However, this fact goes in line with the observation that *E. coli* S1 binds to *Bacillus stearothermophilus* ribosomes and greatly stimulates translation of f2 RNA (52,53).

Cryo-EM structure of the S1_{NTD} on the ribosome

We have determined a cryo-EM structure of an *E. coli* ribosome stalled during translation of the ErmCL leader peptide (Figure 3A), at a resolution of ~ 8 Å (Supplementary Figure S3A). Fitting of the crystal structure of *E. coli* 70S ribosome (40) revealed additional unassigned densities located in the cleft between the head and platform on the solvent side of the small subunit, adjacent to S2 (Figure 3A; Supplementary Figure S3B and C). We attributed these additional densities to part of S1, which was biochemically shown to be present in our ErmCL-ribosome complex (Supplementary Figure S3D). The location of the additional density is in agreement with the localization of S1 based on immunoelectron microscopy (15) and cross-linking mass spectrometry (10). Moreover, fitting the crystal structure of the chimeric S2-S1_{NTD} complex to the cryo-EM map of the ErmCL-ribosome complex based on a structural alignment between S2 from the chimeric S2-S1_{NTD} complex (yellow in Figure 3B) and S2 from the *E. coli* 70S ribosome (orange in Figure 3B) places the S1_{NTD} into one of the unassigned densities (blue in Figure 3B). Subsequently, we generated a molecular model for the complete *E. coli* S1_{D1} (Figure 3C) based on the high sequence homology with the N-terminal segment of eukaryotic initiation factor IF2 α , which adopts an OB domain fold (43). After fitting of S1_{D1}, an additional density remains (Figure 3C), which would be compatible in size with domain D2 of S1 (S1_{D2}, Figure 3E), however, an unambiguous fitting of the OB-like fold of S1_{D2} was not possible due to the lack of resolution and apparent flexibility within this region of the map.

Notably, the additional density attributed to S1 that was recently observed in the *E. coli* SecM-stalled ribosome-channel complex (54) is in excellent agreement with our localization of S1 (Supplementary Figure S3F). In contrast, with the exception of some density for S1_{NTH}, the cryo-EM map of an *E. coli* ribosome at 11.5 Å (45) reveals little or no density for S1_{D1} (Figure 3D). This was surprising since a previous localization of S1 (23) was based on a difference

map between the 11.5 Å *E. coli* cryo-EM map (45) and the crystal structure of the *T. thermophilus* 30S subunit, which lacks S1 (44). In order to address this discrepancy, we re-generated a difference map between the 11.5 Å *E. coli* cryo-EM map and the crystal structure of the *T. thermophilus* 30S subunit, yielding a difference density with features similar to that reported previously (Supplementary Figure S4A). In addition, we also generated a difference map between the 11.5 Å *E. coli* cryo-EM map and the crystal structure of the *E. coli* 70S ribosome (40), which revealed that a large portion of the density attributable to S1 in the 11.5 Å *E. coli* cryo-EM map (23) was in fact due to the *E. coli* ribosomal protein S21, which is absent in the *T. thermophilus* 30S subunit (Supplementary Figure S4B). Moreover, aligning the crystal structures of the *E. coli* 70S ribosome containing mRNA and tRNAs (40) indicates that, after subtraction of density attributable to S21, the remaining density is mostly due to the mRNA and the 3' end of the 16S rRNA (Supplementary Figure S4A and B). In contrast, when difference density maps are generated between the cryo-EM map of the ErmCL-ribosome and the *E. coli* or *T. thermophilus* 30S subunits, additional density that is not present in the 11.5 Å *E. coli* cryo-EM map, is observed that we have attributed to S1_{D1} and S1_{D2} (Supplementary Figure S4C and D). The close proximity of S1_{D1} and S1_{D2} to the 3' end of the 16S rRNA (Supplementary Figure S4C and D) is supported by crosslinks to this region from S1 (55,56).

In addition to contacts with the mRNA and 3' end of the 16S rRNA, the electron density of the cryo-EM map of the ErmCL-ribosome complex also reveals that S1 establishes two contacts with S2, contact one (C1) from the S1_{NTH} and an additional contact (C2) from S1_{D1} (Figure 3C). The contact C1 is consistent with the interactions between the S1_{NTH} and the β -hairpin and helix $\alpha 1$ of S2, and contact C2 would be compatible with the interaction observed between S1_{D1} in the vicinity of the zinc binding motif observed in the crystal structure of the chimeric S2-S1_{NTD} complex (Figure 2B and C). Thus, we believe that the interactions between S1 and S2 within the chimeric S2-S1_{NTD} complex are physiologically relevant and reflect the interactions between S1 and S2 that are observed on the ribosome.

The π -stacking interaction between S1_{NTH} and S2 is essential for ribosome binding

To determine the significance of the hydrophobic and electrostatic contacts for the S1-S2 interaction, we scrutinized the binding potential of different S1_{NTD} mutants to the ribosome (Figure 4A and B) or to purified protein S2 (Figure 4C and D). To evaluate the importance of the π -stacking interactions we removed the aromatic rings of Phe5 and Phe9 by substituting phenylalanine by alanine residues (Figure 4B and D; S1_{NTD}F5A, S1_{NTD}F9A). The role of the salt bridges between the core domain of S1_{NTD} and S2 to ribosome binding was assessed by charge reversal mutations of residues Lys43 and Asp39, respectively (Figure 4B and D; S1_{NTD}K43E, S1_{NTD}D39K). The pull down experiments using either His-tagged ribosomes (33) (Figure 4B) or FLAG-tagged S1_{NTD} variants (Figure 4D) revealed that in the absence of the π -stacking interaction *via* the aromatic rings of either Phe5 or Phe9, protein S1_{NTD} can neither interact

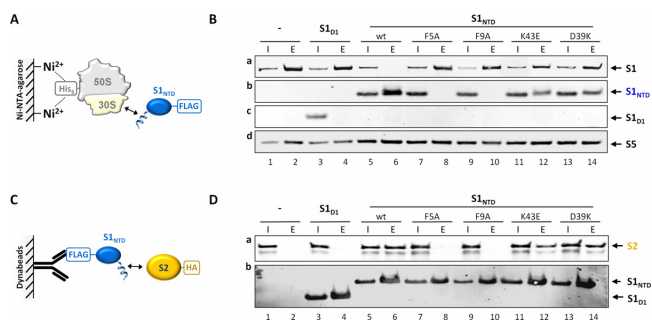


Figure 4. The π -stacking interaction between S1_{NTH} and S2 is pivotal for binding of S1 to the ribosome (A and B) and protein S2 (C and D). Schematic depiction of the co-purification experiments using either His-tagged ribosomes (33) (A) or FLAG-tagged protein S1_{NTD} variants (C). (B) Equal amounts of S30 extract (Input; lanes 1, 3, 5, 7, 9, 11 and 13) and ribosomes (Elution; lanes 2, 4, 6, 8, 10, 12 and 14) purified from *E. coli* strain JE28 before (lanes 1 and 2) and after synthesis of proteins S1_{D1} (lanes 3 and 4), S1_{NTD} (lanes 5 and 6), S1_{NTD}F5A (lanes 7 and 8), S1_{NTD}F9A (lanes 9 and 10), S1_{NTD}K43E (lanes 11 and 12), S1_{NTD}D39K (lanes 13 and 14) were tested for the presence of the respective S1 variants indicated to the right by western blot analysis using anti-S1₁₀₆ antibodies (panels a–c). Protein S5 (panel d) served as loading control. (D) Under the same conditions exemplified in (B) S100 extracts were prepared and supplemented with purified HA-tagged protein S2 (input; lanes 1, 3, 5, 7, 9, 11 and 13). After incubation the FLAG-tagged protein S1 variants were immunoprecipitated by anti-FLAG antibodies (elution; lanes 2, 4, 6, 8, 10, 12 and 14; panel a) and the co-purification of protein S2 was determined by western blot analysis using anti-HA antibodies (panel b). The amounts of protein S1 variants were analysed employing anti-S1₁₀₆ antibodies.

with the ribosome (Figure 4B, panel b, lanes 8 and 10) nor with S2 (Figure 4D, panel a, lanes 8 and 10). In contrast, the mutations of residues involved in electrostatic interactions within the globular domain of S1_{NTD} exhibited only a minor effect on the assembly of S1_{NTD} to the ribosome, since the amounts of proteins S1_{NTD}K43E and S1_{NTD}D39K that co-purified with the ribosome (Figure 4B, panel b, lanes 12 and 14) were only slightly reduced when compared to S1_{NTD} (Figure 4B, panel b, lane 6). Correspondingly, the co-precipitation of S2 was only marginally affected when proteins S1_{NTD}K43E and S1_{NTD}D39K were used (Figure 4D, panel a, lanes 12 and 14). Taken together with the results shown in Figure 1, these data demonstrate that the stable S1_{NTD}–S2 interaction is primarily based on π -stacking conferred by the phenylalanine residues within the S1_{NTH} and the phenylalanine residue at position 32 within the globular domain of S2. The salt bridges between S1_{D1} and the globular domain of S2 seem to play a minor role, possibly by stabilizing the interaction during a potential reorganization of the S1 structure upon mRNA binding.

Free S1_{NTS} binds to the 30S ribosomal subunit

Given the crucial role of the S1_{NTH} in ribosome binding, we hypothesized that its interaction with S2 is the primary anchoring point for S1 on the 30S subunit of the ribosome. To corroborate this assumption we assessed whether free S1_{NTS} can interact with the 30S subunit and consequently impair binding of full length S1. To this end, we employed an ultrafiltration assay described in ‘Materials and Methods’ section using a FITC-labelled S1_{NTS} derivative to facilitate the detection of the peptide. Upon centrifugation,

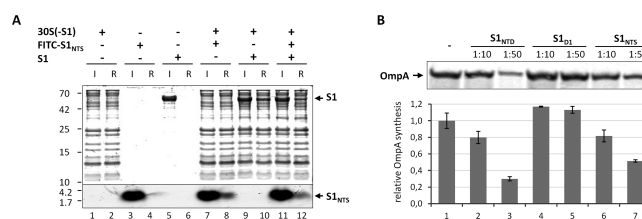


Figure 5. Free S1_{NTS} binds to the ribosome and interferes with translation of the canonical *ompA* mRNA. (A) Purified S1-depleted 30S ribosomes (30S(-S1)) were incubated in the absence (lanes 1 and 2) or in the presence of FITC labelled S1_{NTS} (lanes 7 and 8), native protein S1 (lanes 9 and 10) or both (lanes 11 and 12). Likewise, FITC labelled S1_{NTS} (lanes 3 and 4) or native S1 (lanes 5 and 6) were incubated in the absence of ribosomes. Before (input; lanes 1, 3, 5, 7, 9 and 11) and after ultrafiltration using 100 kDa MWCO Amicon concentrators (Millipore) samples were taken and the presence of the respective proteins and the S1_{NTS} peptide in the ribosome fraction (ribosome fraction; lanes 2, 4, 6, 8, 10 and 12) was determined by SDS-PAGE. (B) *In vitro* translation of *ompA* mRNA in the absence (lane 1) or in the presence of a 10- or 50-fold molar excess over ribosomes of S1_{NTD} (lanes 2 and 3), S1_{D1} (lanes 4 and 5) or S1_{NTS} (lanes 6 and 7), respectively. The assay was performed in triplicate and one representative autoradiograph is shown. Graph representing the quantification of three independent assays is given below. Error bars represent the standard deviation of the mean.

the 30S subunits are retained on the filter (Figure 5A, lane 2), whereas free S1_{NTS} peptide (Figure 5A, lane 4) and full-length S1 (Figure 5A, lane 6) pass through the membrane. As expected, in the presence of S1-depleted 30S subunits (30S(-S1)), the S1_{NTS} peptide (Figure 5A, lane 8) and full-length S1 (Figure 5A, lane 10) were detected in the retained ribosome fraction, indicating an interaction with the ribosomal subunit. Moreover, the concomitant addition of the FITC–S1_{NTS} peptide and protein S1 reduces the amount of both molecules in the ribosome fraction (Figure 5A, lane 12), corroborating the assumption that they compete for the same binding site on the 30S subunit.

S1_{NTS} but not S1_{D1} inhibits translation of canonical *ompA* mRNA *in vitro*

Previously, we have shown that the synthesis of S1_{NTD} inhibits bulk mRNA translation in *E. coli in vivo* presumably because the protein binds to the ribosome and blocks assembly of native S1 (18). Given that the binding of S1 to the ribosome is dictated by the S1_{NTS}, we next determined whether the S1_{NTS} peptide could also functionally interfere with canonical mRNA translation. Thus, we performed an *in vitro* translation assay employing the canonical *ompA* mRNA, translation of which is strictly dependent on the presence of S1 on the ribosome (8). As shown previously (18) and in contrast to the globular S1_{D1} lacking the S1_{NTS} (Figure 5B, lanes 4 and 5), the presence of the S1_{NTD} including S1_{NTS} interferes with translation of the *ompA* mRNA *in vitro* (Figure 5B, lanes 2 and 3). Remarkably and in line with our assumption, the addition of a 10- or 50-fold molar excess of the S1_{NTS} peptide over the ribosome likewise results in reduction of OmpA synthesis by 20 and 50%, respectively (Figure 5B, lanes 6 and 7).

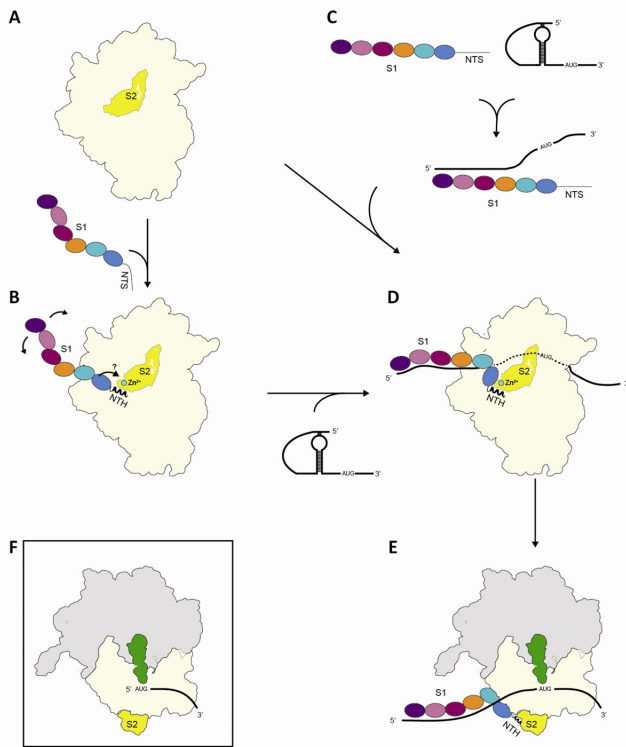


Figure 6. Schematic model showing the interaction of S1 with the 30S subunit. (A) In the free form the N-terminal segment of the multidomain protein S1 (spheres indicating the domains are colour-coded as in Figure 1A) is unstructured. (B) S1 can either interact with the globular domain of protein S2 (in yellow) on the 30S subunit (in light yellow) primarily via the N-terminal helix $S1_{NTH}$, which adopts an α -helical conformation upon binding to S2 through a ‘folding upon binding’ mechanism (48). In this position, the protein can move in a ribosome-independent manner to scan for RNA molecules or (C) S1 can interact directly with the mRNA, facilitate unfolding of the mRNA, and its delivery to the ribosome (5–7). (D) Binding of mRNA induces a rearrangement of the S1 domains D3–D5 (12) that might facilitate the correct positioning of the mRNA possibly supported by the salt bridges between $S1_{D1}$ and S2, leading to the formation of the (E) translation initiation complex. It is still in question whether the presence of the Zn^{2+} ion (green sphere) affects the affinity or the topology of S1 on the ribosome, what could potentially influence the activity or selectivity of the ribosome for specific mRNAs. (F) Post-translational protein modifications within the region of the $S1_{NTH}$ or the S2 protein could likewise influence the affinity of S1 for the ribosome. Thereby, S1-depleted ribosomes that are selective for translation of lmrRNAs could be present under specific conditions.

DISCUSSION

One hallmark of ribosomal protein S1 is its unique flexibility, which was suggested already more than 30 years ago (57,58). As a result, the full-length protein is not amenable to structural analysis and was thus intentionally removed from the ribosome before crystallization (44), resulting in the fact that the S1–ribosome interface hitherto remained enigmatic. Here, we present the first detailed structural analysis of the S1–S2 interface that can be rationalized in terms of the following model. The short N-terminal segment of protein S1 is intrinsically structurally disordered in solution (Figure 6A and Supplementary Figure S1A). It folds partially into a perfect helical structure upon in-

teraction with the globular domain of S2 (Figure 6C) via π -stacking involving two highly conserved phenylalanine residues of S1 (Supplementary Figure S5). Due to the flexible hinge region, the protein in its elongated conformation can scan the surrounding of the ribosome for mRNA molecules, thereby increasing the sphere of ribosome action (Figure 6C). In some situations, S1 may interact with the mRNA and initiate unfolding of secondary structures in the absence of the ribosome (5,6) as well as aid in delivery of the mRNA to the ribosome (Figure 6B) (7). As revealed by NMR and SAXS analyses, binding of RNA molecules induces a topological rearrangement of the S1 domains D3–D5 (12), which might further contribute to an overall reorganization of protein S1 on the ribosome, possibly supported by the salt bridges at the boundary between the globular domains of S1 and S2, or potentially induced by the suggested interaction of the protein S1 with the 3'-terminal region of the 16S rRNA (17) (Figures 2C and 6D). Thereby, S1 could be contracted in order to position the mRNA close to the mRNA track on the 30S subunit (Figure 6D) to facilitate formation of the translation initiation complex (Figure 6E) (7).

During the preparation of this manuscript the structure of the Q β replicase comprising the β -subunit, EF-Tu, EF-Ts and the N-terminal half of S1 was published (22). Interestingly, again domains D1 and D2 function to anchor S1 on the β -subunit and all residues involved in the interaction with the ribosome are likewise contacting the Q β replicase. Nevertheless, several differences in the nature of interactions are evident. In contrast to the stabilizing π -stacking interaction on the ribosome, the N-terminal segment of S1 is localized in a hydrophobic pocket of the Q β replicase, which results in an extension of the helical structure of the $S1_{NTH}$ and concomitantly with an enlargement of the interaction surface. Likewise, the charged S1 residues, Asp39 and Lys43, that form the salt bridges with the globular domain of S2, are involved in interaction with the Q β replicase. Asp39 interacts with two Arg residues in the replicase, whereas Lys43 is involved in the interaction with the main chain carbonyl group of Ile199. Again, this interaction surface is extended as the S1 residue Gly41 forms an additional hydrogen bond with the main chain amide group of Ile199. Taken together, these results suggest that the Q β replicase could directly compete with S2 for the same binding sites on protein S1.

In the course of this study, we also determined the Zn^{2+} binding pocket in the globular domain of ribosomal protein S2 (Figure 2C). Among the biological relevant transition metals, zinc is peculiar as it is redox inert and shows a versatile coordination chemistry, and can hence be used as a structural or catalytic cofactor. In protein S2, the Zn^{2+} ion is coordinated in an octahedral geometry by monodentate carboxylates of three aspartic acid residues (Asp188, Asp204, Asp205), one histidine residue (His18) and two water molecules (Figure 2C). Notably, these residues are conserved across Proteobacteria and Firmicutes, indicating the importance of the presence of Zn^{2+} (Supplementary Figure S6). A search in the MESPEUS database (59) of three-dimensional metal biosites revealed the only similar coordination sphere in the L-rhamnose isomerase from *Pseudomonas stutzeri* (60), where the substrate binding site con-

tains two metal cations. The Zn²⁺ binding site that is similar to the one found in S2 is considered to have a structural role, since it stabilizes the local structure of the protein and facilitates the correct orientation of the substrate. Thus, in the S1/S2 complex the Zn²⁺ ion might lack a catalytic activity but rather plays a structural role. However, the zinc binding pocket is located at the S1–S2 interface, with the Asp188 residue being properly positioned for the coordination of the zinc ion by the salt bridge with the Lys43 residue of S1 (Figure 2C), which resides within the highly conserved loop region connecting β -strands 2 and 3 (Supplementary Figure S5). This result raises the possibility that the S1–ribosome interaction might be modulated by the presence of Zn²⁺ ions (Figure 6C and D). Thus, besides the regulation of gene expression *via* metal responsive transcription factors, the intracellular zinc concentration could likewise affect ribosome specificity and thereby directly modulate the translome. This hypothesis, which could add another level of complexity to the regulation of protein synthesis in response to zinc homeostasis, is currently under investigation.

Recently, evidence is accumulating that ribosome heterogeneity provides a fast and energy efficient pathway for bacteria to adapt protein synthesis to adverse conditions (18,61). In particular, several studies addressed the functional specificity of S1-depleted ribosomes for translation of lmrRNAs (9,62,63). Given the formation of lmrRNAs during stress conditions (61), it is conceivable that conditional post-translational protein modifications affect the small boundary between proteins S1 and S2. Thereby, the affinity of the protein for the ribosome might be reduced and S1-depleted ribosomes could be generated, which are responsible for translation of lmrRNAs (Figure 6F). Concomitantly, free protein S1 might participate in other tasks, as already suggested either in the stabilization of certain transcripts (64) or in trans-translation (65). This assumption is supported by a comparative proteome analysis that revealed the differential acetylation of several r-proteins including S1 and S2 during exponential or stationary growth phase (66). Moreover, a recent study performed to decipher the phosphoproteome of *E. coli* during growth in minimal medium (67) indicates that several residues of protein S1 are differentially phosphorylated in response to the growth phase. Interestingly, the modification of residue Thr2, which is located in close proximity to the N-terminal ribosome anchoring helix, was only observed in late stationary phase. Moreover, Ser44, which is juxtaposed to Lys43 that mediates the salt bridge involving the S2 zinc binding pocket, is highly phosphorylated at late stationary phase. Thus, we envisage that the negative charge introduced by the phosphorylation of Ser44 could contribute to a reorientation of Lys43, and thereby impair the formation of the respective salt bridge. This idea is supported by results indicative for the accumulation of free ribosomal proteins S1 and L7/L12 during stationary phase (68). Interestingly, the interaction of proteins L7/L12 with the ribosome is mechanistically similar to the S1-ribosome interaction. Proteins L7/L12 likewise bind to the ribosome *via* a short N-terminal domain which is connected to the functional domain by a flexible and unstructured linker (69). Notably, this N-terminal ribosome

binding domain is modified in a growth phase dependent manner, which affects the stability of the interaction (70). Taken together, we hypothesize that the small boundary between proteins S1 and S2 could represent a target for modification in response to the growth-phase or environmental conditions, which might affect the affinity of S1 for the ribosome and consequently contributes to ribosome heterogeneity thereby fine-tuning protein synthesis.

ACCESSION NUMBERS

The coordinates and the structure factors were deposited in the Protein Data Bank with accession code 4TOI and the cryo-EM map was deposited in the EMBank with accession code EMD-6211.

SUPPLEMENTARY DATA

Supplementary Data are available at NAR Online.

ACKNOWLEDGEMENTS

The authors would like to thank Mathias Madalinski (Protein Chemistry Facility IMP/IMBA/GMI, Vienna) for synthesis of the FITC labelled S1_{NTS} peptide, and Oliviero Carugo (University of Vienna and University of Pavia) for help with the analysis of the zinc binding site. All members of the I.M. laboratory, especially Tanino G. Albanese, are acknowledged for helpful discussions and contributions. We thank the staff of X-ray beamlines (ID14-1, ID14-4 and ID23-2) at ESRF in Grenoble and of I04 at Diamond in Oxford, for their excellent support.

FUNDING

Austrian Science Fund (FWF) [P20112-B03, P22249-B20, W1207-B09, F4316-B09 to I.M.]; Deutsche Forschungsgemeinschaft (DFG) [FOR2805/WI3285/2-1 to D.N.W.]; National Institutes of Health [R01GM095737 to D.N.W.]; University of Vienna (to I.G.); European Community's Seventh Framework Programme (FP7/2007–2013) under BioStruct-X [283570]. Funding for open access charge: FWF [P20112-B03, P22249-B20, W1207-B09, F4316-B09 to I.M.].

Conflict of interest statement. None declared.

REFERENCES

- Sørensen, M.A., Fricke, J. and Pedersen, S. (1998) Ribosomal protein S1 is required for translation of most, if not all, natural mRNAs in *Escherichia coli* in vivo. *J. Mol. Biol.*, **280**, 561–569.
- Schuwirth, B.S., Borovinskaya, M.A., Hau, C.W., Zhang, W., Vila-Sanjurjo, A., Holton, J.M. and Cate, J.H. (2005) Structures of the bacterial ribosome at 3.5 Å resolution. *Science*, **310**, 827–834.
- Sykes, M.T. and Williamson, J.R. (2009) A complex assembly landscape for the 30S ribosomal subunit. *Annu. Rev. Biophys.*, **38**, 197–215.
- Boni, I.V., Isaeva, D.M., Musychenko, M.L. and Tzareva, N.V. (1991) Ribosome-messenger recognition: mRNA target sites for ribosomal protein S1. *Nucleic Acids Res.*, **19**, 155–162.
- Qu, X., Lancaster, L., Noller, H.F., Bustamante, C. and Tinoco, I. Jr (2012) Ribosomal protein S1 unwinds double-stranded RNA in multiple steps. *Proc. Natl. Acad. Sci. U.S.A.*, **109**, 14458–14463.

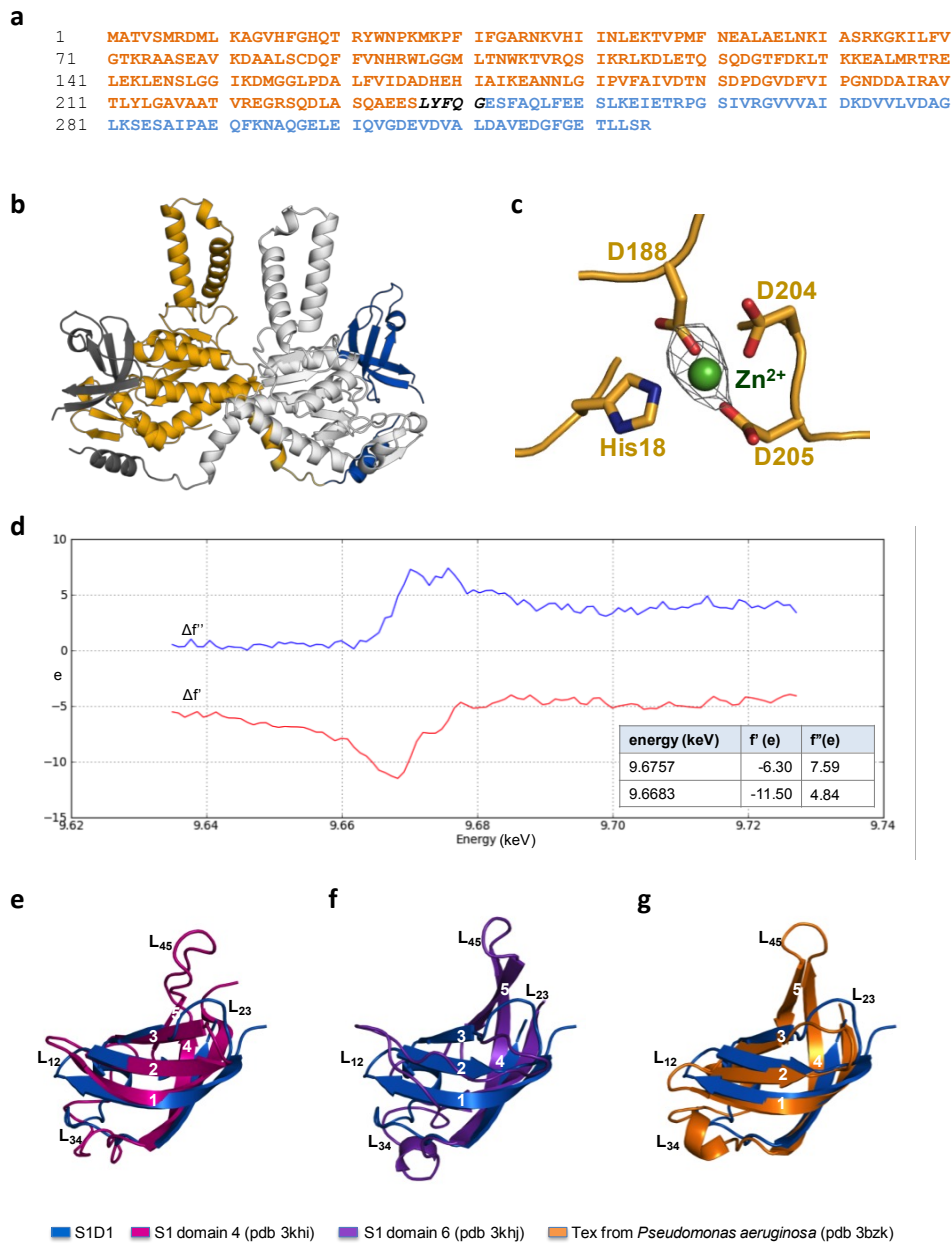
6. Rajkowsch, L. and Schroeder, R. (2007) Dissecting RNA chaperone activity. *RNA*, **13**, 2053–2060.
7. Duval, M., Korepanov, A., Fuchsbaauer, O., Fechter, P., Haller, A., Fabbretti, A., Choulier, L., Micura, R., Klaholz, B.P., Romby, P. *et al.* (2013) *Escherichia coli* ribosomal protein S1 unfolds structured mRNAs onto the ribosome for active translation initiation. *PLoS Biol.*, **11**, e1001731.
8. Tedin, K., Resch, A. and Bläsi, U. (1997) Requirements for ribosomal protein S1 for translation initiation of mRNAs with and without a 5' leader sequence. *Mol. Microbiol.*, **25**, 189–199.
9. Moll, I., Grill, S., Gründling, A. and Bläsi, U. (2002) Effects of ribosomal proteins S1, S2 and the DeaD/CsdA DEAD-box helicase on translation of leaderless and canonical mRNAs in *Escherichia coli*. *Mol. Microbiol.*, **44**, 1387–1396.
10. Lauber, M.A., Rappsilber, J. and Reilly, J.P. (2012) Dynamics of ribosomal protein S1 on a bacterial ribosome with cross-linking and mass spectrometry. *Mol. Cell. Proteomics*, **11**, 1965–1976.
11. Subramanian, A.R. (1983) Structure and functions of ribosomal protein S1. *Prog. Nucleic Acids Res. Mol. Biol.*, **28**, 101–142.
12. Aliprandi, P., Sizun, C., Perez, J., Mareuil, F., Caputo, S., Leroy, J.L., Odaert, B., Laalami, S., Uzan, M. and Bontems, F. (2008) S1 ribosomal protein functions in translation initiation and ribonuclease RegB activation are mediated by similar RNA-protein interactions: an NMR and SAXS analysis. *J. Biol. Chem.*, **283**, 13289–13301.
13. Salah, P., Bisaglia, M., Aliprandi, P., Uzan, M., Sizun, C. and Bontems, F. (2009) Probing the relationship between Gram-negative and Gram-positive S1 proteins by sequence analysis. *Nucleic Acids Res.*, **37**, 5578–5588.
14. Bycroft, M., Hubbard, T.J., Proctor, M., Freund, S.M. and Murzin, A.G. (1997) The solution structure of the S1 RNA binding domain: a member of an ancient nucleic acid-binding fold. *Cell*, **88**, 235–242.
15. Walleczek, J., Albrecht-Ehrlich, R., Stöffler, G. and Stöffler-Meilicke, M. (1990) Three-dimensional localization of the NH₂- and carboxyl-terminal domain of ribosomal protein S1 on the surface of the 30 S subunit from *Escherichia coli*. *J. Biol. Chem.*, **265**, 11338–11344.
16. McGinness, K.E. and Sauer, R.T. (2004) Ribosomal protein S1 binds mRNA and tmRNA similarly but plays distinct roles in translation of these molecules. *Proc. Natl. Acad. Sci. U.S.A.*, **101**, 13454–13459.
17. Laughrea, M. and Tam, J. (1991) Interaction of ribosomal protein S1 and initiation factor IF3 with the 3' major domain and the decoding site of the 30S subunit of *Escherichia coli*. *Biochemistry*, **30**, 11412–11420.
18. Byrgazov, K., Manoharadas, S., Kaberdina, A.C., Vesper, O. and Moll, I. (2012) Direct interaction of the N-terminal domain of ribosomal protein S1 with protein S2 in *Escherichia coli*. *PLoS One*, **7**, e32702.
19. Boni, I.V., Zlatkin, I.V. and Budowsky, E.I. (1982) Ribosomal protein S1 associates with *Escherichia coli* ribosomal 30-S subunit by means of protein-protein interactions. *Eur. J. Biochem.*, **121**, 371–376.
20. Wahba, A.J., Miller, M.J., Niveleau, A., Landers, T.A., Carmichael, G.G., Weber, K., Hawley, D.A. and Slobin, L.I. (1974) Subunit I of G beta replicase and 30 S ribosomal protein S1 of *Escherichia coli*. Evidence for the identity of the two proteins. *J. Biol. Chem.*, **249**, 3314–3316.
21. Vasilyev, N.N., Kutlubaeva, Z.S., Ugarov, V.I., Chetverina, H.V. and Chetverin, A.B. (2013) Ribosomal protein S1 functions as a termination factor in RNA synthesis by Qbeta phage replicase. *Nat. Commun.*, **4**, 1781.
22. Takeshita, D., Yamashita, S. and Tomita, K. (2014) Molecular insights into replication initiation by Qbeta replicase using ribosomal protein S1. *Nucleic Acids Res.*, **42**, 10809–10822.
23. Sengupta, J., Agrawal, R.K. and Frank, J. (2001) Visualization of protein S1 within the 30S ribosomal subunit and its interaction with messenger RNA. *Proc. Natl. Acad. Sci. U.S.A.*, **98**, 11991–11996.
24. Kabsch, W. (2010) Xds. *Acta Crystallogr. D Biol. Crystallogr.*, **66**, 125–132.
25. Evans, P.R. and Murshudov, G.N. (2013) How good are my data and what is the resolution? *Acta Crystallogr. D Biol. Crystallogr.*, **69**, 1204–1214.
26. Karplus, P.A. and Diederichs, K. (2012) Linking crystallographic model and data quality. *Science*, **336**, 1030–1033.
27. Long, F., Vagin, A.A., Young, P. and Murshudov, G.N. (2008) BALBES: a molecular-replacement pipeline. *Acta Crystallogr. D Biol. Crystallogr.*, **64**, 125–132.
28. Adams, P.D., Afonine, P.V., Bunkoczi, G., Chen, V.B., Davis, I.W., Echols, N., Headd, J.J., Hung, L.W., Kapral, G.J., Grosse-Kunstleve, R.W. *et al.* (2010) PHENIX: a comprehensive Python-based system for macromolecular structure solution. *Acta Crystallogr. D Biol. Crystallogr.*, **66**, 213–221.
29. Murshudov, G.N., Skubak, P., Lebedev, A.A., Pannu, N.S., Steiner, R.A., Nicholls, R.A., Winn, M.D., Long, F. and Vagin, A.A. (2011) REFMAC5 for the refinement of macromolecular crystal structures. *Acta Crystallogr. D Biol. Crystallogr.*, **67**, 355–367.
30. Emsley, P. and Cowtan, K. (2004) Coot: model-building tools for molecular graphics. *Acta Crystallogr. D Biol. Crystallogr.*, **60**, 2126–2132.
31. Chen, V.B., Arendall, W.B. 3rd, Headd, J.J., Keedy, D.A., Immormino, R.M., Kapral, G.J., Murray, L.W., Richardson, J.S. and Richardson, D.C. (2010) MolProbity: all-atom structure validation for macromolecular crystallography. *Acta Crystallogr. D Biol. Crystallogr.*, **66**, 12–21.
32. DeLano, W.L. (2002) *The PyMOL Molecular System*. DeLano Scientific, San Carlos, CA.
33. Ederth, J., Mandava, C.S., Dasgupta, S. and Sanyal, S. (2009) A single-step method for purification of active His-tagged ribosomes from a genetically engineered *Escherichia coli*. *Nucleic Acids Res.*, **37**, e15.
34. Suryanarayana, T. and Subramanian, A.R. (1983) An essential function of ribosomal protein S1 in messenger ribonucleic acid translation. *Biochemistry*, **22**, 2715–2719.
35. Horinouchi, S. and Weisblum, B. (1980) Posttranscriptional modification of mRNA conformation: mechanism that regulates erythromycin-induced resistance. *Proc. Natl. Acad. Sci. U.S.A.*, **77**, 7079–7083.
36. Becker, M., Gzyl, K.E., Altamirano, A.M., Vuong, A., Urban, K. and Wieden, H.J. (2012) The 70S ribosome modulates the ATPase activity of *Escherichia coli* YchF. *RNA Biol.*, **9**, 1288–1301.
37. Frank, J., Radermacher, M., Penczek, P., Zhu, J., Li, Y., Ladjadj, M. and Leith, A. (1996) SPIDER and WEB: processing and visualization of images in 3D electron microscopy and related fields. *J. Struct. Biol.*, **116**, 190–199.
38. Chen, J.Z. and Grigorieff, N. (2007) SIGNATURE: a single-particle selection system for molecular electron microscopy. *J. Struct. Biol.*, **157**, 168–173.
39. Dönhöfer, A., Franckenberg, S., Wickles, S., Berninghausen, O., Beckmann, R. and Wilson, D.N. (2012) Structural basis for TetM-mediated tetracycline resistance. *Proc. Natl. Acad. Sci. U.S.A.*, **109**, 16900–16905.
40. Dunkle, J.A., Xiong, L., Mankin, A.S. and Cate, J.H. (2010) Structures of the *Escherichia coli* ribosome with antibiotics bound near the peptidyl transferase center explain spectra of drug action. *Proc. Natl. Acad. Sci. U.S.A.*, **107**, 17152–17157.
41. Pettersen, E.F., Goddard, T.D., Huang, C.C., Couch, G.S., Greenblatt, D.M., Meng, E.C. and Ferrin, T.E. (2004) UCSF Chimera—a visualization system for exploratory research and analysis. *J. Comput. Chem.*, **25**, 1605–1612.
42. Soding, J., Biegert, A. and Lupas, A.N. (2005) The HHpred interactive server for protein homology detection and structure prediction. *Nucleic Acids Res.*, **33**, W244–248.
43. Nonato, M.C., Widom, J. and Clardy, J. (2002) Crystal structure of the N-terminal segment of human eukaryotic translation initiation factor 2alpha. *J. Biol. Chem.*, **277**, 17057–17061.
44. Wimberly, B.T., Brodersen, D.E., Clemons, W.M. Jr, Morgan-Warren, R.J., Carter, A.P., Vornrhein, C., Hartsch, T. and Ramakrishnan, V. (2000) Structure of the 30S ribosomal subunit. *Nature*, **407**, 327–339.
45. Gabashvili, I.S., Agrawal, R.K., Spahn, C.M., Grassucci, R.A., Svergun, D.I., Frank, J. and Penczek, P. (2000) Solution structure of the *E. coli* 70S ribosome at 11.5 Å resolution. *Cell*, **100**, 537–549.
46. Giraud, P., Crechet, J.B., Uzan, M., Bontems, F. and Sizun, C. (2014) Resonance assignment of the ribosome binding domain of *E. coli* ribosomal protein S1. *Biomol. NMR Assign.*, DOI:10.1007/s12104-014-9554-2.

47. Katayama, A., Tsujii, A., Wada, A., Nishino, T. and Ishihama, A. (2002) Systematic search for zinc-binding proteins in *Escherichia coli*. *Eur. J. Biochem.*, **269**, 2403–2413.
48. Wright, P.E. and Dyson, H.J. (2009) Linking folding and binding. *Curr. Opin. Struct. Biol.*, **19**, 31–38.
49. Johnson, S.J., Close, D., Robinson, H., Vallet-Gely, I., Dove, S.L. and Hill, C.P. (2008) Crystal structure and RNA binding of the Tex protein from *Pseudomonas aeruginosa*. *J. Mol. Biol.*, **377**, 1460–1473.
50. McGaughey, G.B., Gagne, M. and Rappe, A.K. (1998) pi-Stacking interactions. Alive and well in proteins. *J. Biol. Chem.*, **273**, 15458–15463.
51. Krissinel, E. and Henrick, K. (2007) Inference of macromolecular assemblies from crystalline state. *J. Mol. Biol.*, **372**, 774–797.
52. Isono, K. and Isono, S. (1976) Lack of ribosomal protein S1 in *Bacillus stearothermophilus*. *Proc. Natl. Acad. Sci. U.S.A.*, **73**, 767–770.
53. Isono, S. and Isono, K. (1975) Role of ribosomal protein S1 in protein synthesis: effects of its addition to *Bacillus stearothermophilus* cell-free system. *Eur. J. Biochem.*, **56**, 15–22.
54. Park, E., Menetret, J.F., Gumbart, J.C., Ludtke, S.J., Li, W., Whynot, A., Rapoport, T.A. and Akey, C.W. (2014) Structure of the SecY channel during initiation of protein translocation. *Nature*, **506**, 102–106.
55. Kenner, R.A. (1973) A protein-nucleic acid crosslink in 30S ribosomes. *Biochem. Biophys. Res. Commun.*, **51**, 932–938.
56. Czernilofsky, A.P., Kurland, C.G. and Stoffler, G. (1975) 30S ribosomal proteins associated with the 3'-terminus of 16S RNA. *FEBS Lett.*, **58**, 281–284.
57. Moore, P.B. and Laughrea, M. (1979) The conformational properties of ribosomal protein S1. *Nucleic Acids Res.*, **6**, 2355–2361.
58. Chu, Y.G. and Cantor, C.R. (1979) Segmental flexibility in *Escherichia coli* ribosomal protein S1 as studied by fluorescence polarization. *Nucleic Acids Res.*, **6**, 2363–2379.
59. Harding, M.M. and Hsin, K.Y. (2014) Mespeus—a database of metal interactions with proteins. *Methods Mol. Biol.*, **1091**, 333–342.
60. Yoshida, H., Yamada, M., Ohyama, Y., Takada, G., Izumori, K. and Kamitori, S. (2007) The structures of L-rhamnose isomerase from *Pseudomonas stutzeri* in complexes with L-rhamnose and D-allose provide insights into broad substrate specificity. *J. Mol. Biol.*, **365**, 1505–1516.
61. Vesper, O., Amitai, S., Belitsky, M., Byrgazov, K., Kaberdina, A.C., Engelberg-Kulka, H. and Moll, I. (2011) Selective translation of leaderless mRNAs by specialized ribosomes generated by MazF in *Escherichia coli*. *Cell*, **147**, 147–157.
62. Moll, I., Grill, S., Gualerzi, C.O. and Bläsi, U. (2002) Leaderless mRNAs in bacteria: surprises in ribosomal recruitment and translational control. *Mol. Microbiol.*, **43**, 239–246.
63. Moll, I., Resch, A. and Blasi, U. (1998) Discrimination of 5'-terminal start codons by translation initiation factor 3 is mediated by ribosomal protein S1. *FEBS Lett.*, **436**, 213–217.
64. Delvillani, F., Papiani, G., Deho, G. and Briani, F. (2011) S1 ribosomal protein and the interplay between translation and mRNA decay. *Nucleic Acids Res.*, **39**, 7702–7715.
65. Bordeau, V. and Felden, B. (2002) Ribosomal protein S1 induces a conformational change of tmRNA; more than one protein S1 per molecule of tmRNA. *Biochimie*, **84**, 723–729.
66. Yu, B.J., Kim, J.A., Moon, J.H., Ryu, S.E. and Pan, J.G. (2008) The diversity of lysine-acetylated proteins in *Escherichia coli*. *J. Microbiol. Biotechnol.*, **18**, 1529–1536.
67. Soares, N.C., Spat, P., Krug, K. and Macek, B. (2013) Global dynamics of the *Escherichia coli* proteome and phosphoproteome during growth in minimal medium. *J. Proteome Res.*, **12**, 2611–2621.
68. Ramagopal, S. (1976) Accumulation of free ribosomal proteins S1, L7, and L12 in *Escherichia coli*. *Eur. J. Biochem.*, **69**, 289–297.
69. Bocharov, E.V., Sobol, A.G., Pavlov, K.V., Korzhnev, D.M., Jaravine, V.A., Gudkov, A.T. and Arseniev, A.S. (2004) From structure and dynamics of protein L7/L12 to molecular switching in ribosome. *J. Biol. Chem.*, **279**, 17697–17706.
70. Gordiyenko, Y., Deroo, S., Zhou, M., Videler, H. and Robinson, C.V. (2008) Acetylation of L12 increases interactions in the *Escherichia coli* ribosomal stalk complex. *J. Mol. Biol.*, **380**, 404–414.

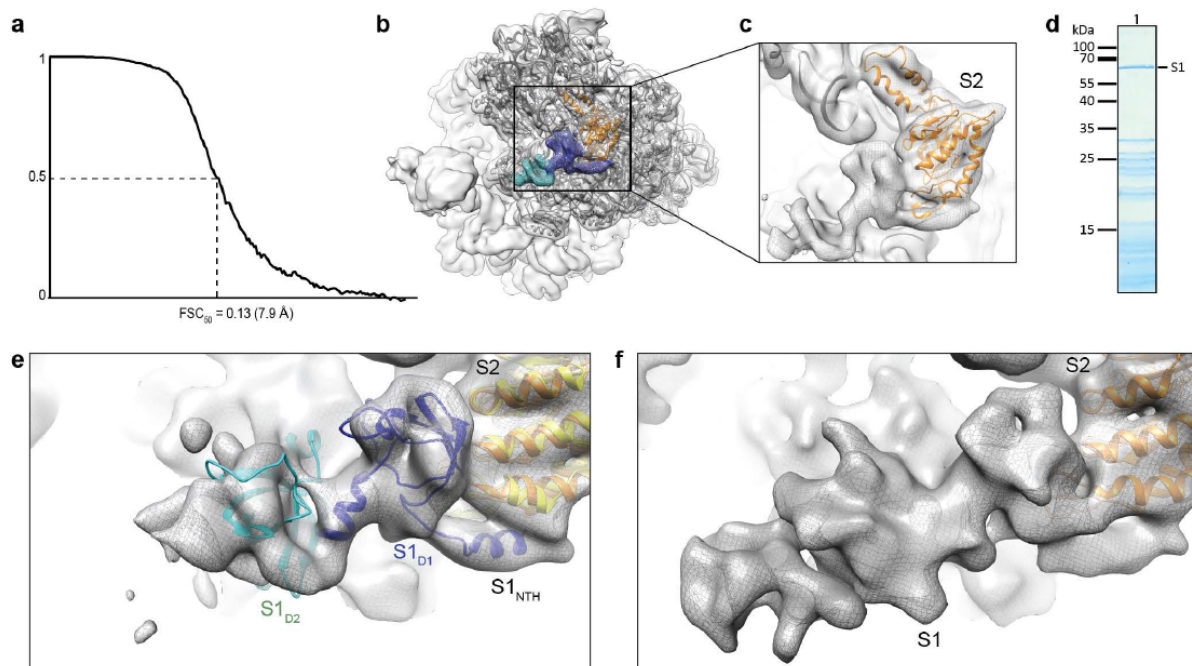
SUPPLEMENTARY DATA

Structural basis for the flexible interaction of protein S1 with the *Escherichia coli* ribosome

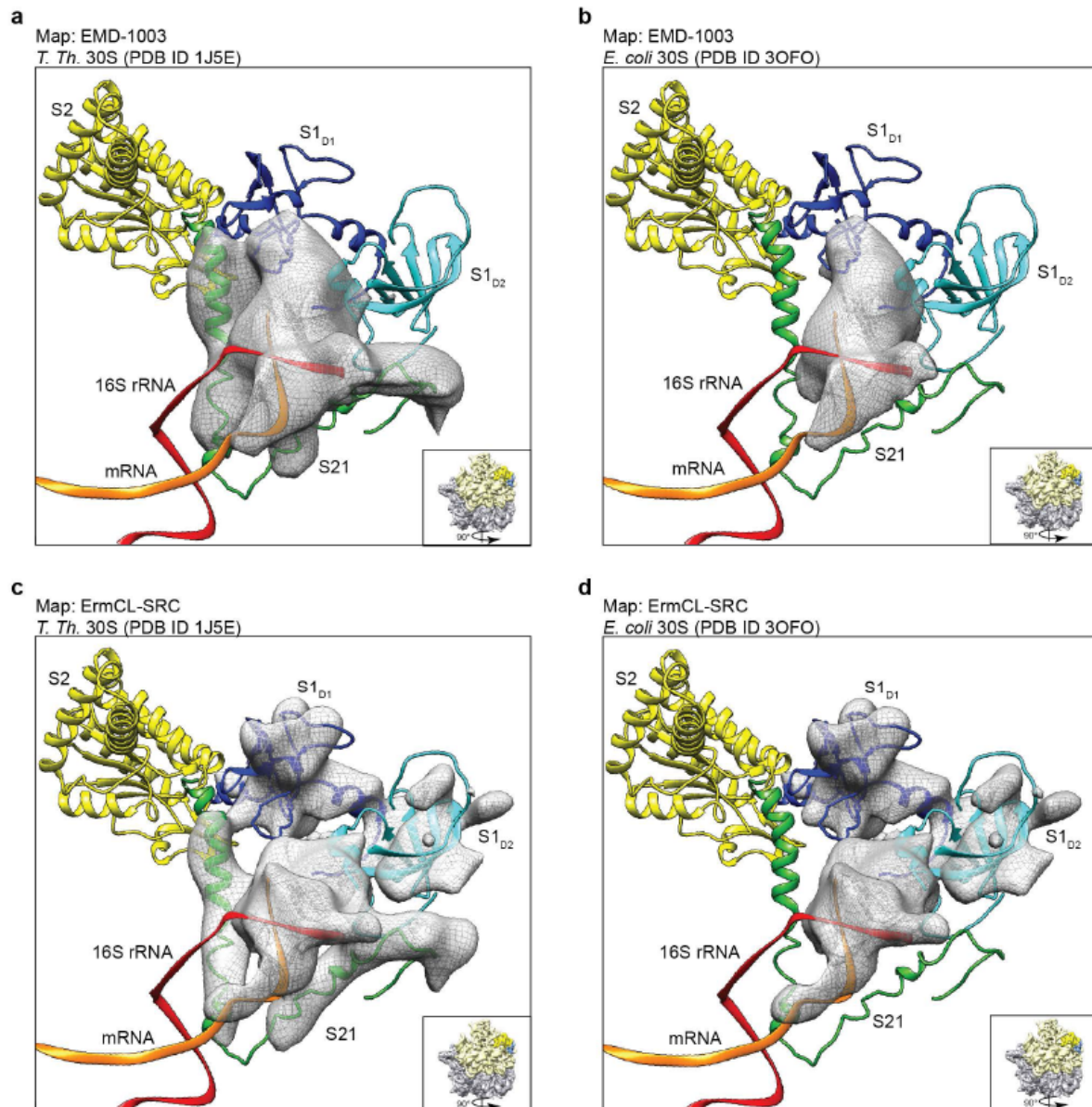
Konstantin Byrgazov¹, Irina Grishkovskaya², Stefan Arenz³, Nicolas Coudeville²,
Hannes Temmel¹, Daniel N. Wilson³, Kristina Djinovic-Carugo^{2,4} and Isabella Moll^{1‡}



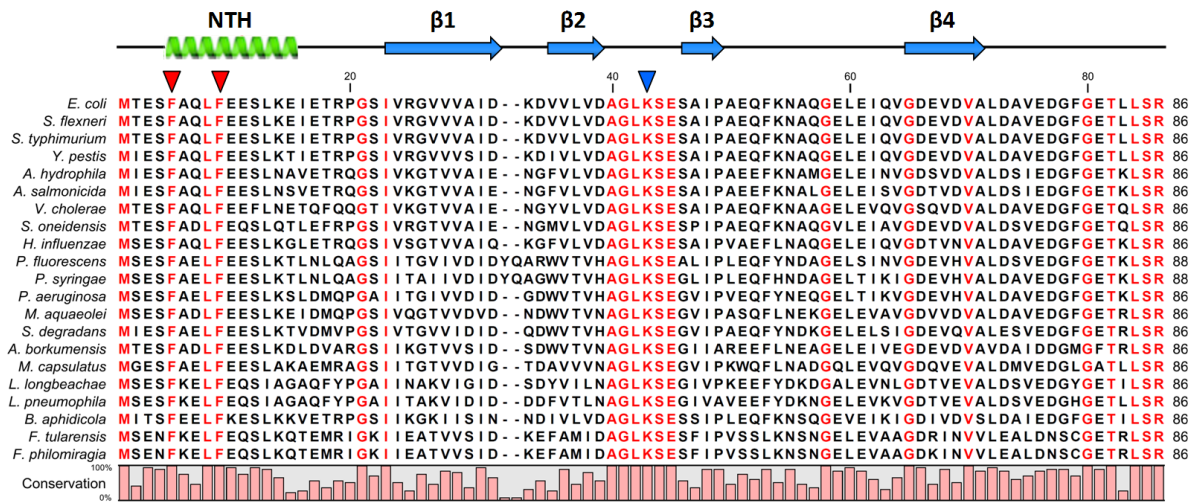
Supplementary Figure S2. Crystal structure analysis of the chimeric S2-S1_{NTD} protein. **(A)** Amino acid sequence of the chimeric S2-S1_{NTD} protein used for the crystal structure analysis. The sequences corresponding to protein S2 (yellow), the flexible linker (black and italics) and protein S1_{NTD} (blue) are indicated. **(B)** Dimer of the chimeric S2-S1_{NTD} protein formed by inter-molecular interaction, where S2 interacts with S1_{NTD} of the symmetry mate. S2 and S1_{NTD} of one monomer are indicated in yellow and blue, and of the second monomer in light and dark grey, respectively. **(C)** Anomalous difference Fourier map showing the position of the Zn²⁺ ion contoured at 3.5 σ . The anomalous data was collected to 3 Å resolution at ID23-1 ESRF (Grenoble, France) at wavelength 1.28 Å (9.68 keV). **(D)** X-ray energy scan around the absorption edge of Zn (red) and its first derivative depicted in blue. The energy is given in keV. Comparison of the structure of protein S1_{NTD} with the domains D4 **(E)** and D6 **(F)** of protein S1 from *E. coli* and the S1 domain of the RNA binding protein Tex from *P. aeruginosa* **(G)**.



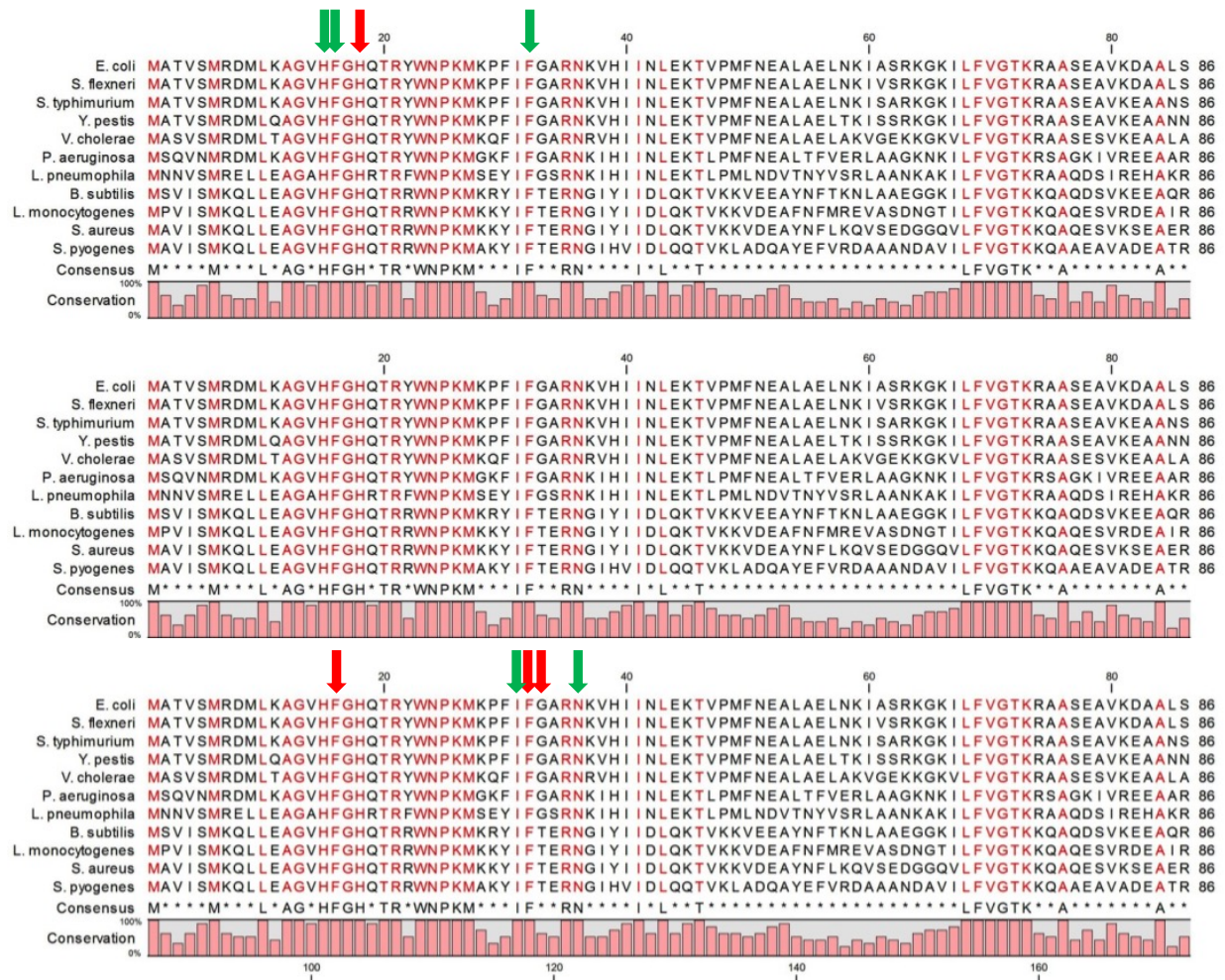
Supplementary Figure S3. Binding position of S1 on the *E. coli* 70S ribosome. **(A)** The average resolution of the cryo-EM map of the ErmCL-ribosome complex was 7.9 Å as determined using the Fourier shell correlation (FSC) cut-off value of 0.5. **(B)** Overview of the cryo-EM map of the ErmCL-ribosome complex (grey mesh), with rigid-body fitted crystal structure of the 30S subunit (pdb accession code 3ofo) from the *E. coli* 70S ribosome (1) (dark grey). Ribosomal protein S2 is colored orange and highlighted electron densities for S1_{D1} (blue) and S1_{D2} (cyan). **(C)** Inset from (B) showing extra unaccounted for density in the cryo-EM map of the ErmCL-ribosome complex (grey mesh) adjacent to S2 (orange). **(D)** InstantBlue (Expedeon) stained 15% SDS polyacrylamide gel electrophoresis of the ErmCL-ribosome complex, indicating the presence of ribosomal protein S1 at ~60 kDa. **(E)** Cryo-EM map (grey mesh) of the ErmCL-ribosome complex containing additional density for domain 1 (S1_{D1}, blue) and domain 2 (S1_{D2}, cyan) of ribosomal protein S1. The model for S1_{D1} was obtained by aligning S2 (yellow) of the chimeric S2-S1_{NTD} with S2 (orange) from an *E. coli* 30S subunit (pdb accession code 3ofo) (1) fitted to the cryo-EM map (grey mesh) as a rigid body. The model was refined for the complete S1_{NTD} based on homology with eIF2α (pdb accession code 1kl9) (2) and fitted so as to maintain interactions between S1 and S2 as observed in the chimeric crystal structure, but also constrained by the electron density of the cryo-EM map (grey mesh). A tentative model for S1_{D2} (cyan) was generated based on homology with eIF2α (pdb accession code 1kl9) (2) and fitted into the density. **(F)** Electron density map (grey mesh) of a SecM-stalled ribosome-channel complex (3) with fitted crystal structure for S2 (orange) from an *E. coli* 30S subunit (pdb accession code 3ofo) (1).



Supplementary Figure S4. Comparison of cryo-EM electron densities for S1 on the *E. coli* 70S ribosome. Difference electron density maps (grey mesh) calculated by **(A)** subtracting the filtered map for *T. thermophilus* 30S subunit (PDB ID 1J5E (4)) from EMD-1003 (5), or from **(B)** the ErmCL-SRC map as well as by subtracting the filtered map for *E. coli* 30S subunit (pdb accession code 3ofo (1)) from **(C)** EMD-1003 (5), or from **(D)** the ErmCL-SRC map. The relative positions of ribosomal protein S21 (green) (pdb accession code 3ofo (1)), 16S rRNA (red) and mRNA (orange) from (pdb accession code 4gd2 (6)), as well as S2 (S1_{NTD}-S2; yellow), S1 domain 1 (S1_{NTD}-S2; blue) and domain 2 (tentative placement of model, which was generated based on homology with eIF2 α (pdb accession code 1k19 (2), cyan).



Supplementary Figure S5. Multiple sequence alignment of the S1_{NTD} protein of several representatives of the class of γ -Proteobacteria. The 100% conserved residues are indicated in red. The Phe5 and Phe9 residues involved in the π -stacking interaction with S2 and the Lys43 residue contacting the zinc binding pocket of S2 are marked by red and blue arrow heads, respectively. The position of the NTH (green helix) and the four β -strands (blue arrows) as determined by crystallography are indicated above. The amino acid alignment was generated using CLC Genomics Workbench software [<http://www.clcbio.com/>].



Supplementary Figure S6. Multiple sequence alignment of the S2 protein of several representatives of the γ -Proteobacteria and Firmicutes. The 100% conserved residues are indicated in red. The residues involved in zinc-binding are indicated by red arrows and the residues contacting the S1_{NTD} are indicated by green arrows. The amino acid alignment was generated using CLC Genomics Workbench software [<http://www.clcbio.com/>].

SUPPLEMENTARY TABLES

Supplementary Table S1. Bacterial strains and plasmids used in this study

	Relevant features	Source or reference
<i>E. coli</i> strains:		
JE28	MG1655:: <i>rpL-his</i>	(7)
Tuner	F ⁻ <i>ompT hsdS_B (r_B⁻ m_B⁻) gal dcm lacY1</i>	Novagen
Tuner(DE3)	F ⁻ <i>ompT hsdS_B (r_B⁻ m_B⁻) gal dcm lacY1(DE3)</i>	Novagen
Plasmids:		
pProEX-HTb	vector for Trc driven gene expression	Invitrogen
pProEX-S2-HA	encodes his- and HA-tagged S2 WT	this study
pProEX-S2-S1 _{NTD}	encodes his-tagged S2-S1 _{NTD}	this study
pPro-S1 ₈₆ ^F	encodes FLAG-tagged S1 ₈₆	this study
pPro-S1 ₁₀₆ ^F	encodes FLAG-tagged S1 ₁₀₆	(8)
pPro-S1 ₁₉₋₈₆ ^F	encodes FLAG-tagged S1 ₁₉₋₈₆	this study
pPro-S1 ₁₉₋₁₀₆ ^F	encodes FLAG-tagged S1 ₁₉₋₁₀₆	this study
pPro-S1 ^F	encodes FLAG-tagged S1	(8)
pPro-S1 ₁₉₋₅₅₇ ^F	encodes FLAG-tagged S1 ₁₉₋₅₅₇	this study
pPro-S1 ₈₇₋₅₅₇ ^F	encodes FLAG-tagged S1 ₈₇₋₅₅₇	(8)
pPro-S1 _{NTSΦ106-557}	encodes FLAG-tagged S1 _{NTSΦ106-557}	this study
pPro-S1 ₈₆ ^F _{F5A}	encodes FLAG-tagged S1 ₈₆ , F5A	this study
pPro-S1 ₈₆ ^F _{F9A}	encodes FLAG-tagged S1 ₈₆ , F9A	this study
pPro-S1 ₈₆ ^F _{D39K}	encodes FLAG-tagged S1 ₈₆ , D39K	this study
pPro-S1 ₈₆ ^F _{K43E}	encodes FLAG-tagged S1 ₈₆ , K43E	this study
pET22b	vector for T7 driven over expression	Novagen
pET-S1 ₁₀₆	pET derivative encoding for his-tagged S1 ₁₀₆	this study
pET-S1 ₈₆	pET derivative encoding for his-tagged S1 ₈₆	this study
pET-S1 ₁₉₋₈₆	pET derivative encoding for his-tagged S1 ₁₉₋₈₆	this study
pKS0325	<i>ompA</i> gene under control of T7-promoter	(9)

Supplementary Table S2. Oligonucleotides used in this study

P1	TATAGGCGCCGAATTCGATGCAACTGTTTCC	fwd primer to clone S2-HA
P2	TATACTCGAGTTAAGCGTAATCTGGAACATC GTACTCAGCTTCTACG	rev primer to clone S2-HA
P3	TATAAAGCTTATATTTTCAGGGTGAATCTTTT GCTCAACTC	fwd primer to clone S2-S1NTD
P4	TATAAAGCTTTTACAGCAGAGTTTCACCG	rev primer to clone S2-S1NTD
P5	P-GAAACTGTTACCGGTGTTATC	fwd primer to remove S1 _{D1} -coding sequence
P6	P-ACCCGGGCGGGTTTCG	rev primer to remove S1 _{D1} -coding sequence
P7	P-CCGGGTTCTATCGTTCCG	fwd primer to remove the first 18 codons of <i>rpsA</i>
P8	P-CATGGTCTGTTTCCTGTG	rev primer to remove the first 18 codons of <i>rpsA</i>
P9	P-GACTATAAGGATGACG	fwd primer to remove the sequence coding for S1 ₈₇₋₁₀₆
P10	P-CAGCAGAGTTTCAC	rev primer to remove the sequence coding for S1 ₈₇₋₁₀₆
P11	TATACATATGACTGAATCTTTTGCTC	fwd primer to amplify <i>rpsA</i> from the 1 st codon
P12	TATACATATGACCCGCCGGGTTCC	fwd primer to amplify <i>rpsA</i> sequence from the 19th codon
P13	TATACTCGAGTTCAGCATCTTCGTAAGC	rev primer to amplify <i>rpsA</i> until 106 th codon
P14	TATACTCGAGCAGCAGAGTTTCAC	rev primer to amplify <i>rpsA</i> until 86 th codon
P15	P-CTCTCAAAGAGTTGAGCGGCAGATTCAG	rev primer to introduce the mutation F5A
P16	P-CTCTCCGCGAGTTGAGCAAAAGATTCAG	rev primer to introduce the mutation F9A
P17	P-TCCTAAAAGAAATCGAAACCCGCCCG	fwd primer to introduce the mutations F5A and F9A
P18	P-GTTAAAGCTGGTCTGAAATCTG	fwd primer to introduce the mutation D39K
P19	P-GTTGACGCTGGTCTGGAATCTG	fwd primer to introduce the mutation K43E
P20	P-CAGTACTACGTCTTTGTGCGATAG	rev primer to introduce the mutations D39K and K43E

Supplementary Table S3. The PISA interface analysis.

	S2	S1_{NTD}	S2/S1_{NTH}	S1_{NTH}	S2/S1_{D1}	S1_{D1}
Number of atoms	90 (4.8%)	81 (16.8%)	48 (2.6%)	42 (13.6%)	42 (2.2%)	39 (11.1%)
Number of residues	22 (9.2%)	23 (35.9%)	12 (5%)	12 75%	11 (4.6%)	11 (22.9%)
Solvent-accessible area (Å²)	725 (5.6%)	870 (15.7%)	402.3 (3.1%)	456.6 (25.7%)	322.7 (2.5%)	413.5 (11%)
Solvation energy gain [kcal/mol]	-2 (0.9%)	-4.8 (10.9%)	-2.3 (1.1%)	-5.5 (83.2%)	0.3 (0.1%)	0.7 (-1.9%)
P-value	0.495	0.397	0.311	0.176	0.703	0.818

SUPPLEMENTARY REFERENCES

1. Dunkle, J.A. and Cate, J.H. (2010) Ribosome structure and dynamics during translocation and termination. *Annu. Rev. Biophys.*, **39**, 227-244.
2. Nonato, M.C., Widom, J. and Clardy, J. (2002) Crystal structure of the N-terminal segment of human eukaryotic translation initiation factor 2alpha. *J. Biol. Chem.*, **277**, 17057-17061.
3. Park, E., Menetret, J.F., Gumbart, J.C., Ludtke, S.J., Li, W., Whynot, A., Rapoport, T.A. and Akey, C.W. (2014) Structure of the SecY channel during initiation of protein translocation. *Nature*, **506**, 102-106.
4. Wimberly, B.T., Brodersen, D.E., Clemons, W.M., Jr., Morgan-Warren, R.J., Carter, A.P., Vornrhein, C., Hartsch, T. and Ramakrishnan, V. (2000) Structure of the 30S ribosomal subunit. *Nature*, **407**, 327-339.
5. Gabashvili, I.S., Agrawal, R.K., Spahn, C.M., Grassucci, R.A., Svergun, D.I., Frank, J. and Penczek, P. (2000) Solution structure of the *E. coli* 70S ribosome at 11.5 Å resolution. *Cell*, **100**, 537-549.
6. Dunkle, J.A., Wang, L., Feldman, M.B., Pulk, A., Chen, V.B., Kapral, G.J., Noeske, J., Richardson, J.S., Blanchard, S.C. and Cate, J.H. (2011) Structures of the bacterial ribosome in classical and hybrid states of tRNA binding. *Science*, **332**, 981-984.
7. Ederth, J., Mandava, C.S., Dasgupta, S. and Sanyal, S. (2009) A single-step method for purification of active His-tagged ribosomes from a genetically engineered *Escherichia coli*. *Nucleic Acids Res.*, **37**, e15.
8. Byrgazov, K., Manoharadas, S., Kaberdina, A.C., Vesper, O. and Moll, I. (2012) Direct interaction of the N-terminal domain of ribosomal protein S1 with protein S2 in *Escherichia coli*. *PLoS One*, **7**, e32702.
9. Ried, G., Koebnik, R., Hindennach, I., Mutschler, B. and Henning, U. (1994) Membrane topology and assembly of the outer membrane protein OmpA of *Escherichia coli* K12. *Mol. Gen. Genet.*, **243**, 127-135.

The proline-rich antimicrobial peptide Onc112 inhibits translation by blocking and destabilizing the initiation complex

A Carolin Seefeldt^{1,2,6}, Fabian Nguyen^{3,6}, Stéphanie Antunes^{1,4,6}, Natacha Pérébaskine^{1,2}, Michael Graf³, Stefan Arenz³, K Kishore Inampudi^{1,2}, Céline Douat^{1,4}, Gilles Guichard^{1,4}, Daniel N Wilson^{3,5} & C Axel Innis^{1,2}

The increasing prevalence of multidrug-resistant pathogenic bacteria is making current antibiotics obsolete. Proline-rich antimicrobial peptides (PrAMPs) display potent activity against Gram-negative bacteria and thus represent an avenue for antibiotic development. PrAMPs from the oncocin family interact with the ribosome to inhibit translation, but their mode of action has remained unclear. Here we have determined a structure of the Onc112 peptide in complex with the *Thermus thermophilus* 70S ribosome at a resolution of 3.1 Å by X-ray crystallography. The Onc112 peptide binds within the ribosomal exit tunnel and extends toward the peptidyl transferase center, where it overlaps with the binding site for an aminoacyl-tRNA. We show biochemically that the binding of Onc112 blocks and destabilizes the initiation complex, thus preventing entry into the elongation phase. Our findings provide a basis for the future development of this class of potent antimicrobial agents.

Antimicrobial peptides form a diverse group of molecules that are produced as part of the innate immune response of all multicellular organisms¹. Among these, PrAMPs have garnered considerable attention as a possible means of countering the rapid increase in bacterial resistance to classical antibiotics^{2,3}. Unlike many peptides that kill bacteria by disrupting their cell membrane, PrAMPs are transported into the cytoplasm by specialized transporters, such as SbmA in Gram-negative bacteria^{4,5}, where they inhibit specific intracellular targets. Given that such transport mechanisms are absent in mammalian cells, and only limited interactions with intracellular eukaryotic proteins have been detected, PrAMPs are generally considered to be nontoxic⁶ and therefore an attractive alternative to existing antimicrobials. Interestingly, some PrAMPs can cross the blood-brain barrier to selectively target brain cells, thus further highlighting their potential for the treatment of cerebral infections or for brain-specific drug delivery⁷.

Initial efforts to locate bacterial targets for PrAMPs led to the identification of the heat-shock protein DnaK as the prime candidate for inhibition⁸. Short proline-rich peptides (of 18–20 amino acids (aa)) such as oncocin, drosocin, pyrrolicorin or apidaecin were previously shown to bind to this bacterial chaperone in a stereospecific manner, thus leading to the development of improved PrAMP derivatives with increased affinity for DnaK^{9–12}. However, subsequent studies into the antimicrobial properties of PrAMPs¹³ have suggested that these peptides are likely to use additional modes of action to inhibit growth. For example, a C-terminally truncated version of the apidaecin 1b peptide results in a loss of antimicrobial activity but no observable decrease

in DnaK binding or cellular uptake¹³. Similarly, oncocin (Onc72 and Onc112) and apidaecin (Api88 and Api137) derivatives were found to inhibit the growth of a *dnaK*-deletion strain as efficiently as that of the *dnaK*-containing parental strain¹⁴. Further investigation revealed that these PrAMPs have an additional target within the bacterial cell, namely the ribosome¹⁴. Although such PrAMPs have been shown to bind to the ribosome and inhibit translation¹⁴, the mechanism by which they inhibit translation has so far not been determined.

Here, we set out to address this issue by obtaining a 3.1-Å-resolution X-ray crystallography structure of the *Thermus thermophilus* 70S ribosome (*Th70S*) in complex with a peptidyl (P)-site-bound deacylated tRNA^{iMet} and Onc112, a representative of the oncocin family of PrAMPs produced by the milkweed bug (*Oncopeltus fasciatus*)¹⁵. The structure reveals that the N-terminal residues 1–12 of Onc112 bind to the upper region of the ribosomal exit tunnel, overlapping the binding site for the CCA end of an aminoacyl (A)-site tRNA at the peptidyl transferase center. Consistently with this, we showed biochemically that Onc112 allows translation to initiate but destabilizes the initiation complex and thus prevents subsequent entry of affected ribosomes into the translation-elongation phase. Moreover, we demonstrated that although truncation of the C-terminal portion of Onc112 is dispensable for ribosome binding, it is essential for antimicrobial activity. We believe that these findings will provide an excellent basis for the design of improved antibacterial compounds, either peptidic or peptidomimetic, that inhibit translation by targeting the ribosomal exit tunnel.

¹Institut Européen de Chimie et Biologie, Université de Bordeaux, Pessac, France. ²INSERM U869, Bordeaux, France. ³Gene Center, Department of Biochemistry, University of Munich, Munich, Germany. ⁴Université de Bordeaux, CNRS, Institut Polytechnique de Bordeaux, UMR 5248, Institut de Chimie et Biologie des Membranes et des Nano-objets (CBMN), Pessac, France. ⁵Center for Integrated Protein Science Munich (CiPSM), University of Munich, Munich, Germany.

⁶These authors contributed equally to this work. Correspondence should be addressed to C.A.I. (axel.innis@inserm.fr) or D.N.W. (wilson@lmb.uni-muenchen.de).

Received 26 February; accepted 22 April; published online 18 May 2015; doi:10.1038/nsmb.3034

RESULTS

Onc112 binds in a reverse orientation within the exit tunnel

We obtained the structure herein referred to as *Tth70S*–Onc112 by soaking the 19-aa Onc112 peptide (VDKPPYLPRPRPPPrIYNr-NH₂, in which r denotes D-arginine) into crystals of *Tth70S* ribosomes in complex with a P-site-bound deacylated tRNA_i^{Met} and a short mRNA (Table 1). Using a minimally biased $F_o - F_c$ map calculated after refinement of a model comprising *Tth70S* ribosomes, tRNA_i^{Met} and mRNA but lacking Onc112, we could see clear density that could be attributed to the N-terminal two-thirds of the Onc112 peptide (Fig. 1). Interestingly, the peptide is bound inside the tunnel with a reversed orientation relative to the growing polypeptide chain during protein synthesis, i.e., with its N terminus located near the peptidyl transferase center and its C terminus extending into the exit tunnel toward the constriction formed by ribosomal proteins L4 and L22. Despite the reversed orientation, the location of the Onc112 peptide overlaps to varying extents with the path of nascent polypeptide chains that have been visualized within the ribosomal tunnel^{16–18} (Supplementary Fig. 1). The conformation of Onc112 bound to the ribosome is extended, in a manner similar to but distinct from that observed previously for oncocin in complex with DnaK¹⁰ (Supplementary Fig. 2). Our CD studies suggest that, in solution, the Onc112 peptide adopts an essentially random conformation, with short stretches of poly(Pro)II helix, specifically, 6% α -helix, 54% random coil, 30% PPII and 6% β -sheet (Supplementary Fig. 3).

Interaction between Onc112 and 23S rRNA of the exit tunnel

Comparison of the *Tth70S*–Onc112 structure with that of a *Tth70S* ribosome featuring tRNA_i^{Met} bound to the P site¹⁹ reveals that several nucleotides of the 23S rRNA undergo a conformational change upon binding of Onc112 to the ribosome (Fig. 2a). U2506 shifts to occupy a position similar to that observed upon binding of aminoacyl-tRNA to the A site of the ribosome^{20,21}. In the presence of Onc112, U2585, which is very flexible in many crystal structures, adopts a defined position similar to that modeled in the structure of a vacant *Escherichia coli* 70S ribosome²². In addition, A2062 shifts to provide space for Onc112, adopting a similar conformation to that observed previously in the presence of the ErmBL nascent chain²³. Thus, binding of Onc112 to the ribosome is accompanied by an induced fit involving several 23S rRNA nucleotides that are generally known for their dynamic behavior within the peptidyl transferase center and ribosomal tunnel.

Electron density for the Onc112 peptide was strongest for residues Val1–Pro8 and became weaker after Pro10, thus making it difficult to model the peptide beyond Pro12 (Fig. 1). We observed three sets of interactions between the N-terminal 10 aa of Onc112 and nucleotides of the 23S rRNA (Fig. 2b). The first set involves aa 1–3 of Onc112 and encompasses eight potential hydrogen-bond interactions (Fig. 2b,c). Val1 of Onc112 can form three hydrogen bonds with nucleotides of the 23S rRNA; two via its α -amine to the N3 atom of C2573 and the O3' atom of C2507; and one via its carbonyl oxygen to the N4 atom of C2573. Three additional hydrogen bonds are possible between the side chain carboxylic acid of Asp2 and the N1 and N2 atoms of G2553 or the 2'-OH of C2507. The positively charged side chain of Lys3 extends into a negatively charged cavity, displacing a hydrated magnesium ion that is present at this site in other *Tth70S* ribosome structures²⁰, and it interacts with the backbone phosphates of A2453 (Fig. 2c) and U2493 (not shown). Substitution of Val1, Asp2 and especially Lys3 by alanine in Onc72 leads to a loss of antimicrobial activity¹⁰, whereas, as expected, a D2E mutant of Onc112 retained both *in vitro* and *in vivo* activity (Supplementary Fig. 4). The K3A

Table 1 Data collection and refinement statistics

<i>Tth70S</i> –Onc112 ^a	
Data collection	
Space group	$P2_12_12_1$
Cell dimensions	
<i>a</i> , <i>b</i> , <i>c</i> (Å)	209.30, 452.29, 624.12
α , β , γ (°)	90.0, 90.0, 90.0
Resolution (Å)	50 (3.1)
R_{merge}	25.5% (166.4%)
$I / \sigma I$	5.47 (0.95)
Completeness (%)	99.1 (98.8)
Redundancy	3.8 (3.6)
Refinement	
Resolution (Å)	3.1
No. reflections	3,999,403
$R_{\text{work}} / R_{\text{free}}$	23.08 / 27.13
No. atoms	
Protein / RNA	91,758 / 195,737
Ligand/ion	2,333
B factors	
Protein / RNA	64.81 / 63.15
Ligand/ion	51.31
r.m.s. deviations	
Bond lengths (Å)	0.015
Bond angles (°)	0.809

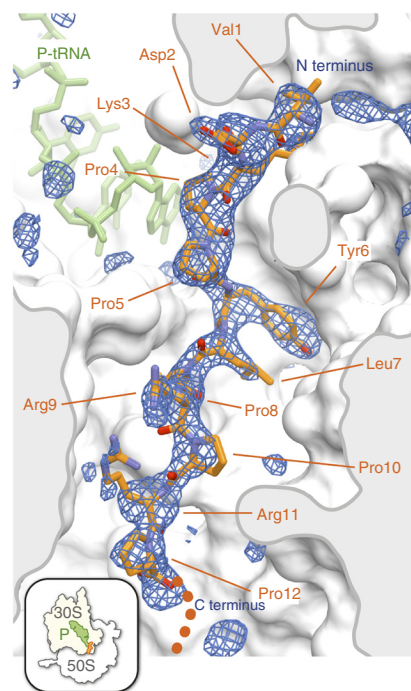
^aStructure determined from a single crystal.

substitution in Onc72 reduced its ribosome binding affinity by a factor of 4.3 and lowered the half-maximal inhibitory concentration (IC₅₀) for *in vitro* translation more than 18-fold¹⁴.

The second set of interactions involves the side chains of Tyr6 and Leu7 of Onc112 (Fig. 2b,d). The aromatic side chain of Tyr6 establishes a π -stacking interaction with C2452 of the 23S rRNA (Fig. 2d). In addition, the side chain hydroxyl of Tyr6 hydrogen-bonds with an undetermined ion that is coordinated by the backbone phosphate of U2506 and the O2 atoms of C2452 and U2504. The hydrophobic cavity occupied by the Tyr6 side chain also accommodates the side chain of Leu7 of Onc112, which packs against the phenol moiety of Tyr6, whereas the backbone of Leu7 forms two hydrogen bonds with U2506 (Fig. 2b,d). The compact hydrophobic core formed by Tyr6 and Leu7 is likely to be key in anchoring the Onc112 peptide to the tunnel because mutagenesis experiments have shown that alanine substitution of either residue in Onc72 reduces the ribosome binding affinity by a factor of 7 and results in a complete loss of inhibitory activity on translation *in vitro*¹⁴. In contrast, mutation of Leu7 in Onc112 to cyclohexylalanine, which would preserve the hydrophobic environment, resulted in retention of inhibitory activity on translation *in vitro* but unexpectedly led to a loss of antimicrobial activity (Supplementary Fig. 4).

Additional interactions with the ribosome encompass the PRPRP motif of Onc112 (Fig. 2b) and include a π -stacking interaction between the guanidino group of Arg9 of Onc112 and the base of C2610 (Fig. 2e). Although substitution of Arg11 with alanine in Onc72 also reduces the ribosome binding affinity and inhibitory properties of the peptide¹⁴, we observed very little density for the side chain of this residue, thus suggesting that it could be important for the overall electrostatic properties of the peptide rather than for a defined interaction with the ribosome (Fig. 1). The high conservation of the 23S rRNA nucleotides that comprise the ribosome-binding site of Onc112 is consistent with the broad spectrum of antimicrobial

Figure 1 Onc112-binding site within the exit tunnel of the ribosome. Transverse section of the exit tunnel of the *Tth70S* ribosome showing the binding site for the Onc112 peptide (orange). Minimally biased $F_o - F_c$ difference map contoured at $+3.0\sigma$ (blue) is observable for the first 12 amino acids of Onc112 (**VDKPPYLPRPRPPRRrY**Nr-NH₂; residues 1–12 are bold and underlined). Initiator tRNA^{Met} bound at the P site is shown in green. Inset shows the view chosen to display the Onc112 peptide relative to the complete 70S ribosome.



activity displayed by this and related PrAMPs against a range of Gram-negative bacteria^{10,24}.

Onc112 allows translation to initiate but blocks elongation

Comparison of the *Tth70S*–Onc112 structure with that of the *Tth70S* ribosome in the preattack state of peptide-bond formation²⁰ indicated that the binding of Onc112 to the ribosome would prevent accommodation of the CCA end of an incoming aminoacyl-tRNA via steric occlusion of the ribosomal A site at the peptidyl transferase center (Fig. 3a). Indeed, Asp2 of Onc112 directly interacts with G2553, a residue located within helix H92 of the 23S rRNA, termed the A loop, that normally stabilizes the A site tRNA at the peptidyl transferase center via Watson-Crick base-pairing with nucleotide C75 of its CCA end.

In order to determine the step of translation that Onc112 inhibits, we performed cell-free protein synthesis and monitored the location of the ribosomes on the mRNA (Fig. 3b and Supplementary Data Set 1), by using toe-printing assays^{25,26}. In the absence of Onc112 or antibiotic, ribosomes were able to initiate at the AUG start codon and translate through the open reading frame, but they became trapped on the downstream isoleucine codon because isoleucine was omitted from the translation mix. In the presence of the antibiotics clindamycin or thiostrepton, ribosomes accumulated at the start codon and could not translate down to the isoleucine codon because these antibiotics prevent delivery and/or accommodation of the first aminoacyl-tRNA directly following the initiation codon²⁷. We observed similar results when performing the toe-printing assay with increasing concentrations of the Onc112 peptide, namely a loss

of the band corresponding to ribosomes stalled at the isoleucine codon and an increase in the band corresponding to the ribosomes accumulating at the start codon. These findings indicate that Onc112 allows subunit joining and formation of the 70S initiation complex but prevents accommodation of the first aminoacyl-tRNA at the A site, as suggested by steric overlap between Onc112 and an A-site tRNA (Fig. 3a). This contrasts with a bona fide translation-initiation inhibitor, such as edeine, which interferes with the stable binding of fMet-tRNA^{Met} to the 30S subunit and thus prevents 70S initiation-complex formation²⁸, in agreement with the lack of a toe-print band at the start codon in the presence of edeine (Fig. 3b).

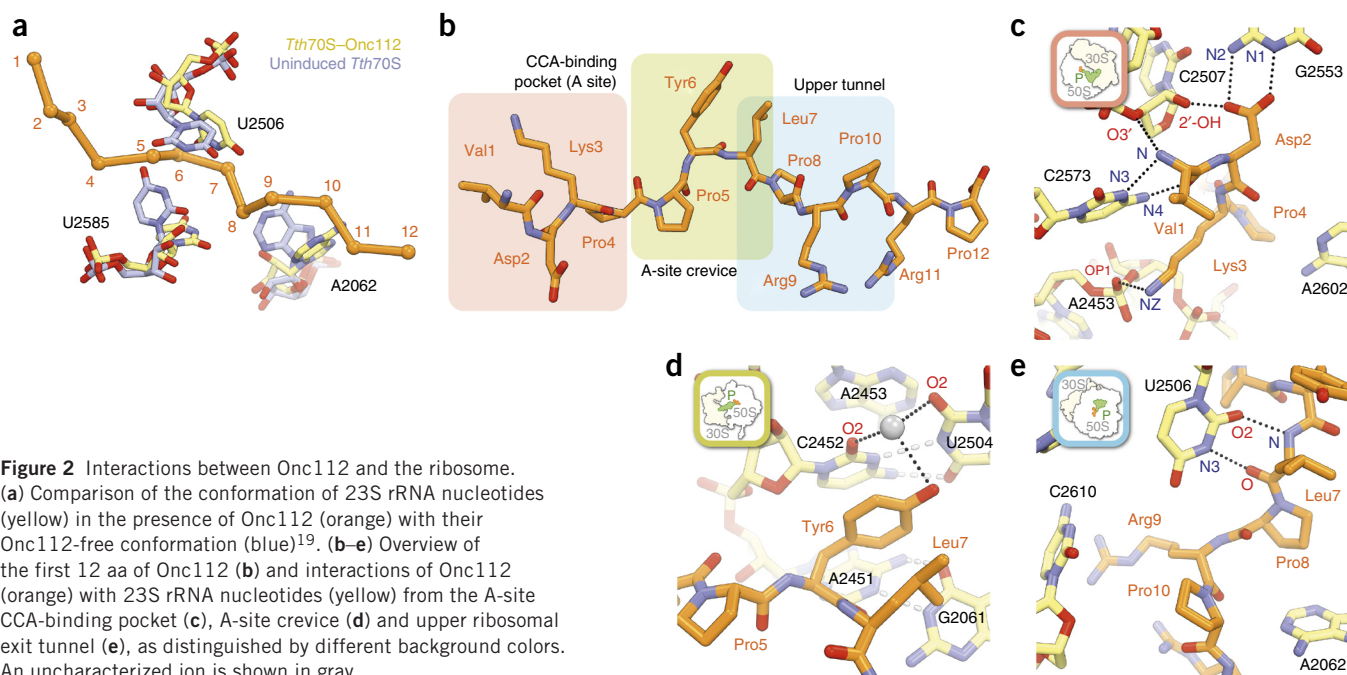
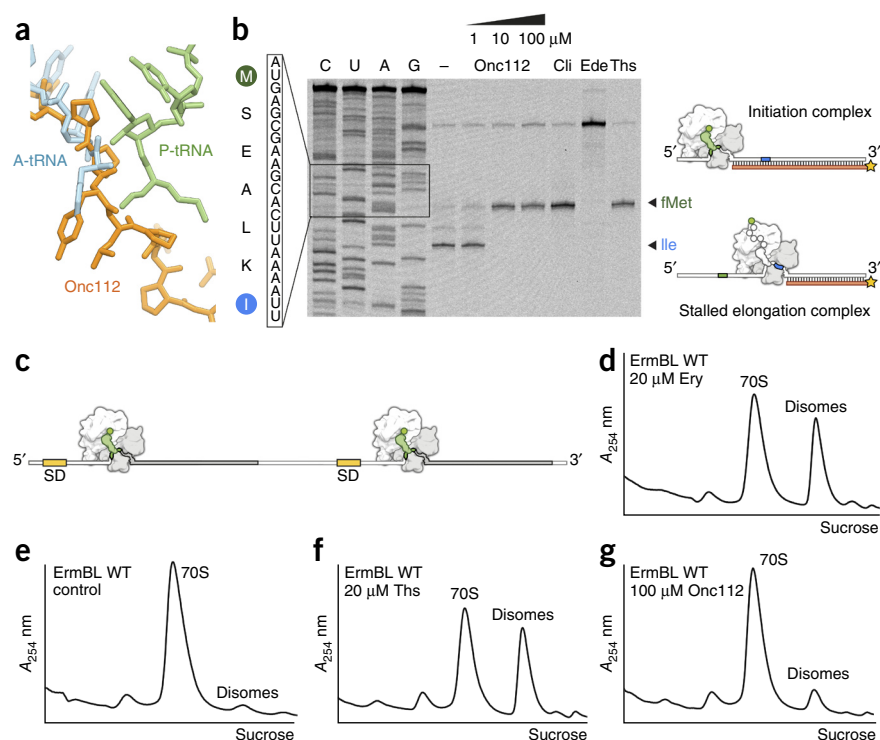


Figure 2 Interactions between Onc112 and the ribosome. (a) Comparison of the conformation of 23S rRNA nucleotides (yellow) in the presence of Onc112 (orange) with their Onc112-free conformation (blue)¹⁹. (b–e) Overview of the first 12 aa of Onc112 (b) and interactions of Onc112 (orange) with 23S rRNA nucleotides (yellow) from the A-site CCA-binding pocket (c), A-site crevice (d) and upper ribosomal exit tunnel (e), as distinguished by different background colors. An uncharacterized ion is shown in gray.

Figure 3 Onc112 blocks and destabilizes the initiation complex. **(a)** Structural comparison of Phe-tRNA^{Phe} (blue) in the A site and fMet-tRNA^{Met} in the P site (green)²⁰ with the binding site of Onc112 (orange). **(b)** Toe-printing assay performed in the absence (–) or presence of increasing concentrations (1 μ M, 10 μ M and 100 μ M) of Onc112, 50 μ M clindamycin (Cli), 50 μ M edeine (Ede) or 100 μ M thiostrepton (Ths). Sequencing lanes for C, U, A and G and the sequence surrounding the toe-print bands (arrows) when ribosomes accumulate at the AUG start codon (green, initiation complex) or the isoleucine codon (blue, stalled elongation complex) are included for reference, as illustrated graphically. The uncropped gel image for the toe-printing assay is in **Supplementary Data Set 1**. **(c–g)** Schematic **(c)** showing the dicistronic ErmBL mRNA that was used to monitor disome formation with sucrose gradients in the presence **(d)** or absence **(e)** of 20 μ M erythromycin (Ery) or the presence of 20 μ M thiostrepton **(f)** or 100 μ M Onc112 **(g)**. In **c**, SD denotes the Shine-Dalgarno sequence. A, absorbance.



Onc112 destabilizes the translation-initiation complex

We noticed that the toe-print bands at the start codon in the presence of Onc112 were consistently weaker than those observed in the presence of clindamycin or thiostrepton (**Fig. 3b** and data not shown), thus suggesting that Onc112 may also perturb the placement of fMet-tRNA₁^{Met} at the P site. In the *Tth70S*–Onc112 structure, the P-site tRNA is uncharged, and its terminal A76 residue undergoes a conformational change that positions it ~3.4 Å away from the Onc112 peptide. *In vivo*, however, we would expect fMet-tRNA₁^{Met} to bind to the peptidyl transferase center in the same manner as in the *Tth70S* ribosome preattack complexes²⁰, such that the formyl group of the fMet moiety would sterically clash with residues Tyr6 and Leu7 of the Onc112 peptide (**Fig. 3a**). Consequently, we used sucrose gradients to monitor disome formation upon translating a dicistronic ErmBL mRNA *in vitro*, in order to investigate the stability of the translation-initiation complex formed in the presence of Onc112 (**Fig. 3c–g**). As a positive control, we performed translation in the presence of the macrolide antibiotic erythromycin, which acts synergistically with the ErmBL polypeptide

chain within the ribosomal tunnel to stall translation at a specific site on the mRNA²⁹. Because the mRNA was dicistronic, two stalled ribosomes on a single mRNA led to the formation of disomes that could be visualized on a sucrose gradient (**Fig. 3d**), as shown previously^{16,23}. We observed negligible disome formation in the absence of erythromycin because the ribosomes rapidly translated the short ORF and were released from the mRNA (**Fig. 3e**). As expected, thiostrepton, which allows 70S initiation-complex formation but prevents elongation (**Fig. 3b**), also led to efficient disome formation (**Fig. 3f**). In contrast, the presence of Onc112, even at concentrations as high as 100 μ M, resulted in only a small increase in disomes (**Fig. 3g**). This leads us to suggest that the 70S initiation complexes formed in the presence of Onc112 are unstable, presumably because the Onc112 peptide encroaches onto fMet-tRNA₁^{Met}, thus causing it to dissociate from the ribosome under the nonequilibrium conditions (centrifugation and sucrose density) used in the disome assay.

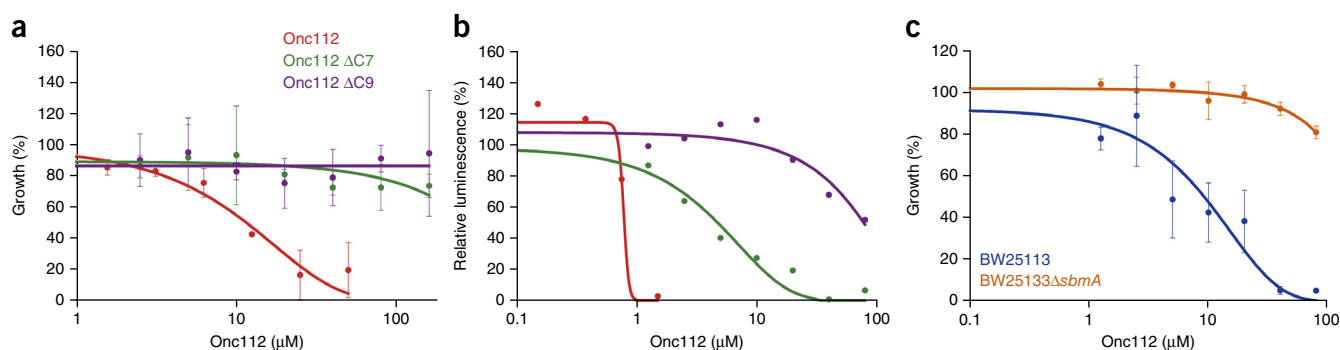
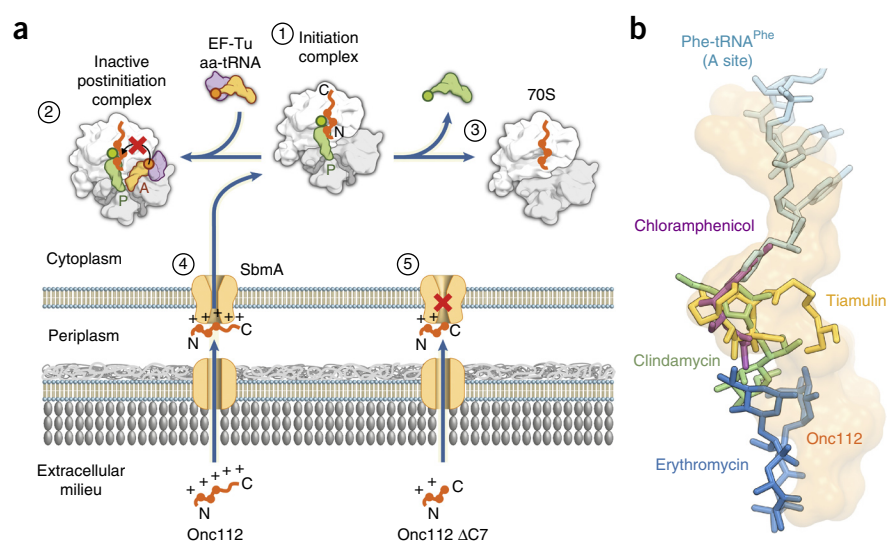


Figure 4 Characterization of Onc112, its C-terminally truncated derivatives and its membrane transporter in Gram-negative bacteria. **(a,b)** Effect of Onc112 (red) and C-terminally truncated Onc112 derivatives Onc112 Δ C7 (green) and Onc112 Δ C9 (purple) on overnight growth of *E. coli* strain BL21(DE3) **(a)** and the luminescence resulting from the *in vitro* translation of Fluc **(b)**. **(c)** Effect of Onc112 on overnight growth of *E. coli* strain BW25113 (blue) or BW25113 Δ sbmA (orange). In **a** and **c**, error bars represent mean \pm s.d. for triplicate experiments, whereas the experiment in **b** was performed in duplicate, with the plotted points representing the mean value. The growth or luminescence measured in the absence of peptide was assigned as 100% in all cases.

Figure 5 Mechanism of action and overlap of Onc112 with antibiotics that target the large subunit of the ribosome. **(a)** Model for the mechanism of action of Onc112. (1) Onc112 binds within the exit tunnel of the ribosome with a reverse orientation relative to a nascent polypeptide chain. (2) Onc112 allows formation of a translation-initiation complex but prevents accommodation of the aminoacyl-tRNA (aa-tRNA) at the A site of the peptidyl transferase center. (3) The initiation complex is destabilized, thus leading to dissociation of the fMet-tRNA_i^{Met} from the P site. Although full-length Onc112 can efficiently penetrate the bacterial cell membrane by using the SbmA transporter (4), C-terminal truncation of Onc112 reduces its antimicrobial activity (5), presumably owing to impaired uptake. **(b)** Relative binding position of Onc112 (orange) on the ribosome, compared with those of well-characterized translation inhibitors chloramphenicol (purple)^{32,33}, clindamycin (green)³³, tiamulin (yellow)³⁴ and erythromycin (blue)^{32,33} as well as an A site-bound Phe-tRNA^{Phe} (ref. 20).



Onc112 C terminus is needed for uptake, not ribosome binding

The lack of density for the C terminus of Onc112 (residues 13–19) hinted that this region is dispensable for ribosome binding, yet its high degree of conservation suggested that it may nevertheless be necessary for antimicrobial activity. In order to assess the role of the C-terminal region of Onc112, we prepared truncated versions of this peptide, Onc112 Δ C7 and Onc112 Δ C9, which lacked the last 7 and 9 aa, respectively. We then determined the half-minimal inhibitory concentration (MIC₅₀) for the growth of *E. coli* strain BL21(DE3) in the presence of full-length Onc112 and compared it with those of the truncated Onc112 Δ C7 and Onc112 Δ C9 derivatives (Fig. 4a). As expected, the full-length Onc112 displayed good activity, inhibiting growth with an MIC₅₀ of 10 μ M, a value similar to that reported previously¹⁴. In contrast, truncation of 7 or 9 aa from the C terminus of Onc112 led to a complete loss of inhibitory activity, even at concentrations above 100 μ M (Fig. 4a). To ascertain whether the truncated Onc112 peptides could still bind to the ribosome and inhibit translation, we monitored *in vitro* translation of firefly luciferase (Fluc) by measuring luminescence after 60 min of translation in the presence of increasing concentrations of either full-length Onc112 or the truncated Onc112 Δ C7 and Onc112 Δ C9 derivatives (Fig. 4b). As expected, the full-length peptide displayed excellent activity, inhibiting translation of Fluc with an IC₅₀ of 0.8 μ M (Fig. 4b), a value similar to that reported when the same system was used for well-characterized translation inhibitors such as chloramphenicol³⁰. In contrast to their lack of antimicrobial activity (Fig. 4a), both truncated Onc112 peptides displayed some inhibitory activity with the *in vitro*-translation system (Fig. 4b), albeit with a reduced efficiency relative to that of full-length Onc112. Specifically, the Onc112 Δ C7 peptide consisting of residues 1–12 of Onc112 had an IC₅₀ of 5 μ M, which was only six times greater than that of full-length Onc112, a result consistent with our structure-based prediction that these residues comprise the major ribosome binding determinants. In contrast, the Onc112 Δ C9 peptide consisting of aa 1–10 of Onc112 had an IC₅₀ of 80 μ M, which was 16 times greater than that of Onc112 Δ C7 and two orders of magnitude greater than that of full-length Onc112. These results illustrate the contribution of Arg11 to efficient ribosome binding and translation inhibition, as reported previously¹⁴.

Although the inner-membrane protein SbmA has been shown to be responsible for the uptake of the eukaryotic PrAMPs Bac7 and PR39 (refs. 4,5), the only insect PrAMP tested so far was apidaecin Ib⁴. In order to assess the role of SbmA in the uptake of Onc112, we compared the growth of an *E. coli* strain lacking the *sbmA* gene (Δ *sbmA*) with the parental strain BW25113 in the presence of increasing concentrations of Onc112 (Fig. 4c). As expected, the full-length Onc112 displayed excellent activity against the susceptible SbmA-containing parental strain, inhibiting growth with an MIC₅₀ of 8 μ M (Fig. 4c), a value similar to that observed with the BL21(DE3) strain (Fig. 4a). In contrast, the Δ *sbmA* strain displayed increased resistance to Onc112, such that even with 100 μ M Onc112, growth was reduced by only 20% (Fig. 4c). These findings indicate that SbmA is indeed necessary for the uptake of Onc112 into Gram-negative bacteria, such as *E. coli*, and provide further support for the proposition that the SbmA transporter is involved in the mechanism of action of the entire group of the PrAMPs⁴.

DISCUSSION

From our structural and biochemical data, we propose a model to explain the mechanism by which PrAMPs such as oncocin inhibit translation (Fig. 5a). We have shown that the binding of Onc112 to the ribosomal exit tunnel allows formation of the 70S initiation complex but prevents accommodation of the aminoacyl-tRNA into the A site (Fig. 5a, steps 1 and 2). Additionally, we propose that Onc112 destabilizes the postinitiation complex by inducing dissociation of fMet-tRNA_i^{Met} from the P site (Fig. 5a, step 3). Finally, our data also suggest that positively charged residues distributed along the entire length of the Onc112 sequence are necessary for ensuring the efficient SbmA-mediated uptake of Onc112 into the cell, whereas residues from the N-terminal moiety of Onc112 are responsible for targeting this peptide to the ribosome (Fig. 5a, steps 4 and 5). We believe that this mechanism of action is likely to be the same for other PrAMPs, such as drosocin, pyrrothocorin and apidaecin, which share many of the residues of Onc112 that are important for its ribosome binding and antimicrobial function.

The binding site for Onc112 within the ribosomal exit tunnel overlaps with the binding sites for a majority of the antibiotics that target the large subunit of the ribosome (Fig. 5b), such as the

chloramphenicols, pleuromutilins (for example, tiamulin) and lincosamides (for example, clindamycin), which inhibit peptide-bond formation by preventing the correct positioning of the tRNA substrates, as well as the macrolides (for example, erythromycin), which abort translation by interfering with the movement of the nascent polypeptide chain through the ribosomal exit tunnel²⁷. Given the substantial spatial overlap that exists between the binding sites for these antibiotics and the regions of the tunnel that interact with Onc112 (Fig. 5b) and presumably with several other PrAMPs, it appears likely that such antimicrobial peptides represent a vast, untapped resource for the development of new therapeutics. Several strategies have been pursued to design improved or entirely new antimicrobials that target the exit tunnel of the ribosome³¹. One approach consists of modifying existing antibiotics to create semisynthetic compounds that possess enhanced antimicrobial properties, including better affinity for mutated or modified ribosomes, the ability to evade drug modification or degradation pathways, increased solubility, improved uptake and reduced efflux. Other strategies involve designing chimeric antibiotics from drugs with adjacent binding sites (for example, macrolide-chloramphenicol or linezolid-sparsomycin) or developing entirely new scaffolds, as exemplified by the oxazolidinone linezolid. The ability to produce new scaffolds based on peptides, such as Onc112, that display potent activity against a diverse range of Gram-negative bacteria represents an exciting avenue for the development of future antimicrobials.

METHODS

Methods and any associated references are available in the [online version of the paper](#).

Accession codes. Coordinates and structure factors have been deposited in the Protein Data Bank under accession code **4ZER**.

Note: Any Supplementary Information and Source Data files are available in the [online version of the paper](#).

ACKNOWLEDGMENTS

We thank the staff at the European Synchrotron Radiation Facility (beamline ID-29) for help during data collection and B. Kauffmann and S. Massip at the Institut Européen de Chimie et Biologie for help with crystal freezing and screening. We also thank C. Mackereth for discussions and advice. This research was supported by grants from the Agence Nationale pour la Recherche (ANR-14-CE09-0001 to C.A.I., G.G. and D.N.W.), Région Aquitaine (2012-13-01-009 to C.A.I.), the Fondation pour la Recherche Médicale (AJE201133 to C.A.I.), the European Union (PCIG14-GA-2013-631479 to C.A.I.), the CNRS (C.D.) and the Deutsche Forschungsgemeinschaft (FOR1805, WI3285/4-1 and GRK1721 to D.N.W.). Predoctoral fellowships from the Direction Générale de l'Armement and Région Aquitaine (S. Antunes) and INSERM and Région Aquitaine (A.C.S.) are gratefully acknowledged.

AUTHOR CONTRIBUTIONS

A.C.S. performed structure solution, model building and analysis. N.P. prepared and crystallized ribosomes. N.P. and C.A.I. collected X-ray crystallography data. F.N. performed growth and *in vitro*-translation inhibition assays. S. Antunes and C.D. synthesized the peptides and performed NMR, CD and electrospray ionization high-resolution MS experiments. M.G. performed toe-printing assays. S. Arenz performed disome assays. K.K.I. prepared tRNA^{Met}. G.G., D.N.W. and C.A.I. designed experiments, interpreted data and wrote the manuscript.

COMPETING FINANCIAL INTERESTS

The authors declare no competing financial interests.

Reprints and permissions information is available online at <http://www.nature.com/reprints/index.html>.

1. Wang, G. *et al.* Antimicrobial peptides in 2014. *Pharmaceuticals (Basel)* **8**, 123–150 (2015).

- Casteels, P., Ampe, C., Jacobs, F., Vaeck, M. & Tempst, P. Apidaecins: antibacterial peptides from honeybees. *EMBO J.* **8**, 2387–2391 (1989).
- Li, W. *et al.* Proline-rich antimicrobial peptides: potential therapeutics against antibiotic-resistant bacteria. *Amino Acids* **46**, 2287–2294 (2014).
- Mattiuazzo, M. *et al.* Role of the *Escherichia coli* SbmA in the antimicrobial activity of proline-rich peptides. *Mol. Microbiol.* **66**, 151–163 (2007).
- Runti, G. *et al.* Functional characterization of SbmA, a bacterial inner membrane transporter required for importing the antimicrobial peptide Bac7 (1–35). *J. Bacteriol.* **195**, 5343–5351 (2013).
- Hansen, A., Schäfer, I., Knappe, D., Seibel, P. & Hoffmann, R. Intracellular toxicity of proline-rich antimicrobial peptides shuttled into mammalian cells by the cell-penetrating peptide penetratin. *Antimicrob. Agents Chemother.* **56**, 5194–5201 (2012).
- Stalmans, S. *et al.* Blood-brain barrier transport of short proline-rich antimicrobial peptides. *Protein Pept. Lett.* **21**, 399–406 (2014).
- Otvos, L. *et al.* Interaction between heat shock proteins and antimicrobial peptides. *Biochemistry* **39**, 14150–14159 (2000).
- Czihal, P. *et al.* Api88 is a novel antibacterial designer peptide to treat systemic infections with multidrug-resistant Gram-negative pathogens. *ACS Chem. Biol.* **7**, 1281–1291 (2012).
- Knappe, D. *et al.* Rational design of oncocin derivatives with superior protease stabilities and antibacterial activities based on the high-resolution structure of the oncocin-DnaK complex. *ChemBioChem* **12**, 874–876 (2011).
- Zahn, M. *et al.* Structural studies on the forward and reverse binding modes of peptides to the chaperone DnaK. *J. Mol. Biol.* **425**, 2463–2479 (2013).
- Zahn, M. *et al.* Structural identification of DnaK binding sites within bovine and sheep bactenecin Bac7. *Protein Pept. Lett.* **21**, 407–412 (2014).
- Berthold, N. & Hoffmann, R. Cellular uptake of apidaecin 1b and related analogs in Gram-negative bacteria reveals novel antibacterial mechanism for proline-rich antimicrobial peptides. *Protein Pept. Lett.* **21**, 391–398 (2014).
- Krizsan, A. *et al.* Insect-derived proline-rich antimicrobial peptides kill bacteria by inhibiting bacterial protein translation at the 70 S ribosome. *Angew. Chem. Int. Ed. Engl.* **53**, 12236–12239 (2014).
- Schneider, M. & Dorn, A. Differential infectivity of two *Pseudomonas* species and the immune response in the milkweed bug, *Oncopeltus fasciatus* (Insecta: Hemiptera). *J. Invertebr. Pathol.* **78**, 135–140 (2001).
- Arenz, S. *et al.* Drug sensing by the ribosome induces translational arrest via active site perturbation. *Mol. Cell* **56**, 446–452 (2014).
- Bischoff, L., Berninghausen, O. & Beckmann, R. Molecular basis for the ribosome functioning as an L-tryptophan sensor. *Cell Reports* **9**, 469–475 (2014).
- Shao, S. & Hegde, R.S. Reconstitution of a minimal ribosome-associated ubiquitination pathway with purified factors. *Mol. Cell* **55**, 880–890 (2014).
- Jenner, L. *et al.* Structural basis for potent inhibitory activity of the antibiotic tigecycline during protein synthesis. *Proc. Natl. Acad. Sci. USA* **110**, 3812–3816 (2013).
- Polikanov, Y.S., Steitz, T.A. & Innis, C.A. A proton wire to couple aminoacyl-tRNA accommodation and peptide-bond formation on the ribosome. *Nat. Struct. Mol. Biol.* **21**, 787–793 (2014).
- Schmeing, T.M., Huang, K.S., Strobel, S.A. & Steitz, T.A. An induced-fit mechanism to promote peptide bond formation and exclude hydrolysis of peptidyl-tRNA. *Nature* **438**, 520–524 (2005).
- Schuwirth, B.S. *et al.* Structures of the bacterial ribosome at 3.5 Å resolution. *Science* **310**, 827–834 (2005).
- Arenz, S. *et al.* Molecular basis for erythromycin-dependent ribosome stalling during translation of the ErmBL leader peptide. *Nat. Commun.* **5**, 3501 (2014).
- Knappe, D. *et al.* Oncocin (VDKPPYLPRPRPRRIYNR-NH2): a novel antibacterial peptide optimized against Gram-negative human pathogens. *J. Med. Chem.* **53**, 5240–5247 (2010).
- Hartz, D., McPheeters, D.S., Traut, R. & Gold, L. Extension inhibition analysis of translation initiation complexes. *Methods Enzymol.* **164**, 419–425 (1988).
- Starosta, A.L. *et al.* Translational stalling at polyproline stretches is modulated by the sequence context upstream of the stall site. *Nucleic Acids Res.* **42**, 10711–10719 (2014).
- Wilson, D.N. The A–Z of bacterial translation inhibitors. *Crit. Rev. Biochem. Mol. Biol.* **44**, 393–433 (2009).
- Dinos, G. *et al.* Dissecting the ribosomal inhibition mechanisms of edeine and pactamycin: the universally conserved residues G693 and C795 regulate P-site RNA binding. *Mol. Cell* **13**, 113–124 (2004).
- Vázquez-Laslop, N., Ramu, H., Klepacki, D., Kannan, K. & Mankin, A.S. The key function of a conserved and modified rRNA residue in the ribosomal response to the nascent peptide. *EMBO J.* **29**, 3108–3117 (2010).
- Starosta, A.L. *et al.* Interplay between the ribosomal tunnel, nascent chain, and macrolides influences drug inhibition. *Chem. Biol.* **17**, 504–514 (2010).
- Wilson, D.N. Ribosome-targeting antibiotics and mechanisms of bacterial resistance. *Nat. Rev. Microbiol.* **12**, 35–48 (2014).
- Bulkley, D., Innis, C.A., Blaha, G. & Steitz, T.A. Revisiting the structures of several antibiotics bound to the bacterial ribosome. *Proc. Natl. Acad. Sci. USA* **107**, 17158–17163 (2010).
- Dunkle, J.A., Xiong, L., Mankin, A.S. & Cate, J.H. Structures of the *Escherichia coli* ribosome with antibiotics bound near the peptidyl transferase center explain spectra of drug action. *Proc. Natl. Acad. Sci. USA* **107**, 17152–17157 (2010).
- Schlünzen, F., Pyetan, E., Fucini, P., Yonath, A. & Harms, J.M. Inhibition of peptide bond formation by pleuromutilins: the structure of the 50S ribosomal subunit from *Deinococcus radiodurans* in complex with tiamulin. *Mol. Microbiol.* **54**, 1287–1294 (2004).

ONLINE METHODS

Peptide synthesis. Commercially available reagents were used throughout without purification. *N,N*-dimethylformamide (DMF, peptide synthesis-quality grade) was purchased from Carlo Erba, and piperidine and trifluoroacetic acid (TFA) were purchased from Alfa Aesar. Rink amide PS resin was purchased from PolyPeptide Laboratories. *N,N'*-diisopropylcarbodiimide (DIC), Oxyma and all standard *N*-Fmoc-protected L and D amino acids were purchased from Iris Biotech. *N*-Fmoc-cyclohexylalanine-OH (Fmoc-Cha-OH) was purchased from PolyPeptide laboratories. RP-HPLC-quality acetonitrile (CH₃CN, Sigma-Aldrich) and MilliQ water were used for RP-HPLC analyses and purification. Analytical RP-HPLC analyses were performed on a Dionex U3000SD with a Macherey-Nagel Nucleodur column (4.6 × 100 mm, 3 μm) at a flow rate of 1 ml min⁻¹ at 50 °C. The mobile phase was composed of 0.1% (v/v) TFA-H₂O (solvent A) and 0.1% TFA-CH₃CN (solvent B). Purification was performed on a Gilson GX-281 with a Macherey-Nagel Nucleodur VP250/21 100–5 C18ec column (21 × 250 mm, 5 μm) at a flow rate of 20 mL min⁻¹. The solid-phase syntheses of peptides were conducted on an automated Liberty Blue System synthesizer (CEM μWaves S.A.S.). ¹H NMR spectra were recorded on a DPX-400 NMR spectrometer (Bruker Biospin) with a vertical 9.4T narrow-bore/ultrashield magnet operating at 400 MHz for ¹H observation by means of a 5-mm direct QNP ¹H/¹³C/³¹P/¹⁹F probe with gradient capabilities (Supplementary Fig. 5). ESI-MS analyses were carried out on a Thermo Exactive from the Mass Spectrometry Laboratory at the European Institute of Chemistry and Biology (UMS 3033-IECB), Pessac, France (Supplementary Fig. 5).

All peptides were synthesized on Rink Amide PS resin (0.79 mmol/g) with a five-fold excess of reagents for the coupling step (0.2 M *N*-Fmoc-amino acid solution (in DMF) with 0.5 M DIC (in DMF) and 1.0 M Oxyma (in DMF)). Coupling of *N*-Fmoc-protected L- and D-arginine-OH was performed twice at 25 °C without microwaves for 1,500 s. Other amino acid couplings were performed first at 90 °C, 170 W, 115 s then at 90 °C, 30 W, 110 s. Fmoc removal was performed with a solution of 20% piperidine in DMF at 75 °C with 155 W for 15 s then 90 °C, 35 W, 50 s. After completion of the synthesis, the peptide resin was washed three times with DCM. Cleavage was performed by treatment with 5 mL of a freshly prepared TFA/TIS/H₂O solution for 240 min at room temperature. The resin was then filtered off, and the TFA solution was concentrated under reduced pressure. The crude products were precipitated as TFA salts in the presence of Et₂O and purified with the appropriate gradient (10–30% of B in 20 min) by semipreparative RP-HPLC. The compounds were freeze dried, and TFA was exchanged with HCl by two repetitive freeze-drying cycles in 0.1 N HCl solution³⁵.

The list of peptides prepared for this study and details concerning their synthesis is as follows:

Onc112. H-Val-Asp-Lys-Pro-Pro-Tyr-Leu-Pro-Arg-Pro-Arg-Pro-Arg-(D-Arg)-Ile-Tyr-Asn-(D-Arg)-NH₂ (2,389.85 g mol⁻¹). Synthesis of *Onc112* (0.1-mmol scale): 24 mg (10% yield); RP HPLC *t*_R 4.11 min (gradient 10–50% of B in 10 min); ESI HRMS (*m/z*): found 1,195.70 [M + 2H]²⁺, 797.47 [M + 3H]³⁺, 598.35 [M + 4H]⁴⁺, and 478.88 [M + 5H]⁵⁺.

Onc112 ΔC7. H-Val-Asp-Lys-Pro-Pro-Tyr-Leu-Pro-Arg-Pro-Arg-Pro-NH₂ (1,433.73 g mol⁻¹). Synthesis of *Onc112 ΔC7* (0.15-mmol scale): 79.4 mg (37% yield); RP HPLC *t*_R 3.54 min (gradient 10–50% of B in 10 min); ESI HRMS (*m/z*): [M + H]⁺ calcd for C₆₇H₁₀₈H₂₀O₁₅, 1,433.83758 found 1,433.84017, with 717.42 [M + 2H]²⁺ and 478.61 [M + 3H]³⁺.

Onc112 ΔC9. H-Val-Asp-Lys-Pro-Pro-Tyr-Leu-Pro-Arg-Pro-NH₂ (1,180.42 g mol⁻¹). Synthesis of *Onc112 ΔC9* (0.1-mmol scale): 22.6 mg (19% yield); RP HPLC *t*_R 4.78 min (gradient 10–50% of B in 10 min); ESI HRMS (*m/z*): [M + H]⁺ calcd for C₅₆H₈₉H₁₅O₁₃, 1,180.63370 found 1,180.68368, with [M + 2H]²⁺ 590.84 and [M + 3H]³⁺ 394.23.

Onc112 D2E. H-Val-Glu-Lys-Pro-Pro-Tyr-Leu-Pro-Arg-Pro-Arg-Pro-Arg-(D-Arg)-Ile-Tyr-Asn-(D-Arg)-NH₂ (2,403.88 g mol⁻¹). Synthesis of *Onc112 D2E* (0.05-mmol scale): 11.6 mg (10% yield); RP HPLC *t*_R 5.75 min (gradient 10–50% of B in 10 min); ESI HRMS (*m/z*): found 1316.70 [M + 2H]²⁺, 840.14 [M + 3H]³⁺ and 601.86 [M + 4H]⁴⁺.

Onc112 L7Cha. H-Val-Asp-Lys-Pro-Pro-Tyr-Cha-Pro-Arg-Pro-Arg-Pro-Arg-(D-Arg)-Ile-Tyr-Asn-(D-Arg)-NH₂ (2,429.92 g mol⁻¹). Synthesis of *Onc112 L7Cha* (0.05-mmol scale): 6.9 mg (6% yield); RP HPLC *t*_R 5.28 min (gradient 10–50% of B in 10 min); ESI HRMS (*m/z*): found 1,252.18 [M + 2H]²⁺, 822.80 [M + 3H]³⁺ and 608.36 [M + 4H]⁴⁺.

CD spectroscopy. CD spectra of peptides were recorded on a J-815 Jasco spectropolarimeter (Jasco France). Data are expressed in terms of total molar ellipticity in deg cm² dmol⁻¹. CD spectra for the *Onc112* peptide were acquired at four different concentrations in phosphate buffer (pH 7.6, 10 mM) between 180 and 280 nm with a rectangular quartz cell with a path length of 1 mm (Hellma 110-QS 1 mm) averaging over two runs. Secondary-structure proportion was estimated from the CD spectra with the deconvolution program CDFriend (S. Buchoux (Unité de Génie Enzymatique et Cellulaire, UMR 6022 CNRS-Université de Picardie Jules Verne) and E. Dufourc (Université de Bordeaux, CNRS, Institut Polytechnique de Bordeaux, UMR 5248 Institut de Chimie et Biologie des Membranes et des Nano-objets (CBMN); available upon request), unpublished). This program uses standard curves obtained for each canonical structure (α-helix, β-sheet, helix-polyproline type II and random coil) with L_iK_j (alternated hydrophobic leucine and hydrophilic/charged lysine residues) peptides of known length, secondary structure and CD spectra. The program implements a simulated annealing algorithm to get the best combination of α-helix, β-sheet, helix-II and random coil that exhibits the lowest normalized r.m.s. deviation with respect to the experimental spectrum^{36–38}. The algorithm yielded the following assessment for the *Onc112* peptide: 54% random coil, 30% helix-PPII, 6% α-helix and 6% β-sheet content.

Purification of *T. thermophilus* 70S ribosomes. *Th70S* ribosomes were purified as described previously³⁹ and resuspended in buffer containing 5 mM HEPES-KOH, pH 7.5, 50 mM KCl, 10 mM NH₄Cl, and 10 mM Mg(CH₃COO)₂ to yield a final concentration of 26–32 mg/mL. For storage, *Th70S* ribosomes were flash frozen in liquid nitrogen and kept at –80 °C.

Preparation of mRNA and tRNA^{iMet}. Synthetic mRNA with the sequence 5'-GGC AAG GAG GUA AAA AUG CGU UUU CGU-3' was obtained from Eurogentec. This mRNA contains a Shine-Dalgarno sequence and an AUG start codon followed by several additional codons. *E. coli* tRNA^{iMet} was overexpressed in *E. coli* HB101 cells and purified as described previously⁴⁰.

Complex formation. A ternary complex containing *Th70S* ribosomes, mRNA and deacylated tRNA^{iMet} was formed by mixing of 5 μM *Th70S* ribosomes with 10 μM mRNA and incubating at 55 °C for 10 min. For the next step, 20 μM tRNA^{iMet} was added, and the mixture was incubated at 37 °C for 10 min. Before the complexes for crystallization were used, the sample was incubated at room temperature for at least 15 min. All complexes were centrifuged briefly before use for crystallization. The final buffer conditions were 5 mM HEPES-KOH, pH 7.6, 50 mM KCl, 10 mM NH₄Cl and 10 mM Mg(CH₃COO)₂.

Crystallization. Published conditions were used as a starting point for screening crystallization conditions by vapor diffusion in sitting-drop trays at 20 °C (refs. 20,39). Crystallization drops consisted of 3 μl of ternary complex and 3–4 μl of reservoir solution containing 100 mM Tris-HCl, pH 7.6, 2.9% (v/v) PEG 20000, 7–10% (v/v) MPD and 175 mM arginine. Crystals appeared within 2–3 d and grew to ~1,000 × 100 × 100 μm within 7–8 d. For cryoprotection, the concentration of MPD was increased in a stepwise manner to yield a final concentration of 40% (v/v). The ionic composition during cryoprotection was 100 mM Tris-HCl, pH 7.6, 2.9% (v/v) PEG 20000, 50 mM KCl, 10 mM NH₄Cl and 10 mM Mg(CH₃COO)₂. *Th70S*–*Onc112* complexes were obtained by soaking 10–20 μM of *Onc112* dissolved in the final cryoprotection solution overnight at 20 °C. Crystals were then flash frozen in a nitrogen cryostream at 80 K for subsequent data collection.

Data collection and processing. Diffraction data were collected at beamline ID29 of the European Synchrotron Radiation Facility (ESRF) in Grenoble, France. A complete data set was obtained by merging 0.1° oscillation data collected at 100 K with a wavelength of 0.97625 Å from multiple regions of the same crystal. Initial data processing, including integration and scaling, were performed with XDS⁴¹. All of the data collected could be indexed in the *P*2₁2₁ space group, with unit-cell dimensions around 210 Å × 450 Å × 625 Å and an asymmetric unit containing two copies of the *Th70S* ribosome.

Model building and refinement. Initial phases were obtained by molecular replacement performed with Phaser⁴². The search model was obtained from

a high-resolution structure of the *Thh70S* ribosome (PDB 4Y4O). Restrained crystallographic refinement was carried out with Phenix⁴³ and consisted of a single cycle of rigid-body refinement followed by multiple cycles of positional and individual *B*-factor refinement. Rigid bodies comprised four domains from the small 30S subunit (head, body, spur and helix h44) and three domains from the large 50S subunit (body, L1 stalk and the C terminus of ribosomal protein L9). Noncrystallographic symmetry restraints between the two copies of the *Thh70S* ribosome in the asymmetric unit were also applied during refinement. After confirming that a single tRNA was bound to the P site and that additional density corresponding to the Onc112 peptide was visible inside the exit tunnel in a minimally biased $F_o - F_c$ map, a model for Onc112 was built with Rapper⁴⁴ and Coot⁴⁵. The models for the tRNA and mRNA were obtained from a high-resolution structure of the *Thh70S* ribosome preattack complex (PDB 1VY4). Further refinement and model validation were carried out in Phenix and on the MolProbity server⁴⁶, respectively. In the final model, 0.65% of protein residues were classified as Ramachandran outliers, and 94.38% had favorable backbone conformations.

In vitro-translation assay. The inhibition of firefly luciferase (Fluc) synthesis by Onc112 was assessed with an *E. coli* lysate-based transcription-translation coupled assay (RTS100, 5Prime) as described previously for other translational inhibitors³⁰. Briefly, 6- μ L reactions, with or without Onc112/antibiotic were mixed according to the manufacturer's description and incubated for 1 h at 30 °C with shaking (1,000 r.p.m.). 1 μ L of each reaction was stopped with 7 μ L kanamycin (50 μ g/ μ L) and then diluted with 40 μ L of luciferase assay substrate (Promega) into a white 96-well chimney flat-bottom microtiter plate (Greiner). The luminescence was then measured with a Tecan Infinite M1000 plate reader. Relative values were determined by defining the luminescence value of the sample without inhibitor as 100%.

Growth inhibition assays. Determination of the minimal inhibitory concentration (MIC) of Onc112 was performed as described previously for other antibiotics³⁰. Specifically, an overnight culture of *E. coli* strain BL21(DE3) (Invitrogen), BW25113 or Keio deletion strain BW25113 Δ *sbmA* (plate 61, well 10E)⁴⁷ was diluted 1:100 to an OD₆₀₀ of ~0.02, and 200 μ L of the diluted cells was then transferred into individual wells of a 96-well plate (Sarstedt). Either 10 μ L of Onc112, Onc112 derivative peptide or water was added to each well. Plates were then incubated overnight in a thermomixer (Eppendorf) at 37 °C/350 r.p.m. The OD₆₀₀ was measured in a Tecan Infinite M1000 plate reader, and the relative growth was calculated by defining the growth of samples without antibiotic as 100%.

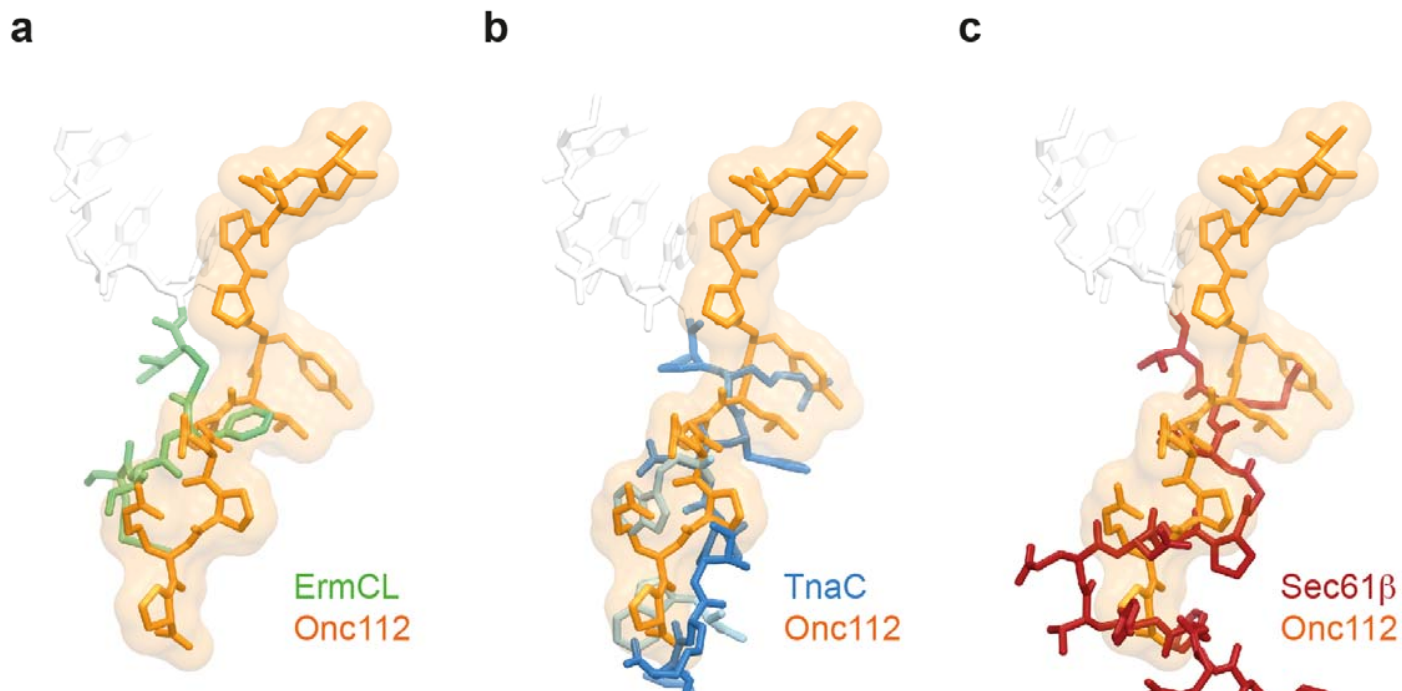
Toe-printing assay. The position of the ribosome on the mRNA was monitored with a toe-printing assay based on an *in vitro*-coupled transcription-translation system with the PURExpress *in vitro* protein synthesis kit (NEB)²⁶. Briefly, each translation reaction consisted of 1 μ L solution A, 0.5 μ L Δ isoleucine + tryptophan amino acid mixture, 0.5 μ L tRNA mixture, 1.5 μ L solution B, 1 μ L (0.5 pmol) hns40aa template: (5'-*ATTAATACGACTC**ACTATAGGGATATAAGGAGGA**AAACATATGAGCGAAGCACTTAA**ATTCTGAACAACATCCGTACTC**TTCGTGCGCAGGCAAGAGAATGTACACTTGA**AACGCTGGAAGAAAT**GCTGGA**AAAAATAGAAAGTTGTTGTTAACGAACGTTGGATTTGTAA**GTGATAGAATTCTATCGTTAATAAGCAAAATTCATTATAACC*-3', with start codon ATG, catch isoleucine codon ATT and stop codon TAA in bold, the hns40aa ORF underlined and primer-binding sites in italics) and 0.5 μ L additional agents (nuclease-free water, Onc112 or antibiotics). Translation was performed in the absence of isoleucine at 37 °C for 15 min at 500 r.p.m. in 1.5-mL reaction tubes. Ile-tRNA aminoacylation was further prevented by the use of the

Ile-tRNA synthetase inhibitor mupirocin. After translation, 2 pmol Alexa647-labeled NV-1 toe-print primer (5'-GGTTATAATGAATTTTGCTTATTAAC-3') was added to each reaction and incubated at 37 °C without shaking for 5 min. Reverse transcription was performed with 0.5 μ L of AMV RT (NEB), 0.1 μ L dNTP mix (10 mM) and 0.4 μ L Pure System Buffer and incubated at 37 °C for 20 min. Reverse transcription was quenched and RNA degraded by addition of 1 μ L 10 M NaOH and incubation for at least 15 min at 37 °C and then was neutralized with 0.82 μ L of 12 M HCl. 20 μ L toe-print resuspension buffer and 200 μ L PN1 buffer were added to each reaction before treatment with a QIAquick Nucleotide Removal Kit (Qiagen). The Alexa647-labeled DNA was then eluted from the QIAquick columns with 80 μ L of nuclease-free water. A vacuum concentrator was used to vaporize the solvent, and the Alexa647-labeled DNA was then dissolved into 3.5 μ L of formamide dye. The samples were heated to 95 °C for 5 min before being applied onto a 6% polyacrylamide (19:1) sequencing gel containing 7 M urea. Gel electrophoresis was performed at 40 W and 2,000 V for 2 h. The GE Typhoon FLA9500 imaging system was subsequently used to scan the polyacrylamide gel.

Disome formation assay. The disome formation assay was performed as described previously^{16,23}. Briefly, *in vitro* translation of the 2xermBL construct was performed with the Rapid Translation System RTS 100 *E. coli* HY Kit (Roche). Translations were carried out for 1 h at 30 °C and then analyzed on 10–55% sucrose-density gradients (in a buffer containing 50 mM HEPES-KOH, pH 7.4, 100 mM KOAc, 25 mM Mg(OAc)₂ and 6 mM β -mercaptoethanol) by centrifugation at 154,693g (SW-40 Ti, Beckman Coulter) for 2.5 h at 4 °C.

Figure preparation. Figures showing electron density and atomic models were generated with PyMOL (<http://www.pymol.org/>).

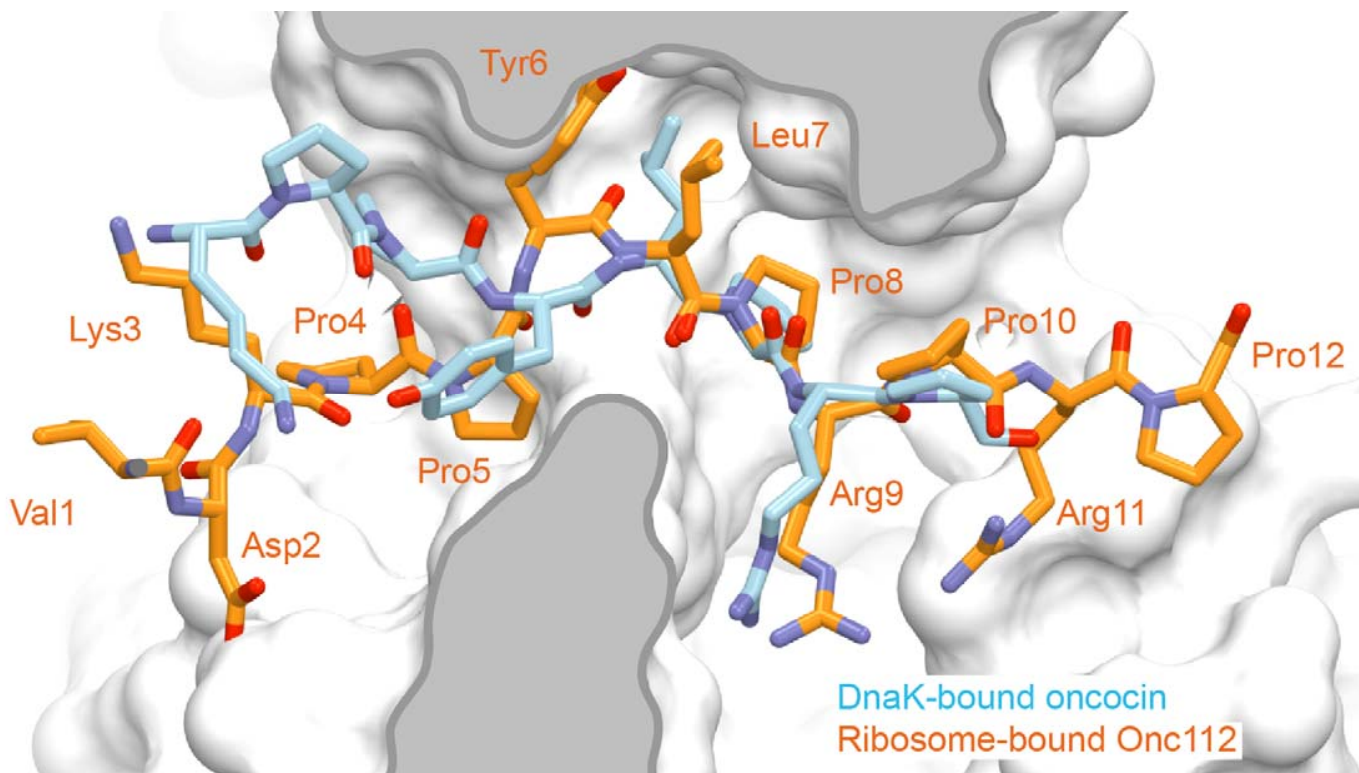
35. Brazier, S.P., Ramesh, B., Haris, P.I., Lee, D.C. & Srai, S.K. Secondary structure analysis of the putative membrane-associated domains of the inward rectifier K⁺ channel ROMK1. *Biochem. J.* **335**, 375–380 (1998).
36. Jean-François, F. *et al.* Variability in secondary structure of the antimicrobial peptide Cateslytin in powder, solution, DPC micelles and at the air-water interface. *Eur. Biophys. J.* **36**, 1019–1027 (2007).
37. Jobin, M.L. *et al.* The enhanced membrane interaction and perturbation of a cell penetrating peptide in the presence of anionic lipids: toward an understanding of its selectivity for cancer cells. *Biochim. Biophys. Acta* **1828**, 1457–1470 (2013).
38. Khemtémourian, L., Buchoux, S., Aussenac, F. & Dufourc, E.J. Dimerization of Neu/Erb2 transmembrane domain is controlled by membrane curvature. *Eur. Biophys. J.* **36**, 107–112 (2007).
39. Selmer, M. *et al.* Structure of the 70S ribosome complexed with mRNA and tRNA. *Science* **313**, 1935–1942 (2006).
40. Schmitt, E., Blanquet, S. & Mechulam, Y. Crystallization and preliminary X-ray analysis of *Escherichia coli* methionyl-tRNA^{Met} formyltransferase complexed with formyl-methionyl-tRNA^{Met}. *Acta Crystallogr. D Biol. Crystallogr.* **55**, 332–334 (1999).
41. Kabsch, W. Xds. *Acta Crystallogr. D Biol. Crystallogr.* **66**, 125–132 (2010).
42. McCoy, A.J. *et al.* Phaser crystallographic software. *J. Appl. Crystallogr.* **40**, 658–674 (2007).
43. Adams, P.D. *et al.* PHENIX: a comprehensive Python-based system for macromolecular structure solution. *Acta Crystallogr. D Biol. Crystallogr.* **66**, 213–221 (2010).
44. de Bakker, P.I., DePristo, M.A., Burke, D.F. & Blundell, T.L. *Ab initio* construction of polypeptide fragments: accuracy of loop decoy discrimination by an all-atom statistical potential and the AMBER force field with the Generalized Born solvation model. *Proteins* **51**, 21–40 (2003).
45. Emsley, P. & Cowtan, K. Coot: model-building tools for molecular graphics. *Acta Crystallogr. D Biol. Crystallogr.* **60**, 2126–2132 (2004).
46. Chen, V.B. *et al.* MolProbity: all-atom structure validation for macromolecular crystallography. *Acta Crystallogr. D Biol. Crystallogr.* **66**, 12–21 (2010).
47. Baba, T. *et al.* Construction of *Escherichia coli* K-12 in-frame, single-gene knockout mutants: the Keio collection. *Mol. Syst. Biol.* **2**, 2006.0008 (2006).



Supplementary Figure 1

Overlap of Onc112 with nascent polypeptide chains in the ribosome exit tunnel.

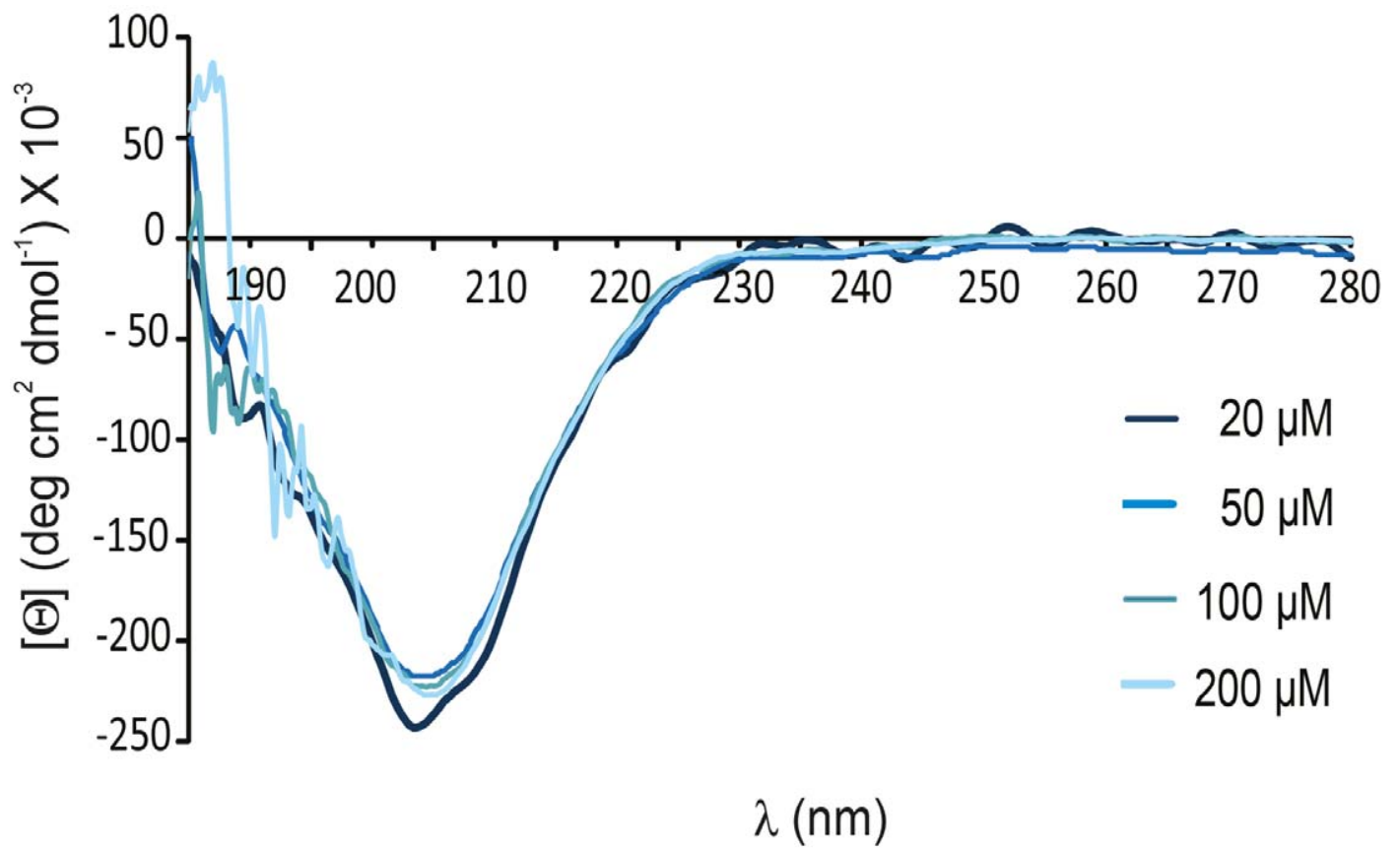
Comparison of the binding position of Onc112 (orange) with (a) ErmCL (green), (b) TnaC (blue) and Sec61 β (red) nascent chains. In (a)-(c), the CCA-end of the P-tRNA is shown in white and in (b) the two tryptophan molecules are in cyan.



Supplementary Figure 2

Comparison of *Tth70S*–Onc112 with the DnaK–oncocin complex.

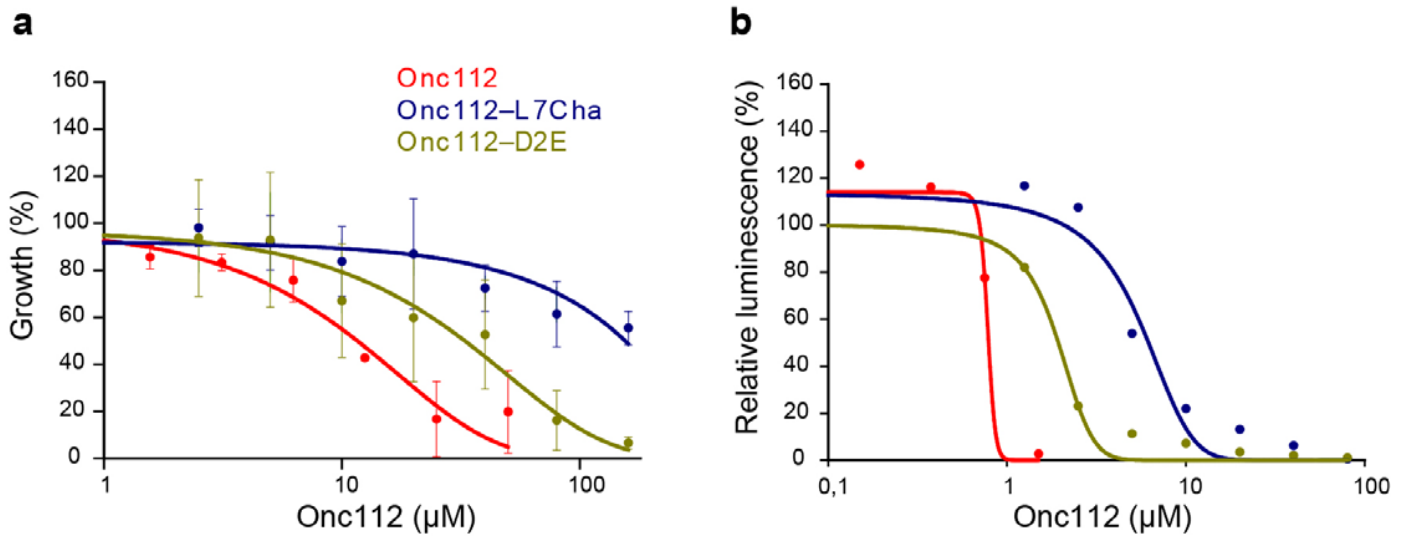
The conformation of residues Lys3–Pro10 of the Oncocin peptide O2 (cyan, $\text{VDKPPYLPRPRPPROIYNO-NH}_2$, where O represents ornithine) in complex with DnaK (white surface representation) was compared with residues Val1–Pro12 of Onc112 (orange) from the ribosome-bound Onc112 structure.



Supplementary Figure 3

Conformation of the Onc112 peptide in solution.

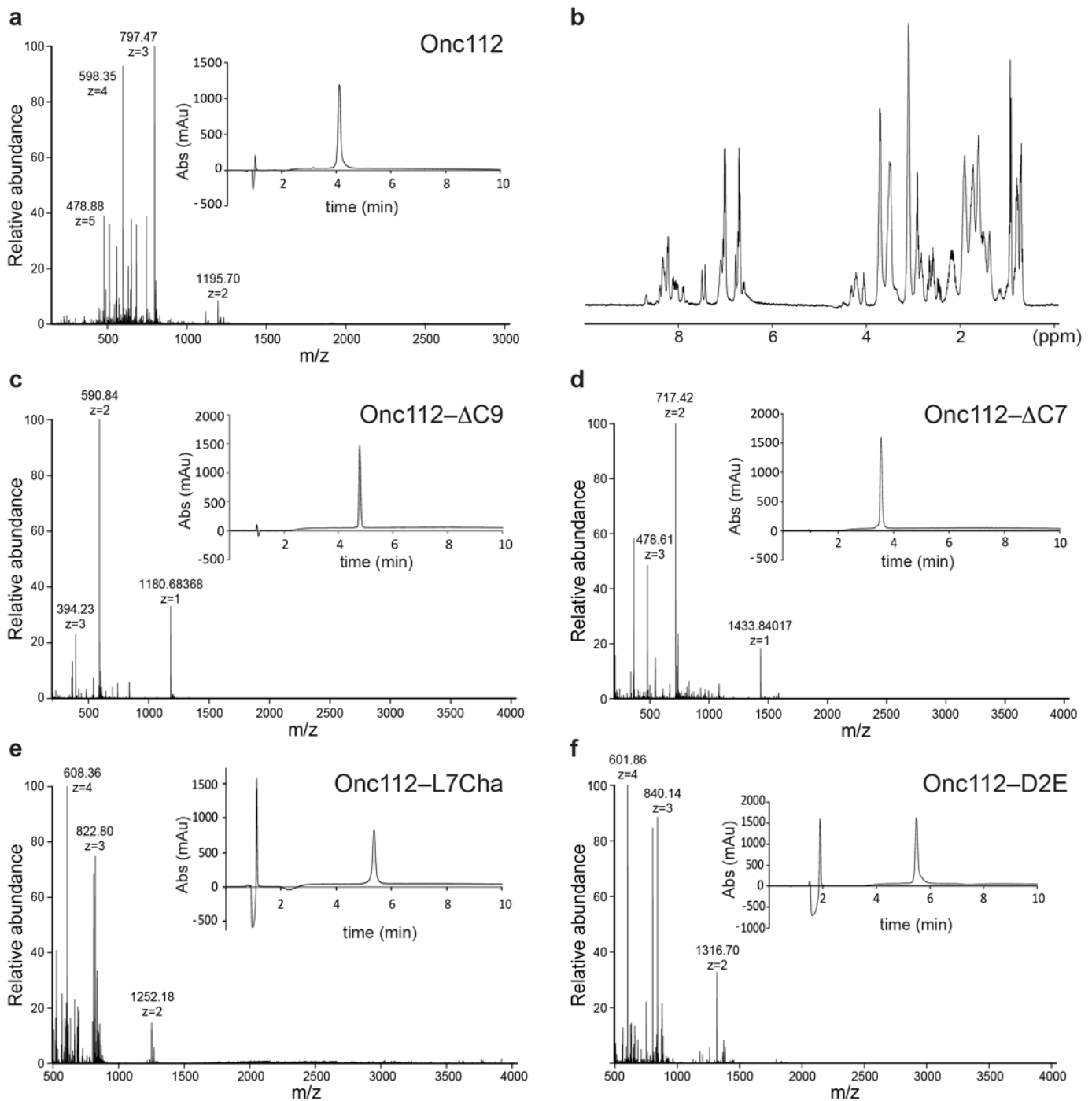
Far-UV circular dichroism (CD) spectra of the Onc112 peptide at concentrations ranging from 20 to 200 μM .



Supplementary Figure 4

Inhibitory activity of Onc112 peptide derivatives.

(a-b) Effect of Onc112 (red) and Onc112 derivatives Onc112-L7Cha (blue) and Onc112-D2E (olive) on (a) the overnight growth of *E. coli* strain BL21(DE3) and (b) the luminescence resulting from the *in vitro* translation of firefly luciferase (Fluc). In (a), the error bars represent the standard deviation (s.d.) from the mean for a triplicate experiment (n=3). In (b), the experiment was performed in duplicate (n=2). The growth or luminescence measured in the absence of peptide was assigned as 100%.



Supplementary Figure 5

Validation of Onc112 and derivatives.

(a) Electrospray ionization high resolution mass spectrometry (ESI-HRMS) and reverse phase (RP) high performance liquid chromatography (HPLC), and (b) ^1H nuclear magnetic resonance (NMR) spectra of the Onc112 peptide. (c-f) ESI-HRMS and RP HPLC of the (c) Onc112- ΔC9 , (d) Onc112- ΔC7 , (e) Onc112-L7Cha and (f) Onc112-D2E peptides.

Review

Fabian Nguyen, Agata L. Starosta, Stefan Arenz, Daniel Sohmen, Alexandra Dönhöfer and Daniel N. Wilson*

Tetracycline antibiotics and resistance mechanisms

Abstract: The ribosome and protein synthesis are major targets within the cell for inhibition by antibiotics, such as the tetracyclines. The tetracycline family of antibiotics represent a large and diverse group of compounds, ranging from the naturally produced chlortetracycline, introduced into medical usage in the 1940s, to second and third generation semi-synthetic derivatives of tetracycline, such as doxycycline, minocycline and more recently the glycylycylcline tigecycline. Here we describe the mode of interaction of tetracyclines with the ribosome and mechanism of action of this class of antibiotics to inhibit translation. Additionally, we provide an overview of the diverse mechanisms by which bacteria obtain resistance to tetracyclines, ranging from efflux, drug modification, target mutation and the employment of specialized ribosome protection proteins.

Keywords: glycylycylcline; resistance; ribosome; tetracycline; tigecycline; translation.

*Corresponding author: Daniel N. Wilson, Gene Center and Department of Biochemistry, University of Munich, Feodor-Lynenstr. 25, D-81377 Munich, Germany; and Center for Integrated Protein Science Munich (CiPSM), University of Munich, Feodor-Lynenstr. 25, D-81377 Munich, Germany, e-mail: wilson@lmb.uni-muenchen.de
Fabian Nguyen, Agata L. Starosta, Stefan Arenz, Daniel Sohmen and Alexandra Dönhöfer: Gene Center and Department of Biochemistry, University of Munich, Feodor-Lynenstr. 25, D-81377 Munich, Germany

Introduction: the ribosome as a target for antibiotics

The ribosome is one of the major targets within the bacterial cell for antibiotics, with a diverse range of antibiotics that have been discovered and shown to inhibit a variety of distinct steps during protein synthesis (Sohmen et al., 2009a,b; Wilson, 2009, 2013). This wealth of biochemical and structural data has demonstrated that the majority of

antibiotics interact with the functional centers of the ribosome: Many clinically important antibiotics bind at or near to the peptidyltransferase center (PTC) on the large ribosomal subunit where peptide bond formation occurs; these include the chloramphenicols, pleuromutilins (retapamulin), oxazolidinones (linezolid), lincosamides (lincomycin), macrolides (erythromycin), ketolides (telithromycin) and streptogramins (quinupristin and dalfopristin). On the small ribosomal subunit, antibiotic binding sites are clustered along the path of the mRNA and tRNAs, for example, spectinomycin, streptomycin, aminoglycosides (kanamycin), tuberactinomycins (viomycin) and tetracyclines (doxycycline) (Sohmen et al., 2009a,b; Wilson, 2009, 2013). This review focuses on the latter class of antibiotics, the tetracyclines, which bind at the decoding center of the small subunit, i.e., where the codon of the mRNA is recognized by the anticodon of the tRNA. There have been many excellent reviews on different aspects of tetracycline inhibition and tetracycline resistance mechanisms (Roberts, 1996; Chopra and Roberts, 2001; Connell et al., 2003b; Thaker et al., 2010; Nelson and Levy, 2011), so here we focus on the most recent biochemical and structural insights with an emphasis on aspects related directly to the translation machinery.

The tetracycline class of antibiotics

Discovery and chemical structure of tetracyclines

The first compound belonging to the tetracycline family, chlortetracycline, was discovered in 1948 by Dr. Benjamin Duggar working at Lederle Laboratories (American Cyanamid) (Duggar, 1948). Chlortetracycline (Figure 1A) was isolated from *Streptomyces aureofaciens*, and called aureomycin because of the gold coloring of the bacteria (Duggar, 1948). Shortly afterwards, in the early 1950s Alexander Finlay from Pfizer discovered oxytetracycline

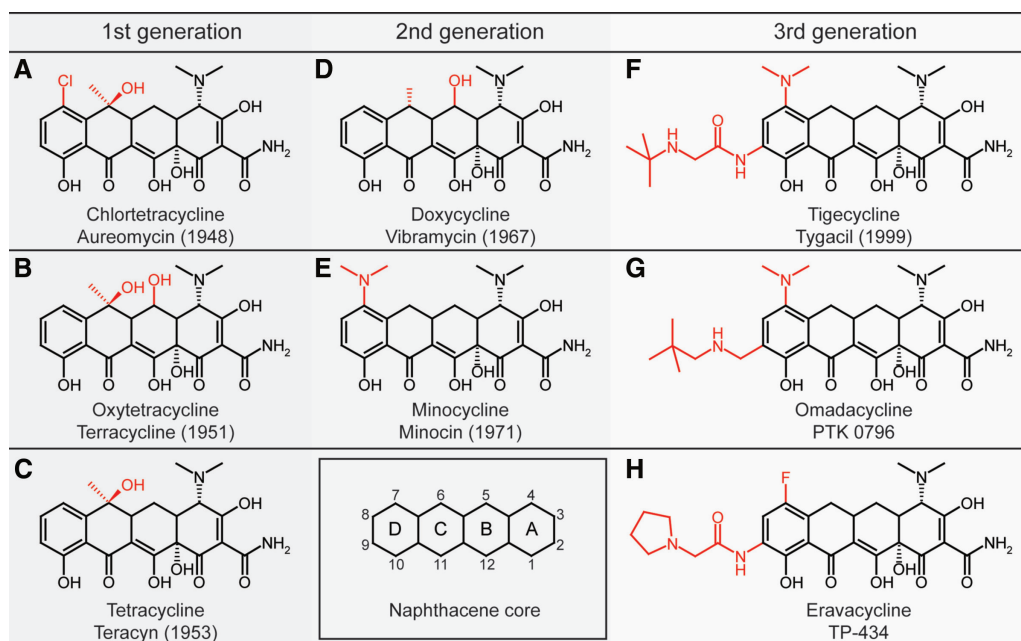


Figure 1 Chemical structures of tetracyclines.

Chemical structures of (A–C) first generation tetracyclines. (A) chlortetracycline (aureomycin), (B) oxytetracycline (terracycline) and (C) tetracycline (teracyclin), (D–E) second generation tetracyclines; (D) doxycycline (vibramycin) and (E) minocycline (minocin), and (F–G) third generation tetracyclines; (F) the glycyloxy tetracycline tigecycline (tygacil), (G) the aminomethyl tetracycline omadacycline (PTK 0796) and (H) the fluorocycline eravacycline (TP-434). The numbers in parentheses indicates the year the antibiotic was discovered/reported. The inset of the DCBA naphthalene core provides the carbon atom assignments for rings A–D.

(Figure 1B), a secondary metabolite of soil bacteria *Streptomyces rimosus* from the Terra Haute, Indiana, and therefore called ‘terramycin’ (Finlay et al., 1950). Although both antibiotics were already on the market, their chemical structure remained elusive until 1953. The chemical structures of chlortetracycline and oxytetracycline (Figure 1A and B) were the results of joint efforts of a Pfizer team, together with the Nobel Prize laureate, Robert B. Woodward (Stephens et al., 1952, 1954; Hochstein et al., 1953).

The basis of these structures is the DCBA naphthalene core comprising four aromatic rings (inset to Figure 1), therefore this family of antibiotics was named ‘tetracyclines’ (Stephens et al., 1952). It was noted that compared with oxytetracycline, chlortetracycline lacks a hydroxyl group at the C5 position of ring B and has a chlorine atom substituent present at the C7 position of ring D (Figure 1A and B). Moreover, as a result of chemical modifications, Pfizer-Woodward described C7-deschloro derivative of chlortetracycline, with a higher potency against bacterial pathogens, which was called ‘tetracycline’ (Figure 1C, teracyclin) (Conover et al., 1953), because it is the simplest member of the ‘tetracycline’ family of antibiotics. Subsequently, tetracycline was also detected in the broth of *S. aureofaciens* (Backus et al., 1954) and

S. rimosus (Perlman et al., 1960), consistent with the discovery that tetracycline is a precursor of chlortetracycline (McCormick et al., 1960).

Soon after the discovery of first generation tetracyclines, Pfizer and Lederle began developing the second generation tetracycline compounds with improved pharmacokinetic properties, increased antimicrobial potency and decreased toxicity. A series of chemical modifications of ring C led Pfizer to the semi-synthesis of methacycline (Boothe et al., 1959; Blackwood et al., 1961), which was further used as a precursor for the synthesis of doxycycline (Figure 1D; Vibramycin) (C6-deoxy-tetracycline) (Stephens et al., 1963), one of the most commonly used tetracyclines to date. Additionally, Lederle analyzed biogenesis mutants of chlortetracycline in *S. aureofaciens*, and discovered the precursor demeclocycline (C6-demethyl-C7-chlorotetracycline) (McCormick et al., 1957), which was further reduced to sancycline (C6-demethyl-C6-deoxytetracycline), a tetracycline with the minimal chemical features necessary to retain antimicrobial activity (McCormick et al., 1960). Subsequently, sancycline was converted to C7-amino-sancycline or minocycline (Figure 1E; Minocin) (Martell and Boothe, 1967), the most powerful tetracycline of that period, and the last tetracycline to be introduced into the market in the 20th century.

Emerging antibiotic resistance renewed interest in the development of a third generation of tetracyclines. In the late 1980s, Lederle (later Wyeth) reopened the tetracycline program. Already known tetracycline derivatives were re-evaluated and their action revisited according to the recent knowledge about tetracycline action (Tally et al., 1995), leading to a focus on modifications of the C7 and C9 positions of ring D of the tetracycline core. The breakthrough came with the synthesis of a series of C9-aminotetracyclines bearing a glycyloxy moiety (Sum et al., 1994), leading to the development of a new class of third generation tetracyclines, referred to as glycyloxytetracyclines. A glycyloxy derivative of minocycline, tigecycline (Figure F; Tygacyl) (Petersen et al., 1999), with a *t*-butyl amine group was one of the most potent antimicrobials and is the first tetracycline introduced into the market in over 40 years. Currently, two additional third generation tetracyclines are in phase III clinical trials: Omadacycline (PTK 0796; Figure 1G) is a 9-alkylaminomethyl derivative of minocycline (aminomethylcycline) (Draper et al., 2013) and was developed by Paratek Pharmaceuticals, which applies transition metal-based chemistry to produce tetracycline derivatives (Nelson et al., 2003). Conversely, Tetrphase Pharmaceuticals utilized Meyers' chemistry (Sun et al., 2008) to obtain the fluorocycline eravacycline (TP-434; Figure 1H), which bears C7-fluoro and C9-pyrrolidinoacetamido modifications of ring D (Grossman et al., 2012).

The binding site of tetracycline on the 30S subunit and 70S ribosome

X-ray structures of tetracycline in complex with the *Thermus thermophilus* 30S subunit provided the first direct visualization of the drug binding sites (Figure 2A) (Brodersen et al., 2000; Pioletti et al., 2001). In the first study, the crystals were soaked in 80 μM tetracycline and the structure determined to 3.4 Å revealed two tetracycline binding sites on the 30S subunit (Brodersen et al., 2000). By contrast, in the second study crystals were soaked in 4 μM tetracycline and the resulting structure at 4.5 Å reported six distinct tetracycline binding sites (Pioletti et al., 2001). However, only one tetracycline binding site was common between the two studies, termed the 'primary binding site' (Tet1), which is located at the base of the head of the 30S subunit (Figure 2A), and was subsequently verified biochemically (Connell et al., 2002). The identification of multiple lower occupancy secondary binding sites (Tet2) was not unexpected, as earlier biochemical evidence indicated that tetracyclines have multiple binding sites on the small and large subunit (Gale et al., 1981). For example,

tetracycline binding enhances the reactivity of U1052 and C1054 of the 16S rRNA present in the primary binding site, but also protects the nucleotide A892, located in one of the secondary binding sites, from chemical modification (Moazed and Noller, 1987). Recently, an X-ray structure of tetracycline bound to an initiation complex comprising the *T. thermophilus* 70S ribosome bound with P-site tRNA^{Met} and mRNA was determined at 3.5 Å (Jenner et al., 2013). Interestingly, only one molecule of tetracycline was bound to the 70S ribosome, namely at the primary binding site (Figure 2B) and no secondary binding sites were observed (Jenner et al., 2013), re-emphasizing the higher affinity and occupancy of the primary binding site relative to the secondary binding sites.

In the primary binding site, tetracycline utilizes the hydrophilic surface of the molecule to interact with the irregular minor groove of helix 34 (h34) and the loop of h31 of the 16S rRNA (Figure 2C). This is consistent with the observations that alterations of the hydrophilic surface (C1–C4, C10–C12) of tetracycline abolish the antimicrobial activity of the drug, whereas the hydrophobic surface (C5–C9) is more amenable to modification without loss of inhibitory activity (Nelson, 2001), as seen in many natural product tetracyclines (Figure 1). The hydrophilic side of tetracycline establishes hydrogen-bond interactions with the phosphate-oxygen atoms of nucleotides C1054, G1197 and G1198 in h34 of the 16S rRNA, directly and/or via coordination of a magnesium ion (Mg1) (Figure 2C) (Brodersen et al., 2000; Pioletti et al., 2001; Jenner et al., 2013). The possibility of an additional magnesium ion (Mg2) mediating the interaction between the phosphate backbone of G966 in h31 and ring A of tetracycline was proposed based on the recent 70S structure (Jenner et al., 2013). These findings are consistent with the earlier studies indicating the importance of divalent magnesium for binding of tetracycline to the ribosome (White and Cantor, 1971).

The interaction of tetracycline with the backbone of the rRNA, rather than by establishing sequence-specific nucleobase interactions (Figure 2C), is consistent with the broad-spectrum activity of tetracycline antibiotics (Bradford and Jones, 2012). The single interaction between ring D of tetracycline and the nucleobase of C1054 of the 16S rRNA involves stacking interactions (Figure 2C) and is therefore unlikely to be sequence-specific. The high structural conservation of the tetracycline binding site in eukaryotic ribosomes (Ben-Shem et al., 2011) is consistent with the documented inhibitory activity of tetracycline against eukaryotic translation *in vitro* (Budkevich et al., 2008). Thus, antibiotic uptake probably makes a larger contribution to the natural resistance of eukaryotic cells to tetracyclines.

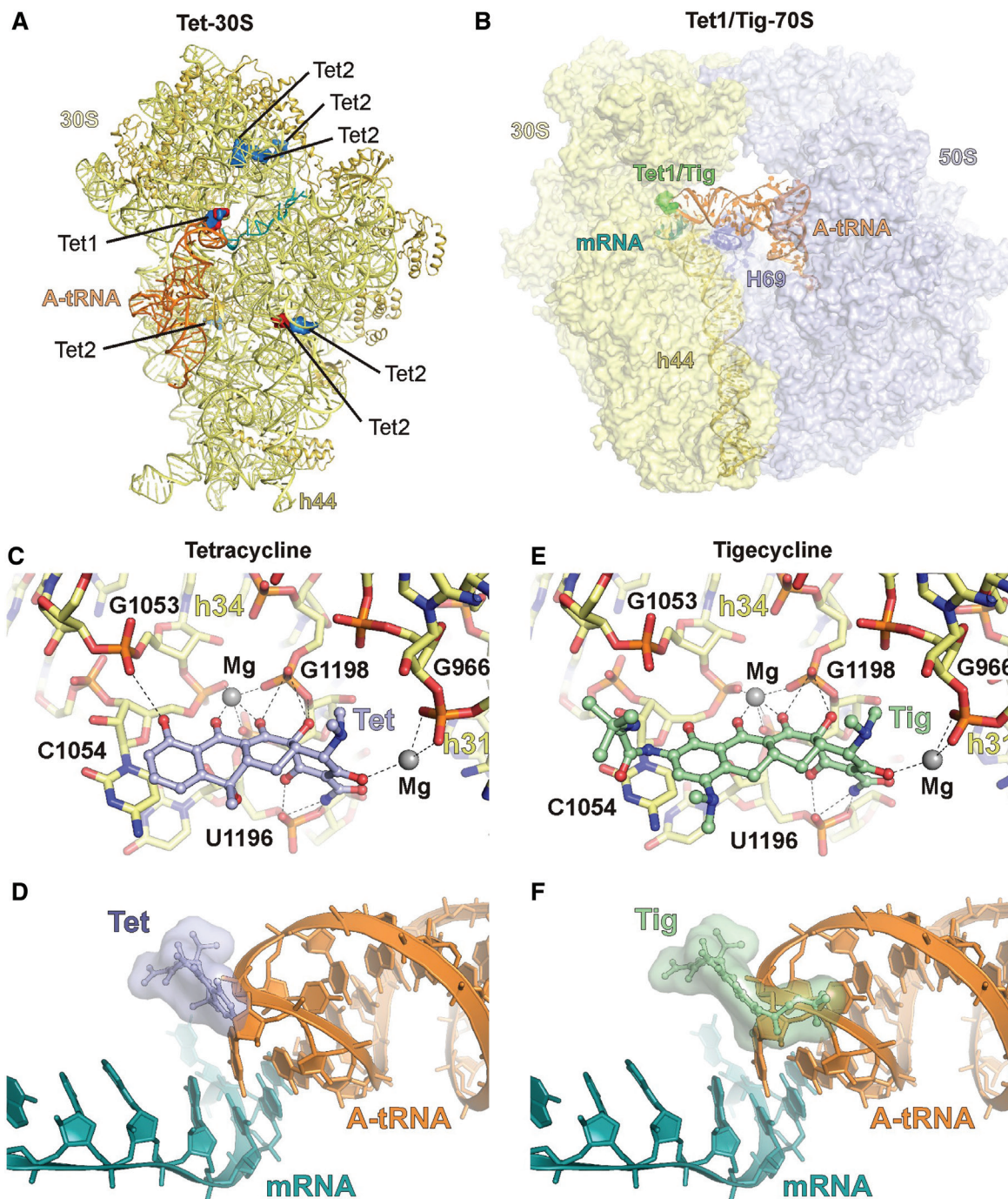


Figure 2 Binding site of tetracyclines on the ribosome.

(A) Primary (Tet1) and secondary (Tet2) binding sites of tetracycline on the 30S subunit (Brodersen et al., 2000; Pioletti et al., 2001). (B) Binding site of tetracycline/tigecycline (Tet1/Tig) on the 70S ribosome (30S, yellow; 50S, blue) (Jenner et al., 2013) relative to mRNA (teal), A-tRNA (orange) (Voorhees et al., 2009). h44 of the 16S rRNA and H69 of the 23S rRNA are indicated for reference. (C) Interaction of tetracycline within the primary binding site (Jenner et al., 2013). The charged side of tetracyclines coordinates magnesium ions to interact with the backbone of residues h34 and h31. (D) Binding position of tetracycline (Jenner et al., 2013) relative to mRNA (teal) and A-tRNA (orange) (Voorhees et al., 2009). (E) Interaction of tigecycline within the primary binding site, illustrating the additional interaction between the C9-substitution of tigecycline and C1054 of the 16S rRNA (Jenner et al., 2013). (F) Binding position of tigecycline (Jenner et al., 2013) relative to mRNA (teal) and A-tRNA (orange) (Voorhees et al., 2009).

The mechanism of action of tetracyclines during translation

During translation, aminoacyl-tRNAs are delivered to the ribosome by the elongation factor EF-Tu. A proof-reading process ensues that monitors correctness of the interaction between the anticodon of the aminoacyl-tRNA and the A-site codon of the mRNA. Selection of the correct or cognate tRNA stimulates the GTP hydrolysis activity of EF-Tu, resulting in conformational changes in EF-Tu that lead to dissociation of EF-Tu·GDP from the ribosome, and the concomitant accommodation of the aminoacyl-tRNA into the A-site. The primary binding site of tetracycline is located within the decoding center of the small subunit and overlaps in position with the anticodon loop of an A-site bound tRNA (Figure 2B and D). Specifically, rings C and D of tetracycline sterically clash with the first nucleotide of the anticodon of the tRNA that interacts with the third (or wobble) base of the A-site codon of the mRNA (Figure 2D). The competition for ribosome binding between tetracycline and A-tRNA was observed during the crystallization of the tetracycline-70S complex, where initial co-crystallization studies using 60 μM tetracycline and five-fold excess of tRNA^{Met} (over ribosomes) led to non-specific binding of tRNA^{Met} to the A-site, rather than tetracycline (Jenner et al., 2013). To obtain electron density for tetracycline, co-crystallization experiments were performed with higher concentrations of tetracycline (300 μM) coupled with lower excess (1.5-fold) of tRNA^{Met}. These findings are consistent with biochemical experiments demonstrating that tetracycline inhibits binding of tRNAs to the ribosomal A-site, but not the ribosome-stimulated EF-Tu GTPase activity (Gale et al., 1981; Blanchard et al., 2004). Specifically, single molecule FRET experiments indicate that in the presence of tetracycline (40 μM ; $10\times K_d$), aminoacyl-tRNA accommodation is efficiently blocked, resulting in repetitive ternary complex binding and release events (Blanchard et al., 2004; Geggier et al., 2010; Jenner et al., 2013). Indeed, the overlap between tetracycline and A-tRNA is similar regardless of whether the A-tRNA is still bound to EF-Tu in an initial selection state or whether the A-tRNA has fully accommodated into the A-site on the 70S ribosome.

Second generation tetracycline derivatives: doxycycline and minocycline

Second generation tetracyclines, such as doxycycline and, in particular, minocycline, exhibit superior antimicrobial

activities compared to tetracycline against a range of Gram-negative (e.g., *Escherichia coli* and *Pseudomonas aeruginosa*) and especially Gram-positive (*Staphylococcus aureus* and *Enterococcus faecalis*) bacteria (Bradford and Jones, 2012), including some strains of tetracycline-resistant bacteria (Testa et al., 1993; Sum et al., 1994). Consistently, minocycline has a ~20-fold higher affinity to the ribosome than tetracycline (but 5-fold lower than tigecycline) and inhibits *in vitro* translation 2–7-fold more efficiently than tetracycline (Bergeron et al., 1996; Olson et al., 2006). The similarity in chemical structure between minocycline and tetracycline (Figure 1) and the ability of minocycline to compete with tetracycline for ribosome binding (Olson et al., 2006), suggests that minocycline binds analogously to the ribosome as tetracycline. Presumably the improved binding properties of minocycline result from presence of the C7-dimethylamido group on ring D that may facilitate stacking interactions with C1054 (Figure 2C). Additionally, second generation tetracyclines, such as minocycline, are more lipophilic than their parent compounds and as a result display better absorption and pharmacokinetic parameters (Agwuh and MacGowan, 2006).

Third generation tetracycline derivatives: glycylicyclines and tigecycline

The third generation of tetracycline derivatives includes the glycylicyclines, which bear an N,N-dimethylglycylamido (DMG) moiety on the C9 position of ring D (Figure 1F) (Barden et al., 1994; Sum et al., 1994). Compared to first (e.g., tetracycline) and second generation tetracyclines (e.g., minocycline), the 9-DMG derivatives of minocycline (termed tigecycline or DMG-MINO) (Figure 1F) and sancycline (DMG-DMDOT) display improved inhibitory activities against a wide range of Gram-positive and negative bacteria and in particular have similar minimal inhibitory concentrations against susceptible and resistant bacterial strains (Testa et al., 1993; Barden et al., 1994; Sum et al., 1994). Consistently, glycylicyclines, such as tigecycline, exhibit ~10–30 fold lower half inhibitory concentrations (IC_{50}) during *in vitro* translation compared with tetracycline (Bergeron et al., 1996; Olson et al., 2006; Grossman et al., 2012; Jenner et al., 2013) as well as having improved ribosome binding properties. Specifically, DMG-DMDOT and DMG-DOX bind to the ribosome with a ~5-fold higher affinity than tetracycline (Bergeron et al., 1996), whereas tigecycline has been reported to have a ~10–100-fold higher binding affinity for the ribosome compared to tetracycline (Olson et al., 2006; Grossman et al., 2012; Jenner et al., 2013).

A 3.3 Å resolution X-ray structure of tigecycline bound to the *T. thermophilus* 70S ribosome reveals that tigecycline binds to the decoding center on the 30S subunit analogously to tetracycline (Figure 2B) (Jenner et al., 2013). No secondary binding sites were observed (Jenner et al., 2013). Moreover, unlike tetracycline, crystallization in the presence of 60 μM tigecycline and 5-fold excess of tRNA^{Met} (over ribosomes) was sufficient to yield clear electron density for the drug and prevent non-specific binding of tRNA^{Met} to the A-site, thus re-emphasizing the higher binding affinity of tigecycline for the ribosome compared to tetracycline. As expected, based on the common features of the chemical structures of tetracycline and tigecycline (Figure 1C and F), tigecycline uses the polar face of the drug to establish an analogous network of hydrogen-bond interactions with two Mg²⁺ ions and the phosphate-oxygen backbone of h34 and h31 of the 16S rRNA (Figure 2E). The similarity in binding site of tigecycline with tetracycline is also supported by the competition between tigecycline and tetracycline for ribosome binding (Olson et al., 2006; Grossman et al., 2012; Jenner et al., 2013), as well as the similarity in chemical footprinting and hydroxyl-radical cleavage patterns generated in the presence of either drug (Moazed and Noller, 1987; Bauer et al., 2004). However, in the case of tigecycline, ~10-fold lower concentrations of the drug were required compared to tetracycline in order to generate the same modification patterns (Bauer et al., 2004).

The major differences between tigecycline and tetracycline are the 7-dimethylamido and 9-t-butylglycylamido substitutions attached to ring D of tigecycline (Figure 1F). While the 7-dimethylamido moiety does not appear to establish interactions with the ribosome, the glycyl nitrogen atom of the 9-t-butylglycylamido moiety of tigecycline stacks with the π-orbital of nucleobase C1054 (Figure 2E). The remainder of the 9-t-butylglycylamido moiety of tigecycline adopts a very rigid conformation (although it does not make any apparent contact with the ribosome), which may contribute to the stacking interaction with C1054. Indeed, the interaction of tigecycline with C1054 appears to further enhance the stacking interaction between C1054 and U1196 (Figure 2E), similar to what is seen when tRNA is bound to the A-site (Schmeing et al., 2009). Thus, the stacking interaction between the 9-t-butylglycylamido moiety of tigecycline and C1054 and U1196, which is lacking or less optimal in tetracycline (Figure 2E), provides a structural basis for the improved ribosome binding properties of tigecycline. Additionally, the 9-t-butylglycylamido moiety of tigecycline significantly increases the steric overlap of tigecycline and the anticodon loop of the A-tRNA (Figure 2F), compared to the modest overlap observed between tetracycline and the A-tRNA (Figure 2D). Collectively, the enhanced binding affinity of tigecycline,

together with the increased steric overlap with the A-tRNA, provides a likely explanation for the increased effectiveness of tigecycline (2 μM) to prevent stable binding of the ternary complex EF-Tu·GTP·aa-tRNA to the A-site, compared to 40 μM tetracycline (Jenner et al., 2013).

Third generation tetracycline derivatives: omadacycline and eravacycline

Two additional third generation tetracycline derivatives with C9 substitutions on ring D, which display broad-spectrum activity against tetracycline-susceptible and -resistant bacterial strains, are in phase III clinical trials. Omadacycline is an aminomethylcycline (Figure 1G) developed by Paratek Pharmaceuticals (Boston, MA, USA; Draper et al., 2013). Competition studies with radiolabeled tetracycline indicate that omadacycline has a 2-fold higher affinity for the ribosome than tetracycline and, consistently, omadacycline inhibits *in vitro* translation at 2-fold lower drug concentrations than tetracycline (Draper et al., 2013; Jenner et al., 2013). Eravacycline (Tetraphase Pharmaceuticals, Watertown, MA) is a glycylcycline bearing a fluorine atom at position C7 and a pyrrolidinoacetamido group at the C9 of ring D (Figure 1H). Competition studies with radiolabelled tetracycline indicate that eravacycline has 10-fold higher affinity for the ribosome than tetracycline and inhibits *in vitro* translation at 4-fold lower drug concentrations than tetracycline (Grossman et al., 2012). The similar ribosome binding affinity of eravacycline (0.2 μM) and tigecycline (0.2 μM) (Grossman et al., 2012; Jenner et al., 2013) and the reduced affinity of compounds with amide bond replacements in the 9-position, such as omadacycline (2 μM) (Draper et al., 2013; Jenner et al., 2013) and 9-propylpyrrolidyl-7-fluorocycline (4 μM) (Jenner et al., 2013) is consistent with an important role of the amide to strengthen the stacking interactions of the C9 substitution with C1054. Introduction of an additional aromatic ring E to generate pentacyclines (Sun et al., 2010) also improves the binding and inhibitory properties of the drug relative to tetracycline (Jenner et al., 2013), further supporting the hypothesis that stacking interactions with C1054 enhance the binding and inhibitory properties of tetracycline derivatives.

Tetracycline resistance mechanisms

There are four main mechanisms by which bacteria can acquire resistance to tetracyclines (Table 1). In addition, innate mechanisms exist because some bacteria

Table 1 Tetracycline resistance determinants.

Efflux		Ribosomal protection	Degradation	rRNA mutations
<i>tetA</i>	<i>tet31</i>	<i>tetM</i>	<i>tetX</i>	G1058C
<i>tetB</i>	<i>tet33</i>	<i>tetO</i>	<i>tet37</i>	A926T
<i>tetC</i>	<i>tet35</i>	<i>tetQ</i>		G927T
<i>tetD</i>	<i>tet38</i>	<i>tetS</i>		A928C
<i>tetE</i>	<i>tet39</i>	<i>tetT</i>		ΔG942
<i>tetG</i>	<i>tet40</i>	<i>tetW</i>		
<i>tetH</i>	<i>tet41</i>	<i>tetB(P)</i>		
<i>tetJ</i>	<i>tet42</i>	<i>tet32</i>		
<i>tetK</i>	<i>tet45</i>	<i>tet36</i>		
<i>tetL</i>	<i>tetAB(46)</i>	<i>tet44</i>		
<i>tetA(P)</i>	<i>tcr3</i>	<i>otrA</i>		
<i>tetV</i>	<i>otrC</i>	<i>tet</i>		
<i>tetY</i>	<i>otrB</i>			
<i>tetZ</i>				
<i>tet30</i>				

are naturally more resistant to tetracyclines due to differences in the permeability of the cell membrane. For example, Gram-negative bacteria are naturally resistant to several antibiotics because of the presence of a lipopolysaccharide containing outer membrane layer. In addition, the presence of small molecule transporters can also act on drugs to differing extents in different bacteria, conferring resistance by pumping the drugs out of the cell. Of the acquired resistance mechanisms, the most prevalent tetracycline resistance mechanism is efflux, with 28 distinct classes of efflux pumps identified so far (Table 1). Following closely are the so-called ribosome protection proteins, which bind to the ribosome and remove the drug from its binding site, with 12 distinct classes reported (Table 1). Less prevalent resistance mechanisms include two distinct genes that encode monooxygenases, which modify tetracyclines and promote their degradation, and mutations within the 16S rRNA that reduce the binding affinity of the drug for the ribosome (Table 1). In addition, a novel tetracycline resistance determinant, *tetU*, encoded on the plasmid pKq10 in *E. faecium* has been reported to confer some tetracycline resistance (Ridenhour et al., 1996), however, a recent study questions the validity of this conclusion (Caryl et al., 2012).

Efflux pumps to expel tetracycline from the cell

The 28 different classes of efflux pumps (Table 1) present in Gram-negative and Gram-positive bacteria fall into seven

defined groups based primarily on sequence homology (Guillaume et al., 2004). By far the largest group are the group 1 drug-H⁺ antiporters containing 12 transmembrane helices, and comprise the well characterized tetracycline efflux pumps, such as TetA, the most frequently occurring tetracycline-resistance determinant in Gram-negative bacteria. Although no structures exist for tetracycline efflux pumps, the high homology of the group 1 efflux pumps like TetA with the major facilitator superfamily (MFS) of secondary active transporters, implies a similar membrane topology and structural ‘inward-outward’ mechanism of action within the cell membrane (Figure 3A). Such efflux proteins exchange a proton (H⁺) for the tetracycline molecule against a concentration gradient (Piddock, 2006). Most tetracycline efflux pumps confer resistance to tetracycline, but are less effective against second generation doxycycline and minocycline, and confer little or no resistance to third generation glycylicylines, such as tigecycline (Chopra and Roberts, 2001). For example, the MIC of *E. coli* strain DH10B expressing the TetA efflux pump is >128 μg/ml for tetracycline, 32 μg/ml for doxycycline, 8 μg/ml for minocycline and 1 μg/ml for tigecycline (Grossman et al., 2012). Nevertheless, laboratory-derived mutations in *tetA* and *tetB* have been generated that can confer some glycylicylines resistance, but at the expense of tetracycline resistance (Guay et al., 1994).

In many cases, there is a fitness cost associated with the expression of antibiotic resistance genes, therefore many bacteria regulate the expression of the resistance gene(s) using translational attenuation, transcriptional attenuation and translational coupling (Chopra and Roberts, 2001). Another mechanism that is used for regulation of *tet* resistance genes is negative control by a Tet repressor protein (TetR) (Hillen and Berens, 1994; Saenger et al., 2000). In the absence of tetracycline, TetR binds as a homodimer to two tandemly orientated *tet* operators to block transcription of the efflux pump (Figure 3B), such as observed in the structure of the TetR-DNA complex (Figure 3C) (Orth et al., 2000). However, in the presence of tetracycline, the drug binds to TetR, which dissociates from the *tet* operator, thus inducing transcription and induction of expression of the TetA efflux pump (Figure 3B) (Saenger et al., 2000). In some cases, the *tetR* gene is also encoded directly in front of the efflux pump, and therefore TetR will rebind the *tet* operator only when insufficient amounts of tetracycline are in the cell and re-block transcription of its own gene and that of the downstream efflux pump (Hillen and Berens, 1994). Crystal structures of tetracycline in complex with the TetR homodimer reveal that tetracycline binds to the C-terminal effector-binding domain and induces conformational changes in

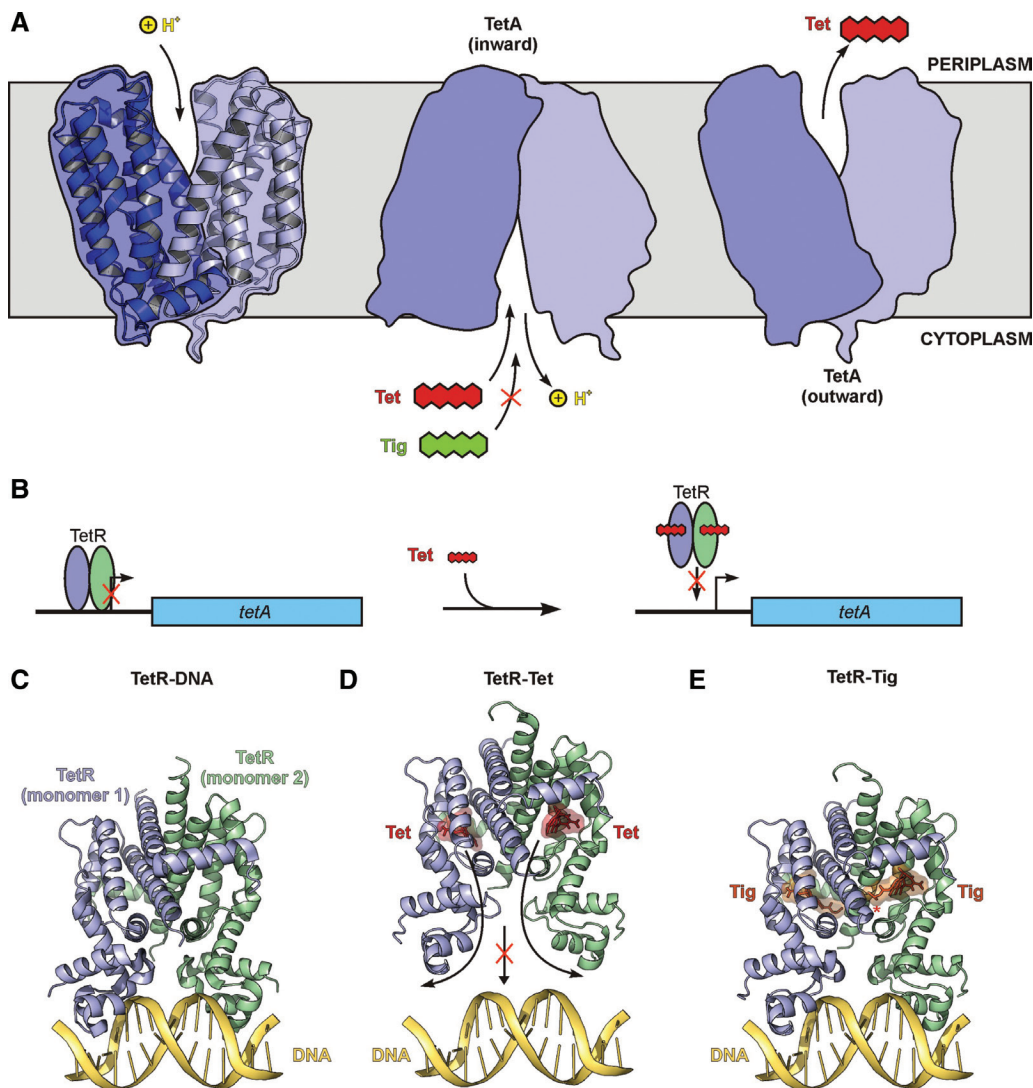


Figure 3 TetR-mediated regulation of the tetracycline resistance TetA efflux pump.

(A) Schematic for mechanism of action of efflux pump TetA, illustrating that efflux of tetracycline (but not tigecycline) is coupled to proton transport. The homology model for the TetA efflux pump was generated by HHPred (Söding et al., 2005) based on similarity with the proton-driven MFS transporter YajR from *Escherichia coli* (PDB ID 2WDO) (Jiang et al., 2013). (B) Schematic for TetR-mediated regulation of TetA, illustrating that tetracycline binding to the TetR homodimer leads to activation of transcription of the *tetA* gene. (C–E) Structures of TetR homodimer in complex with (C) DNA (Orth et al., 2000), (D) tetracycline (Hinrichs et al., 1994; Kisker et al., 1995) and (E) tigecycline (Orth et al., 1999). In (D), the binding of tetracycline to the C-terminal effector domain induces conformational changes in the DNA-binding domain (arrowed) that leads to loss of interaction with the DNA.

the N-terminal helix-turn-helix DNA-binding domain of TetR (Hinrichs et al., 1994; Kisker et al., 1995). The conformational changes lead to an increase in the separation of the DNA-binding domains such that interaction with the *tet* operator sequence of the DNA is precluded (Figure 3D) (Orth et al., 2000; Saenger et al., 2000). Although glycyclines, such as tigecycline, can bind to the C-terminal effector-binding domain of TetR, this interaction induces only a limited conformational change in the DNA-binding domain (Figure 3E) (Orth et al., 1999), consistent with the reduced (5-fold) induction of TetR-regulated TetA

expression observed in the presence of tigecycline compared to tetracycline (Orth et al., 1999).

Modification of tetracyclines leads to drug degradation

The *tetX* and *tet37* tetracycline resistance determinants encode FAD-requiring monooxygenases (Figure 4A) that confer resistance to tetracyclines through modification of the drug (Speer et al., 1991; Yang et al., 2004). The

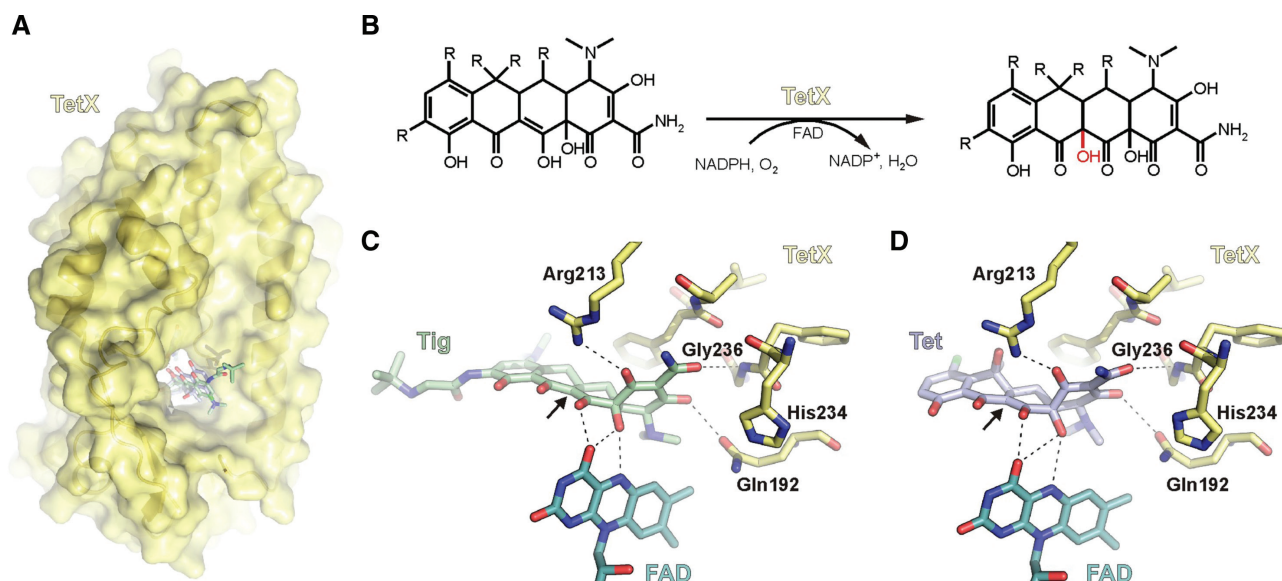


Figure 4 Tetracycline resistance via drug modification and degradation.

(A) Overlay of structures of the TetX monooxygenase (yellow) in complex with tigecycline (green) (Volkers et al., 2013) or tetracycline (blue) (Volkers et al., 2011). (B) Reaction pathway for TetX-mediated hydroxylation of tetracycline, which requires cofactors FAD, NADPH₂ and O₂. (C–D) FAD and residues of TetX recognize moieties of ring A and B of (C) tigecycline (Volkers et al., 2013) and (D) tetracycline (Volkers et al., 2011) to mediate hydroxylation of position C11a (arrowed), which leads to degradation of the drugs.

monooxygenases utilize NADPH and O₂ to hydroxylate position C11a located between ring B and C of tetracyclines (Figure 4B). The hydroxylated form of the drug has significantly altered chemical properties that perturb the magnesium coordination properties of the drug and presumably therefore reduce the drugs affinity for the ribosome. Moreover, the hydroxylated tetracycline undergoes a non-enzymatic decomposition. The requirement of O₂ for the monooxygenase activity means that the resistance mechanism only operates in bacteria growing in aerobic conditions.

Crystal structures indicate that monooxygenases, such as TetX, recognize the common core of the tetracyclines, specifically moieties present on rings A and B of the drug (Volkers et al., 2011, 2013), thus explaining why these enzymes also modify tetracycline derivatives, such as the glycyclcline tigecycline (Moore et al., 2005), which has an identical ring A and B arrangement as tetracycline (Figure 1C and F). Moreover, the ring D substitutions present in glycyclclines protrude from the active site (Figure 4A) and therefore do not prevent binding and modification of these derivatives by the TetX enzyme (Volkers et al., 2013). While C11a-hydroxytigecycline has an MIC of 64 µg/ml against *E. coli* compared to 0.5 µg/ml for tigecycline, the presence of the *tetX* gene in *E. coli* results in an MIC of only 2 µg/ml for tigecycline but 128 µg/ml for tetracycline (Moore et al., 2005; Grossman et al., 2012). This suggests that even if tigecycline is a substrate

for TetX, the enzymatic reaction is severely impaired with tigecycline compared to tetracycline. Furthermore, there have not been any reports to date of TetX in clinical isolates conferring tetracycline resistance therefore, at present, TetX is unlikely to influence the effectiveness of new glycyclclines, such as tigecycline.

Ribosome mutations conferring resistance to tetracyclines

Mutations conferring resistance to tetracycline antibiotics have been reported within the 16S rRNA. The first reported mutation was a G1058C substitution in h34 of the 16S rRNA of clinical isolates of the Gram-positive bacteria *Propionibacterium acnes* (Ross et al., 1998). These bacterial isolates encode three homozygous copies of the rRNA bearing the G1058C substitution, resulting in an increased MIC for tetracycline as well as for doxycycline and minocycline (Ross et al., 1998). Some resistance (4-fold increase in MIC) to tetracycline was also observed when the 16S rRNA operon bearing the G1058C substitution was overexpressed from a plasmid in a wildtype *E. coli* strain bearing seven copies of the susceptible 16S rRNA operon (Ross et al., 1998). Overexpression of the G1058C rRNA operon in an *E. coli* strain lacking the seven rRNA operons produced an 8-fold increase in MIC for tetracycline and tigecycline (Bauer et al., 2004). Consistently, tetracycline has a lower affinity for ribosomes

bearing the G1058C mutations than wildtype ribosomes (Nonaka et al., 2005). In wildtype bacterial ribosomes, G1058 forms a base-pair interaction with U1199 in h34, which would be disrupted by a G1058C mutation. Therefore, the decreased affinity of tetracycline for G1058C containing ribosomes most likely results from local conformational perturbations of the neighboring nucleotides G1197 and G1198 that are involved in direct interactions with tetracycline as well as in the coordination of a Mg^{2+} ion (Figure 2C).

Tetracycline resistance mutations have also been identified within the stem loop of helix 31 of the 16S rRNA in *Helicobacter pylori* strains, with the triple mutation A965U/G966U/A967C conferring high-level resistance against tetracycline (Dailidienė et al., 2002; Trieber and Taylor, 2002) as well as an increased MIC for doxycycline and minocycline (Gerrits et al., 2002). Overexpression of the ${}_{965}\text{AGA-UUC}_{967}$ triple mutation containing rRNA operon in an *E. coli* strain lacking the seven rRNA operons produced a 4-fold increased MIC for tetracycline and tigecycline (Bauer et al., 2004). Studies performing systematic site-directed mutagenesis of positions 965–967 indicate that the strength of the tetracycline resistance was generally proportional to the severity of the changes relative to the wildtype sequence, i.e., with single and double mutations tending to confer lower level resistance than triple mutations (Gerrits et al., 2003; Nonaka et al., 2005). Consistently, binding of tetracycline was the least efficient to ribosomes bearing the triple mutation (AGA-UUC), although still reduced for ribosomes bearing single mutations (e.g., AGC or GGA) when compared with wildtype (AGA) ribosomes (Nonaka et al., 2005). The decreased affinity of tetracycline for ribosomes bearing mutations in positions 965–967 most likely arises from perturbations in the conformation of the loop of helix 31, thus disrupting the interaction between the phosphate-oxygen of G966 of the 16S rRNA and the Mg^{2+} ion that is coordinated by ring A of tetracycline (Figure 2C). It is noteworthy that although the AGA-UUC triple mutation and G1058C cause a similar fold increase in the MIC for tigecycline and tetracycline, the absolute MIC₉₀ of tigecycline for G1058C (1 $\mu\text{g}/\text{ml}$) and AGA-UUC (0.5 $\mu\text{g}/\text{ml}$) is still 16-fold lower when compared with the respective MIC₉₀s for tetracycline (Bauer et al., 2004), consistent with the increased affinity and effectiveness of tigecycline over tetracycline.

Factor-assisted protection: ribosome protection proteins

To date, there are 12 distinct classes of ribosome protection proteins (RPPs) that confer resistance to tetracycline

(Table 1), with the best-characterized being TetO and TetM (reviewed by Connell et al., 2003a). TetO is usually found on plasmids present in *Campylobacter* species, but has also been discovered chromosomally in several Gram-positive organisms, e.g., *Streptococcus* and *Staphylococcus* (Roberts, 1994). In contrast, TetM, which is usually present on conjugative transposons (such as Tn916 and Tn1545), was first identified in *Streptococcus* sp., but has subsequently been found in a wide variety of Gram-positive and Gram-negative species (Roberts, 1994). The different classes of RPPs have high homology with one another; for example, TetO from *Campylobacter jejuni* displays >75% identity (>85% similarity) with TetM from *E. faecalis*. The presence of mosaic RPPs comprising regions from distinct RPP classes have also been reported, for example the novel mosaic *tetS/M* gene identified in foodborne strains of *Streptococcus bovis* (Barile et al., 2012). In general, RPPs are thought to have derived from *otrA*, which confers tetracycline resistance in the natural producer of oxytetracycline, *Streptomyces rimosus* (Doyle et al., 1991).

Sequence alignments indicate that RPPs are GTPases with the most significant homology (~25% identity and ~35% similarity) to translation factor EF-G (Burdett, 1991), which has allowed homology models for RPPs such as TetM to be generated (Dönhöfer et al., 2012) (Figure 5A–D). However, RPPs, such as TetM, cannot complement temperature sensitive *E. coli* EF-G (or *B. subtilis* EF-Tu) mutants (Burdett, 1991) and thus RPPs are considered paralogs of EF-G that have attained the specialized function to improve translation in the presence of tetracycline (Connell et al., 2003a) (Figure 5E). Analogous to EF-G, biochemical studies indicate that TetM and TetO bind to both GTP and GDP (Burdett, 1991; Taylor et al., 1995), and that mutation of the conserved Asn128 of the nucleotide binding G4 motif within the G domain of TetO results in reduced tetracycline resistance (Grewal et al., 1993), consistent with the importance of GTP binding for RPP action. Moreover, binding of TetO and TetM to the ribosome requires GTP or GDPNP, and does not occur with GDP (Dantley et al., 1998; Trieber et al., 1998). The GTPase activities of both TetM and TetO are stimulated (10–20-fold) by the presence of ribosomes (Burdett, 1991; Taylor et al., 1995; Connell et al., 2003b), however the release of tetracycline from the ribosome by TetM or TetO can occur in the presence of non-hydrolyzable GTP analogs, such as GDPNP (Burdett, 1996; Trieber et al., 1998; Connell et al., 2002). This indicates that GTP hydrolysis is not strictly necessary for tetracycline release, but rather for dissociation of the RPP from the ribosome. Curiously, the ribosome-dependent GTPase of TetM, but not of EF-G, is slightly stimulated by the presence (up to 1 mM) of tetracycline (Burdett, 1996). In contrast, the

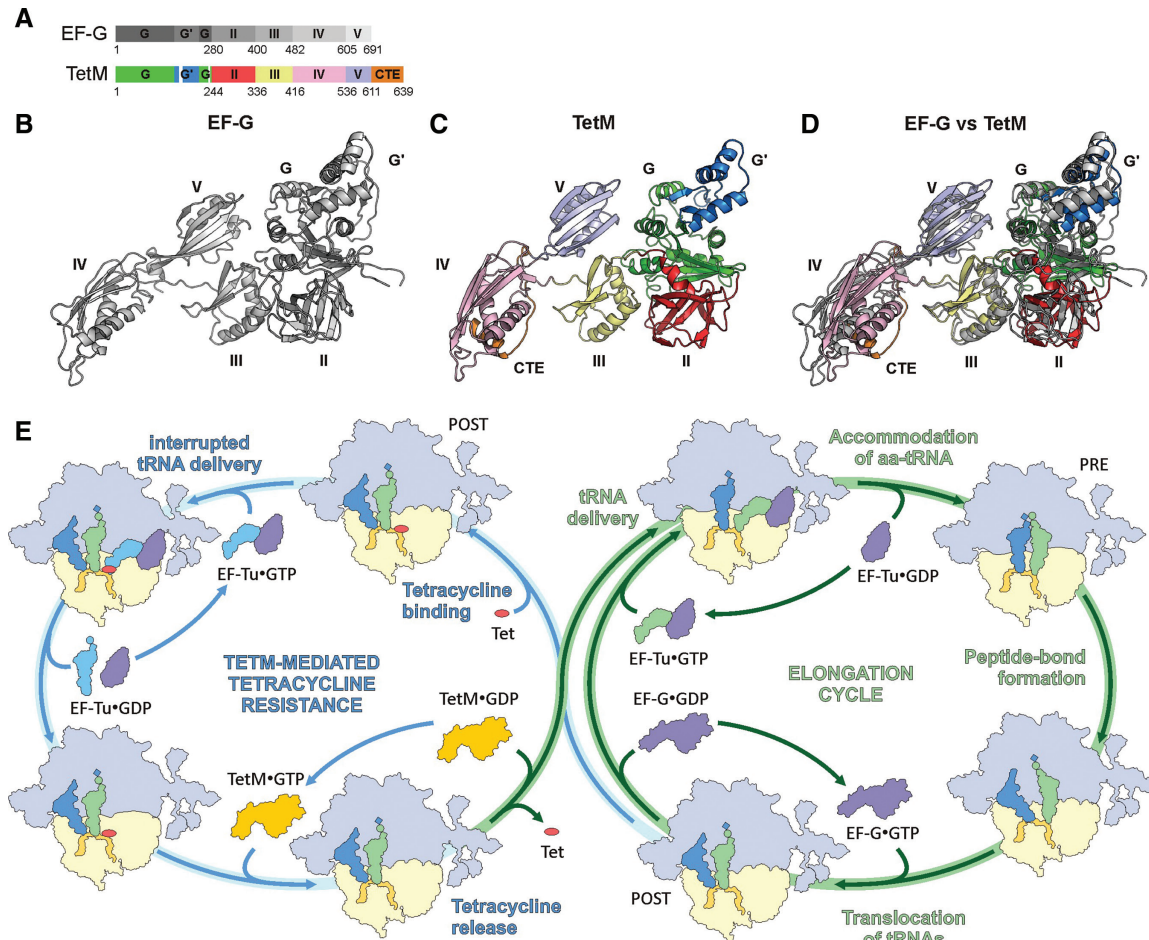


Figure 5 Tetracycline resistance mediated by ribosome protection proteins.

(A) Schematic comparing the domain arrangement of EF-G and the RPP TetM. (B–D) Comparison of (B) the crystal structure of *Thermus thermophilus* EF-G (PDB ID 2WRI) (Gao et al., 2009) with a homology model for TetM [colored as in (A); PDB ID 3J25 (Dönhöfer et al., 2012)] and (D) superimposition of (B) and (E). (E) Schematic illustrating the translation elongation cycle (green) and cycle of tetracycline inhibition and TetM-mediated tetracycline resistance (blue).

ribosome-dependent GTPase activity of TetM and TetO is inhibited by thiostrepton (Connell et al., 2003b; Starosta et al., 2009; Mikolajka et al., 2011) and the toxin α -sarcin (Connell et al., 2003b), as observed previously for other translation factors, such as EF-G (Wilson, 2009).

TetO binds preferentially to the POST translational state ribosome (Connell et al., 2003b), which is expected as during translation elongation, it is the POST state ribosome that is stabilized by the action of tetracycline to prevent delivery of aa-tRNA to the ribosomal A-site (Figure 5E). Cryo-electron microscopy (EM) structures of TetM (Figure 6A) and TetO (Figure 6B) in complex with ribosome reveal that RPPs occupy a similar binding site as EF-G (Figure 6C) (Spahn et al., 2001; Dönhöfer et al., 2012; Li et al., 2013), consistent with the competition observed between TetM and EF-G for ribosome binding (Dantley et al., 1998). As EF-G binds to the PRE translational state and specifically stabilizes

a rotated ribosome with hybrid site tRNAs before converting it into a POST state (Figure 5E), RPPs are unlikely to compete with EF-G during translation in the cell. Competition between RPPs and EF-G/EF-Tu might however explain the inhibition observed when high concentrations of RPPs are used in *in vitro* translation systems (Trieber et al., 1998).

Although no crystal structures of RPPs exist to date, the cryo-EM structure of the TetM-70S complex (Figure 6A) was sufficiently resolved (~ 7 Å resolution) as to allow docking of a molecular model for the TetM protein, generated based on homology with EF-G (Figure 5A–D) (Dönhöfer et al., 2012). This exercise led to the discovery of a conserved C-terminal extension (CTE) in RPPs that adopts a short α -helix, which is absent in EF-G (Figure 5A–D). Truncation of the CTE abolished the ability of TetM to confer resistance to tetracycline in *E. coli*, indicating the critical importance of the

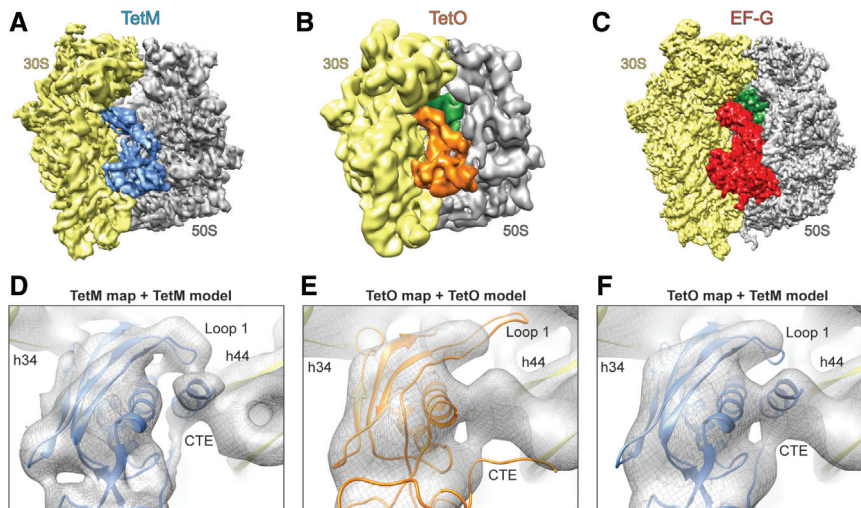


Figure 6 Structures of TetM, TetO and EF-G in complex with the 70S ribosome.

(A–C) Cryo-EM structures of (A) TetM (blue) (Dönhöfer et al., 2012) and (B) TetO (orange) (Li et al., 2013) on the ribosome, compared with (C) the binding position of EF-G (red) (Gao et al., 2009). (D–F) Cryo-EM map (grey) of the (D) TetM-70S (Dönhöfer et al., 2012) complex or (E, F) TetO-70S (Li et al., 2013) complex, with molecular model for domain IV of (D, F) TetM (blue) (Dönhöfer et al., 2012) and (E) TetO (orange) (Li et al., 2013).

short α -helix for TetM function (Dönhöfer et al., 2012). On the ribosome, the CTE of TetM is observed to be sandwiched between domain IV of TetM and helix 44 (h44) of the 16S rRNA (Figure 6D), consistent with chemical patterns in h44 observed upon TetO binding (Connell et al., 2002; Dönhöfer et al., 2012). Although the CTE of TetO was modeled differently in the 10 Å resolution cryo-EM structure of the TetO-70S complex (Figure 6E) (Li et al., 2013), the electron density of the TetO-70S map suggests that the CTE of TetO does in fact adopt a short α -helix and interact with h44 as observed in the TetM-70S structure (Figure 6D and E), and consistent with the high identity (>75%) between TetM and TetO. A similar discrepancy was also observed for loop 1 of domain IV, which was modeled in an extended conformation in the TetO-70S complex (Figure 6D) and proposed to form, together with surrounding rRNA nucleotides, a corridor which the tetracycline molecule navigates during its release from the ribosome (Li et al., 2013). However, careful inspection of the cryo-EM maps of both the TetO and TetM complexes does not support an extended conformation, but rather suggests that loop 1 adopts a kinked conformation for both TetO and TetM in order to establish interactions with the CTE (Figure 6D and E). In contrast, both the TetO-70S and TetM-70S structures are in agreement with respect to an interaction between loop 2 of domain IV and nucleotides in h34 (Dönhöfer et al., 2012; Li et al., 2013), consistent with the chemical protections of h34 observed upon TetO binding to the ribosome (Connell et al., 2002; Connell et al., 2003b).

In the first cryo-EM structure of a TetO-70S complex at 16 Å, density for TetO was not observed to overlap with tetracycline in the primary binding site, leading to the proposal that the RPPs remove tetracycline from the ribosome, not directly, but by inducing a local disturbance in h34 (Spahn et al., 2001). However, the subsequent higher resolution RPP-70S structures reveal that loop 3 of domain IV interacts with the vicinity of C1054 of the 16S rRNA (Dönhöfer et al., 2012; Li et al., 2013), and thus directly encroaches upon the binding site of tetracycline (Figure 7A and B), and more extensively tigecycline (Figure 7C) (Jenner et al., 2013). This suggests that residues within loop 3 of RPPs are involved in directly dislodging tetracycline from its binding site. Alanine scanning mutagenesis of loop 3 of domain IV of TetM however did not reveal any single critical amino acid, but rather the double Y506A/Y507A mutation was required to abolish TetM-mediated tetracycline resistance (Dönhöfer et al., 2012). Surprisingly, despite the high sequence conservation of loop 3 across different RPPs (Figure 7D), a single mutation Y507A was reported to inactivate *C. jejuni* TetO (Li et al., 2013). The system used to assess the tetracycline resistance however yielded only ~2-fold changes in MIC for the wildtype TetO protein (Li et al., 2013), whereas >10-fold differences were observed with wildtype TetM (Dönhöfer et al., 2012). Therefore, a reanalysis of *C. jejuni* TetO and *Listeria monocytogenes* TetS was performed, revealing that like TetM, these RPPs confer a >10-fold increase in MIC compared to the parental strain, and that while the

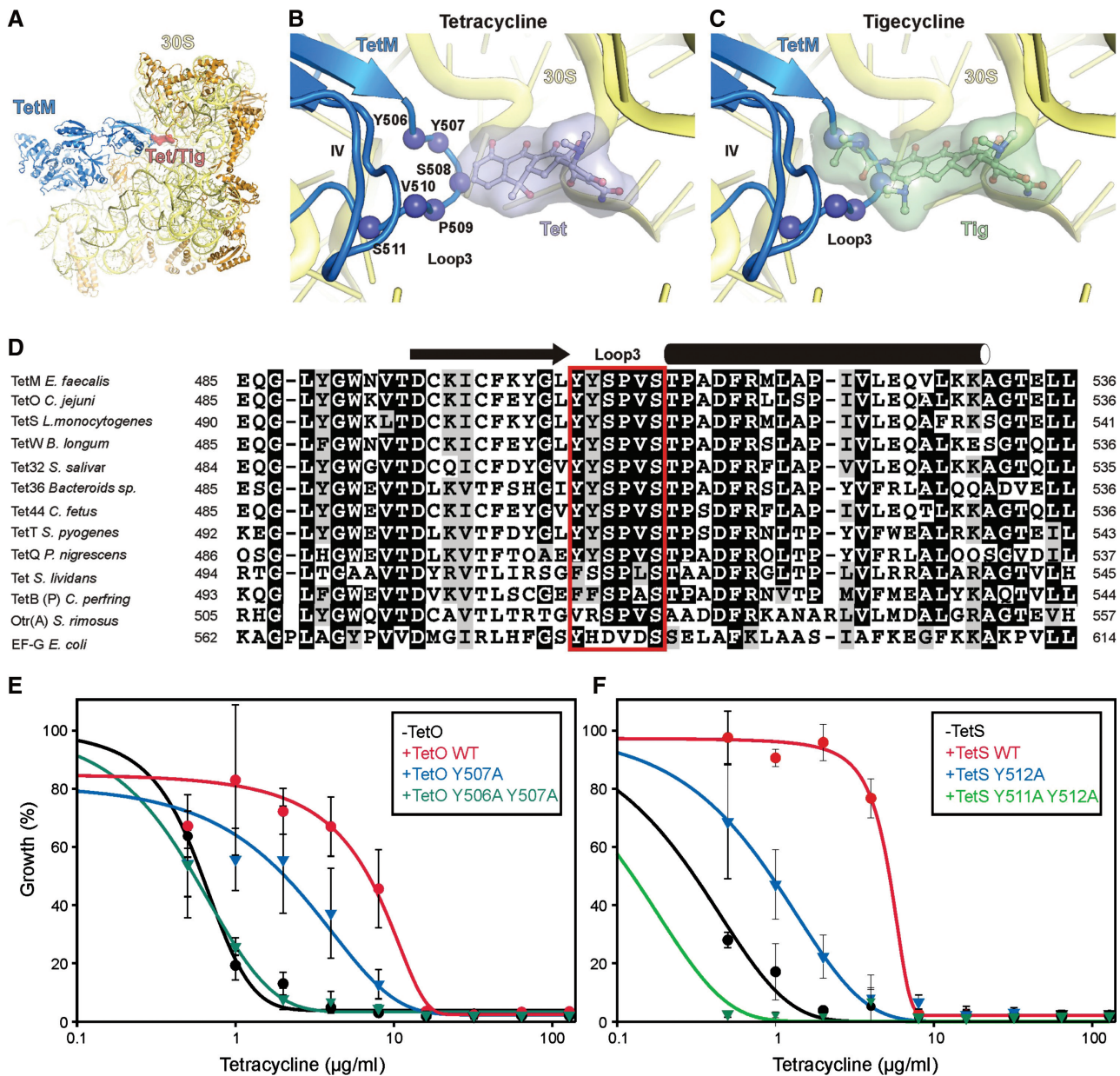


Figure 7 The role of Loop 3 of domain IV of RPPs for tetracycline resistance.

(A) Overview of relative position of TetM (blue) (Dönhöfer et al., 2012), tetracycline/tigecycline (red) (Jenner et al., 2013) and 30S subunit (yellow). (B–C) Relative binding positions of loop 3 of domain IV of TetM (Dönhöfer et al., 2012) compared to (B) tetracycline (blue) and (C) tigecycline (green) (Jenner et al., 2013). (D) Sequence alignment of RPPs showing conservation of loop 3 (red box) of domain IV (black boxes indicate identical residues, grey boxes indicate similar residues). (E–F) Growth curves of wildtype *E. coli* strain BL21 (-TetO or -TetS, black) in the presence of increasing concentrations of tetracycline (0–128 µg/ml) compared with the WT strain harboring a plasmid encoding wildtype (E) *C. jejuni* TetO (+TetO WT, red) or (F) *L. monocytogenes* TetS (+TetS WT, red), or single (blue) or double (green) mutants. Experiments were performed as described in (Dönhöfer et al., 2012).

single mutation Y507A reduces the MIC, the Y506A/Y507A double mutation was necessary to completely inactivate TetO and TetS (Figure 7E and F), as reported previously for TetM (Dönhöfer et al., 2012). Based on these findings, it is tempting to speculate that these aromatic tyrosine residues in loop 3 establish stacking interactions with

C1054 to dislodge tetracycline from its binding, however, higher resolution structures of RPP·70S complexes will be required to validate this hypothesis.

The enhancement of C1054 to chemical modification that is observed upon TetO binding remains subsequent to dissociation of TetO from the ribosome, suggesting that

RPPs may imprint a defined conformation of C1054 in the ribosome, which on one the hand prevents rebinding of tetracycline and on the other hand favors delivery of the aa-tRNA by EF-Tu (Connell et al., 2002, 2003a,b). In this context, it is interesting to note that mutations in the *miaA* gene of *E. coli* interfere with the ability of TetM and TetO to confer tetracycline resistance (Burdett, 1993; Taylor et al., 1998). The *miaA* gene encodes an enzyme involved in the modification of tRNA position A37, which is located 3' adjacent to the anticodon of tRNAs that decode codons starting with U (Esberg and Bjork, 1995). The modification [2-methylthio-N₆-(D₂-isopentenyl)adenosine] has been shown to stabilize the anticodon-codon interaction by improving stacking interactions (Vacher et al., 1984), and the lack of this modification significantly reduces the affinity of these tRNAs for the ribosome as well as reducing the efficiency and fidelity of translation (Vacher et al., 1984; Esberg and Bjork, 1995). Thus, the lower level of tetracycline resistance in *E. coli* *miaA* mutants suggests that RPP induced alterations within the decoding site that promote binding of modified tRNAs are unfavourable for binding of the unmodified aminoacyl-tRNAs.

Although RPPs increase the MIC for tetracycline, doxycycline and minocycline, these proteins have little or no effect on the potency of third generation tetracyclines,

such tigecycline, eravacycline and omadacycline (Grossman et al., 2012; Draper et al., 2013; Jenner et al., 2013). The ability of third generation tetracyclines to overcome TetM action does not appear to be related only to an increase in binding affinity compared to tetracycline, since omadacycline displays a similar affinity to azacycline, which does not overcome TetM action (Jenner et al., 2013). The C9-moiety of the third generation tetracyclines might therefore contribute not only to the binding affinity of the drug, but also enhance the on-rate of the drug as well as sterically hinder residues within loop 3 of the TetM from accessing nucleotide C1054 to dislodge the drug from its binding site on the ribosome (Figure 7C). It will be interesting to see whether alterations within loop 3 of domain IV can give rise to RPPs that confer resistance against third generation tetracyclines, such as tigecycline.

Acknowledgments: This work was supported by Deutsche Forschungsgemeinschaft FOR1805 (Grant WI3285/2-1 to D.N.W.) and the European Molecular Biology Organisation (EMBO) Young Investigator Programme (D.N.W.); A.L.S. is funded by an AXA Research Fund Postdoctoral Fellowship.

Received December 6, 2013; accepted January 30, 2014; previously published online February 5, 2014

References

- Agwuh, K.N. and MacGowan, A. (2006). Pharmacokinetics and pharmacodynamics of the tetracyclines including glycylicyclines. *J. Antimicrob. Chemother.* *58*, 256–265.
- Backus, E.J., Duggar, B.M., and Campbell, T.H. (1954). Variation in *Streptomyces aureofaciens*. *Ann. NY Acad. Sci.* *60*, 86–101.
- Barden, T.C., Buckwalter, B.L., Testa, R.T., Petersen, P.J., and Lee, V.J. (1994). "Glycylcyclines". 3. 9-Aminodoxycyclinecarboxamides. *J. Med. Chem.* *37*, 3205–3211.
- Barile, S., Devirgiliis, C., and Perozzi, G. (2012). Molecular characterization of a novel mosaic tet(S/M) gene encoding tetracycline resistance in foodborne strains of *Streptococcus bovis*. *Microbiology* *158*, 2353–2362.
- Bauer, G., Berens, C., Projan, S., and Hillen, W. (2004). Comparison of tetracycline and tigecycline binding to ribosomes mapped by dimethylsulphate and drug-directed Fe²⁺ cleavage of 16S rRNA. *J. Antimicrob. Chemother.* *53*, 592–599.
- Ben-Shem, A., Garreau de Loubresse, N., Melnikov, S., Jenner, L., Yusupova, G., and Yusupov, M. (2011). The structure of the eukaryotic ribosome at 3.0 Å resolution. *Science* *334*, 1524–1529.
- Bergeron, J., Ammirati, M., Danley, D., James, L., Norcia, M., Retsema, J., Strick, C.A., Su, W.G., Sutcliffe, J., and Wondrack, L. (1996). Glycylcyclines bind to the high-affinity tetracycline ribosomal binding site and evade Tet(M)- and Tet(O)-mediated ribosomal protection. *Antimicrob. Agents Chemother.* *40*, 2226–2228.
- Blackwood, R.K., Beereboom, J.J., Rennhard, H.H., von Wittenau, M.S., and Stephens, C.R. (1961). 6-methylenetetracyclines. 1. a new class of tetracycline antibiotics. *J. Am. Chem. Soc.* *83*, 2773–2775.
- Blanchard, S.C., Gonzalez, R.L., Kim, H.D., Chu, S., and Puglisi, J.D. (2004). tRNA selection and kinetic proofreading in translation. *Nat. Struct. Mol. Biol.* *11*, 1008–1014.
- Boothe, J.H., Kende, A.S., Fields, T.L., and Wilkinson, R.G. (1959). Total synthesis of tetracyclines. I. (±)-dedimethylamino-12a-deoxy-6-demethylanhydrochlortetracycline. *J. Am. Chem. Soc.* *81*, 1006–1007.
- Bradford, P.A., and Jones, C.H. (2012). Tetracyclines. In: *Antibiotic Discovery and Development*, Dougherty, T.J. and Puccim, M.J., eds. (New York: Springer), pp. 147–179.
- Brodersen, D.E., Clemons, W.M., Carter, A.P., Morgan-Warren, R.J., Wimberly, B.T., and Ramakrishnan, V. (2000). The structural basis for the action of the antibiotics tetracycline, pactamycin, and hygromycin B on the 30S ribosomal subunit. *Cell* *103*, 1143–1154.
- Budkevich, T.V., El'skaya, A.V., and Nierhaus, K.H. (2008). Features of 80S mammalian ribosome and its subunits. *Nucleic Acids Res.* *36*, 4736–4744.
- Burdett, V. (1991). Purification and characterization of Tet(M), a protein that renders ribosomes resistant to tetracycline. *J. Biol. Chem.* *266*, 2872–2877.

- Burdett, V. (1993). transfer-RNA modification activity is necessary for Tet(M)-mediated tetracycline resistance. *J. Bacteriol.* *175*, 7209–7215.
- Burdett, V. (1996). Tet(M)-promoted release of tetracycline from ribosomes is GTP dependent. *J. Bacteriol.* *178*, 3246–3251.
- Caryl, J.A., Cox, G., Trimble, S., and O'Neill, A.J. (2012). “tet(U)” is not a tetracycline resistance determinant. *Antimicrob. Agents Chemother.* *56*, 3378–3379.
- Chopra, I. and Roberts, M. (2001). Tetracycline antibiotics: mode of action, applications, molecular biology, and epidemiology of bacterial resistance. *Microbiol. Mol. Biol. Rev.* *65*, 232–260.
- Connell, S.R., Trieber, C.A., Stelzl, U., Einfeldt, E., Taylor, D.E., and Nierhaus, K.H. (2002). The tetracycline resistance protein Tet(O) perturbs the conformation of the ribosomal decoding centre. *Mol. Microbiol.* *45*, 1463–1472.
- Connell, S.R., Tracz, D.M., Nierhaus, K.H., and Taylor, D.E. (2003a). Ribosomal protection proteins and their mechanism of tetracycline resistance. *Antimicrob. Agents Chemother.* *47*, 3675–3681.
- Connell, S.R., Trieber, C.A., Dinos, G.P., Einfeldt, E., Taylor, D.E., and Nierhaus, K.H. (2003b). Mechanism of Tet(O)-mediated tetracycline resistance. *EMBO J.* *22*, 945–953.
- Conover, L.H., Moreland, W.T., English, A.R., Stephens, C.R., and Pilgrim, F.J. (1953). Terramycin. XI. Tetracycline. *J. Am. Chem. Soc.* *75*, 4622–4623.
- Dailidienė, D., Bertoli, M.T., Miculevičienė, J., Mukhopadhyay, A.K., Dailidė, G., Pascasio, M.A., Kupcinskis, L., and Berg, D.E. (2002). Emergence of tetracycline resistance in *Helicobacter pylori*: multiple mutational changes in 16S ribosomal DNA and other genetic loci. *Antimicrob. Agents Chemother.* *46*, 3940–3946.
- Dantley, K., Dannelly, H., and Burdett, V. (1998). Binding interaction between Tet(M) and the ribosome: requirements for binding. *J. Bacteriol.* *180*, 4089–4092.
- Dönhöfer, A., Franckenberg, S., Wickles, S., Berninghausen, O., Beckmann, R., and Wilson, D.N. (2012). Structural basis for TetM-mediated tetracycline resistance. *Proc. Natl. Acad. Sci. USA* *109*, 16900–16905.
- Doyle, D., McDowall, K.J., Butler, M.J., and Hunter, I.S. (1991). Characterization of an oxytetracycline-resistance gene, *otrA*, of *Streptomyces rimosus*. *Mol. Microbiol.* *5*, 2923–2933.
- Draper, M.P., Weir, S., Macone, A., Donatelli, J., Trieber, C.A., Tanaka, S.K., and Levy, S.B. (2013). The mechanism of action of the novel aminomethylcycline antibiotic omadacycline. *Antimicrob. Agents Chemother.* Sep 16. [Epub ahead of print] doi: 10.1128/AAC.01066-13.
- Duggar, B.M. (1948). Aureomycin; a product of the continuing search for new antibiotics. *Ann. NY Acad. Sci.* *51*, 177–181.
- Esberg, B. and Bjork, G.R. (1995). The methylthio group (ms(2)) of N-6-(4-hydroxyisopentenyl)-2-methylthioadenosine (ms(2)io(6)A) present next to the anticodon contributes to the decoding efficiency of the tRNA. *J. Bacteriol.* *177*, 1967–1975.
- Finlay, A.C., Hobby, G.L., P'an, S.Y., Regna, P.P., Routien, J.B., Seeley, D.B., Shull, G.M., Sobin, B.A., Solomons, I.A., Vinson, J.W., et al. (1950). Terramycin, a new antibiotic. *Science* *111*, 85.
- Gale, E.F., Cundliffe, E., Reynolds, P.E., Richmond, M.H., and Waring, M.J. (1981). Antibiotic inhibitors of ribosome function. In: *The Molecular Basis of Antibiotic Action* (Bristol, UK: John Wiley and Sons), pp. 278–379.
- Gao, Y.G., Selmer, M., Dunham, C.M., Weixlbaumer, A., Kelley, A.C., and Ramakrishnan, V. (2009). The structure of the ribosome with elongation factor G trapped in the posttranslocational state. *Science* *326*, 694–699.
- Geggie, P., Dave, R., Feldman, M.B., Terry, D.S., Altman, R.B., Munro, J.B., and Blanchard, S.C. (2010). Conformational sampling of aminoacyl-tRNA during selection on the bacterial ribosome. *J. Mol. Biol.* *399*, 576–595.
- Gerrits, M.M., de Zoete, M.R., Arents, N.L., Kuipers, E.J., and Kusters, J.G. (2002). 16S rRNA mutation-mediated tetracycline resistance in *Helicobacter pylori*. *Antimicrob. Agents Chemother.* *46*, 2996–3000.
- Gerrits, M.M., Berning, M., Van Vliet, A.H., Kuipers, E.J., and Kusters, J.G. (2003). Effects of 16S rRNA gene mutations on tetracycline resistance in *Helicobacter pylori*. *Antimicrob. Agents Chemother.* *47*, 2984–2986.
- Grewal, J., Manavathu, E.K., and Taylor, D.E. (1993). Effect of mutational alteration of Asn-128 in the putative GTP-binding domain of tetracycline resistance determinant Tet(O) from *Campylobacter jejuni*. *Antimicrob. Agents Chemother.* *37*, 2645–2649.
- Grossman, T.H., Starosta, A.L., Fyfe, C., O'Brien, W., Rothstein, D.M., Mikolajka, A., Wilson, D.N., and Sutcliffe, J.A. (2012). Target- and resistance-based mechanistic studies with TP-434, a novel fluorocycline antibiotic. *Antimicrob. Agents Chemother.* *56*, 2559–2564.
- Guay, G.G., Tuckman, M., and Rothstein, D.M. (1994). Mutations in the tetA(B) gene that cause a change in substrate specificity of the tetracycline efflux pump. *Antimicrob. Agents Chemother.* *38*, 857–860.
- Guillaume, G., Ledent, V., Moens, W., and Collard, J.M. (2004). Phylogeny of efflux-mediated tetracycline resistance genes and related proteins revisited. *Microb. Drug Resist.* *10*, 11–26.
- Hillen, W. and Berens, C. (1994). Mechanisms underlying expression of Tn10 encoded tetracycline resistance. *Annu. Rev. Microbiol.* *48*, 345–369.
- Hinrichs, W., Kisker, C., Duvel, M., Muller, A., Tovar, K., Hillen, W., and Saenger, W. (1994). Structure of the Tet repressor-tetracycline complex and regulation of antibiotic resistance. *Science* *264*, 418–420.
- Hochstein, F.A., Stephens, C.R., Conover, L.H., Regna, P.P., Pasternack, R., Gordon, P.N., Pilgrim, F.J., Brunings, K.J., and Woodward, R.B. (1953). The structure of terramycin_{1,2}. *J. Am. Chem. Soc.* *75*, 5455–5475.
- Jenner, L., Starosta, A.L., Terry, D.S., Mikolajka, A., Filonava, L., Yusupov, M., Blanchard, S.C., Wilson, D.N., and Yusupova, G. (2013). Structural basis for potent inhibitory activity of the antibiotic tigecycline during protein synthesis. *Proc. Natl. Acad. Sci. USA* *110*, 3812–3816.
- Jiang, D., Zhao, Y., Wang, X., Fan, J., Heng, J., Liu, X., Feng, W., Kang, X., Huang, B., Liu, J., et al. (2013). Structure of the YajR transporter suggests a transport mechanism based on the conserved motif A. *Proc. Natl. Acad. Sci. USA* *110*, 14664–14669.
- Kisker, C., Hinrichs, W., Tovar, K., Hillen, W., and Saenger, W. (1995). The complex formed between Tet repressor and tetracycline-Mg²⁺ reveals mechanism of antibiotic resistance. *J. Mol. Biol.* *247*, 260–280.
- Li, W., Atkinson, G.C., Thakor, N.S., Allas, U., Lu, C.C., Chan, K.Y., Tenson, T., Schulten, K., Wilson, K.S., Hauryliuk, V., et al. (2013). Mechanism of tetracycline resistance by ribosomal protection protein Tet(O). *Nat. Commun.* *4*, 1477.

- Martell, M.J., Jr. and Boothe, J.H. (1967). The 6-deoxytetracyclines. VII. Alkylated aminotetracyclines possessing unique antibacterial activity. *J. Med. Chem.* *10*, 44–46.
- McCormick, J.R.D., Sjolander, N.O., Hirsch, U., Jensen, E.R., and Doerschuk, A.P. (1957). A new family of antibiotics: the demethyltetracyclines. *J. Am. Chem. Soc.* *79*, 4561–4563.
- McCormick, J.R.D., Hirsch, U., Sjolander, N.O., and Doerschuk, A.P. (1960). Cosynthesis of tetracyclines by pairs of *Streptomyces aureofaciens* mutants. *J. Am. Chem. Soc.* *82*, 5006–5007.
- Mikolajka, A., Liu, H., Chen, Y., Starosta, A.L., Marquez, V., Ivanova, M., Cooperman, B.S., and Wilson, D.N. (2011). Differential effects of thiopeptide and orthosomycin antibiotics on translational GTPases. *Chem. Biol.* *18*, 589–600.
- Moazed, D. and Noller, H.F. (1987). Interaction of antibiotics with functional sites in 16S ribosomal RNA. *Nature* *327*, 389–394.
- Moore, I.F., Hughes, D.W., and Wright, G.D. (2005). Tigecycline is modified by the flavin-dependent monooxygenase TetX. *Biochemistry* *44*, 11829–11835.
- Nelson, M.L. (2001). The chemistry and cellular biology of the tetracyclines. In: *Tetracyclines in Biology, Chemistry and Medicine*, M.L. Nelson, W. Hillen, and R.A. Greenwald, eds. (Switzerland: Birkhäuser Verlag), pp. 3–63.
- Nelson, M.L. and Levy, S.B. (2011). The history of the tetracyclines. *Ann. N.Y. Acad. Sci.* *1241*, 17–32.
- Nelson, M.L., Ismail, M.Y., McIntyre, L., Bhatia, B., Viski, P., Hawkins, P., Rennie, G., Andorsky, D., Messersmith, D., Stapleton, K., et al. (2003). Versatile and facile synthesis of diverse semisynthetic tetracycline derivatives via Pd-catalyzed reactions. *J. Org. Chem.* *68*, 5838–5851.
- Nonaka, L., Connell, S.R., and Taylor, D.E. (2005). 16S rRNA mutations that confer tetracycline resistance in *Helicobacter pylori* decrease drug binding in *Escherichia coli* ribosomes. *J. Bacteriol.* *187*, 3708–3712.
- Olson, M.W., Ruzin, A., Feyfant, E., Rush, T.S., 3rd, O'Connell, J., and Bradford, P.A. (2006). Functional, biophysical, and structural bases for antibacterial activity of tigecycline. *Antimicrob. Agents Chemother.* *50*, 2156–2166.
- Orth, P., Schnappinger, D., Sum, P.E., Ellestad, G.A., Hillen, W., Saenger, W., and Hinrichs, W. (1999). Crystal structure of the tet repressor in complex with a novel tetracycline, 9-(N,N-dimethylglycylamido)-6-demethyl-6-deoxy-tetracycline. *J. Mol. Biol.* *285*, 455–461.
- Orth, P., Schnappinger, D., Hillen, W., Saenger, W., and Hinrichs, W. (2000). Structural basis of gene regulation by the tetracycline inducible Tet repressor-operator system. *Nat. Struct. Biol.* *7*, 215–219.
- Perlman, D., Heuser, L.J., Dutcher, J.D., Barrett, J.M., and Boska, J.A. (1960). Biosynthesis of tetracycline by 5-hydroxy-tetracycline-producing cultures of *Streptomyces rimosus*. *J. Bacteriol.* *80*, 419–420.
- Petersen, P.J., Jacobus, N.V., Weiss, W.J., Sum, P.E., and Testa, R.T. (1999). In vitro and in vivo antibacterial activities of a novel glycylycylamine, the 9-t-butylglycylamido derivative of minocycline (GAR-936). *Antimicrob. Agents Chemother.* *43*, 738–744.
- Piddock, L.J. (2006). Multidrug-resistance efflux pumps-not just for resistance. *Nat. Rev. Microbiol.* *4*, 629–636.
- Pioletti, M., Schlunzen, F., Harms, J., Zarivach, R., Gluhmann, M., Avila, H., Bashan, A., Bartels, H., Auerbach, T., Jacobi, C., et al. (2001). Crystal structures of complexes of the small ribosomal subunit with tetracycline, edeine and IF3. *EMBO J.* *20*, 1829–1839.
- Ridenhour, M.B., Fletcher, H.M., Mortensen, J.E., and Daneo-Moore, L. (1996). A novel tetracycline-resistant determinant, tet(U), is encoded on the plasmid pKq10 in *Enterococcus faecium*. *Plasmid* *35*, 71–80.
- Roberts, M.C. (1994). Epidemiology of tetracycline-resistance determinants. *Trends Microbiol.* *2*, 353–357.
- Roberts, M.C. (1996). Tetracycline resistance determinants: Mechanisms of action, regulation of expression, genetic mobility, and distribution. *FEMS Microbiol. Rev.* *19*, 1–24.
- Ross, J.I., Eady, E.A., Cove, J.H., and Cunliffe, W.J. (1998). 16S rRNA mutation associated with tetracycline resistance in a Gram-positive bacterium. *Antimicrob. Agents Chemother.* *42*, 1702–1705.
- Saenger, W., Orth, P., Kisker, C., Hillen, W., and Hinrichs, W. (2000). The tetracycline repressor—a paradigm for a biological switch. *Angew Chem. Int. Ed. Engl.* *39*, 2042–2052.
- Schmeing, T.M., Voorhees, R.M., Kelley, A.C., Gao, Y.G., Murphy, F.V.T., Weir, J.R., and Ramakrishnan, V. (2009). The crystal structure of the ribosome bound to EF-Tu and aminoacyl-tRNA. *Science* *326*, 688–694.
- Söding, J., Biegert, A., and Lupas, A.N. (2005). The HHpred interactive server for protein homology detection and structure prediction. *Nucleic Acids Res.* *33*, W244–W248.
- Sohmen, D., Harms, J.M., Schlunzen, F., and Wilson, D.N. (2009a). Enhanced SnapShot: Antibiotic inhibition of protein synthesis II. *Cell* *139*, 212–212 e211.
- Sohmen, D., Harms, J.M., Schlunzen, F., and Wilson, D.N. (2009b). SnapShot: antibiotic inhibition of protein synthesis I. *Cell* *138*, 1248 e1241.
- Spahn, C.M., Blaha, G., Agrawal, R.K., Penczek, P., Grassucci, R.A., Trieber, C.A., Connell, S.R., Taylor, D.E., Nierhaus, K.H., and Frank, J. (2001). Localization of the ribosomal protection protein Tet(O) on the ribosome and the mechanism of tetracycline resistance. *Mol. Cell* *7*, 1037–1045.
- Speer, B.S., Bedzyk, L., and Salyers, A.A. (1991). Evidence that a novel tetracycline resistance gene found on two *Bacteroides* transposons encodes an NADP-requiring oxidoreductase. *J. Bacteriol.* *173*, 176–183.
- Starosta, A.L., Qin, H., Mikolajka, A., Leung, G.Y., Schwinghammer, K., Nicolaou, K.C., Chen, D.Y., Cooperman, B.S., and Wilson, D.N. (2009). Identification of distinct thiopeptide-antibiotic precursor lead compounds using translation machinery assays. *Chem Biol* *16*, 1087–1096.
- Stephens, C.R., Conover, L.H., Hochstein, F.A., Regna, P.P., Pilgrim, F.J., Brunings, K.J., and Woodward, R.B. (1952). Terramycin. VIII. Structure of aureomycin and terramycin. *J. Am. Chem. Soc.* *74*, 4976–4977.
- Stephens, C.R., Conover, L.H., Pasternack, R., Hochstein, F.A., Moreland, W.T., Regna, P.P., Pilgrim, F.J., Brunings, K.J., and Woodward, R.B. (1954). The structure of Aureomycin1. *J. Am. Chem. Soc.* *76*, 3568–3575.
- Stephens, C.R., Beereboom, J.J., Rennhard, H.H., Gordon, P.N., Murai, K., Blackwood, R.K., and von Wittenau, M.S. (1963). 6-Deoxytetracyclines. IV.1,2 Preparation, C-6 Stereochemistry, and Reactions. *J. Am. Chem. Soc.* *85*, 2643–2652.
- Sum, P.E., Lee, V.J., Testa, R.T., Hlavka, J.J., Ellestad, G.A., Bloom, J.D., Gluzman, Y., and Tally, F.P. (1994). Glycylyclines. 1. A new generation of potent antibacterial agents through modification of 9-aminotetracyclines. *J. Med. Chem.* *37*, 184–188.

- Sun, C., Wang, Q., Brubaker, J.D., Wright, P.M., Lerner, C.D., Noson, K., Charest, M., Siegel, D.R., Wang, Y.M., and Myers, A.G. (2008). A robust platform for the synthesis of new tetracycline antibiotics. *J. Am. Chem. Soc.* *130*, 17913–17927.
- Sun, C., Hunt, D.K., Clark, R.B., Lofland, D., O'Brien, W.J., Plamondon, L., and Xiao, X.Y. (2010). Synthesis and antibacterial activity of pentacyclines: a novel class of tetracycline analogs. *J. Med. Chem.* *54*, 3704–3731.
- Tally, F.T., Ellestad, G.A., and Testa, R.T. (1995). Glycylcyclines: a new generation of tetracyclines. *J. Antimicrob. Chemother.* *35*, 449–452.
- Taylor, D.E., Jerome, L.J., Grewal, J., and Chang, N. (1995). Tet(O), a protein that mediates ribosomal protection to tetracycline, binds, and hydrolyses GTP. *Can. J. Microbiol.* *41*, 965–970.
- Taylor, D.E., Trieber, C.A., Trescher, G., and Bekkering, M. (1998). Host mutations (*miaA* and *rpsL*) reduce tetracycline resistance mediated by Tet(O) and Tet(M). *Antimicrob. Agents Chemother.* *42*, 59–64.
- Testa, R.T., Petersen, P.J., Jacobus, N.V., Sum, P.E., Lee, V.J., and Tally, F.P. (1993). *In vitro* and *in vivo* antibacterial activities of the glycylcyclines, a new class of semisynthetic tetracyclines. *Antimicrob. Agents Chemother.* *37*, 2270–2277.
- Thaker, M., Spanogiannopoulos, P., and Wright, G.D. (2010). The tetracycline resistome. *Cell. Mol. Life Sci.* *67*, 419–431.
- Trieber, C.A. and Taylor, D.E. (2002). Mutations in the 16S rRNA genes of *Helicobacter pylori* mediate resistance to tetracycline. *J. Bacteriol.* *184*, 2131–2140.
- Trieber, C.A., Burkhardt, N., Nierhaus, K.H., and Taylor, D.E. (1998). Ribosomal protection from tetracycline mediated by Tet(O) interaction with ribosomes is GTP-dependent. *Biol. Chem.* *379*, 847–855.
- Vacher, J., Grosjean, H., Houssier, C., and Buckingham, R.H. (1984). The effect of point mutations affecting *Escherichia coli* tryptophan tRNA on anticodon-anticodon interactions and on UGA suppression. *J. Mol. Biol.* *177*, 329–342.
- Volkers, G., Palm, G.J., Weiss, M.S., Wright, G.D., and Hinrichs, W. (2011). Structural basis for a new tetracycline resistance mechanism relying on the TetX monooxygenase. *FEBS Lett.* *585*, 1061–1066.
- Volkers, G., Damas, J.M., Palm, G.J., Panjikar, S., Soares, C.M., and Hinrichs, W. (2013). Putative dioxygen-binding sites and recognition of tigecycline and minocycline in the tetracycline-degrading monooxygenase TetX. *Acta Crystallogr. D Biol. Crystallogr.* *69*, 1758–1767.
- Voorhees, R.M., Weixlbaumer, A., Loakes, D., Kelley, A.C., and Ramakrishnan, V. (2009). Insights into substrate stabilization from snapshots of the peptidyl transferase center of the intact 70S ribosome. *Nat. Struct. Mol. Biol.* *16*, 528–533.
- White, J.P. and Cantor, C.R. (1971). Role of magnesium in the binding of tetracycline to *Escherichia coli* ribosomes. *J. Mol. Biol.* *58*, 397–400.
- Wilson, D.N. (2009). The A-Z of bacterial translation inhibitors. *Crit. Rev. Biochem. Mol. Biol.* *44*, 393–433.
- Wilson, D.N. (2013). Ribosome-targeting antibiotics and bacterial resistance mechanisms. *Nat. Rev. Microbiol.* *12*, 35–48.
- Yang, W., Moore, I.F., Koteva, K.P., Bareich, D.C., Hughes, D.W., and Wright, G.D. (2004). TetX is a flavin-dependent monooxygenase conferring resistance to tetracycline antibiotics. *J. Biol. Chem.* *279*, 52346–52352.

Cryo-EM structure of the tetracycline resistance protein TetM in complex with a translating ribosome at 3.9-Å resolution

Stefan Arenz^a, Fabian Nguyen^a, Roland Beckmann^{a,b}, and Daniel N. Wilson^{a,b,1}

^aGene Center and Department for Biochemistry, University of Munich, 81377 Munich, Germany; and ^bCenter for integrated Protein Science Munich (CiPSM), University of Munich, 81377 Munich, Germany

Edited by Peter B. Moore, Yale University, New Haven, CT, and approved March 20, 2015 (received for review January 28, 2015)

Ribosome protection proteins (RPPs) confer resistance to tetracycline by binding to the ribosome and chasing the drug from its binding site. Current models for RPP action are derived from 7.2- to 16-Å resolution structures of RPPs bound to vacant or nontranslating ribosomes. Here we present a cryo-electron microscopy reconstruction of the RPP TetM in complex with a translating ribosome at 3.9-Å resolution. The structure reveals the contacts of TetM with the ribosome, including interaction between the conserved and functionally critical C-terminal extension of TetM with a unique splayed conformation of nucleotides A1492 and A1493 at the decoding center of the small subunit. The resolution enables us to unambiguously model the side chains of the amino acid residues comprising loop III in domain IV of TetM, revealing that the tyrosine residues Y506 and Y507 are not responsible for drug-release as suggested previously but rather for intrafactor contacts that appear to stabilize the conformation of loop III. Instead, Pro509 at the tip of loop III is located directly within the tetracycline binding site where it interacts with nucleotide C1054 of the 16S rRNA, such that RPP action uses Pro509, rather than Y506/Y507, to directly dislodge and release tetracycline from the ribosome.

ribosome | antibiotic | tetracycline | resistance | TetM

The ribosome is one of the major targets for antibiotics within the bacterial cell (1, 2). A well-characterized class of broad-spectrum antibiotics in clinical use are the tetracyclines, which bind to elongating ribosomes and inhibit delivery of the EF-Tu•GTP•aa-tRNA ternary complex to the A-site (1, 3). X-ray crystal structures of ribosomal particles in complex with tetracycline have revealed that the primary drug binding site is located in helix 34 (h34) of the 16S rRNA, overlapping the binding position of the anticodon-stem loop of an A-site tRNA (4–6). The widespread use of tetracyclines has led to an increase in tetracycline resistance among clinically relevant pathogenic bacteria, thus limiting the medical utility of many members of this class (7). Drug efflux and ribosome protection are the most common tetracycline resistance mechanisms acquired by bacteria (8) and have led to the development of the third generation of tetracycline derivatives, such as tigecycline, which display enhanced antimicrobial activity and overcome both the efflux and ribosome protection resistance mechanisms (6, 9–11).

To date, there are 12 distinct classes of ribosome protection proteins (RPPs) that confer resistance to tetracycline, with the most prevalent and best characterized being TetO and TetM (3, 8, 12). The different classes of RPPs have high homology with one another; for example, *Campylobacter jejuni* TetO displays >75% identity (>85% similarity) with *Enterococcus faecalis* TetM. Based on the presence of conserved nucleotide binding motifs, RPPs are grouped together within the translation factor superfamily of GTPases (13). Accordingly, TetO and TetM catalyze the release of tetracycline from the ribosome in a GTP-dependent manner (14, 15). Biochemical studies indicate that, although GTPase activity is necessary for multiturnover of RPPs, GTP hydrolysis is not strictly required to dislodge tetracycline

because the drug is also released when nonhydrolysable GTP analogs are used (14, 15).

Nonhydrolysable GTP analogs have been used to trap RPPs on the ribosome for structural analysis by cryo-EM. The first structure of an RPP-ribosome complex was a cryo-EM reconstruction of a TetO•70S complex at 16-Å resolution. This structure revealed that TetO binds analogously to the ribosome as translation elongation factor EF-G (16), consistent with the significant homology (~25/35% identity/similarity) between RPPs and EF-G (17). Because the electron density for TetO did not come within 6 Å of the tetracycline-binding site (16), TetO was suggested to chase the drug from the ribosome by inducing conformational changes within h34 (12, 16, 18). In contrast, two subsequent structures at higher resolution, a TetM•70S complex at 7.2 Å (19) and a TetO•70S complex at 9.6 Å (20), revealed electron density for the RPPs directly overlapping with the tetracycline binding site. Based on the homology with EF-G, molecular models for the RPPs were generated and docked into the cryo-EM maps, suggesting that residues within loop III of domain IV of TetM/TetO come into direct contact with the tetracycline molecule (19, 20). Consistently, mutagenesis studies identified specific residues within loop III that are critical for RPP activity (19–21), in particular the conserved tyrosine residues Y506 and Y507 (19, 20). However, the exact role of these tyrosine residues and a detailed molecular understanding of the mechanism by which RPPs dislodge tetracycline from its binding site was not possible at the reported resolutions.

Here we present a cryo-EM structure of TetM in complex with a translating ribosome at an average resolution of 3.9 Å. Local

Significance

The ribosome, the protein-synthesizing machine in the cell, is a major target for antibiotics, such as tetracyclines. The widespread usage of tetracyclines has led to an increase in tetracycline resistance amongst medically relevant pathogenic bacteria, limiting their utility. Many bacteria obtain tetracycline resistance via ribosome protection proteins, such as TetM and TetO, that bind to the ribosome and chase tetracycline from its binding site. We have determined a structure of TetM bound to a translating ribosome at 3.9 Å, providing molecular insight into how TetM interacts with the ribosome to dislodge the drug from its binding site.

Author contributions: S.A., F.N., and D.N.W. designed research; S.A. and F.N. performed research; S.A., F.N., R.B., and D.N.W. analyzed data; and S.A. and D.N.W. wrote the paper.

The authors declare no conflict of interest.

This article is a PNAS Direct Submission.

Freely available online through the PNAS open access option.

Data deposition: The atomic coordinates have been deposited in the Protein Data Bank (PDB), www.pdb.org (PDB ID code 3J9Y), and the cryo-EM map has been deposited in the Electron Microscopy Data Bank (EMDB), www.emdatabank.org (EMDB ID code EMD-6311).

¹To whom correspondence should be addressed. Email: wilson@genzentrum.lmu.de.

This article contains supporting information online at www.pnas.org/lookup/suppl/doi:10.1073/pnas.1501775112/-DCSupplemental.

resolution calculations indicate that the majority of the core of the ribosome and domain IV of TetM extends toward 3.5 Å, enabling bulky side chains to be modeled. We provide a detailed account of the interactions between TetM and the ribosome, in particular revealing a complex network of interactions of the C-terminal helix and domain IV of TetM with the ribosomal decoding site and intersubunit bridge B2a. The structure reveals that Pro509 at the tip of loop III, rather than the previously identified tyrosine Y506 and Y507, overlaps the binding site of tetracycline and is therefore directly involved in releasing tetracycline from the ribosome.

Results and Discussion

Cryo-EM Structure and Molecular Model of a TetM•RNC. In our previous study (19), the TetM•70S complex was formed using vacant 70S ribosomes, which led to high heterogeneity because the vacant ribosomes adopted both rotated and nonrotated states. Moreover, because TetM only interacts with the nonrotated ribosomes, the heterogeneity reduced the overall occupancy of TetM on the ribosome. A further reduction in occupancy resulted from the presence of tigecycline, the binding of which (contrary to initial expectations; refs. 16 and 19) was mutually exclusive with TetM binding (19). As a result, the final reconstruction of the TetM•70S complex was derived from only 52,701 (12%) of the initial 406,687 particles and yielded a resolution of 7.2 Å (19). To reduce sample heterogeneity and increase the TetM occupancy, we omitted tigecycline and formed a complex between TetM and a translating, rather than vacant, 70S ribosome. We have previously prepared and determined cryo-EM structures of 70S ribosomes stalled during translation of Erm leader peptides by the presence of the macrolide antibiotic erythromycin (22–24). These studies revealed that the ErmCL-stalled ribosome is an ideal substrate for TetM binding because the ribosome adopts a nonrotated conformation with a peptidyl-tRNA in the P-site and a vacant A-site (22, 24). Therefore, the ErmCL-stalled ribosomes

were bound with TetM in presence of the nonhydrolysable GTP analog, GDCPP, and the resulting sample was subjected to multi-particle cryo-EM (*Materials and Methods*).

Data were collected on a Titan Krios transmission electron microscope, fitted with a Falcon II direct electron detector, and processed with the SPIDER software package (25). After removal of nonaligning and edge particles, in silico sorting revealed the presence of two subpopulations of ribosomes bearing peptidyl-tRNA in the P-site, and either a vacant A-site (25%) or an A-site occupied by TetM (75%) (*SI Appendix, Fig. S1A*). The latter volume, which we term the TetM•ribosome nascent chain complex (TetM•RNC), contained 78,186 particles and was refined further to produce a final cryo-EM map of the TetM•RNC (Fig. 1A) with an average resolution of 3.9 Å (based on the Fourier shell correlation cutoff at 0.143, *SI Appendix, Fig. S1B*). Similar to our recent cryo-EM structure of the ErmCL-RNC (22), local resolution calculations indicate that the ribosomal core of the TetM•RNC extends to 3.5 Å (*SI Appendix, Fig. S1C and D*). The resolution of domains I–V of TetM was predominantly between 3.5–4.5 Å (Fig. 1B), but with some regions extending to >5 Å, indicating flexibility as observed recently for other ribosome-bound ligands (26–29). Strand separation in β -sheets and the pitch of helices is observed, allowing a more accurate and complete backbone model to be presented for all 639 residues in domains I–V of TetM (Fig. 1C).

Moreover, the high resolution of the ribosome enabled us to more precisely map the sites of interaction with TetM (Fig. 1D and *SI Appendix, Table S1*) compared with previous reports (16, 19, 20). Overall, the interactions of TetM are similar to those for translation GTPases, such as EF-G (30), such that on the 50S subunit, the G domain of TetM contacts the sarcin-ricin loop (SRL, H95 of the 23S rRNA) and ribosomal protein L6, whereas the G' subdomain interacts with one of the C-terminal domains of L7 (Fig. 1D and E and *SI Appendix, Fig. S2A–F*). Domain V of TetM inserts into the cleft formed by H43/H44 of the

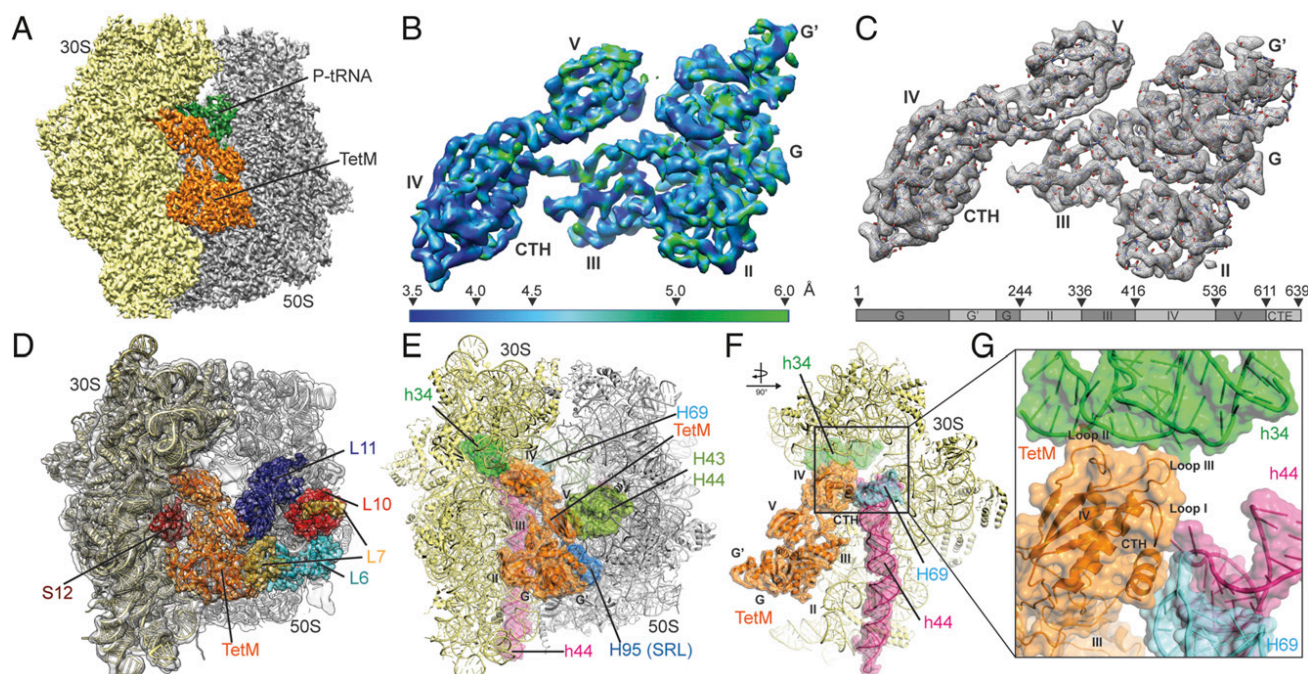


Fig. 1. Cryo-EM reconstruction of TetM•RNC. (A) Cryo-EM density map of the TetM•RNC, with TetM (orange), 30S (yellow), 50S (gray), and P-tRNA (green). (B and C) Extracted cryo-EM density for TetM colored according to local resolution (B) and with fitted polyaniline model into the density (gray mesh) for domains I (G domain), G' subdomain, II, III, IV, V, and C-terminal extension (CTE) (C). (D) Overview of the TetM•RNC showing cryo-EM density with fitted models for 30S (yellow) and 50S (gray) subunits, and TetM (orange). Ribosomal proteins contacting TetM are colored (S12, brown; L6, cyan; L7, yellow; L10, red; L11, violet). (E) Model for the TetM•RNC with rRNA helices that interact with TetM colored (h34, green; h44, pink; H43/H44, dark green; H69, light blue; H95, dark blue). (F) Side-view of E. (G) Side view of E with zoom onto 16S rRNA helices h34 (green) and h44 (pink) and 23S rRNA helix H69 (blue) that directly interact with domain IV and the CTH of TetM (orange).

23 rRNA and L11, overlapping the binding site of thiostrepton (31) (*SI Appendix, Fig. S2 A–F*) and explaining the inhibition of TetM by this antibiotic (32–34). On the small subunit, domain III of TetM contacts ribosomal protein S12 (Fig. 1 *D* and *E*), whereas domain IV of TetM wedges between the head and body of the 30S, reaching into the decoding center where contacts with h34 (head) and h44 (body) of the 16S rRNA are observed, as well as between the C-terminal extension of TetM and H69 of the 23S rRNA (Fig. 1 *F* and *G*).

Interaction of Domain IV of TetM with the 30S Subunit. Domain IV of TetM comprises a four-stranded β -sheet and two α -helices, with an overall $\beta\beta\alpha\beta\alpha$ topology. Three loops (termed Loop I, II, and III) protrude from the distal end of domain IV of TetM (Fig. 2*A*). The proline-rich loop I, located between β_2 and β_3 , was modeled differently in the recent TetM- and TetO-bound ribosome structures (3, 19, 20). In our structure, loop I adopts a bent conformation to establish interactions with the C-terminal helix α_{CTE} of TetM (Fig. 2*A*), similar to that predicted previously for TetM (19), but quite unlike the extended conformation suggested for TetO (20) (*SI Appendix, Fig. S3 A–D*). We believe that a bent conformation of loop I of TetO would be more consistent with the electron density for the TetO•70S complex as well as with the high sequence conservation between TetO and TetM (*SI Appendix, Fig. S3 A–F*). Moreover, the extended conformation modeled for the TetO•70S structure is incompatible with the presence of mRNA (*SI Appendix, Fig. S3A*), suggesting that loop I is unlikely to form part of a corridor that tetracycline navigates during its release from the ribosome (20).

The density for Loop II between β_4 and α_4 is poorly ordered, however interaction with helix 34 of the 16S rRNA is apparent, with residues Ser465 and Leu466 of TetM coming into close proximity with the backbone of C1209 and the nucleobase of C1214 (Fig. 2*B*). This finding is in agreement with the protection of C1214 from DMS modification upon TetO binding to the ribosome (18, 32). With the exception of Gly467, the residues of loop II are not highly conserved and mutagenesis of these residues exhibited only moderate effects on TetM activity (*SI Appendix, Fig. S3 G and H*). We note, however, that shortening of the loop by removal of two amino acids was previously shown to completely inactivate TetO (20).

Interaction of TetM at the Ribosomal Decoding Site. The C-terminal extension (CTE) of TetM comprises a short 11-aa α -helix (residues 627–637) connected to domain V by a flexible linker (Fig. 2*C*), consistent with previous reports (19). Sequence alignments, secondary structure predictions, as well as the electron density for the TetO•70S complex (*SI Appendix, Fig. S4 A–F*) lead us to suggest that the topology of the CTE observed here for TetM is a conserved feature of all RPPs. The C-terminal helix (CTH) is likely to stabilize domain IV of TetM on the ribosome, as we observe contact between the CTH and A1913 located at the tip of H69 of the 23S rRNA (Fig. 2*C*). A1913 adopts a very defined position, similar to that observed when A-tRNA or A/T-tRNA (in complex with EF-Tu) is bound to the ribosome (35, 36) (Fig. 2*D* and *SI Appendix, Fig. S4 G and H*), but distinct from the conformation observed in the absence of A-tRNA where A1913 inserts into h44 of the 16S rRNA (6) (Fig. 2*D*). Although nucleotides A1492 and A1493 of h44 exhibit some flexibility

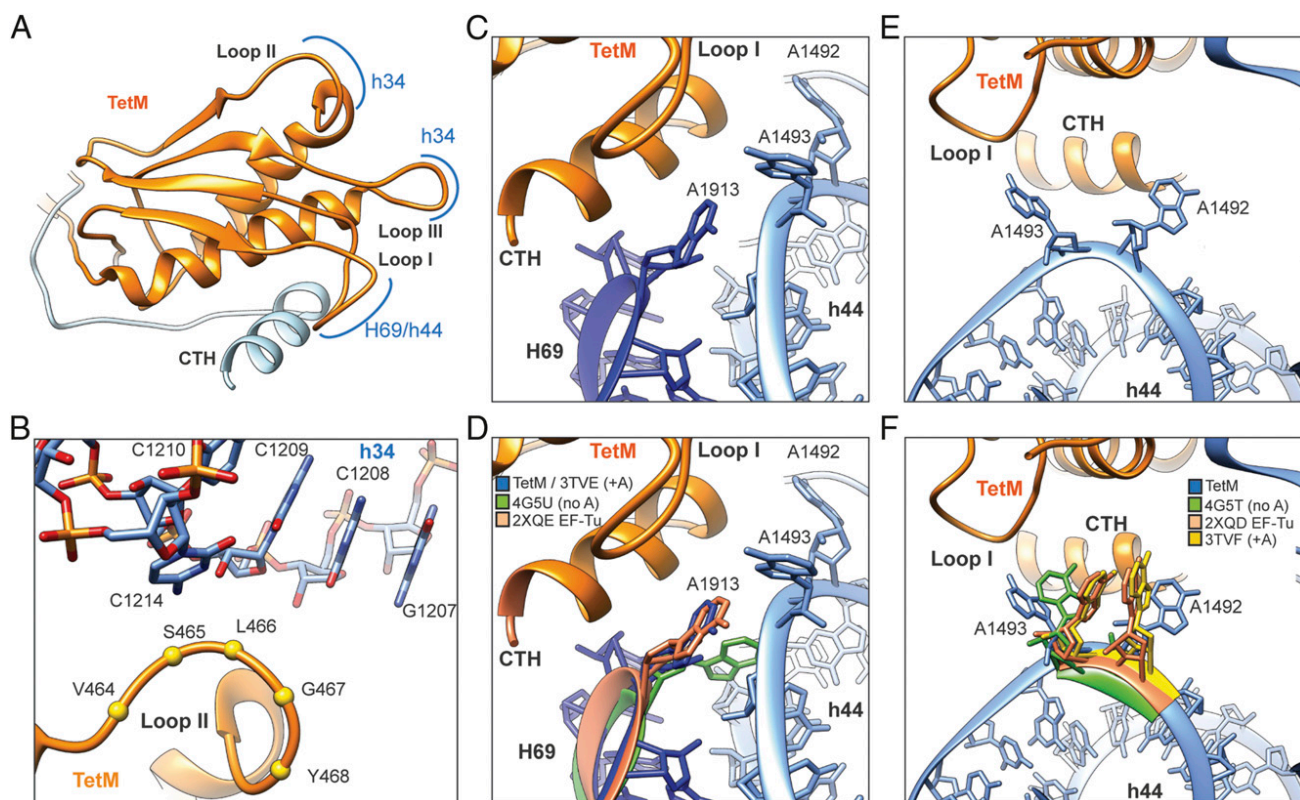


Fig. 2. Interactions of domain IV and the CTH of TetM. (*A*) Overview of domain IV (orange) and the C-terminal extension (cyan) of TetM, indicating interaction of loops I–III with rRNA helices h34, h44 and H69 as well as loop I with the C-terminal helix (CTH) of TetM. (*B*) Proximity of loop II residues ($C\alpha$ atoms shown as yellow spheres) to the nucleotides C1209, C1051 and C1214 of h34 of the 16S rRNA. (*C* and *D*) Interaction of the CTH of TetM (orange) with nucleotide A1913 of H69 of 23S rRNA (deep blue). In *D*, the positions of A1913 with ribosome lacking A-tRNA (green, PDB 4G5U; ref. 6) or containing A-tRNA (blue, PDB 3TVE; ref. 36) or A/T-tRNA (pink, PDB 2XQE; ref. 35) are shown. (*E* and *F*) Flipped-out conformations of nucleotides A1492 and A1493 of h44 of the 16S rRNA (blue) upon TetM (orange) binding to the ribosome. In *F*, the positions of A1492 and A1493 with ribosome lacking A-tRNA (green, PDB 4G5T; ref. 6) or containing A-tRNA (blue, PDB 3TVF; ref. 36) or A/T-tRNA (pink, PDB 2XQD; ref. 35) are shown.

(SI Appendix, Fig. S4 I and J), both nucleotides clearly adopt preferred conformations when TetM is bound, such that both nucleotides are flipped-out of h44 and extend toward Loop I and the CTH, respectively, of TetM (Fig. 2E). The flipping of A1492 and A1493 by TetM binding was suggested previously at 7.2 Å (19) to resemble the conformation observed during decoding of the mRNA-tRNA duplex (35–37) (Fig. 2F). At higher resolution, however, it is evident that the exact conformations of A1492 and A1493 are distinct and the nucleotides adopt an unusual splayed conformation (Fig. 2E and F), which to our knowledge has not been observed before. The most similar conformation for A1493 was observed in the P-tRNA bound ribosome with a vacant A-site (Fig. 2F); however, in this structure, A1492 remains buried within h44. Although the resolution of the previous TetO•70S structures (16, 20) was insufficient to unambiguously assign the conformational state of A1492 and A1493, biochemical studies suggest that binding of TetO to the ribosome also flips A1493 from h44, as indicated by exposure of A1408 of the 16S rRNA to DMS modification (18, 19). Because removal of the CTH by truncation of 17 amino acids inactivates TetM (19), it is likely that the interaction of TetM, and presumably TetO, with A1492 and A1493 is critical for stabilization of the RPP on the ribosome.

Pro509 of Loop III of TetM Directly Encroaches Upon the Tetracycline-Binding Site. Loop III of TetM linking $\beta 5_4$ to helix αB_4 is the best resolved part of the TetM structure with a local resolution predominantly around 3.5 Å, which enabled the bulky aromatic sidechains, such as tyrosines and phenylalanines, to be modeled (Fig. 3A and B). In contrast to the previous TetM/O•70S reconstructions at lower resolution (19, 20), where the density for Loop III was ambiguous (SI Appendix, Fig. S5A and B), we are confident of the register of the amino acids within Loop III of TetM as well as the orientation of the side chains in most cases (Fig. 3A and B and SI Appendix, Fig. S5C). Based on this model, Pro509 at the tip of loop III stacks against C1054 within h34 of the 16S rRNA (Fig. 3C), explaining the protection of C1054 from DMS modification observed upon TetO binding to the ribosome (18). C1054 comprises part of the primary tetracycline-

binding site and establishes stacking interactions with ring D of tetracycline (4–6) (Fig. 3D). Our structure indicates that Pro509 of Loop III of TetM clashes with tetracycline and is therefore directly responsible for dislodging the drug from the ribosome (Fig. 3D). This contrasts with previous suggestions that the two conserved tyrosines, Y506 and Y507, within loop III of TetM are directly involved in tetracycline release (19, 20). It is worth noting that although Pro509 is identical in all available RPP sequences, Y506 and Y507 are substituted with Phe/Val and Ser/Phe/Arg, respectively, in some RPPs (SI Appendix, Fig. S5D). Our structure would also suggest that shortening loop III would remove the overlap with tetracycline, consistent with the lack of activity of TetO mutants where two residues were deleted from loop III (20). Although tigecycline exhibits an even greater overlap with TetM (Fig. 3E), we believe that, in addition to the increased affinity of tigecycline compared with tetracycline (10, 11, 38), the C9-glycyl substituent of tigecycline hinders access of the loop III residues to C1054 and thus contributes to tigecyclines ability to overcome TetM-mediated resistance (6, 11).

Stabilization of Loop III Is Critical for TetM Activity. Given that Ser508 and Pro509 located at the tip of Loop III are invariant in all available RPP sequences (SI Appendix, Fig. S5D), it is somewhat surprising that these and neighboring residues can be mutated to alanine with little or no effect on RPP activity (3, 19). Similarly, the double SP508-509/AA and triple SPV508-510/AAA mutants of TetM were also shown to retain tetracycline resistance activity (19). In silico mutagenesis based on our refined model indicated that if loop III of the triple SPV508-510/AAA mutant adopts the same conformation as the wildtype TetM then the backbone of Ala509 would maintain a steric clash with tetracycline (Fig. 4A), providing a possible explanation for the retention in activity of the mutant. In contrast, mutation of Y506/Y507 completely inactivates TetM/TetO (3, 19, 20), indicating an important role for these tyrosine residues. Indeed, in our structure, both tyrosines are involved in intradomain interactions linking loop III with loops I and II (Fig. 4B). Specifically, Y507 comes within 3.5 Å of E435 within loop I and the side chain OH of Y506 is within hydrogen bonding distance to

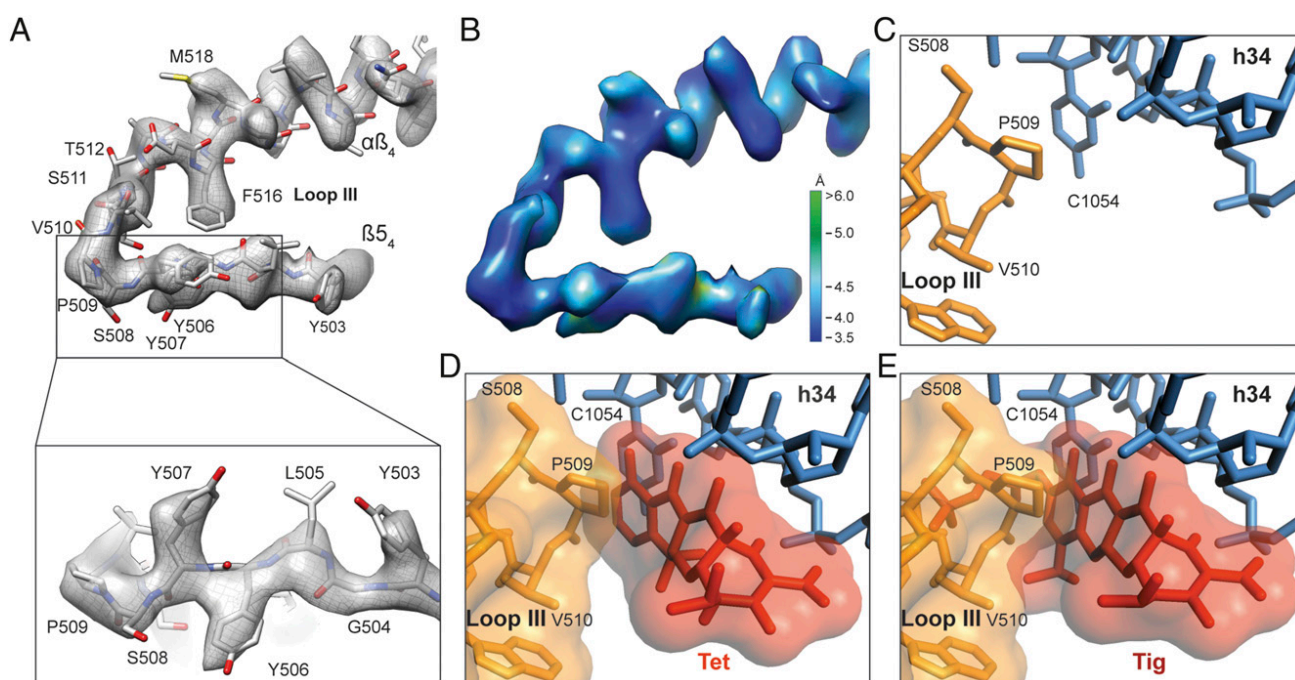


Fig. 3. The role of loop III in TetM in tetracycline resistance. (A and B) Extracted Cryo-EM density of loop III of domain IV in TetM (gray mesh) with molecular model for loop III (A) and colored according to local resolution (B). (C) Stacking interaction of P509 at the tip of loop III (orange) with nucleotide C1054 of h34 of the 16S rRNA (blue). (D and E) Comparison of the binding positions of loop III of TetM domain IV (orange) with (D) tetracycline (Tet) and (E) tigecycline (Tig; ref. 6).

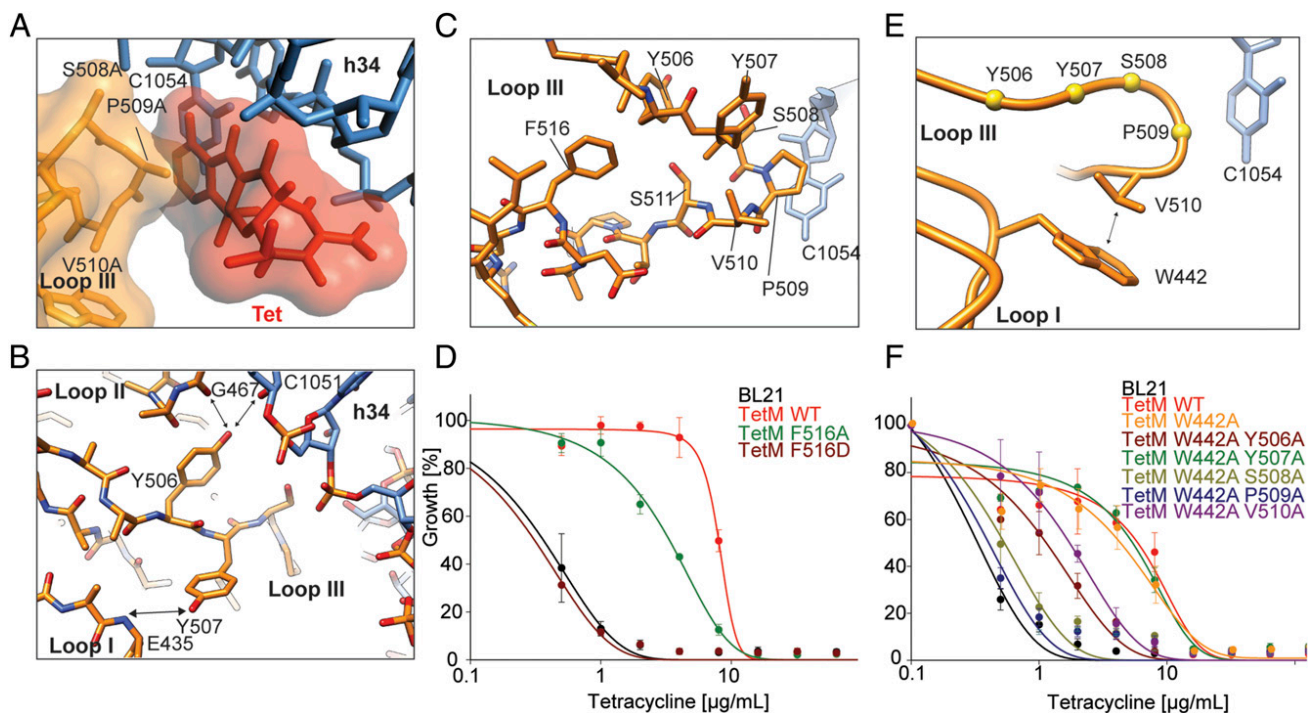


Fig. 4. Stabilization of loop III in TetM via intra-TetM interactions ensures TetM activity. (A) Relative binding position of TetM triple mutant SPV508-510AAA (orange) and tetracycline (Tet, red; ref. 6). (B) Tyrosine residues Y506 and Y507 of loop III of TetM domain IV (orange) stabilize the conformation of loop III via interactions with G467 of loop II, 16S rRNA residue C1051 and residue E435 of loop I, respectively. (C) Localization of TetM residue F516 within the hydrophobic pocket formed by loop III. (D) Growth curves of wildtype *E. coli* strain BL21 (black) in the presence of increasing concentrations of tetracycline (0–128 $\mu\text{g/mL}$) compared with the wildtype strain harboring a plasmid encoding wildtype TetM (red) and TetM single mutants F516A (green) and F516D (brown). (E) Interaction between the sidechain V510 of loop III of TetM with the invariant tryptophan (W442) located in loop I. (F) as in D but with TetM mutant W442A (orange) and the double mutants W442A/Y506A (brown), W442A/Y507A (green), W442A/S508A (olive), W442A/P509A (blue) and W442A/V510A (violet). In D and F, the error bars represent the SD from the mean for three independent experiments.

the carbonyl of G467 in loop II, as well as to the ribose 2' OH of C1051 in h34 of the 16S rRNA (Fig. 4B). Collectively, these results suggest that the role of Y506 and Y507 within loop III is to stabilize the conformation of loop III.

To further investigate the importance of the stabilization of loop III for TetM activity, we analyzed the activity of two additional TetM mutants: The first mutations were introduced at position F516. F516 is invariant in all RPP sequences (SI Appendix, Fig. S5D), and the phenylalanine side chain is well resolved within the hydrophobic core of loop III, where it clamps the proximal end of helix αB_4 to the distal end of strand βS_4 (Figs. 3A and 4C). To monitor activity of TetM, the growth of wild-type *Escherichia coli* strain BL21 (–TetM) in the presence of increasing concentrations of tetracycline (0–128 $\mu\text{g/mL}$) was

compared with the same strain bearing a plasmid overexpressing either *Enterococcus faecalis* TetM (+TetM) or one of the TetM variants (Fig. 4D). In the absence of TetM, the wild-type *Escherichia coli* strain (black circles) is sensitive to tetracycline with a minimal inhibitory concentration (MIC_{50}) of $\sim 0.6 \mu\text{g/mL}$, whereas as before (19), overexpression of *Enterococcus faecalis* TetM (red circles) raises the MIC_{50} by 14-fold to $\sim 10 \mu\text{g/mL}$ (Fig. 4D). Although mutation of F516 to alanine (F516A) had a modest affect on TetM activity ($\text{MIC}_{50} \sim 3 \mu\text{g/mL}$), mutation of F516 to the negatively charged Asp (F516D) led to a complete loss of activity (Fig. 4D), consistent with the importance of F516 for providing a hydrophobic environment to maintain the defined conformation of loop III necessary for tetracycline release. Another possible source of stabilization of Loop III is the

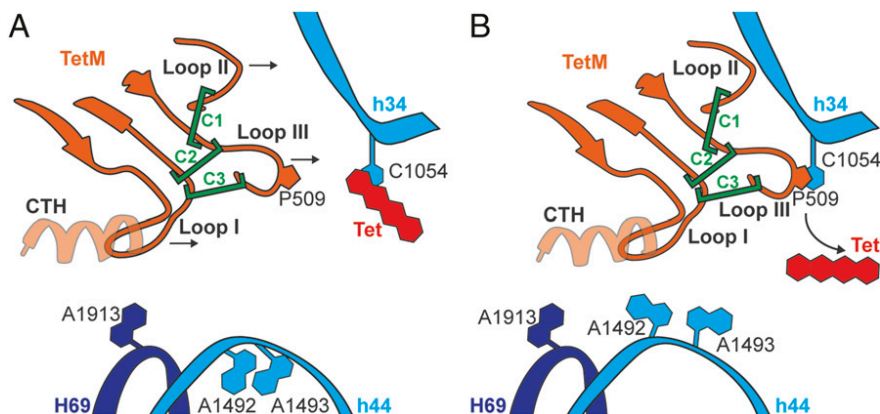


Fig. 5. Schematic model for TetM-mediated tetracycline resistance. (A and B) Upon TetM binding to tetracycline bound ribosomes, the proline residue P509 located at the tip of loop III of domain IV is directly responsible for chasing the drug off the ribosome by interacting with its binding site nucleotide C1054 of the 16S rRNA. (B) TetM binding to the ribosome leads to interaction of the C-terminal helix (CTH) with 23S rRNA nucleotide A1913 (dark blue) and induces 16S rRNA decoding nucleotides A1492 and A1493 (blue) to flip out of helix 44 (h44) of the 16S rRNA. Intramolecular interactions that stabilize the conformation of loop III are represented as green clamps with C1 illustrating the interaction Y506/G467, C2 for Y507/E435 and C3 for V510/W442.

interaction between the side chain of V510 and an invariant tryptophan (W442) located within loop I (Fig. 4E). Although mutation of W442 to alanine (W442A) alone did not affect the activity of TetM, the presence of the W442A mutation made loop III sensitive to secondary mutations. In particular, mutations of S508 or P509 to alanine in the context of W442A abolished TetM activity (Fig. 4F), whereas wild-type activity was observed for TetM with single S508A or P509A mutations (19). Collectively, these results illustrate the importance of the structural integrity of loop III in the positioning residues S508 and P509 located at the tip of loop III, which is necessary for efficient tetracycline resistance.

Conclusion

In conclusion, our structure enables a molecular model to be presented for how TetM confers resistance to tetracycline by dislodging the drug from its binding site on the ribosome (Fig. 5A and B): Specifically, Pro509 within loop III of domain IV of TetM directly overlaps in position with ring D of tetracycline and thus dislodges the drug from the ribosome. TetM is proposed to prevent rebinding of tetracycline by altering the conformation of nucleotides such as C1054 within the drug binding site that persist following TetM dissociation (12, 18, 19, 32). Within the constraints of the current resolution, TetM does not appear to alter the conformation of C1054 to prevent drug rebinding (*SI Appendix, Fig. S5E*), however, we cannot rule out that such an alteration occurs during GTP hydrolysis and dissociation of TetM from the ribosome. Previous studies identified two conserved tyrosines within loop III of TetM as being important for tetracycline resistance (3, 19, 20). Here we show that these tyrosine residues are not directly involved in displacing the drug

from its binding site, but rather act like clamps (termed C1 and C2) that stabilize the loop III of domain IV of TetM by establishing intradomain interactions with loop I and II of TetM (Fig. 5A). We also identify an additional clamp C3 between loop I and III that is important for stabilization of loop III. Additionally, domain IV of TetM is positioned on the ribosome for tetracycline displacement via interaction of loop I and the CTH with residues located within intersubunit bridge B2a, namely, A1913 of H69 of the 23S rRNA and a splayed conformation of decoding site nucleotides A1492 and A1493 (Fig. 5B). We believe that the molecular details and mechanism of action reported here for TetM will be conserved for other ribosome protection proteins, such as TetO, that also confer resistance to tetracycline.

Materials and Methods

Enterococcus faecalis TetM was purified as described (34) and bound to ErmCL-RNC (22). Cryo-EM data were collected using the EPU software on a Titan Krios TEM (FEI) and processed using the SPIDER software package (25). The backbone model of *Enterococcus faecalis* TetM was initially generated using HHPred (39), then manually fitted using Chimera (40) and refined using Coot (41) and PHENIX (42). A structure of the *Escherichia coli* 70S ribosome (43) was fitted the cryo-EM density using Chimera (40), manually adjusted and then refined with Coot (41). Site-specific mutations were introduced into the *tetM* gene using KOD Xtreme Hot Start Polymerase according to the manufacturers instructions and minimal inhibitory concentrations were determined as described (11, 19). Detailed materials and methods can be found in the *SI Appendix, SI Materials and Methods*.

ACKNOWLEDGMENTS. We thank Rishi Matadeen and Sacha DeCarlo for data collection at the NeCEN facility (Leiden, Netherlands) and Dr. A. L. Starosta for helpful comments. This work was supported by the Deutsche Forschungsgemeinschaft GRK1721 and FOR1805 (WI3285/3-1, to D.N.W.).

- Wilson DN (2009) The A-Z of bacterial translation inhibitors. *Crit Rev Biochem Mol Biol* 44(6):393–433.
- Wilson DN (2014) Ribosome-targeting antibiotics and mechanisms of bacterial resistance. *Nat Rev Microbiol* 12(1):35–48.
- Nguyen F, et al. (2014) Tetracycline antibiotics and resistance mechanisms. *Biol Chem* 395(5):559–575.
- Brodersen DE, et al. (2000) The structural basis for the action of the antibiotics tetracycline, pactamycin, and hygromycin B on the 30S ribosomal subunit. *Cell* 103(7):1143–1154.
- Pioletti M, et al. (2001) Crystal structures of complexes of the small ribosomal subunit with tetracycline, edeine and IF3. *EMBO J* 20(8):1829–1839.
- Jenner L, et al. (2013) Structural basis for potent inhibitory activity of the antibiotic tigecycline during protein synthesis. *Proc Natl Acad Sci USA* 110(10):3812–3816.
- Roberts MC (2005) Update on acquired tetracycline resistance genes. *FEMS Microbiol Lett* 245(2):195–203.
- Chopra I, Roberts M (2001) Tetracycline antibiotics: Mode of action, applications, molecular biology, and epidemiology of bacterial resistance. *Microbiol Mol Biol Rev* 65(2):232–260.
- Chopra I (2002) New developments in tetracycline antibiotics: Glycylcyclines and tetracycline efflux pump inhibitors. *Drug Resist Updat* 5(3–4):119–125.
- Bergeron J, et al. (1996) Glycylcyclines bind to the high-affinity tetracycline ribosomal binding site and evade Tet(M)- and Tet(O)-mediated ribosomal protection. *Antimicrob Agents Chemother* 40(9):2226–2228.
- Grossman TH, et al. (2012) Target- and resistance-based mechanistic studies with TP-434, a novel fluorocycline antibiotic. *Antimicrob Agents Chemother* 56(5):2559–2564.
- Connell SR, Tracz DM, Nierhaus KH, Taylor DE (2003) Ribosomal protection proteins and their mechanism of tetracycline resistance. *Antimicrob Agents Chemother* 47(12):3675–3681.
- Leipe DD, Wolf YI, Koonin EV, Aravind L (2002) Classification and evolution of P-loop GTPases and related ATPases. *J Mol Biol* 317(1):41–72.
- Burdett V (1996) Tet(M)-promoted release of tetracycline from ribosomes is GTP dependent. *J Bacteriol* 178(11):3246–3251.
- Trieber CA, Burkhardt N, Nierhaus KH, Taylor DE (1998) Ribosomal protection from tetracycline mediated by Tet(O): Tet(O) interaction with ribosomes is GTP-dependent. *Biol Chem* 379(7):847–855.
- Spahn CM, et al. (2001) Localization of the ribosomal protection protein Tet(O) on the ribosome and the mechanism of tetracycline resistance. *Mol Cell* 7(5):1037–1045.
- Burdett V (1991) Purification and characterization of Tet(M), a protein that renders ribosomes resistant to tetracycline. *J Biol Chem* 266(5):2872–2877.
- Connell SR, et al. (2002) The tetracycline resistance protein Tet(o) perturbs the conformation of the ribosomal decoding centre. *Mol Microbiol* 45(6):1463–1472.
- Dönhöfer A, et al. (2012) Structural basis for TetM-mediated tetracycline resistance. *Proc Natl Acad Sci USA* 109(42):16900–16905.
- Li W, et al. (2013) Mechanism of tetracycline resistance by ribosomal protection protein Tet(O). *Nat Commun* 4:1477.
- Thakor NS, et al. (2008) Chimeras of bacterial translation factors Tet(O) and EF-G. *FEBS Lett* 582(9):1386–1390.
- Arenz S, et al. (2014) Drug sensing by the ribosome induces translational arrest via active site perturbation. *Mol Cell* 56(3):446–452.
- Arenz S, et al. (2014) Molecular basis for erythromycin-dependent ribosome stalling during translation of the ErmBL leader peptide. *Nat Commun* 5:3501.
- Byrgazov K, et al. (2015) Structural basis for the interaction of protein S1 with the *Escherichia coli* ribosome. *Nucleic Acids Res* 43(1):661–673.
- Frank J, et al. (1996) SPIDER and WEB: Processing and visualization of images in 3D electron microscopy and related fields. *J Struct Biol* 116(1):190–199.
- Fernández IS, Bai XC, Murshudov G, Scheres SH, Ramakrishnan V (2014) Initiation of translation by cricket paralysis virus IRES requires its translocation in the ribosome. *Cell* 157(4):823–831.
- Hussain T, et al. (2014) Structural changes enable start codon recognition by the eukaryotic translation initiation complex. *Cell* 159(3):597–607.
- Voorhees RM, Fernández IS, Scheres SH, Hegde RS (2014) Structure of the mammalian ribosome-Sec61 complex to 3.4 Å resolution. *Cell* 157(7):1632–1643.
- Shao S, Brown A, Santhanam B, Hegde RS (2015) Structure and assembly pathway of the ribosome quality control complex. *Mol Cell* 57(3):433–444.
- Gao YG, et al. (2009) The structure of the ribosome with elongation factor G trapped in the posttranslational state. *Science* 326(5953):694–699.
- Harms JM, et al. (2008) Translational regulation via L11: Molecular switches on the ribosome turned on and off by thiostrepton and micrococin. *Mol Cell* 30(1):26–38.
- Connell SR, et al. (2003) Mechanism of Tet(O)-mediated tetracycline resistance. *EMBO J* 22(4):945–953.
- Starosta AL, et al. (2009) Identification of distinct thiopeptide-antibiotic precursor lead compounds using translation machinery assays. *Chem Biol* 16(10):1087–1096.
- Mikolajka A, et al. (2011) Differential effects of thiopeptide and orthostomycin antibiotics on translational GTPases. *Chem Biol* 18(5):589–600.
- Voorhees RM, Schmeing TM, Kelley AC, Ramakrishnan V (2010) The mechanism for activation of GTP hydrolysis on the ribosome. *Science* 330(6005):835–838.
- Demeshkina N, Jenner L, Westhof E, Yusupov M, Yusupova G (2012) A new understanding of the decoding principle on the ribosome. *Nature* 484(7393):256–259.
- Ogle JM, Carter AP, Ramakrishnan V (2003) Insights into the decoding mechanism from recent ribosome structures. *Trends Biochem Sci* 28(5):259–266.
- Olson MW, et al. (2006) Functional, biophysical, and structural bases for antibacterial activity of tigecycline. *Antimicrob Agents Chemother* 50(6):2156–2166.
- Soding J, Biegert A, Lupas AN (2005) The HHPred interactive server for protein homology detection and structure prediction. *Nucleic Acids Res* 33(Web server issue):W244–W248.
- Pettersen EF, et al. (2004) UCSF Chimera—a visualization system for exploratory research and analysis. *J Comput Chem* 25(13):1605–1612.
- Emsley P, Cowtan K (2004) Coot: Model-building tools for molecular graphics. *Acta Crystallogr D Biol Crystallogr* 60(Pt 12 Pt 1):2126–2132.
- Adams PD, et al. (2010) PHENIX: A comprehensive Python-based system for macromolecular structure solution. *Acta Crystallogr D Biol Crystallogr* 66(Pt 2):213–221.
- Fischer N, et al. (2015) Structure of the *E. coli* ribosome-EF-Tu complex at <3 Å resolution by C-corrected cryo-EM. *Nature*, 10.1038/nature14275.

Supporting Information

Arenz et al

SI Materials and Methods

Purification of TetM protein

Enterococcus faecalis TetM from TnFO1 (Q47810) was cloned into pET-46 Ek/LIC (Novagene) with an N-terminal 6x histidine tag. The plasmid was transformed into *E. coli* BL21(DE3) (Novagene) and incubated at 37°C/120 rpm overnight in 20 mL LB medium containing 100 µg/mL ampicillin. A volume of 20 mL overnight culture was used to inoculate 1.6 L of LB medium containing 100 µg/mL ampicillin. The culture was grown at 37°C/120 rpm to an OD₆₀₀ of 0.3. The temperature was then reduced to 30°C and 16 mL of ethanol was added until the OD₆₀₀ value reached 0.6. Expression of TetM was induced by adding 1.6 ml of 1mM IPTG. After 2hrs, cells were harvested by centrifugation at 3000 x g for 15 min at 4°C and subsequently resuspended in 25 mL Lysis buffer (50 mM NaH₂PO₄, 300 mM NaCl, 5 mM Imidazole, pH 8.0). Cells were lysed using the M-110L Microfluidizer (Microfluidics) and the lysate cleared by centrifugation at 17000 x g for 15 min at 4°C. The cleared lysate was then incubated at 4°C for 1h with 1 mL Ni-NTA agarose beads (Machery-Nagel) and loaded onto a 20 mL Econopac Chromatography column (Biorad). Beads were washed twice with 5 mL Wash buffer (50 mM NaH₂PO₄, 300 mM NaCl, 10 mM Imidazole, pH 8.0) and eluted in 2 mL Elution buffer (50 mM NaH₂PO₄, 300 mM NaCl, 250 mM Imidazole, pH 8.0). The eluate was further purified by gel filtration using a Superdex™ 75 pg column (Amersham) and GF buffer (50 mM Hepes, 100 mM KCl, 200 mM NaCl, 10 mM MgCl₂, 5 mM β-Mercaptoethanol, 10% Glycerol).

Site directed mutagenesis

Site directed mutagenesis was performed using the whole plasmid PCR method. Primers are attached in **Supplementary Table 2**. *E. faecalis tetM* on pET-46 Ek/LIC (Novagene) was used as a template. Double mutants W442A + loop III were produced using loop III mutants as templates (1). KOD Xtreme™ Hot Start Polymerase (Novagene) was used in the following PCR program: 94°C 2 min; 20x (98°C 10sec, 63°C 30sec, 68°C 7min); 68°C 7min.

Generation and purification of ErmCL-SRC

ErmCL-SRC was generated following the same procedure as previously described (2). The 2*XermCL* construct contained a T7 promoter followed by a strong ribosome binding site (RBS) spaced by 7 nucleotides (nts) to the ATG start codon of the first *ermCL* cistron. A linker of 22

nts separated the stop codon of the first *ermCL* cistron and the start codon of the second *ermCL* cistron. The linker also comprised the strong RBS 7 nts upstream of the ATG start codon of the second *ermCL* cistron, enabling initiation of translation independent from the first *ermCL* cistron. Each *ermCL* cistron encoded amino acids 1-19 corresponding to ErmCL leader peptide (Genbank accession number V01278) present on macrolide resistance plasmid pE194 (3, 4). *In vitro* translation of the *2xermCL* construct was performed using the Rapid Translation System RTS 100 *E. coli* HY Kit (Roche) and was carried-out in the presence of 10 μ M erythromycin (ERY) for 1h at 30 °C. The ErmCL-SRC was purified from the disome fractions on sucrose gradients and concentrated using Amicon Ultra-0.5 mL Centrifugal Filters (Millipore). Monosomes of the ErmCL-SRC were obtained by annealing a short DNA oligonucleotide (5'-ttctctctataaaaact-3', Metabion) to the linker between the *ermCL* cistrons of the disomes, generating a DNA-RNA hybrid that was cleaved by RNase H (NEB) treatment in buffer A at 25°C for 1h. The ErmCL-SRC monosomes were then purified and concentrated using the Amicon Ultra-0.5 mL Centrifugal Filters (Millipore).

Generation of TetM•RNCs

The ErmCL-SRC (0.5 μ M) was incubated with a 4-fold excess (2 μ M) of purified recombinant TetM protein in the presence of 500 μ M GDPCP in buffer A (50 mM HEPES-KOH, pH7.4, 100 mM KOAc, 25 mM Mg(OAc)₂, 6 mM β -mercaptoethanol, 100 μ M evernimicin and 10 μ M erythromycin) for 30 min at 30°C. Thereafter, the binding reaction was diluted using buffer A to yield a final ribosome concentration of 4 A₂₆₀/ml for cryo-grid preparation.

Cryo-electron microscopy and single particle reconstruction

The TetM•RNC (4 A₂₆₀/ml) was applied to 2 nm pre-coated Quantifoil R3/3 holey carbon supported grids and vitrified using a Vitrobot Mark IV (FEI Company). Data collection was performed using the EPU software at NeCEN (Leiden, Netherlands) on a Titan Krios transmission electron microscope (TEM) (FEI, Holland) equipped with a Falcon II direct electron detector at 300 kV with a magnification of 125,085x, a pixelsize of 1.108 Å and a defocus range of 0.9-2.2 μ m. The data were provided as a series of seven frames (dose per frame is 4 e⁻/Å²) from which we summed frames 1-6 (accumulated dose of 24 e⁻/Å²) after alignment using Motion Correction software (5). Images were processed using a frequency-limited refinement protocol that helps prevent over-fitting (6), specifically by truncation of high frequencies (in this case at 7-8 Å using a Butterworth filter). Power spectra and defocus values were determined using the SPIDER TF ED command and recorded images were manually inspected for good areas and power-spectra quality. Data were processed further using the

SPIDER software package (7), in combination with an automated workflow as described previously (8). After initial, automated particle selection based on the program SIGNATURE (9), initial alignment was performed with 127,205 particles, using *E. coli* 70S ribosome as a reference structure (2). After removal of noisy particles (22,207 particles), the dataset could be sorted into two main subpopulations using an incremental K-means-like method of unsupervised 3D sorting (10): The first subpopulation (26,814 particles; 25%) was defined by the presence of stoichiometric density for P-site tRNA. The second, major subpopulation (78,186 particles; 75%) was defined by the presence of stoichiometric densities for P-tRNA and TetM (**SI Appendix, Figure S1A**), and could be refined further to produce a map with an average resolution of 3.9 Å (0.143 FSC, **SI Appendix, Figure S1B**). The final refined map was subjected to the program EMBFACTOR (11) in order to apply an automatically determined negative B-factor for sharpening of the map. Local resolution calculations were performed using Resmap (12) revealing that the resolution of the majority of the core of the 30S and 50S subunits extended to 3.5 Å (**SI Appendix, Figure S1C**).

Molecular modelling and map-docking procedures

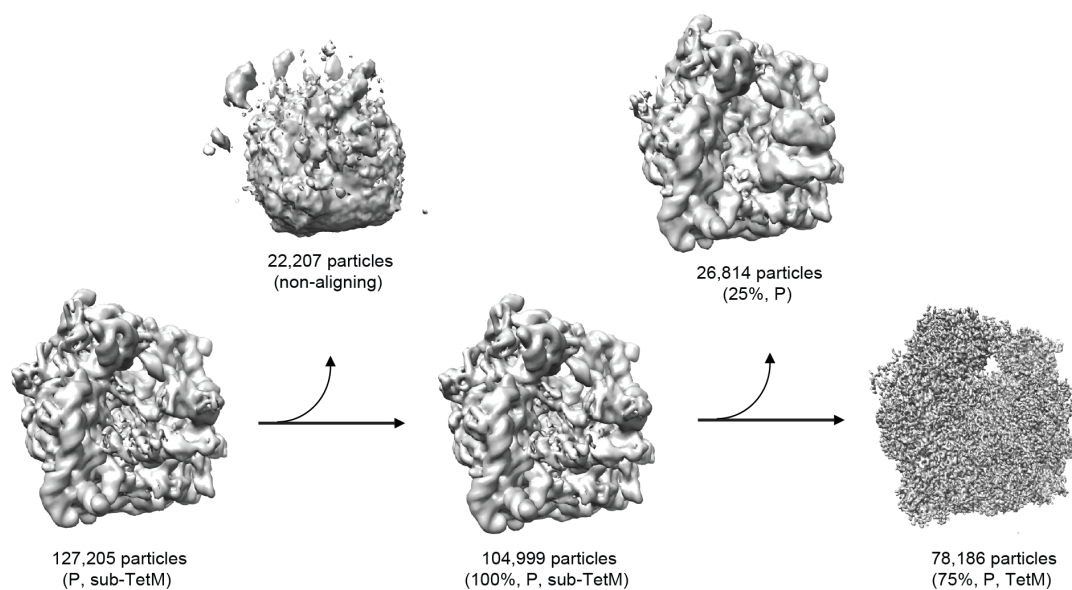
The initial molecular model for the 70S ribosome of the TetM•RNC was based on the cryo-EM structure of an *E. coli* 70S ribosome (PDB ID 5AFI, (13)). The 30S and 50S subunits were fitted as rigid bodies and were manually adjusted and refined in Coot (14). The model for the C-terminal domain of L7 was based on a rigid body fit of the NMR structure of L7/L12 (1RQU, (15)). The molecular model for TetM was initially based on a homology model using EF-G as a template (generated by HHPred (16) and Modeller (17)). The model was split into five domains, which were individually fitted into the EM density as rigid bodies and then manually adjusted and refined using Coot (14) and PHENIX (18). Since the resolution of domains I-III and V of TetM was insufficient to model the amino acid side chains, only a backbone trace was generated. Domain IV of TetM was resolved up to 3.5 Å allowing the bulky amino acid side-chains in loop III to be modelled.

Figure preparation

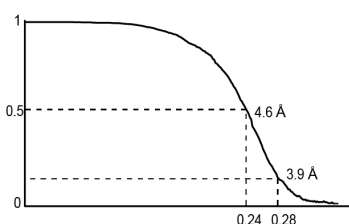
Figures showing electron densities and atomic models were generated using UCSF Chimera (19) and PyMOL Molecular Graphics System (Version 1.5.0.4 Schrödinger, LLC).

Supplementary Figures

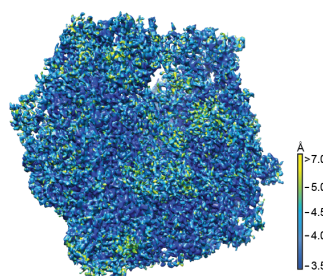
A



B



C



D

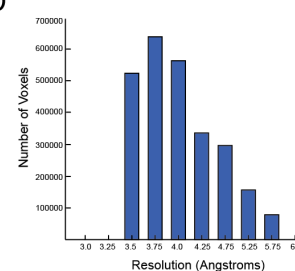


Figure S1 Cryo-EM reconstruction of the TetM•RNC. (A) *In silico* sorting of the TetM•RNC dataset. After removal of non-aligning and edge particles, sorting of the dataset yielded two homogenous sub-datasets. The vast majority of the particles (75%; 78,186 particles in total) contained stoichiometric density for P-tRNA as well as for TetM and this subpopulation was chosen for refinement. (B) Fourier-shell correlation curve of the refined final map, indicating the average resolution of the TetM•RNC is 3.9 Å. (C) Overview of the TetM•RNC colored according to the local resolution as calculated using ResMap (12). (D) Histogram generated by ResMap showing the number of voxels of the cryo-EM map of the TetM•RNC distributed across the resolution bins ranging from 3.5 Å to 6.0 Å.

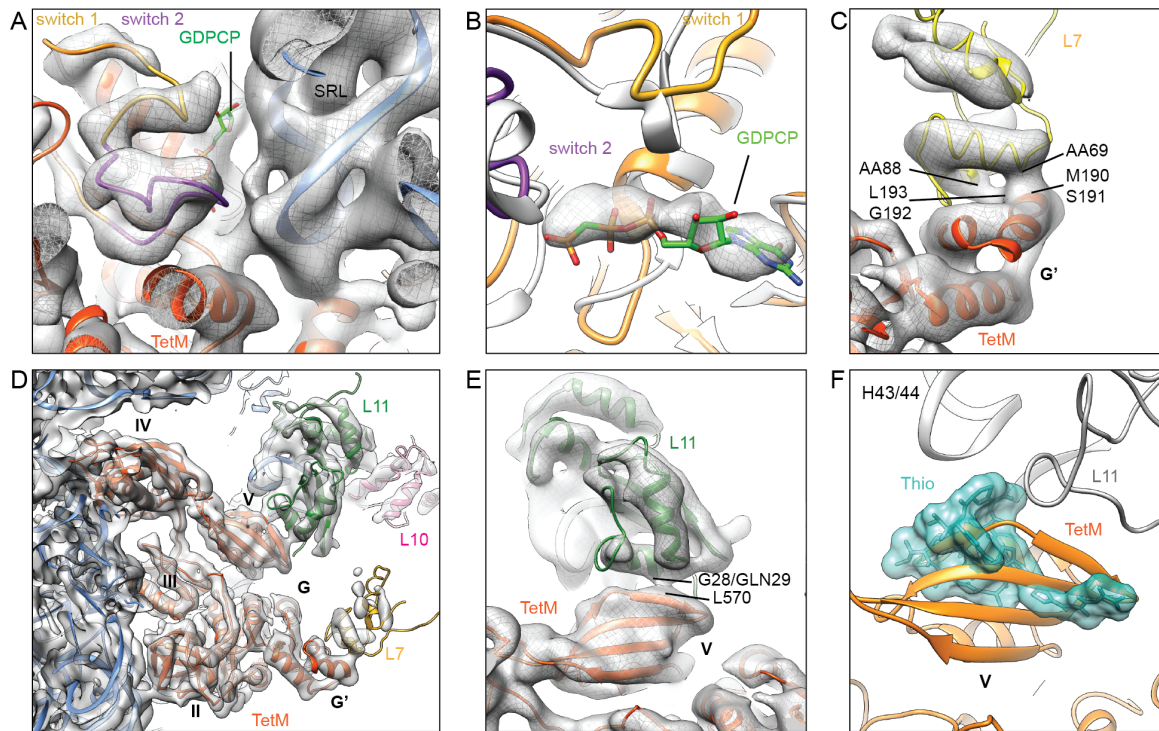


Figure S2 Interaction of TetM with the large ribosomal subunit. (A) Interaction of the G domain of TetM with the sarcin-ricin loop (SRL) of the 23S rRNA (blue). The switch 1 (yellow) and switch 2 (purple) loops are indicated, as is the putative position for the GDPCP molecule (green). (B) Comparison of the conformation of switch 1 and 2 loops of TetM with equivalent region of EF-G (PDB ID 4CR1). Putative density for GDPCP molecule (grey mesh) corresponds with the position of the GDPNP molecule (green) from the EF-G structure (PDB ID 4CR1) aligned to the TetM based on the G domain. (C) Interaction between the C-terminal domain of L7/L12 (yellow) and the G' domain of TetM (orange). (D) Overview of TetM (orange) showing interaction with L7 (yellow) and L11 (green). (E) Interaction between L11 (green) and domain V of TetM (orange). (F) Overlap in the binding site of domain V of TetM (orange) with the antibiotic thioStrepton (cyan). In panels (A) and (C-E), the cryo-EM density for the TetM-RNC is shown as a grey mesh.

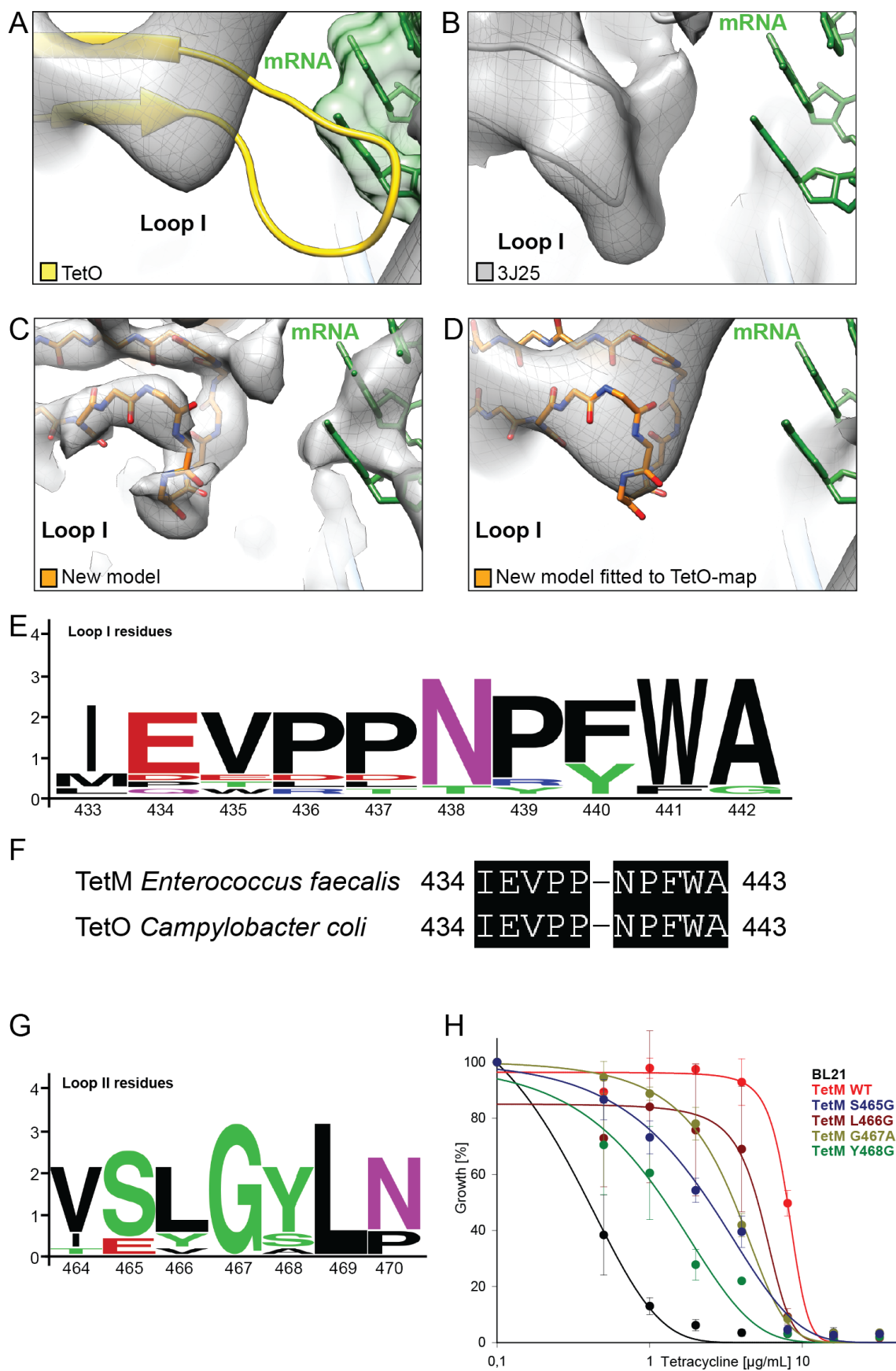


Figure S3 Analysis of loops I and II of domain IV of TetM. (A-D) Cryo-EM map (grey mesh) of (A, D) TetO•70S complex (20), (B) TetM•70S complex (1) and (C) TetM•RNC, with molecular model for loop I of domain IV of (A) TetO (yellow, (20)), (B) TetM (grey, PDB

3J25, (1)) and (C, D) the revised molecular model for loop I of domain IV of TetM based on the cryo-EM map of the TetM•RNC at 3.9 Å resolution (orange). (E) Logo-Plot of residues 433-443 of loop I of domain IV of TetM, numbered according to *Enterococcus faecalis* TetM. (F) Sequence alignment of residues 433-443 of loop I of *Enterococcus faecalis* TetM and *Campylobacter coli* TetO. (G) Logo-plot of residues 464-470 forming loop II of TetM domain IV. (H) Growth curves of wildtype *E. coli* strain BL21 (black) in the presence of increasing concentrations of tetracycline (0-128 µg/ml) compared with the wildtype strain harboring a plasmid encoding wildtype TetM (red) or TetM single mutants S465G (blue), L466G (brown), G467A (olive) and Y468G (green).

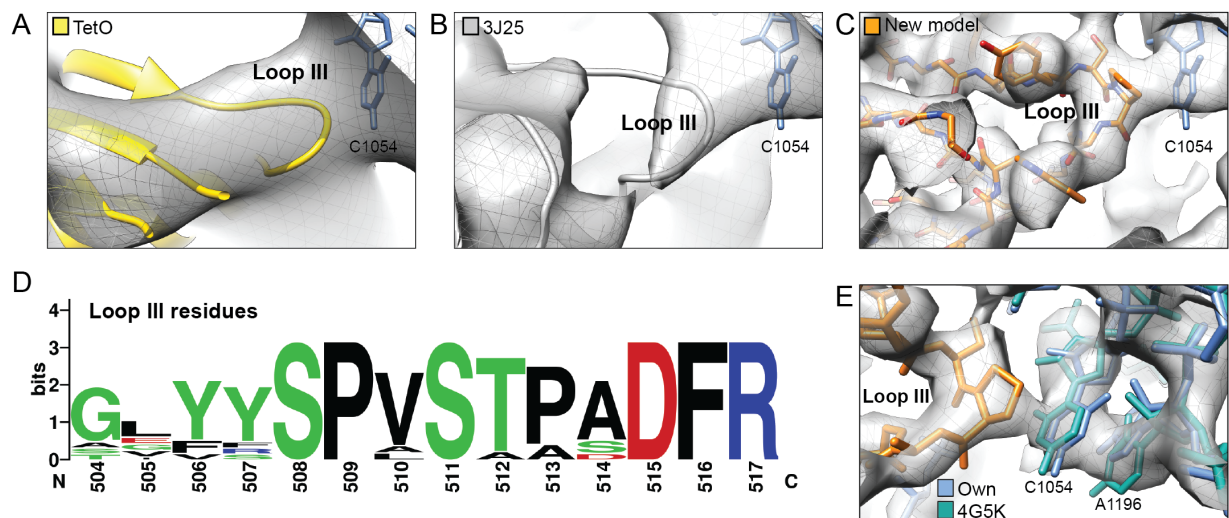


Figure S5 Structures of loop III of domain IV in TetO and TetM. (A-C) Cryo-EM map (grey mesh) of (A) TetO•70S complex (20), (B) TetM•70S complex (1) and (C) TetM•RNC, with molecular model for loop III of domain IV of (A) TetO (yellow, (20)), (B) TetM (grey, PDB 3J25, (1)) and (C) the revised molecular model for loop I of domain IV of TetM based on the cryo-EM map of the TetM•RNC at 3.9 Å resolution (orange). (D) Logo-Plot of residues 504-517 of loop III of domain IV of TetM, numbered according to *Enterococcus faecalis* TetM. (E) Cryo-EM density (grey mesh) the TetM•RNC with molecular models for TetM (orange), and a comparison of the conformation of C1054 of the 16S rRNA from the TetM•RNC (blue) with the tetracycline-bound conformation (cyan, (21)).

Supplementary Table 1

TetM			Ribosome	
Domain	Region	Residue	Region	Residue
G				
	loop between 1 ₁ and A ₁	V12	23S rRNA, H95 (SRL)	G2661
	loop between A ₁ and 2 ₁	G53	23S rRNA, H95 (SRL)	G2663
	loop between 3 ₁ and B ₁	H78	23S rRNA, H95 (SRL)	A2662
	loop between 4 ₁ and C ₁	K102	23S rRNA, H95 (SRL)	A2657
	C1	A107	23S rRNA, H95 (SRL)	G2661
	loop between 5 ₁ and D ₁	Q132	23S rRNA, H95 (SRL)	A2657
	loop between 5 ₁ and D ₁	G134	L6	V91, G92
G'	B _G	M190,S191	L7-CTD, helix α 4	V69
	B _G	G192,L193	L7-CTD, helix α 4	V88
II	3 ₂	R278	16S rRNA, h5 (body)	U368
	5 ₂	T292	16S rRNA, h5 (body)	U358
	6 ₂	L304	16S rRNA, h5 (body)	A55
III	A ₃	D363	S12	H77
IV	loop II between 4 ₄ and A ₄	S465, L466, G467	16S rRNA, h34 (head)	backbone C1214, C1209, C1051
	loop III between 5 ₄ and B ₄	Y506, S508, P509	16S rRNA, h34 (head)	backbone C1051 U1052, C1054
	loop III between 5 ₄ and B ₄	P513	16S rRNA, h18 (body)	C518
	loop III between 5 ₄ and B ₄	R517	16S rRNA, h18 (body)	C519
V	A5	Y555	23S rRNA, H43/H44	A1095
	A5	K560	23S rRNA, H89	U2473
	2 ₅	L570	L11 3 ₁₀ -helix	G28, Q29
	B5	T594, F595	L6	K175, K176
	B5	T594, F595	23S rRNA, H95 (SRL)	A2660
	B5	N598, G599	23S rRNA, H95 (SRL)	A2660
CTE	loop between 4 ₅ and C ₅	R627	S12	L49
	C ₅	R632	23S rRNA, H69	C1913
	C ₅	F635, N636	23S rRNA, H69	C1914

Supplementary Table 2

Construct	Primer sense/ antisense (5' – 3')
TetM W442A	5'-GTGCCGCAAATCCTTTCGCGGCTTCCATTGGTTTATCTGTATCACCGCTTC-3' 5'-GATAAACCAATGGAAGCCGCGAAAGGATTTGGCGGCACTTCGATGTGAATG-3'
TetM S465G	5'-CAGTATGAGAGCTCGGTTGGCCTTGGATACTTAAATCAATCATTTC-3' 5'-GATTTAAGTATCCAAGGCCAACCGAGCTCTCATACTGCATTCCAC-3'
TetM L466G	5'-GAGAGCTCGGTTTCTGGCGGATACTTAAATCAATCATTTCAAAATG-3' 5'-GATTGATTTAAGTATCCGCCAGAAACCGAGCTCTCATACTGCATTTC-3'
TetM G467A	5'-GAGCTCGGTTTCTCTTGGCTACTTAAATCAATCATTTCAAAATGCAG-3' 5'-GAAATGATTGATTTAAGTACGCCAAGAGAAACCGAGCTCTCATACTGCATTTC-3'
TetM Y468G	5'-CTCGGTTTCTCTTGGAGGCTTAAATCAATCATTTCAAAATGCAG-3' 5'-GAAATGATTGATTTAAGCCTCCAAGAGAAACCGAGCTCTCATACT-3'
TetM F516A	5'-GTTAGTACCCAGCAGATGGCGGGATGCTTGCTCCTATTGTATTGGAAC-3' 5'-CAATAGGAGCAAGCATCCGCGCATCTGCTGGGGTACTAACAGGGCTATAG-3'
TetM F516D	5'-GTTAGTACCCAGCAGATGATCGGATGCTTGCTCCTATTGTATTGGAAC-3' 5'-CAATAGGAGCAAGCATCCGATCATCTGCTGGGGTACTAACAGGGCTATAG-3'

References

1. Dönhöfer A, *et al.* (2012) Structural basis for TetM-mediated tetracycline resistance. *Proc. Natl. Acad. Sci. USA* 109(42):16900-16905.
2. Arenz S, *et al.* (2014) Drug Sensing by the Ribosome Induces Translational Arrest via Active Site Perturbation. *Mol Cell* 56(3):446-452.
3. Iordanescu S (1976) Three distinct plasmids originating in the same *Staphylococcus aureus* strain. *Archives roumaines de pathologie experimentales et de microbiologie* 35(1-2):111-118.
4. Narayanan CS & Dubnau D (1985) Evidence for the translational attenuation model: ribosome-binding studies and structural analysis with an in vitro run-off transcript of *ermC*. *Nucleic Acids Res* 13(20):7307-7326.
5. Li X, *et al.* (2013) Electron counting and beam-induced motion correction enable near-atomic-resolution single-particle cryo-EM. *Nat Methods* 10(6):584-590.
6. Scheres SH & Chen S (2012) Prevention of overfitting in cryo-EM structure determination. *Nat Methods* 9(9):853-854.
7. Frank J, *et al.* (1996) SPIDER and WEB: processing and visualization of images in 3D electron microscopy and related fields. *J Struct Biol* 116(1):190-199.
8. Becker T, *et al.* (2012) Structural basis of highly conserved ribosome recycling in eukaryotes and archaea. *Nature* 482(7386):501-506.
9. Chen JZ & Grigorieff N (2007) SIGNATURE: a single-particle selection system for molecular electron microscopy. *J. Struct. Biol.* 157(1):168-173.
10. Loerke J, Giesebrecht J, & Spahn CM (2010) Multiparticle cryo-EM of ribosomes. *Methods Enzymol* 483:161-177.
11. Fernandez JJ, Luque D, Caston JR, & Carrascosa JL (2008) Sharpening high resolution information in single particle electron cryomicroscopy. *J Struct Biol* 164(1):170-175.
12. Kucukelbir A, Sigworth FJ, & Tagare HD (2014) Quantifying the local resolution of cryo-EM density maps. *Nat Methods* 11(1):63-65.
13. Fischer N, *et al.* (2015) Structure of the *E. coli* ribosome-EF-Tu complex at <3 Å resolution by C-corrected cryo-EM. *Nature*.
14. Emsley P & Cowtan K (2004) Coot: Model-Building Tools for Molecular Graphics. *Acta Crystallographica Section D - Biological Crystallography* 60:2126-2132.
15. Bocharov EV, *et al.* (2004) From structure and dynamics of protein L7/L12 to molecular switching in ribosome. *J. Biol. Chem.* 279(17):17697-17706.
16. Soding J, Biegert A, & Lupas AN (2005) The HHpred interactive server for protein homology detection and structure prediction. *Nucleic Acids Res* 33(Web Server issue):W244-248.
17. Eswar N, Eramian D, Webb B, Shen MY, & Sali A (2008) Protein structure modeling with MODELLER. *Methods Mol Biol* 426:145-159.
18. Adams PD, *et al.* (2010) PHENIX: a comprehensive Python-based system for macromolecular structure solution. *Acta Crystallogr D Biol Crystallogr* 66(Pt 2):213-221.
19. Pettersen EF, *et al.* (2004) UCSF Chimera - A Visualization System for Exploratory Research and Analysis. *J. Comput. Chem.* 25(13):1605-1612.
20. Li W, *et al.* (2013) Mechanism of tetracycline resistance by ribosomal protection protein Tet(O). *Nat. Commun.* 4:1477.
21. Jenner L, *et al.* (2013) Structural basis for potent inhibitory activity of the antibiotic tigecycline during protein synthesis. *Proc Natl Acad Sci U S A* 110(10):3812-3816.

ARTICLE

Received 28 Jan 2014 | Accepted 24 Feb 2014 | Published 24 Mar 2014

DOI: 10.1038/ncomms4501

Molecular basis for erythromycin-dependent ribosome stalling during translation of the ErmBL leader peptide

Stefan Arenz¹, Haripriya Ramu², Pulkit Gupta², Otto Berninghausen¹, Roland Beckmann^{1,3}, Nora Vázquez-Laslop², Alexander S. Mankin² & Daniel N. Wilson^{1,3}

In bacteria, ribosome stalling during translation of ErmBL leader peptide occurs in the presence of the antibiotic erythromycin and leads to induction of expression of the downstream macrolide resistance methyltransferase ErmB. The lack of structures of drug-dependent stalled ribosome complexes (SRCs) has limited our mechanistic understanding of this regulatory process. Here we present a cryo-electron microscopy structure of the erythromycin-dependent ErmBL-SRC. The structure reveals that the antibiotic does not interact directly with ErmBL, but rather redirects the path of the peptide within the tunnel. Furthermore, we identify a key peptide-ribosome interaction that defines an important relay pathway from the ribosomal tunnel to the peptidyltransferase centre (PTC). The PTC of the ErmBL-SRC appears to adopt an uninduced state that prevents accommodation of Lys-tRNA at the A-site, thus providing structural basis for understanding how the drug and the nascent peptide cooperate to inhibit peptide bond formation and induce translation arrest.

¹Gene Center, Department for Biochemistry, University of Munich, Feodor-Lynen Strasse 25, 81377 Munich, Germany. ²Center for Pharmaceutical Biotechnology, University of Illinois, Chicago, Illinois 60607, USA. ³Center for integrated Protein Science Munich (CiPSM), University of Munich, Feodor-Lynen Strasse 25, 81377 Munich, Germany. Correspondence and requests for materials should be addressed to A.S.M. (email: shura@uic.edu) or to D.N.W. (email: wilson@lmb.uni-muenchen.de).

During protein synthesis, nascent polypeptide chains can modulate the efficiency of translation¹. Nascent polypeptide-mediated translation regulation can be an intrinsic property of the nascent chain¹ or can depend on the additional presence of a ligand, for example, a macrolide antibiotic such as erythromycin (ERY)^{2,3}. Biochemical and genetic studies of several drug-dependent regulatory peptides have provided initial models for how interactions within the ribosomal tunnel can relay back to the peptidyltransferase centre (PTC) to induce translation arrest^{2,3}. Interestingly, biochemical characterization of distinct Erm leader peptide-stalled ribosome complexes (SRCs) indicates that fundamental differences exist in their mechanisms of translational arrest: for example, mutations of 23S rRNA nucleotides A2062 and A2503 abolish stalling with ErmAL1 and ErmCL, but have no influence on ErmBL- and ErmDL-mediated translation arrest⁴. Furthermore, different regulatory peptides appear to have a different sensitivity to the chemical structure of the antibiotic^{4–6}. The lack of structural information has made it difficult to explain these conceptually important distinctions and provide models of drug-dependent stalling to a sufficient level of molecular detail.

Here we have characterized structurally and biochemically the requirements for ribosome stalling during translation of the ErmBL leader peptide. Similar to other inducible macrolide resistance genes, *ermB* is controlled by programmed arrest of translation of the leader peptide ErmBL (Fig. 1a). Previous studies demonstrated that polymerization of the ErmBL nascent chain halts when the Asp codon (D10) of the *ermBL* open-reading frame (ORF) enters the ribosomal P-site and the Lys (K11) codon is placed in the A-site^{4,7} (Fig. 1a). Consistently, our findings indicate that the ErmBL-SRC contains an ErmBL-transfer RNA in the P-site and Lys-tRNA in the A-site, and thus stalling results

from inability of the ribosome to catalyse peptide bond formation. On the basis of our cryo-electron microscopy (EM) structure of the ErmBL-SRC, we suggest that peptide bond formation does not occur because the accommodation of Lys-tRNA at the A-site of the PTC is corrupted. Moreover, we identify critical residues in ErmBL and in the ribosome, which we propose to be important for maintaining the PTC in an uninduced and thus inactive state.

Results

Cryo-EM structure of the ErmBL-SRC. To assess whether the ErmBL-SRC contains the nascent chain attached to tRNA^{Asp} in the P-site or to tRNA^{Lys} in the A-site, *in vitro* translation of ErmBL was performed in the presence of ERY and either radiolabelled aspartate or lysine. Analysis of the ErmBL nascent chain shows that radiolabelled Asp, but not Lys, was incorporated into the peptidyl-tRNA of the SRC (Fig. 1b). Thus, the ribosome stalls because it is unable to catalyse formation of a peptide bond between the 10-amino-acid-long ErmBL nascent chain attached to the tRNA^{Asp} in the P-site and the incoming Lys-tRNA^{Lys} (Fig. 1a). To unravel the structural basis for ErmBL-mediated stalling, we generated ErmBL-SRC for analysis using cryo-EM. For previous structures of drug-independent SRCs, the nascent chains were of sufficient length to exit the ribosomal tunnel, enabling purification of the SRC using N-terminal affinity tags^{8–10}. In contrast, the peptides controlling macrolide resistance genes, including the 10-amino-acid-long ErmBL nascent chain, are too short to exit the tunnel, making preparation of SRC by N-terminal affinity tagging impossible. Consequently, we established a SRC purification technique employing a bicistronic (2 × *ermBL*) messenger RNA (mRNA) bearing two *ermBL* ORFs.

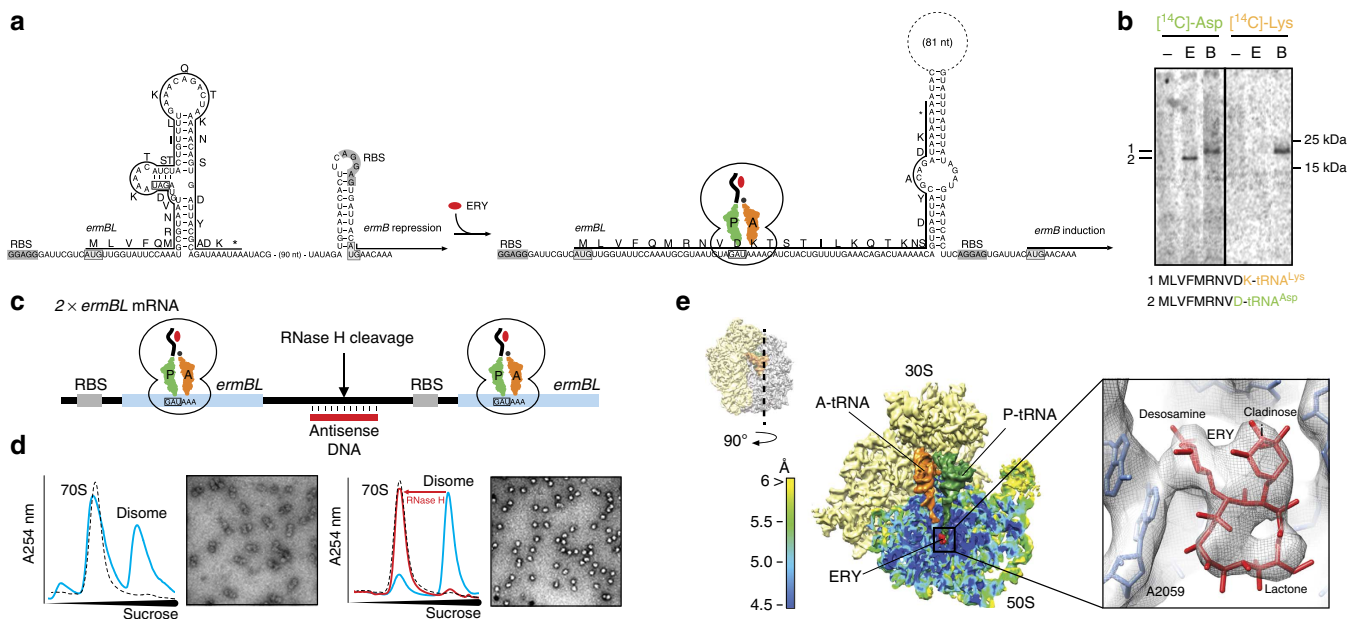


Figure 1 | Cryo-EM structure of the ErmBL-stalled ribosome complex. (a) Schematic for *ermBL*-dependent regulation of *ermB* translation in the presence of erythromycin (ERY). (b) *In vitro* translation of ErmBL using either ¹⁴C-Asp or ¹⁴C-Lys in the absence (–) or presence (E) of 50 μM ERY. In the control samples (B), where translation was carried out in the absence of ERY, but in presence of borrelidin (a Thr-tRNA synthetase inhibitor), translation arrest occurred after an 11-amino-acid nascent chain was polymerized (such that codon 12 is in the A-site, which is one codon further compared with the natural stall site), thereby providing a mobility marker and confirming ¹⁴C-Lys incorporation in the absence of ERY. (c) The bicistronic 2 × *ermBL* mRNA was translated *in vitro* in the presence of 10 μM ERY to generate ErmBL-SRC disomes. (d) Complementary DNA oligo and RNase H cleavage converts disomes to monosomes, as shown by sucrose density centrifugation and negative stain EM. (e) Surface and cross-section of the ErmBL-SRC, containing 30S (yellow), 50S (coloured according to local resolution), A-tRNA (orange), P-tRNA (green) and ERY (red). Inset shows electron density for ERY (grey mesh) with fitted crystal structure (PDB3OFR)¹¹.

The ORFs were separated by a 22-nucleotide linker and each had a strong ribosome-binding site (RBS) (Fig. 1c). *In vitro* translation of $2 \times ermBL$ leads to the formation of disomes (one ribosome per cistron, two ribosomes per mRNA), as evident from sucrose gradient analysis and negative-stain EM (Fig. 1d). Importantly, disome formation is strictly dependent on the presence of ERY and does not occur on monocistronic *ermBL* mRNAs (Supplementary Fig. 1). To avoid orientation bias during cryo-EM analysis, the disomes were converted into monosomes by cleavage of the linker using an antisense DNA oligonucleotide and RNase H (Fig. 1c,d).

Cryo-EM and single-particle reconstruction of the resulting ErmBL-SRC, coupled with *in silico* sorting (Supplementary Fig. 2), yielded one major homogeneous subpopulation of ribosomes bearing tRNAs in the A- and P-sites (Fig. 1e). Local resolution indicates that most of the ErmBL-SRC map, in particular the core region encompassing the PTC and ribosomal tunnel, reaches a resolution of 4.5 Å (Fig. 1e and Supplementary Fig. 3). Consistent with this resolution, distinct features of the electron density for ERY, such as the lactone ring, desosamine and cladinose sugars, can be unambiguously resolved (Fig. 1e). Moreover, rigid-body fitting of the crystal structure of ERY in complex with the *Escherichia coli* ribosome¹¹ indicates that the drug is bound to its canonical position^{11,12} in the ErmBL-SRC (Fig. 1e).

The path of ErmBL through the ribosomal tunnel. Additional density in the ErmBL-SRC, which we assign to the ErmBL

nascent chain, is observed within the ribosomal tunnel extending from the CCA-end of the P-tRNA (Fig. 2a). Unlike the nascent chains of TnaC⁸ and SecM¹⁰ that extend throughout the entire length of ribosomal tunnel (Fig. 2b,c), the 10-amino-acid-long ErmBL occupies only the upper third of this conduit (Fig. 2a). Moreover, the unique path of the ErmBL nascent chain enables it to bypass the tunnel-bound ERY (Fig. 2d). In contrast, the nascent chains of SecM- and TnaC-SRC, as well as of other ribosome-nascent chain complexes^{9,13–15}, adopt conformations that would be sterically obstructed by the drug (Fig. 2e,f). Although *ermBL* translation by the ERY-bound ribosome stalls at the 10th codon, the conformation of the ErmBL polypeptide within the tunnel (Fig. 2a) illustrates the general principle of how a specific subset of polypeptides can bypass ERY to be translated on drug-bound ribosomes¹⁶.

Closer examination of the ErmBL-SRC structure indicates an apparent lack of contact between ErmBL and ERY (Fig. 2d). This is distinct from the direct interaction between the nascent chain and the drug that was proposed for ErmCL, based on the observation that removal or modification of the C3 cladinose sugar abolishes ErmCL stalling^{17,18}. Therefore, we tested whether ErmBL stalling is sensitive to structural modifications of the antibiotic cofactor. In excellent agreement with the structural predictions, ErmBL stalling could be induced not only by ERY, but also by a wide range of tunnel-binding macrolides, including those which failed to induce ErmCL-SRC formation¹⁷, for example, solithromycin, which lacks the C3 cladinose, as well as oleandomycin and ITR-054, which contain alterations of the C3

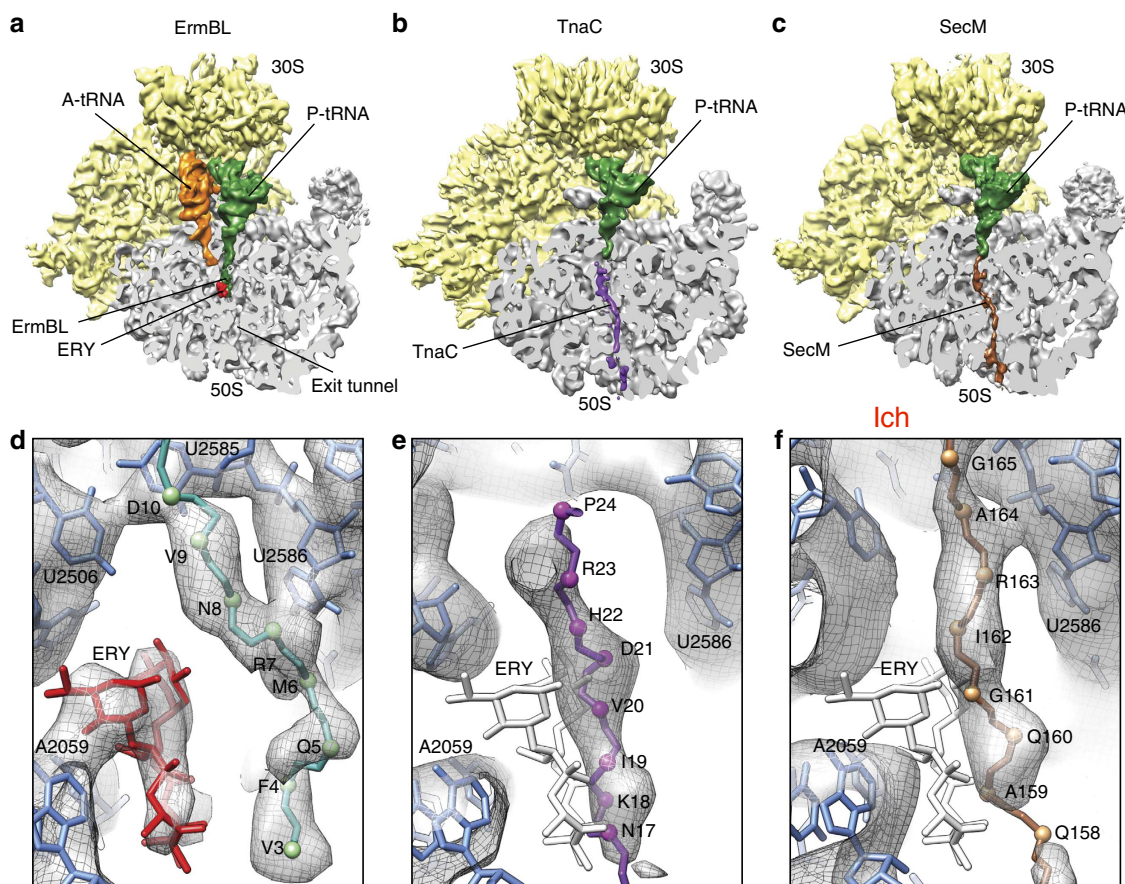


Figure 2 | Path of the ErmBL compared with TnaC and SecM nascent chains. (a–c) Comparison of cryo-EM structures of ErmBL-SRC, TnaC-SRC⁸ and SecM-SRC¹⁰, with a transverse section of the 50S subunit (grey) displaying the path of the respective nascent chains through the ribosomal tunnel. (d–f) Paths of the (d) ErmBL (teal), (e) TnaC⁸ (purple) and (f) SecM¹⁰ (brown) nascent chains. Erythromycin (ERY)¹¹ is coloured red in (d) ErmBL-SRC, whereas the superimposed position of ERY is coloured white in (e) TnaC-SRC and (f) SecM-SRC.

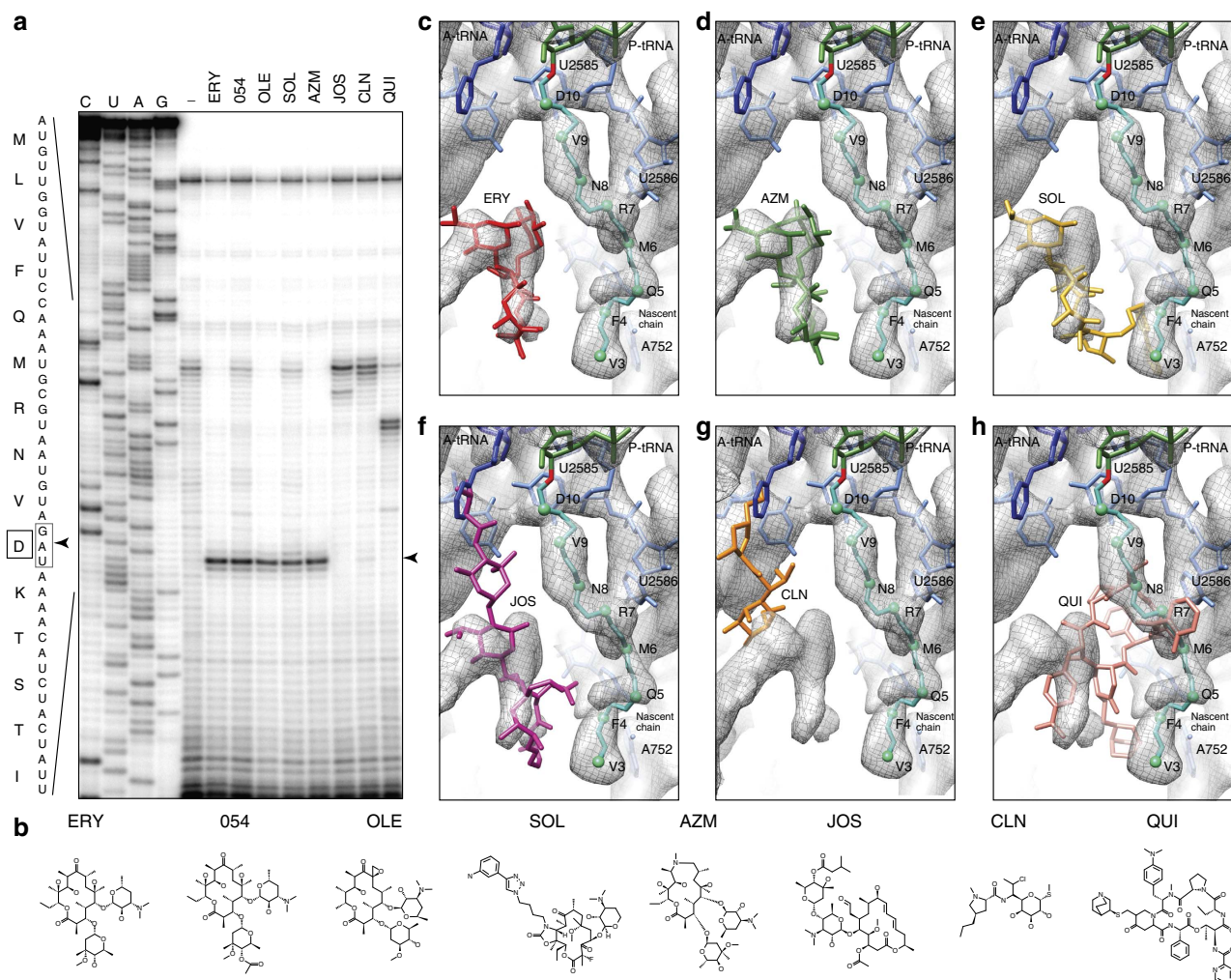


Figure 3 | Superimposition of various antibiotics relative to ErmBL. (a) Detection of ribosome stalling by toe-printing during translation of *ermBL*, in the presence of the antibiotics erythromycin (ERY), ITR-054 (054), oleandomycin (OLE), solithromycin (SOL), azithromycin (AZM), josamycin (JOS), clindamycin (CLN) and quinupristin (QUI). The arrowed toe-print band indicates that ErmBL arrests translation with the Asp (D10) codon (boxed) located in the P-site. (b) Chemical structures of ERY, macrolides ITR-054 (054), OLE, the ketolide SOL and the azalide AZM compared with the macrolide JOS, the lincosamide CLN and the streptogramin B QUI. Differences between ERY and respective drugs are highlighted. (c) ErmBL-SRC map (grey mesh) with molecular model for ErmBL-tRNA (teal), 23S rRNA (blue) and ERY (red, PDB3OFR¹¹). (d–h) as in (c), but with relative binding positions of (d) AZM (green, PDB1M1K¹⁹), (e) SOL (yellow, PDB3ORB⁴²), (f) JOS (purple, PDB2O44), (g) CLN (orange, PDB3OFZ¹¹) and (h) QUI (pink, PDB1SM1 (ref. 20)).

sugar (Fig. 3). As expected, antibiotics josamycin and clindamycin, which overlap with the A-site and inhibit formation of the first peptide bond^{11,12,19} (Fig. 3), and quinupristin, which overlaps with the path of ErmBL^{12,20} (Fig. 3), did not allow the drug-bound ribosome to reach the *ermBL* stall site (Fig. 3).

Interaction between ErmBL and the ribosomal tunnel. To ascertain which residues of ErmBL interact with the ribosomal tunnel, a model for nascent chain was built (Fig. 4a). Since the resolution does not allow us to model sidechains, we present only a backbone model for the ErmBL nascent chain. On the basis of this model, three interactions with the ribosomal tunnel are predicted: one from the C terminus (V9–D10) of ErmBL with U2585, a second in the vicinity of R7 with U2586 and a third between F4 and U2609 (Fig. 4a). Local resolution indicates that the C terminus of ErmBL (M6–D10) is very stable, providing more confidence in the placement of the backbone model, whereas in contrast, the N-terminal residues (M1–Q5) are flexible

to such an extent that modelling of M1 and L2 was not possible due to lack of density and alternative models for the N-terminal are therefore possible (Fig. 4b). Consistently, alanine-scanning mutagenesis of ErmBL demonstrated that C-terminal residues, namely, R7 and V9–D10, are critical for stalling, whereas the N-terminal residues are not (Fig. 4c). The most distal contact from the PTC between F4 and U2609 (Fig. 4a,b) does not appear to be functionally important because neither the F4A mutation, nor the U2609C alteration affected the efficiency of stalling (Fig. 4c; Supplementary Fig. 4).

In contrast, the second contact, between R7 and U2586, plays an important role, since disruption of this interaction by the R7A mutation in ErmBL significantly diminishes stalling (Fig. 4a,c). Strikingly, changes in the ribosomal interacting partner (U2586A/G/C) were able to restore the efficiency of translation arrest for the ErmBL-R7A mutant (Fig. 4d). The fact that the U2586 mutations (U2586A/G/C) were unable to restore stalling for the ErmBL-V9A or -D10A mutants (Fig. 4e) and that stalling of the ErmBL-R7A mutant could not be compensated by alterations of the neighbouring tunnel nucleotide A2062 (Fig. 4f)

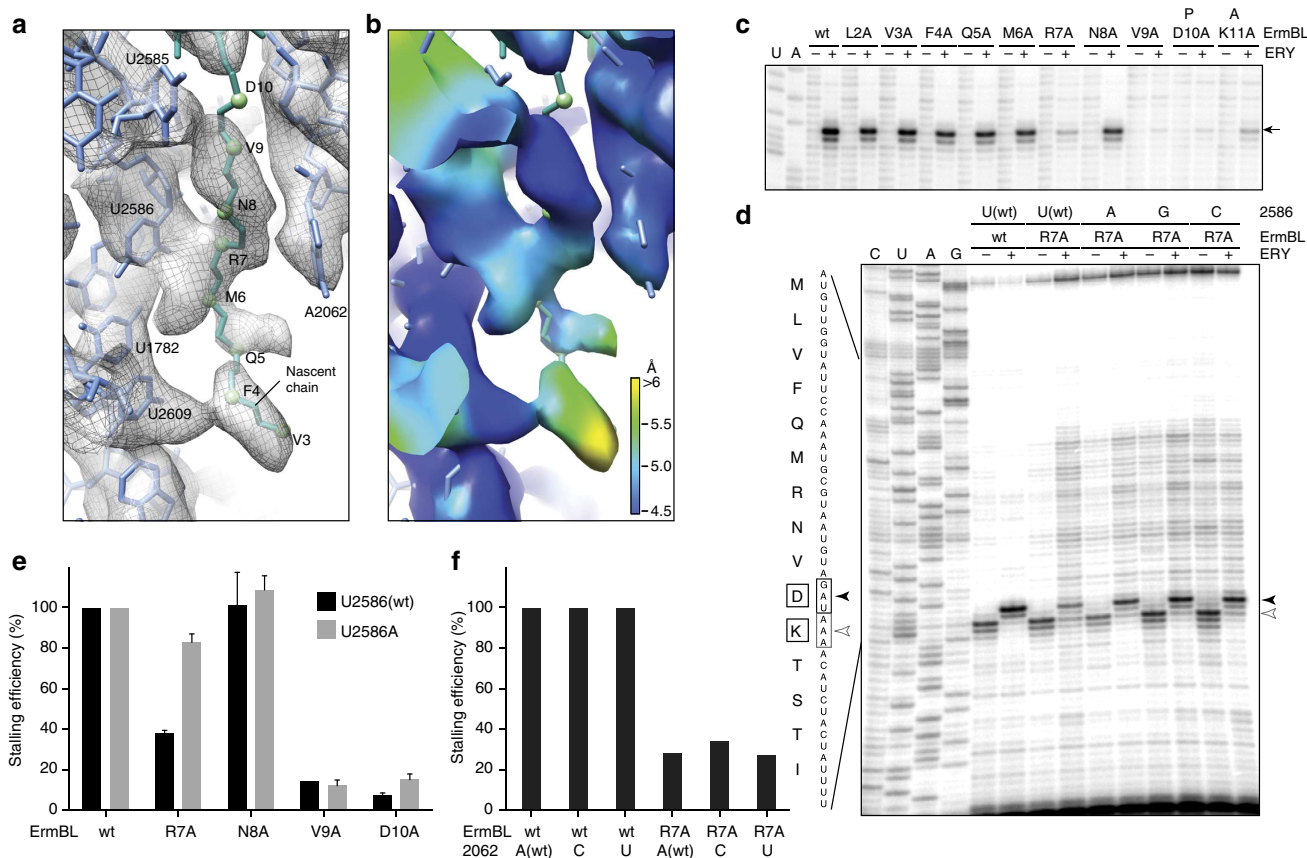


Figure 4 | Interactions of the ErmBL nascent chain with the ribosome. (a) Interactions of ErmBL (teal) with 23S rRNA (blue) within the exit tunnel of the ribosome. (b) Local resolution map of view shown in (a). (c) Alanine-scanning mutagenesis of ErmBL and effect of mutant peptides on ribosome stalling (arrowed) in the presence (+) and absence (-) of erythromycin (ERY) as determined by toe-printing. (d) Toe-printing of wild type (wt) and mutant (R7A) ErmBL on *E. coli* ribosomes with wt or mutated 23S rRNA nucleotide 2586, in the presence (+) or absence (-) of ERY. All the reactions contained borrelidin, a Thr-tRNA synthetase inhibitor, which, in the absence of ERY-dependent arrest at the Asp (D10) codon, causes translation arrest at the Lys (K11) codon. (e) Influence of the U2586A mutation on stalling efficiency with the wt and mutant ErmBL peptides (an average of two independent experiments; error bars represent the standard deviation of the mean). (f) The mutations of A2062 do not affect ErmBL stalling, nor rescue stalling impaired by the R7A mutation.

re-emphasizes the specificity and importance of the R7-U2586 interaction for the mechanism of ErmBL stalling. This also provides support for our model for the C-terminal portion of the ErmBL nascent chain and in particular the placement of R7. Notably, the identity of the tunnel nucleotide A2062, which is critical for ErmCL- and ErmAL1-mediated ribosome stalling, was not important for the formation of the ErmBL-SRC^{4,18} (Fig. 4e and Supplementary Fig. 4). The ErmBL-SRC structure shows the lack of direct contact between A2062 and the nascent chain (Fig. 4b), providing a plausible explanation for the clear distinction between the drug-dependent translation arrest directed by different stalling peptides.

The conformation of the PTC of the ErmBL-SRC. The third contact between the ErmBL nascent chain and the ribosome engages the peptide residues V9/D10 with U2585 of the 23S rRNA. Previous crystallographic analysis of model complexes showed that accommodation of the CCA-end of the A-site tRNA requires movement of the PTC nucleotides U2584 and U2585 to achieve the ‘induced fit’ state of the PTC and provide room for the A-tRNA^{21–23} (Fig. 5a). The crystal structures of the 50S structure with the PTC in either the uninduced or the induced state were fitted to the electron density for the 50S subunit of the ErmBL-SRC as a rigid body (Fig. 5a). Together with difference

electron density maps (Supplementary Fig. 5), this procedure suggests that U2584 and U2585 have not shifted sufficiently and remain in an uninduced-like conformation in the ErmBL-SRC, probably due to the interaction of U2585 with the ErmBL nascent chain. The local resolution of the ErmBL map is 4.5 Å, which is sufficient to distinguish movements of 0.9–1.1 Å^{24–26}. Because the differences in the nucleotide positions between the induced and uninduced states are in the order of 1–2 Å, we are rather confident that our data would allow us to conclude that the functional state of the PTC in ErmBL-SRC differs from its classic induced state.

Although higher resolution will be necessary to validate the exact placement of the PTC residues, its deviation from the fully functional state in the ErmBL-SRC and unaccommodated state of the A-tRNA (Fig. 5a) provide an explanation for the translational arrest, since the fully accommodated state is required for efficient nucleophilic attack and fast peptide bond formation (Fig. 5b). Moreover, an unaccommodated state of A-tRNA in the ErmBL-SRC is consistent with the finding that Lys encoded by the A-site codon of the SRC is not incorporated into the ErmBL nascent chain (Fig. 1b). Although the density corresponding to the A-site amino acid was mostly lacking, we verified biochemically that the A-site tRNA fully retains its aminoacyl moiety through the entire purification protocol (Supplementary Fig. 6). Therefore, we believe that the lack of density reflects the flexibility

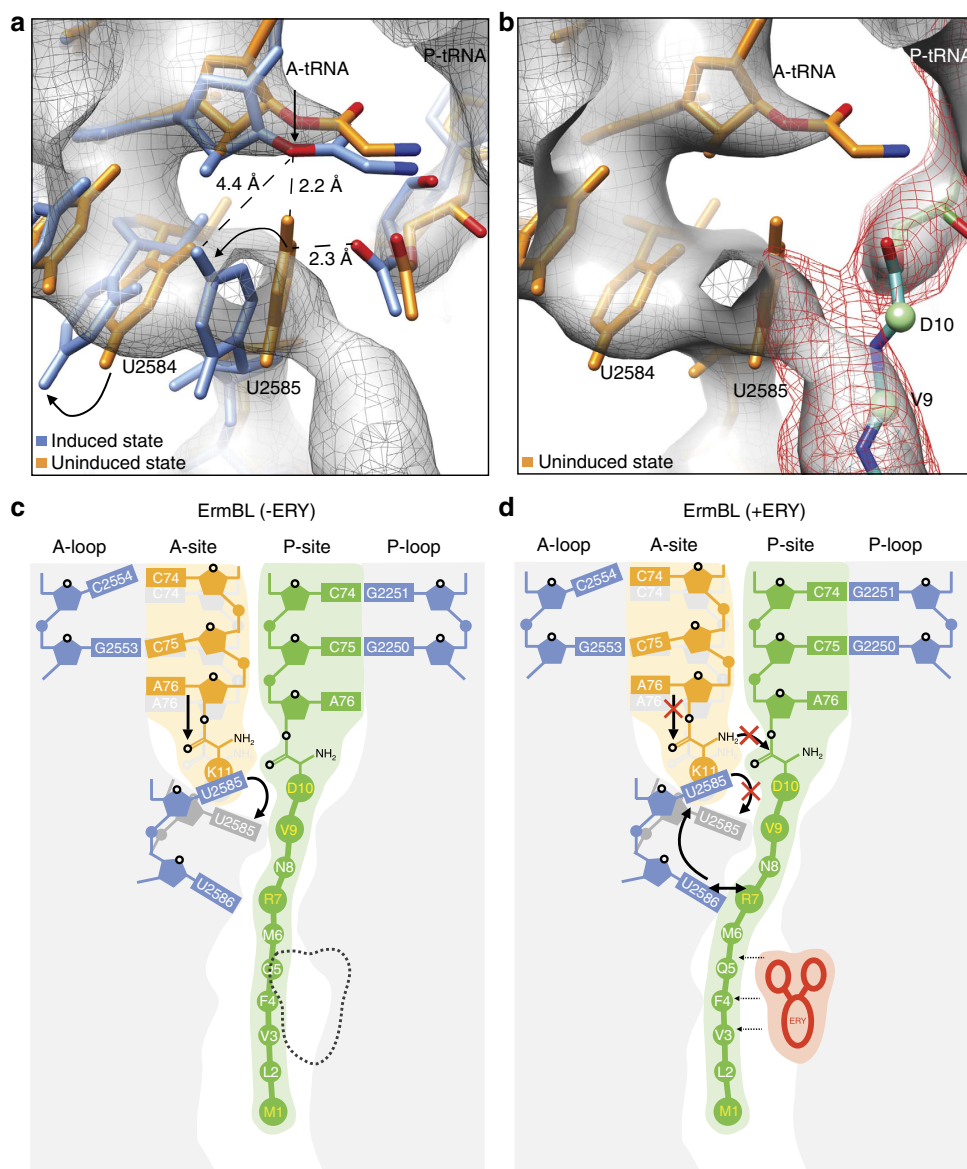


Figure 5 | The uninduced state of the PTC and an unaccommodated A-tRNA in the ErmBL-SRC prevent peptide bond formation. (a,b) During accommodation of the A-tRNA, U2585 and U2584 undergo conformational changes (arrowed) necessary for peptide bond formation^{21–23}. In the ErmBL-SRC, the electron density suggests that U2585 retains an unaccommodated state (orange, PDB1VQ6)^{21–23}, thus preventing proper placement of the A-tRNA in the PTC (blue, PDB1VQN)^{21–23}. (b) Electron density between the ErmBL nascent chain (dark mesh) and U2585 indicates that the C-terminal amino acids of ErmBL directly interact with U2585, likely restricting its movement. (c,d) Model for the translation of ErmBL (c) in the absence of erythromycin (ERY) (canonical translation), and (d) translation arrest in the presence of ERY (stalling). In (d), the drug restricts the conformational space available for the ErmBL nascent chain such that interactions with U2586 and U2585 are established. We propose that this prevents movement of U2585 from the uninduced to induced state, and thus hinders accommodation of the A-tRNA and peptide bond formation.

of the Lys residue of the A-tRNA and reinforces the notion of the ‘inappropriate’ placement of the PTC acceptor substrate (Fig. 5a,b). Because the ribosome accelerates peptide bond formation primarily through accurate positioning of the reacting components^{27,28}, high flexibility of the acceptor substrate would be incompatible with fast peptidyl transfer. Mutation of the SRC acceptor amino acid from lysine to alanine reduced the efficiency of translation arrest (Fig. 4c), suggesting that the nature of the A-tRNA amino acid influences the ability of aminoacyl-tRNA to be accommodated in the A-site.

Discussion

Our biochemical and structural insights allow us to propose a model for the concerted action of the drug and the nascent chain

in inhibiting the PTC functions: During canonical translation, for example, of ErmBL in the absence of ERY, the nascent polypeptide chain passes freely through the ribosomal tunnel, exploring many conformations most of which are compatible with efficient peptide bond formation. However, in the presence of the macrolide molecule, the path of the nascent chain is restricted because some of the previously accessible routes are obstructed by the drug. In the constrained conformational space the peptide is compelled to establish specific and long-lived contacts with the tunnel wall (R7-U2586) and at the PTC (V9-D10 with U2585) (Fig. 5c). These contacts stabilize the improper (uninduced) state of U2585, which in turn precludes accommodation of the Lys-tRNA in the A-site and thus prevents peptide bond formation (Fig. 5d).

In conclusion, our analysis of the ErmBL-SRC establishes a basic framework for understanding how the combined action of the nascent peptide and a small molecule cofactor may induce programmed translation arrest. It will be interesting to extend these insights by comparing the ErmBL-SRC structure with other drug-dependent SRCs, such as ErmCL, which have principally different antibiotic- and tunnel sensor requirements. Collectively, it appears that there are several alternative ways to inhibit translation via the cooperative action of nascent peptides and tunnel-binding antibiotics.

Methods

Generation and purification of ErmBL-SRC. The $2 \times ermBL$ construct was synthesized (Eurofins, Martinsried, Germany) such that it contained a T7 promoter followed by a strong RBS spaced by 7 nucleotides (nts) to the ATG start codon of the first *ermBL* cistron (Fig. 1a). A linker of 22 nts separated the stop codon of the first *ermBL* cistron and the start codon of the second *ermBL* cistron (Fig. 1c). The linker also comprised the strong RBS 7 nts upstream of the ATG start codon of the second *ermBL* cistron, enabling initiation of translation independent from the first *ermBL* cistron (Fig. 1c). Each *ermBL* cistron encoded amino acids 1–17 corresponding to ErmBL leader peptide (Genbank accession number K00551) present on macrolide resistance plasmid pAM77 (ref. 29). The complete sequence of $2 \times ermBL$ construct is:

```
5'-TAATACGACTCACTATAGGGAGTTTTATAAGGAGGAAAAAATATGTTGGTAT
TCCAAATGCGTAATGTAGATAAAAACATCTACTATTTTGAATAAAAGTTTATA
AGGAGGAAAAAATATGTTGGTATTCCAAATGCGTAATGTAGATAAAAACATC
TACTATTTTGAATAAA-3'
```

(T7 promoter, italics; RBS, bold; ErmBL ORF, shaded grey with GAT codon in P-site of stalled ribosome shown in bold; annealing site for complementary DNA oligonucleotide, underlined). *In vitro* translation of the $2 \times ermBL$ construct was performed using the Rapid Translation System RTS 100 *E. coli* HY Kit (Roche; Cat. No. 3246817). Translations were carried out in the presence of 10 μ M ERY for 1 h at 30 °C. Control reactions were performed in the absence of ERY as well as using a monocistronic *ermBL* construct (Supplementary Fig. 1). Translation reactions were analysed on sucrose density gradients (10–55% sucrose in a buffer A, containing 50 mM HEPES-KOH, pH 7.4, 100 mM KOAc, 25 mM Mg(OAc)₂, 6 mM β -mercaptoethanol, 10 μ M ERY and 1 \times Complete EDTA-free Protease Inhibitor cocktail (Roche)) by centrifugation at 154,693g (SW-40 Ti, Beckman Coulter) for 2.5 h at 4 °C (Fig. 1d). For ErmBL-SRC purification, disome fractions were collected using a Gradient Station (BioComp) with an Econo UV Monitor (Biorad) and a FC203B Fraction Collector (Gilson). Purified ErmBL-SRC disomes were concentrated by centrifugation using Amicon Ultra-0.5 ml Centrifugal Filters (Millipore) according to the manufacturer's protocol. To obtain monosomes of the ErmBL-SRC, a short DNA oligonucleotide (5'-ttcctcttaaact-3', Metabion) was annealed to the linker between the *ermBL* cistrons of the disomes, generating a DNA–RNA hybrid that could be cleaved by RNase H (New England Biolabs) treatment in buffer A at 25 °C for 1 h (Fig. 1c). The RNase H-cleaved disome material was directly applied to the cryo-grids without any further purification.

Aminoacylation status of tRNA^{Lys} in the ErmBL-SRC. RNA from three A₂₆₀ units of the disome peak, subjected to exactly the same procedures as required for preparation for cryo-EM, was extracted by acidic phenol, ethanol precipitated and dissolved in 6 μ l NaOAc, pH 4.0. The isolated RNA was then resolved by electrophoresis in an 8 cm long (1 mm thick) 14% acidic denaturing gel³⁰ alongside with deacylated tRNA^{Lys} and aminoacyl-tRNA markers. After electrophoresis for 24 h at 50 V in the cold room, the RNA was transferred to a Hybond N+ membrane (GE Healthcare) by electroblotting and probed with a [³²P]-5'-labelled DNA oligonucleotide complementary to tRNA^{Lys}: (GTCGTGCAGGATTCGAACCTGCGACCAATTGATTAAGTCAACTGC TCTACCAACTGAGCTAACGACCC).

Negative-stain EM. Ribosomal particles were diluted in buffer A to a final concentration of 0.5 A₂₆₀ ml⁻¹. One drop of each sample was deposited on a carbon-coated grid. After 30 s, grids were washed with distilled water and then stained with three drops of 2% aqueous uranyl acetate for 15 s. The remaining liquid was removed by touching the grid with filter paper. Micrographs were taken using a Morgagni transmission electron microscope (FEI Company), 80 kV, wide angle 1 K charge-coupled device at direct magnifications of 72 K.

Cryo-EM and single-particle reconstruction. Monosomes of the ErmBL-SRC were applied to 2 nm pre-coated Quantifoil R3/3 holey carbon-supported grids and vitrified using a Vitrobot Mark IV (FEI Company). Data collection was performed on a Titan Krios transmission electron microscope (FEI Company) under low-dose conditions (about 20 e⁻ per Å²) at a nominal magnification of $\times 75,000$ with a

nominal defocus between -1 and -3.5 μ m. Images were collected at 200 keV at a magnification of $\times 148,721$ at the plane of charge-coupled device using a TemCam-F416 CMOS camera (TVIPS GmbH, 4,096 \times 4,096 pixel, 15.6 μ m pixel, 1 s per full frame), resulting in an image pixel size of 1.0605 Å (object scale). Data collection was facilitated by the semi-automated software EM-TOOLS (TVIPS GmbH) as described³¹. Contrast-transfer functions were determined using the SPIDER TF ED command and recorded images were manually inspected for good areas and power-spectra quality. Data were processed further using the SPIDER software package³², in combination with an automated workflow as described previously³¹. After initial, automated particle selection based on the programme SIGNATURE³³, initial alignment was performed with 1,344,100 particles, using *E. coli* 70S ribosome as a reference structure³⁴. After removal of noisy particles (527,625 particles; 39%), the data set could be sorted into three main subpopulations (Supplementary Fig. 2) using an incremental K-means-like method of unsupervised 3D sorting³⁵: the first subpopulation (353,318 particles; 26%) was defined by the presence of the L1 stalk adopting an 'in' conformation and the presence of non-stoichiometric density for tRNAs in the A-, P- and E-sites. The second and third subpopulations were defined by the presence of the L1 stalk adopting an 'out' conformation and the absence of density for the E-tRNA. The minor subpopulation contained only P-tRNA, but due to the small particle numbers (113,413 particles; 8%) could only be refined to ~ 7 Å resolution (with a Fourier shell correlation (FSC) cutoff of 0.5). In contrast, the major subpopulation (349,744 particles; 26%) contained both A- and P-tRNAs and could be refined to an average resolution of 6.6 Å (0.5 FSC) and a local resolution extending to 4.5 Å for the core of the 30S and 50S subunit (Supplementary Fig. 3). Local resolution was computed within a softened sphere (radius of 22 Å) at each voxel, as described previously³⁶, using the 0.5 FSC of two reconstructions; namely, from the first 50% of the particles and then the remaining 50%.

Molecular modelling and map-docking procedures. The molecular model for the ribosomal proteins and rRNA of the ErmBL-SRC was based on the 50S subunit from the crystal structure of ERY bound to the *E. coli* 70S ribosome (PDB3OFR)¹¹ and obtained by performing a rigid-body fit into the cryo-EM density map of the ErmBL-SRC using UCSF Chimera³⁷ (fit in map function). The conformations of 23S rRNA nucleotides U2584 and U2585 were taken from the equivalent nucleotides of the *Haloarcula marismortui* 50S subunit in complex with the unaccommodated A-site tRNA mimic (PDB1VQ6)^{21,22} after the PDB was fitted as a rigid body into the ErmBL-SRC density map. The conformation of U2506 was similar to the equivalent nucleotide of the *H. marismortui* 50S subunit in complex with the accommodated A-site tRNA mimic (PDB1VQN)^{21,22}, however, required manual rotation of the base to prevent clashing with the unaccommodated position of U2585. In contrast, the conformation of A2062 present in the ErmBL-SRC is unique, being distinct from the tunnel 'in' (PDB3CC2)³⁸ and tunnel 'out' (PDB1VQ6)^{21,22} conformations observed in previously reported ribosome structures. The conformation of A2062 in the ErmBL-SRC is most closely related to conformations of this nucleotide observed in the *Thermus thermophilus* 70S ribosome (PDB2J01)³⁹. To investigate the conformational state of the PTC of the ErmBL-SRC, crystal structures of *H. marismortui* 50S subunit in complex with model peptide bond substrates (Fig. 5a,b) were fitted into the cryo-EM density map of the ErmBL-SRC as a rigid body using UCSF Chimera³⁷. The model for the ErmBL nascent polypeptide chain was generated and manually fitted into the density using Coot⁴⁰. PDBs for the unaccommodated (PDB1VQ6) and accommodated (PDB1VQN) state of the PTC were filtered to 4.5 Å to using the Molmap function in Chimera. Difference electron density maps were then calculated by subtracting the filtered maps for 1VQ6 from 1VQN (Supplementary Fig. 5a) or ErmBL from 1VQN (Supplementary Fig. 5b).

Figure preparation. Figures showing electron densities and atomic models were generated using UCSF Chimera³⁷.

Toe-printing assay. The DNA templates containing T7 promoter, RBS and the ErmBL-coding ORF (wild type or the mutants) were generated by crossover PCR. The toe-printing analysis of drug-dependent ribosome stalling was carried out as described¹⁸. Briefly, the DNA templates (0.1 pmol) were used in a total volume of 5 μ l of PURExpress (New England Biolabs) cell-free transcription–translation reactions. Samples were incubated for 15 min at 37 °C, followed by addition of the [³²P]-labelled NV1 toe-printing primer designed to anneal ~ 100 nucleotides downstream from the anticipated ribosome-stalling site. The primer was extended by reverse transcriptase and the reaction products were analysed in sequencing gels. In experiments with mutant ribosomes, the 'Δ ribosome' version of the PURExpress kit was supplemented with ribosomes (10 pmol per reaction) isolated from the SQ171 *E. coli* strain carrying the plasmid expressing *E. coli rrmB* operon with the engineered mutations in the 23S rRNA gene. Mutant ribosomes were purified as described⁴¹.

Cell-free translation and analysis of peptidyl tRNA. Translation of the *ermBL* ORF for peptidyl tRNA analysis was carried out in the *E. coli* S30 cell-free transcription–translation system (Promega). PCR-generated DNA template carrying the *ermBL* gene (shown in blue) under the control of the *Ptac* promoter (green) had the following structure:

acggatccttgacaattaatcatcggtcgtataatgtgtggaattgtgagaggaggaaa
 acatatgttggatttccaatgctgaatgtagataaaacatctactattttgaaataa
 M L V F Q M R N V D K T S T I L K *

The DNA template (0.1–0.5 pmol) was translated in a 5 µl reaction containing 100 µCi of [¹⁴C]-Asp or [¹⁴C]-Lys (specific activity of both: 208 mCi mmol⁻¹) (American Radio Chemicals) following the manufacturer's protocol. When required, translation reactions were carried out in the presence of 50 µM ERY or borrelidin. After 30 min incubation at 37 °C, samples were analysed in a 16% bis-tris polyacrylamide gel using MES running buffer (as described in http://openwetware.org/Sauer:bis-Tris_SDS_PAGE based on US patent 6,162,338). Gels were dried and exposed overnight to a phosphorimager screen.

References

- Ito, K. & Chiba, S. Arrest peptides: cis-acting modulators of translation. *Annu. Rev. Biochem.* **82**, 171–202 (2013).
- Ramu, H., Mankin, A. & Vazquez-Laslop, N. Programmed drug-dependent ribosome stalling. *Mol. Microbiol.* **71**, 811–824 (2009).
- Vázquez-Laslop, N., Ramu, H. & Mankin, A. S. in *Ribosomes. Structure, function, evolution.* (eds Rodnina, M. V., Wintermeyer, W. & Green, R.) 377–392 (Springer-Verlag, 2011).
- Vázquez-Laslop, N., Ramu, H., Klepacki, D., Kannan, K. & Mankin, A. S. The key function of a conserved and modified rRNA residue in the ribosomal response to the nascent peptide. *EMBO J.* **29**, 3108–3117 (2010).
- Mayford, M. & Weisblum, B. The ermC leader peptide: amino acid alterations leading to differential efficiency of induction by macrolide-lincosamide-streptogramin B antibiotics. *J. Bacteriol.* **172**, 3772–3779 (1990).
- Kamimiyama, S. & Weisblum, B. Induction of erm2V by 16-membered-ring macrolide antibiotics. *Antimicrob. Agents Chemother.* **41**, 530–534 (1997).
- Min, Y. H., Kwon, A. R., Yoon, E. J., Shim, M. J. & Choi, E. C. Translational attenuation and mRNA stabilization as mechanisms of erm(B) induction by erythromycin. *Antimicrob. Agents Chemother.* **52**, 1782–1789 (2008).
- Seidelt, B. *et al.* Structural insight into nascent polypeptide chain-mediated translational stalling. *Science* **326**, 1412–1415 (2009).
- Bhushan, S. *et al.* Structural basis for translational stalling by human cytomegalovirus (hCMV) and fungal arginine attenuator peptide (AAP). *Mol. Cell* **40**, 138–146 (2010).
- Bhushan, S. *et al.* SecM-stalled ribosomes adopt an altered geometry at the peptidyltransferase center. *PLoS Biol.* **19**, e1000581 (2011).
- Dunkle, J. A., Xiong, L., Mankin, A. S. & Cate, J. H. Structures of the Escherichia coli ribosome with antibiotics bound near the peptidyl transferase center explain spectra of drug action. *Proc. Natl Acad. Sci. USA* **107**, 17152–17157 (2010).
- Tu, D., Blaha, G., Moore, P. & Steitz, T. Structures of MLSBK antibiotics bound to mutated large ribosomal subunits provide a structural explanation for resistance. *Cell* **121**, 257–270 (2005).
- Becker, T. *et al.* Structure of monomeric yeast and mammalian Sec61 complexes interacting with the translating ribosome. *Science* **326**, 1369–1373 (2009).
- Bhushan, S. *et al.* alpha-Helical nascent polypeptide chains visualized within distinct regions of the ribosomal exit tunnel. *Nat. Struct. Mol. Biol.* **17**, 313–317 (2010).
- Frauenfeld, J. *et al.* Cryo-EM structure of the ribosome-SecYE complex in the membrane environment. *Nat. Struct. Mol. Biol.* **18**, 614–621 (2011).
- Kannan, K. & Mankin, A. S. Macrolide antibiotics in the ribosome exit tunnel: species-specific binding and action. *Ann. NY Acad. Sci.* **1241**, 33–47 (2012).
- Vázquez-Laslop, N. *et al.* Role of antibiotic ligand in nascent peptide-dependent ribosome stalling. *Proc. Natl Acad. Sci. USA* **108**, 10496–10501 (2011).
- Vázquez-Laslop, N., Thum, C. & Mankin, A. S. Molecular mechanism of drug-dependent ribosome stalling. *Mol. Cell* **30**, 190–202 (2008).
- Hansen, J. L. *et al.* The structures of four macrolide antibiotics bound to the large ribosomal subunit. *Mol. Cell* **10**, 117–128 (2002).
- Harms, J., Schluenzen, F., Fucini, P., Bartels, H. & Yonath, A. Alterations at the peptidyl transferase centre of the ribosome induced by the synergistic action of the streptogramins dalfopristin and quinupristin. *BMC Biol.* **2**, 4 (2004).
- Schmeing, T. M., Huang, K. S., Kitchen, D. E., Strobel, S. A. & Steitz, T. A. Structural insights into the roles of water and the 2' hydroxyl of the P site tRNA in the peptidyl transferase reaction. *Mol. Cell* **20**, 437–448 (2005).
- Schmeing, T. M., Huang, K. S., Strobel, S. A. & Steitz, T. A. An induced-fit mechanism to promote peptide bond formation and exclude hydrolysis of peptidyl-tRNA. *Nature* **438**, 520–524 (2005).
- Simonovic, M. & Steitz, T. A. A structural view on the mechanism of the ribosome-catalyzed peptide bond formation. *Biochim. Biophys. Acta* **1789**, 612–623 (2009).

- Baker, T. S. & Johnson, J. E. Low resolution meets high: towards a resolution continuum from cells to atoms. *Curr. Opin. Struct. Biol.* **6**, 585–594 (1996).
- Rossmann, M. G. Fitting atomic models into electron-microscopy maps. *Acta Crystallogr. D Biol. Crystallogr.* **56**, 1341–1349 (2000).
- Fabiola, F. & Chapman, M. S. Fitting of high-resolution structures into electron microscopy reconstruction images. *Structure* **13**, 389–400 (2005).
- Polacek, N., Gaynor, M., Yassin, A. & Mankin, A. S. Ribosomal peptidyl transferase can withstand mutations at the putative catalytic nucleotide. *Nature* **411**, 498–501 (2001).
- Sievers, A., Beringer, M., Rodnina, M. V. & Wolfenden, R. The ribosome as an entropy trap. *Proc. Natl Acad. Sci. USA* **101**, 7897–7901 (2004).
- Horinouchi, S., Byeon, W. H. & Weisblum, B. A complex attenuator regulates inducible resistance to macrolides, lincosamides, and streptogramin type B antibiotics in Streptococcus sanguis. *J. Bacteriol.* **154**, 1252–1262 (1983).
- Jester, B. C., Leventgood, J. D., Roy, H., Ibba, M. & Devine, K. M. Nonorthologous replacement of lysyl-tRNA synthetase prevents addition of lysine analogues to the genetic code. *Proc. Natl Acad. Sci. USA* **100**, 14351–14356 (2003).
- Becker, T. *et al.* Structural basis of highly conserved ribosome recycling in eukaryotes and archaea. *Nature* **482**, 501–506 (2012).
- Frank, J. *et al.* SPIDER and WEB: processing and visualization of images in 3D electron microscopy and related fields. *J. Struct. Biol.* **116**, 190–199 (1996).
- Chen, J. Z. & Grigorieff, N. SIGNATURE: a single-particle selection system for molecular electron microscopy. *J. Struct. Biol.* **157**, 168–173 (2007).
- Dönhöfer, A. *et al.* Structural basis for TetM-mediated tetracycline resistance. *Proc. Natl Acad. Sci. USA* **109**, 16900–16905 (2012).
- Loerke, J., Giesebrecht, J. & Spahn, C. M. Multiparticle cryo-EM of ribosomes. *Methods Enzymol.* **483**, 161–177 (2010).
- Lasker, K. *et al.* Molecular architecture of the 26S proteasome holocomplex determined by an integrative approach. *Proc. Natl Acad. Sci. USA* **109**, 1380–1387 (2012).
- Pettersen, E. F. *et al.* UCSF Chimera—a visualization system for exploratory research and analysis. *J. Comput. Chem.* **25**, 1605–1612 (2004).
- Blaha, G., Gurel, G., Schroeder, S. J., Moore, P. B. & Steitz, T. A. Mutations outside the anisomycin-binding site can make ribosomes drug-resistant. *J. Mol. Biol.* **379**, 505–519 (2008).
- Selmer, M. *et al.* Structure of the 70S ribosome complexed with mRNA and tRNA. *Science* **313**, 1935–1942 (2006).
- Emsley, P. & Cowtan, K. Coot: model-building tools for molecular graphics. *Acta Crystallogr. D Biol. Crystallogr.* **60**, 2126–2132 (2004).
- Ohashi, H., Shimizu, Y., Ying, B. W. & Ueda, T. Efficient protein selection based on ribosome display system with purified components. *Biochem. Biophys. Res. Commun.* **352**, 270–276 (2007).
- Llano-Sotelo, B. *et al.* Binding and action of CEM-101, a new fluoroketolide antibiotic that inhibits protein synthesis. *Antimicrob. Agents Chemother.* **54**, 4961–4970 (2010).

Acknowledgements

This research was supported by grants from the NIHGM104370 (to A.S.M. and N.V.-L.), Deutsche Forschungsgemeinschaft W13285/2-1 (D.N.W.) and the EMBO young investigator grant (to D.N.W.).

Author contributions

D.N.W., N.V.-L. and A.S.M. designed the research; S.A., H.R. and P.G. performed the research. O.B. collected the EM data and S.A., H.R., P.G., R.B., N.V.-L., A.S.M. and D.N.W. analysed the data. N.V.-L., A.S.M. and D.N.W. wrote the paper.

Additional information

Accession codes: The cryo-EM map and associated molecular model of the ErmBL-SRC have been deposited in the EM databank under accession code EMD-5771 and the protein databank under PDB code 3J5L

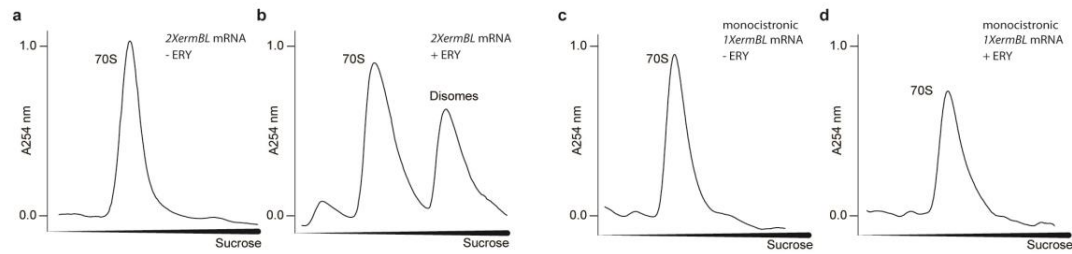
Supplementary Information accompanies this paper at <http://www.nature.com/naturecommunications>

Competing financial interests: The authors declare no competing financial interests.

Reprints and permission information is available online at <http://npg.nature.com/reprintsandpermissions/>

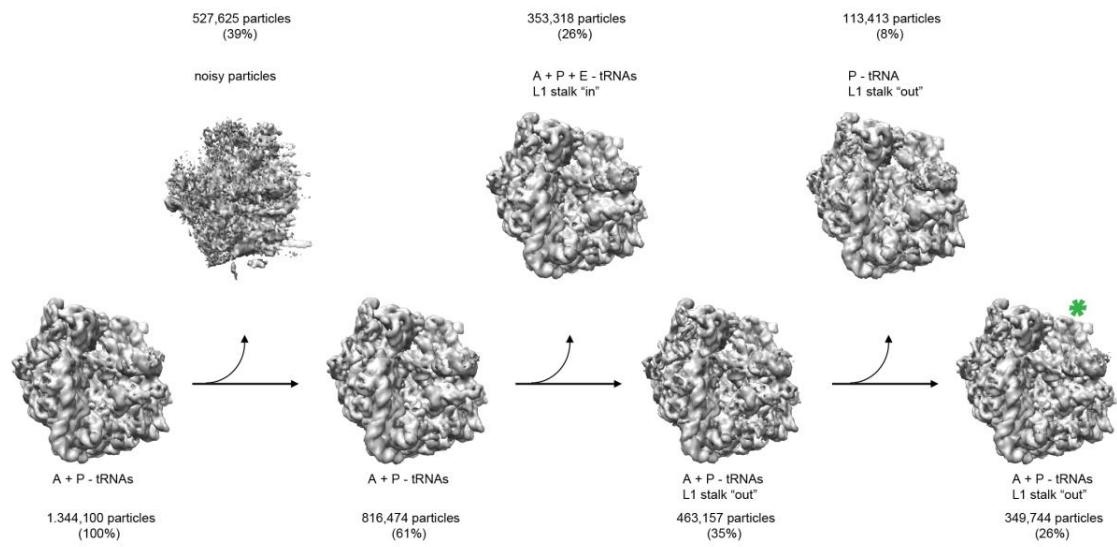
How to cite this article: Arenz, S. *et al.* Molecular basis for erythromycin-dependent ribosome stalling during translation of the ErmBL leader peptide. *Nat. Commun.* 5:3501 doi: 10.1038/ncomms4501 (2014).

Supplementary Figures



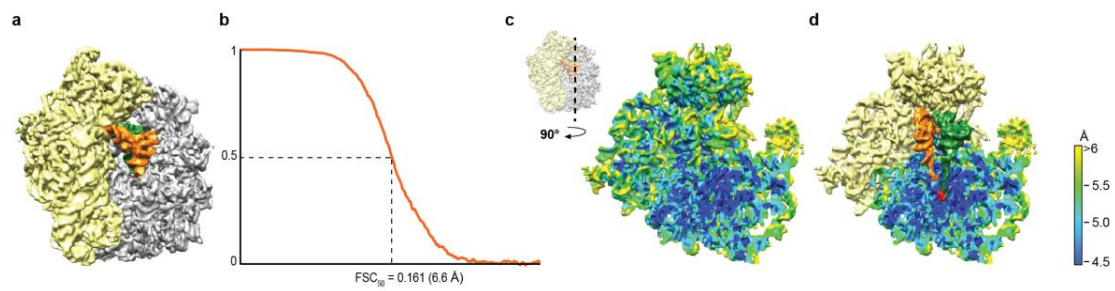
Supplementary Figure 1 Generation of ErmBL-SRC disomes

a, Sucrose gradient profiles of *in vitro* translation reactions of the bicistronic *ermBL* mRNA performed in the **(a)** absence and **(b)** presence of 10 μ M erythromycin. **c**, Sucrose gradient profiles of *in vitro* translation reactions of the monocistronic *ermBL* mRNA performed in the **(c)** absence or **(d)** presence of 10 μ M erythromycin.



Supplementary Figure 2 *In silico* sorting of the ErmBL-SRC

During the processing of the cryo-EM dataset of the ErmBL-SRC, several subpopulations of 70S ribosomes with differences in their tRNA occupancy and their conformational state could be separated subsequent to removal of noisy particles. The predominant homogenous population (26%) with stoichiometric occupancy of A- and P-tRNAs (marked by a green asterisk) was chosen for refinement.



Supplementary Figure 3 Average and local resolution determination of the ErmBL-SRC.

a, Overview of the ErmBL-SRC with 30S (yellow), 50S (grey), A-tRNA (orange) and P-tRNA (green) highlighted. **b**, Average resolution of the ErmBL-SRC was 6.6 Å using the Fourier shell correlation (FSC) cut-off value of 0.5. **c**, Local resolution displayed on the ErmBL-SRC with the 50S subunit cut (as depicted in inset) to reveal the ribosomal tunnel. **d**, as in c, but with 30S (yellow), A-tRNA (orange), P-tRNA (green) and erythromycin (red) highlighted for reference.

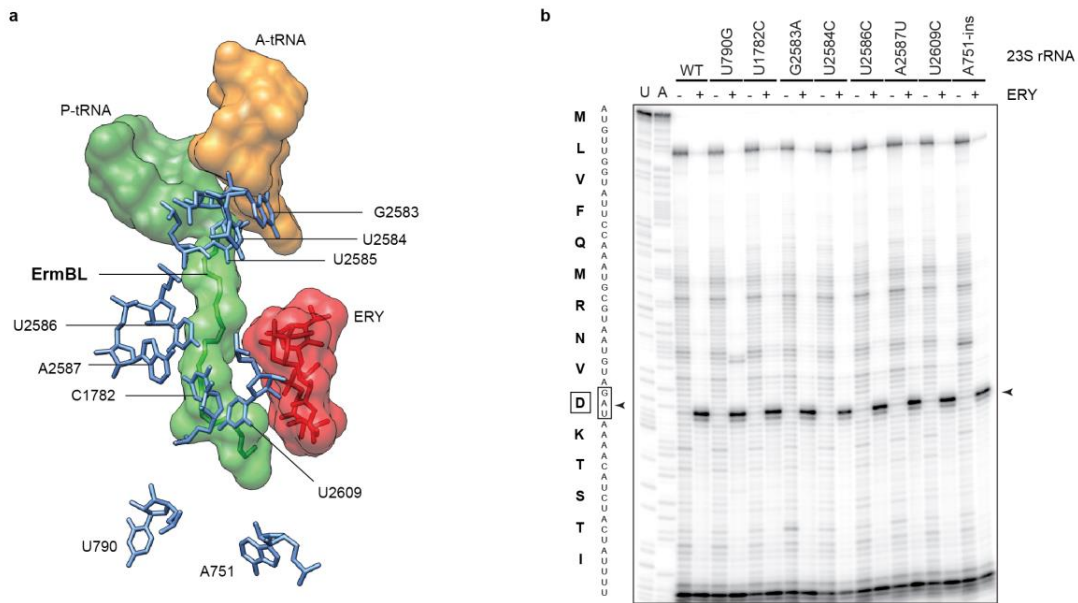


Figure 4 Mutations of 23S rRNA residues do not affect ErmBL-stalling.

23S rRNA nucleotides were chosen for mutagenesis on the basis of their proximity to the ErmBL nascent chain (a) and the ability of the mutant ribosomes to support cell growth. Mutant rRNA was expressed from an *rrnB* operon on a plasmid in the SQ171 strain that lacks chromosomal *rrn* alleles^{1,2} and the mutant ribosomes were isolated followed the published procedures³. b, The ribosomes were used in toeprinting assays, which were run in the absence (-) or presence (+) of 50 μ M of erythromycin (Ery). The toeprint band indicated by the arrow represents ribosomes arrested with the Asp (D10) *ermBL* codon in the P site.

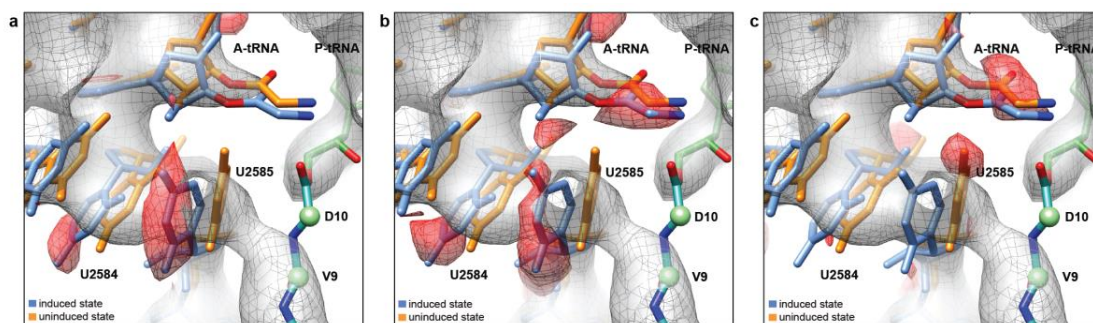


Figure 5 Difference density maps of ErmBL-SRC

a, Electron density maps were generated for the uninduced (orange, PDB1VQ6)⁴⁻⁶ and induced (blue, PDB1VQN)⁴⁻⁶ state of the PTC and a difference density map was generated (red mesh). Overlaid is the cryo-EM density map of the ErmBL-SRC (grey mesh). **b**, Electron density map was generated for the induced (blue, PDB1VQN)⁴⁻⁶ state of the PTC and a difference density map was generated (red mesh) by subtracting the cryo-EM density map of the ErmBL-SRC. For reference the uninduced state of the PTC (orange, PDB1VQ6)⁴⁻⁶ and the cryo-EM density map of the ErmBL-SRC (grey mesh) is also included. **c**, Electron density map was generated for the uninduced (orange, PDB1VQ6)⁴⁻⁶ state of the PTC and a difference density map was generated (red mesh) by subtracting the cryo-EM density map of the ErmBL-SRC. For reference the induced state of the PTC (blue, PDB1VQN)⁴⁻⁶ and the cryo-EM density map of the ErmBL-SRC (grey mesh) is also included. The cross correlation coefficient between the nucleobase of U2584 increases from 70% to 94% when comparing the fit between the induced and uninduced state with the ErmBL map.

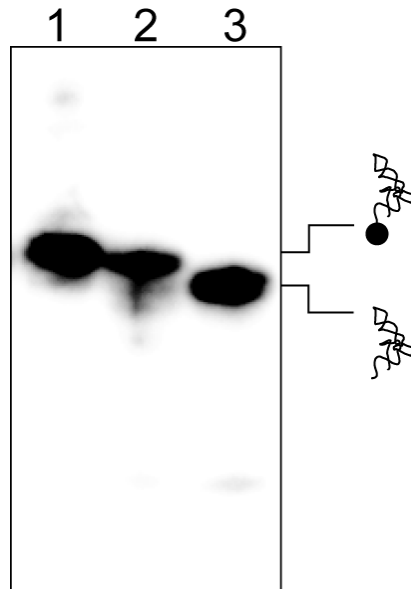


Figure 6 The ErmBL-SRC contains Lys-tRNA^{Lys} in the A-site and not deacylated tRNA^{Lys}. Analysis of the aminacylation status of the A-site bound tRNA^{Lys} in the ErmBL-SRC. Total RNA was extracted from the disome (ErmBL-SRC) material, fractionated in a denaturing acidic gel and subjected to Northern blotting using an oligonucleotide probe specific for tRNA^{Lys} (lane 1). Lys-tRNA^{Lys} marker (lane 2) was prepared by incubating total *E. coli* tRNA with a mixture of aminoacyl-tRNA synthetases in the PURExpress cell-free translation system lacking ribosomes (New England Biolabs). Total *E. coli* tRNA was used as deacylated tRNA^{Lys} marker (lane 3).

Supplemental References

- 1 Bollenbach, T., Quan, S., Chait, R. & Kishony, R. Nonoptimal microbial response to antibiotics underlies suppressive drug interactions. *Cell* **139**, 707-718 (2009).
- 2 Asai, T., Zaporjets, D., Squires, C. & Squires, C. L. An Escherichia coli strain with all chromosomal rRNA operons inactivated: complete exchange of rRNA genes between bacteria. *Proc Natl Acad Sci U S A* **96**, 1971-1976. (1999).
- 3 Ohashi, H., Shimizu, Y., Ying, B. W. & Ueda, T. Efficient protein selection based on ribosome display system with purified components. *Biochem Biophys Res Commun* **352**, 270-276 (2007).
- 4 Schmeing, T. M., Huang, K. S., Kitchen, D. E., Strobel, S. A. & Steitz, T. A. Structural insights into the roles of water and the 2' hydroxyl of the P site tRNA in the peptidyl transferase reaction. *Mol. Cell* **20**, 437-448 (2005).
- 5 Schmeing, T. M., Huang, K. S., Strobel, S. A. & Steitz, T. A. An induced-fit mechanism to promote peptide bond formation and exclude hydrolysis of peptidyl-tRNA. *Nature* **438**, 520-524 (2005).
- 6 Simonovic, M. & Steitz, T. A. A structural view on the mechanism of the ribosome-catalyzed peptide bond formation. *Biochim Biophys Acta* **1789**, 612-623 (2009).

Drug Sensing by the Ribosome Induces Translational Arrest via Active Site Perturbation

Stefan Arenz,¹ Sezen Meydan,² Agata L. Starosta,¹ Otto Berninghausen,¹ Roland Beckmann,^{1,3} Nora Vázquez-Laslop,² and Daniel N. Wilson^{1,3,*}

¹Gene Center and Department for Biochemistry, University of Munich, Feodor-Lynenstr. 25, 81377 Munich, Germany

²Center for Pharmaceutical Biotechnology, University of Illinois, Chicago, Chicago, IL 60607, USA

³Center for integrated Protein Science Munich (CIPSM), University of Munich, Feodor-Lynenstr. 25, 81377 Munich, Germany

*Correspondence: wilson@imb.uni-muenchen.de

<http://dx.doi.org/10.1016/j.molcel.2014.09.014>

SUMMARY

During protein synthesis, nascent polypeptide chains within the ribosomal tunnel can act in *cis* to induce ribosome stalling and regulate expression of downstream genes. The *Staphylococcus aureus* ErmCL leader peptide induces stalling in the presence of clinically important macrolide antibiotics, such as erythromycin, leading to the induction of the downstream macrolide resistance methyltransferase ErmC. Here, we present a cryo-electron microscopy (EM) structure of the erythromycin-dependent ErmCL-stalled ribosome at 3.9 Å resolution. The structure reveals how the ErmCL nascent chain directly senses the presence of the tunnel-bound drug and thereby induces allosteric conformational rearrangements at the peptidyltransferase center (PTC) of the ribosome. ErmCL-induced perturbations of the PTC prevent stable binding and accommodation of the aminoacyl-tRNA at the A-site, leading to inhibition of peptide bond formation and translation arrest.

INTRODUCTION

Nascent polypeptide-mediated translation regulation can be an intrinsic property of the nascent chain or require an additional ligand, such as an amino acid or antibiotic (Ramu et al., 2009; Vázquez-Laslop et al., 2011a). Similar to other inducible macrolide resistance genes, the *Staphylococcus aureus* *ermC* gene is controlled by programmed arrest during translation of the upstream *ermCL* leader peptide (Horinouchi and Weisblum, 1980; Iordănescu, 1976; Shivakumar et al., 1980) (Figure 1A): In the absence of erythromycin, ErmC expression is repressed because the ribosome-binding site (RBS) and AUG start codon of the *ermC* mRNA are sequestered in a stem-loop structure (Figure 1A). However, in the presence of subinhibitory concentrations of erythromycin, ribosomes translating the ErmCL leader peptide become stalled, leading to an alternative stem-loop structure in the mRNA that exposes the RBS and start codon of the *ermC* gene and thus allows ribosome binding and induction of ErmC expression (Figure 1A).

Previous studies demonstrated that polymerization of the ErmCL nascent chain halts because the ribosome is unable to catalyze peptide bond formation between the 9 aa long ErmCL-tRNA^{Ile} (codon 9) in the ribosomal P-site and Ser-tRNA^{Ser} (codon 10) in the A-site (Johansson et al., 2014; Vázquez-Laslop et al., 2008) (Figure 1A). Mutations of specific ErmCL amino acid residues located in the ribosomal exit tunnel of the ErmCL-SRC reduce or abolish stalling, as do mutations of certain rRNA nucleotides that comprise the tunnel wall (Johansson et al., 2014; Mayford and Weisblum, 1989; Vázquez-Laslop et al., 2008, 2010, 2011b). Additionally, the chemical structure of the macrolide antibiotic can influence ribosome stalling (Vázquez-Laslop et al., 2008, 2011b). Collectively, these findings indicate that ribosome stalling results from interactions between the ErmCL leader peptide, the macrolide, antibiotic and components of the ribosomal tunnel (Vázquez-Laslop et al., 2011a); however, a structural basis for this complex interplay is lacking.

To elucidate the nature of these interactions and ascertain how they lead to inactivation of the PTC of the ribosome, we generated ErmCL-SRC for structural analysis by cryo-electron microscopy (EM). The structure reveals the path of the ErmCL nascent polypeptide chain and its interactions with specific 23S rRNA nucleotides U2506, U2586, and A2062 within the ribosomal tunnel. Moreover, ErmCL is observed to directly interact with the cladinose sugar of erythromycin, thus revealing how the nascent chain monitors the presence of the tunnel-bound drug. Collectively, these interactions appear to stabilize a unique conformation of the ErmCL nascent chain that induces global rearrangements at the peptidyltransferase center (PTC) of the ribosome, which in turn prevent stable binding and accommodation of the A-tRNA, and thus induce translational arrest.

RESULTS

Cryo-EM Structure of the ErmCL-SRC

The ErmCL-SRC was generated by translation of a dicistronic *2XermCL* mRNA in the presence of 10 μM erythromycin using an *E. coli* lysate-based in vitro translation system. The ErmCL-SRC disomes were isolated by sucrose gradient purification, converted to monosomes, and directly applied to cryogrids (Figure S1 available online), as performed previously for the ErmBL-SRC (Arenz et al., 2014). Data collection was performed on a Titan Krios TEM fitted with the Falcon II direct electron detector (FEI, Netherlands), and images were processed with SPIDER

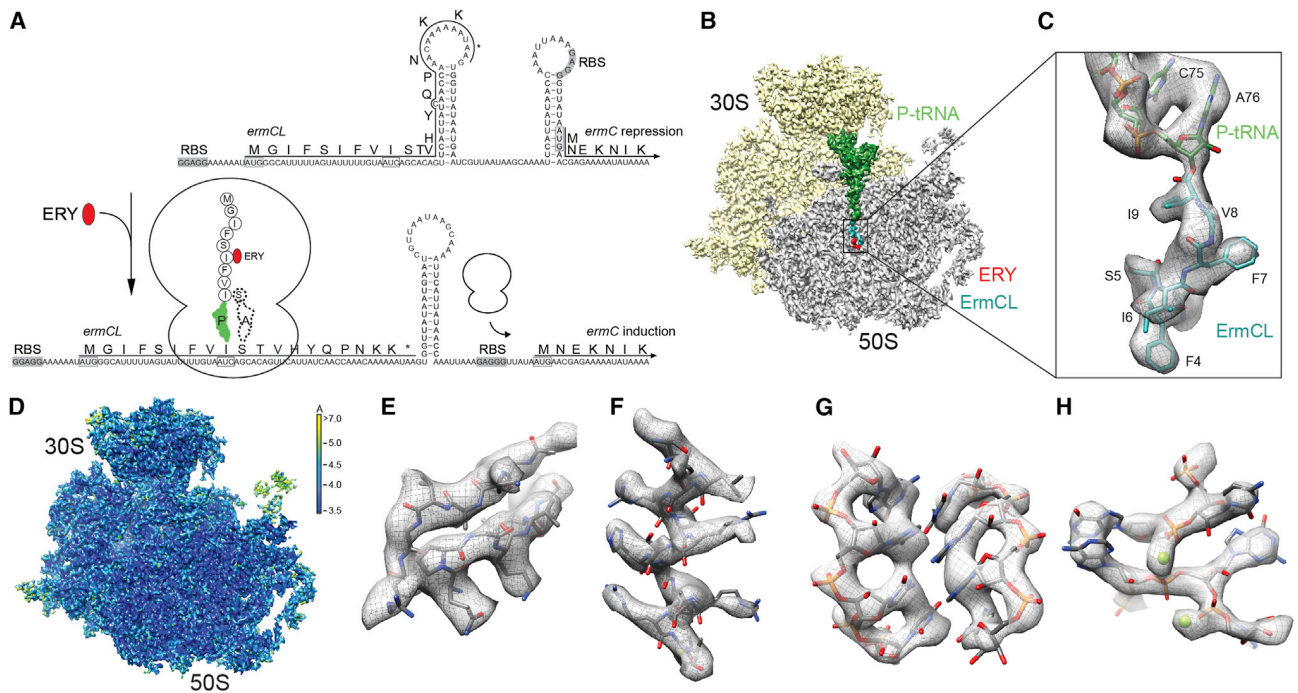


Figure 1. Cryo-EM Structure of the ErmCL-SRC

(A) Schematic for *ermCL*-dependent regulation of *ermC* translation in the presence of erythromycin (ERY).

(B) Transverse section of the ErmCL-SRC, with 30S (yellow), 50S (gray), P-tRNA (green), ErmCL (teal), and ERY (red).

(C) Zoom showing electron density (gray) and model for the ErmCL nascent chain (teal) attached to CCA-end of the P-tRNA (green).

(D) As (B), but colored according to local resolution.

(E–H) Examples of electron density in the ErmCL-SRC map including (E) β strands and (F) α helix in ribosomal proteins, (G) rRNA helix, and (H) coordinated Mg^{2+} ions. See also Figure S1.

(Frank et al., 1996) (see Experimental Procedures). In silico sorting of cryo-EM images yielded one major homogeneous subpopulation of ribosomes bearing a P-tRNA but lacking A-tRNA (Figures 1B and 1C), which contrasts with the previous cryo-EM reconstruction of the ErmBL-SRC that contained tRNAs in both the A- and P-sites (Arenz et al., 2014). The ErmCL-SRC has an average resolution of 3.9 Å, while local resolution calculations indicate that the ribosomal core reaches 3.5 Å (Figures 1D and S1). Rigid-body docking of crystallographic structures of the *E. coli* ribosome (Pulk and Cate, 2013) reveals excellent agreement with the cryo-EM map, such as strand separation in β sheets (Figure 1E) and the pitch of α helices (Figure 1F) within the ribosomal proteins, as well as density for the majority of the amino acid side chains (Figures 1E and 1F). Additionally, the rRNA backbone and nucleotides are well-resolved, as well as the position of many magnesium ions (Figures 1G and 1H). The distinct features of the electron density allowed the CCA-end of the P-tRNA to be accurately placed and a model for residues 3–9 of the ErmCL leader peptide to be built de novo (Figure 1C).

Critical Interactions of ErmCL with Components of the Ribosomal Tunnel

The overall path of the ErmCL nascent chain within the ribosomal tunnel is shifted toward erythromycin when compared with the path of ErmBL (Arenz et al., 2014) (Figure S2). Four sites of con-

tact are observed between the ErmCL nascent chain and components of the ribosomal tunnel (Figures 2A, 2B, and S3): At the C terminus of ErmCL, U2506 interacts with V8 and stacks upon the aromatic side chain of F7, whereas I6 interacts with U2586 (Figure 2A). These contacts are likely to be important, since mutations to alanine in the conserved “IFVI” motif (I6–I9) of ErmCL severely reduce ribosome stalling (Johansson et al., 2014; Vázquez-Laslop et al., 2008). Although mutation of U2586 to A, C, or G did not affect wild-type ErmCL stalling (Figure 2C), the stalling efficiency of the I6A-ErmCL mutant could be partially rescued by the U2586 mutations (Figure 2C). This functional interplay between U2586 and I6 is consistent with the direct interaction observed in the structure (Figure 2A). To investigate this contact further, we generated all possible amino acid substitutions at position 6 of ErmCL and monitored the efficiency of stalling by toe-printing (Figure S4). The results indicated that the hydrophobic amino acids M, V, and L (and to a lesser extent the charged amino acid E) at position 6 maintained efficient ribosome stalling, whereas all other substitutions further reduced the stalling efficiency.

An interaction is also observed from the N terminus of ErmCL with A2062 (Figure 2D); however, due to the poor density (indicating flexibility) of the N terminus (Figure S3), we can only tentatively assign this interaction with A2062 to I3 and could not model the very N-terminal residues M1–G2. While alanine scanning mutagenesis indicates that the nature of the N-terminal residues

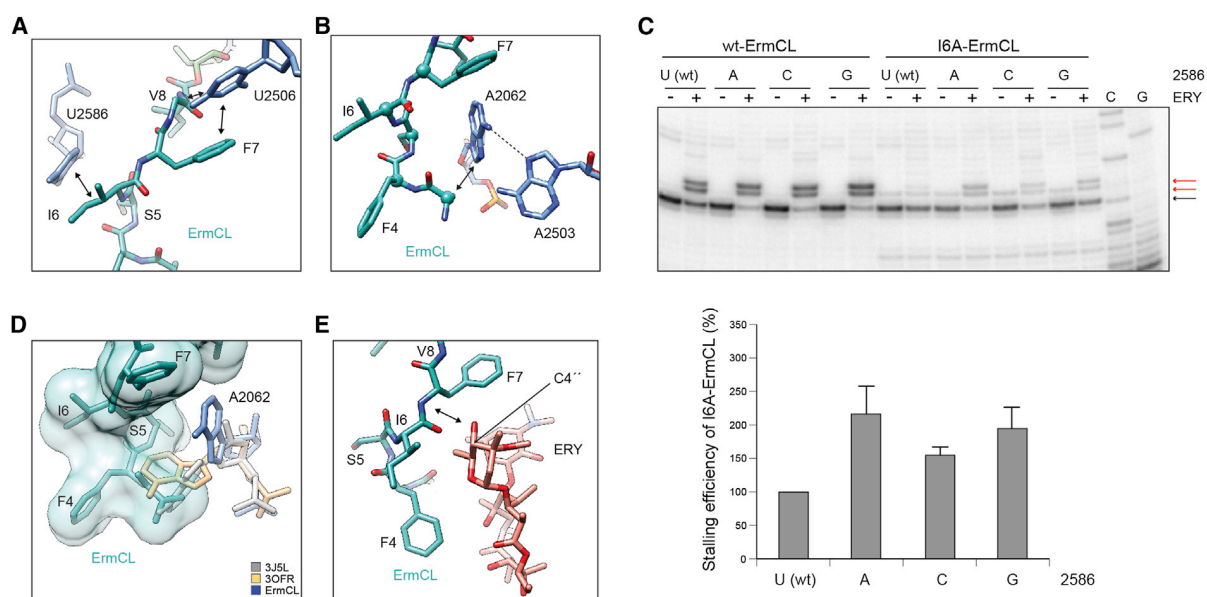


Figure 2. Interaction of the ErmCL Nascent Chain within the Ribosomal Tunnel

(A and B) ErmCL (teal) contacts (arrowed) with 23S rRNA nucleotides (A) U2506, U2586, and (B) A2062.

(C) Toe-printing of wild-type (wt) and mutant (I6A) ErmCL translation on *E. coli* ribosomes with wt (U2586) or U2586A/C/G mutants, in the presence (+) or absence (-) of ERY. All reactions contained the Thr-tRNA synthetase inhibitor borrelidin, which halts translation at the Thr (T11) codon in the absence of ERY-induced arrest at the Ile (I9) codon. Error bars represent one SD of the mean.

(D) Spacefill representation of ErmCL (teal) illustrating the steric clash with A2062 positions from PDB3OFR (Dunkle et al., 2010) (yellow) and ErmBL-SRC (PDB ID 3J5L, gray) (Arenz et al., 2014). For comparison, the A2062 position in ErmCL-SRC is shown (blue).

(E) Sensing of the C3 cladinose sugar of ERY (Dunkle et al., 2010) (red) by the ErmCL nascent chain (teal). See also Figures S2–S4.

G2–S5 is not critical for ribosome stalling (Johansson et al., 2014; Vázquez-Laslop et al., 2008), truncation of more than two N-terminal residues of ErmCL notably reduced stalling (Vázquez-Laslop et al., 2008), suggesting that the I3 position is at least sterically important for the stalling mechanism. In this regard, we note that in the ErmCL-SRC, A2062 is stabilized in a conformation that lies flat against the tunnel wall (Figures 2B and S3), whereas the A2062 conformation that protrudes into the tunnel lumen observed in the majority of ribosome structures (Vázquez-Laslop et al., 2010), including the ErmBL-SRC (Arenz et al., 2014), would sterically clash with the ErmCL nascent chain (Figure 2D). In the flat conformation, the N7 of A2062 is within hydrogen bonding distance of the exocyclic amino group of A2503 (Figure 2B), suggesting that the steric role of the N terminus of ErmCL may be to induce the previously noted interaction between A2062 and A2503 (Vázquez-Laslop et al., 2010). Consistently, mutations of A2062U/C or A2503G dramatically reduce ErmCL stalling (Vázquez-Laslop et al., 2010; Vázquez-Laslop et al., 2008). In the absence of conformational changes with previously proposed relays from A2062/A2503 back to the PTC (Vázquez-Laslop et al., 2010), we favor a model whereby A2062/A2503 exert an effect on the PTC via the ErmCL nascent chain.

Drug Sensing by the ErmCL Nascent Chain within the Ribosomal Tunnel

In the ErmCL-SRC, erythromycin is bound in the canonical position (Dunkle et al., 2010; Tu et al., 2005), as observed previously

in the ErmBL-SRC (Arenz et al., 2014). However, unlike the ErmBL-SRC (Arenz et al., 2014), direct contact is observed between ErmCL and the drug (Figures 2E and S3), possibly between the backbone N of F7 and the C4''-OH of the cladinose sugar of erythromycin; however, higher resolution will be required to verify this. Biochemical experiments support ErmCL monitoring for the presence and the structure of the drug; specifically, ErmCL-mediated stalling was observed in the presence of other cladinose-containing macrolides but not in the presence of ketolide antibiotics, such as telithromycin, which lack the C3-cladinose (Vázquez-Laslop et al., 2008, 2011b) (Figure S4). Moreover, macrolides bearing modifications of the C3-cladinose are also impaired for ErmCL-mediated ribosome stalling (Vázquez-Laslop et al., 2011b).

Inactivation of the PTC of the Ribosome by ErmCL

To understand how the interaction of ErmCL with erythromycin and rRNA components of the exit tunnel prevents stable binding of the A-tRNA and therefore leads to inhibition of peptidyl-transfer, we compared the PTC of the ErmCL-SRC with crystal structures of the ribosome in different states of peptide bond formation (Schmeing et al., 2002, 2005a, 2005b; Voorhees et al., 2009) (Figure 3A). While the overall conformation of the PTC is similar between ErmCL and the crystal structures, a few clear differences are evident. In the fully functional ribosome, U2585 rotates by 19° upon A-tRNA accommodation (i.e., when moving from the unaccommodated [uninduced] to the accommodated [induced] state) (Schmeing et al., 2002, 2005a,

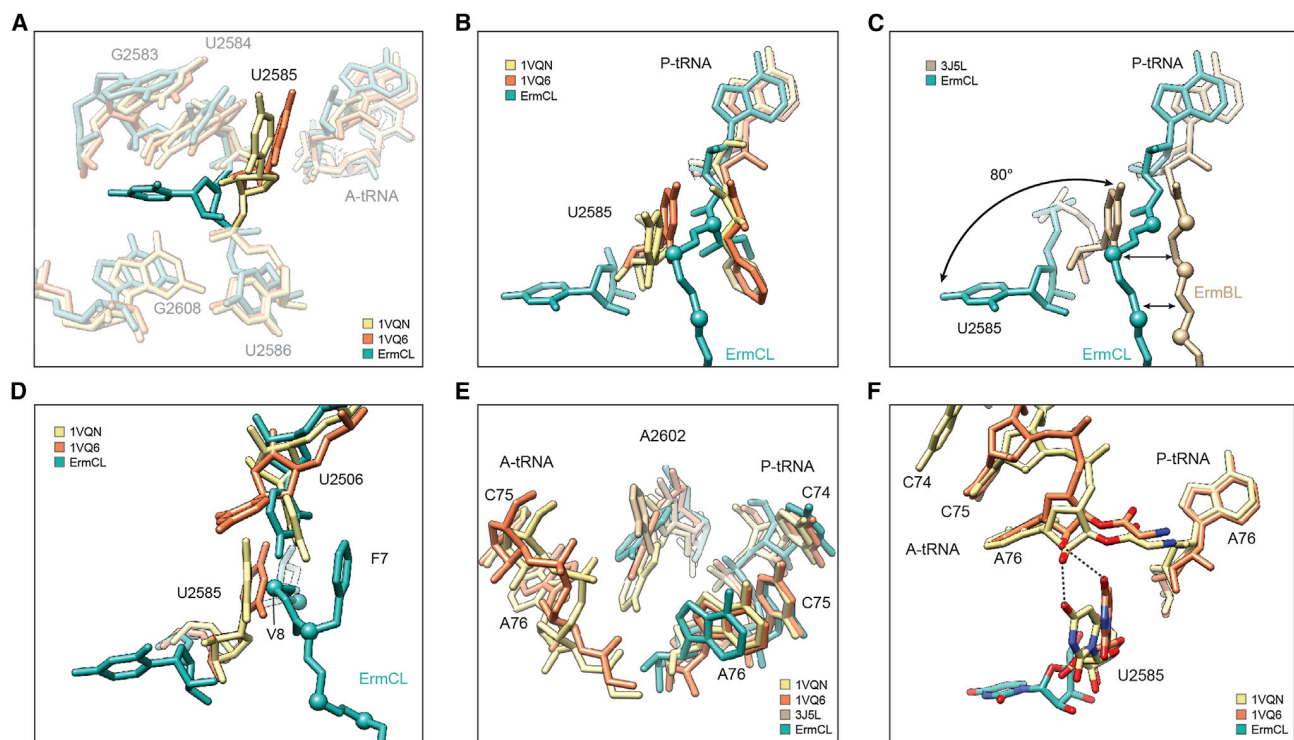


Figure 3. Conformational Changes at the PTC of the ErmCL-SRC

(A and B) Flipped conformation of 23S rRNA nucleotide U2585 in ErmCL-SRC (teal) compared to canonical position of U2585 in the uninduced (PDB1VQ6, orange) and induced (PDB1VQN, yellow) states of the PTC (Schmeing et al., 2005a, 2005b).

(C) Comparison of ErmCL (teal) and ErmBL (PDB3J5L, tan) (Arenz et al., 2014) nascent chains and respective U2585 positions.

(D and E) Relative positions of (D) U2585 and U2506, and (E) A2602 in ErmCL-SRC (teal), uninduced (PDB1VQ6, orange), and induced (PDB1VQN, yellow) states of the PTC (Schmeing et al., 2005a, 2005b). In (E), A2602 position of ErmBL-SRC (PDB3J5L, tan) (Arenz et al., 2014) is included for reference.

(F) The flipped U2585 position in ErmCL-SRC (teal) prevents stabilization of the A-tRNA as observed in the uninduced (PDB1VQ6, orange) and induced (PDB1VQN, yellow) state of the PTC (Schmeing et al., 2005a, 2005b). See also Figure S3.

2005b) (Figure 3A). Surprisingly, U2585 adopts a dramatically different conformation in ErmCL-SRC, such that it is rotated by 80° compared to the unaccommodated state, and is flipped into a pocket formed by U2584/G2583 and G2608 (Figures 3A and 3B). This is reminiscent of the large rotation (180°) of U2585 observed upon streptogramin binding to the *Deinococcus radiodurans* 50S subunit (Harms et al., 2004); however, the final position is distinct (Figure S3). The positions of U2585 in the fully accommodated state would sterically clash with the ErmCL nascent chain, which may be the cause of the flipped state of U2585 in the ErmCL-SRC (Figure 3B). This contrasts with the ErmBL-SRC, where the path of the ErmBL nascent chain is compatible with (and even proposed to stabilize) the position of U2585 in the unaccommodated state (Arenz et al., 2014) (Figure 3C).

In the *Haloarcula marismortui* 50S crystal structures, U2506 is also observed to undergo a shift upon A-tRNA accommodation, such that the base interacts with U2585 (Schmeing et al., 2002, 2005a, 2005b) (Figure 3D). In the ErmCL-SRC, U2506 adopts a position similar to (but distinct from) U2506 in the accommodated state, which establishes interactions with residues V8 and F7 of ErmCL and is thereby presumably stabilized by the shifted conformation of the nascent chain (Figure 3D). Further-

more, A2602 is observed to undergo a slight shift upon A-tRNA accommodation (Figure 3E). In the ErmCL-SRC, A2602 appears to adopt a defined position (Figure S3), similar to the unaccommodated state but slightly shifted toward the A-tRNA (Figure 3E), which may also influence A-tRNA stability. During binding and accommodation of the A-tRNA, the ribose 2'OH of A76 maintains hydrogen bonding distance to the C4 oxygen of U2585 (Schmeing et al., 2005a; Schmeing et al., 2005b; Schmeing et al., 2002), which is also observed for the unaccommodated A-tRNA in the ErmBL-SRC (Arenz et al., 2014). In contrast, this contact is not possible with the flipped position of U2585 in the ErmCL-SRC (Figure 3F).

DISCUSSION

Collectively, our biochemical and structural findings lead us to propose a model for ErmCL-mediated drug-dependent ribosome stalling (Figure 4): While the exact conformation of the ErmCL peptide within the ribosomal tunnel in the absence of erythromycin has yet to be determined, biochemical studies indicate that peptide bond formation between Ser-tRNA in the A-site and the ErmCL-tRNA in the P-site can occur (Johansson et al., 2014; Vázquez-Laslop et al., 2008) (Figure 4A).

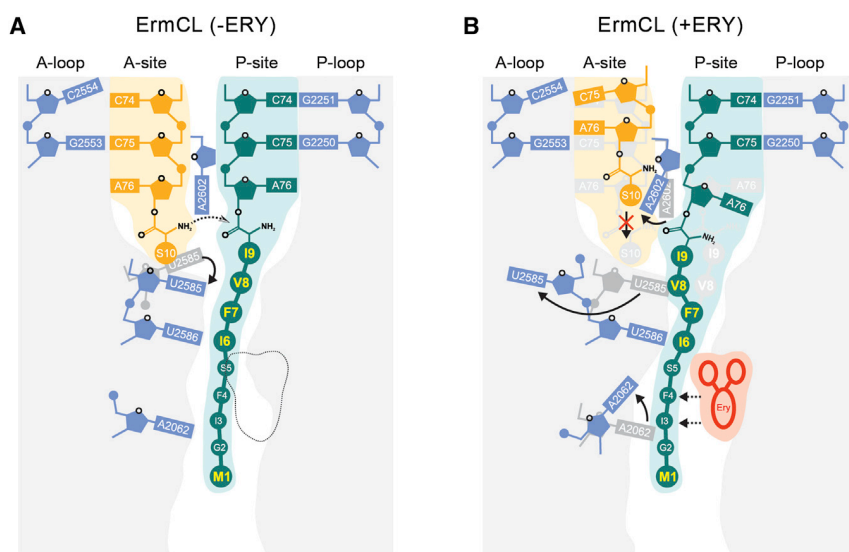


Figure 4. Schematic Model of ErmCL-Mediated Translation Arrest

(A) In the absence of erythromycin (-ERY), Ser-tRNA accommodates at the A-site enabling peptide bond formation with the ErmCL-tRNA in the P-site.

(B) In contrast, in the presence of erythromycin, the ErmCL nascent chain adopts a distinct conformation that promotes conformational rearrangements of 23S rRNA nucleotides A2062 and A2602 and, most dramatically, flipping of U2585. Collectively, this global rearrangement of the PTC prevents stable binding and accommodation of Ser-tRNA at the ribosomal A-site and thus results in translational arrest.

However, in the presence of erythromycin, the ErmCL nascent chain interacts with the drug and adopts a unique conformation that is stabilized via interactions with specific rRNA components of the tunnel such as U2586, U2506, and A2062 (Figure 4B). In this stalled state, the ErmCL nascent chain precludes the canonical position of U2585 and promotes an alternative flipped conformation, which together with shifted P-tRNA and A2602 positions remodels the PTC making it unfavorable for the A-tRNA to fully accommodate and therefore leads to dissociation and translation arrest (Figure 4B). The absence of Ser-tRNA in the A-site of the ErmCL-SRC (Figure 1B) is consistent with previous single-molecule fluorescence experiments demonstrating that the A-site of ErmCL-SRC has a reduced capability to stably bind A-tRNA (Johansson et al., 2014). This contrasts with the structures of ErmBL- and SecM-stalled ribosomes, where stable tRNA binding was observed at the ribosomal A-site (Arenz et al., 2014; Bhushan et al., 2011).

In conclusion, our study illustrates how the ribosome can employ the ErmCL nascent chain to monitor the presence of erythromycin and induce allosteric conformational rearrangements within the PTC active site, leading to translational stalling and regulation of expression of downstream genes. The distinct mechanisms of drug sensing and active site perturbation utilized by ErmCL and ErmBL (Arenz et al., 2014) raise the question as to whether similar mechanisms are utilized by other drug-dependent stalling systems.

EXPERIMENTAL PROCEDURES

Generation and Purification of ErmCL-SRC

ErmCL-SRC were generated following the same procedure as previously described (Arenz et al., 2014). The *2xermCL* construct was synthesized (Eurofins, Martinsried) such that it contained a T7 promoter followed by a strong ribosome binding site (RBS) spaced by 7 nt to the ATG start codon of the first *ermCL* cistron. A linker of 22 nt separated the stop codon of the first *ermCL* cistron and the start codon of the second *ermCL* cistron. The linker also comprised the strong RBS 7 nt upstream of the ATG start codon of the second *ermCL* cistron, enabling initiation of translation independent from the first *ermCL* cistron. Each

ermCL cistron encoded amino acids 1–19 corresponding to ErmCL leader peptide (GenBank accession number V01278) present on macrolide resistance plasmid pE194 (Iordănescu, 1976; Narayanan and Dubnau, 1985). The complete sequence of the *2xermCL* construct is as follows:

5'-TAATACGACTCACTATAGGGAGTTTTATAAGGAGGAAAAAATATGGGC

ATTTTTAGTATTTTTGTAATCAGCACAGTTCATTATCAACCAACAAAAAATA

AAGTTTTATAAGGAGGAAAAAATATGGGCATTTTTAGTATTTTTGTAATCAG

CAGAGTTCATTATCAACCAACAAAAAATAA-3' (T7 Promoter, italics; RBS, bold; the ATC codon in the P-site of the stalled ribosome is shown in bold; annealing site for complementary DNA oligonucleotide, underlined).

In vitro translation of the *2xermCL* construct was performed using the Rapid Translation System RTS 100 *E. coli* HY Kit (5PRIME; catalog number 2401110).

Translation reactions were analyzed on sucrose density gradients (10%–55% sucrose in a buffer A, containing 50 mM HEPES-KOH [pH 7.4], 100 mM KOAc, 25 mM Mg(OAc)₂, 6 mM β-mercaptoethanol, 10 μM erythromycin, and 1 × Complete EDTA-free Protease Inhibitor cocktail [Roche]) by centrifugation at 154,693 × *g* (SW-40 Ti, Beckman Coulter) for 3 hr at 4°C. For ErmCL-SRC purification, disome fractions were collected using a Gradient Station (Biocomp) with an Econo UV Monitor (Biorad) and a FC203B Fraction Collector (Gilson). Purified ErmCL-SRC disomes were concentrated by centrifugation through Amicon Ultra-0.5 ml Centrifugal Filters (Merck-Millipore) according to the manufacturer's protocol. To obtain monosomes of the ErmCL-SRC, a short DNA oligonucleotide (5'-ttctctctataaaact-3', Metabion) was annealed to the linker between the *ermCL* cistrons of the disomes, generating a DNA-RNA hybrid that could be cleaved by RNase H (NEB) treatment in buffer A at 25°C for 1 hr. After cleavage of the disomes, ErmCL-SRC monosomes were again purified and concentrated by centrifugation through Amicon Ultra-0.5 ml Centrifugal Filters (Merck-Millipore) according to the manufacturer's protocol.

Negative-Stain EM

Ribosomal particles were diluted in buffer A to final concentrations of 0.5 *A*₂₆₀/ml up to 5 *A*₂₆₀/ml in order to determine the optimal ribosome density for cryo-EM. One drop of each sample was deposited on a carbon-coated grid. After 30 s, grids were washed with distilled water and then stained with three drops of 2% aqueous uranyl acetate for 15 s. The remaining liquid was removed by touching the grid with filter paper. Micrographs were taken using a Morgagni transmission electron microscope (FEI), 80 kV, wide angle 1K CCD at direct magnifications of 72K.

Cryo-EM and Single-Particle Reconstruction

A total of 4 *A*₂₆₀/ml monosomes of the ErmCL-SRC were applied to 2 nm pre-coated Quantifoil R3/3 holey carbon supported grids and vitrified using a Vitrobot Mark IV (FEI Company). Data collection was performed at NeCEN (Leiden) on a Titan Krios transmission electron microscope (TEM) (FEI, Eindhoven)

equipped with a Falcon II direct electron detector at 300 kV with a magnification of 125,085 \times , a pixel size of 1.108 Å, and a defocus range of 0.7–1.2 μm . The data are provided as a series of seven frames (dose per frame of 4 $\text{e}^-/\text{Å}^2$) from which we summed frames 2–5 (accumulated dose of 20 $\text{e}^-/\text{Å}^2$) after alignment using Motion Correction software (Li et al., 2013). Images were processed using a frequency-limited refinement protocol that helps prevent overfitting (Scheres and Chen, 2012), specifically by truncation of high frequencies (in this case, at 8 Å). As reported and expected (Scheres and Chen, 2012), we find that using this processing regime the 0.143 FSC value provides a good indicator for the true average resolution of the map. Additionally, the local resolution of the map was calculated using ResMap (Kucukelbir et al., 2014). Power-spectra and defocus values were determined using the SPIDER TF ED command, and recorded images were manually inspected for good areas and power-spectra quality. Data were processed further using the SPIDER software package (Frank et al., 1996), in combination with an automated workflow as described previously (Becker et al., 2012). After initial, automated particle selection based on the program SIGNATURE (Chen and Grigorieff, 2007), initial alignment was performed with 419,113 particles using *E. coli* 70S ribosome as a reference structure (Arenz et al., 2014). After removal of noisy particles (47,340 particles; 11%), the data set could be sorted into two main subpopulations using an incremental K-means-like method of unsupervised 3D sorting (Loerke et al., 2010):

The major subpopulation (285,841 particles; 68%) was defined by the presence of stoichiometric densities for P-tRNA and could be refined to an average resolution of 3.9 Å (0.143 FSC) and a local resolution extending to 3.5 Å for the core of the 30S and 50S subunit as computed using ResMap (Kucukelbir et al., 2014) (Figure S1). The final map was subjected to the program EM-BFACTOR (Fernández et al., 2008) in order to apply an automatically determined negative B-factor for sharpening of the map.

Molecular Modeling and Map-Docking Procedures

The molecular model for the ribosomal proteins and rRNA of the ErmCL-SRC is based on the molecular model for the 50S subunit from the recent crystal structure of the *E. coli* 70S ribosome (PDB ID 4KIX) (Pulk and Cate, 2013) and obtained by performing a rigid body fit into the cryo-EM density map of the ErmCL-SRC using UCSF Chimera (Pettersen et al., 2004) (fit in map function). Similarly, the position of erythromycin was identical to that observed previously (Dunkle et al., 2010; Tu et al., 2005) and obtained by rigid body fit of PDB3OFR (Dunkle et al., 2010) into the cryo-EM density map of the ErmCL-SRC. The overall fit of the crystal structures were in very good agreement with the electron density of ErmCL-SRC, and since exclusively the conformations of important nucleotides of the PTC and the exit tunnel are crucial to interpret the molecular mechanism leading to stalling on ErmCL, only these 23S rRNA nucleotides (A2602, G2583, U2584, U2585, U2586, U2506, and A2062), were manually shifted/rotated where necessary into their respective densities using Coot (Emsley and Cowtan, 2004), whereas the rest of the rigid-body-fitted crystal structure remained unchanged. The conformation of A2602 observed in ErmCL-SRC is distinct from the “up” conformation observed in ErmBL-SRC (PDB3J5L) (Arenz et al., 2014) and from the “down” conformation (in PDB1VQN) (Schmeing et al., 2005a, 2005b). As such, its conformation resembles an intermediate state between “up” and “down.” The conformation of U2506 is similar to its conformation in (PDB1VQN) (Schmeing et al., 2005a, 2005b); however, slight manual rotation of the base was required to get an optimal fit. Different conformations of A2062—e.g., the “down” (PDB2WRJ) (Gao et al., 2009) and “tunnel-in” (PDB3I8F) (Jenner et al., 2010)—conformations sterically clash with the ErmCL nascent chain, whereas the “up” conformation present in the *Haloarcula marismortui* 50S subunit in complex with model peptide bond substrates (e.g., PDB1VQN) (Schmeing et al., 2005a, 2005b) was similar to the conformation of A2062 observed in the ErmCL-SRC. Most notably, U2585 adopts a unique and novel “flipped out” position, which is very different to previously observed positions for U2585 (i.e., U2585 in the uninduced [PDB1VQ6] or [PDB1VQN] induced state of the PTC) (Schmeing et al., 2005a, 2005b). In the novel, “flipped-out” conformation, U2585 is rotated approximately 80° when compared to its canonical position. In order to regularize the rRNA backbone surrounding U2585, neighboring nucleotides G2583, U2584, and U2586 were slightly adjusted in the model for ErmCL-SRC. Besides 23S rRNA nucle-

otides, the CCA-end of the P-tRNA, in particular A76, was manually adjusted in order to fit the density, since previously reported conformations observed in crystal structures of the *Haloarcula marismortui* 50S subunit in complex with model peptide bond substrates did not fit the density when fitted as a rigid body together with the 50S subunit. The molecular model for the ErmCL nascent polypeptide chain was modeled and refined into the density using Coot (Emsley and Cowtan, 2004).

Figure Preparation

Figures showing electron densities and atomic models were generated using UCSF Chimera (Pettersen et al., 2004).

Toe-Printing Assay

The DNA templates containing T7 promoter, ribosome binding site, and the ErmCL coding ORF (wild-type or the mutants) were generated by crossover PCR. The toeprinting analysis of drug-dependent ribosome stalling was carried out as described (Vázquez-Laslop et al., 2008). Briefly, the DNA templates (0.1 pmol) were used in a total volume of 5 μl of PURExpress (NEB) cell-free transcription-translation reactions. Samples were incubated for 15 min at 37°C, followed by addition of the [^{32}P]-labeled NV1 toe-printing primer designed to anneal ~100 nt downstream from the anticipated ribosome stalling site. The primer was extended by reverse transcriptase, and the reaction products were analyzed in sequencing gels. In experiments with mutant ribosomes, the “ Δ ribosome” version of the PURExpress kit was supplemented with ribosomes (10 pmol per reaction) isolated from the SQ171 *E. coli* strain carrying the plasmid expressing *E. coli rrmB* operon with the engineered mutations in the 23S rRNA gene. Wild-type and mutant ribosomes were purified as described (Ohashi et al., 2007).

ACCESSION NUMBERS

The cryo-EM map and associated atomic coordinates have been deposited in the EMDB and PDB with the accession codes EMDB-6057 and PDB ID 3J7Z, respectively.

SUPPLEMENTAL INFORMATION

Supplemental Information includes four figures and can be found with this article online at <http://dx.doi.org/10.1016/j.molcel.2014.09.014>.

ACKNOWLEDGMENTS

We thank Rishi Matadeen and Sacha DeCarlo for data collection at the NeCEN facility (Leiden) and Charlotte Ungewickell and Dorota Klepacki for expert technical assistance. This research was supported by grants from the NIH (GM106386 to N.V.-L. and R01GM095737 to D.N.W.) and the Deutsche Forschungsgemeinschaft (FOR1805, WI3285/3-1, and GRK1721 to D.N.W.).

Received: July 15, 2014

Revised: September 8, 2014

Accepted: September 11, 2014

Published: October 8, 2014

REFERENCES

- Arenz, S., Ramu, H., Gupta, P., Berninghausen, O., Beckmann, R., Vázquez-Laslop, N., Mankin, A.S., and Wilson, D.N. (2014). Molecular basis for erythromycin-dependent ribosome stalling during translation of the ErmBL leader peptide. *Nat. Commun.* 5, 3501.
- Becker, T., Franckenberg, S., Wickles, S., Shoemaker, C.J., Anger, A.M., Armache, J.P., Sieber, H., Ungewickell, C., Berninghausen, O., Daberkow, I., et al. (2012). Structural basis of highly conserved ribosome recycling in eukaryotes and archaea. *Nature* 482, 501–506.
- Bhushan, S., Hoffmann, T., Seidelt, B., Frauenfeld, J., Mielke, T., Berninghausen, O., Wilson, D.N., and Beckmann, R. (2011). SecM-stalled ribosomes adopt an altered geometry at the peptidyl transferase center. *PLoS Biol.* 9, e1000581.

- Chen, J.Z., and Grigorieff, N. (2007). SIGNATURE: a single-particle selection system for molecular electron microscopy. *J. Struct. Biol.* *157*, 168–173.
- Dunkle, J.A., Xiong, L., Mankin, A.S., and Cate, J.H. (2010). Structures of the *Escherichia coli* ribosome with antibiotics bound near the peptidyl transferase center explain spectra of drug action. *Proc. Natl. Acad. Sci. USA* *107*, 17152–17157.
- Emsley, P., and Cowtan, K. (2004). Coot: model-building tools for molecular graphics. *Acta Crystallogr. D Biol. Crystallogr.* *60*, 2126–2132.
- Fernández, J.J., Luque, D., Castón, J.R., and Carrascosa, J.L. (2008). Sharpening high resolution information in single particle electron cryomicroscopy. *J. Struct. Biol.* *164*, 170–175.
- Frank, J., Radermacher, M., Penczek, P., Zhu, J., Li, Y., Ladjadi, M., and Leith, A. (1996). SPIDER and WEB: processing and visualization of images in 3D electron microscopy and related fields. *J. Struct. Biol.* *116*, 190–199.
- Gao, Y.G., Selmer, M., Dunham, C.M., Weixlbaumer, A., Kelley, A.C., and Ramakrishnan, V. (2009). The structure of the ribosome with elongation factor G trapped in the posttranslocational state. *Science* *326*, 694–699.
- Harms, J.M., Schlünzen, F., Fucini, P., Bartels, H., and Yonath, A. (2004). Alterations at the peptidyl transferase centre of the ribosome induced by the synergistic action of the streptogramins dalfoipristin and quinupristin. *BMC Biol.* *2*, 4.
- Horinouchi, S., and Weisblum, B. (1980). Posttranscriptional modification of mRNA conformation: mechanism that regulates erythromycin-induced resistance. *Proc. Natl. Acad. Sci. USA* *77*, 7079–7083.
- Iordănescu, S. (1976). Three distinct plasmids originating in the same *Staphylococcus aureus* strain. *Arch. Roum. Pathol. Exp. Microbiol.* *35*, 111–118.
- Jenner, L.B., Demeshkina, N., Yusupova, G., and Yusupov, M. (2010). Structural aspects of messenger RNA reading frame maintenance by the ribosome. *Nat. Struct. Mol. Biol.* *17*, 555–560.
- Johansson, M., Chen, J., Tsai, A., Kornberg, G., and Puglisi, J.D. (2014). Sequence-dependent elongation dynamics on macrolide-bound ribosomes. *Cell Rep.* *7*, 1534–1546.
- Kucukelbir, A., Sigworth, F.J., and Tagare, H.D. (2014). Quantifying the local resolution of cryo-EM density maps. *Nat. Methods* *11*, 63–65.
- Li, X., Mooney, P., Zheng, S., Booth, C.R., Braunschweig, M.B., Gubbens, S., Agard, D.A., and Cheng, Y. (2013). Electron counting and beam-induced motion correction enable near-atomic-resolution single-particle cryo-EM. *Nat. Methods* *10*, 584–590.
- Loerke, J., Giesebrecht, J., and Spahn, C.M. (2010). Multiparticle cryo-EM of ribosomes. *Methods Enzymol.* *483*, 161–177.
- Mayford, M., and Weisblum, B. (1989). ermC leader peptide. Amino acid sequence critical for induction by translational attenuation. *J. Mol. Biol.* *206*, 69–79.
- Narayanan, C.S., and Dubnau, D. (1985). Evidence for the translational attenuation model: ribosome-binding studies and structural analysis with an in vitro run-off transcript of ermC. *Nucleic Acids Res.* *13*, 7307–7326.
- Ohashi, H., Shimizu, Y., Ying, B.W., and Ueda, T. (2007). Efficient protein selection based on ribosome display system with purified components. *Biochem. Biophys. Res. Commun.* *352*, 270–276.
- Petersen, E.F., Goddard, T.D., Huang, C.C., Couch, G.S., Greenblatt, D.M., Meng, E.C., and Ferrin, T.E. (2004). UCSF Chimera—a visualization system for exploratory research and analysis. *J. Comput. Chem.* *25*, 1605–1612.
- Pulk, A., and Cate, J.H. (2013). Control of ribosomal subunit rotation by elongation factor G. *Science* *340*, 1235970.
- Ramu, H., Mankin, A., and Vázquez-Laslop, N. (2009). Programmed drug-dependent ribosome stalling. *Mol. Microbiol.* *71*, 811–824.
- Scheres, S.H., and Chen, S. (2012). Prevention of overfitting in cryo-EM structure determination. *Nat. Methods* *9*, 853–854.
- Schmeing, T.M., Seila, A.C., Hansen, J.L., Freeborn, B., Soukup, J.K., Scaringe, S.A., Strobel, S.A., Moore, P.B., and Steitz, T.A. (2002). A pre-translocational intermediate in protein synthesis observed in crystals of enzymatically active 50S subunits. *Nat. Struct. Biol.* *9*, 225–230.
- Schmeing, T.M., Huang, K.S., Kitchen, D.E., Strobel, S.A., and Steitz, T.A. (2005a). Structural insights into the roles of water and the 2' hydroxyl of the P site tRNA in the peptidyl transferase reaction. *Mol. Cell* *20*, 437–448.
- Schmeing, T.M., Huang, K.S., Strobel, S.A., and Steitz, T.A. (2005b). An induced-fit mechanism to promote peptide bond formation and exclude hydrolysis of peptidyl-tRNA. *Nature* *438*, 520–524.
- Shivakumar, A.G., Hahn, J., Grandi, G., Kozlov, Y., and Dubnau, D. (1980). Posttranscriptional regulation of an erythromycin resistance protein specified by plasmic pE194. *Proc. Natl. Acad. Sci. USA* *77*, 3903–3907.
- Tu, D., Blaha, G., Moore, P.B., and Steitz, T.A. (2005). Structures of MLSBK antibiotics bound to mutated large ribosomal subunits provide a structural explanation for resistance. *Cell* *121*, 257–270.
- Vázquez-Laslop, N., Thum, C., and Mankin, A.S. (2008). Molecular mechanism of drug-dependent ribosome stalling. *Mol. Cell* *30*, 190–202.
- Vázquez-Laslop, N., Ramu, H., Klepacki, D., Kannan, K., and Mankin, A.S. (2010). The key function of a conserved and modified rRNA residue in the ribosomal response to the nascent peptide. *EMBO J.* *29*, 3108–3117.
- Vázquez-Laslop, N., Ramu, H., and Mankin, A.S. (2011a). Nascent peptide-mediated ribosome stalling promoted by antibiotics. In *Ribosomes. Structure, function, evolution*, M.V. Rodnina, W. Wintermeyer, and R. Green, eds. (Wien, New York: Springer-Verlag), pp. 377–392.
- Vázquez-Laslop, N., Klepacki, D., Mulhearn, D.C., Ramu, H., Krasnykh, O., Franzblau, S., and Mankin, A.S. (2011b). Role of antibiotic ligand in nascent peptide-dependent ribosome stalling. *Proc. Natl. Acad. Sci. USA* *108*, 10496–10501.
- Voorhees, R.M., Weixlbaumer, A., Loakes, D., Kelley, A.C., and Ramakrishnan, V. (2009). Insights into substrate stabilization from snapshots of the peptidyl transferase center of the intact 70S ribosome. *Nat. Struct. Mol. Biol.* *16*, 528–533.

Molecular Cell, Volume 56

Supplemental Information

Drug Sensing by the Ribosome Induces

Translational Arrest via Active Site Perturbation

**Stefan Arenz, Sezen Meydan, Agata L. Starosta, Otto Berninghausen, Roland Beckmann,
Nora Vázquez-Laslop, and Daniel N. Wilson**

SUPPLEMENTAL FIGURES

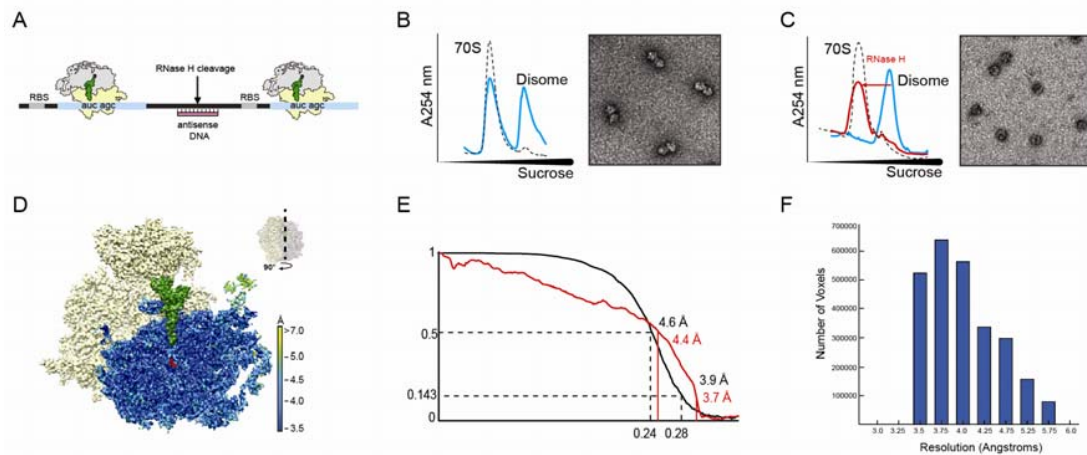


Figure S1 Average and local resolution determination of the ErmCL-SRC, related to Figure 1. (A) Schematic for *ermCL*-dependent regulation of *ermC* translation in the presence of erythromycin (ERY). (B,C) The bicistronic *2XermCL* mRNA was translated *in vitro* in the presence of 10 μ M ERY in order to generate (B) ErmCL-SRC disomes, which were (C) converted to monosomes by annealing of complementary DNA oligo and RNase H cleavage, as shown by sucrose density centrifugation and negative stain EM. (D) Local resolution (Kucukelbir et al., 2014) displayed on the ErmCL-SRC with a transverse section through the 50S subunit (as depicted in the insert), 30S (yellow), P-tRNA (green) and erythromycin (red). (E) Average resolution of the ErmCL-SRC was 4.6 Å using the Fourier shell correlation (FSC) cut-off value of 0.5. Since the microscopy images were processed in the absence of spatial frequencies higher than 8 Å, the FSC cut-off value of 0.143 was used for average resolution determination of 3.9 Å (Scheres and Chen, 2012). The overall fit of the 50S model to the ErmCL-SRC map is indicated by the FSC calculation between the model and map (red curve). (F) Histogram generated by ResMap (Kucukelbir et al., 2014) showing that the local resolution of the final map predominantly ranges from 3.5-4.0 Å.

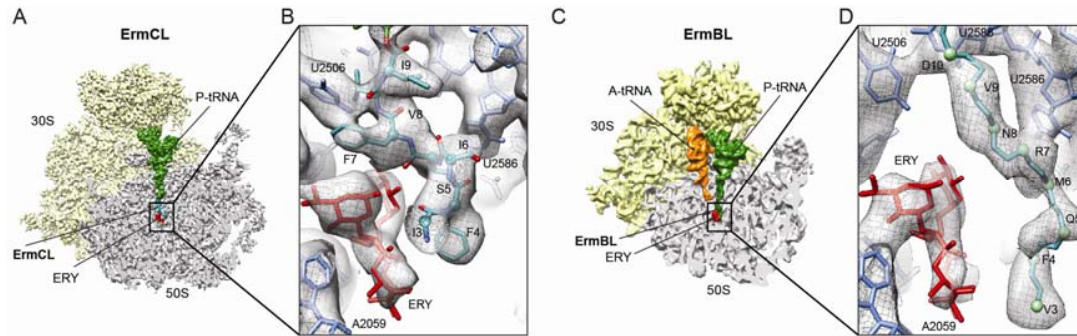


Figure S2 Comparison of the path of the ErmCL and ErmBL nascent chains through the ribosomal tunnel, related to Figure 2. (A-D) Comparison of cryo-EM structures of (A,B) ErmCL-SRC and (C,D) ErmBL-SRC (Arenz et al., 2014) with 30S (yellow) and transverse section of the 50S subunit (grey), illustrating the path of the respective nascent polypeptide chains through the ribosomal tunnel. Enlargements with density (grey mesh) and molecular models for the ErmCL (teal) and ErmBL (green) nascent chains, erythromycin (ERY, red) and 23S rRNA nucleotides (blue).

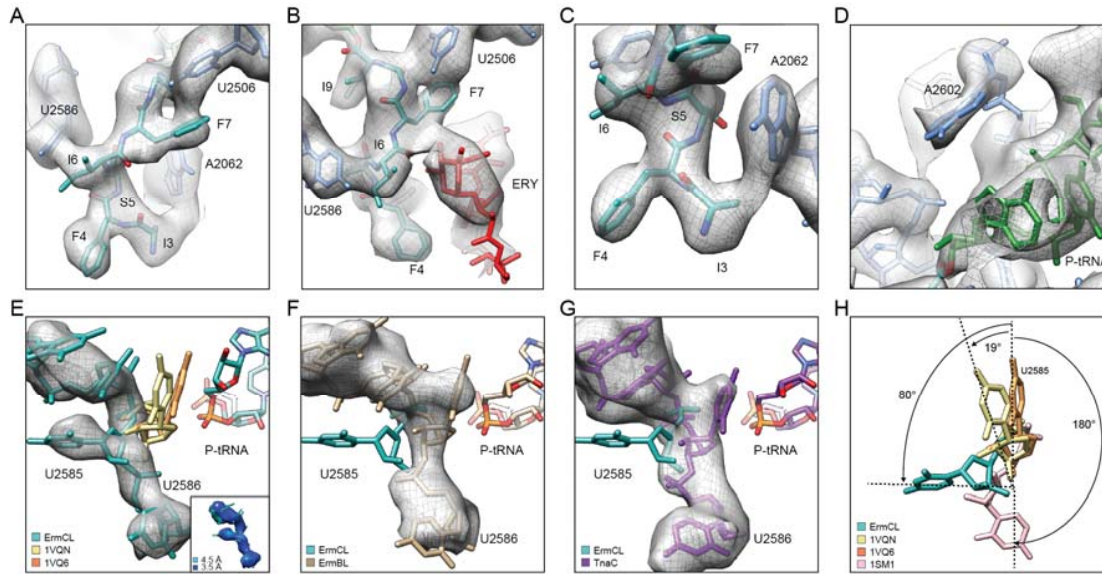


Figure S3 Electron density for selected regions of the PTC and tunnel, related to Figure 2 and 3. (A-C) Views of the ErmCL nascent chain (teal), 23S rRNA nucleotides (blue), and erythromycin (Dunkle et al., 2010) (red) in the ribosomal tunnel of the ErmCL-SRC. Views identical to those shown in Fig. 2A,B,E, respectively, but including electron density (grey mesh). (D) Electron density (grey mesh) for the defined position of A2602 in the ErmCL-SRC. (E) Unique conformation of 23S rRNA nucleotide U2585 in ErmCL-SRC (teal) compared to its positions observed in the uninduced (PDB1VQ6, orange) and induced (PDB1VQN, yellow) state of the PTC (Schmeing et al., 2005a; Schmeing et al., 2005b). Insert show electron density for nucleotides G2583-U2586 coloured according to local resolution (Kucukelbir et al., 2014). (F,G) Electron density for G2583-U2586 in (F) ErmBL-SRC (Arenz et al., 2014) and (G) TnaC-SRC indicating the absence of electron density for the flipped position of U2585 and presence of electron density for canonical position of U2585. (H) Comparison of U2585 conformations in the uninduced (PDB1VQ6, orange) and induced (PDB1VQN, yellow) state of the PTC (Schmeing et al., 2005a; Schmeing et al., 2005b), as well as in ErmCL-SRC (teal) and streptogramin-bound ribosomes (PDB1SM1) (Harms et al., 2004).

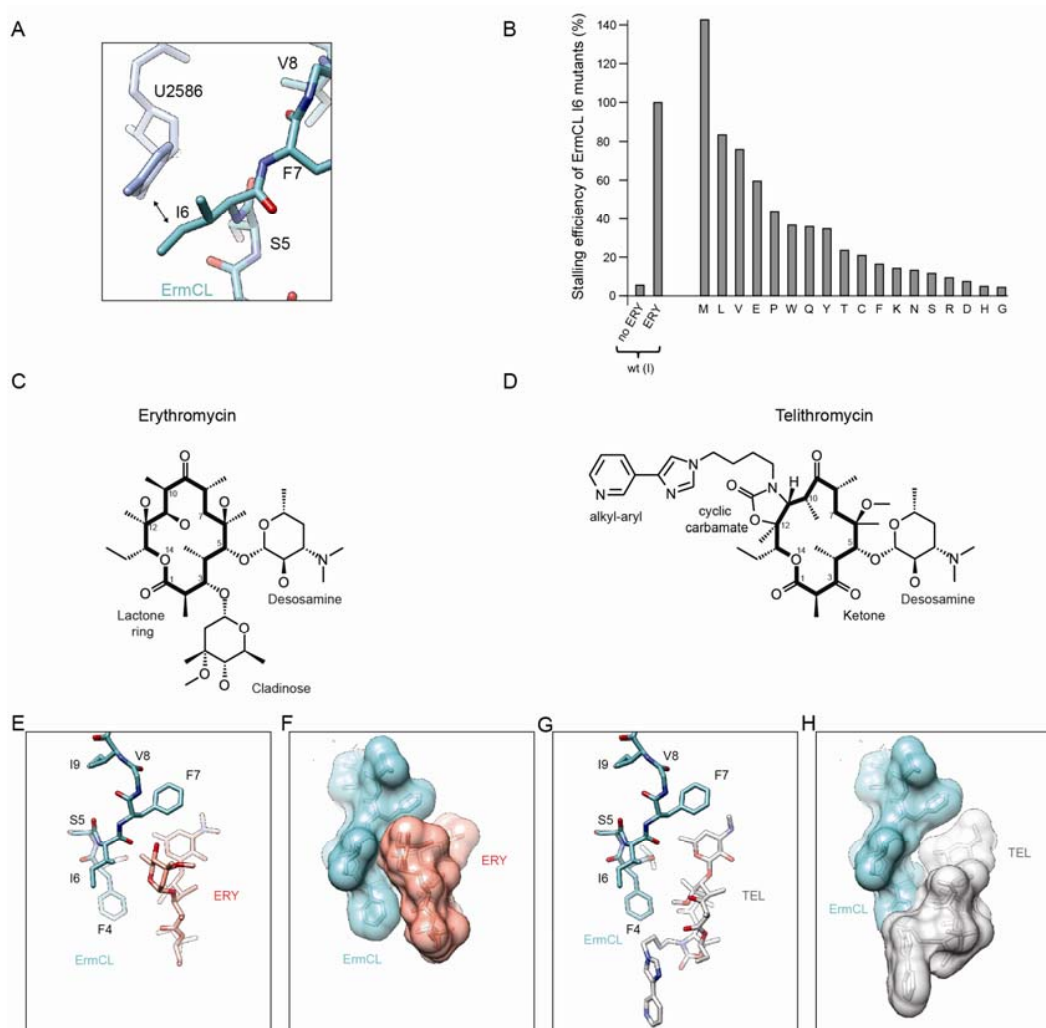


Figure S4 Superimposition of telithromycin antibiotic relative to ErmCL, related to Figure 2. (A) Interaction between I6 and U2586 in the ErmCL-SRC. (B) Quantification of the stalling efficiency of mutations at position I6 of ErmCL based on toe-printing assays. (C,D) Chemical structures of (C) erythromycin (ERY) and (D) telithromycin (TEL) showing, various alterations of the lactone ring and the absence of the C3 cladinose sugar in telithromycin. (E-H) Relative position of (E,F) erythromycin and (G,H) telithromycin to ErmCL. Spacefill representations of ErmCL and (F) ERY (Dunkle et al., 2010) and (H) TEL (Dunkle et al., 2010) illustrate the proximity of the C3 cladinose sugar of erythromycin to ErmCL, which is absent in the superimposition of telithromycin due to the lack of the C3 cladinose.

SUPPLEMENTAL REFERENCES

- Arenz, S., Ramu, H., Gupta, P., Berninghausen, O., Beckmann, R., Vazquez-Laslop, N., Mankin, A.S., and Wilson, D.N. (2014). Molecular basis for erythromycin-dependent ribosome stalling during translation of the ErmBL leader peptide. *Nat Commun* *5*, 3501.
- Dunkle, J.A., Xiong, L., Mankin, A.S., and Cate, J.H. (2010). Structures of the *Escherichia coli* ribosome with antibiotics bound near the peptidyl transferase center explain spectra of drug action. *Proc Natl Acad Sci U S A* *107*, 17152-17157.
- Harms, J., Schluenzen, F., Fucini, P., Bartels, H., and Yonath, A. (2004). Alterations at the peptidyl transferase centre of the ribosome induced by the synergistic action of the streptogramins dalbavancin and quinupristin. *BMC Biol.* *2*, 4.
- Kucukelbir, A., Sigworth, F.J., and Tagare, H.D. (2014). Quantifying the local resolution of cryo-EM density maps. *Nat Methods* *11*, 63-65.
- Scheres, S.H., and Chen, S. (2012). Prevention of overfitting in cryo-EM structure determination. *Nat Methods* *9*, 853-854.
- Schmeing, T.M., Huang, K.S., Kitchen, D.E., Strobel, S.A., and Steitz, T.A. (2005a). Structural insights into the roles of water and the 2' hydroxyl of the P site tRNA in the peptidyl transferase reaction. *Mol. Cell* *20*, 437-448.
- Schmeing, T.M., Huang, K.S., Strobel, S.A., and Steitz, T.A. (2005b). An induced-fit mechanism to promote peptide bond formation and exclude hydrolysis of peptidyl-tRNA. *Nature* *438*, 520-524.

Alternate conformation of a nascent chain in the ribosomal tunnel induces P-tRNA perturbation and inhibition of peptide bond formation

Stefan Arenz¹, C. Axel Innis^{2,3}, Roland Beckmann^{1,4} and Daniel N. Wilson^{1,4*}

¹Gene Center and Department for Biochemistry, University of Munich, Feodor-Lynenstr. 25, 81377 Munich, Germany

²Institut Européen de Chimie et Biologie, Univ. Bordeaux, 33607, Pessac, France

³INSERM U869, 33000 Bordeaux, France

⁴Center for integrated Protein Science Munich (CiPSM), University of Munich, Feodor-Lynenstr. 25, 81377 Munich, Germany.

*Correspondence: wilson@lmb.uni-muenchen.de

Running title: Nascent chain induced translation arrest

SUMMARY

During protein synthesis, nascent polypeptide chains within the ribosomal tunnel can act in *cis* to induce ribosome stalling and regulate expression of downstream genes. The *Streptococcus sanguis* ErmBL leader peptide induces stalling in the presence of clinically important macrolide antibiotics, erythromycin and telithromycin, leading to the induction of the resistance methyltransferase ErmB. Here, we report cryo-electron microscopy structures at 3.6 Å resolution of ErmBL-stalled ribosome complexes in the presence of erythromycin, with or without Lys-tRNA bound in the A-site. The structures reveal that the ErmBL nascent chain adopts an unusual conformation within the ribosomal tunnel, with the C-terminal Asp10 sidechain in a previously unseen rotated position. While the Lys-tRNA in the A-site is optimally positioned, peptide bond formation cannot occur because the ribose A76 of the peptidyl-tRNA in the P-site is shifted from its canonical position. Thus, in addition to a structural basis for polypeptide-mediated translational arrest, these reconstructions also provide structural insight into the fundamental mechanism of peptide bond formation.

INTRODUCTION

Ribosomes are the protein synthesizing machines of the cell. The active site for peptide bond formation, the peptidyltransferase center (PTC) is located on the large ribosomal subunit^{1,2}. During translation elongation, peptide bond formation occurs when a peptidyl-tRNA is located at the P-site and an aminoacyl-tRNA at the A-site of the PTC. The α -amino group of the aminoacyl-tRNA makes a nucleophilic attack onto the carbonyl carbon of the peptidyl-tRNA, transferring the peptidyl moiety onto the A-tRNA and prolonging the nascent polypeptide chain by one amino acid^{1,2}. As the nascent polypeptide chain is synthesized, it passes through a tunnel located on the large ribosomal subunit and emerges on the solvent side where protein folding occurs³. A growing body of evidence has revealed that the ribosomal tunnel is not a passive conduit for the nascent polypeptide chain but rather plays an important role in protein folding, co-translational targeting and translation regulation³.

Nascent polypeptide-mediated translation regulation can be an intrinsic property of the nascent chain, such that the amino acid sequence of the polypeptide is sufficient to modulate the rate of translation, and in some cases even induce translation arrest⁴. Well-characterized bacterial examples include the MifM and SecM leader peptides, which interact with the ribosomal tunnel to induce translational stalling^{5,6} and thereby regulate expression of a downstream gene in the operon^{4,7}. Nascent polypeptide-mediated translation regulation can also require the presence of an additional ligand or co-factor^{4,8,9}. Well-characterized examples include the TnaC leader peptide, which requires the presence of free tryptophan for stalling to occur^{10,11}, and the Erm leader peptides, which induce translation stalling in the presence of the macrolide antibiotics^{8,9}.

In the case of Erm peptides, the translational arrest in the leader peptide leads to expression of the downstream macrolide resistance determinant, usually a methyltransferase that confers resistance by methylating A2058, a 23S ribosomal RNA nucleotide that comprises part of the macrolide binding site within the ribosomal tunnel. For example, in *Streptococcus sanguis* the expression of the ErmB methyltransferase is controlled by programmed arrest during translation of the upstream *ermBL* leader peptide¹²⁻¹⁴ (**Figure 1A**): In the absence of erythromycin, ErmB expression is repressed because the ribosome-binding site (RBS) and AUG start codon of the *ermB* mRNA are

sequestered in a stem-loop structure (**Figure 1A**). However, in the presence of sub-inhibitory concentrations of erythromycin, ribosomes translating the ErmBL leader peptide become stalled, leading to an alternative stem-loop structure in the mRNA that exposes the RBS and start codon of the *ermB* gene and thus allows ribosome binding and induction of ErmB expression (**Figure 1A**). The drug-dependent nature of the stalling ensures that expression only occurs when the drug is present, which is critical for survival because of the fitness cost associated with the methylation of A2058¹⁵.

Previous studies demonstrated that polymerization of the ErmBL nascent chain halts because the ribosome is unable to catalyze peptide bond formation between the 10 amino acid long ErmBL-tRNA^{Asp} (codon 10) in the ribosomal P-site and Lys-tRNA^{Lys} (codon 11) in the A-site¹⁶ (**Figure 1A**). The ErmBL-dependent translational arrest occurs with both macrolides (e.g. erythromycin) and ketolides (e.g. telithromycin)¹⁶, which contrasts with other leader peptides, such as ErmCL, where stalling is specific for macrolides^{9,17}. Mutagenesis studies identified four residues within ErmBL (Arg7, Val9-Lys11) that are critical for stalling¹⁶. Interestingly, the compromised stalling efficiency of the ErmBL-R7A mutant could be rescued by compensatory mutations within U2586 (but not A2062) of the 23S rRNA. The first structural insights into how the ErmBL leader peptide, the macrolide antibiotic and the ribosomal tunnel cooperate to inactivate the PTC of the ribosome were derived from a cryo-electron microscopy (cryo-EM) structure of the ErmBL-SRC at 4.5-6.6 Å resolution¹⁶. On the basis of this structure, it was suggested that peptide bond formation cannot occur because the ErmBL nascent chains stabilizes an uninduced state of the ribosome that prevents accommodation of Lys-tRNA at the A-site.

Here we present cryo-EM structures of the ErmBL-stalled ribosome complex in the presence and absence of A-tRNA, with a resolution of 3.1-3.6 Å. The structures reveal a complex network of potential hydrogen bonding interactions between the C-terminal region of ErmBL and nucleotides of the 23S rRNA, explaining the importance of these residues for translational stalling. The ErmBL nascent chain adopts a unique path within the ribosomal tunnel that enables it to bypass the tunnel-bound macrolide. The unique path of ErmBL arise because of an unusual rotated conformation of the C-terminal Asp10 residue, which is unlike that seen previously in any cryo-EM or X-ray crystallography structures. The conformation of the ErmBL nascent chain induces

distortions in the terminal A76 of the P-tRNA, preventing nucleophilic attack by the accommodated A-tRNA, and thus leading to translation arrest. In addition to providing insights into nascent chain mediated translation arrest, the ErmBL-stalled ribosome structures also provide fundamental insight into the mechanism of peptide bond formation.

RESULTS AND DISCUSSION

Cryo-EM structures of ErmBL-stalled ribosome complexes

The ErmBL-stalled ribosomal complexes (SRCs) were generated by translation of a dicistronic *2XermBL* mRNA in the presence of 20 μ M erythromycin using an *E. coli* lysate-based *in vitro* translation system. The ErmBL-SRC disomes were then isolated by sucrose gradient purification, converted to monosomes, re-isolated and applied to cryogrids, as described previously^{16,18}. Data collection was performed on a Titan Krios TEM fitted with the Falcon II direct electron detector (FEI, Netherlands) and images were processed with SPIDER¹⁹ (see Experimental Procedures). *In silico* sorting of cryo-EM images yielded two major homogeneous subpopulations of ribosomes bearing P-tRNA and E-tRNAs, but differing in the presence (termed ErmBL-APE-SRC; 85,393 particles, 33%) or absence (termed ErmBL-PE-SRC; 75,839 particles, 30%) of A-tRNA (**Figure 1B** and **Figure S1**). Both subpopulations could be refined to an average resolution of 3.6 Å (using a Fourier shell correlation (FSC) cut-off of 0.143, **Figure S2**), with local resolution calculations indicating that the ribosomal core reaches towards 3.1 Å (**Figure 1C** and **Figure S2**). At this resolution, base separation is clearly observed for rRNA nucleotides (**Figure 1D**), as is the density for the majority of the amino acid side chains in ribosomal proteins (**Figure 1E**). Density is also observed for the lysyl side chain attached to the CCA-end of the A-tRNA as well as for the ErmBL leader peptide attached to CCA-end of the P-tRNA (**Figure 1F**).

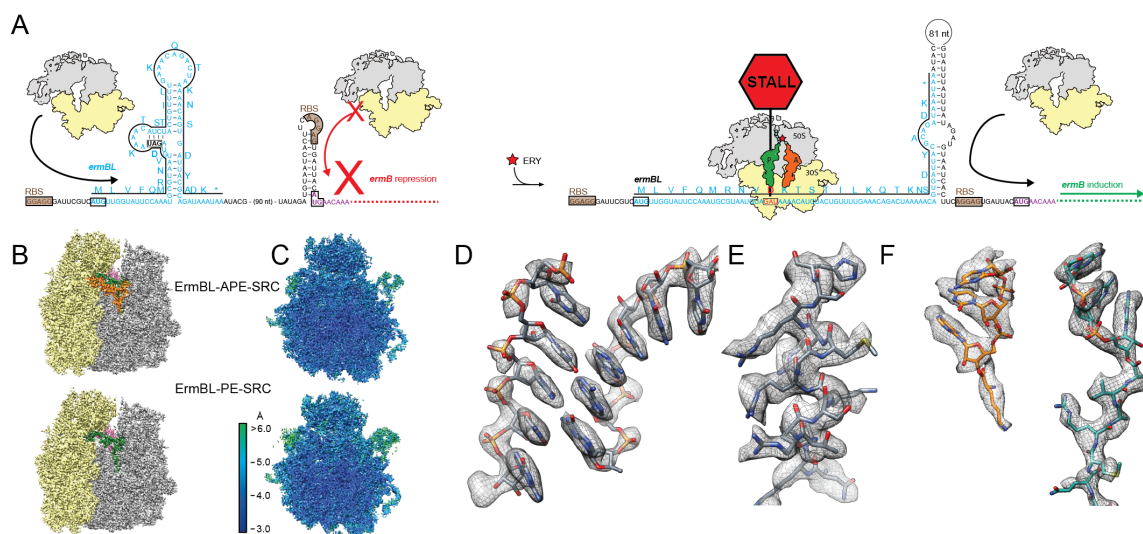


Figure 1 Cryo-EM structure of the ErmBL-SRC. (A) Schematic for *ermBL*-dependent regulation of *ermB* translation in the presence of erythromycin (ERY). (B) Cryo-EM maps of the ErmBL-APE-SRC and ErmBL-PE-SRC, with 30S (yellow), 50S (grey), A-tRNA (orange), P-tRNA (green) and E-tRNA (magenta). (C) Transverse sections of the cryo-EM maps of the ErmBL-APE-SRC and ErmBL-PE-SRC, coloured according to local resolution. (D-F) Examples of electron density (grey mesh) of the ErmBL-APE-SRC map illustrating (D) base separation within an rRNA helix, (E) side chains of a ribosomal protein α -helix, (F) aminoacylated-CCA-end of the A-tRNA (orange) and ErmBL-peptide attached to the CCA-end of the P-tRNA (green).

A molecular model for the ErmBL nascent chain

The ErmBL nascent chains of both ErmBL-SRCs were well resolved within the ribosomal tunnel, as indicated by local resolution (Figure 2A,B and Figure S3). Moreover, the electron density for ErmBL in the ErmBL-PE-SRC was basically identical to that in the ErmBL-APE-SRC (Figure S3), indicating that the presence of the A-tRNA does not influence the conformation of the ErmBL nascent chain. With the exception of the side chain of Asn8 for which we observe no density, we are able to present a complete model for the ErmBL nascent chain residues Val3-Asp10. In contrast, the N-terminus of ErmBL appears to be flexible, consistent with the worse local resolution of this region, thus preventing the N-terminal Met1 residue from being modeled and allowing only the backbone for Leu2 to be tentatively assigned (Figure 2A,B and Figure S3). The overall backbone trace of the ErmBL nascent chain within the ribosomal tunnel reported here is similar to the path reported previously for ErmBL based on a 4.5-6.6 Å

cryo-EM map ¹⁶ (**Figure S4**). Specifically, ErmBL adopts a unique conformation that enables it to by-pass the macrolide erythromycin bound within the tunnel without contacting it (**Figure 2C**). This is consistent with biochemical studies demonstrating that ErmBL stalling occurs with a variety of different macrolides and thus appears insensitive to the chemical nature of the drug ¹⁶. The ErmBL path is distinct from that reported for the drug-dependent ErmCL stalling peptide ¹⁸, which establishes intimate interactions with the drug (**Figure 2D**), consistent with the findings that ErmCL stalling occurs with macrolide antibiotics containing a C3-cladinose sugar, such as erythromycin, but not with ketolides, such as telithromycin that lack the C3-cladinose ^{9,17}. This contrasts with the available structures of other polypeptide chains within the ribosomal tunnel ^{5,6,20-24}, which revealed paths that would be sterically obstructed by the presence of the macrolide, as exemplified here by the TnaC nascent chain ²⁰ (**Figure 2E**). As noted ¹⁶, the path of the ErmBL illustrates the principle as to how specific amino acid sequences allow translation of a subset of proteins, even in the presence of a macrolide-obstructed tunnel ^{25,26}.

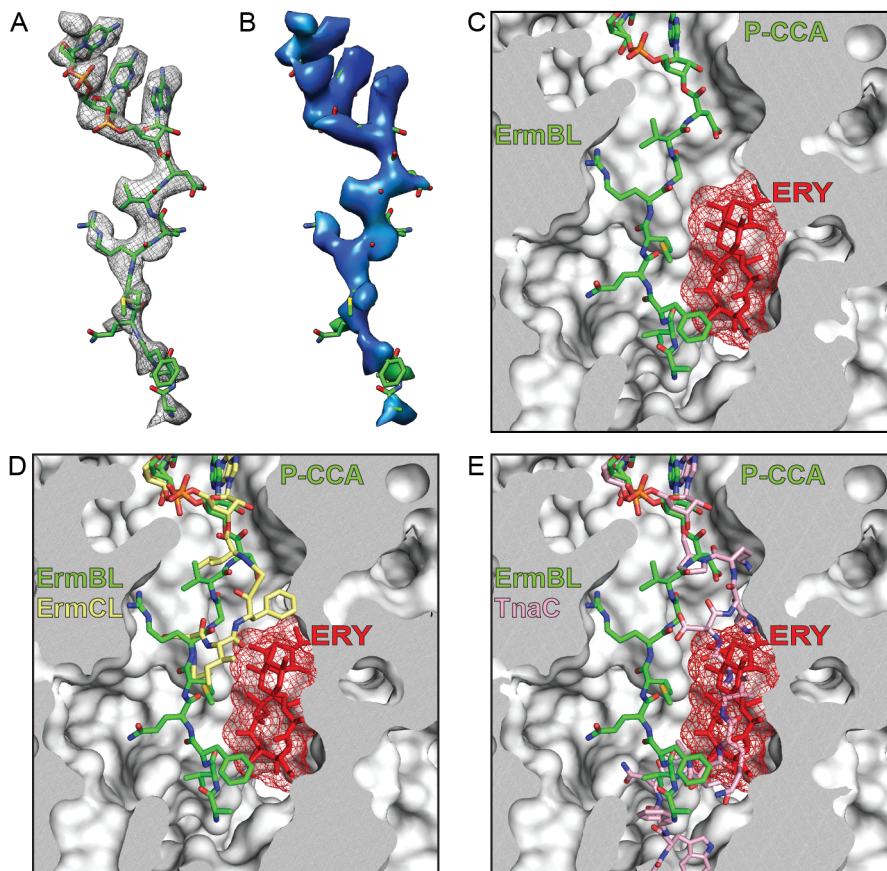


Figure 2 Path of ErmBL within the ribosomal tunnel. (A,B) Atomic model of ErmBL nascent chain including the CCA-end of the P-tRNA (green) with electron density represented as (A) grey mesh and (B) coloured according to local resolution. (C,E) Transverse sections of the ribosomal tunnel (grey) illustrating the path of (C) ErmBL (green), relative to (D) ErmCL (yellow, ¹⁸) and (E) TnaC (pink, ²⁰), and ERY (red mesh).

Interactions of ErmBL within the ribosomal tunnel

In contrast to the previous reconstruction of ErmBL ¹⁶, the significantly higher resolution of the ErmBL-SRCs reported here permits a detailed analysis of the interactions of ErmBL nascent chain with components of the ribosomal tunnel (**Figure 3A**). The majority of the interactions are localized within the last four C-terminal amino acids of ErmBL, namely Arg7-Asp10, which collectively establish a total of nine potential hydrogen bond interactions with nucleotides of the 23S rRNA: Asp10 can form three hydrogen bonds, one from the backbone carboxyl oxygen with the N3 of U2585 and two from the side chain oxygens of Asp10 with the N1 and/or N2 of G2061 as well as the N3 of U2506 (**Figure 3B**). These interactions are likely to be important since

mutation of Asp10 to Ala abolishes translational stalling¹⁶. The backbone carboxyl of Asn8 is within hydrogen bonding distance of the ribose 2'OH of A2062, whereas no density is observable for the side chain, consistent with the report that Asn8Ala mutations do not affect ErmBL stalling¹⁶. Indeed, we note that the most favored rotamers for the Asn side chain would sterically clash with the desosamine sugar of erythromycin, presumably causing the Asn8 sidechain to adopt multiple other less defined states, explaining the absence of density (**Figure 3C**).

The well-resolved density for the Arg7 side chain can be explained by the multiple interactions that this positively charged residue establishes by protruding into a negatively charged rRNA pocket of the tunnel wall (**Figure 3D**). Specifically, four hydrogen bonds are possible with the two terminal amino groups of Arg7, namely to the phosphate oxygens of A2063 and A2441, the bridging ribose oxygen of A2439 and the ribose 2'OH of U2586 (**Figure 3D**). In addition, the backbone of NH of Arg7 is within hydrogen bonding distance of the O2 of U2586. While mutation of Arg7Ala abolishes stalling, compensatory mutations of U2586 were able to restore stalling¹⁶, supporting the intimate association between these two entities. What is unclear from the structure is why the Val9Ala mutation also abolishes ErmBL stalling activity¹⁶. In the ErmBL-SRC, the sidechain of Val9 is well resolved, yet does not appear to come into close proximity of any components of the ribosomal tunnel (**Figure 3E**). We speculate that the Val9 side chain may therefore be important for indirectly promoting the correct conformation of the ErmBL nascent chain: one possibility is that Val9 provides some steric constraints that are necessary for the Arg7 side chain to be optimally oriented, since these two residues spatially neighbor each other within the ribosomal tunnel.

In contrast to the C-terminus, the N-terminal half of ErmBL (residues Leu2-Met6) are not critical for stalling and can individually be mutated to alanine without loss of activity¹⁶. This is consistent with the poor density and worse local resolution in this region, suggesting that the N-terminus of ErmBL is flexible and does not adopt a single defined conformation. The sequence of the N-terminus MLVFQM is also very hydrophobic and therefore provides limited possibilities for hydrogen bonding interactions. Instead, the Phe4 and Met6 side chains appear to pack against the U2609-A752 and U1782-U2586 base pairs, respectively (**Figure 3E**). The only potential

hydrogen bonding interactions are from the backbone carboxyl of Val5 and the C9 hydroxyl of the lactone ring of erythromycin. However, the lactone ring itself is relatively poorly resolved in this region and therefore it is hard to envisage how this could be an important stabilizing interaction.

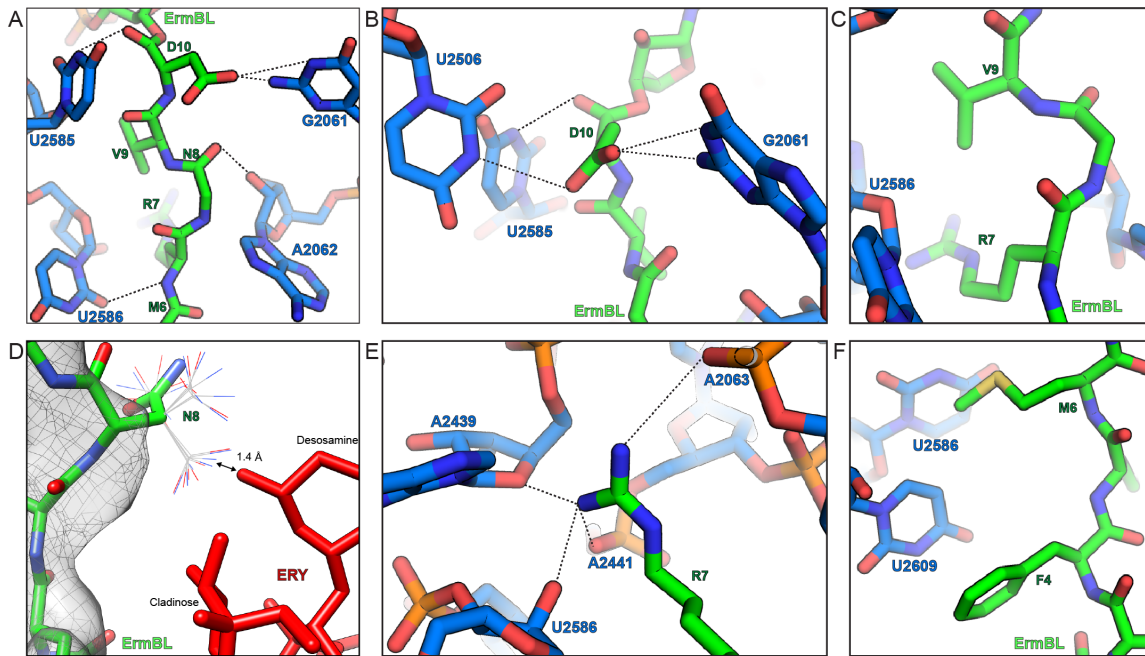


Figure 3 Interaction of the ErmBL nascent chain within the ribosomal tunnel. (A-F) Interactions of ErmBL (green) with 23S rRNA nucleotides (blue). In (D) different rotamers of the N8 side chain are illustrated, cryo-EM map of the ErmBL-SRC is shown as a grey mesh and ERY is shown in red. Potential hydrogen bonds are indicated as dashed lines.

Rotation of Asp10 and an alternate path of the ErmBL

To understand how interactions of ErmBL within the ribosomal tunnel lead to translational arrest by preventing peptide bond formation with the incoming Lys-tRNA in the A-site, we compared the ErmBL-SRC with all available X-ray crystallography structures of ribosomal states with aminoacylated-tRNAs in the P-site. To date, this consists of structures of the *Haloarcula marismortui* 50S subunits bearing CC-puromycin (CC-pmn) or CC-Phe-caproic-acid-biotin (CC-pcb) tRNA analogs²⁷⁻³⁰ and of *Thermus thermophilus* 70S ribosomes bearing fMet-tRNA³¹ or Phe-tRNA². In every single case, the side chain of the Phe or fMet attached the P-tRNA is observed having the same orientation (**Figure 4A,B**), namely, pointing towards the direction of A2062. Surprisingly, the Asp10 side chain attached the P-tRNA in the ErmBL-SRC is rotated by 180°

compared to the Phe/fMet side chains in the crystal structures (**Figure 4A,B**), with the consequence that the ErmBL nascent chain is oriented towards A2062. One possibility is that this simply reflects differences between a peptidyl-tRNA as in the case of ErmBL and an aminoacyl-tRNA as in the crystal structures, therefore, we also compared the ErmBL-SRC with structures of other ribosomal states bearing peptidyl-tRNAs in the P-site. There are currently four available cryo-EM structures of ribosomes bearing peptidyl-tRNAs of sufficient resolution so as to be able to determine the orientation of the amino acid attached to the P-tRNA, namely, the TnaC-SRC²⁰, ErmCL-SRC¹⁸, Sec61beta²⁴ and the MifM-SRC⁵. In all four structures, the amino acid side chain attached the P-tRNA is oriented analogously to the Phe/fMet side chain in the crystal structures (**Figure 4C-F**). This finding suggests that the difference is not related to the length of the peptide on the P-tRNA, and also excludes difference in species since the ErmCL- and TnaC-SRC were also formed using *E. coli* ribosomes^{18,20}. Moreover, the rotation is unlikely to be related to the nature of the amino acid since an Asp residue is also directly attached to the P-tRNA in the MifM-SRC⁵. This leads us to conclude that the 180° rotation of the Asp10 residue in the ErmBL-SRC is likely to be a consequence of its context within the ErmBL nascent chain. It would therefore seem logical to assume that the interactions that stabilize the ErmBL in a specific conformation have an important influence on mediating the rotated state of Asp10 and/or *vice versa*.

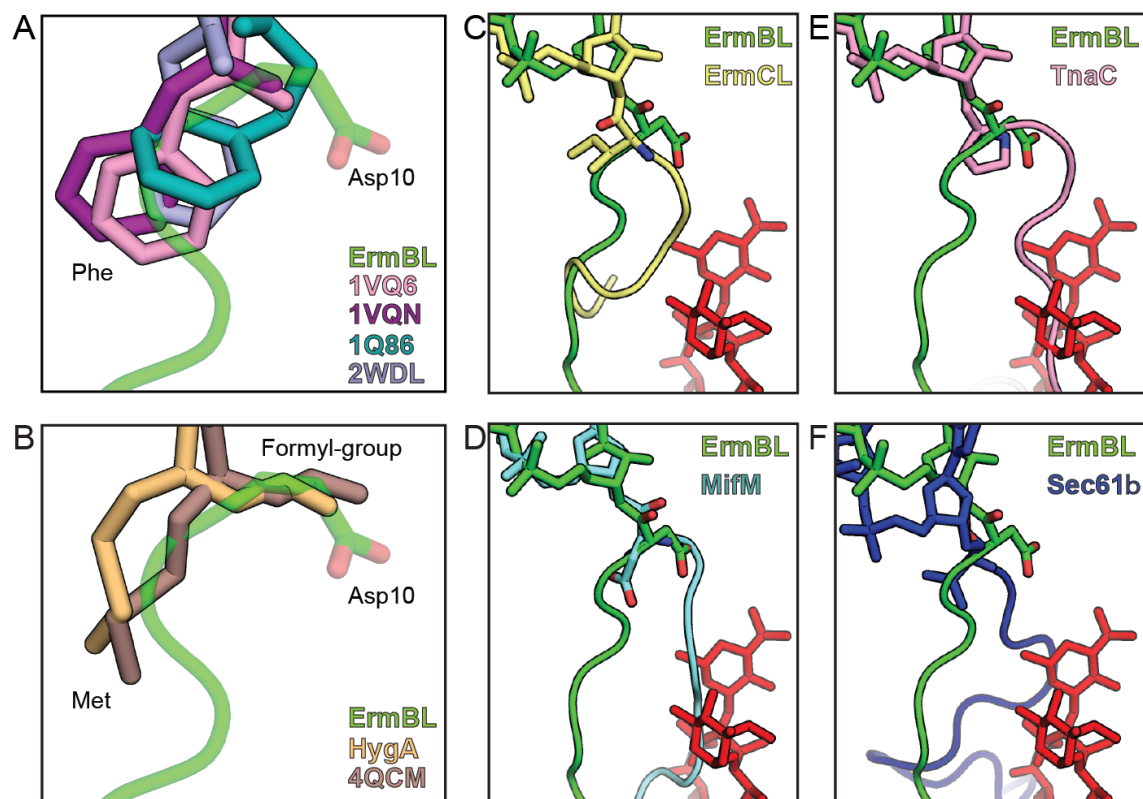


Figure 4 Rotation of the C-terminal amino acid and an alternate path for ErmBL. (A-B) Orientation of ErmBL and Asp10 side chain (green), compared with (A) CC-Phe-caproic-acid-biotin (CC-pcb), CC-puromycin (CC-Pmn) tRNA analogs (²⁹, PDB 1VQ6, pink and 1VQN, purple, ²⁷, PDB 1Q86, teal), or Phe-tRNA (², PDB 2WDL, blue), or with (B) *Thermus thermophilus* 70S ribosomes bearing fMet-tRNA (³¹, PDB 4QCM, brown, (Polikanov 2015 in press), PDB 4Z3R, yellow). (C-F) Alternate path of ErmBL (green) compared to (C) ErmCL (¹⁸, PDB 3J7Z, yellow), (D) MifM (⁵, PDB 3J9W, light blue), (E) TnaC (²⁰, PDB 4UY8, pink) and (F) Sec61β (²⁴, PDB 3J92, dark blue) relative to the position of ERY (red).

A-tRNA accommodation at the PTC of the ErmBL-SRC

To understand how the unorthodox pathway of the ErmBL nascent chain could lead to inhibition of peptidyl-transferase activity, we compared the PTC of the ErmBL-SRC with crystal structures of the ribosome in different states of peptide bond formation ²⁸⁻³¹. Initially, we focused on the A-tRNA, since it was previously proposed that ErmBL stabilized an unaccommodated Lys-tRNA at the A-site of the PTC ¹⁶. In contrast to the previous study, the higher resolution enables us to more accurately place the CCA-end of the A-tRNA and also model the lysyl moiety (**Figure 5A**), which was not observed before. Comparison of the position of the CCA-end of the Lys-tRNA in ErmBL-SRC with the unaccommodated C-pmn (**Figure 5B**) and accommodated CC-pmn (**Figure 5C**)

on the *H. marismortui* 50S subunit²⁸⁻³⁰, as well as with accommodated CCA-end of the Phe-tRNA in the *T. thermophilus* pre-attack complexes^{2,31}, suggests that the Lys-tRNA in the ErmBL-SRC is in a fully or near-fully accommodated state. The A-tRNA is shifted by 1.3 Å between the unaccommodated and accommodated state, when measuring the displacement using the ribose oxygen atom (**Figure 5D**). In comparison, the Lys-tRNA in the ErmBL-SRC is shifted by 0.9 Å and 0.6 Å relative to the unaccommodated and accommodated state, respectively.

Accommodation of the A-tRNA is accompanied by corresponding conformational changes within the 23S rRNA nucleotides of the PTC, specifically, shifts in U2506 and U2584-U2585 are thought to be diagnostic for A-tRNA binding²⁸⁻³⁰. In the ErmBL-PE-SRC, there is no clear density for U2506 (**Figure 5E**), however, upon binding of Lys-tRNA to the A-site, as in the ErmBL-APE-SRC, U2506 adopts a defined conformation (**Figure 5F**), which is similar to that observed in the accommodated state (**Figure 5G**). In both the ErmBL-SRC structures, the density for U2585 is weaker than other PTC nucleotides, but appears to predominantly adopt an intermediate position between the accommodated and unaccommodated U2585 states (**Figure 5H**). We note that regardless of whether the Lys-tRNA is fully or near-fully accommodated, the refined model of the Lys-tRNA in the ErmBL-APE-SRC positions the α -amino group similarly to the accommodated pre-attack A-tRNAs (arrowed in **Figure 5C**) ready for nucleophilic attack of the P-tRNA. However, the presence of the lysyl moiety on the A-tRNA is alone sufficient to indicate that the nucleophilic attack has not occurred, consistent with the previous biochemical evidence indicating that the lysine amino acid does not get incorporated into the ErmBL nascent chain¹⁶.

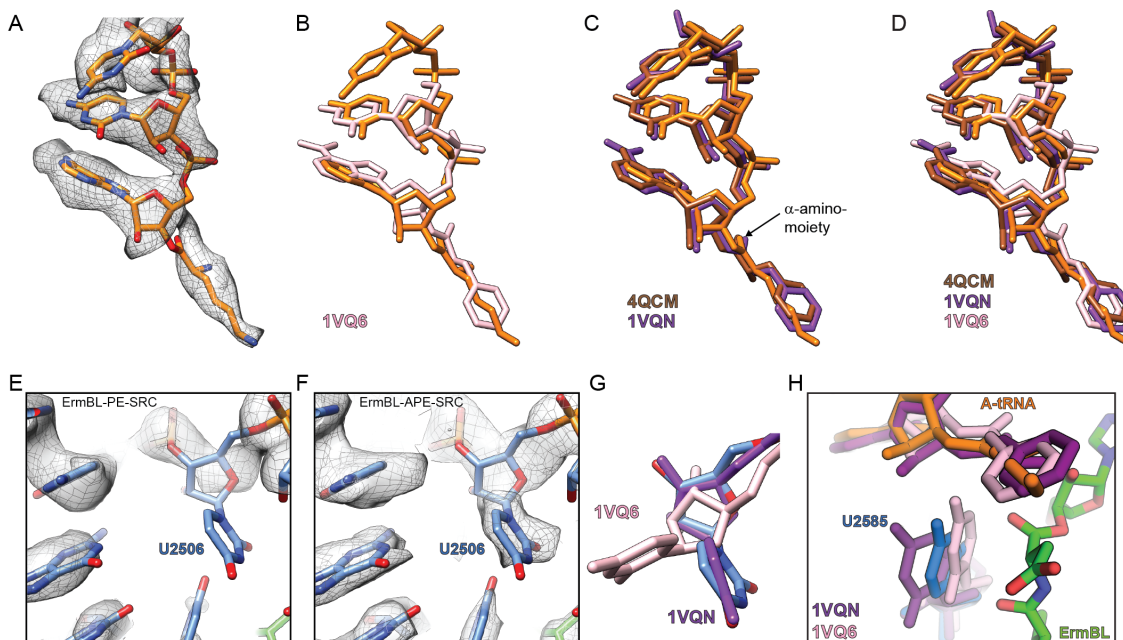


Figure 5 A-site tRNA accommodation at the PTC of the ErmBL-APE-SRC. (A-D) Atomic model for the CCA-end of the A-site tRNA (orange) in the ErmBL-APE-SRC with (A) electron density (grey mesh), compared with (B) unaccommodated (²⁹, PDB 1VQ6, pink) and (C) accommodated A-tRNA states (³¹, PDB 4QCM, brown; ²⁹ PDB 1VQN, purple), and (D) with both. (E-G) Position of 23S rRNA nucleotide U2506 (blue) in (E) ErmBL-PE-SRC and (F) ErmBL-APE-SRC including electron density (grey mesh) and (G) compared with the uninduced (²⁹, PDB 1VQ6, pink) and induced (²⁹, PDB 1VQN, purple) states of the PTC. (H) Comparison of 23S rRNA nucleotide U2585 in ErmBL-APE-SRC (blue), the uninduced (²⁹, PDB 1VQ6, pink) and induced (²⁹, PDB 1VQN, purple) states of the PTC. The nascent chain and A-tRNA in ErmBL are shown in green and orange, respectively.

Perturbation of the P-tRNA by ErmBL prevents peptide bond formation

Comparison of the CCA-end of the P-tRNA in the ErmBL-SRC (Figure 6A,B) with the accommodated position of CC-Pmn²⁹, Phe-tRNA² or fMet-tRNA³¹ reveals a shift of 1-2 Å for the ribose and nucleobase of A76 (Figure 6C,D), which was also evident at lower resolution¹⁶. This suggests that peptide bond formation may be prevented because of a perturbed position of the P-tRNA, rather than an unaccommodated A-tRNA as proposed previously¹⁶. We note that the distance for the nucleophilic attack of the α -amino group of the Lys-tRNA onto the carbonyl-carbon of the P-tRNA is 4.1 Å in the ErmBL-SRC (Figure 6E), whereas the equivalent distances in the pre-attack complexes are 3.2-3.3 Å^{2,31} (Figure 6F).

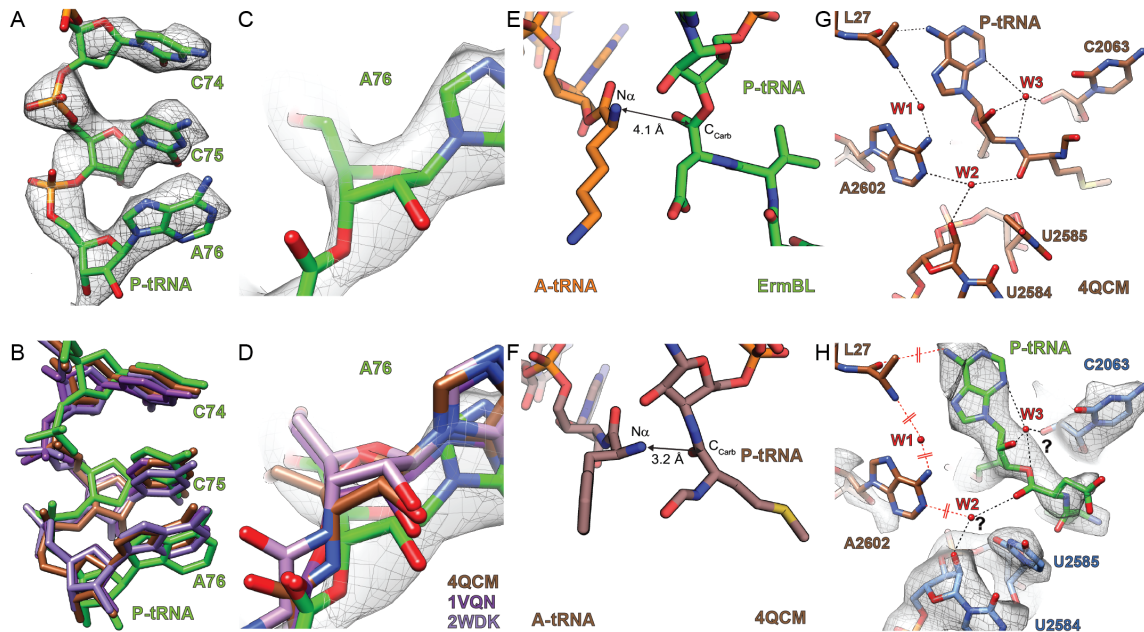


Figure 6 Perturbation of the P-tRNA by ErmBL prevents peptide bond formation. (A-D) Atomic model for the CCA-end of the P-site tRNA (green), including (A,C,D) electron density (grey mesh), in the ErmBL-APE-SRC, and compared with (B) P-tRNAs in the pre-peptide bond formation state (³¹, PDB 4QCM, brown; ², PDB 2WDK, blue), with (C,D) zoom onto the ribose of A76. (E,F) Relative orientation of the A-site α -amino group and the P-site carbonyl carbon in (E) ErmBL-APE-SRC and (F) the pre-attack state (³¹, PDB 4QCM, brown). (G,H) Network of hydrogen bonds creating a proton wire that enables peptide bond formation, according to Polikanov et al ³¹.

The most recent model for peptide bond formation, based on high resolution X-ray crystallography structures, suggests that for the nucleophilic attack to proceed, proton transfer is necessary from the attacking nucleophile to a water molecule (W1) via a proton wire formed by the 2' -OH of the P-site A76 ribose and the 2' -OH of A2451 ³¹ (Figure 6G). In the pre-attack complexes, nucleotide A2602 and the N-terminal regions of L27 become ordered ^{2,31}, which together with the OP1 of A76 of the A-tRNA and the 2' OH of A2451, coordinate W1 ³¹ (Figure 6G). In the ErmBL-SRC, we observe no density for A2602 or for the N-terminus of L27, suggesting that the W1 is not coordinated (Figure 6H). Stabilization of the very N-terminus of L27 has only been observed in the pre-attack structures due to interaction of the side chain of His3 of L27 with the O1P of C75 of the A-tRNA and the backbone carboxyl of Ala2 of L27 with the N6 of A76 of the P-tRNA ^{2,31}. This simultaneous interaction of L27 with the A- and P-tRNA is not possible in the ErmBL-SRC because of the shifted position of the nucleobase of A76 of the P-

tRNA (**Figure 6H**). Moreover, the positioning of the ribose 2' OH of the A76 of the P-tRNA is also critical for peptide bond formation³²⁻³⁴, and therefore it is easy to envisage how perturbations of the ribose positioning of the P-tRNA as seen in ErmBL can disrupt the proton shuttle/wire.

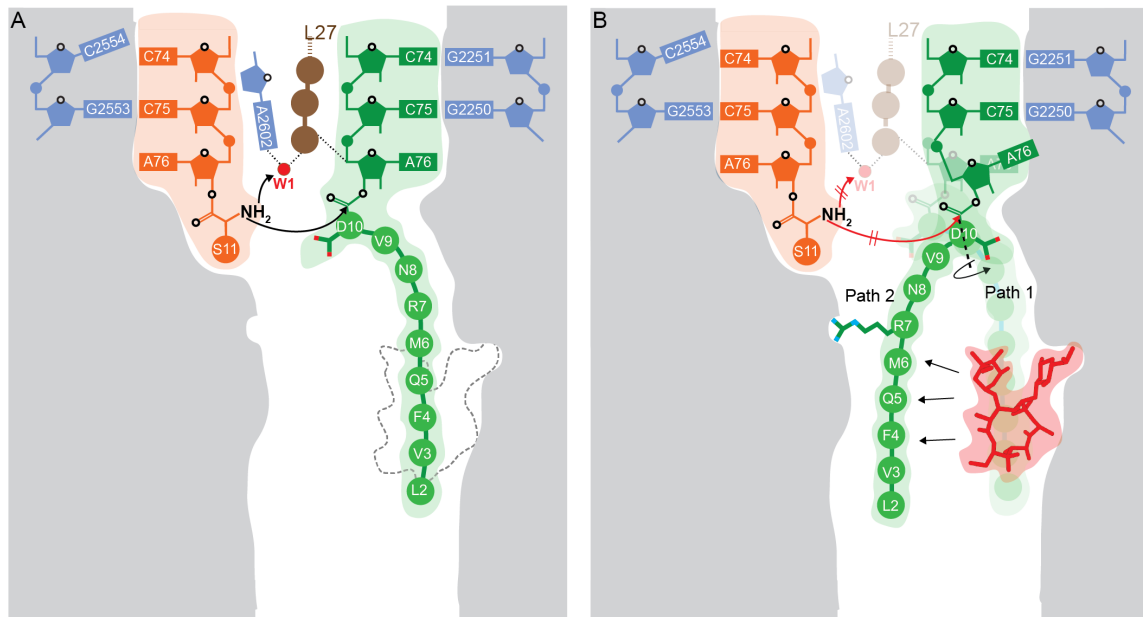


Figure 7 Model for ErmBL-mediated translation arrest.

CONCLUSION

Based on our cryo-EM structures of the ErmBL-SRC, we propose a model for how the ErmBL nascent chain, together with the macrolide erythromycin and components of the ribosomal tunnel, interplay to inactivate the PTC and induce translational arrest (**Figure 7**). In the absence of erythromycin, crystal structures suggest that following accommodation of an aminoacyl-tRNA at the A-site of the PTC, the α -amino group of the A-tRNA is positioned to make nucleophilic attack onto the carbonyl-carbon of the peptidyl-tRNA in the P-site (**Figure 7A**). For this nucleophilic attack to proceed, proton transfer is necessary from the attacking nucleophile to a water molecule (W1, which is coordinated by L27 and A2602), via a proton wire formed by the 2' -OH of the P-site A76 ribose and the 2' -OH of A2451 (**Figure 7A**). In all structures to date, the side chain of the C-terminal amino acid, which is attached to the P-tRNA, is oriented such that all nascent polypeptide chains follow a similar pathway through the ribosomal tunnel. This canonical pathway, which we term pathway P1, is sterically occluded by the presence of macrolide antibiotics, explaining why this class of antibiotics induces peptidyl-tRNA drop-off for most nascent polypeptide chains³⁵⁻³⁷

In the presence of erythromycin, we propose that the conformations adopted by ErmBL are restricted, presumably due to the reduced diameter of the ribosomal tunnel, which in turn promotes interaction of critical residues, such as Arg7 of ErmBL, with 23S rRNA nucleotides on one side of the ribosomal tunnel (**Figure 7B**). In addition, we observe that Asp10 of ErmBL adopts an unusual rotated conformation, which together with the Arg7 interaction, stabilizes the ErmBL nascent chain in an alternative pathway P2, rather than using the canonical pathway P1. Pathway P2 is directed away from the tunnel-bound drug, providing an explanation as to why ErmBL-stalling occurs with both macrolides and ketolides¹⁶. In contrast to previous suggestions¹⁶, the Lys-tRNA in the ErmCL-SRC appears to be sufficiently accommodated at the A-site of the PTC such that nucleophilic attack onto the P-tRNA is possible (**Figure 7B**). Instead, we observe that the A76 ribose of the P-tRNA is perturbed, presumably as a consequence of the unusual rotation of Asp10 and conformation of the ErmBL nascent chain. We propose that the perturbed A76 of the P-tRNA prevents coordination of the water molecules necessary for catalyzing peptide bond formation (**Figure 7B**)³¹, in agreement with the lack of density

for A2602 and the N-terminus of L27, which ultimately traps the ribosome in a pre-attack state and thereby stalls translation.

In conclusion, this study illustrates how the ribosome can employ the ErmBL nascent chain, together with antibiotic erythromycin, to prevent peptide bond formation via P-tRNA perturbation. Inhibition by P-tRNA perturbation has been suggested previously for the SecM stalling sequence⁶, however the limited resolution precluded a molecular basis for this stalling mechanism. Recent cryo-EM structures of the drug-dependent ErmCL-SRC have revealed a completely unrelated mechanism of PTC silencing, namely, via inducing allosteric conformational rearrangements within the PTC active site¹⁸. It will be interesting to investigate other drug-dependent stalling systems to ascertain whether these systems use similar mechanisms to induce translational arrest or whether further novel mechanisms will be discovered.

EXPERIMENTAL PROCEDURES

Generation and purification of ErmBL-SRC

ErmBL-SRC were generated following the same procedure as previously described¹⁶. The *2XermBL* construct was synthesized (Eurofins, Martinsried, Germany) such that it contained a T7 promoter followed by a strong ribosome binding site (RBS) spaced by 7 nucleotides (nts) to the ATG start codon of the first *ermBL* cistron. A linker of 22 nts separated the stop codon of the first *ermBL* cistron and the start codon of the second *ermBL* cistron. The linker also comprised the strong RBS 7 nts upstream of the ATG start codon of the second *ermBL* cistron, enabling initiation of translation independent from the first *ermBL* cistron. Each *ermBL* cistron encoded amino acids 1-17 corresponding to ErmBL leader peptide (Genbank accession number K00551) present on macrolide resistance plasmid pAM77 from *Streptococcus sanguis* strain a1³⁸. The complete sequence of *2XermBL* construct is:

5'-*TAATACGACTCACTATAGGGAGTTTTATAAGGAGGAAAAATATGTTGGTAT*
TCCAAATGCGTAATGTAGATAAAAACATCTACTATTTTGAAATAAAGTTTTATA
AGGAGGAAAAATATGTTGGTATTCCAAATGCGTAATGTAGATAAAAACATC
TACTATTTTGAAATAA-3' (T7 Promoter, italics; RBS, bold; ErmBL ORF, shaded

grey with GAT codon in P-site of stalled ribosome shown in bold; Annealing site for complementary DNA oligonucleotide, underlined). *In vitro* translation of the *2XermBL* construct was performed using the Rapid Translation System RTS 100 *E. coli* HY Kit (5PRIME; Cat. No. 2401110). Translation reactions were analyzed on sucrose density gradients (10%-55% sucrose in a buffer A, containing 50 mM HEPES-KOH, pH 7.4, 100 mM KOAc, 25 mM Mg(OAc)₂, 6 mM β-mercaptoethanol, 10 μM erythromycin and 1× Complete EDTA-free Protease Inhibitor cocktail (Roche)) by centrifugation at 154,693 x g (SW-40 Ti, Beckman Coulter) for 3 h at 4°C. For ErmBL-SRC purification, disome fractions were collected using a Gradient Station (Biocomp) with an Econo UV Monitor (Biorad) and a FC203B Fraction Collector (Gilson). Purified ErmBL-SRC disomes were concentrated by centrifugation through Amicon Ultra-0.5 mL Centrifugal Filters (Merck-Millipore) according to the manufacturer's protocol. To obtain monosomes of the ErmBL-SRC, a short DNA oligonucleotide (5'-ttcctcctataaaact-3', Metabion) was annealed to the linker between the *ermBL* cistrons of the disomes, generating a DNA-

RNA hybrid that could be cleaved by RNase H (NEB) treatment in buffer A at 25°C for 1h. After cleavage of the disomes, ErmBL-SRC monosomes were again purified and concentrated by centrifugation through Amicon Ultra-0.5 mL Centrifugal Filters (Merck-Millipore) according to the manufacturer's protocol.

Negative-stain electron microscopy

Ribosomal particles were diluted in buffer A to final concentrations of 0.5 A₂₆₀/ml up to 5 A₂₆₀/ml in order to determine the optimal ribosome density for cryo-EM. One drop of each sample was deposited on a carbon-coated grid. After 30 seconds, grids were washed with distilled water and then stained with 3 drops of 2% aqueous uranyl acetate for 15 seconds. The remaining liquid was removed by touching the grid with filter paper. Micrographs were taken using a Morgagni transmission electron microscope (FEI), 80 kV, wide angle 1K CCD at direct magnifications of 72K.

Cryo-electron microscopy and single particle reconstruction

4 A₂₆₀/ml monosomes of the ErmBL-SRC were applied to 2 nm pre-coated Quantifoil R3/3 holey carbon supported grids and vitrified using a Vitrobot Mark IV (FEI Company). Data collection was performed at NeCEN (Leiden, Netherlands) on a Titan Krios transmission electron microscope (TEM) (FEI, Eindhoven, Netherlands) equipped with a Falcon II direct electron detector at 300 kV with a magnification of 125,085x, a pixel size of 1.108 Å and a defocus range of 0.7-1.2 µm. The data are provided as a series of seven frames (dose per frame of 4 e⁻/Å²) from which we summed frames 2-5 (accumulated dose of 28 e⁻/Å²) after alignment using Motion Correction software³⁹. Images were processed using a frequency-limited refinement protocol that helps prevent over-fitting⁴⁰, specifically by truncation of high frequencies (in this case at 8 Å). As reported and expected⁴⁰, we find that using this processing regime the 0.143 FSC value provides a good indicator for the true average resolution of the map. Additionally, the local resolution of the map was calculated using ResMap⁴¹. Power-spectra and defocus values were determined using the SPIDER TF ED command and recorded images were manually inspected for good areas and power-spectra quality. Data were processed further using the SPIDER software package¹⁹, in combination with an automated

workflow as described previously⁴². After initial, automated particle selection based on the program SIGNATURE⁴³, initial alignment was performed with 285,462 particles, using *E. coli* 70S ribosome as a reference structure¹⁶. After removal of noisy particles (30,093 particles; 11%), the dataset of 255,369 particles could be sorted into two main subpopulations using an incremental K-means-like method of unsupervised 3D sorting (**Figure S1**)⁴⁴: A minor sub-population (94,139 particles, 37%) containing stoichiometric density for the P-tRNA, lacking E-tRNA (L1 stalk in the “out” position) and containing sub-stoichiometric density for the A-tRNA, which was not sorted further due to the low particle numbers. The major subpopulation (161,231 particles; 63%) was defined by the presence of stoichiometric densities for P- and E-tRNAs but sub-stoichiometric density for the A-tRNA. This population was further sorted into two additional sub-populations, both containing stoichiometric densities for the P- and E-tRNAs (L1 stalk in the “in” position) and differing by the presence (termed ErmBL-APE-SRC) or absence of A-tRNA (ErmBL-PE-SRC). Both sub-populations could be refined to an average resolution of 3.6 Å (0.143 FSC) and a local resolution extending towards 3.0 Å for the core of the 30S and 50S subunit as computed using ResMap⁴¹ (**Figure S2**). The final maps were subjected to the program EM-BFACTOR⁴⁵ in order to apply an automatically determined negative B-factor for sharpening of the map.

Molecular modeling and map-docking procedures

The molecular model for the ribosomal proteins and rRNA of the ErmBL-SRC is based on the molecular model for the 50S subunit from the recent crystal structure of the *E. coli* 70S ribosome (PDB ID 4KIX)⁴⁶ and obtained by performing a rigid body fit into the cryo-EM density map of the ErmCL-SRC using UCSF Chimera⁴⁷ (fit in map function). Similarly, the position of erythromycin was identical to that observed previously^{48,49} and obtained by rigid body fit of PDB3OFR⁴⁹ into the cryo-EM density map of the ErmCL-SRC. The overall fit of the crystal structures were in very good agreement with the electron density of ErmCL-SRC and since exclusively the conformations of important nucleotides of the PTC and the exit tunnel are crucial to interpret the molecular mechanism leading to stalling on ErmCL, only these 23S rRNA nucleotides (A2602, G2583, U2584, U2585, U2586, U2506, A2062), were manually shifted/rotated where

necessary into their respective densities using Coot⁵⁰, whereas the rest of the rigid-body-fitted crystal structure remained unchanged. The conformation of A2602 observed in ErmCL-SRC is distinct from the “up” conformation observed in ErmBL-SRC (PDB3J5L)¹⁶ and from the “down” conformation in (PDB1VQN)^{28,29} as such its conformation resembles an intermediate state between “up” and “down”. The conformation of U2506 is similar to its conformation in (PDB1VQN)^{28,29}, however slight manual rotation of the base was required to get an optimal fit. Different conformations of A2062, e.g. the “down” (PDB2WRJ)⁵¹ and “tunnel-in” (PDB3I8F)⁵² conformations sterically clash with the ErmCL nascent chain, whereas the “up” conformation present in the *Haloarcula marismortui* 50S subunit in complex with model peptide bond substrates (e.g. PDB1VQN)^{28,29} was similar to the conformation of A2062 observed in the ErmCL-SRC. Most notably, U2585 adopts a unique and novel “flipped out” position, which is very different to previously observed positions for U2585, i.e. U2585 in the uninduced (PDB1VQ6) or (PDB1VQN) induced state of the PTC^{28,29}. In the novel, “flipped-out” conformation U2585 is rotated approximately 80° when compared to its canonical position. In order to regularize the rRNA backbone surrounding U2585, neighboring nucleotides G2583, U2584 and U2586 were slightly adjusted in the model for ErmCL-SRC. Besides 23S rRNA nucleotides, the CCA-end of the P-tRNA, in particular A76, was manually adjusted in order to fit the density, since previously reported conformations observed in crystal structures of the *Haloarcula marismortui* 50S subunit in complex with model peptide bond substrates did not fit the density when fitted as a rigid body together with the 50S subunit. The molecular model for the ErmCL nascent polypeptide chain was modeled and refined into the density using Coot⁵⁰.

Figure preparation

Figures showing electron densities and atomic models were generated using UCSF Chimera⁴⁷.

SUPPLEMENTAL INFORMATION

Supplemental Information includes Figures S1-S4 and Supplemental References can be found with this article online at <http://...>

ACCESSION NUMBERS

The cryo-EM maps and associated atomic coordinates have been deposited in the EMDB and PDB with the accession codes EMDB-XXX and PDB-XXX (ErmBL-APE-SRC) and EMDB-YYY and PDB ID YYY (ErmBL-AP-SRC).

ACKNOWLEDGMENTS

We thank Rishi Matadeen and Sacha DeCarlo for data collection at the NeCEN facility (Leiden, Netherlands) and Charlotte Ungewickell and Dorota Klepacki for expert technical assistance. This research was supported by grants from the NIH (GM104370 to N.V-L. and R01GM095737 to D.N.W.) and the Deutsche Forschungsgemeinschaft (FOR1805, WI3285/3-1 and GRK1721 to D.N.W.).

REFERENCES

- 1 Simonovic, M. & Steitz, T. A. A structural view on the mechanism of the ribosome-catalyzed peptide bond formation. *Biochimica et biophysica acta* **1789**, 612-623 (2009).
- 2 Voorhees, R. M., Weixlbaumer, A., Loakes, D., Kelley, A. C. & Ramakrishnan, V. Insights into substrate stabilization from snapshots of the peptidyl transferase center of the intact 70S ribosome. *Nat Struct Mol Biol* **16**, 528-533 (2009).
- 3 Wilson, D. N. & Beckmann, R. The ribosomal tunnel as a functional environment for nascent polypeptide folding and translational stalling. *Curr. Opin. Struct. Biol.* **21**, 1-10 (2011).
- 4 Ito, K. & Chiba, S. Arrest peptides: cis-acting modulators of translation. *Annu. Rev. Biochem.* **82**, 171-202 (2013).
- 5 Sohmen, D. *et al.* Structure of the *Bacillus subtilis* 70S ribosome reveals the basis for species-specific stalling. *Nat Commun* **6**, 6941, doi:10.1038/ncomms7941 (2015).
- 6 Bhushan, S. *et al.* SecM-stalled ribosomes adopt an altered geometry at the peptidyltransferase center. *PLoS Biol.* **19**, e1000581 (2011).
- 7 Ito, K., Chiba, S. & Pogliano, K. Divergent stalling sequences sense and control cellular physiology. *Biochemical and biophysical research communications* **393**, 1-5 (2010).
- 8 Ramu, H., Mankin, A. & Vazquez-Laslop, N. Programmed drug-dependent ribosome stalling. *Molecular microbiology* **71**, 811-824 (2009).
- 9 Vázquez-Laslop, N., Ramu, H. & Mankin, A. S. in *Ribosomes. Structure, function, evolution* (eds M. V. Rodnina, W. Wintermeyer, & R. Green) 377-392 (Springer-Verlag, 2011).
- 10 Gong, F., Ito, K., Nakamura, Y. & Yanofsky, C. The mechanism of tryptophan induction of tryptophanase operon expression: tryptophan inhibits release factor-mediated cleavage of TnaC-peptidyl-tRNA(Pro). *Proc. Natl. Acad. Sci. U S A* **98**, 8997-9001 (2001).
- 11 Gong, F. & Yanofsky, C. Instruction of translating ribosome by nascent peptide. *Science* **297**, 1864-1867 (2002).
- 12 Iordanescu, S. Three distinct plasmids originating in the same *Staphylococcus aureus* strain. *Arch Roum Pathol Exp Microbiol* **35**, 111-118 (1976).
- 13 Horinouchi, S. & Weisblum, B. Posttranscriptional modification of mRNA conformation: mechanism that regulates erythromycin-induced resistance. *Proceedings of the National Academy of Sciences of the United States of America* **77**, 7079-7083 (1980).
- 14 Shivakumar, A. G., Hahn, J., Grandi, G., Kozlov, Y. & Dubnau, D. Posttranscriptional regulation of an erythromycin resistance protein specified by plasmic pE194. *Proceedings of the National Academy of Sciences of the United States of America* **77**, 3903-3907 (1980).
- 15 Gupta, P., Sothiselvam, S., Vazquez-Laslop, N. & Mankin, A. S. Deregulation of translation due to post-transcriptional modification of rRNA explains why erm genes are inducible. *Nat. Commun.* **4**, 1984 (2013).
- 16 Arenz, S. *et al.* Molecular basis for erythromycin-dependent ribosome stalling during translation of the ErmBL leader peptide. *Nat Commun* **5**, 3501, doi:10.1038/ncomms4501 (2014).

- 17 Vazquez-Laslop, N., Thum, C. & Mankin, A. S. Molecular mechanism of drug-
dependent ribosome stalling. *Mol Cell* **30**, 190-202 (2008).
- 18 Arenz, S. *et al.* Drug sensing by the ribosome induces translational arrest via active
site perturbation. *Mol Cell* **56**, 446-452, doi:10.1016/j.molcel.2014.09.014 (2014).
- 19 Frank, J. *et al.* SPIDER and WEB: processing and visualization of images in 3D
electron microscopy and related fields. *J Struct Biol* **116**, 190-199 (1996).
- 20 Bischoff, L., Berninghausen, O. & Beckmann, R. Molecular basis for the ribosome
functioning as an L-tryptophan sensor. *Cell Rep* **9**, 469-475,
doi:10.1016/j.celrep.2014.09.011 (2014).
- 21 Bhushan, S. *et al.* alpha-Helical nascent polypeptide chains visualized within distinct
regions of the ribosomal exit tunnel. *Nat Struct Mol Biol* **17**, 313-317 (2010).
- 22 Seidelt, B. *et al.* Structural insight into nascent polypeptide chain-mediated
translational stalling. *Science* **326**, 1412-1415 (2009).
- 23 Bhushan, S. *et al.* Structural basis for translational stalling by human
cytomegalovirus (hCMV) and fungal arginine attenuator peptide (AAP). *Mol. Cell* **40**,
138-146 (2010).
- 24 Shao, S., Brown, A., Santhanam, B. & Hegde, R. S. Structure and assembly pathway
of the ribosome quality control complex. *Mol Cell* **57**, 433-444,
doi:10.1016/j.molcel.2014.12.015 (2015).
- 25 Kannan, K., Vazquez-Laslop, N. & Mankin, A. S. Selective protein synthesis by
ribosomes with a drug-obstructed exit tunnel. *Cell* **151**, 508-520 (2012).
- 26 Kannan, K. *et al.* The general mode of translation inhibition by macrolide antibiotics.
Proceedings of the National Academy of Sciences of the United States of America **111**,
15958-15963, doi:10.1073/pnas.1417334111 (2014).
- 27 Hansen, J. L., Schmeing, T. M., Moore, P. B. & Steitz, T. A. Structural insights into
peptide bond formation. *Proc. Natl. Acad. Sci. USA* **99**, 11670-11675 (2002).
- 28 Schmeing, T. M., Huang, K. S., Kitchen, D. E., Strobel, S. A. & Steitz, T. A.
Structural insights into the roles of water and the 2' hydroxyl of the P site tRNA in the
peptidyl transferase reaction. *Mol. Cell* **20**, 437-448 (2005).
- 29 Schmeing, T. M., Huang, K. S., Strobel, S. A. & Steitz, T. A. An induced-fit
mechanism to promote peptide bond formation and exclude hydrolysis of peptidyl-
tRNA. *Nature* **438**, 520-524 (2005).
- 30 Schmeing, T. M. *et al.* A pre-translocational intermediate in protein synthesis
observed in crystals of enzymatically active 50S subunits. *Nat. Struct. Biol.* **9**, 225-
230 (2002).
- 31 Polikanov, Y. S., Steitz, T. A. & Innis, C. A. A proton wire to couple aminoacyl-
tRNA accommodation and peptide-bond formation on the ribosome. *Nat Struct Mol
Biol* **21**, 787-793, doi:10.1038/nsmb.2871 (2014).
- 32 Dorner, S., Panuschka, C., Schmid, W. & Barta, A. Mononucleotide derivatives as
ribosomal P-site substrates reveal an important contribution of the 2'-OH to activity.
Nucleic acids research **31**, 6536-6542 (2003).
- 33 Weinger, J. S., Parnell, K. M., Dorner, S., Green, R. & Strobel, S. A. Substrate-
assisted catalysis of peptide bond formation by the ribosome. *Nat. Struct. Mol. Biol.*
11, 1101-1106 (2004).
- 34 Zaher, H. S., Shaw, J. J., Strobel, S. A. & Green, R. The 2'-OH group of the peptidyl-
tRNA stabilizes an active conformation of the ribosomal PTC. *EMBO J* **30**, 2445-
2453, doi:10.1038/emboj.2011.142 (2011).

- 35 Menninger, J. & Otto, D. Erythromycin, carbomycin and spiramycin inhibit protein synthesis by stimulating the dissociation of peptidyl-tRNA from ribosomes. *Antimicrob. Agents Chemother.* **21**, 811-818. (1982).
- 36 Otaka, T. & Kaji, A. Release of (oligo)peptidyl-tRNA from ribosomes by erythromycin A. *Proc. Natl. Acad. Sci. USA* **72**, 2649-2652. (1975).
- 37 Tenson, T., Lovmar, M. & Ehrenberg, M. The mechanism of action of macrolides, lincosamides and streptogramin B reveals the nascent peptide exit path in the ribosome. *J. Mol. Biol.* **330**, 1005-1014 (2003).
- 38 Horinouchi, S., Byeon, W. H. & Weisblum, B. A complex attenuator regulates inducible resistance to macrolides, lincosamides, and streptogramin type B antibiotics in *Streptococcus sanguis*. *J. Bacteriol.* **154**, 1252-1262 (1983).
- 39 Li, X. *et al.* Electron counting and beam-induced motion correction enable near-atomic-resolution single-particle cryo-EM. *Nat Methods* **10**, 584-590, doi:10.1038/nmeth.2472 (2013).
- 40 Scheres, S. H. & Chen, S. Prevention of overfitting in cryo-EM structure determination. *Nat Methods* **9**, 853-854, doi:10.1038/nmeth.2115 (2012).
- 41 Kucukelbir, A., Sigworth, F. J. & Tagare, H. D. Quantifying the local resolution of cryo-EM density maps. *Nat Methods* **11**, 63-65, doi:10.1038/nmeth.2727 (2014).
- 42 Becker, T. *et al.* Structural basis of highly conserved ribosome recycling in eukaryotes and archaea. *Nature* **482**, 501-506 (2012).
- 43 Chen, J. Z. & Grigorieff, N. SIGNATURE: a single-particle selection system for molecular electron microscopy. *J. Struct. Biol.* **157**, 168-173 (2007).
- 44 Loerke, J., Giesebrecht, J. & Spahn, C. M. Multiparticle cryo-EM of ribosomes. *Methods Enzymol* **483**, 161-177, doi:10.1016/S0076-6879(10)83008-3 (2010).
- 45 Fernandez, J. J., Luque, D., Caston, J. R. & Carrascosa, J. L. Sharpening high resolution information in single particle electron cryomicroscopy. *J Struct Biol* **164**, 170-175, doi:10.1016/j.jsb.2008.05.010 (2008).
- 46 Pulk, A. & Cate, J. H. Control of ribosomal subunit rotation by elongation factor G. *Science* **340**, 1235970, doi:10.1126/science.1235970 (2013).
- 47 Pettersen, E. F. *et al.* UCSF Chimera - A Visualization System for Exploratory Research and Analysis. *J. Comput. Chem.* **25**, 1605-1612 (2004).
- 48 Tu, D., Blaha, G., Moore, P. & Steitz, T. Structures of MLSBK antibiotics bound to mutated large ribosomal subunits provide a structural explanation for resistance. *Cell* **121**, 257-270 (2005).
- 49 Dunkle, J. A., Xiong, L., Mankin, A. S. & Cate, J. H. Structures of the *Escherichia coli* ribosome with antibiotics bound near the peptidyl transferase center explain spectra of drug action. *Proceedings of the National Academy of Sciences of the United States of America* **107**, 17152-17157 (2010).
- 50 Emsley, P. & Cowtan, K. Coot: Model-Building Tools for Molecular Graphics. *Acta Crystallographica Section D - Biological Crystallography* **60**, 2126-2132 (2004).
- 51 Gao, Y. G. *et al.* The structure of the ribosome with elongation factor G trapped in the posttranslocational state. *Science* **326**, 694-699 (2009).
- 52 Jenner, L. B., Demeshkina, N., Yusupova, G. & Yusupov, M. Structural aspects of messenger RNA reading frame maintenance by the ribosome. *Nat Struct Mol Biol* **17**, 555-560 (2010).

SUPPLEMENTARY INFORMATION

Table 1: Refinement and Model Statistics

Data Collection and Refinement	ErmBL-APE-SRC	ErmBL-PE-SRC
Particles	85,393	75,839
Pixel size (Å)	1.108	1.108
Defocus range (µm)	1.0-2.4	1.0-2.4
Voltage (kV)	300	300
Electron dose (e ⁻ /Å ²)	28	28
Map sharpening B factor (Å ²)	-147.40	-140.09
Resolution (Å, 0.143 FSC)	3.6	3.6
Model Composition		
Non-hydrogen atoms	146778	145176
Protein residues	5626	5626
RNA bases	4761	4696
Validation (proteins)		
Poor rotamers (%)	0.00	0.00
Ramachandran outliers (%)	2.68	2.68
Ramachandran favored (%)	89.95	89.99
Bad backbone bonds (%)	0.00	0.00
Bad backbone angles	0.00	0.00
MolProbity score	1.89 (81 st percentile)	1.88 (82 nd percentile)
Validation (nucleic acids)		
Correct sugar puckers (%)	99.67	99.78
Bad backbone conformations (%)	14.18	14.30
Bad bonds (%)	1.06	1.06
Bad angles	0.00	0.00
Clashscore, all atoms	6.11 (90th percentile)	5.99 (90th percentile)

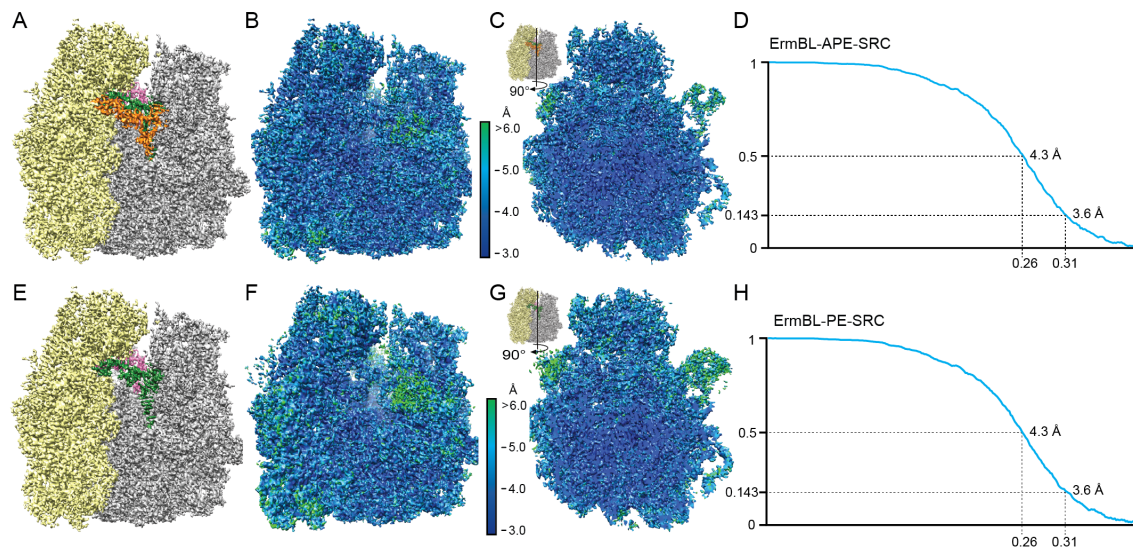


Figure S2 Average and local resolution determination of ErmBL-SRC's (A-D) Cryo-EM reconstruction of (A) ErmBL-APE-SRC bearing A-tRNA (orange), P-tRNA (green) and E-tRNA (pink) and (B) the surface or (C) the transverse section coloured according to local resolution. (D) Average resolution of the ErmBL-APE-SRC was 4.3 Å using the Fourier shell correlation (FSC) cut-off value of 0.5. Due to image processing in the absence of spatial frequencies higher than 8 Å, the FSC value of 0.143 was used for average resolution determination of 3.9 Å⁴⁰. (E-H) Cryo-EM reconstruction of (E) ErmBL-APE-SRC bearing A-tRNA (orange), P-tRNA (green) and E-tRNA (pink) and (F) the surface or (G) the transverse section coloured according to local resolution. (H) Average resolution of the ErmBL-APE-SRC was 4.3 Å using the Fourier shell correlation (FSC) cut-off value of 0.5. Due to image processing in the absence of spatial frequencies higher than 8 Å, the FSC value of 0.143 was used for average resolution determination of 3.9 Å (Scheres and Chen, 2012).

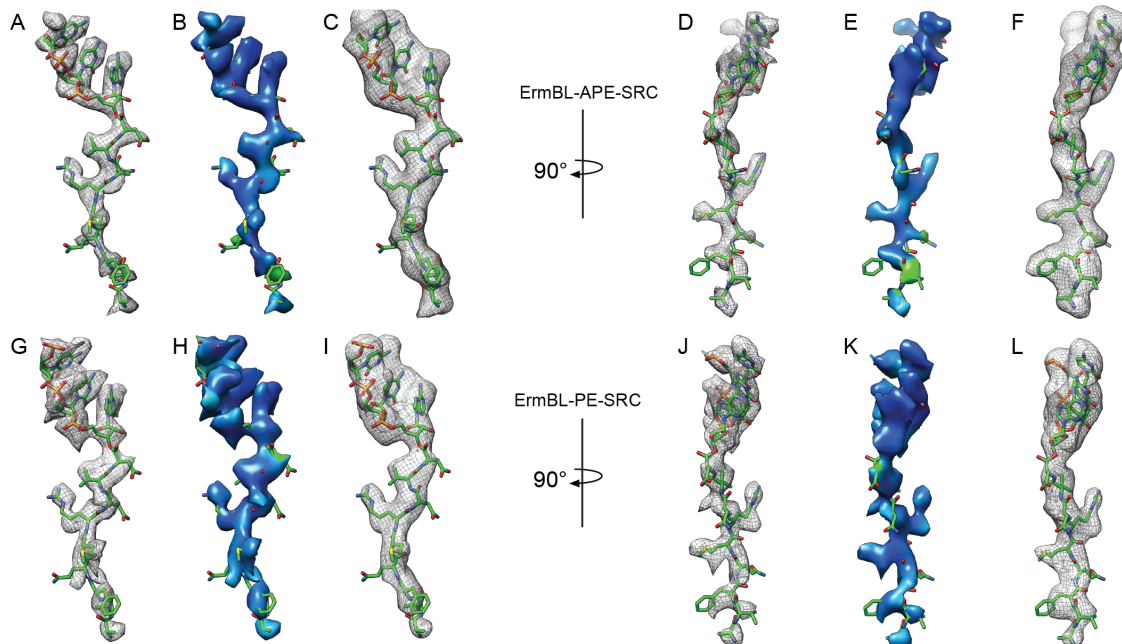


Figure S3 Cryo-EM densities for the ErmBL nascent chain in both ErmBL-SRCs (A-L) Isolated cryo-EM densities with atomic model for ErmBL nascent chains (green) from (A-F) ErmBL-APE-SRC and (G-L) ErmBL-PE-SRC with electron density (B,E,H,K) coloured according to local resolution or (C,F,I,L) filtered to 4-5 Å.

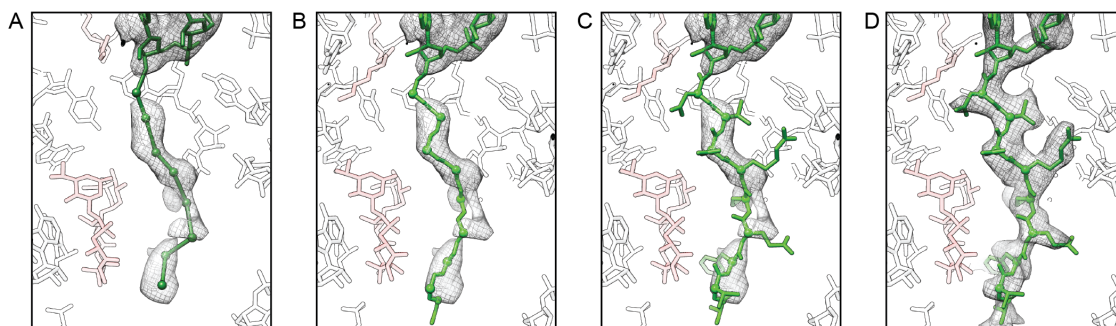


Figure S4 Improvement ErmBL-SRC map and model. (A-C) Isolated cryo-EM density (grey mesh) of the initial ErmBL-SRC reconstruction (¹⁶, EMD-5771) with C α backbone trace (A) of initially reported for ErmBL nascent chain (PDB 3J5L, green) and (B) of the new atomic model and (C) including amino acid side chains. (D) Isolated cryo-EM density (grey mesh) of the new ErmBL-APE SRC reconstruction including atomic model for ErmBL nascent chain residues V3-D10 (green).